Use as Original 9/27/96

SEP 3 0 1996

ENGINEERING DATA TRANSMITTAL

Page 1 of 1

1. EDT № 613758

2. To: (Receiving Organization) FSAR Development	3. From: (Originating Organization) Safety Issue Resolution	4. Related EDT No.: N/A
5. Proj./Prog./Dept./Div.:	6. Design Authority/ Design Agent/Cog. Engr.: D.R. Bratzel	7. Purchase Order No.: N/A
8. Originator Remarks: This report presents an in-depth technical review of the potential for nuclear criticality to occur in Hanford defense waste tanks during safe storage operations.		9. Equip./Component No.: N/A
		10. System/Bldg./Facility: N/A
11. Receiver Remarks: 11A. Design Baseline Document? [] Yes [X] No		12. Major Assm. Dwg. No.: N/A
		13. Permit/Permit Application No.: N/A
		14. Required Response Date: N/A

15. DATA TRANSMITTED

(A) Item No.	(B) Document/Drawing No.	(C) Sheet No.	(D) Rev. No.	(E) Title or Description of Data Transmitted	(F) Approval Designator	(G) Reason for Transmittal	(H) Originator Disposition	(I) Receiver Disposition
1	WHC-SD-WM-TI-757		0	Fluid Dynamics, Particulate Segregation, Chemical Processes, Natural Ore Analog and Tank Inventory Discussions that Relate to the Potential for Criticality in Hanford Tanks	SQ			

16. KEY

Approval Designator (F)	Reason for Transmittal (G)		Disposition (H) & (I)	
E, S, Q, D or N/A (see WHC-CM-3-5, Sec.12.7)	1. Approval 2. Release 3. Information	4. Review 5. Post-Review 6. Dist. (Receipt Acknow. Required)	1. Approved 2. Approved w/comment 3. Disapproved w/comment	4. Reviewed no/comment 5. Reviewed w/comment 6. Receipt acknowledged

17. SIGNATURE/DISTRIBUTION
(See Approval Designator for required signatures)

(G) Reason	(H) Disp.	(J) Name (K) Signature (L) Date (M) MSIN	(G) Reason	(H) Disp.	(J) Name (K) Signature (L) Date (M) MSIN
		Design Authority	1	1	S. J. Eberlein for 9/27/96
		Design Agent			
1	1	Cog.Eng. D. R. Bratzel 9/18/96			
1	1	Cog. Mgr. R. J. Cash 9/27/96			
1	1	QA J. W. Hagan 9/27/96			
1	1	Safety L. M. Calderon 9/27/96			
		Env.			

18.	19.	20.	21. DOE APPROVAL (if required)
D. R. Bratzel 9/18/96 Signature of EDT Originator Date	G. J. Dunford 9/18/96 Authorized Representative for Receiving Organization Date	R. J. Cash 9/27/96 Design Authority/ Cognizant Manager Date	Ctrl. No. [] Approved [] Approved w/comments [] Disapproved w/comments

BD-7400-172-2 (05/96) GEF097

Fluid Dynamics, Particulate Segregation, Chemical Processes, Natural Ore Analog and Tank Inventory Discussions that Relate to the Potential for Criticality in Hanford Tanks

R. J. Serne
G. A. Whyatt
S. V. Mattigod
Y. Onishi
P. G. Doctor
B. N. Bjornstad
M. R. Powell
L. M. Liljegren
J. H. Westsik, Jr.
N. J. Aimo
K. P. Recknagle
G. R. Golcar
T. B. Miley
G. R. Holdren
Pacific Northwest National Laboratory, Richland, WA 99352

D.W. Jeppson
R.K. Biyani
G.S. Barney
Westinghouse Hanford Company, Richland, WA 99352

U.S. Department of Energy Contract DE-AC06-87RL10930

EDT/ECN: ~~603229~~ 613758 X7. 9/30/96 UC:

TRADEMARK DISCLAIMER. Reference herein to any specific commercial product, process, or service by trade name, trademark, manufacturer, or otherwise, does not necessarily constitute or imply its endorsement, recommendation, or favoring by the United States Government or any agency thereof or its contractors or subcontractors.

Printed in the United States of America. To obtain copies of this document, contact: WHC/BCS Document Control Services, P.O. Box 1970, Mail stop H6-08, Richland WA 99352, Phone (509) 372-2420; Fax (509) 376-4989.

DATE: HANFORD RELEASE ID: 2.
STA: 4
SEP 30 1996

Release Approval 9/27/96 Date Release Stamp

Approved for Public Release

Org Code: 8M700
B&R Code:

Charge Code: N1696
Total Pages: ~~xxx~~ 352 kmd 9/27/96

Key Words: Hanford Tank Farms, Criticality Safety Basis, Fissile Materials

Abstract:

This report presents an in-depth review of the potential for nuclear criticality to occur in Hanford defense waste tanks during past, current and future safe storage and maintenance operations. The report also briefly discusses the potential impacts of proposed retrieval activities, although retrieval was not a main focus of scope. After thorough review of fluid dynamic aspects that focus on particle segregation, chemical aspects that focus on solubility and adsorption processes that might concentrate plutonium and/or separate plutonium from the neutron absorbers in the tank waste, and ore-body formation and mining operations, the interdisciplinary team has come to the conclusion that there is negligible risk of nuclear critically under existing storage conditions in Hanford Site underground waste storage tanks. Further, for the accident scenarios considered an accidental criticality is incredible.

The executive summary and summaries at the end of each section in which substantial analyses, calculations or literature interpretations were performed provide more detailed findings and support for these conclusions.

TRADEMARK DISCLAIMER. Reference herein to any specific commercial product, process, or service by trade name, trademark, manufacturer, or otherwise, does not necessarily constitute or imply its endorsement, recommendation, or favoring by the United States Government or any agency thereof or its contractors or subcontractors.

Printed in the United States of America. To obtain copies of this document, contact: WHC/BCS Document Control Services, P.O. Box 1970, Mail stop H6-08, Richland WA 99352, Phone (509) 372-2420; Fax (509) 376-4989.

Release Approval — Date 9/27/96

DATE:
STA: 4
HANFORD RELEASE
ID: 2.
SEP 30 1996

Release Stamp

Approved for Public Release

WHC-SD-WM-TI-757
Revision 0

Fluid Dynamic Particulate Segregation, Chemical Processes, and Natural Ore Analog Discussions that Relate to the Potential for Criticality in Hanford Tanks

Prepared for the U.S. Department of Energy
Office of Environmental Restoration and
Waste Management

Westinghouse
Hanford Company Richland, Washington

Management and Operations Contractor for the
U.S. Department of Energy under Contract DE-AC06-87RL10930

Approved for Public Release

Document Title: FLUID DYNAMIC PARTICULATE SEGREGATION, CHEMICAL PROCESSES, AND NATURAL ORE ANALOG DISCUSSIONS THAT RELATE TO THE POTENTIAL FOR CRITICALITY IN HANFORD TANKS

Prepared by:

R. J. Serne — 9-19-96 Date
Staff Scientist, Applied Geology and Geochemistry Group
Pacific Northwest National Laboratory

G. A. Whyatt — 9-23-96 Date
Senior Development Engineer, Chemical Separations & Slurry Processing Group
Pacific Northwest National Laboratory

S. V. Mattigod — 9/19/96 Date
Senior Research Scientist, Applied Geology and Geochemistry Group
Pacific Northwest National Laboratory

Y. Onishi — 9/23/96 Date
Program Manager, Hydrology Group
Pacific Northwest National Laboratory

D. W. Jeppson — 9/23/96 Date
Process Engineering
Westinghouse Hanford Company

Reviewed by:

J. W. Brothers — 9/19/96 Date
Program Manager, Project Management Group
Pacific Northwest National Laboratory

Approved by:

D. R. Bratzel — 9/23/96 Date
Criticality Safety Project, TWRS Safety Issue Resolution
Westinghouse Hanford Company

ACKNOWLEDGMENTS

The authors wish to thank Ed Lipke, Bob Cash, Dave Nyham, and especially Dave Bratzel of Westinghouse Hanford Company for funding this work and keeping us focused on the key objectives. We wish to thank Don Alexander from the U.S. Department of Energy, Richland Operations Office for introducing us to the technical issue and programmatic history. His insight and preliminary analyses gave us a good foundation from which to venture forward. We wish to thank Joe Brothers from the Pacific Northwest National Laboratory Program Office for guiding us on protocols, for being our laison to the Westinghouse Hanford Company financial and program groups, for being our advocate in several programmatic meetings, and for reviewing the draft document.

Numerous scientists, engineers, and project managers freely shared their related work, both published and drafts, and helped guide us to other important literature or issues. Among these willing helpers we wish to recognize John Lafemina, Reza Shekarriz, Jun Liu, Brian Rapko, Penny Colton, Jim Campbell, Greg Lumetta, Jack Ryan, and Linfeng Rao of Pacific Northwest National Laboratory and Cal Delegard, Harry Babad, Bob Marusich, Terry Vail, George Reddick, John Harris, III, Kayle Boomer and Chuck Rogers of Westinghouse Hanford Company. Other technical materials and ideas were provided by Dave Hobbs and Major Thompson of Westinghouse Savannah River and Steve Agnew of Los Alamos National Laboratory.

We wish to acknowledge the stimulating discussions that we had with outside consultants, other Hanford Site staff members, and formal reviewers, who were often unknown to us, but whose comments on draft material helped sharpen the final report. Some of the participants include Arlin Postma (private consultant), Nabil Morcos (Idaho National Engineering Laboratory), Dick Vorehm (M. Chew & Associates), Wally Schulz (W23 Company), Roland Felt, Carole Sohn, and Harry Calley (U.S. Department of Energy), Jess Greenborg, Lou Rodgers, and Alan Waltar (Westinghouse Hanford Company), Rob Tayloe (Battelle Columbus) and Andy Prichard (Pacific Northwest National Laboratory).

Finally we wish to thank Mary Curry and Maggi Nielson of Boeing Computer Services Richland for editing the document and preparing many of the figures for duplication, formatting the report, and coordinating all other prepublication tasks.

This page intentionally left blank.

EXECUTIVE SUMMARY

This report uses information compiled and critically assimilated by the staffs at the Pacific Northwest National Laboratory (PNNL) and Westinghouse Hanford Company (WHC) to evaluate the potential for nuclear criticality to occur in Hanford Site defense waste tanks during present waste storage and under some selected accident scenarios. The report also addresses active operations such as tank cascading, and operation of air-lift circulators to cool the contents of self-boiling tanks to evaluate whether they could have created conditions that would predispose the tanks toward criticality events during inactive storage.

Our critical review found no scenarios or physical and chemical processes that would likely lead to a criticality event. While numerical probabilities for a criticality event have not been attempted, the possibility of such an event during the continued waste storage or future maintenance and retrieval operations is judged to be very remote. The conclusions presented in the following paragraphs support our overall conclusion.

SUPPORTING CONCLUSIONS

Fissile material and the bulk of the neutron absorbers are present in the sludge phase in Hanford Site tanks. The sludge particles are very small grains of crystalline and amorphous hydrous oxides, phosphates, carbonates, and other minor compounds. The particles readily agglomerate and coagulate into larger clusters in the high-pH and high-ionic-strength tank environment. The agglomerated material is cohesive in terms of fluid dynamic properties. Cohesive material is not easily suspended by low-energy physical disturbances and does not promote fluid transport through settled beds. This latter property minimizes convective transport of dissolved material or fine-grained suspended particles through the settled sludge.

Transmission electron microscopy [TEM] characterization of the sludge clearly shows that the sludge primary particles are submicron in size and that agglomeration into larger clusters has occurred. The primary particles agglomorate randomly, rather than selectively with particles of similar composition. Most of the agglomerates appear to be random mixtures of primary particles that are held together by physical forces controlled by innate surface charges, particle size, and the chemical nature of the surrounding fluids. Theoretical discussions that support the TEM observations are found in Appendix A.

Sedimentation studies and inferred particle-size characterization using visual and light-scattering techniques indicate that the sludge particles range from a few microns to hundreds of microns in size. These observations are consistent with the TEM information only if the material is agglomerated into larger clusters.

Sludge agglomerates are likely to be broken up by vigorous mixer pump and jet-fluid sluicing operations associated with retrieval; reagglomeration of particles is expected to occur rapidly during settling of the sludge in receiver tanks or after the mixer pumping ceases. As long as the aqueous

fluid chemical environment is kept at pH values greater than 10 and the ionic strength is kept at values greater than 0.1 molar, the fissile and neutron absorbers should readily reagglomerate. Because the neutron absorbers are present in much higher concentrations than the fissile material, the agglomerates should contain ample neutron absorbing properties to keep the sludge subcritical.

Our review of chemical processes and available sludge characterization data did not identify the form in which the fissile material in the tanks exists. It could be as discrete solids controlled by solubility relationships or it could be bound to sludge adsorbent surfaces such as iron and aluminum hydrous oxides. Theoretical arguments to support both mechanisms were presented because available data is too sparse to clearly choose which mechanism is more likely. However, it is well established that the solubility of plutonium in the various tank chemical environments is well below that needed to promote a criticality event in solution. The available tank supernate solution data clearly corroborates this conclusion. The effects of many chemical variables including ionic strength, pH, inorganic and organic competing ligands, and radiolysis were reviewed and arguments presented to show that they cannot lead to the necessary high solubility.

The chemical and physical conditions necessary to create natural ore bodies were reviewed. We concluded that tank environments are not similar to the natural environments that promote ore-body formation. The time scale, finite size of the tanks, and the relatively low mass transport into and out of tanks precludes the formation of an anthropogenic ore body. Further, most natural ore bodies are formed at temperatures and pressures that are well beyond those found in tanks and are generally formed over millions of years.

The sludge primary particles, including some theoretical estimates of the size of discrete particles of plutonium hydrous oxides, if they exist, are much smaller than the size of minerals that can be readily separated and concentrated by mineral processing techniques. Further, specialized mineral processing techniques such as flotation, require a narrow chemical environment in the supporting liquid and special organic reagents to carry the selected mineral to the floating layer. The high ionic strength, high pH and types of organics in the tank are not similar to the conditions required for successful flotation.

To provide defense-in-depth, we also performed numerous fluid dynamic calculations assuming that the fissile particles were not agglomerated with neutron absorbers or adsorbed onto the surfaces of neutron absorbers. The calculations assumed that fissile and neutron absorbers agglomerated only with themselves to form particles whose size was the same as distributions measured by light-scattering and visual-settling techniques. We then performed quantitative calculations using both one- and three-dimensional conceptual models and codes. Chapters 3 through 6 present the calculations that show, for the most realistic cases, that the level of segregation of fissiles from neutron absorbers was about a factor of 2.5. The concentration necessary to reach criticality is estimated to be about 20, based on the highest measured concentration of plutonium in tank sludge.

Some worst case simple-settling calculations were performed that did lead to separation factors larger than 20. The scenario required that the

plutonium be present as the finest grained particles in the sludge at the highest concentration for any tank at the Hanford Site and that no interparticle type agglomeration occurred. Further, the neutron absorbers were the larger particles in the sludge distribution. In this extreme case we assumed that all the neutron absorbers settled first and the plutonium slowly settled on top to form a thin, fissile-rich layer. Even though the thin layer exceeded the 2.6 g/L safe plutonium concentration for infinite geometry, the layer was of a uniform pancake shape far below the 240 g/ft^2 necessary to go critical.

The evidence shows no indication that such large separation factors could be reached by any of the past tank operations, including tank-to-tank transfers, cascading, salt-well pumping, and air-lift circulation. Further, in-tank mixing and jet-sluicing operations that are planned in the future will not produce fluid dynamic conditions that would lead to such large separation factors.

A set of experiments was designed that would provide the necessary data to determine whether the plutonium present in the tanks is discrete solid phases or is adsorbed onto the surfaces of the ubiquitous neutron absorbers such as iron and aluminum hydroxide. The experiments would also determine whether the plutonium-bearing particles would tend to separate from the other sludge particles, especially the better neutron absorbers, during settling from suspensions.

This page intentionally left blank.

CONTENTS

1.0 INTRODUCTION 1-1
1.1 FLUID DYNAMIC CALCULATIONS 1-3
1.2 CHEMISTRY OF SOLID AND LIQUID PHASES 1-4
1.3 NATURAL ORE DEPOSIT ANALOG 1-5
1.4 ORE PROCESSING TECHNIQUES 1-6

2.0 PHYSICAL PROCESSES RELATED TO SOLID SEGREGATION 2-1
2.1 SOLID TRANSPORT MECHANISMS 2-1
2.1.1 Solid Properties 2-1
2.1.3 Controlling Parameters for Solid Transport 2-9
2.1.4 Initiation of Solid Motion 2-9
2.1.5 Critical Condition for Cohesive Solids 2-10
2.1.6 Bed Forms 2-11
2.1.7 Solid/Sediment Discharge Rate Formulas 2-11
2.1.8 Solid Transport, Deposition, and Resuspension 2-13

3.0 SUMMARY OF FEATURES INCLUDED IN TEMPEST MODELS 3-1
3.1 TEMPEST FLUID DYNAMIC MODEL 3-1
3.1.1 Limitations of the TEMPEST Model 3-4
3.2 COMPARISON OF INPUT AND TANK WASTE CHARACTERIZATION DATA 3-4
3.2.1 Viscosity 3-5
3.2.2 Yield Stress 3-6

4.0 PARTICLE SEGREGATION MODELING IN HANFORD WASTE TANKS WITH TEMPEST AND STOMP CODES 4-1
4.1 WASTE SLUICING AND TANK PUMP-OUT OPERATIONS 4-2
4.1.1 Tank Waste Sluicing 4-3
4.1.2 Slurry Pump-Out Operation 4-3
4.2 SLURRY RECEIVING TANK OPERATIONS (ORIGINAL TANK FILLING, CASCADING, TANK TRANSFERS/ADDITIONS) 4-6
4.2.1 Analytical Solution Predictions (Most Representative of the Cascading Process and Tank Filling with Slurry Containing Low Suspended Solids) 4-6
4.2.2 TEMPEST Modeling For Waste Tank AY-102 4-8
4.3 MIXER JET PUMP OPERATION (PROPOSED FOR TANK SY-102) 4-10
4.4 SALT WELL PUMPING 4-13
4.5 AIR LIFT CIRCULATORS 4-14
4.5.1 Estimation of Air-Induced Liquid Flow 4-14
4.5.2 Liquid and Solid Movement 4-15
4.6 THERMAL EFFECTS 4-16

5.0 SCOPING RESULTS FOR STAGNANT SETTLING CASE 5-1
5.1 SIMPLIFIED SEDIMENTATION MODEL 5-1
5.2 SIMULATION RESULTS 5-3
5.2.1 Bounding Sensitivity Analysis 5-3
5.2.2 Hindered Settling Effect 5-4
5.2.3 Interpretation of Results from One-Dimensional Settling Calculations 5-5

CONTENTS (cont)

6.0 EVALUATION OF 1/12-SCALE DATA FROM MIXING UNIFORMITY TESTS 6-2
6.1 SCALED EXPERIMENTS 6-2
6.2 TEST PROCEDURE 6-3
6.3 PROPERTIES OF WELL-MIXED SIMULANTS 6-3
6.4 EFFECT OF PUMP POWER ON THE DIAMETER OF SUSPENDED PARTICLES 6-4
6.5 SETTLED SOLIDS 6-5
6.6 IMPLICATIONS 6-6

7.0 CHEMICAL PROCESSES THAT CONTROL FATE OF PLUTONIUM AND NEUTRON ABSORBERS 7-1
7.1 SOLUTION SPECIES 7-1
7.1.1 Redox Status 7-1
7.1.2 Hydrolysis 7-2
7.1.3 Complexation 7-3
7.1.4 Ionic Strength Effects 7-4
7.1.5 Temperature Effects 7-5
7.1.6 Radiolysis Effects 7-5
7.2 SOLUBILITY 7-7
7.2.1 Precipitation of Plutonium Hydroxide Phase 7-7
7.2.2 Organics Present in Hanford Site Tanks and their Influence on Solubility and Plutonium Speciation 7-10
7.2.3 Effects of Other Parameters on Plutonium Solubility 7-14
7.2.4 Solid Solution Phases 7-15
7.2.5 Crystallization and Particle Size of Precipitated Phases 7-17
7.3 ADSORPTION 7-21
7.3.1 Introduction 7-22
7.3.2 Adsorption Substrates in the Waste Tank Environment 7-24
7.3.3 Tetravalent Plutonium Adsorption on Iron and Aluminum Oxide/hydroxide Substrates 7-27

8.0 INTRODUCTION TO NATURAL ORE DEPOSIT EFFORTS 8-1
8.1 INTRODUCTION AND BACKGROUND 8-1
8.2 ORE-FORMING PROCESSES 8-2
8.2.1 Natural Ore-Forming Processes 8-2
8.2.2 Potential Ore-Forming Processes in Waste Tanks 8-4
8.3 NATURALLY OCCURRING RADIOGENIC MINERALS 8-7
8.4 DATA NEEDS 8-8

9.0 PROPERTIES OF GENERATED WASTE RELEVANT TO CRITICALITY HAZARD 9-1
9.1 OBJECTIVE/SCOPE 9-1
9.2 BACKGROUND 9-1
9.2.1 Wastes from Plutonium Separations and Finishing Operations at Hanford 9-1
9.2.2 Operational Controls on Waste Transfer 9-3
9.2.3 Waste Properties Relevant to Criticality Hazard . . . 9-4
9.2.4 Activity Status of Tanks 9-4

CONTENTS (cont)

9.3 WASTE STREAM CHARACTERIZATION 9-4
9.3.1 Hanford Defined Waste 9-5
9.3.2 PUREX 9-6
9.3.3 Thorium Fuel Waste to Tank Farms 9-11
9.3.4 REDOX 9-13
9.3.5 Bismuth Phosphate Process Wastes 9-14
9.3.6 Uranium Recovery Waste Stream 9-14
9.3.7 Plutonium Finishing Plant Waste 9-15
9.4 PLUTONIUM AND ABSORBER CONCENTRATIONS IN WASTE 9-15
9.5 DISCUSSION OF ACTIVE TANKS (DOUBLE-SHELL TANKS) 9-17
9.5.1 Waste in Tanks AW-103 and AW-105 9-18
9.5.2 Waste in Tank AW-106 9-19
9.5.3 Waste in Tank AY-101 9-20
9.5.4 Waste in Tanks AZ-101 and AZ-102 9-21
9.5.5 Waste in Tank SY-102 9-22
9.6 SUMMARY AND CONCLUSIONS 9-23

10.0 LABORATORY EXPERIMENTS TO SUPPORT CRITICALITY ISSUES 10-1
10.1 ADSORPTION EXPERIMENTS 10-1
10.2 SOLID-SOLUTION FORMATION EXPERIMENTS 10-2
10.3 PLUTONIUM SOLID PHASE FORMATION EXPERIMENTS 10-3
10.4 TESTS ON ACTUAL HANFORD WASTE TANK SLUDGES 10-3

11.0 REFERENCES 11-1

APPENDICES

APPENDIX A FLOCCULATIONS OF WASTE PARTICLES
APPENDIX B GRAVITY CONCENTRATION
APPENDIX C ANALYSIS TO DETERMINE THE VOLUME OF AIR ENTRAINED BY A SINGLE AIR LIFT CIRCULATOR
APPENDIX D PATHWAYS OF IRON HYDROXIDES, OXYHYDROXIDES, AND OXIDES
APPENDIX E FUEL PROCESSED AT PUREX AND PUREX-TO-TANK FARM WASTE TRANSFER DATA SINCE 1983
APPENDIX F CONCENTRATION RATIO OF PLUTONIUM (IV) HYROXYCARBONATE AND PLUTONIUM (IV) HYDROXY-EDTA COMPEXES

LIST OF FIGURES

2-1 Drag Coefficient of Spheres as a Function of Reynolds Number F2-1
2-2 Shields Diagram F2-2
2-3 Comparison of Predicted and Observed Total Sediment Discharges for the Colorado River at Taylor's Ferry, Colorado F2-3
3-1 Comparison of TEMPEST Model Predictions and 102-SY Characterization Data for Various Water-Sludge Dilutions F3-1
4-1 Predicted Vertical Distributions of Flow (m/s) and Solid 9 Concentration (kg/m^3) on Vertical Plane 14 (9 O'clock Position) of the Hole at 7 Simulation Minutes F4-1
4-2 Predicted Horizontal Distributions of Flow (m/s) and Solid 9 Concentration (kg/m^3) at Bottom of the Hole at 7 Simulation Minutes F4-2
4-3 Predicted Horizontal Distributions of Flow (m/s) and Solid 5 Concentration (kg/m^3) at Bottom of the Hole at 7 Simulation Minutes. F4-3
4-4 Predicted Horizontal Distributions of Flow (m/s) and Solid 5 Concentrations (kg/m^3) at Top of the Hole at 7 Simulation Minutes F4-4
4-5 Predicted Horizontal Distributions of Flow (m/s) and Solid 1 Concentration (kg/m^3) at Bottom of the Hole at 7 Simulation Minutes F4-5
4-6 Predicted Vertical Distributions of Flow (m/s) and Solid 9 Concentration (kg/m^3) on Vertical Plane 14 (9 O'clock Position) of the Hole without Yield Stress at 7 Simulation Minutes F4-6
4-7 Predicted Vertical Distributions of Flow (m/s) and Solid 9 Concentration (kg/m^3) on Vertical Plane 14 (9 O'clock Position) of the Hole without Yield Stress at 20 Simulation Minutes F4-7
4-8 Predicted Vertical Distributions of Flow (m/s) and Solid 5 Concentration (kg/m^3) on Vertical Plane 9 Containing One of the 1-in. Nozzles in Tank AY-102 at 1 Simulation Hour F4-8
4-9 Predicted Horizontal Distributions of Flow (m/s) and Solid 5 Concentration (kg/m^3) at 15 inches Above the Bottom of Tank AY-102 at 25 Simulation Minutes F4-9
4-10 Predicted Horizontal Distributions of Flow (m/s) and Solid 5 Concentration (kg/m^3) at 23 Inches above the Bottom of Tank AY-102 at 1 Simulation Hour F4-10
4-11 Predicted Horizontal Distributions of Flow (m/s) and Solid 5 Concentration (kg/m^3) on the Plane Containing Four 1-in. Nozzles in Tank AY-102 at 1 Simulation Hour F4-11
4-12 Close-up of Predicted Horizontal Distributions of Flow (m/s) and Solid 5 Concentration (kg/m^3) on the Plane Containing Four 1-in. Nozzles in Tank AY-102 at 1 Simulation Hour F4-12

LIST OF FIGURES (cont)

4-13 Predicted Horizontal Distributions of Flow (m/s) and Solid 5 Concentration (kg/m^3) at the Top of Tank AY-102 at 1 Simulation Hour F4-13
4-14 Predicted Vertical Distribution of Flow (m/s) and Solid 1 Concentration (kg/m^3) on Vertical Plane 9 Containing One of the 1-in. Nozzles in Tank AY-102 at 1 Simulation Hour F4-14
4-15 Predicted Horizontal Distributions of Flow (m/s) and Solid 1 Concentration (kg/m^3) at 23 Inches Above the Bottom of Tank AY-102 at 1 Simulation Hour F4-15
4-16 Predicted Vertical Distributions of Flow (m/s) and Solid 9 Concentration (kg/m^3) on Vertical Plane 9 Containing One of the 1-in. Nozzles in Tank AY-102 at 1 Simulation Hour F4-16
4-17 Predicted Horizontal Distributions of Flow (m/s) and Solid 9 Concentration (kg/m^3) at 23 Inches Above the Bottom of Tank AY-102 at 1 Simulation Hour F4-17
4-18 Predicted Maximum Solid Segregation for Solids 1, 5, and 9 at 23 Inches Above the Bottom of Tank AY-102 Over 1 Simulation Hour F4-18
4-19 Predicted Three-Dimensional Distribution of Solid 9 Volume Fractions After 2 Minutes of Mixer Pump Operation for Initially Settled Sludge F4-19
4-20 Predicted Three-Dimensional Distribution of Solid 9 Volume Fractions after 30 Minutes of Miser Pump Operation for Initially Settled Sludge F4-21
4-21 Predicted Three-Dimensional Distribution of Solid 9 Volume Fractions After 1.5 Hours of Mixer Pump Operation for Initially Settled Sludge F4-23
4-22 Predicted Vertical Distributions of Flow (m/s) and Solid 7 Concentrations (kg/m^3) on Vertical Plane 11 (12:30 Clock Position) with Sludge Initially Fully Mixed With Supernate at 1.5 Simulation Hours F4-25
4-24 Predicted Horizontal Distributions of Flow (m/s) and Solid 7 Concentration (kg/m^3) at the Bottom of Tank With Sludge Initially Fully Mixed With Supernate at 1.5 Simulation Hours F4-27
4-25 Predicted Horizontal Distributions of Flow (m/s) and Solid 1 Concentrations (kg/m^3) at the Bottom of Tank With Sludge Initially Fully Mixed With Supernate at 1.5 Simulation Hours F4-28
4-26 Predicted Vertical Distributions of Flow (m/s) and Solid 4 Concentration (kg/m^3) on Vertical Plane 9 (2 O'clock Position) in with Off-Center Jet at 5 Simulation Minutes F4-29
4-27 Predicted Horizontal Distributions of Flow (m/s) and Solid 4 Concentrations (kg/m^3) at the Bottom of Tank with Off-Center Jet at 5 Simulation Minutes F4-30
4-28 Predicted Vertical Distributions of Flow (m/s) and Solid 4 (with 10 Times Greater Settling Velocity) Concentration (kg/m3) on Vertical Plane 9 (2 O'clock Position) with Off-Center Jet at 5 Simulation Minutes F4-31
4-29 Predicted Horizontal Distributions of Flow (m/s) and Solid 4 (with 10 Times Greater Settling Velocity) Concentrations (kg/m3) at the Bottom of Tank with Off-Center Jet at 5 Simulation Minutes . . . F4-32

LIST OF FIGURES (cont)

4-31 TEMPEST Predicted Velocity Field for Sludge Slurry at Bottom of Tank While Air Lift Circulators are Running F4-34
4-32 Temperature Profile and Velocity Profile for Heat Convection Simulation (Base Case) F4-35
4-33 Temperature Profile and Velocity Profile for Heat Convection Simulation Range (High-Heat-Generation Case) F4-36
7-1 Distribution of Pu(IV)-Hydroxycarbonate Species as a Function of pH at Fixed Total Carbonate Concentration of 1.0 M F7-1
7-2 Distribution of Pu(IV)-Hydroxycarbonate Species as a Function of Total Carbonate Concentration at a Fixed pH of 8.5 . . . . . F7-2
7-3 Computed Distribution of Pu(IV) Aqueous Species as a Function of pH at a Fixed Carbonate Concentration of 0.001 M F7-3
7-4 Computed Distribution of Pu(IV) Aqueous Species as a Function of pH at a Fixed Carbonate Concentration of 0.05 M F7-4
7-5 Experimental Data for Solubility of $PuO_2 \bullet xH_2O$ as a Function of pH and Total Carbonate Concentration F7-5
7-6 Hanford Waste Stream Data Compared with the Experimental Equilibrium Solubility of $PuO_2 \bullet xH_2O$ F7-6
7-7 Hanford Waste Tank Supernatant Data Compared with Experimental Solubility Data for Solubility of Freshly Precipitated and Aged $PuO_2 \bullet xH_2O$ Solid F7-7
7-8 Experimental Data for Decontamination Factor of Plutonium in Cladding Removal Waste as a Function of Added Lanthanum Concentration F7-8
7-9 Adsorption Isotherms for Pu(IV) Adsorption on Goethite at Fixed Electrolyte Concentration F7-9
7-10 Adsorption Isotherms for Th(IV) Adsorption on Goethite at Fixed Electrolyte Concentration F7-10
7-11 Experimental Data for Pu(IV) Adsorption on Goethite as a Function of Total Dissolved Carbonate Concentration at a Fixed pH Value of 8.6 . . . . . F7-11
7-12 Experimental Data for Th(IV) Adsorption of Goethite Function of Total Dissolved Carbonate Concentration at a Fixed pH Value of 9.0 . . . . . F7-12
7-13 Estimated Pu(IV) Adsorption Envelope as a Function of pH and Total Dissolved Carbonate Concentration F7-13
7-14 Estimated Pu(IV) Adsorption Isopleths with pH and Total Dissolved Carbonate as Variables F7-15
7-15 Estimated Pu(IV) Adsorption Isopleths as a Function of Total Dissolved Carbonate Concentration and at Various Fixed pH Values F7-17
8-1 Settling Velocities for Gold Particles of Various Sizes and Degrees of Flatness F8-1
9-1 Schematic for the 28 DSTs at the Hanford Site F9-1
9-2 Schematic for the Two Types of SSTs at the Hanford Site F9-2
9-3 Schematic of Tank AW-103 Showing Waste Introduction Location . . F9-3

LIST OF TABLES

2-1	Solid Size Classification	T2-1
2-2	Values of the Exponent Constant α in Hindering Fall Velocity	T2-2
2-4	Guidelines for Selection of Independent and Dependent Variables in Alluvial Streams	T2-2
2-5	Critical Shear Stresses for Cohesive Sediments	T2-3
2-6	Shear Strength of Aggregates	T2-3
2-7	Input Data Requirements and Output for Some Sediment Discharge Formulas	T2-4
2-8	Evaluation of Six Sediment Discharge Formulas for Five Rivers	T2-5
2-9	Cohesive Sediment Erosion Parameters	T2-5
2-10	Cohesive Sediment Deposition Parameters	T2-5
4-1	Particle Size Distributions of Tank C-106 Sludge	T4-1
4-2	Maximum Segregation over the Initial Conditions Near the Bottom of the Hole	T4-1
4-3	Particle Size Distributions of Tank SY-102 Sludge	T4-2
4-4	Power Law Curve Fit Parameters for Tank SY-102 Wastes	T4-2
4-4	Simulation Input Parameters	T4-3
4-5	Maximum Segregation Over the Initial Conditions near the SY-102 Tank Bottom	T4-3
5-1	Particle Size Volume Distributions Used in Modeling	T5-1
5-2	Maximum Factor Increases in PuO_2 Mass Fraction in Sediment Layer	T5-2
5-3	Bounding Sensitivity Cases for Maximum PuO_2 Particle Size	T5-2
5-4	Factor Increase in Mass Fraction Solids Concentration for Various Particles With and Without the Effect of Hindered Settling	T5-3
6-1	Particle Sizes and Viscosity of Simulants Used in Experiments	T6-1
6-2	The Effect of Pump Power on the Size of Suspended Particles	T6-2
6-3	Particle Diameters in Settled Solids for Simulant S2	T6-3
7-1	Oxidation-Reduction Potentials for Plutonium	T7-1
7-2	Stability Constants for Hydrolytic Species of Pu(IV)	T7-1
7-3	Stability Constants for Pu(IV) Complexes	T7-2
7-4	Probable Stochiometries of Pu(IV)-OH-CO_3 Mixed Ligand Aqueous Species	T7-2
7-5	Total Dissolved Plutonium, Carbonate, and Hydroxyl Concentrations in Supernatants and Drainable Liquids from Single- and Double-Shell Tanks at the Hanford Site	T7-3
7-6	Organic Content (by Class) in Tank SY-101	T7-4
7-7	Average Organic Content of SY-101 Core Samples	T7-5
7-8	Organic Carbon Analyses for Tank SY-103 Samples	T7-6
7-9	Summary of Organic Types in Tank Samples wt.%	T7-6
7-10	Organic Compounds and Other Inorganic Species Found in Organic Layer of Tank C-103	T7-8
7-11	Analysis of Supernate Solution in Tank C-103	T7-9
7-12	Organic Carbon Analyses on Tank C-103 Samples	T7-10
7-13	Organic Species Identified in Tank AN-107 Supernate Solution	T7-11
7-14	Organic Species Measured in Tanks C-102 and C-204	T7-13
7-15	Organic Species Measured in Tank BY-108	T7-14

LIST OF TABLES (cont)

7-16 Solid Solution Compounds Pu(IV) T7-14
7-17 Differences in Ionic Radii Between Pu(IV) and Potential Solid Solution Forming Ions in Hanford Site Waste Streams (%) T7-15
8-1 Comparison of Naturally Occurring Ore Deposits T8-1
8-2 Ore-Forming Processes T8-3
9-1 Plutonium Production by Plant T9-1
9-2 Tank Diameters T9-1
9-3 Minimum Subcriticality Mass Ratio for Selected Absorber Materials T9-2
9-4 Single-Shell Tank Plutonium Inventory Comparison T9-3
9-5 Double-Shell Tank Estimated Plutonium Inventory Comparison . . . T9-11
9-6 Tanks With Enough Fissile Material To Warrant Further Consideration T9-12
9-7 Fuel Processed at PUREX and Associated Waste Volumes T9-13
9-8 Zirconium-Clad Fuels Processed at PUREX T9-13
9-9 Decladding Waste Sludge Formation in AW-103 and -105 Receiver Tanks T9-14
9-10 Plutonium and Associated Insoluble Absorbers in Zirflex Decladding Waste T9-14
9-11 Neutralized Zirflex Current Acid Waste Transferred from TK-F16 . T9-15
9-12 Sources and Quantity of Some Insoluble Absorbers in the NZCAW . . T9-16
9-13 Sludge Volume Formed in Tanks from NZCAW T9-17
9-14 PUREX Canyon Sump Waste Plus Ammonia Scrubber Bottoms Accumulated in Tank F-18 . . . . . T9-18
9-15 Organic Wash Waste Transferred from Tanks TK-G8 and TK-R8 . . . . T9-19
9-16 Aluminum Cladding Waste T9-20
9-17 Sludge Formation in Receiving Tanks from Aluminum Cladding Removal Waste T9-20
9-18 Sources and Quantity of Some Insoluble Absorbers in the NCAW . . T9-21
9-19 Neutralized Current Acid Waste from Aluminum Clad Fuel Processing T9-22
9-20 Thorium-Aluminum Coating Waste from TK-E5 . . . . . T9-23
9-21 Thorium - Neutralized 1WW Waste from TK-F18 . . . . . T9-24
9-22 Thorium - Organic Wash Waste from TK-G8 and TK-R8 . . . . . T9-25
9-23 Thorium - Canyon Sump Waste from Tank TK-F18 . . . . . T9-26
9-24 Thorium - Flush and Lab Waste from PUREX T9-26
9-25 Typical REDOX Waste Compositions T9-27
9-26 Typical Bismuth Phosphate Waste Composition T9-28
9-27 Volume and Composition of Uranium Recovery Waste T9-29
9-28 Plutonium Criticality Ratios - Single-Shell Tanks T9-30
9-29 Neutron Absorber-to-Plutonium Mass Ratios for Solids in Double-Shell Tank T9-35
9-30 Supernatant Plutonium Concentration for Double Shell Tanks with more than 10 kg of plutonium T9-36
9-31 AW-103 and AW-105 Tank Waste Analysis T9-37
9-32 AW-103 and AW-105 Sludge Insoluble Neutron Absorber-to-Plutonium Ratios T9-37
9-33 AY-101 Sludge Analysis and Insoluble Absorber to Plutonium Mass Ratios T9-38
9-34 AZ-101 Tank Sludge Analysis Compared to Projections from Process Records T9-38

LIST OF TABLES (cont)

9-35 AZ-101 Sludge Insoluble Neutron Absorber-to-Plutonium Ratios . . T9-39
9-36 Tank SY-102 Sludge Insoluble Neutron Absorber Analysis and Comparison to Projections from Process Records T9-39
9-37 SY-102 Sludge Insoluble Neutron Absorber to Plutonium Ratios . . T9-40

TERMS

CFD	computational fluid dynamics
DST	double-shell tank
HDW	Hanford (Site) Defined Waste
HLW	high-level waste
HTCE	Historical Tank Content Estimate
LANL	Los Alamos National Laboratory
LMWA	low-molecular-weight organic acid
MOX	mixed oxide (fuel)
MT	metric ton
NCAW	neutralized current acid waste
NMC	nuclear material control
NPH	normal paraffin hydrocarbons
NZCAW	neutralized zirflex current acid waste
PFP	Plutonium Finishing Plant
PNNL	Pacific Northwest National Laboratory
PRTR	plutonium recycle test reactor
PUREX	Plutonium-Uranium Extraction (Plant)
PWR	Shippingport reactor fuels
REDOX	Reduction-Oxidation
SNL	Savannah River National Laboratory
SST	single-shell tank
TBP	tributyl phosphate
TCR	Tank Characterization Reports
TOC	total organic carbon
WHC	Westinghouse Hanford Company

1.0 INTRODUCTION

This report uses information compiled and critically assembled by the staffs at the Pacific Northwest National Laboratory (PNNL) and Westinghouse Hanford Company (WHC) to evaluate the potential for nuclear criticality to occur in Hanford Site defense waste tanks during present waste storage and under some selected accident scenarios. The report also addresses active operations, such as tank cascading and operation of air-lift circulators to cool the contents of self-boiling tanks, to evaluate whether they could have created conditions that would predispose the tanks to criticality events during the inactive storage mode. Some analyses of past operations' fluid dynamics use conceptual models and data relevant to future retrieval operations because they have fluid-dynamic and particle-segregation characteristics similar to those of future operations.

Our report is organized as follows.

- Chapter 2.0 describes the fluid dynamic separation processes.
- Chapter 3.0 briefly describes the conceptual model and processes included in the TEMPEST code that was used.
- Chapter 4.0 provides the results of the TEMPEST calculations.
- Chapter 5.0 contains some results from simplified one-dimensional settling calculations.
- Chapter 6.0 contains data from observations of particle segregation in 1/12th scale mixer pump testing.
- Chapter 7.0 describes aqueous speciation, solubility, and adsorption processes that affect the potential for criticality from waste deposition and retrieval activities in the Hanford Site waste tanks.
- Chapter 8.0 examines how natural ore deposits form and the potential for such natural processes to analogously form enriched zones of fissile materials inside the waste tanks.
- Chapter 9.0 tabulates the tank inventory and waste process chemistry that bounds the chemical process discussions presented in Chapter 7 and neutronics calculations presented in companion reports such as Bratzel et al. (1996), Rogers et al. (1996), and Waltar et al. (1996).
- Chapter 10.0 discusses laboratory tests that are recommended to provide further data specific to the Hanford Site tanks. Such data should generate more definite conclusions about the dominant chemical mechanisms that influence the fate of plutonium and neutron absorbers in the tanks.
- Chapter 11.0 is the list of references.

- Appendix A presents a theoretical description of agglomeration and the variables that influence it. It also discusses sludge characterization results that used TEM to show that agglomeration is occurring in tanks.

- Appendix B reviews mineral ore processing techniques used to separate trace quantities of valuable material from the common bulk rock.

- Appendix C presents detailed calculations to support the values for bubble velocities used in Chapter 4.0 to evaluate the impact of air-lift circulators on particle separation.

- Appendix D presents details on characterization of tank sludge mineralogy, particle size and leaching attributes that support discussions presented in Chapter 7.0.

- Appendix E presents data on various PUREX reprocessing campaigns that support the discussions found in Chapter 9.0.

- Appendix F presents the concentration ratio calculations for Pu(IV) hydroxycarbonate and Pu(IV) hydroxy-EDTA complex concentrations.

The first five technical sections of the report describe our evaluations of processes that influence the degree of segregation between fissile material (primarily ^{239}Pu) and neutron absorbers. Reviews of fluid dynamic processes set the stage for describing various computer, simple analytical, and physical model exercises to quantify the degree of particle segregation that could occur during current "safe-storage" and tank maintenance, and during past tank-filling operations.

This study originally had two purposes. The first was to use available chemistry information to establish that the neutron absorbers and plutonium are in the same particles. The second was to show that the potential for fluid-dynamic processes to segregate the plutonium does not exist. If these goals had been met, the fluid dynamic work described would not have been necessary to assure that conditions in the waste tanks are subcritical. Further, it appears unlikely that the assertion that a strong, permanent (over the 40+ years of waste aging) chemical bonding between the plutonium and neutron absorbers exists can be proven using existing data. However, recent analyses on agglomeration do support physical association of the fissile and neutron absorbers in the settled sludge layers and during resettling of sludge after vigorous resuspension. Finally, we see merit in evaluating all the potential processes that bear on the problem to perhaps develop several lines of reasoning and "defense in depth" regarding the potential for criticality in Hanford Site waste tanks. To achieve this, much of the report covers fluid dynamics constructs and calculations.

Throughout the criticality analyses, we have assumed agreement that the only phase in which criticality events would be plausible is the tank waste sludge phase. As discussed in Bratzel et al. (1996) and Waltar et al. (1996), the solubility of plutonium in tank supernate liquid is too low for enough plutonium to homogenously dissolve and lead to criticality in the liquid

phase. Also, the ability of salt cake to adsorb plutonium, or to retain enough plutonium-containing pore liquid is limited to the extent that plutonium concentrations needed for criticality cannot be attained. Therefore, we concentrate our analyses on the behavior of plutonium and neutron absorbers in the sludge and its interstitial liquid phases in the waste tanks.

Finally, after a review of the available data, we wish to inform the reader that the available data on the particle size and mineralogy of discrete types of compounds (e.g., plutonium-rich, iron-rich, aluminum-rich, etc.) in the sludge stored in the Hanford Site waste tanks is very limited. The speciation of plutonium in tank supernate solutions also has not been evaluated. Without such information, performing definitive thermodynamic or fluid dynamic calculations is difficult. We performed the calculations using assumptions based on expert opinion and rationale explained in the report. We hope that we have explained the rationale adequately for the reader to assess the validity and merit of our conclusions.

1.1 FLUID DYNAMIC CALCULATIONS

Some evidence indicates that discrete hydrous plutonium oxide particles may exist in the Hanford Site tanks as small particles relative to the bulk sludge, which also exhibits a rather limited particle size range (from submicron to a few hundred microns). This will greatly reduce the potential for significant segregation and localized accumulations. This developing argument assumes that knowledge on particle sizes of "fresh" sludge does not directly apply to "aged" sludge. Further, much of the current knowledge relies on laboratory tests on simulated sludges that are considered to be fresh. Direct measurements of the chemical speciation of plutonium and neutron absorbers and sludge rheological properties using aged sludge are sparse. Without a conclusive understanding on whether the plutonium and key neutron absorbers within sludge exist as discrete mineral phases or amorphous gels, we decided to emphasize the potential importance of inertial segregation.

The fluid dynamics portion of our review addresses general potential particle segregation issues using cases that are specific to Hanford Site tanks. We chose this approach to save time. The following specific cases will be used:

- Retrieving sludge waste tank C-106 by sluicing
- Settling the retrieved sludge in tank AY-102
- Mixing the sludge in tank SY-102 with variable energy inputs followed by pump shut-off.

Also, physical and chemical attributes of sludge from tank C-106 were used to calculate the effects of salt-well pumping and sludge heat generation.

From these specific calculations and earlier literature specific to tank operations (i.e., use of air-lift circulators), we infer conditions for other operations such as tank-to-tank transfers of sludge slurry, cascading, mixer pump operation and salt well pumping. The work performed in the solid segregation area is broken down into the following categories:

- Complex multidimensional fluid dynamic modeling
- Simplified analytical models
- Evaluation of 1/12-scale data
- Evaluation of related segregation technologies.

A primary thrust was to set up and execute TEMPEST (see Eyler et al. 1993 and Trent and Eyler 1993) fluid dynamic models to simulate portions of the retrieval processes that are believed to have the greatest potential for concentrating plutonium-enriched particles from other sludge particles. Preliminary results that cover the first few hours of TEMPEST simulations are included. More work is being performed specific to retrieval and will be reported in Whyatt et al. (1996). We emphasize that our early TEMPEST calculations appear to be approaching steady state and that the results may represent the long-term state of the waste tanks, but we will certainly monitor the continuing work .

1.2 CHEMISTRY OF SOLID AND LIQUID PHASES

Several activities were performed, including a computer literature review on chemical, geochemical, and thermodynamic topics that pertain to understanding the chemical reactions such as plutonium solubility/precipitation, plutonium adsorption/desorption, and plutonium separation from known neutron absorbers that are present in the tank wastes at concentrations hundreds to thousands of times higher than plutonium. Finally, using thermodynamic constructs we performed equilibrium (solubility) calculations to estimate the likely conditions in tanks with high plutonium inventories and large driving forces that could influence plutonium distribution (e.g., high heat, high carbonate, and low free hydroxide).

We have determined that the key chemical processes that are important to assessing the potential for nuclear criticality are solubility/precipitation and adsorption/desorption of plutonium onto neutron absorbers. Several parameters or variables influence these two processes; important ones are included in our critical review. Both processes can be quantified by evaluating the distribution of the constituent of interest (e.g., plutonium or a selected neutron absorber such as iron) between the existing solid phase and solution phase. Therefore, our discussions include reviews of how important parameters influence species in solution and in solid phases. Important parameters that are included and effect both solution and solid are as follows:

1. Hydrolysis—pH effects
2. Soluble inorganic and organic complexation
3. Radiolysis

4. Redox
5. Ionic strength
6. Temperature effects on parameters 1 through 5
7. Time (aging, recrystallization).

To complete the critical review we collected available literature germane to the waste tank environments using computer literature searches of technical journals, reports, and databases, available Hanford topical reports, operating contractor internal memos, and important issues offered by numerous outside review teams that oversaw waste-tank operations at the Hanford Site. Each report or resource was then read and pertinent notes prepared that distill the information to key facts describing mechanistic tests and hypotheses about each parameter's effects on solubility and adsorption or direct observations and data that can be used to corroborate/compare with the hypotheses.

The available literature on the nature of plutonium and neutron absorbers within the waste tank sludge and supernate solutions is insufficient to conclusively determine whether the plutonium is present in sludge as adsorbed species on the surfaces of the major sludge hydrous oxides (e.g., iron, manganese, chromium, and aluminum) or as discrete crystalline or amorphous solid phases. If the plutonium molecules are chemically adsorbed onto the hydrous oxide sludge, enough neutron absorber should always accompany the plutonium to inhibit criticality. If the plutonium molecules are present as discrete plutonium compounds such as hydrous plutonium oxide or as solid solutions with other large cations (such as zirconium, lanthanum, and bismuth) in hydroxide or phosphate compounds, the enriched plutonium particles could be segregated from the more ubiquitous hydrous oxides of the common metals (iron, aluminum, manganese, etc.) during mechanical disturbances that resuspend particles. Depending on the size and density of the plutonium-rich particles and neutron absorber particles, differential settling of the various particles could lead to segregation and concentration, perhaps to the extent that criticality might occur. Our assessment led to two hypotheses. Both are explained in Chapter 7.0, but the reader can decide which seems more likely. To be thorough we consider both hypotheses as plausible and rely upon the fluid dynamics discussions to evaluate whether mechanical forces are sufficient to promote the degree of particle segregation needed to allow the sludge to go critical.

1.3 NATURAL ORE DEPOSIT ANALOG

Some processes occurring in Hanford defense nuclear waste tanks may be analogous to those in which a trace material becomes highly enriched by naturally occurring processes. In the case of Hanford waste tanks we are interested in processes whereby fissile particulate matter (i.e., precipitates of plutonium) could be concentrated. The common types of ore deposits are those that form near the earth's surface and those that form under high temperature and pressure deep underground. However, we should note that natural ore bodies and waste in Hanford Site tanks are significantly different. The most significant difference is that a natural ore body forms over thousands to millions of years, while waste has been stored in tanks for, at most, four to five decades. Another difference is that the processes that occur in hydrothermal ore deposits that form at great depth and high

temperature (300-600 °C) and pressure do not apply to near-surface Hanford Site waste tanks, the contents of which are generally at or below 100 °C, and under relatively low (atmospheric) pressure.

1.4 ORE PROCESSING TECHNIQUES

The mining literature was reviewed to determine if the mechanisms that achieve gravity separations are applicable to separating plutonium-rich particles from neutron-absorber sludge particles in the tanks. Chapters 4.0, 5.0 and 6.0 present our critical analyses, using various fluid dynamic tools, of the potential for particle separation in tanks. We state in several places that the these analyzes do not include all possible mechanisms and processes, such as momentum-driven processes that are too complicated to be easily reduced to simple mathematical algorithms. We reviewed some of these difficult-to-quantify processes that challenge existing mathematical algorithms. We are particularly looking for evidence that ore-milling processes that are engineered to separate different particles could occur spontaneously within tanks during the various operations used to transfer or retrieve waste, remove liquid, or to remove heat from tanks. Our goal is to review ore milling operations to understand their basic principles and to evaluate whether past and future Hanford Site tank operations could reproduce the necessary conditions and driving forces.

2.0 PHYSICAL PROCESSES RELATED TO SOLID SEGREGATION

Solid particle movement affects the transport of tank waste both indirectly and directly. Indirectly, sediment transport changes properties and rheology (e.g., density, viscosity, shear stress, bottom roughness, and heat transfer coefficient) of the waste mixture in waste tanks. These changes in turn affect the flow velocities of particles and solution and also the temperature distribution within the tanks. Changes in temperature distribution may also affect the solubility of some chemicals causing precipitation or dissolution of specific chemical compounds. This affects particle size, solid and fluid densities, and rheology found in the tanks.

Natural processes in tanks can directly suspend and transport solids by creating flow (from, for example, buoyancy caused by heat and the presence of gases. Human activities related to waste tank maintenance (e.g., mixer jet-pumps and injection of new wastes into tanks) also can cause particle transport. Suspended solids settle in different locations, depending on how well flow transports specific solids. Both suspended and bottom solids can adsorb dissolved wastes, then migrate and settle in a different location in the tank. The potentially nonuniform deposition of contaminated suspended solids and the direct adsorption of soluble contaminants by the bottom sediment may build up the specific solids in the tank bottom. Sludge can be subject to subsequent resuspension or desorption. Contaminant adsorption by solids can also reduce concentrations in supernate solution and bring neutron absorbers present in the waste sludge/salt cake into close contact with insoluble fissile materials. Thus, the effects of mass transfer from solution to solid and vice versa can either increase or decrease the potential for criticality to occur, depending on which reactions dominate.

In this section, we evaluate potential physical processes that could promote segregation of solids in the defense waste tanks on the Hanford Site.

2.1 SOLID TRANSPORT MECHANISMS

Transport, deposition, and resuspension processes can rearrange particle distributions through their complex interdependency with flow, rheology, and bottom roughness or resistance to flow. Hydraulic and environmental engineers have investigated sediment transport in natural environments extensively. This knowledge is useful to assessing particle movement in Hanford Site tanks. Solid/sediment transport is generally controlled by geometric and channel characteristics, fluid properties, flow characteristics, and solid properties (Raudkivi 1967, Graf 1971, Vanoni 1975, Simons and Senturk 1977, Onishi, 1994a).

2.1.1 Solid Properties

2.1.1.1 Solid Types. Solids/sediments are composed of a variety of minerals. In the natural environment (e.g., rivers) the most common mineral is usually quartz, because of its great resistance to weathering and abrasion (Leliavsky 1966, Richards 1982). However, solids in Hanford Site tanks are formed through various chemical reactions and consist of a wide variety of chemical

compounds, e.g., $NaNO_3(s)$, $NaNO_2(s)$, $Al(OH)_3$ (s), and other aluminum, lead, iron, and manganese oxyhydroxides (Reynolds and Herting 1984, Tank Waste Science Panel 1991, Castaing 1994, DiCenso et al. 1995, Onishi and Hudson 1996).

Solid particles can be divided into cohesive and noncohesive solids. Noncohesive solids consist of discrete particles whose movement depends only on particle properties (e.g., size, shape, and density) for given transport and erosion forces (Vanoni 1975, Jansen et al. 1979). The main properties of noncohesive solids that relate to solid/sediment transport are particle size, shape, density, and fall velocity. Sand and gravel are examples of noncohesive sediments. Movement of cohesive solids also depends on the strength of cohesive bonds between particles. They flocculate (or aggregate) and the aggregate properties depend on sediment type, and concentration of ions in the water, and flow conditions (Krone 1962, Mehta et al. 1989). Fine silt and clay are often cohesive sediments. The fine-grained sludges in Hanford Site tanks also are considered to be cohesive particles.

2.1.1.2 Solid Sizes. The most important property of the solid particle is its size (Vanoni 1975, Simons and Senturk 1977). Particle sizes may be defined by volume, weight, fall velocity, and sieve size, and other size parameters such as Feret's diameter, Martin's diameter, and projected area diameter. Because the size and shape of grains in sediments vary over wide ranges, descriptions are based on groupings into different size classes. Table 2-1 shows a commonly used grade scale with associated sieve sizes (Lane 1947, Vanoni 1975). Note that particle behavior on a sieve and the probability of falling through the sieve depend on many factors, e.g., particle size and shape, mesh size and shape, duration of sieving, and sieve loading. Some recommendations for the sieve loading were reported in Shergold (1946) and Jansen et al. (1979). For fine particles the pipet method, which relies on fall velocity to describe particle size, is commonly used. Usually size distributions are plotted as normal or log-normal, and geometric means and standard deviation of the particle distribution are determined.

2.1.1.3 Shape of the Solid Particles. The most pertinent shape parameters are sphericity and roundness. Sphericity is defined as the ratio of surface area of a sphere of the same volume as the particle to the actual surface area of the particle to describe relative motion between the falling particle and the fluid (Wadell 1932, Simons and Senturk 1977). Roundness is the ratio of the average of the corners and edges of a particle to the radius of a circle inscribed in the maximum projected area of the particle (Vanoni 1975). Roundness is important for abrasion, but has a negligible impact on the hydrodynamic behavior of the particles.

Both these parameters tend to decrease with decreasing particle size (Simons and Senturk 1977). Because of practical difficulties in measuring sphericity and roundness, a more common parameter is a shape factor, SF defined as

$$SF = \frac{c}{\sqrt{ab}} \tag{2.1}$$

where a, b, and c are the length of the longest, intermediate and shortest,

mutually perpendicular axes of the particle. The fall velocity can be expressed as a function of SF and a particle Reynolds number (Vanoni 1975), as discussed in Section 2.1.1.5.

2.1.1.4 Specific Weight of the Solid Particles. The specific weight of quartz is 2.65. Other common minerals include feldspar, chert, and carbonates, whose specific weights are 2.55 to 2.76, 2.65, and 2.85, respectively (Vanoni 1975). However, many solids in the waste tanks have different specific weights from these values, e.g., $NaNO_3(s)$ and $NaNO_2(s)$ have specific weights of 2.26 and 2.17, respectively. Aluminum and iron oxides that are present in the Hanford Site tank sludge in the form of boehmite, gibbsite, ferrihydrite, goethite, hematite and magnetite have specific weights of 3.44, 2.4, 3.96, 4.77, 5.26, and 5.18, respectively (Lide 1995). Crystalline PuO_2 is much heavier (specific weight of 11.46), but no value is available for amorphous plutonium hydrous oxide. Further, many solids, including plutonium may be coprecipitated or adsorbed on other solids, and thus may have specific weights significantly lower than that of the pure PuO_2 crystal solids.

2.1.1.5 Fall Velocity of Spheres. The fall velocity of a sphere is given by (Raudkivi 1967, Vanoni 1975)

$$w^2 = \frac{4}{3}\,\frac{g d_s}{C_D}\left(\frac{\rho_s - \rho}{\rho}\right) \tag{2.2}$$

where C_D = drag coefficient
d_s = sediment diameter
g = gravitational acceleration
w = fall velocity
ρ = density of fluid
ρ_s = solid particle.

Rouse (1937a, b) presented the drag coefficient as a function of a particle's Reynolds number or the auxiliary scale of the nondimensionalized submerged weight of the particle, as shown in Figure 2-1. A particle Reynolds number, R, and submerged weight, F, shown in Figure 2-1 are calculated using Equations 2.3 and 2.4.

$$R = \frac{w d_s}{\nu} \tag{2.3}$$

$$F = \frac{\pi d_s^3}{6}(\gamma_s - \gamma) \tag{2.4}$$

where ν = kinematic viscosity
γ_s = specific weight of the solid
γ = specific weight of the liquid
d_s = sediment diameter.

Rouse (1937b) also presented the fall velocity of a quartz sphere as a function of particle size and water temperature or particle Reynolds number, as reported by Leliavsky (1966), Raudikivi (1967), Vanoni (1975), and Graf (1971). For a Reynolds number of less than 0.1, the fall velocity, w, is given by the Stokes law

$$w = \frac{g d_s^2}{18\nu} \left(\frac{\gamma_s - \gamma}{\gamma} \right) \tag{2.5}$$

An effect of particle shape on the fall velocity was reported by McNown et al. (1951). They relate the fall velocity as a function of a particle Reynolds number, R, a shape factor, SF, and resistance factor, K, defined as

$$F/(3\pi\mu w d_s) \tag{2.6}$$

where μ is the dynamic viscosity of the fluid.

2.1.1.6 Effects of Solid Concentrations on Fall Velocity. The fall velocities determined by Equations 2.2 and 2.5 are valid for a single spherical particle in a quiescent infinite fluid. If only a few closely spaced particles are in a fluid, they will fall in a group with a velocity that is higher than that of a single particle falling alone. On the other hand, if particles are dispersed throughout the fluid, the interference between neighboring particles will reduce (or hinder) their fall velocity (Raudkivi 1967). Thus the effective size of individual particles decreases with increasing fine sediment concentrations. Simons and Senturk (1977) reported that the main changes in fluid properties caused by increasing the fine sediment concentration are increases in viscosity and specific weight of the sediment-fluid mixture. The hindered settling velocity may be expressed using (Richardson and Zaki 1954, Jansen et al. 1979) as

$$\frac{w}{w_0} = (1-c)^{\alpha} \tag{2.7}$$

where c = sediment concentration
w_0 = fall velocity without sediment concentration effects
α = constant, a function of the particle Reynolds number, R.

The values of α reported by Richardson and Zaki (1954) are shown in Table 2-2.

For cohesive sediment, at higher concentrations, c (e.g., above 300 mg/L), continuing aggregation or break-up of cohesive sediment affect the sediment fall velocity. Another way to express the fall velocity in this case is

$$w = A\, c^{\frac{4}{3}} \tag{2.8}$$

where A is constant. At sediment concentrations above approximately 10 g/L, sediment settling is hindered by the close spacing of settling aggregates. In this case, the resulting fall velocity is commonly expressed by

$$w_h = w\ (1-k_1 c)^5 \tag{2.9}$$

where k_1 = constant,
w_h = hindered fall velocity.
c = sediment concentration.

For laminar flow conditions, simpler expressions are available (Govier and Aziz 1972), including the following Famulado and Happel formula:

$$\frac{w}{w_0} = \frac{1}{1+k_2 c^{\frac{1}{3}}} \tag{2.10}$$

where k_2 = a constant in the range of 1.30 ± 0.24.

2.1.2. Fluid Properties and Flow Characteristics

2.1.2.1 Fluid Properties. The main fluid properties that affect sediment transport (or particle settling velocity) are fluid viscosity and density and, to a lesser extent, heat capacity. Relevant to the Hanford Site tank waste, Mahoney and Trent (1995) obtained the following equation for the liquid viscosities, based on the viscosity data obtained from the literature for $NaNO_3$ solutions:

$$\mu_L = a_4 \exp([a_0 + a_1 C + a_2 C^2]/T) \tag{2.11}$$

where: a_k = coefficients fit from experimental data as shown in Table 2-3
T = solution temperature, (°K)
C = weight percentage (concentration) of the solute.

The correlation is thought to give estimates that are within 10 percent of the actual value for solutions with 0 to 90 wt% $NaNO_3$ in the temperature range from 273 °K to 433 °K.

Mixtures of fluids and sediment with high sediment concentrations likely exhibit non-Newtonian flow characteristics (Govier and Aziz 1972, Trent and Eyler 1993). Many models have been developed for the rheological behavior of non-Newtonian fluids (Mahoney and Trent 1995). These include power law or Ostwald-DeWaele (Bird et al. 1960), Cross (1965), Carreau (Ellwood et al. 1990), biviscous (Kalyon et al. 1993), Bingham (Bird et al. 1960), Casson (Bird et al. 1960), Herschel-Bulkey (Bird et al. 1960), and Gay (Dabak and Yucel 1987) models. A Bingham model for shear stress, for example, is expressed as

$$\tau = -\left\{\mu_\infty + \frac{\tau_0}{\left|\sqrt{\frac{1}{2}\Pi_D}\right|}\right\} D \ for\ \frac{1}{2}\Pi_D > \tau_0^2 \tag{2.12}$$

and $$D=0, \quad for \quad \frac{1}{2}\Pi_D < \tau_0^2 \tag{2.13}$$

where D = shear rate tensor
Π_D = second invariant of the shear rate tensor (see Bird et al. 1960, pg. 102)
| | = scalar portion of the tensor
τ_0 = yield strength
μ_∞ = Newtonian viscosity at high shear rate.

The Bingham model has been used on other Hanford Site tank waste problems (Trent and Eyler 1993, Onishi et al. 1995) but was not used in the analyses presented in this report (see Section 3.0 for more details).

No viscosity correlation for multicomponent, solid-liquid waste mixtures is available because the solid-liquid mixtures and their interactions are so complex. Developing such a relationship for uniform spherical particles has been the subject of numerous theoretical and experimental efforts (Mahoney and Trent 1995). One common approach is to extend Einstein's viscosity relationship to apply at finite particle volume concentrations (Onishi and Hudson 1996). The type of relationship that results is typically of the form

$$\mu_M = \mu_L(1+2.5C_V+14.4C_V^2+\ldots) \tag{2.14}$$

where C_V = the particle volume fraction
μ_M = viscosity of a mixed electrolyte solution
μ_L = viscosity of a pure electrolyte solution (one salt component only).

Similar expressions have been given by a number of authors (e.g., Frankel and Acrivos 1967). Relationships of this form apply for uniform spherical particles with low to moderate particle volume loadings. As the particulate volume loading approaches maximum packing, the predicted viscosities will deviate significantly from those observed. A model of this form does not include any colloidal or large-aspect ratio effects that make the mixture viscosity much more nonlinear than that predicted by Equation 2.14.

Some empirical formulas have been developed to estimate the fluid density for a multicomponent solution (Mahoney and Trent 1995, Onishi and Hudson 1996). For tank wastes, the following formulas for the liquid density, ρ_L (kg/m^3) are suggested by Mahoney and Trent (1995).

$$\rho_L = 1171.8-9.140C-0.7758T+0.4866T^2+4.318m_{OH} \tag{2.15}$$

or its simplified form,

$$\rho_L = 1245.8-9.824C-1.0606T+0.6812T^2 \tag{2.16}$$

where C = the weight percent of the all aqueous species to the total solution weight
m_{OH} = the molality of hydroxide in the solution, and
T = solution temperature, °K.

The slurry mixture density, ρ_M, is a function of the solid and liquid densities, as well as the solids fraction, and can be expressed as (Onishi and Hudson 1996)

$$\rho_M = \frac{\rho_L}{\left(1-\chi_S\left(1-\frac{\rho_L}{\rho_S}\right)\right)} \tag{2.17}$$

where ρ_s = solid particle density, (or volume weighted average density for mixtures)
χ_s = solid mass fraction (weight of solids/weight of total slurry).

Important flow characteristics that are required along with combinations of Equations 2.11 through 2.17to predict particle settling velocities in a mechanically disturbed regime are flow discharge and velocity, depth of fluid, width of flow, energy slope, and shear and yield stresses.

Similar to the density formula (Equation 2.17), single-phase liquid heat capacity, c_{pL}, may be expressed by (Mahoney and Trent 1995)

$$c_{pL} = a_0+a_1C+a_2T+a_3C^2T \tag{2.18}$$

where a_0, a_1, a_2, and a_4 = empirically determined coefficients
T = temperature in degrees kelvin.

Currently no data is available to develop an empirical formula for heat capacity of the multicomponent fluid in Hanford Site tanks. Heat capacities for a liquid-solid (gasless) mixture, C_{PM}, and a bubbly mixture (liquid-solid-gas), C_{PB}, for potential application to the Hanford wastes are estimated in (Mahoney and Trent 1995) as follows:

$$c_{pm} = \frac{n_L\rho_L c_{pL}+(1-n_L)\,\rho_s c_{ps}}{n_L\rho_L+(1-n_L)\,\rho_s} \tag{2.19}$$

and

$$c_{pb} = (1-n_G)\,c_{pm} \tag{2.20}$$

where ρ_L = density of the liquid phase in the mixture,
ρ_s = particle density of the representative solid,
c_{pL} = heat capacity of the representative liquid
c_{ps} = heat capacity of the representative solid,
n_L = porosity that is filled with liquid (volume fraction in the mixture filled with liquid),
n_G = porosity that is filled with gases (volume fraction in mixture filled with gas

2.1.2.2 Flow Characteristics. Important flow characteristics that must be known to predict whether particles will be suspended and potentially separated from other particles during deposition are flow discharge and velocity, depth, width, energy slope, and shear and yield stresses. One of the main

characteristics of the sediment-laden flow is the interaction between flow and sediment transport. For example, in a waste tank, a sufficiently fast flow transports solids. The solids' transport changes the properties and rheology (e.g., density, viscosity, shear stress, bottom roughness, and heat transfer coefficient) of the waste mixture in the tanks (Onishi et al. 1995). These changes in turn affect the flow velocity and temperature distributions. Changes in temperature and chemical species distributions may also affect the solubilities of some chemicals causing either precipitation or dissolution of specific chemical compounds. This affects particle size, solid and fluid densities, and rheology, which in turn affect the flow velocities in the tanks (Onishi and Hudson 1996). The variables controlling particle transport have continual feedback or an interrelationship, therefore, one must be cognizant of these complications when performing either simple or complex calculations.

Flow-sediment interactions have been investigated most intensively in alluvial streams (Leliavsky 1966, Raudkivi 1967, Richards 1982). That flow affects sediment transport, which controls the hydraulic roughness and channel geometry through bed formation and sediment deposition and erosion is well known (Vanoni 1975, Onishi 1994a). The hydraulic roughness and channel geometry, in turn, affect the flow (Simons and Senturk 1977).

For example, multiple flow velocities and sediment transport rates for the same flow depth or discharge in a given channel, depending on the bed form, are common (Nordin 1989). Thus, to predict depth, discharge, and velocity requires knowledge of the relationships among flow parameters, fluid and sediment properties, and the hydraulic roughness or friction factors affected by sediment transport.

To close the loop of interdependency among the flow, sediment transport and hydraulic roughness, numerous methods and formulas are available to predict stage/depth-discharge/velocity relationships and to calculate sediment transport rates in rivers (Onishi 1994a). These relationships and empirical equations are an integral part of numerical sediment transport models/codes (Vanoni 1975; National Research Council 1983; Fan 1988, Onishi 1994a). These stage/depth-discharge/velocity predictors include the following:

- Einstein-Barbarossa (Einstein and Barbarossa 1952)
- Garde-Raju (Garde and Raju 1966)
- Simons-Richardson-Haynie (Simons and Richardson 1966; Haynie and Simons 1968)
- Engelund (1966)
- Znamenskaya (1967)
- Raudkivi (1967)
- Kennedy-Alam-Lovera (Alam and Kennedy 1969; Lovera and Kennedy 1969)
- Maddock (1969)
- Mostafa-McDermid (Mostafa and McDermid 1971)
- Brownlie (1983).

As summarized by Raudkivi (1967), Vanoni (1975), and Onishi (1994a), most of these predictors are based on the concept that a specific variable (e.g., friction factor, hydraulic radius, or cross-sectional area) can be divided into two components, one corresponding to the skin friction (grain roughness), and the other accounting for the form drag (bed forms).

Many of these methods were compared against measured data obtained from the Colorado River in Colorado (Vanoni 1975), the Niobrara River in Nebraska (Vanoni 1975), and the Sacramento River in California (Nakato 1990). These comparisons show wide variations among predictions. These variations are caused by an incomplete understanding of the relationship between bed forms and hydraulic roughness. Among these predictors, Brownlie reveals the best match to the measured data (Onishi 1994a).

2.1.3 Controlling Parameters for Solid Transport

Flow, solid/sediment transport, and bottom roughness and flow-field geometry are interdependent. In general, the following parameters are relevant for the solid/sediment transport (Vanoni 1975, Simons and Senturk 1977):

- Water discharge, Q
- Solid/sediment discharge, Q_s
- Flow channel bottom width, b
- Mean fluid flow depth, d
- Friction factor, f
- Channel plan geometry, m
- Depth/hydraulic radius, r
- Energy gradient, S
- Mean velocity, V
- Fluid kinematic viscosity, ν
- Fluid density, ρ
- Solid particle density, ρ_s
- Mean falling velocity, w
- Geometric mean size of bottom solid material, d_s
- Geometric standard deviation of bottom solid material, σ_s
- Gravitational acceleration constant, g.

Selecting appropriate independent variables as input data is important to obtaining unique solutions for unknowns, the dependent variables, for a specific problem. Table 2-4 provides guidelines for selecting independent variables (Vanoni 1975).

2.1.4 Initiation of Solid Motion

As the flow over a sediment (in our case sludge and/or salt cake) surface increases from zero, flow-induced forces (lift and drag) acting on the solid particle increase. When these forces exceed the submerged weight of the particle, the solid particle starts to move. This critical condition for initiation of motion has been correlated to the velocity using the relationship (Leliavsky 1966)

$$V_{critical} = kW^{1/6} \tag{2.21}$$

where $V_{critical}$ = critical velocity to initiate solid particle movement
k = constant
W = dry particle weight in air.

Subsequently, many researchers, including Shields (1936) and White (1940), correlated the flow intensity controlling initial particle movement and the subsequent sediment transport rate to velocity, shear stress, or stream power (product of shear stress and velocity), as summarized by Leliavsky (1966), Henderson (1966), Raudkivi (1967), Vanoni (1975), Graf (1971), Simons and Senturk (1977), Jansen et al. (1979), and Richards (1982). Assuming that the initiation of motion is determined by bed shear stress (τ_o), the specific weight difference ($\gamma_s - \gamma$) between sediment and water, d_s, ρ, and ν, the following dimensional analysis yields the well-known Shields diagram for the initiation of motion (Shields 1936).

$$\frac{\tau_o}{(\gamma_s-\gamma)\, d_s} = F\left(\frac{U_* d_s}{\nu}\right) \tag{2.22}$$

where F = functional relationship
U_* = the velocity shear (τ_0/ρ).

Figure 2-2 clearly indicates that particle sizes for the critical shear stresses needed to erode bottom sediments differ significantly. The most easily erodible sediment is a particle having the particle Reynolds number, R of around 10, while very small particles (having smaller particle Reynolds number) exhibit greater resistance to being entrained by a given flow. This is mainly because most small particles are cohesive. Thus, a given flow can clearly segregate specific-sized particles by selectively eroding some solid particles. Further, it is not the smallest particles that are eroded first as the flow rate increases from zero. Because sludge in Hanford tanks is very fine grained and cohesive it will not erode at low fluid velocities as one might intuitively expect.

When flow conditions reach the critical stage of initiating motion, some bottom solid particles start to move. Initially, they roll and slide along the bed with increasing velocity; some jump and hop. These particles make up the "bed load"; the rest of the moving particles that seldom fall back into the interface are the "suspended load." Together these make up the sediment transport.

2.1.5 Critical Condition for Cohesive Solids

Unlike noncohesive solids, the fall velocity and critical shear stress for erosion and deposition of cohesive solids depend not only on the solid properties (e.g., density and diameter), but also on the electrochemical environment of the solid, flow characteristics, and solid past history of transport, deposition, and resuspension, (e.g., phenomena such as flocculation and consolidation) as described in Vanoni (1975). Few studies have been made that address the initiation of movement of cohesive particles and knowledge of these phenomena are very limited (Krone 1962, Partheniades 1962, Onishi et al. 1993, Onishi 1994b).

Since Sundborg (1956) derived the critical shear stress for cohesive solids, some studies have been done that correlate the stress to shear strength, S_v, and plasticity index, I_p. For example, Dunn (1959) conducted measurements with sediments ranging from sand to silty clay, and obtained the

following relationship for critical shear stress for cohesive sediments with a plasticity index between 5 and 16:

$$\tau_{CR} = 0.001\ (S_v + 180) \cdot \tan\ (30 + 1.73 I_p) \qquad (2.23)$$

where S_v = shear strength
I_p = plasticity index.

The critical shear stress increases with the plasticity index, I_p. Some of these studies provided a wide range of critical shear stress for erosion, as shown in Table 2-5.

Another important consideration is the formation of aggregates on the critical shear stress. The larger the aggregation, the smaller the critical shear stress for erosion (Krone 1962). The shear strength of various aggregates, based on a San Francisco Bay sediment, are shown in Table 2-6.

Note that zeroth order aggregates are made up of the sediment particle themselves. The first order aggregate is made up with zeroth aggregates, second-order aggregates are made up with first-order aggregates, and so on. These values clearly indicate that the more the cohesive sediment aggregates, the weaker the bond between the aggregates and the bed sediment, and the lower the critical shear stress needs to be for erosion to start. Section 2.1.8 covers the transport, deposition, and erosion of cohesive sediment in more detail.

2.1.6 Bed Forms

The common bed forms are ripples, bars, dunes, transition, flat bed, and antidunes, listed in the general order of their occurrence with increasing velocity, Froude number, and sediment transport rates (Raudkivi 1967, Vanoni 1975, Jansen et al. 1979). The ripples are the smallest, having wave lengths and heights up to approximately 30 cm and 3 cm, respectively. Bars have wave lengths and heights comparable to the stream channel width and flow depth. Dunes are larger than ripples, but smaller than bars. With increasing velocity, dunes will disappear, forming a flat bed, thus reducing the friction factor/hydraulic roughness significantly. In the transition from dune to flat bed, the bed is mainly covered by low-amplitude ripples and dunes, interspersed with flat bed. Antidunes have a nearly sinusoidal form with a wave length of $2\pi V^2/g$ and variable height depending on flow depth and velocity. Antidunes are always accompanied by in-phase waves of the water surface.

Predictions of the bed forms have been studied theoretically, experimentally, or by field observations (Kennedy 1963, Simons and Richardson 1966). Simons and Richardson (1966) provides the bed form prediction as a function of mean particle diameter and stream power (defined as the product of bottom shear stress and velocity).

2.1.7 Solid/Sediment Discharge Rate Formulas

Many formulas have been developed for calculating solid/sediment discharges of bed materials (mostly non-cohesive sediment), since DuBoys (1879) presented a relationship between sediment discharge, particle mean diameter, and the shear stress acting on the bed. Many of these formulas correlate the sediment discharge to shear stress, velocity, or stream power, as well as fluid and solid properties. For example, DuBoys' formula relates the bed loads to shear stress by (Vanoni 1975)

$$q_s = \chi_o \tau_o (\tau_o - \tau_c) \tag{2.24}$$

where q_s = sediment discharge per unit width (= Q_s/b),
χ_o = coefficient.
τ_o = bed shear stress, and
τ_c = critical bed shear stress for initiation of motion.

The values of τ_c and τ_o are solely functions of a median bed sediment size. Many other formulas, e.g., Meyer-Peter (Meyer-Peter and Muller 1948) and Shields (1936), use a similar concept of correlating the sediment discharge to shear stress. Some relate the sediment discharge directly or indirectly to velocity, including the Einstein bed load function (Einstein 1950) and Colby (1964a,b). Einstein postulated that a sediment particle moves if the instantaneous hydrodynamic lift force exceeds the particle weight, and that the motions should be expressed statistically. A third group of formulas relating to stream power are represented by Engelund and Hansen (1967), Ackers and White (1973), and Yang (1973, 1979). Yang hypothesized that the sediment transport rate is related to the rate of energy dissipation, which in turn can be expressed by the stream power (product of velocity and shear stress), which he called the unit stream power. These formulas have been summarized in many publications (Rouse 1950, Leliavsky 1966, Raudikivi 1967, Graf 1971, Vanoni 1975, Simons and Senturk 1977, Jansen et al. 1979, Richards 1982). Required input data and their output for some formulas are summarized by Nakato (1990), as shown in Table 2-7.

A major problem that the engineer faces is which sediment discharge formula to use to calculate the sediment discharge for given hydraulic and sediment parameters. The following 23 methods are representative sediment discharge formulas applicable to non-cohesive bed sediment under uniform steady conditions and are reviewed by Onishi (1994a):

- DuBoys (DuBoys 1879, Vanoni 1975)
- Schoklitsch (Shulits 1935, Vanoni 1975)
- Shields (Shields 1936, Vanoni 1975)
- Meyer-Peter (Meyer-Peter and Muller 1948, Vanoni 1975)
- Meyer-Peter-Muller (Meyer-Peter and Muller 1948)
- Einstein-Brown (Brown 1950)
- Einstein Bed Load Function (Einstein 1950)
- Laursen (1958)
- Colby (1964a, b)
- Bagnold (1966)
- Blench Regime Formula (Blench 1966)
- Engelund-Hansen (Engelund and Hansen 1967)

- Inglis-Lacey (Inglis 1968)
- Toffaleti (1969)
- Graf (1971)
- Shen-Hung (Shen and Hung 1972)
- Ackers-White (Ackers and White 1973)
- Yang (1973, 1979)
- Maddock (1976)
- Engelund-Fredsoe (Engelund and Fredsoe 1976)
- Karim (Karim and Kennedy 1981)
- Brownlie (1981a, b)
- Van Rijn (1984a, b).

Vanoni (1975) compared the following 13 sediment discharge formulas against observed data for the Colorado River at Taylor's Ferry, Colorado, and Niobrara River near Colby, Nebraska: DuBoys, Schoklitsch, Shields, Meyer-Peter, Meyer-Peter-Muller, Einstein-Brown, Einstein Bed Load Function, Laursen, Colby, Blench Regime Formula, Engelund-Hansen, Inglis-Lacey, and Toffaleti. Predictions made using these formulas and field data vary by several orders of magnitude (See Figure 2-3 for the Colorado River). The Toffaleti, Colby, Inglis-Lacey, and Engelund-Hansen formulas predicted values closer to the measured data for these river conditions than other sediment discharge formulas.

Yang and Molinas (1982) compared the following six formulas against 1,259 data sets from laboratory flumes and five rivers: Colby, Engelund-Hansen, Shen-Hung, Ackers-White, Maddock, and Yang. The five rivers were the Niobrara and Middle Loup Rivers in Nebraska, Mountain Creek in South Carolina, the Rio Grande in New Mexico, and the Mississippi River in Missouri. All six formulas predicted the total sediment load in the rivers within an approximately 200-percent error, as shown in Table 2-8, showing both mean values and the distributions of the ratio of the computed to the measured total sediment load. The Yang and Shen-Hung formulas show the best results, followed by Ackers-White, and Engelund-Hansen. However, the Shen-Hung formula is limited to small rivers because it uses a dimensionally nonhomogeneous parameter (Yang and Molinas 1982).

A series of performance tests of sediment discharge formulas by many researchers clearly demonstrates a wide range of variations and limitations for these formulas. The Engelund-Hansen, Inglis-Lacey, Toffaleti, Ackers-White, and Yang formulas show the most acceptable results over a wide range of flow and sediment conditions (Onishi 1994a). However, users must be very careful to select several formulas and test them for a specific application.

2.1.8 Solid Transport, Deposition, and Resuspension

2.1.8.1. Solid transport. Solid/sediment transport is commonly expressed by the following advection-diffusion equation (National Research Council 1993, Onishi 1994a, 1994b):

$$\frac{\partial c}{\partial t}+\nabla\cdot(uc) = \nabla\cdot(\epsilon\nabla c)+G_s \qquad (2.25)$$

where c= solid concentration
ϵ = dispersion coefficient
G_s = solid erosion and deposition rates.

The erosion and deposition rates are usually formulated separately for cohesive and non-cohesive sediments (Onishi et al. 1993). Most commonly used methods to determine the sediment erosion and deposition rates are discussed in Section 2.1.8.2 (National Research Council 1993, Onishi 1994a).

2.1.8.2 Solid Deposition and Erosion. Particle erosion and deposition depends not only on fluid flow and solid characteristics, but also on actual concentration of solids in the fluid.

For non-cohesive solids

$$G_s = \frac{Q_s - Q_{sa}}{\Delta A} \qquad \text{for erosion (2.26)}$$

$$G_s = \frac{Q_{sa} - Q_s}{\Delta A} \qquad \text{for deposition (2.27)}$$

where ΔA = unit bottom surface area to and from which solid will be deposited or eroded
Q_s= sediment transport capacity for the given flow per unit surface area
Q_{sa}= actual sediment transport rate per unit surface area.

Q_s can be evaluated by various sediment transport discharge formulas (e.g., Einstein 1950, Toffaleti, 1969, Ackers and White 1973, Yang (1979)), as discussed in Section 2.1.7.

For cohesive solids (Partheniades 1962, Krone 1962)

$$G_s = M\left(\frac{\tau_o}{\tau_{CR}} - 1\right) \qquad \text{for erosion (2.28)}$$

$$G_s = w\,c\left(1 - \frac{\tau_o}{\tau_{CD}}\right) \qquad \text{for deposition (2.29)}$$

where M = erodibility coefficient
w = particle(or agglomerate) fall velocity
τ = bed shear stress
τ_{CD}= critical shear stress for deposition
τ_{CR}= critical shear stress for erosion.

The fall velocity, w in Equation 2.29 may be determined by Equation 2.2 or 2.5 if the solids concentration is relatively low and cohesive solids do not form many aggregates. However, as we discussed in Section 2.1.1.5, at higher concentrations (e.g., above 300 mg/L), continuing aggregation or break-up of cohesive solids affects the sediment fall velocity. Thus, the fall velocity becomes a function of solids concentration under this condition (See Equations 2.7 through 2.10).

Teeter (1988) and Krone (1962) conducted experiments specifically to obtain parameters in Equations 2.8, 2.28, and 2.29 with Buzzards Bay (Massachusetts)sand, and Clinch River (Tennessee) sediments. The erosion and deposition parameters values shown in Tables 2-9 and 2-10 are obtained by Teeter's experiments.

Many sediment transport and contaminant transport codes are available that have incorporated these sediment transport, deposition, and erosion formulas to evaluate behavior of sediment and sediment-sorbed contaminants, as evaluated and summarized in National Research Council (1993), Onishi (1994a) and Onishi (1994b).

This page intentionally left blank.

Figure 2-1. Drag Coefficient of Spheres as a Function of Reynolds Number (Rouse 1937b).

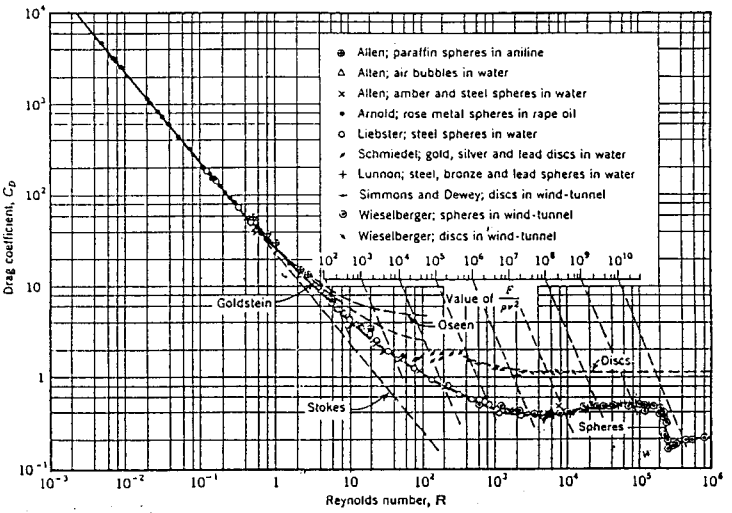

Figure 2-2. Shields Diagram (Shields 1936, Vanoni 1975)

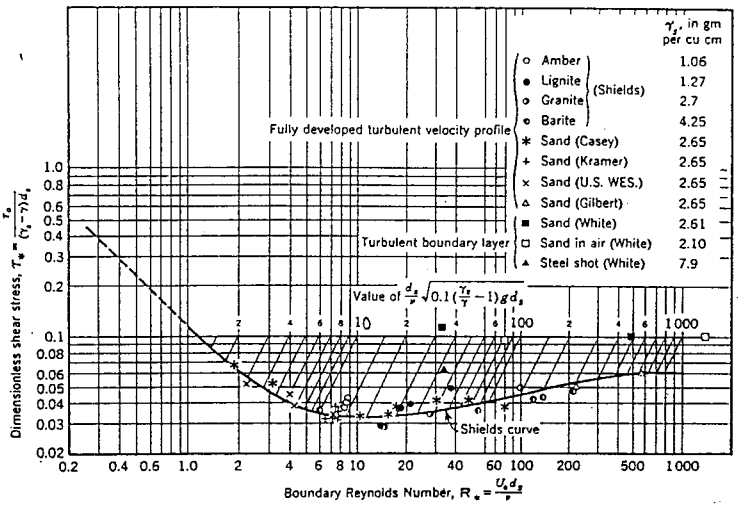

Figure 2-3. Comparison of Predicted and Observed Total Sediment Discharges for the Colorado River at Taylor's Ferry, Colorado (Vanoni, 1975).

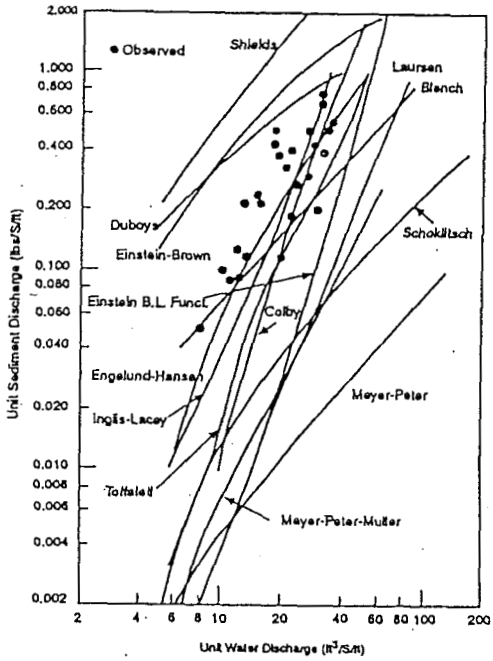

This page intentionally left blank.

Table 2-1. Solid Size Classification
(adopted from Vanoni 1975).

Class Name	Sizes (mm)	Sieve Mesh Opening per in.	
		Tyler	U.S. Standard
Boulders			
very large	4,096 - 2,048		
large	2,048 - 1,024		
medium	1,024 - 512		
small	512 - 256		
Cobbles			
large	256 - 128		
small	128 - 64		
Gravel			
very coarse	64 - 32		
coarse	32 - 16		
medium	16 - 8	2.5	
fine	8 - 4	5	5
very fine	4 - 2	9	10
Sand			
very coarse	2.000 - 1.000	16	18
coarse	1.000 - 0.500	32	35
medium	0.500 - 0.250	60	60
fine	0.250 - 0.125	115	120
very fine	0.125 - 0.062	250	230
Silt			
coarse	0.062 - 0.031		
medium	0.031 - 0.016		
fine	0.016 - 0.008		
very fine	0.008 - 0.004		
Clay			
coarse	0.004 - 0.002		
medium	0.002 - 0.001		
fine	0.001 - 0.0005		
very fine	0.0005 - 0.00024		

Table 2-2. Values of the Exponent Constant α in Hindering Fall Velocity.

Particle Reynolds Number $R = w_0 d_s / \nu$	Exponent Constant α
<0.2	4.65
0.2 - 1.0	$4.35R^{-0.03}$
1.0 - 200	$4.45R^{-0.1}$
>200	2.39

Table 2.3. Coefficients for Equation 2.10 Based on Experimental Measurements of $NaNO_3$ Solutions (Mahoney and Trent [1995])

Coeff.	Value
a_4	5.8044 x 10-6 Pa-s
a_0	1489.9 K
a_1	-0.97874 K
a_2	0.19490 K

Table 2-4. Guidelines for Selection of Independent and Dependent Variables in Alluvial Streams (adopted from Vanoni 1975).

Time frames	Independent variables		Dependent variables	Functional relationships	
	Properties of fluid sediment and others	Flow characteristics		Single values	Multiple values for some ranges
Short-term	ν ρ, ρ_s, d_s, σ_s, w, g	Q, d, m	Q_s, b, r, V, s, f	X	
		d, S, m	Q, Q_s, b, r, V, f		X
		r, S, m	Q, Q_s, b, d, V, f		X
		Q, S, m	Q_s, b, d, r, V, f		X
Long-term	ν, ρ, ρ_s, g	Q, Q_s	m, b, d, r, V, S, f, d_s, σ_s, w,	X	

Table 2-5. Critical Shear Stresses for Cohesive Sediments.

Authors	Critical Shear Stresses N/m^2
Dunn (1959)	0.058 - 0.24
Smerdon and Bearsley (1961)	0.0038 - 0.024
Flaxman (1962)	0.11 - 0.72
Abdel-Rahmann (Vanoni 1975)	0.0072 - 0.043

Table 2-6. Shear Strength of Aggregates.

Orders of Aggregates	Shear strength N/m^2
0	2.2
1	0.39
2	0.14
3	0.14
4	0.082
5	0.036
6	0.020

Table 2-7. Input Data Requirements and Output for Some Sediment Discharge Formulas (Adapted from Nakato 1990).

	Independent Variables		Dependent Variables (Output)
	Properties of Fluid Sediment	Flow Characteristics	
Ackers-White	ν, γ, γ_s, D_{35}	d, d, U_* (or S)	Q_T
Einstein-Brown	ν, γ, γ_s, D_{50}	U_{*b} (or r_b and S)	Q_B
Engelund-Fredsoe	ν, γ, γ_s, D_{50}	V, d, S	Q_B and Q_S
Engelund-Hansen	γ, γ_s, D_{50}	V, U_* (or r_b and S)	Q_T
Inglis-Lacey	ν, γ, γ_s, D_{50}	V, d	Q_T
Karim	ν, γ, γ_s, D_{50}	q, d, S	Q_T
Meyer-Peter-Muller	ν, γ, γ_s, D_{90}, D_{si}, P_i	V, U_{*b} (or r_b and S)	Q_B
Van Rijn	ν, γ, γ_s, D_{16}, D_{50}, D_{84}, D_{90}	V, d, S	Q_B and Q_S
Schoklitsch	D_{si}, P_i	q, S	Q_B
Toffaleti	ν, T, γ, γ_s, D_{65}, D_{si}, P_i	V, d, S	Q_B and Q_S
Yang	ν, γ, γ_s, D_{50}	V, d, S	Q_T

D_{16}, D_{35}, D_{84}, D_{90}, and D_{si} = bed sediment diameter such that 16, 35, 84, 90, and Si percent are finer, respectively

Q_T, Q_B, and Q_S = total, bed, and suspended sediment load, respectively

P_i = ith fraction of bed material group

q = water discharge per unit channel width

γ_b = hydraulic radius of bed only (cross sectional area of flow divided by wetted perimeter)

T = water temperature, °K,

U_* = shear velocity

U_{*b} = shear velocity evaluated at bed surface

Other parameters are as previously defined.

Table 2-8. Evaluation of Six Sediment Discharge Formulas for Five Rivers (Yang and Molinas 1982).

Sediment Discharge Formulas	Ratio of Computed Values to the Measured Total Sediment Load					
	Mean	Frequency of Occurrence (%)				Standard Deviation
		Ratio range				
		0.75-1.25	0.5-1.5	0.25-1.75	0.5-2.0	
Ackers-White	1.50	31	61	75	80	0.80
Corby	0.61	13	29	71	33	0.66
Engelund-Hansen	1.51	34	58	72	79	0.75
Maddock	0.49	24	43	56	45	0.48
Shen-Hung	1.18	43	71	80	81	0.61
Yang	1.12	50	76	95	88	0.44

Table 2-9. Cohesive Sediment Erosion Parameters.

Erosion Variables	Sediment Sizes (mm) $0.002<d_s<0.014$	Sediment Sizes (mm) $0.014<d_s<0.030$	Sediment Sizes (mm) $0.030<d_s<0.072$
τ_{CR} (N/m^2)	0.0060	0.6 - 0.16	> 0.6
M (g/m^2-s)	4.2×10^{-3}	--	--

Table 2-10. Cohesive Sediment Deposition Parameters.

Deposition Variables	Sediment Sizes (mm) $0.002<d_s<0.014$	Sediment Sizes (mm) $0.014<d_s<0.030$	Sediment Sizes (mm) $0.030<d_s<0.072$
τ_{CD}, N/m^2	0.043	0.33	0.42
w, cm/s	6.0×10^{-4}	0.104	0.202
A	1.8×10^{-5}	3.2×10^{-3}	6.4×10^{-3}

This page intentionally left blank.

3.0 SUMMARY OF FEATURES INCLUDED IN TEMPEST MODELS

Section 2.0 presented a general literature review into the fluid dynamic processes that could promote segregation. The first subsection, Section 3.1, describes the features contained within the TEMPEST fluid dynamic model, which was used (see Section 4.0) to perform predictions on particle segregation specific to the Hanford tank ciriticality issue. The second subsection, (Section 3.2), provides a comparison of TEMPEST code input data used in the predictions to actual tank waste properties.

3.1 TEMPEST FLUID DYNAMIC MODEL

The TEMPEST code, as implemented for the simulations described in Section 4.0, simulates an isothermal, incompressible flow in which the density and viscosity are influenced by the concentration of suspended particulates. Implicit within the TEMPEST model is the assumption that the Boussinesq condition is applicable. The Boussinesq approximation assumes that the change in density (in our tank analyses the slurry density) over the time steps used in the code is quite small. This approximation is valid for liquids and suspended solids under natural convection conditions and low velocity flows expected in tank operations such as tank filling, tank-to-tank transfers, air lift circulators, and mixer pump operation. This approximation allows one to simplify the governing equations by treating density as a constant in all terms except the body force terms of momentum equations. The complete equations for conservation of mass and momentum and for treatment of turbulence are documented in Trent and Eyler (1989). Version T.2.10c of the TEMPEST code was used.

Turbulent flow Reynolds stresses are modeled through an effective viscosity. The Prandtl-Kolmogrov hypothesis is used to relate the effective viscosity to velocity and length scales. In this approach, transport equations for the turbulent kinetic energy (k) and the dissipation of turbulent kinetic energy (ϵ) are solved by the k-ϵ model to determine the effective turbulent (eddy) viscosity as:

$$\mu_T = C_\mu \rho k^2/\epsilon \tag{3.1}$$

where

C_μ = constant equal to 0.09
ρ = fluid density
k = turbulent kinetic energy
ϵ = dissipation of turbulent kinetic energy

The baseline fluid density and molecular viscosity are taken as those of water at 37 °C for all TEMPEST code calculations for tanks C-106 and AY-102. The TEMPEST code input values for tank SY-102 were chosen from a measured value of 1.03 g/cm^3 (Dicenso et al. 1995) for the fluid density and an estimated molecular viscosity of the supernate of 1 cP (Onishi and Hudson 1996).

The slurry molecular viscosity is then calculated by multiplying the molecular viscosity of the base fluid by a factor of "a" raised to the power "ß":

$$\mu=\mu_o\ a^{\beta} \tag{3.2}$$

where

μ_o = base fluid viscosity = 0.69 cP or 1.0 cP
a = 105,000
ß = C_v/C_{vmax}
C_v = volume fraction solids in slurry
C_{vmax} = 0.46

The form of this equation was selected in an earlier effort to model the periodic rollover and gas release processes in tank SY-101 (Trent and Michener 1993). The value of "a" is determined by dividing a high viscosity intended to represent a very high solids concentration by a viscosity typical of a more dilute slurry. Reliable data on which to base the value of C_{vmax} is not available. To reliably set this parameter, accurate data is needed for the particle, bulk, and fluid densities for sludge. While a significant amount of data of this type has been taken, it is considered unreliable and clearly in error. For example, Bratzel (1980) examined four analyses of 106-C tank sludge to ensure that measurements were using a consistent basis. The resulting bulk density-particle density data pairs were, in g/cm^3: (1.22, 0.727), (1.324, 1.082), (1.579, 1.495), (1.485, 1.140). In all cases the particle density was less than the bulk density, which is impossible for a settling solid. This casts serious doubt on the validity of the data. Because obtaining a direct measurement for the value of C_{vmax} is difficult, a reasonable value within the same range as values selected previously to model tank SY-101 was chosen. The SY-101 modeling effort produced results similar to observed tank phenomena during mixer pump operation.

The calculated slurry molecular viscosity is used to calculate the fluid transport, but not to adjust the input settling velocity for each particle size used in the model. The impact of high solids concentrations on particle settling velocities is accounted for separately. The molecular viscosity of the slurry is added to the turbulent viscosity and the sum is used in fluid dynamic calculations.

Particle size distributions are modelled in TEMPEST using discrete particle sizes to represent portions of particle size distributions obtained from the characterization of sludge samples. We used data from only two Hanford Site tanks: C-106 and SY-102 (Castaing 1994, DiCenso et al. 1995) for all calculations discussed in Section 4.0. The extent to which the particles within these size distributions may actually be aggregates or flocculants instead of primary particles is unknown. Because we lack specific information on the density of different sized particles, all TEMPEST calculations for cases dealing with tanks C-106 and AY-102 initially assume that the particles have a uniform density of 2.44 g/cm^3 based on C-106 solids' properties (DiCenso et al. 1995). For the TEMPEST calculations on tank SY-102 a particle density of 1.80 g/cm^3 is used based on DiCenso et al. (1995).

Also, the actual shapes of different materials are not known, so all particulates are assumed to be spherical. To some extent, the modeling

results for different assumptions for the particle size, particle density, and shape of a particle can be evaluated by calculating the settling velocity and determining an equivalent diameter for that particle.

The settling velocity of each particle is provided to the code in the form of a velocity that is calculated assuming spherical particles and using Stokes Law (Equation 2.5). These input settling velocities do not include the effects of particle interaction, such as particle flocculation or agglomeration. Particle agglomeration is expected to occur and is discussed in some detail in Appendix A. The TEMPEST model does include the effect of hindered settling. The input settling velocity of each particle is adjusted for the effects of hindered settling based on an equation of the form

$$w_s = w_{so}(1-\beta)^b \tag{3.3}$$

where

w_s = hindered settling velocity
w_{so} = input settling velocity (unhindered settling velocity)
β = C_v/C_{vmax}, with C_{vmax}=0.46
C_v = volume fraction solids in slurry
b = 6.0

This correlation was discussed as Equation 2.6. The value of b for the Stokes Law settling region was provided in Table 2-2 as 4.65. However, using this value resulted in unrealistic settling occurring on top of the existing settled sludge layers in the bottom of the tank in the AY-102 simulation. Therefore, Equation 3.3 was modified. Because the value of C_{vmax} affects the viscosity calculation (see Equation 3.2), we changed the value of b instead to avoid affecting the viscosity. Setting b to 6.0 increased the hindering effect and prevented the unrealistic settling within the sludge layer. This value of 6.0 was used for all simulations reported in Section 4.0. The check made to ensure that the potential error introduced into the settling results would not be unacceptableis discussed in Section 4.3.

In some but not all TEMPEST simulations, a yield stress was introduced into the rheology model. Where used, its inclusion is noted with the results (Section 4.0). The expression used to calculate the yield stress is

$$\tau_{yield} = b_1 \beta^{b_3} \left(\frac{1-e^{-b_2\gamma}}{b_2\gamma+\epsilon}\right)(1-\alpha) \tag{3.4}$$

where

τ_{yield} = calculated yield stress
b_1 = yield stress = 1.5 psi
b_2 = strain coefficient = 50 dimensionless
b_3 = moisture exponent = 25 dimensionless
β = C_v/C_{vmax}
γ = strain rate of fluid
ϵ = a small constant set at 1 E-30
α = volume fraction gas, set to zero for all simulations

The calculated yield stress is added to the stress imparted by the viscosity in response to fluid shear. This yield stress formulation has been implemented with only limited success and the validity of its results is uncertain. However, simulations were performed with and without the yield stress to evaluate its effect on the results. Including the yield stress resulted in numerical problems that, in some cases, required the model to be adjusted further. However, where the code operated properly, the effect on particle segregation was small.

While TEMPEST can model diffusive effects on solutes and particles, the input was intentionally selected to eliminate diffusive effects.

3.1.1 Limitations of the TEMPEST Model

In the TEMPEST model, gravity causes the suspended particles to settle relative to the base fluid. The particle settling velocity is adjusted to account for hindered settling, but otherwise the particles neither accelerate nor decelerate relative to the base fluid. The velocity remains constant. The momentum of the particles is not included in the model. As a result, particles will tend to follow the stream lines even through sudden changes in direction. Several mechanisms that are useful in mineral processing cannot be simulated using TEMPEST. These mechanisms include film concentration, differential acceleration, Bagnold forces, flotation, and interstitial trickling. Appendix B covers mechanisms that the mineral-processing industry uses to achieve separations.

3.2 COMPARISON OF INPUT AND TANK WASTE CHARACTERIZATION DATA

In many cases, no rheological information exists for a tank sludge of interest. Available tank sludge viscosity data typically includes information for only one or two solids concentrations. Therefore, a fluid dynamic model as described in Section 3.1 is needed to estimate properties in a continuous manner for the remaining sludge concentrations. However, the predictions of physical properties used within the model must be comparable to tank waste data where data exist. This section explores the degree to which the fluid property values within the model agree with measurements on actual tank waste.

3.2.1 Viscosity

For the majority of regions in the TEMPEST simulations that have been calculated, the turbulent viscosity is much greater than the molecular viscosity after adjustments have been made for the solids content. Thus, after these two values are added together in the model, the molecular viscosity has little effect on the calculated results for these regions. The molecular viscosity input values and viscosity model predictions become important in the areas of the simulation where velocities are low and solids concentrations are high. The low velocities reduce the magnitude of the turbulent viscosity and the high solids content increases the fluid molecular viscosity.

The value of "a" in Equation 3.2 (105,000) was calculated by dividing a viscosity of 2,500 Pa-s (a value for a very high solids content slurry) by the viscosity of 0.024 Pa-s, which represents a relatively dilute slurry. Willingham (1994) surveyed data on tank sludges, slurries, and supernatants and found sludge viscosities in the range of 30 to 1,800 Pa-s with occasional high values exceeding this range. Thus, the high end viscosity of 2,500 Pa-s appears reasonable for a consolidated sludge. Similarly, values for slurries typically range from 0.010 to 0.070 Pa-s, which is consistent with the lower value of 0.024 Pa-s.

The predictions of the viscosity model can be checked against characterization data for sludge from SY-102. The TEMPEST SY-102 mixer pump model simulates an approximate three-to-one dilution of the settled sludge with supernatant liquid (three parts supernatant liquid to one part sludge). Actual characterization data for one-to-one and two-to-one dilutions of SY-102 sludge with water indicate that the slurry exhibits no yield stress and fits a yield pseudoplastic model (DiCenso et al. 1995). The viscosity model used in TEMPEST is not psuedoplastic, so the viscosity is not shear dependent as long as a yield stress is not specified. The data and the model are compared by using the data-derived model to calculate the apparent viscosity for a range of observed shear rates from the TEMPEST model for one mixer pump operating in the center of the tank. The solids content for the TEMPEST model was determined by assuming that the initial sludge layer had a volume fraction solids of 0.45, which is just below the maximum value of 0.46. This concentration is then diluted three to one with supernatant as the model executes. Figure 3-1 shows this comparison. The range of shear rates observed within a single cross section of the tank was 0.06 to 0.84 s^{-1}. Because the mixer pump problem includes relatively high shear rates, Figure 3-1 also includes values for lower shear rates.

In comparing the TEMPEST predictions and the actual data from tank SY-101 apparent viscositiy for the one-to-one dilution, the TEMPEST model appears somewhat more sensitive to increasing concentration than the available 102-SY characterization data would indicate. The discrepancy is larger at high shear rates and smaller at lower shear rates. The data for the two-to-one dilution appears to be fairly well approximated with the model slightly over-predicting at high shear and under-predicting at low shear. Thus, while the TEMPEST-predicted viscosities of the fully mixed tank may be very close to the data-based predictions, the predicted viscosity in high-concentration,

high-shear regions would be higher than the data for tank 102-SY indicates. The differences in viscosity between TEMPEST predictions and actual data in high shear regions has little impact on fluid dynamic calculations because the turbulent viscosity tends to dominate in these regions.

3.2.2 Yield Stress

The yield stress model in TEMPEST contains several parameters.

- Parameter b_2 (strain coefficient) primarily allows an exponential to function in place of the discontinuous Bingham model. Thus, its value is not selected based on fluid dynamic properties.

- Parameters b_1 (yield stress) and b_3 (moisture exponent) are not based on waste characterization data. They are taken directly from efforts to model the periodic rollover and gas release phenomena occurring in tank 101-SY sludge.

The yield stress model was implemented for a run of the 102-AY model. Examining the calculated yield stresses in the TEMPEST model, the yield stress only appears to become important in the bottom two cells of the problem containing the initial sludge layers. These are the layers where the solids concentrations are highest. In these areas, the yield stress that is added to the viscous stress reaches about 0.07 Pa at a volume fraction solids of 0.29. This is somewhat smaller than the 4.7 Pa yield stress measured for a one-to-one dilution of 102-AY solids with a volume fraction solids estimated to be 0.12. However, the measured value is uncertain because the characterization report does not list the units in which the yield stress was measured. We assumed that the units are the commonly used pascals (WHC 1993).

The validity of the TEMPEST yield model is uncertain. The users manual for the TEMPEST code notes that "The Bingham yield model is in development and testing and should be used with caution in the present version" (Eyler et al. 1993). The difficulty in modeling a yield stress using a Bingham yield model is that the viscosity is predicted to go to infinity when the shear rate drops to zero. Also, a discontinuity occurs at the point where the shear stress is equal to the yield stress (Mahoney and Trent 1995). The approach taken in TEMPEST to avoid these problems is to substitute a stiff exponential for the yield stress. In addition, the yield stress model used in TEMPEST incorporates a dependency on the solids concentration. It should be noted that the particulates in the colloidal size range have the greatest effect on yield stress. Therefore, a simple correlation to volume fraction solids may not be sufficient to predict the yield stresses between different waste slurries.

The yield model was implemented for the AY-102 TEMPEST calculations presented in Section 4.2 to determine if unexpected behaviors might influence the segregation behavior. However, the yield model itself should not be considered an accurate representation of the yield behavior of the sludge. While the cases have been calculated for investigative purposes, the development and validation of the TEMPEST yield model is beyond the scope of the current activity.

The conceptual model described here, including yield stress, viscosity, hindered settling, discrete particle size bin selections was implemented to calculate several specific problems that are described in Section 4.0.

This page intentionally left blank.

Figure 3-1. Comparison of TEMPEST Model Predictions and 102-SY Characterization Data for Various Water-Sludge Dilutions.

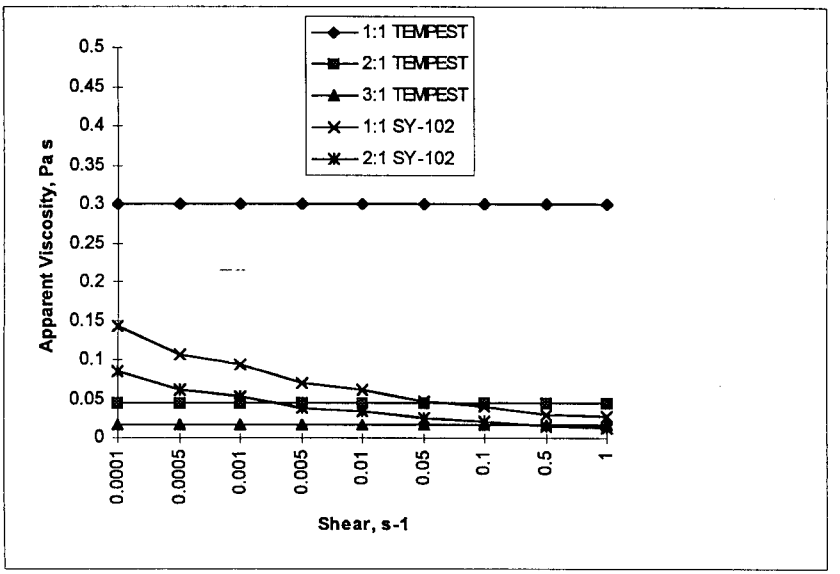

This page intentionally left blank.

4.0 PARTICLE SEGREGATION MODELING IN HANFORD WASTE TANKS WITH TEMPEST AND STOMP CODES

This chapter describes our efforts to determine the amount of particle segregation that might occur when the contents in Hanford Site waste tanks are disturbed as kinetic energy is generated. Kinetic energy can be generated during filling, post-filling operations such as tank transfers or additions, or stirring tank contents to remove heat or material (such as drainable liquid). Energy also is generated by aging processes such as radioactive decay. The potential for particle segregation during the following tank operations is discussed in this chapter:

- Tank filling, including the cascade process where supernate from one tank overflows into a second tank as the volume of slurry input to the first tank exceeds its capacity
- Additions and/or tank-to-tank transfers
- Salt well pumping
- Tank mixing to inhibit episodic gas release (burping, steam release) using mixer pumps or air-lift circulators
- Sludge sluicing and retrieval in anticipation of final pretreatment and disposal.

This chapter also includes the results of TEMPEST and STOMP modeling performed to date. A separate document to be prepared for the WHC retrieval program managers late in fiscal year 1996 will include the final computer modeling results for the specific Tank C-106 retrieval and Tank SY-102 mixing campaigns (Whyatt et al. 1996).

Tank sludge shows some discrete hydrous iron, zirconium, and aluminum oxide and several metal phosphate particles exist in tanks. Crystalline uranium phases have also been found in selected tanks. Thus it is plausible that discrete hydrous plutonium phases might exist in tanks. Details are provided in Chapter 7 and Appendix D. However, direct measurements of the chemical speciation of plutonium and neutron absorbers and on sludge rheological properties are sparse. Because we do not know conclusively whether the plutonium and key neutron absorbers exist predominately as discrete mineral phases or amorphous chemically and physically agglomerated gels, we decided to emphasize the potential importance of inertial segregation of discrete particles. This approach will not allow us to overlook possible fissile material-concentrating mechanisms and should lead to a thorough critical analysis of the criticality issue.

Some of the fluid dynamics analyses presented in this chapter for past operations use conceptual models and data that also are relevant to future retrieval operations such as jet-pump sluicing and retrieval. The specific cases and code input data used rely heavily on the anticipated retrieval and mixing activities and data on the sludges and liquids in tanks AY-102 (the receiver tank for sluiced waste from C-106), C-106, and SY-102.

The particle size distribution in each TEMPEST simulation is represented by either seven or nine discrete particle sizes. The particle sizes were selected to match the particle size distributions based on available data for solids in tanks SY-102 (DiCenso et al. 1995) and C-106 (Castaing 1994).

TEMPEST requires up to 24 hours of computer processing time to create results that represents just 2 to 3 minutes of real time where complicated fluid dynamics are occuring. These results presented here represent only the first tens of minutes of each of the following processes: sluicing of tank C-106, settling of sluiced solids into receiver tank AY-102, and jet-pump mixing of the solids in tank SY-102. Because the models represent such a short time, computer exercises may not show the processes at steady state and the final results could differ from these preliminary findings.

Despite these caveats, our expert opinion is that these results do represent the likely fate of sludge particles in the Hanford Site tanks, and that future calculations made over enough time for the process to reach a steady state will not dramatically change the conclusions presented herein.

The STOMP code was used to evaluate the potential for particle resuspension and transport during salt-well pumping and during heat-generated convection from radioactive decay. Particulars on the STOMP code can be found in White and Oostrom (1996a,b) and Nichols et al. (1996).

4.1 WASTE SLUICING AND TANK PUMP-OUT OPERATIONS

The fate of sludge particles during these types of operations is being evaluated using TEMPEST runs on the C-106 sludge sluicing and pump-out operation. Although the simulations discussed in this section were performed at a fixed temperature, the TEMPEST code can create simulations that consider the influences of the thermal effects caused by the pump and by friction between particles. The physical properties of the sludge waste used in the modeling are taken from Castaing (1994). These include the bulk density of the sludge at approximately 1.45 g/mL and a void volume of approximately 40 percent filled with interstitial solution. The particle density of the sludge was estimated to be 2.4 g/mL. The particle size distribution is shown in Table 4-1.

The average particle size for this sludge sample, based on weight, is about 16 μm. The overlying supernate has a density of 1.03 g/mL. As discussed in Chapter 7.0, plutonium-oxide particles are conservatively estimated to have a particle density of 11.46 g/mL. Some chemists on the team have argued that the amorphous/hydrous plutonium oxide has a particle density closer to 6 g/mL. The settling velocity of the conservative-density Pu particles with a conservative particle size of 11.5 μm is 0.81 mm/s in pure water at 37°C, which corresponds to the settling velocity of solid particles of Size Fraction 5 (see Table 4-1). The less dense hydrous plutonium oxide particle (perhaps a more realistic case) with a realistic particle size of 2-μm diameter has a settling velocity of 0.016 mm/s in pure water at 37 °C. This realistic settling velocity is much slower than those for solid particles of Size Fraction 1 in Table 4-1. Thus very small hydrous Pu oxides with a density of ~6 g/ml would actually settle slower than the particles of Size Fraction 1. Thus, the TEMPEST model results for Solids 5 and 1 will over

predict the actual settling velocity of discrete plutonium-bearing solid behavior in Hanford Site sludge. Because our concern is preferential settling of heavy particles, the analyses presented should over-predict the actual separation of discrete Pu-bearing particles from the rest of the sludge. This should lead to an over-estimation of the potential for criticality in Hanford tanks.

4.1.1 Tank Waste Sluicing

The supernate of tank AY-102 will be injected into tank C-106 to sluice tank C-106 sludge. The velocity at the 1-in. nozzle exit of the sluicer jet is 37 m/s. Because the density of the tank AY-102 supernate is 1.0 g/mL (Castaing 1994), and is much heavier than the air in the tank C-106 head space, the jet velocity is not expected to slow much from the initial velocity of 37 m/s before the jetted water hits the sludge.

The critical velocity of water flow needed to erode the sediment in the natural environment varies significantly with the sediment sizes as discussed in Section 2.1. It varies from approximately 0.2 m/s for the most easily erodible medium sand (diameter of 0.3 mm) to 0.4 m/s for coarse sand (diameter of 2 mm), to 1.3 m/s for medium gravel (diameter of 1 cm), to 2.5 m/s for 1 μm clay (Vanoni 1975, Simons and Senturk 1977). Some of these values are very approximate, especially the critical velocity to erode clay-sized material because of its cohesive nature.

The particle density of most natural sediments is about 2.65 g/mL and the water density at 20°C is 1 g/mL, so the density difference in these natural cases is 1.65 g/mL. The density difference between tank C-106 sludge and tank AY-102 supernate is 1.4 g/mL. The critical velocity for the tank sludge is similar to those in nature, and should be much smaller than 37 m/s. Therefore, with the sluicing jet velocity fixed at 37 m/s, all solid particles directly hit by the jet should be readily and completely resuspended. Finally, sluicing operations are not expected to segregate solid particles.

4.1.2 Slurry Pump-Out Operation

A retrieval pump will withdraw the slurry generated by the sluicing operation at the rate of 300 gal/min. The current plan is to dig a 3-ft-deep 5-ft-diameter hole (well point) in the sludge in tank C-106, from which the slurry pump will extract the material and transfer it to tank AY-102. To simulate this case, the well point is being simulated as a right-circular cylinder 5 ft in diameter and 3 ft high. The well point for withdrawing the sludge provides a location where larger, more dense sludge particles could selectively segregate from the flow and collect at the bottom of the well point. The TEMPEST code is being applied to this case as a full three-dimensional representation. The inlet slurry stream to the hole is assumed to contain 30 wt% solids, which is the maximum capacity of the pump being used. The slurry will be removed by a suction pump 4 in. in diameter. For these calculations, the pump is located at the top center of the cylindrical well point. The actual location of the retrieval pump will be at some elevation within the pit. Moving the suction point to the top of the cylinder is a simplification and probably increases the potential for settling in the bottom

of the well point. This should make our analysis conservative for particle segregation. We divided the solids into 9 size fractions by combining the 25-30 μm and the 30-35 μm sizes as the fifth of the nine size fractions (Table 4-1). This was done because TEMPEST can only handle 9 discrete size categories instead of the 10 discrete sizes available from the actual data. Although all solids are assumed to have particle densities of 2.4 g/mL for the TEMPEST calculations, a real particle's settling velocity can be used determine which of the nine particle bins would be equivalent. Once specific particle size and density information becomes available for actual sludge species, one can easily determine which bin should be used to estimate particle segregation potential without rerunning the code.

Although some solids entering the pump out point will likely be in the form of chunks of aggregated sludge, chunks are not included in the model. Chunks would tend to settle very fast relative to individual particles and would include both fissile material and neutron absorbers. The presence of mixed-particle chunks would, therefore, reduce the segregration of discrete plutonium-rich particles.

We model the slurry as being forced by the sluicing into this hole from a 10 cm-wide by 5 cm deep channel at one edge (the 9 o' clock position on the figures) of the top of the cylindrical hole. The channel is shown in Figure 4.4 because this figure represents the top of the well point. In other figures the channel is not explicitly shown because they represent layers deeper in the hole below the location where the channel meets the well point(hole). The slurry will be withdrawn from the top-center of the hole through a 4-in.-diameter pipe. With the sluicing rate of 300 gal/min, the hole will fill in about 1.5 min. Steady-state flow is expected fairly quickly.

We used the TEMPEST code (Trent and Eyler 1993 and Onishi et al. 1995) to examine the possibility of particle segregation in the bottom of the 3- by 5-ft cylinder dug out by the sluice jet for the pump-out operation. The TEMPEST code and our conceptual model accounts for various physical properties and rheology correlations for non-Newtonian flow and hindered particle settling needed to simulate waste in Hanford Site tanks (see Section 3.0).

The main model parameters for the tank waste transport modeling are those that determine viscosity, particle settling velocities, and yield/shear stress. Specific formulas and values selected for the modeling are shown in Equations 3.1, 3.2, and 3.3 (See Section 3.0). The current TEMPEST version's handling of the yield stress is limited in that it cannot keep sludge that should not get resuspended together for an extended time. Because no measured rheology values are available for the tank C-106 waste, we selected rheology values that were constrained by measured values for tank SY-101 waste and the rheology values that were used in TEMPEST models for mixing SY-101 tank waste (Trent and Michener 1993). Furthermore, because tank waste retrieval operations are not being performed yet, the models cannot be calibrated to specific tanks. However, because we are using the same rheology parameter values that were successfully used by the TEMPEST SY-101 modeling, we feel that this calculated overall behavior valid. Moreover the predicted values of viscosity (approximately 17 cP) for fully mixed waste in Tank SY-102 that relied on the Tank SY-101 rheology matched reasonably well with the measured consistency factor of 0.013-0.014 Pa-s for the mixed SY-102 waste (with the

volume ratio of sludge to supernate of 0.5). This confirms the general validity of the chosen model parameters (DiCenso et al. 1995).

The simulation time step used for the sluicing-pump out modeling was approximately 2 milliseconds. Early simulation results (out to 7 min) show that concentrations of each of the 9 particle-size solids are relatively uniformly distributed within the entire hole. Solid 1, the finest at 5-10 μm, (see Table 4-1) is most uniformly distributed and Solid 9, the coarsest at 50-55 μm, show some nonuniformity.

Figure 4-1 shows predicted distributions of flow (m/s) and Solid 9 concentrations (kg/m3) in a vertical plane extending from the top to the bottom of the hole and from the slurry inlet channel (shown at the right of the figure) to the center of the hole after 7 min from the start of the sluicing. Figure 4-2 shows the horizontal distribution of Solid 9 concentration for the circular plane at the bottom of the hole. As indicated in these figures, predicted concentrations of the Solid 9 after 7 min vary from 22.1 kg/m^3 near the surface to 40.1 kg/m^3 near the bottom, revealing some differential particle settling effects. The major portion of the hole from top to bottom has a Solid 9 particle concentration of approximately 23 kg/m^3. Note that the incoming slurry has a Solid 9 concentration of 22.2 kg/m^3. Thus there is very little change within the bulk of the excavated hole from which the slurry is pumped out of the tank.

Compared to Solid 9, Solid 5 (a medium-sized particle or the conservative representation of plutonium-bearing solids) particle concentrations are even more uniformly distributed than the biggest particles in the hole. Near the bottom of the well point excavation, Solid 5 particle concentrations vary from 20.7 to 21.2 kg/m^3; they vary only from 17.2 to 17.5 kg/m^3 near the top of the hole, as shown in Figures 4-3 and 4-4, respectively. The incoming concentration of Solid 5 is 17.5 kg/m^3. Thus, the concentration increases only slightly near the bottom of the excavation.

For Solid 1 (the more realistic representation of the plutonium-bearing solids), the particle concentration distribution is uniform throughout the hole, ranging from 130 to 131 kg/m^3, with the incoming concentration of 130 kg/m^3. The predicted Solid 1 distribution near the bottom of the excavation is shown in Figure 4-5.

To test the sensitivity of the predictions to the yield stress of the sludge (and the limitation in the TEMPEST code), we also modeled the sluicing-pump out operation with no yield stress. This is equivalent to allowing all the sludge to be moved without the threshold velocity needed to create solid movement. Figure 4-6 shows the predicted Solid 9 particle concentrations after 7 min of sluicing. The predictions for no yield stress show particle concentrations that vary from 22.1 to 40.2 kg/m^3. As the comparison between Figure 4-1 (showing Solid 9 concentrations varying from 22.1 to 40.1 kg/m^3) and Figure 4-6 clearly shows, these results are similar, indicating that the solid movement is insensitive to the selection of yield stress values in these calculations. The gradual solid accumulation at the bottom of the hole is evident in Figure 4-7 after 20 minutes of simulated sluicing (without the yield stress), showing that Solid 9 reached a maximum concentration of 62.5 kg/m^3. This is an increase of 50 percent over the 7-min predictions and an increase in coarse particle concentration at the bottom of the hole of

280 percent over the incoming well-mixed sludge slurry. This value is not the total enrichment factor for Solid 9 particles versus total sludge. Such a calculation requires one to add the concentration of all nine particle sizes to get the bulk sludge concentration.

Predicted maximum solid segregation for Solids 1, 5, and 9 over the incoming slurry concentrations that account for the total sludge settled at various positions near the bottom of the well point excavation are shown in Table 4-2.

Table 4-2 shows the relative concentrations of plutonium-bearing solids for the realistic case and conservative case (Solids 1 or 5, respectively) are actually reduced within the pump-out hole, because the concentration of coarser solids (e.g., Solid 9 with an assumed particle density of 2.4 g/mL) increases slightly under the model test conditions and durationssimulated. For the model results obtained to date , the sluice/pump-out operation does not segregate plutonium-bearing solids in any measurable degree. Apparently the advective fluid flow patterns created by the sluice jet and suction pump completely overcome the tendency of individual particles to settle with different velocities.

These predictions indicate that hardly any segregation of the particles takes place in the horizontal direction (across the cross section at any depth looking down from above the hole). Some concentration of larger particles takes place near the bottom, but the smaller particles (e.g., Solid 1) make up most of the bulk solids, even at the bottom of the hole, if they have the same particle density as the bulk sludge. The sluice/pump-out operation appears unlikely to segregate solid particles in any significant degree, based on these initial results. Once we obtain the actual particle density of the sludge as a function of particle size, we can calculate the individual settling velocities and choose the appropriate bin number. We will be able to reinterpret the TEMPEST code predictions without rerunning the code unless a large portion of the sludge particle density-size values result in calculated settling velocities outside the range shown in Table 4-1.

4.2 SLURRY RECEIVING TANK OPERATIONS (ORIGINAL TANK FILLING, CASCADING, TANK TRANSFERS/ADDITIONS)

We are examining the possibility of solid segregation in a tank receiving sluiced tank wastes via a pipe either from another tank or directly from the process facilities. We selected Tank AY-102 to represent this slurry-receiving operation for the TEMPEST modeling, but the analytical solution predictions are for a generic tank with slurry containing low suspended solids with generic particle size distributions and rheology properties.

4.2.1 Analytical Solution Predictions (Most Representative of the Cascading Process and Tank Filling with Slurry Containing Low Suspended Solids)

An analysis based on potential flow solutions for the fluid velocity in the tank will be applied to predict the preferential segregation of different-sized particles that occurs when dilute slurry is added to a receiver tank.

small particles at dilute concentration. Results are being obtained, and will be provided in a later report.

The analysis method is based on an asymptotic expansion for the particle velocity and concentration field. It is assumed that extremely small particles follow the fluid stream lines perfectly. Larger particles deviate from the fluid velocity field because of finite inertia and settling velocity. This is accounted for in the asymptotic expansion of the particle field and the particle differential equations describing conservation of mass and momentum of the particle phase.

Use of an asymptotic expansion for the particle velocity and concentration fields provides approximate solutions that account for the effects of particle settling relative to the fluid and particle segregation caused by the effects inertia. Particle settling occurs because of gravity; inertial effects arise when particles cannot follow fluid stream lines perfectly. Examples include the tendency of particles to migrate outward during centrifuging operations. Inertial effects could lead to segregation. Currently available codes, including TEMPEST, that treat particles as passive scalars that settle do not account for these inertial effects.

The approximate solutions will be based on fluid velocites that are described by potential flow solutions. The fluid inlet in a receiver tank at the Hanford Site will consist of four jets in a horizontal plane. The jets are oriented 90° apart. Flow from this geometry can be modeled by using the superposition of potential flow solutions. A potential source will be placed at the location of the jet outlet; this will provide the correct total mass flow rate of fluid. However, a potential source results in flow moving out radially so that the magnitude of the velocity is constant on the surface of a sphere surrounding the source and its direction is purely radial. This is not realistic for four horizontal jets. To correct for this, two potential quadrapole solutions will be used.

Potential flow solutions for the velocity obey inviscid transport equations of fluid mechanics and apply approximately when the Reynolds number is very large. These equations are appropriate for modeling the far field effects of jets. However, errors arise in regions with high viscosity, such as boundary layers. This degree of approximation is not necessary in computational fluid dynamics (CFD) codes. Therefore, the method used will account for particle inertial effects, which are not accounted for in TEMPEST, but will not account for viscous effects on the fluid velocity profiles, which are accounted for in TEMPEST. We anticipate that the results will provide an additional bounding calculation. This calculation will allow two independent assessments of particle segretation; this potential flow analysis and the TEMPEST calcuations. Appendix B also contains material that addresses the effects of momentum and inertial flow on particle segregation. As discussed in Appendix B, momentum and inertial forces are used extensively in mineral separation and purification. The various processes using accelerating tables, jigs and other devices use much more energy and specialized conditions than expected in any of the tank operations that were used in the past or contemplated in the future to retrieve sludge from the Hanford site tanks. We expect the results of CFD modeling will also corroborate this conclusion and

support the finding that extensive segregation of plutonium-bearing particles from neutron absorber-bearing particles is unlikely in the Hanford tanks.

4.2.2 TEMPEST Modeling For Waste Tank AY-102

The stream containing 330 gal/min of sludge slurry with 30 wt% solids will be sluiced from tank C-106 into tank AY-102. We assumed that the solids in the slurry have the same size distribution as the tank C-106 sludge (Table 4-1). This presupposes that the jet-nozzle sluicer does not destroy the sludge's original particle size distribution. Tank AY-102 initially contains 1.5 ft of the sludge and 15 ft of supernate above the sludge layer. The sludge in tank AY-102 has a bulk density of 1.4 g/mL (Castaing 1994), and is assumed to have the same particle size distribution as that in tank C-106.

Tank AY-102's inlet pipe has a distributor consisting of four 1-in.-diameter nozzles, oriented at right angles to each other to form a cross in the horizontal plane. The distributor is located 6 ft off the tank center and 13 ft above the tank bottom. A 4-in.-suction pipe to recirculate the tank AY-102 supernate back to tank C-106 for continued feed to the sluice jet is located 22 ft from the center (or 28 ft from the slurry inlet distributor) at the surface of the supernate (16.5 ft above the tank bottom). We located the suction pipe 45° between two of the four injection nozzles. The suction pipe volumetric flow rate for outgoing supernate liquid is set to 300 gal/min to match the incoming slurry discharge. To simplify the simulation and still maintain some conservativeness regarding potential solid setting in the tank, we moved the slurry distributor inlet to the center of tank AY-102, and increased the tank diameter from the actual 75 ft to 81 ft (to account for the inlet's actual location 6 ft off center). This allows us symmetry in the calculation, which cuts down the run times significantly, but still gives us the "right" geometry to the walls and distance between the inlet and supernate outlet suction pump. It is our professional judgement that this simplification will not significantly bias or invalidate the sludge settling results.

We used the TEMPEST code to calculate a full three-dimensional simulation case (with yield stress, but without simulating chemical reactions) with approximately 20-msec time steps. Figure 4-8 shows the predicted vertical distribution of Solid 5 (the conservative plutonium-bearing solid) concentration after 1 simulation hour. The figure shows the slurry plume descending from one of the four nozzles toward the tank bottom and the density current spreading the slurry over the original 1.5-ft-deep tank AY-102 sludge layer. Little mixing with the original tank sludge is predicted. Near the surface of the tank in the supernate, there is very little Solid 5 present. Figures 4-9 and 4-10 show the predicted Solid 5 concentrations on a horizontal plane just above the original AY-102 sludge layer after 25-min and 1-hr simulation times, respectively. The fan-shaped isoconcentration contours reflect the density current movement. These figures show that the jets cause the slurry plume to break into four discrete fingers that hit the tank wall and swivel back toward the tank center. Solid 5 concentration profiles show the accumulated slurry from the four distributor nozzles after 25 min. After 60 min, the Solid 5 concentrations are increased between the four jet pathways and along the tank periphery. Variations of Solid 5 concentrations within this horizontal plane near the original sludge interface vary only

approximately 30 percent (from 5.6 to 7.3 kg/m^3 at 1 hour) across the tank cross section. Particles of all sizes will accumulate steadily in this layer just above the original AY-102 sludge layer. Therefore, the concentrations are expected to increase for all solids, eventually reaching a total volume fraction of 0.46 (C_{vmax}), the value chosen to represent a completely settled sludge layer. Once a layer (represented by grid spacings in the numerical computer calculation) reaches this volume fraction of settled solids, solids that settle later must accumulate in the grid layer just above the layer that has just reached C_{vmax} = 0.46. This sequence is expected to continue until all of the Tank 106-C sluiced slurry has been placed in in Tank AY-102 and settles.

Immediately after being expelled from the 1-in. nozzles, the slurried sludge solids sink rapidly toward the tank bottom. Figures 4-11 and 4-12 show velocity and Solid 5 distributions on the horizontal plane containing the four slurry jet nozzles near the liquid surface. Figure 4-12 covers an expanded radial distance (1.9 m) equal to the distances shown by velocity arrows in Figure 4-11. The closely bunched contours indicate rapid initial mixing. Because the four slurry jets distribute the slurry to slide on the original tank AY-102 sludge surface as a density current, hardly any solids move upward toward the pump suction inlet at the surface. This prevents solids from being recirculated back to tank C-106. This is clearly indicated in Figure 4-13, where Solid 5 concentrations ranging from 1.2 x 10^{-6} kg/m^3 to 2.7 x 10^{-5} kg/m^3 are found in this surface plane.

Other particle size solids show patterns similar to that of Solid 5. Solid 1 (more realistic representation of plutonium-bearing solids) shows an even more uniform distribution (Figures 4-14 and 4-15). Solid 9, the largest particles in the sludge, have somewhat less uniform distribution patterns (Figures 4-16 and 4-17). These simulation results are for 1 hr simulation time (1 hr of sludge entering tank AY-102 after sluicing tank C-102 begins). The predictions indicate that most of the slurry introduced into tank AY-102 will accumulate over the original tank AY-102 sludge layer at the tank bottom.

Figure 4-18 shows the predicted maximum segregation for three of the particle sizes over the initial slurry concentrations on the horizontal layer just above the original tank AY-102 sludge after 1 simulation hour. Solid 5 gradually increases its relative concentrations by up to 1.5, while Solid 1 shows practically no segregation. If we assume that these two particle bins represent the conservative and most representative estimates for plutonium-bearing solids, respectively, the predictions indicate that the slurry-receiving operation does not significantly segregate plutonium-bearing solids in the receiving tank. This conclusion is thought to hold for other operations such as original tank filling, additions to partially filled tanks, cascading, and tank-to-tank transfers within the limits of the modeling assumptions and input values chosen. Any detailed discussion is not viable without more detailed data on the slurry flow rates into tanks, slurry particle concentrations, and the individual particle densities and chemical makeup of sludge of different particle sizes, if differences truly exist.

4.3 MIXER JET PUMP OPERATION (PROPOSED FOR TANK SY-102)

Potential particle segregation during the jet mixer operation in double-shell tanks is being evaluated using tank SY-102 as a representative tank for the jet mixing operation. Tank SY-102 has a sludge layer with a bulk density of 1.56 g/mL; the overlying supernate has a density of 1.03 g/mL (DiCenso et al. 1995). The particle density of the average bulk sludge is 1.80 g/mL. The sludge contains $NaNO_3$(s), $Al(OH)_3$(s), $Na_3PO_4 \cdot 12H_2O$(s), and iron solids (Onishi and Hudson 1996). The particle distribution and calculated unhindered settling (fall) velocity are shown in Table 4-3 (DiCenso et al. 1995). These settling velocities were calculated by assigning fluid viscosity to be 1.0 cP.

The average particle size based on the volume is about 53 μm (DiCenso et al. 1995). In tank SY-102 modeling, we include all seven of these solid fractions. As discussed previously, a conservative estimate is that plutonium solids have a particle density of 11.46 g/mL. Some chemists on the team believe that the amorphous/hydrous plutonium oxide has a particle density closer to 6 g/mL. The unhindered settling velocity of the denser particles (conservative) with a conservative particle size of 11.5 μm is 0.81 mm/s, which corresponds to the settling velocity of solid particles of Size Fraction 4 (Table 4-3). While the less dense particles (perhaps more realistic) with a realistic particle size of 2 μm diameter has a unhindered settling velocity of 0.016 mm/s. This realistic settling velocity is much smaller than those of solid particles of Size Fraction 1 in Table 4-3. Thus, the predicted model results for Solids 4 and 1 can be regarded as conservative and more realistic representatives of plutonium-bearing solid behavior.

The tank SY-102 conceptual model used in TEMPEST simulates the operation of two mixer pumps each with two jet nozzles. The four outlets have 6-in.-diameter nozzles and are placed 17 in. above the tank bottom, with the 15-in. diameter pump suction line positioned 7 in. above the tank bottom. The mixer pumps are located 20 ft from the tank center on opposite ends of a diagonal line through the tank center. Each jet rotates over a half circle at 0.5 rpm and injects fluid into the tank at 60 ft/s.

Tank 102-SY is the most challenging problem currently being modeled. Tank SY-102 TEMPEST runs are three dimensional but are reduced by assuming that the tank is symmetrical, so that only one quadrant of the tank has to be modeled. Using symmetry arguments to simplify the problem makes an implicit assumption that the jets of the two mixer pumps are synchronized and counter-rotating.

We selected the following three TEMPEST test cases for tank SY-102 modeling. All cases assume a three-to-one ratio of supernate liquid to sludge. Currently, we are simulating all three test cases without a threshold yield stress for the settled sludge. Later we plan to model with yield stress (see Whyatt et al. 1996). Cases 1 and 2 were modeled to address concerns that the flow patterns of the jet rotating in 90° increments used in Case 3 might not agitate the overall sludge enough to show significant differences in particle deposition patterns.

- Case 1, Static Sludge. The rotating jet is located in the center of the tank. The simulation begins with the tank sludge sitting on the bottom of the tank.

- Case 2, Mixed Sludge and Supernate. The rotating jet is located in the center of the tank. The simulation begins with the tank sludge fully mixed in the tank supernate.

- Case 3, Off-center Jet. The jet is located 20 ft off center, but discrete 90° changes in mixer pump discharge direction at 30-second intervals simulate a rotation rate of 0.5 rpm. The simulation begins with the tank sludge sitting on the bottom of the tank.

We ran the Case 1 model for 1.5 hr. As the jet mixes the sludge and supernate, all the solid concentrations change with time. However, instead of changing the solid concentrations in the jet at every time step, we only changed the jet solid concentrations several times during the simulation. Thus, the model results at this time are a qualitative representation of the pump mixer operation. The three-dimensional distributions of predicted volume fractions of Solid 9 after the first 2 min, 30 min, and 1.5 hr are shown in Figures 4-19 through 4.21, with color-coded volume fractions . These figures indicate that as the sludge-mixing time progresses, the jet containing the sludge slurry is mixing the sludge and supernate. It takes over 1 hr to mix them fully. Also the stream of slurry exiting the jet eventually hits the tank wall. Because the current TEMPEST has limited success handing yield stress, especially for the sludge to resist initial movement induced by the flow, we assigned the yield stress for the current simulation as zero. This causes some uncertainty in these TEMPEST results that show almost all the bottom sludge as eventually mixed. If the sludge has a significant yield stress before beginning the jet pump mixing, more resistance to sludge movement than is currently modeled could exist. We will further evaluate this uncertainty for the specific retrieval report (see Whyatt et al. 1996).

In Case 2, we evaluated potential particle segregation during continuous pump operation once the sludge and supernate are fully mixed. Internally, TEMPEST-generated calculated viscosity varies from 0.016 to 0.022 Pa-s. Although these values are not directly comparable to available measured rheology data, they are nonetheless similar to measured consistency factors of 0.013-0.014 Pa-s for fully mixed SY-102 tank waste obtained in the laboratory by mixing tank SY-102 sludge with twice the volume of its supernate, as shown in Table 4-4 (DiCenso et al. 1995). A more detailed discussion on rheology was presented in Chapter 3.

The model predicted some settling of Solid 7 (the coarsest solid, with 100-175-μm diameter) and hardly any settling of Solid 1 (the finest solid, with 10-20-μm diameter), as expected. (See Figures 4-22 and 4.23 showing the Solid 7 and 1 distributions at 1.5 simulation hours). Fully mixed concentrations for Solids 1 and 7 are 16.6 kg/m^3 and 9.0 kg/m^3, respectively. Changes from the initial solids concentrations for all other solids, including Solid 4, fall between these two patterns. As indicated in Figures 4-24 and 4.25, accumulation patterns for Solids 7 and 1 on the bottom of the tank also reflect these patterns, showing Solid 7 varying its concentration from 9.1 kg/m^3 near the tank center to 14.2 kg/m^3 along the tank wall, while Solid 1

varies only from 16.6 kg/m^3 to 16.7 kg/m^3, showing no position-sensitive variable accumulation.

Predicted solid maximum segregation (the factor change over the initially assumed well-mixed state) for Solids 1, 4, and 7 is shown in Table 4-5. This table indicates that the relative concentrations of the two presumed plutonium-bearing solids (Solids 1 or 4) are actually reduced near the tank bottom, because the concentration of coarser solids (e.g., Solid 7) increases slightly under the model test conditions and durations tested. According to the model results obtained under the conditions and duration simulated, the mixer pump operation does not segregate the plutonium-bearing solids in any measurable amount once the sludge and supernate are fully mixed and the pump is continuously run.

Case 3, with the off-center jet, requires very small simulation time steps. At 5 simulation minutes, the model predicted that a large portion of the sludge still is not mixed by the jet, as shown in Figures 4-26 and 4-27. The figures depict a vertical slice through the tank at the 2 o'clock position and a horizontal plane at the tank bottom, respectively. They show the particle concentration distributions of Solid 4 (the conservative presumed case for plutonium-rich solids). The particle concentrations shown in Figure 4-26 (vertical slice through the tank) varies from 0.131 kg/m^3 to 21.0 kg/m^3. This result indicates that even though no yield stress is imposed in this case, sludge has not yet been appreciably resuspended mostly because TEMPEST calculates a very large viscosity for the slurry based on the high concentrations of suspended solids. Although we will evaluate the effects of yield stress further, for this early simulation time, TEMPEST shows that the bulk of the sludge has not resuspended and is hardly moving.

To test the effect of particle settling velocity on distribution predictions, we arbitrarily increased the unhindered settling velocity of Solid 4 by 10 times the actual value (0.81 mm/s, see Table 4-3). As before, TEMPEST internally calculated a hindered settling velocity, as affected by the suspended solids concentration. We kept all other solid settling velocities (unhindered) the same as those shown in Table 4-3. The predicted distributions of Solid 4, for this variant on Case 3, are shown in Figures 4-28 and 4-29. The particle concentration for the vertical slice through the tank (at the 2 o'clock position) varies from 0.126 to 21.3 kg/m^3 (see Figure 4-28). Some additional settling occurs with increased settling velocity. However, comparing Figures 4-28 and 4-29 with Figures 4-26 and 4-27 clearly reveals that the tenfold increase in settling velocity for Solid 4 did not significantly change the distribution and accumulation patterns for this particle size in the tank. Note that approximately a hundredfold difference in settling velocity, as seen between Solids 1 and 7, is needed before significantly measurable segregation differences occur between the sludge particles. This sensitivity analysis helps determine how much difference in particle size and density, as they relate to hydrodynamic settling velocity (see Sections 2.1.1.5 and 2.1.1.6 for the relationship), will cause significant differences in settling trends between various types of sludge components.

4.4 SALT WELL PUMPING

Numerical simulations of salt well pumping of a single-shell tank were performed using the STOMP code (White and Oostrom 1996a, 1996b) and certain sludge properties taken from Castaing (1994) for tank C-106. These simulations were performed for two reasons:

- To find the maximum fluid flow velocities caused by salt well pumping
- To assess whether such velocities could promote the particulate transport of plutonium-rich particles.

Input parameters needed for the simulations included: porosity and permeability of the sludge material, as well as the fluid properties and pumping rate. Likely values for porosity range from 30 to 50 percent, while permeability values could range from between 10^{-12} cm^2 and 10^{-15} cm^2. These values were chosen because we assumed that the sludge material has the consistency of wet mud, which has a relatively high porosity, but a very low permeability (e.g., clay). In addition, fluid properties such as viscosity and density were chosen to reflect previous measurements (see Castaing 1994). Accordingly, a fluid density of 1.4 gm/cm^3, and a viscosity of 12.5 cP were used. These properties represent a fluid made primarily of water saturated with $NaNO_3$. Reported pumping rates during salt-well pumping range from less than 0.1 to 5 gal/min.

A worst case scenario, i.e., one that would yield maximum velocities during pumping, was simulated using a porosity of 30 percent, permeability of 10^{-12} cm^2, and a pumping rate of 2 gal/min. Other simulations were performed with different combinations of porosity, permeability, and pumping rate to explore the sensitivity of the resulting velocities to these uncertain parameters. However, a steady pumping rate could not be maintained because the sludge has such low permeability. After an initial pumping period, the sludge around the well stopped yielding fluid to the well. The velocity of fluid movement toward the well when the area right around the pump is pumped dryis very small. This phenomenon actually has been observed in some tanks subjected to salt-well pumping.

Radial flow toward a pumping well is characterized by a very rapid decrease in the magnitude of the fluid velocity as the distance from the well increases (Theis 1935).

Assuming that the initial velocities generated by pumping could mobilize the plutonium-rich particles or the neutron absorber-rich particles near the well, the particles would be pumped out of the tank. This would leave an area in the vicinity of the well with diminished concentrations of either plutonium- or neutron absorber-rich particles. However, because calculated velocities drop markedly as the distance from the well increases, the effect would be very localized. Away from the pump the velocities are so low that no particle resuspension is plausible and, whatever their size, the sludge particles would remain as they were before salt-well pumping.

Simulation results show maximum velocities immediately adjacent to the well of 0.00209 m/s (for a pumping rate of 2 gal/min) during the first minute

of pumping. After this time the sludge around the well dries out and flow decreases. The simulations do not account for the fluid already in the well before pumping starts. As discussed in Sections 2 and 4.1, the critical velocities needed to resuspend particles in natural stream beds range from 0.2 to 2.5 m/s. Further, cohesive particles such as fine-grained clays actually require velocities of a few meters/second. The calculations using the STOMP code suggest that the highest velocities will be three orders of magnitude lower than this value and will occur in an area immediately surrounding the pump for very short durations before the flow drops to essentially zero.

In summary it appears that salt-well pumping has not affected particle segregation if the sludge is fine-grained silt and clay-like. If the sludge maintains these characteristics, any future salt-well pumpling also will not affect particle segregation. If the tank contains only salt cake, the permeabilities would be higher and flow rates could be higher. However, salt cake does not contain significant amounts of plutonium, so salt-cake particle transport is not an issue for criticality.

4.5 AIR LIFT CIRCULATORS

4.5.1 Estimation of Air-Induced Liquid Flow

Figure 4-30 is a schematic of an air lift circulator, or sparger. It is is essentially a pipe within a pipe. Air is forced through the inner pipe and escapes out the bottom where it creates bubbles and entrains liquid and fine particles that rise with the bubbles within the annulus between the two pipes. The buoyancy created by the rising bubbles moves the entrained slurry and creates "convection" cells that pull sludge or slurry from the neighboring volume below and outside the pipes.

The total flow rate of entrained liquid depends on the supply rate of the air, the geometry of the sparger, and the physical properties of the liquid. The flow rate inside the sparger may be predicted by recognizing that the pressure drop calculated for flow outside the sparger must be equal to the pressure drop calculated inside. The pressure drop inside the sparger is related to the flow of entrained slurry.

Hanford Site waste tanks that contain air lift circulators usually have about 22 of these dual-pipe systems. They are arranged in 2 concentric circles around the tank to completely mix the slurry in the tank.

In the Hanford Site tanks, the sparger system's performance is complicated because the liquid is actually a slurry that contains suspended solids. We found no specific correlations in the literature that explicitly consider the characteristics for sparging of solid-liquid suspensions. Therefore, we assumed that the slurry is a liquid with a density and viscosity equal to those of the slurry.

This assumption is justified if the suspended particles are relatively small, which is the case in most, if not all, of the Hanford Site waste tanks. The goal of this section is to determine whether the entrained liquid flow rate used in a TEMPEST prediction documented by Eyler (1983) is reasonable.

The TEMPEST analysis made a similar assumption regarding flow of the mixed slurry. This means that any uncertainty resulting from treating the slurry mixture as a liquid is also embedded in the final results of the earlier TEMPEST simulation for air-lift circulators.

4.5.2. Liquid and Solid Movement

The flow rate of liquid (tank liquor and fine particulates) induced by air bubbles in the air-lift circulators is estimated to be 2,100 gal/min or more. (See Appendix C for details of our analyses to determine whether the velocity of the entrained tank slurry caused by the rising bubbles that Eyler [1983] used [50 ft^2/min in each air-lift circulator] is reasonable.) An older version of the TEMPEST code was used by Eyler (1983) to simulate liquid flow and solid movement in a double-shell tank by imposing the induced liquid velocity of 0.961 ft/s in each circulator. The older version of TEMPEST assumed that viscosity was independent of solid concentrations and that the flow was Newtonian.

The TEMPEST 1/7 tank modeling is based on the symmetry afforded by placing the 22 air lift circulators evenly around the tank in 2 concentric circles. The model assumes that three layers of solids settle at the bottom of the tank when the air lift circulators are not running. Each layer was assumed to have a constant settling velocity of 0.030 m/s (Eyler 1983). As the air-induced liquid flow rises through the outer 30-in. tubes of the air lift circulator, the flow around the tube bottoms (0.76 m above the tank bottom) will entrain sludge into the tubes. This erodes the solids around the tubes. However, the velocity decreases with the distance from the tube bottom perimeter, reducing the velocity near the tank bottom to about 0.05 m/s or less more than 1 m away from each air lift circulator. This behavior also was predicted by the earlier TEMPEST run (See Figure 4-31). As discussed in Chapter 2 and Section 4.1, the critical velocity is about 0.2 m/s for the most easily erodible medium, sand (0.3-mm diameter); 0.4 m/s for coarse sand (2-mm diameter); 1.3 m/s for medium gravel (1-cm diameter); and 2.5 m/s for 1-μm clay (Vanoni 1975, Simons and Senturk 1977).

Based on this behavior, although the older TEMPEST model predicted that uniform mixing and complete sludge resuspension would be achieved throughout the tank after 15 simulation minutes, the actual scouring is probably limited to local areas around the air lift circulators, and many solids located beyond about 1 m from the air circulators will not be resuspended by the induced flow. Most of the solids resuspended by the induced flow will probably follow a local recirculating flow pattern around the tubes, with some small amount of the resuspended solids diffused to settle on the tank bottom on top of solids that do not move when the air lift circulators operate. The probability that this selective settling in zones between the air lift circulators and farther out into the tank could lead to concentration of much sludge material and plutonium-rich sludge in particular is remote. Neutronic criticality calculations suggest that one would need a large volume of fissile material with moderate concentrations of Pu to settle in a spherical geometry for criticality to occur. Some calculations that quantify this statement are found in Bratzel et al. (1996) and Rogers et al. (1996). Based on these reports and our analyis of the relatively small areas of sludge around the 22 air lift circulators in each tank (that contains such devices) that would be actively

resuspended, the potential for criticality to occur is very small.

The tank will be divided into 22 zones (approximately concentric circles around each air lift circulator for which there will be complete resuspension and pancake like settling when the air is shut off) and many interconnected zones just outside the 22 concentric circles where little or no sludge will be resuspended. What little resuspended sludge that "diffuses" over these zones and could preferentially settle would be dispersed around the 22 active zones and would not preferentially settle in any select dead zone. All the dead zones should receive portions of the diffused sludge and the diffused sludge should ultimately settle in pancake-like fashion on sludge that is too far from the air lift circulator bottoms to be entrained or resuspended.

4.6 THERMAL EFFECTS

Numerical simulations of heat convection caused by radioactive decay within a generic tank containing sludge were performed using the code STOMP (White and Oostrom 1996a, 1996b). These simulations had two purposes. The first was to find the maximum flow velocities that could be generated by heat convection cells formed as radionuclides in the waste decay. The second was to assess whether these velocities could promote the transport of plutonium-rich particles.

Several input parameters were needed to conduct the simulations. These include parameters governing the flow of the sludge interstitial fluid and parameters governing heat production and diffusion. These properties represent a fluid consisting primarily of water saturated with $NaNO_3$. Parameters relating to the diffusion of heat include thermal conductivities of both fluid and sludge. The properties and boundary conditions are presented in Table 4-4.

In choosing a constant temperature for the supernate, we assumed that the supernate fluid equilibrates faster (releases heat) than the sludge material because of its higher conductivity. These choices, along with the permeability of the sludge dictate whether fluid convection cells develop within the sludge to transfer heat from the interior of the tank to the boundaries. In the absence of fluid convection cells, heat will be transferred via conduction to the tank boundaries.

It should be noted that actual measurements of the parameters listed in Table 4-4 are either very limited or non-existent.This leads to high uncertainty in the results from the numerical simulations. A sensitivity study with a base case as a reference was considered to explore the effect of different parameter values on the system. However, the many possible combinations of parameter valuesmake such a study impractical until some measurements are taken to limit the number of possible parameter combinations.

Figure 4-32 shows the results of the simulation using the values of the parameters presented in Table 4-4. The simulated domain is axisymmetric (i.e. the center of the tank is at the left). The upper picture is the temperature profile in the tank for the given heat production and heat dissipation through the walls and bottom of the tank. As stated, the supernate solution is assumed to stay set at 40 °C and the heat steadily builds toward the center of

the tank to a maximum of 60 °C. For this simulation, a convection cell develops close to the walls of the tank, where cooling is occurring. Maximum velocities are below 10^{-11} ft/s(<3 · 10^{-12} m/s). Fluid exchange between the sludge and the ponded supernate is also observed; fluid flows upward (out of the sludge) in the center of the tank, and then downward (into the sludge) at the edges of the tank. This isshown in the lower figure in Figure 4-32. The velocities observed are extremely low and would not support any resuspension of sediment. As discussed in Sections 2.1.8 and 4.4, the necessary flow velocity to resuspend and physically transport particles varies from 0.2 to 2.5 m/s. This value is over 10 orders of magnitude higher than the very slow convection cell estimated by these calculations.

An additional simulation using STOMP was performed to investigate the effect of increased heat production within the sludge inside the tank. A heat production rate of 43.2 W/m^3 (from Waltar et al. [1996]) was used. The rate is based on the heat generated in Tank C-106, which is considered the highest heat-generating tank at Hanford. The STOMP simulation yielded extremely high temperatures inside the sludge. These temperatures were well above the boiling point of water (100 °C) in widespread regions in the sludge.

Several points concerning the simulation need to be made. First, the simulation depends entirely on the boundary conditions used. The boundary conditions dictate the rate of heat loss from the sludge/tank, and thus are responsible for the temperature history inside the sludge. The boundary conditions for heat conduction through the tank walls and floor and thermal properties of sludge are highly uncertain. (This applies to all our heat convection simulations).

The second issue concerns how STOMP simulates the upward flow of gas (water vapor) in a homogeneous medium underlying a ponded layer of liquid. Physically this is an unstable situation; gas bubbles migrate upwards along preferred pathways (fingering), while liquid migrates downwards to fill the space left by the gas. In STOMP, however, gas migration in a homogeneous medium is uniformly distributed. STOMP does not simulate the actual gas bubble generation and migration along preferential pathways.

The third issue pertains to tank breathing and whether pressure buildup in the headspace of the tank caused by increased temperatures is allowed to equilibrate with atmospheric pressure. Continued heating of the fluid in the sludge would most likely increase the temperature of the headspace inside the tank, as well as the humidity of the air inside. Venting would allow heat and moisture to escape, which would have to be accounted for in the simulations as boundary conditions.

To achieve pore seepage velocities of 0.2 to 2.5 m/s (the value needed to start particle migration), a hydraulic conductivity of the order 0.1 to 1.0 m/s and a hydraulic gradient of about 1 to 12 would be needed, assuming a porosity of about 50 percent. These values of hydraulic conductivity represent those of gravel with water. (More viscous fluids such as tank liquors would require an even larger permeability.) Clearly, the sludge material does not resemble gravel (i.e., the pore size is much smaller) and the hydraulic gradients induced by heat generation/transfer are several orders of magnitude smaller than 1 to 12.

Research indicates that the sludge is made up of clay-to-silt sized particles, with the bulk of the particles having a size of less than 10 microns. This particle size distribution would yield very small pores (less than 10 μm), which would make the transport of colloids of similar size quite difficult within the stationary sludge matrix.

The results of this simulation indicate that the sludge heats up (see Figure 4-33a) and boils the interstitial fluid, causing the resulting vapor to migrate upward. If the tank is allowed to breathe, the sludge would eventually dry up, and possibly heat up further because evaporative cooling has been lost. The simulation assumed a constant ponded layer of fluid above the sludge top, which allows for a continuous supply of fluid to the sludge. This can be seen in the fluid velocity plot, Figure 4-33b. In general, drying the sludge reduces saturation and, as a result, its hydraulic conductivity, and thus reduces the resulting pore water velocities.

Hypothetically an optimum heat generation rate could exist, which would create a maximum fluid convection within the sludge without making the fluid itself boil. However, investigating this possibility would involve extensive guesswork given the uncertainty in boundary conditions and thermal and hydraulic properties, and the large number of possible combinations.

In summary, we find that the small particle size nature of the Hanford tank sludge, will prohibit convection cell velocities to reach values high enough to entrain fine particles and selectively move particles of different density, size or shape. A criticality induced by particle migration caused by heat generation is implausible. Heat induced changes in solubility of plutonium or neutron absorbers in tank liquids is addressed in Chapter 7.0.

Figure 4-1. Predicted Vertical Distributions of Flow (m/s) and Solid 9 Concentration (kg/m^3) on Vertical Plane 14 (9 O'clock Position) of the Hole at 7 Simulation Minutes.

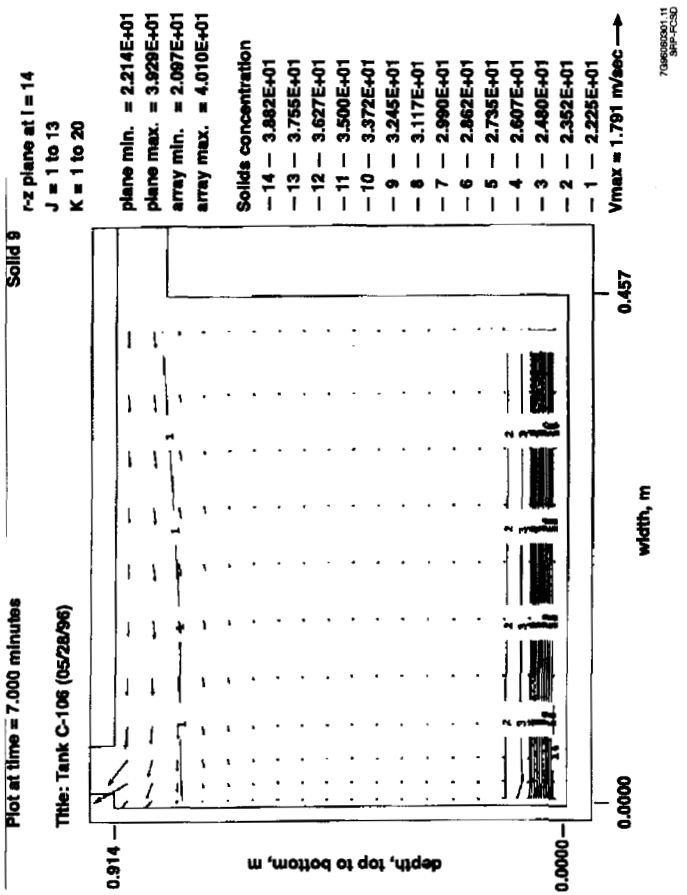

Figure 4-2. Predicted Horizontal Distributions of Flow (m/s) and Solid 9 Concentration (kg/m^3) at Bottom of the Hole at 7 Simulation Minutes.

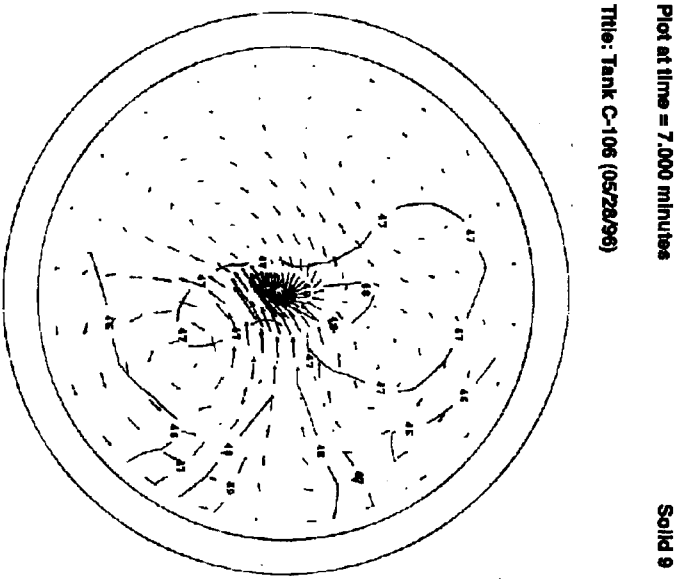

Figure 4-3. Predicted Horizontal Distributions of Flow (m/s) and Solid 5 Concentration (kg/m^3) at Bottom of the Hole at 7 Simulation Minutes.

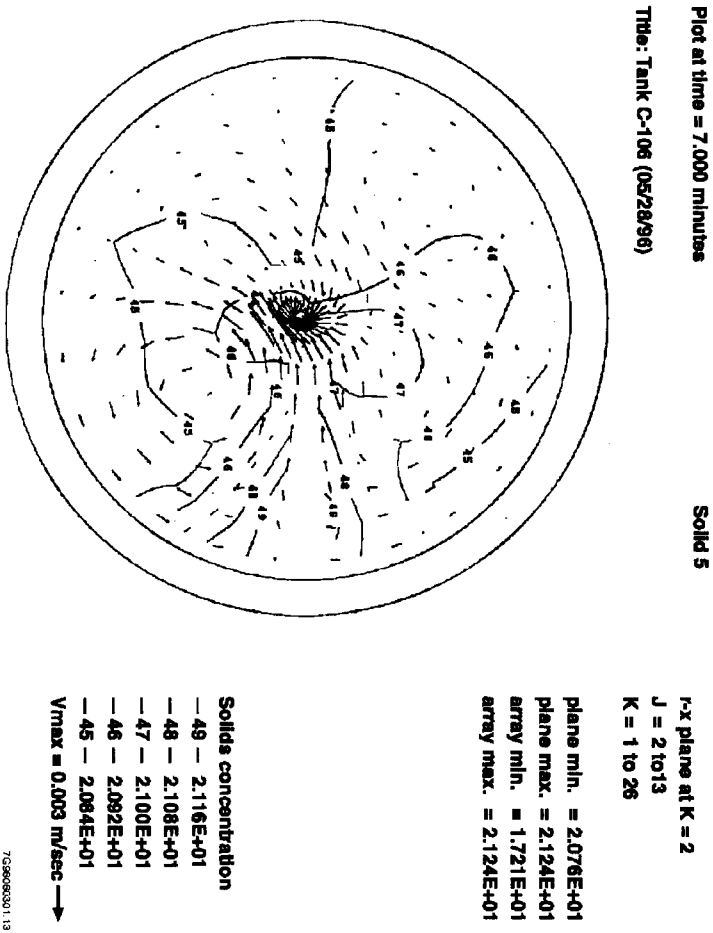

Figure 4-4. Predicted Horizontal Distributions of Flow (m/s) and Solid 5 Concentrations (kg/m^3) at Top of the Hole at 7 Simulation Minutes.

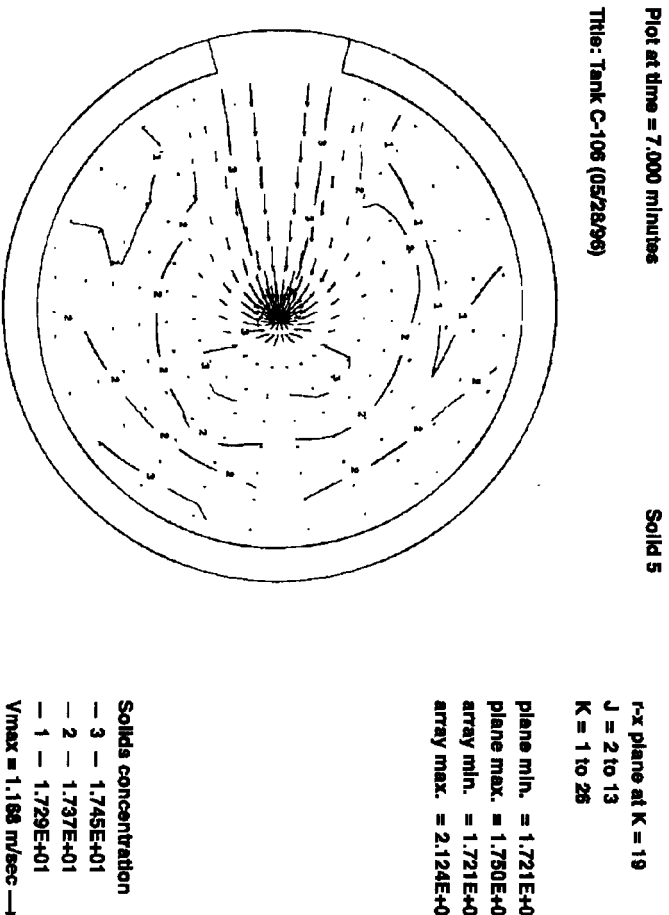

Figure 4-5. Predicted Horizontal Distributions of Flow (m/s) and Solid 1 Concentration (kg/m^3) at Bottom of the Hole at 7 Simulation Minutes.

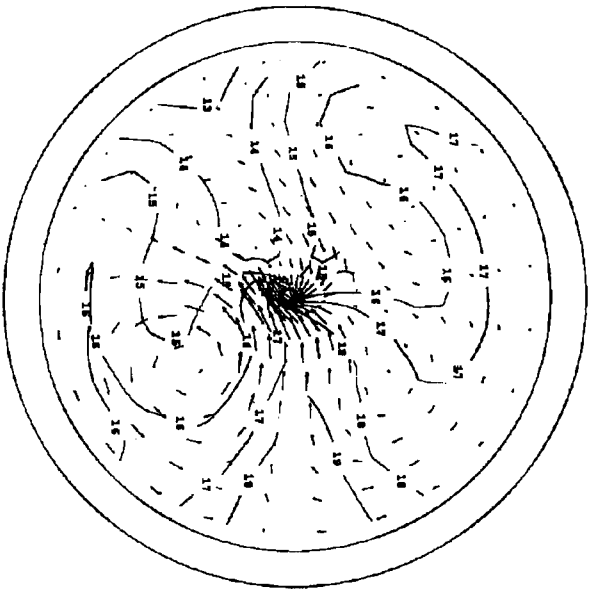

Figure 4-6. Predicted Vertical Distributions of Flow (m/s) and Solid 9 Concentration (kg/m^3) on Vertical Plane 14 (9 O'clock Position) of the Hole without Yield Stress at 7 Simulation Minutes.

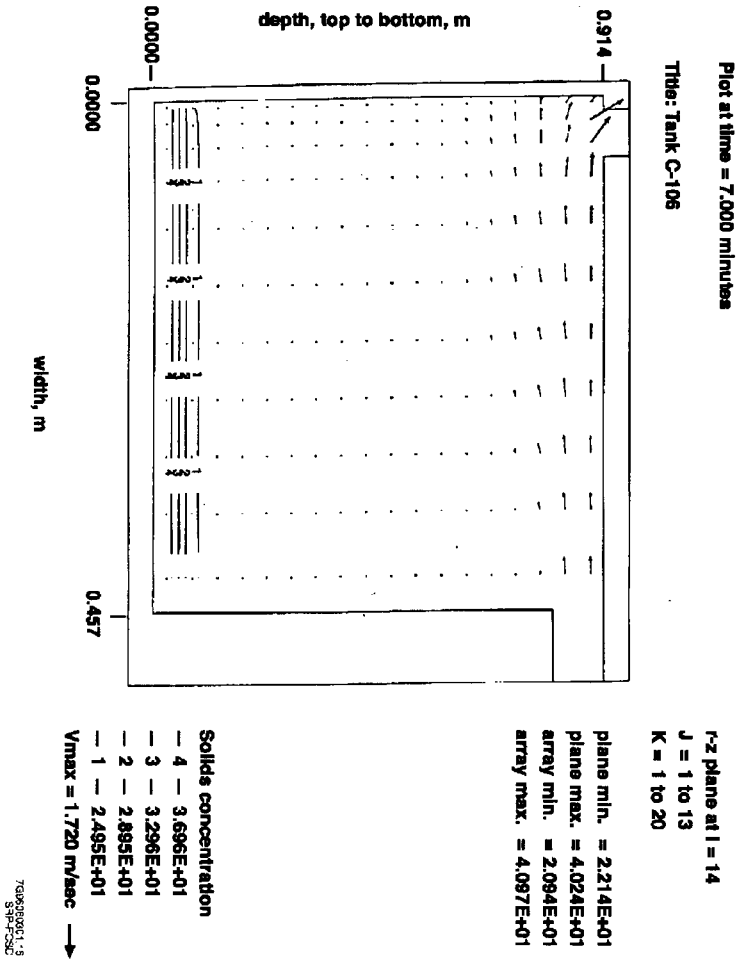

Figure 4-7. Predicted Vertical Distributions of Flow (m/s) and Solid 9 Concentration (kg/m^3) on Vertical Plane 14 (9 O'clock Position) of the Hole without Yield Stress at 20 Simulation Minutes.

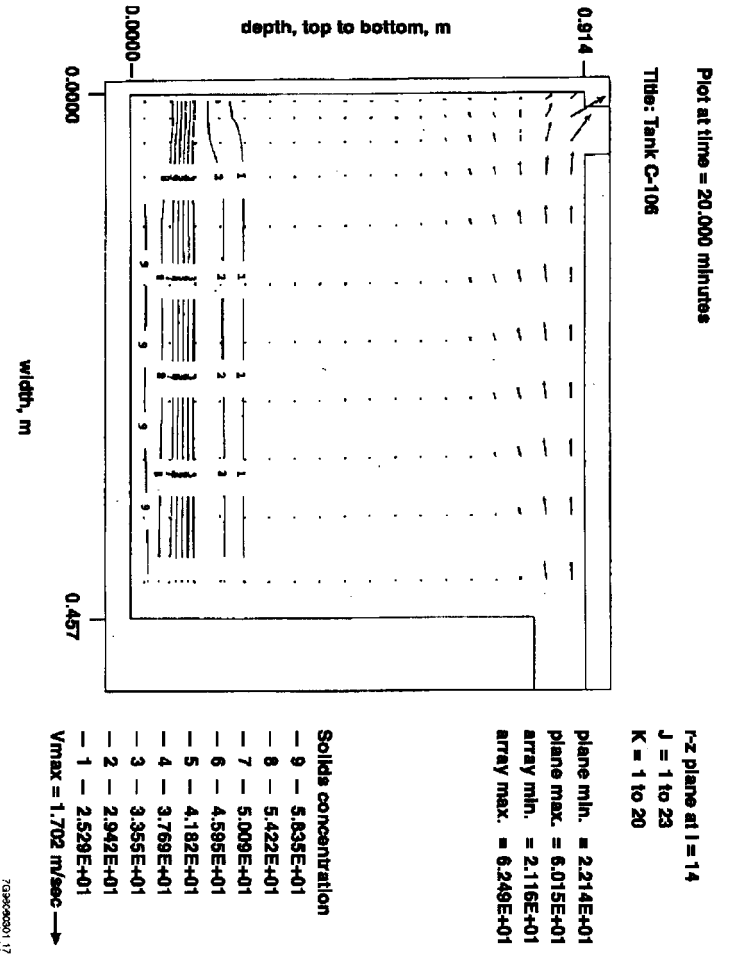

Figure 4-8. Predicted Vertical Distributions of Flow (m/s) and Solid 5 Concentration (kg/m^3) on Vertical Plane 9 Containing One of the 1-in. Nozzles in Tank AY-102 at 1 Simulation Hour.

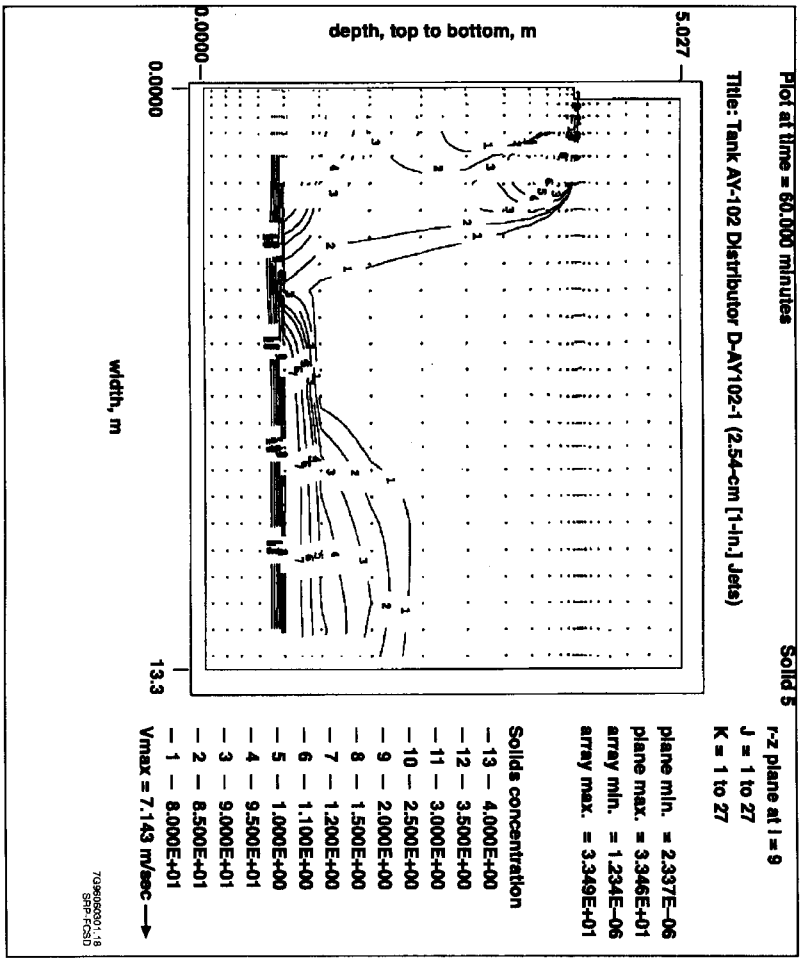

Figure 4-9. Predicted Horizontal Distributions of Flow (m/s) and Solid 5 Concentration (kg/m^3) at 15 inches Above the Bottom of Tank AY-102 at 25 Simulation Minutes.

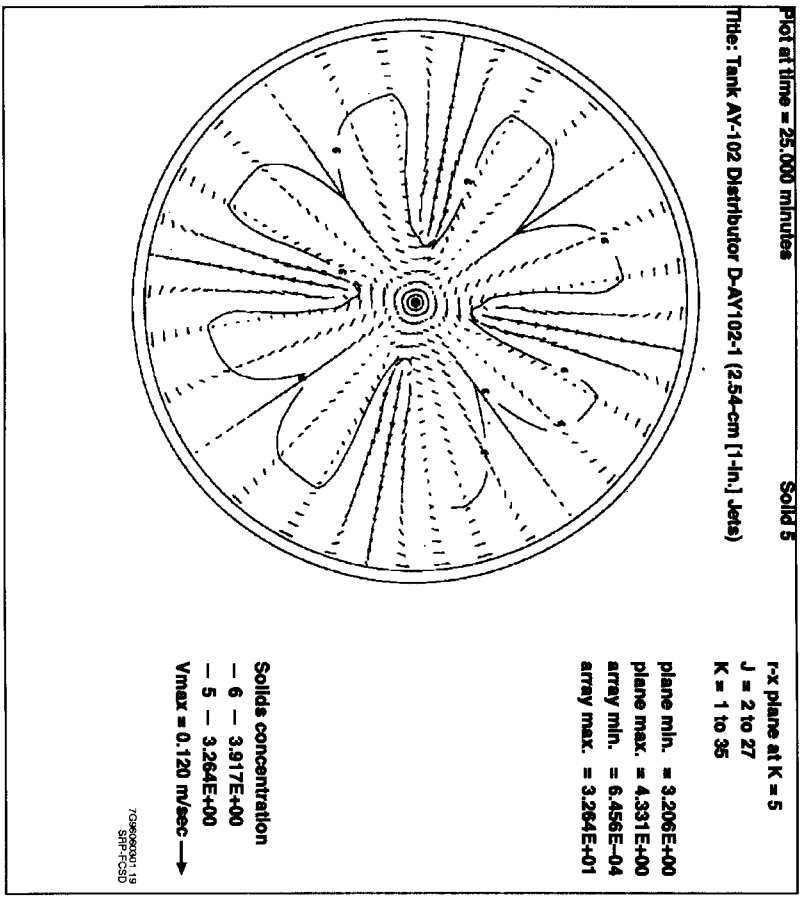

Figure 4-10. Predicted Horizontal Distributions of Flow (m/s) and Solid 5 Concentration (kg/m^3) at 23 Inches above the Bottom of Tank AY-102 at 1 Simulation Hour.

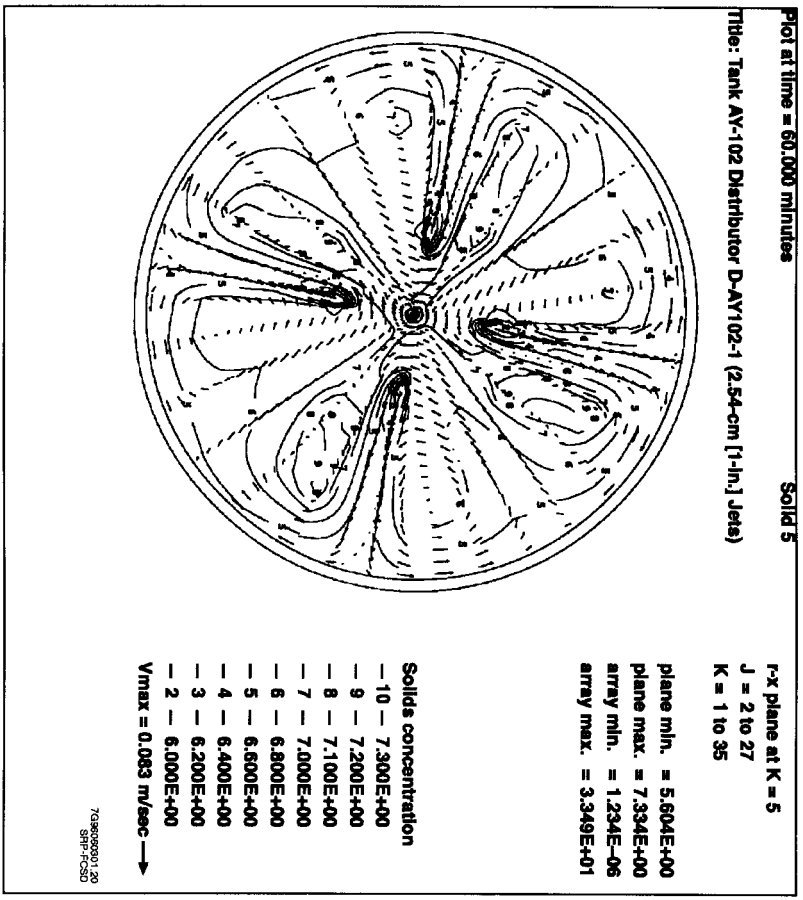

Figure 4-11. Predicted Horizontal Distributions of Flow (m/s) and Solid 5 Concentration (kg/m^3) on the Plane Containing Four 1-in. Nozzles in Tank AY-102 at 1 Simulation Hour.

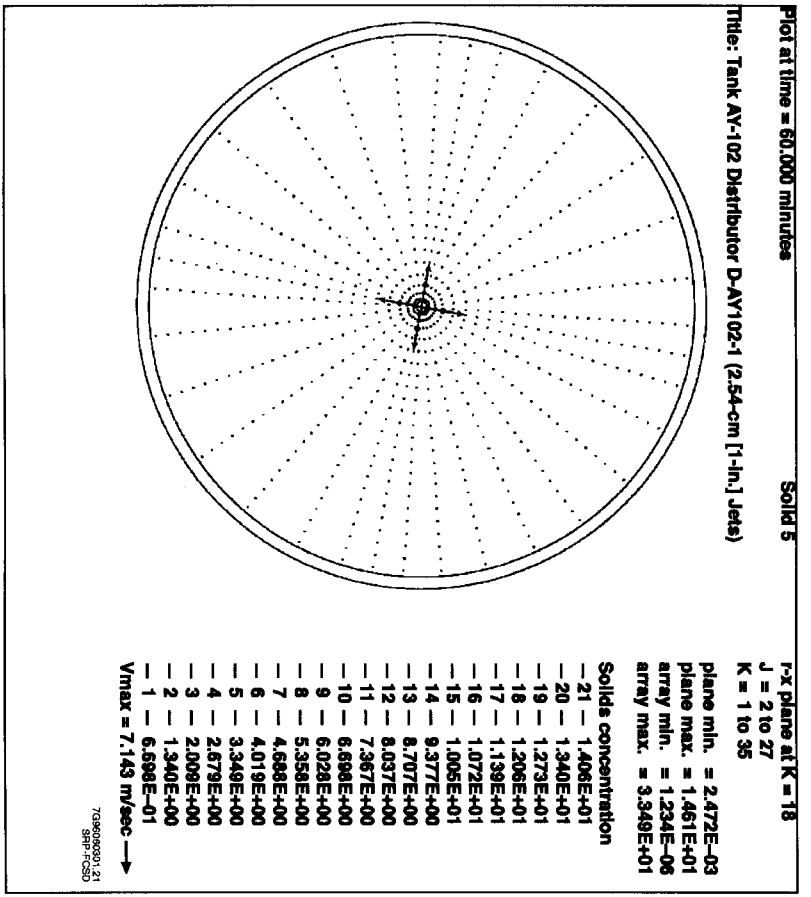

Figure 4-12. Close-up of Predicted Horizontal Distributions of Flow (m/s) and Solid 5 Concentration (kg/m^3) on the Plane Containing Four 1-in. Nozzles in Tank AY-102 at 1 Simulation Hour.

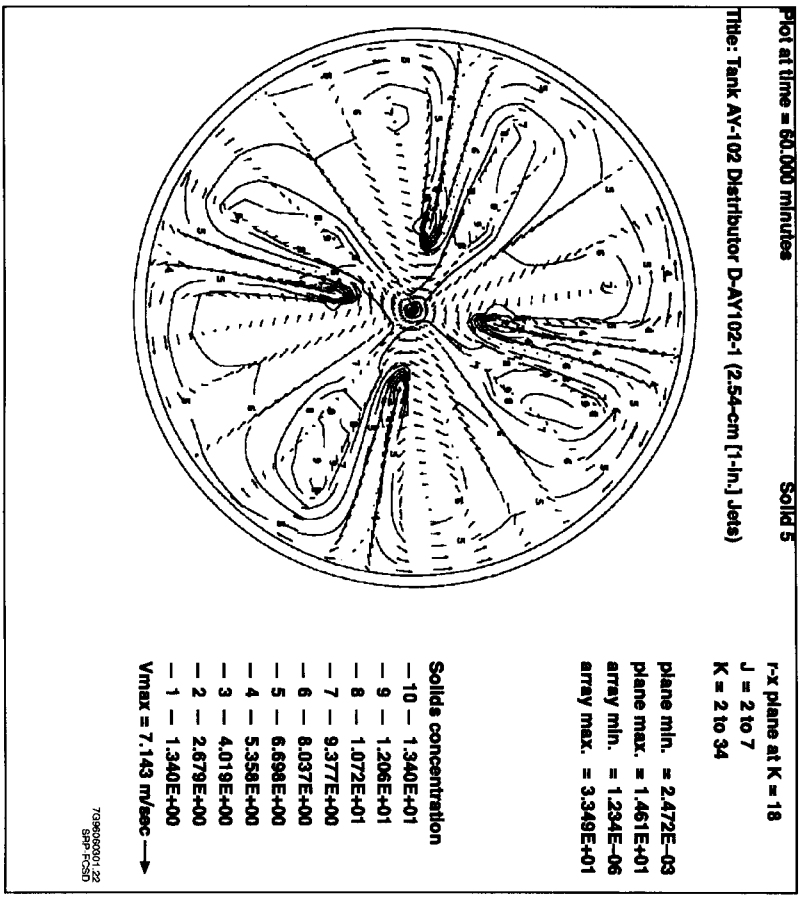

Figure 4-13. Predicted Horizontal Distributions of Flow (m/s) and Solid 5 Concentration (kg/m^3) at the Top of Tank AY-102 at 1 Simulation Hour.

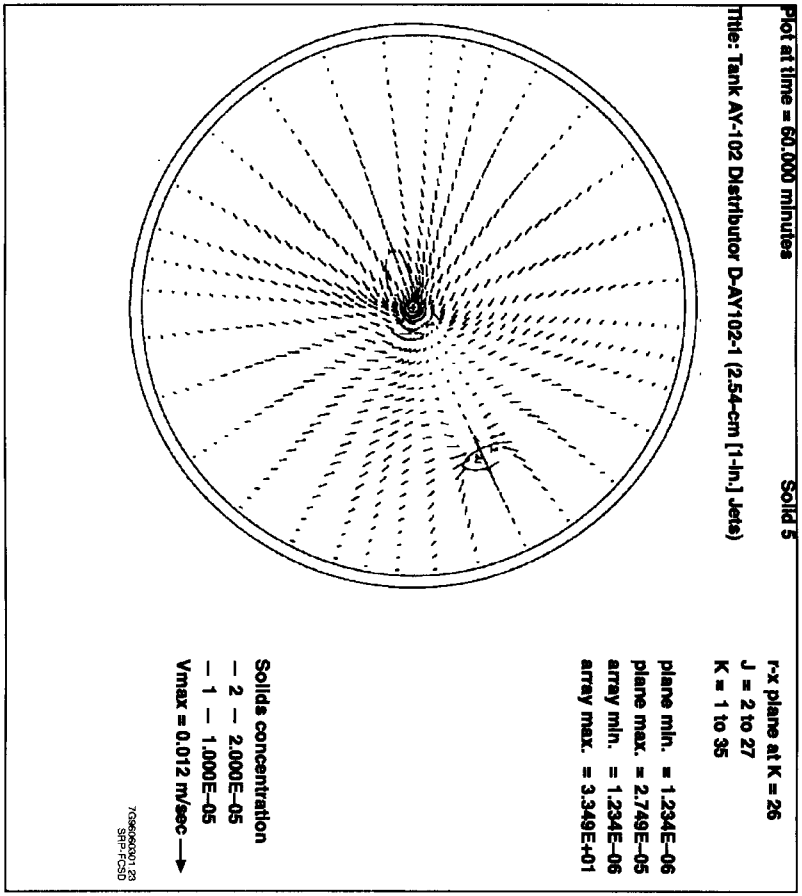

Figure 4-14. Predicted Vertical Distribution of Flow (m/s) and Solid 1 Concentration (kg/m^3) on Vertical Plane 9 Containing One of the 1-in. Nozzles in Tank AY-102 at 1 Simulation Hour.

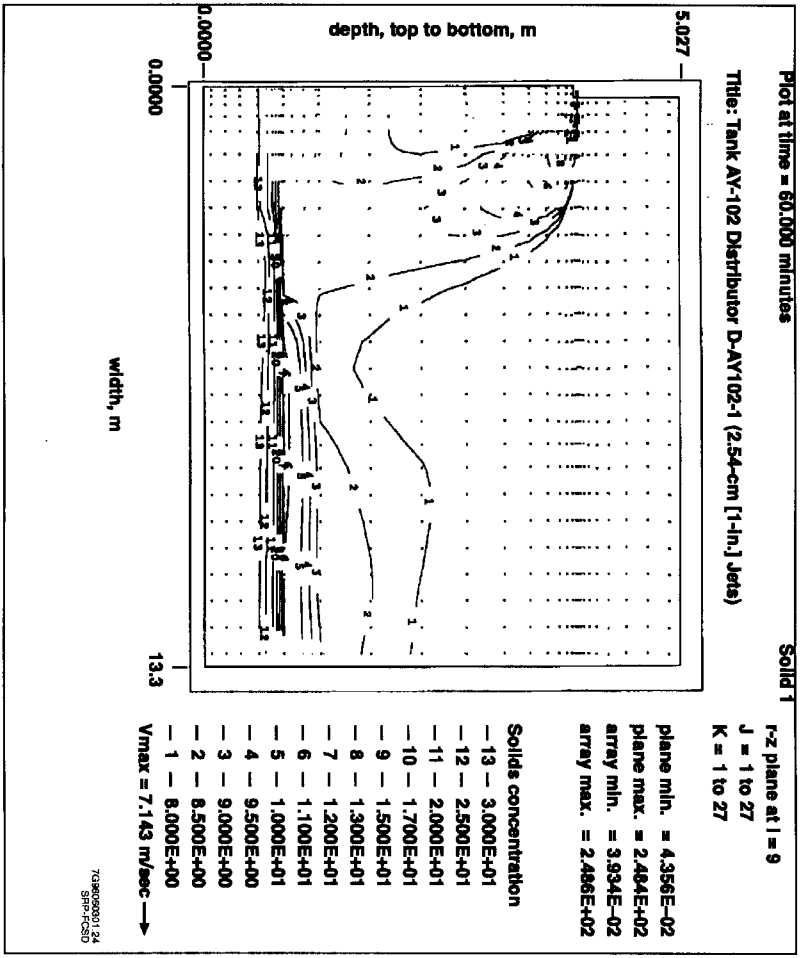

Figure 4-15. Predicted Horizontal Distributions of Flow (m/s) and Solid 1 Concentration (kg/m^3) at 23 Inches Above the Bottom of Tank AY-102 at 1 Simulation Hour.

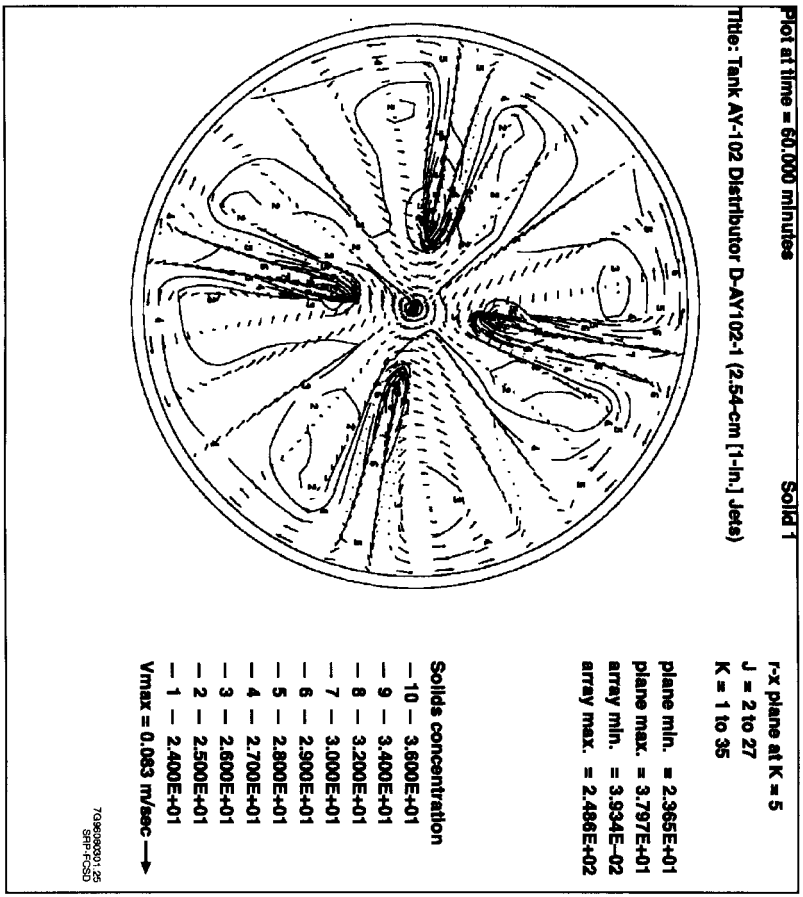

Figure 4-16. Predicted Vertical Distributions of Flow (m/s) and Solid 9 Concentration (kg/m^3) on Vertical Plane 9 Containing One of the 1-in. Nozzles in Tank AY-102 at 1 Simulation Hour.

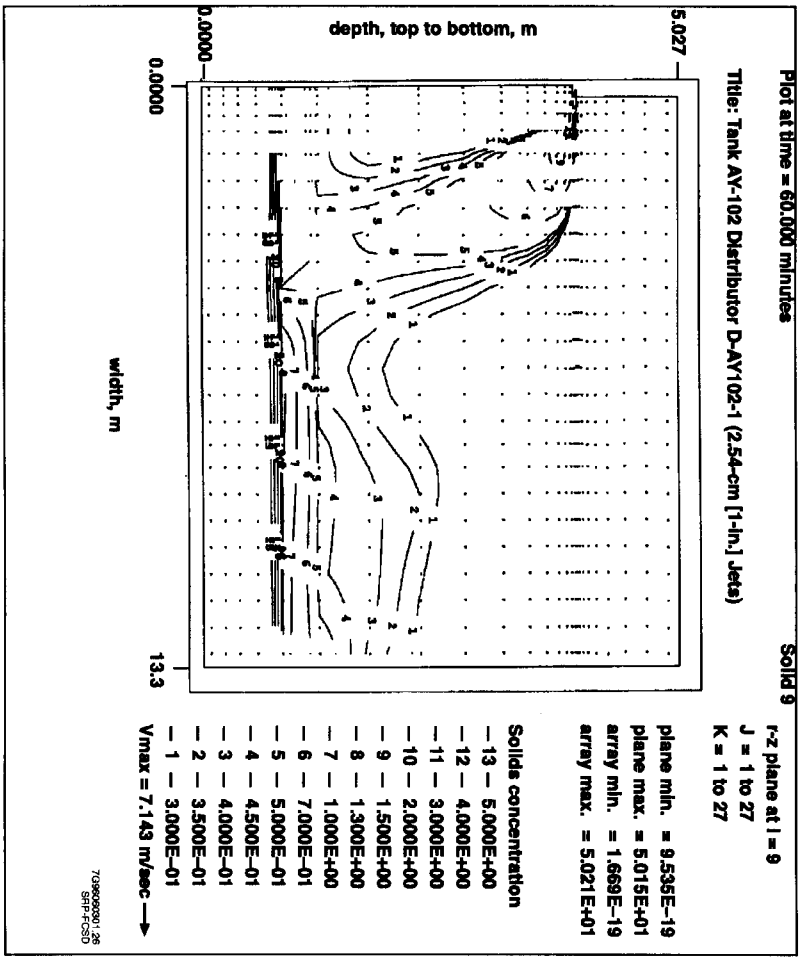

Figure 4-17. Predicted Horizontal Distributions of Flow (m/s) and Solid 9 Concentration (kg/m^3) at 23 Inches Above the Bottom of Tank AY-102 at 1 Simulation Hour.

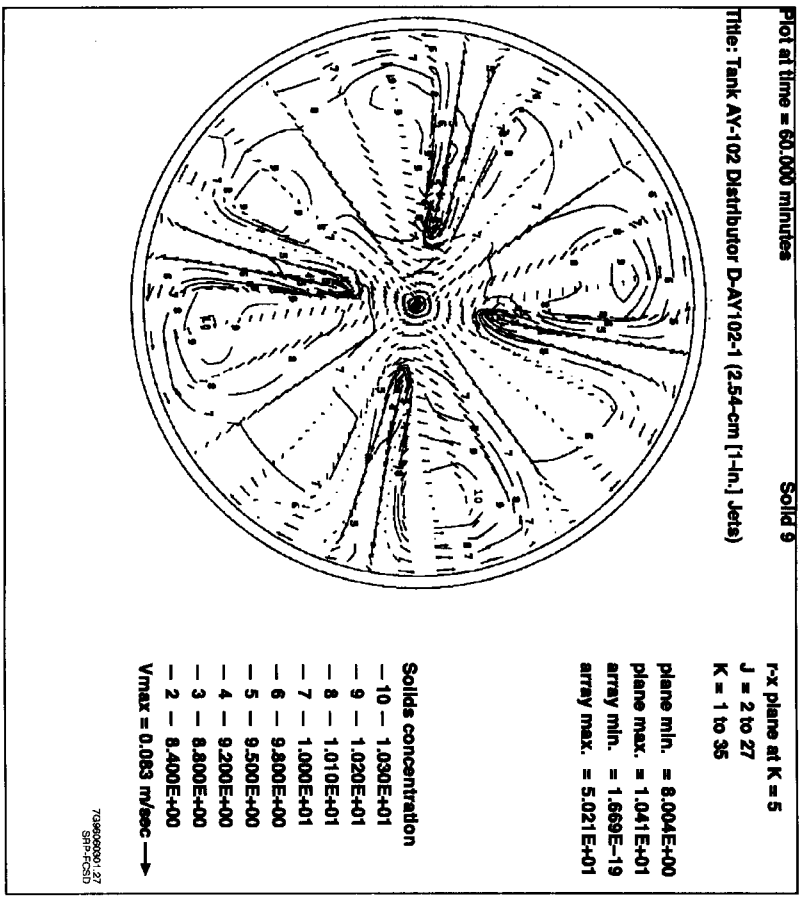

Figure 4-18. Predicted Maximum Solid Segregation for Solids 1, 5 and 9 at 23 Inches Above the Bottom of Tank AY-102 Over 1 Simulation Hour.

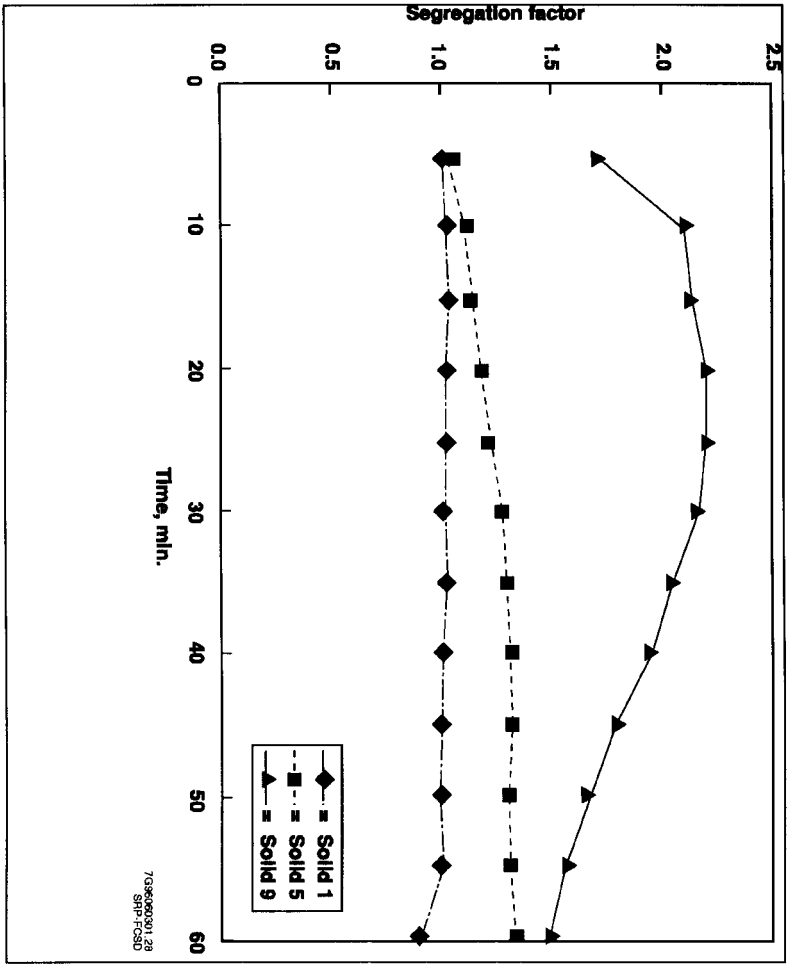

Figure 4-19. Predicted Three-Dimensional Distribution of Solid 9 Volume Fractions After 2 Minutes of Mixer Pump Operation for Initially Settled Sludge.

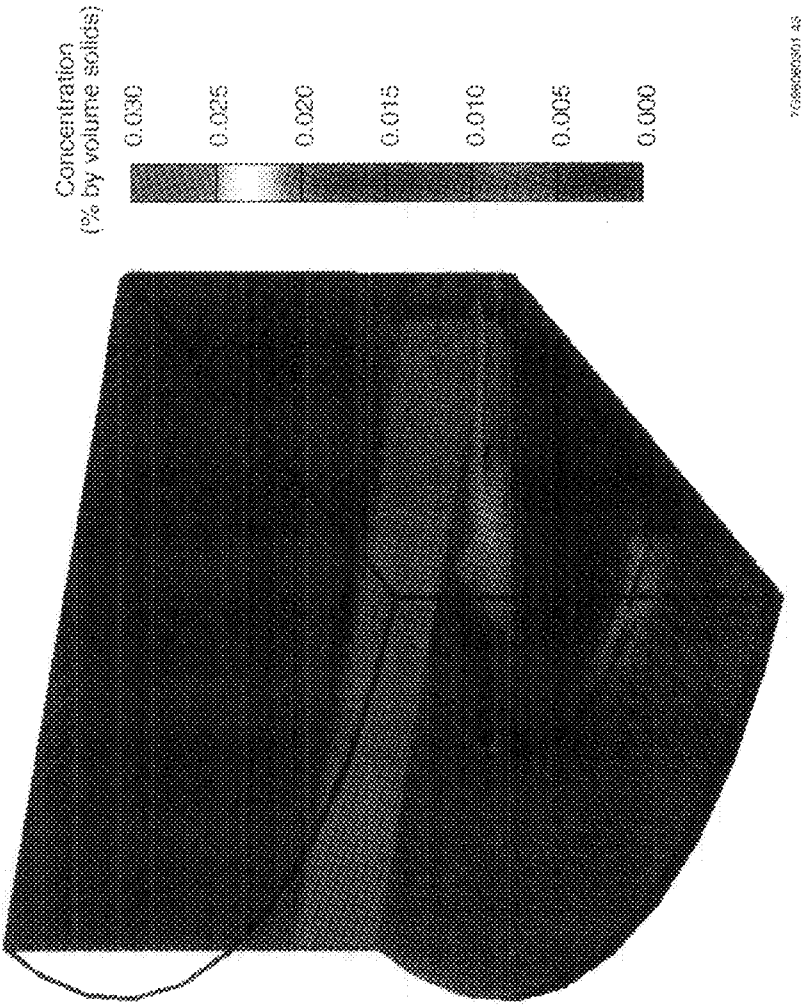

Figure 4-20. Predicted Three-Dimensional Distribution of Solid 9 Volume Fractions After 30 Minutes of Mixer Pump Operation for Initially Settled Sludge.

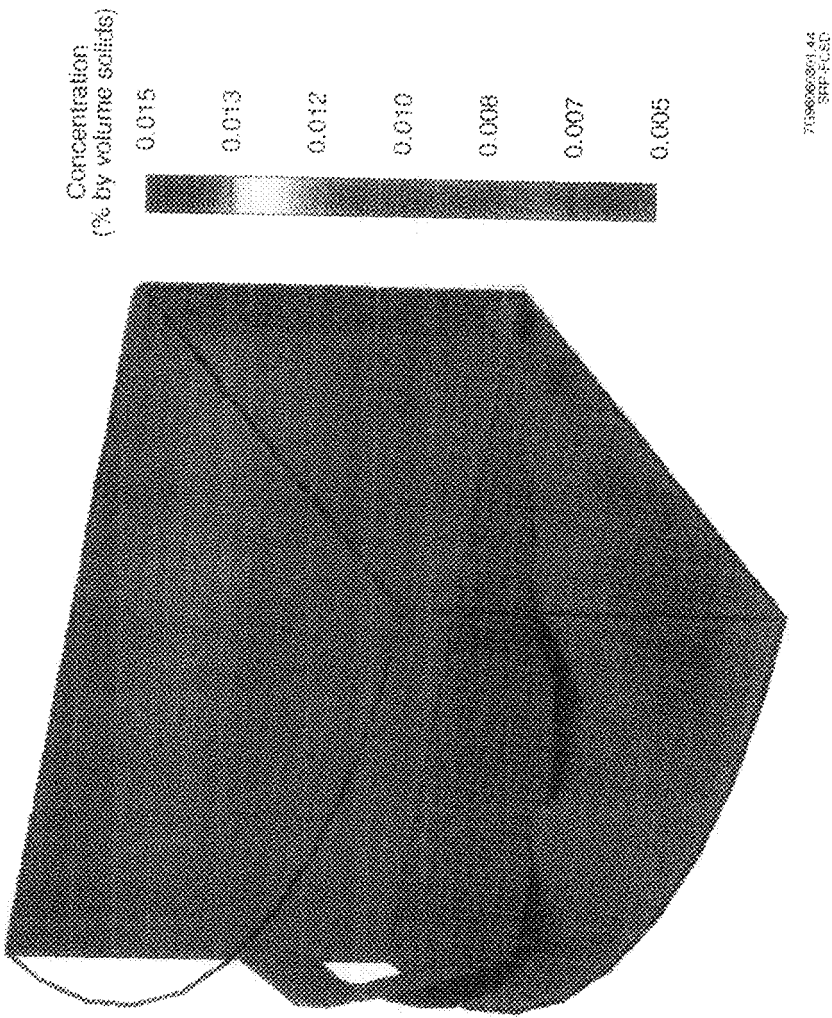

Figure 4-21. Predicted Three-Dimensional Distribution of Solid 9 Volume Fractions After 1.5 Hours of Mixer Pump Operation for Initially Settled Sludge.

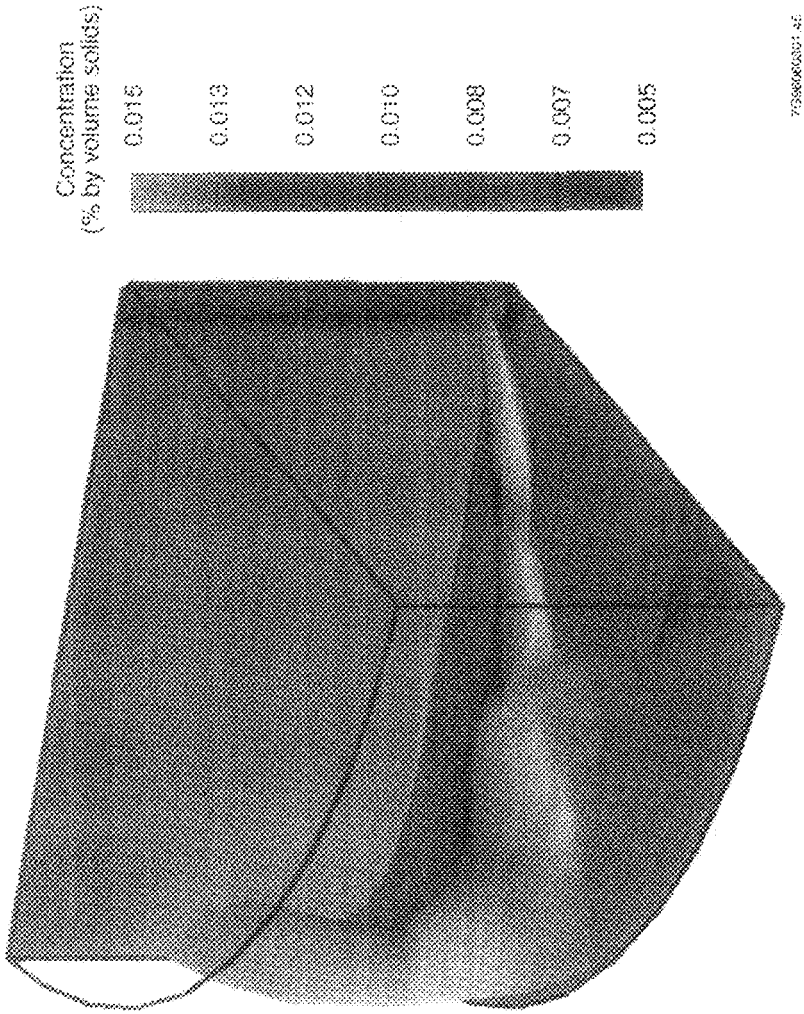

Figure 4-22. Predicted Vertical Distributions of Flow (m/s) and Solid 7 Concentrations (kg/m^3) on Vertical Plane 11 (12:30 Clock Position) with Sludge Initially Fully Mixed With Supernate at 1.5 Simulation Hours.

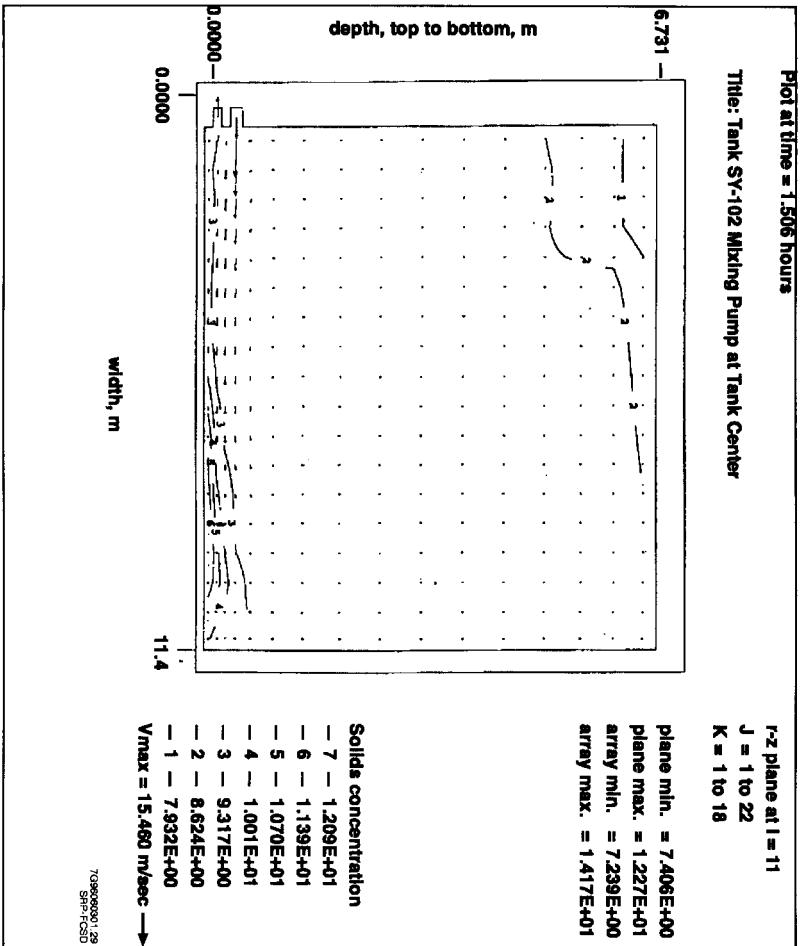

Figure 4-23. Predicted Vertical Distributions of Flow (m/s) and Solid 1 Concentration (kg/m^3) on Vertical Plane 11 (12:30 Clock Position) with Sludge Initially Fully Mixed With Supernate at 1.5 Simulation Hours.

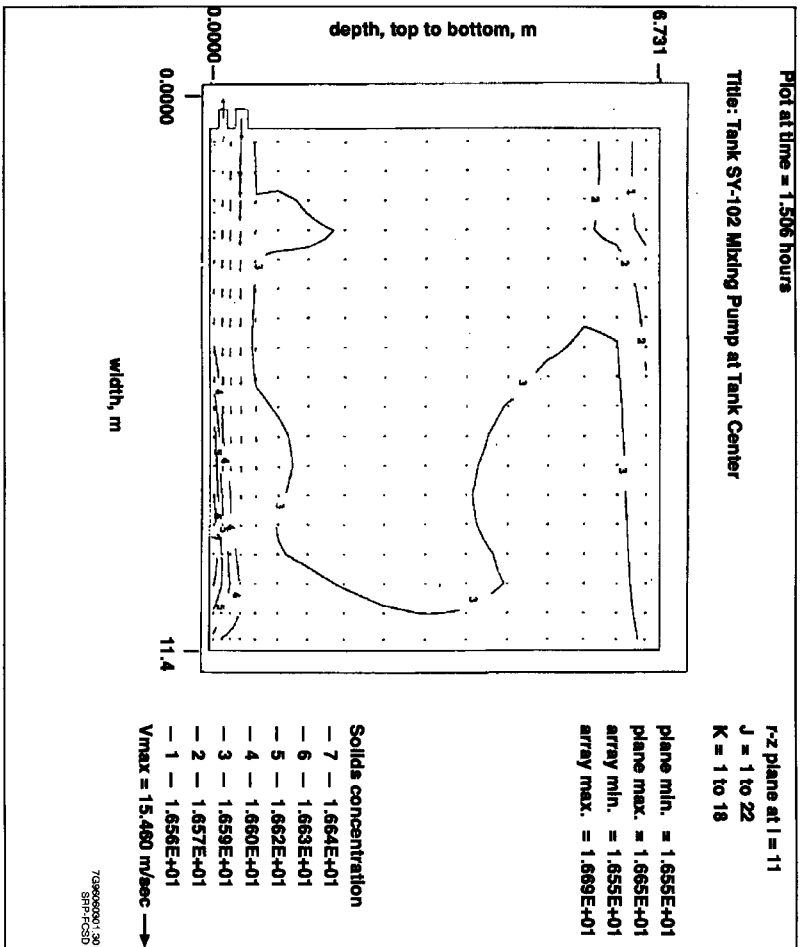

Figure 4-24. Predicted Horizontal Distributions of Flow (m/s) and Solid 7 Concentration (kg/m^3) at the Bottom of Tank With Sludge Initially Fully Mixed With Supernate at 1.5 Simulation Hours.

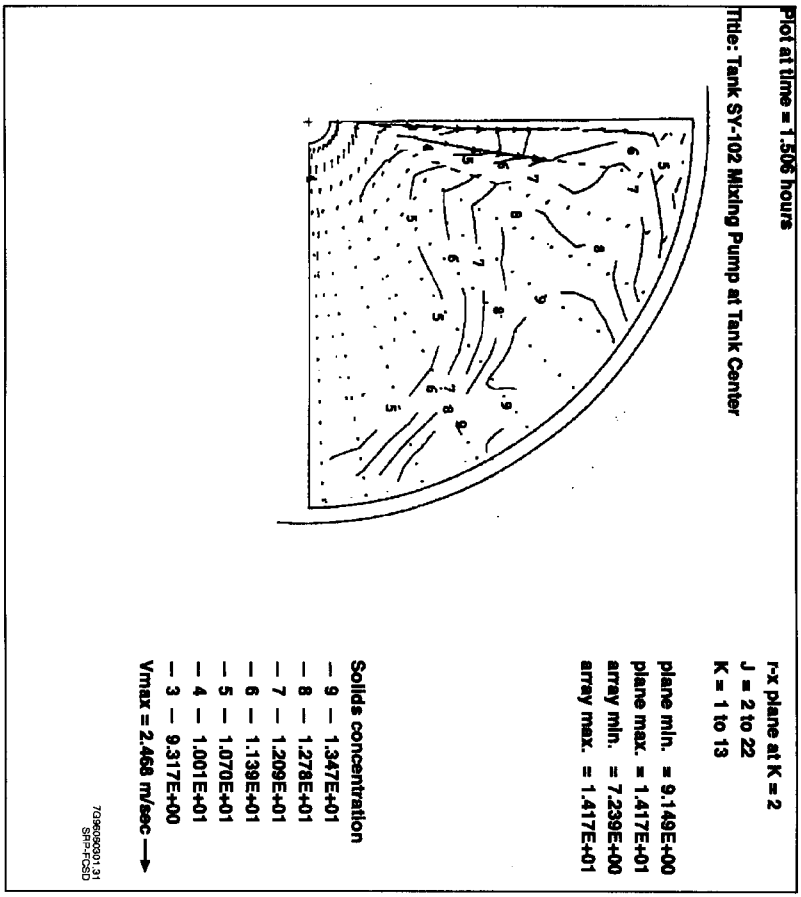

Figure 4-25. Predicted Horizontal Distributions of Flow (m/s) and Solid 1 Concentrations (kg/m^3) at the Bottom of Tank With Sludge Initially Fully Mixed With Supernate at 1.5 Simulation Hours.

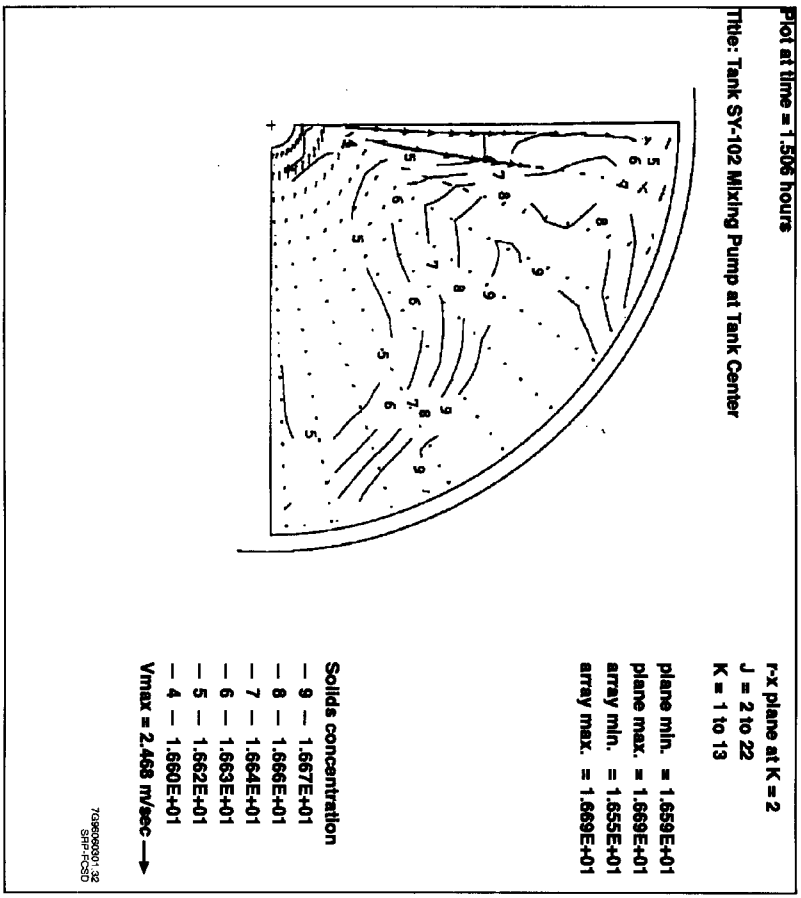

Figure 4-26. Predicted Vertical Distributions of Flow (m/s) and Solid 4 Concentration (kg/m^3) on Vertical Plane 9 (2 O'clock Position) in with Off-Center Jet at 5 Simulation Minutes.

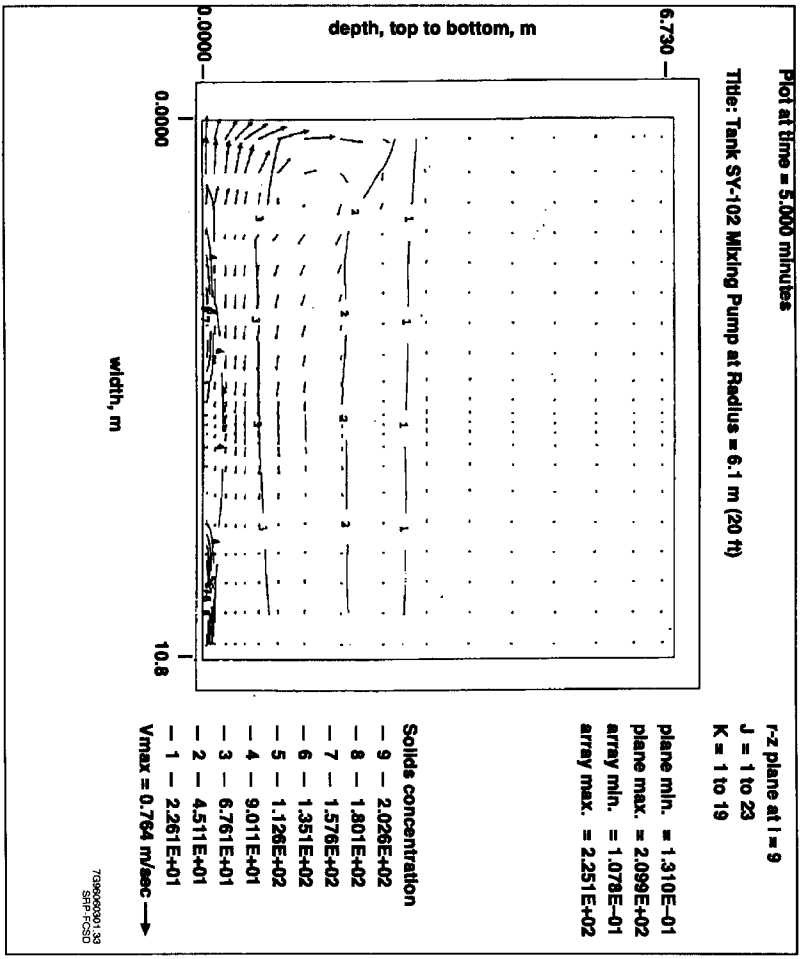

Figure 4-27. Predicted Horizontal Distributions of Flow (m/s) and Solid 4 Concentrations (kg/m^3) at the Bottom of Tank with Off-Center Jet at 5 Simulation Minutes.

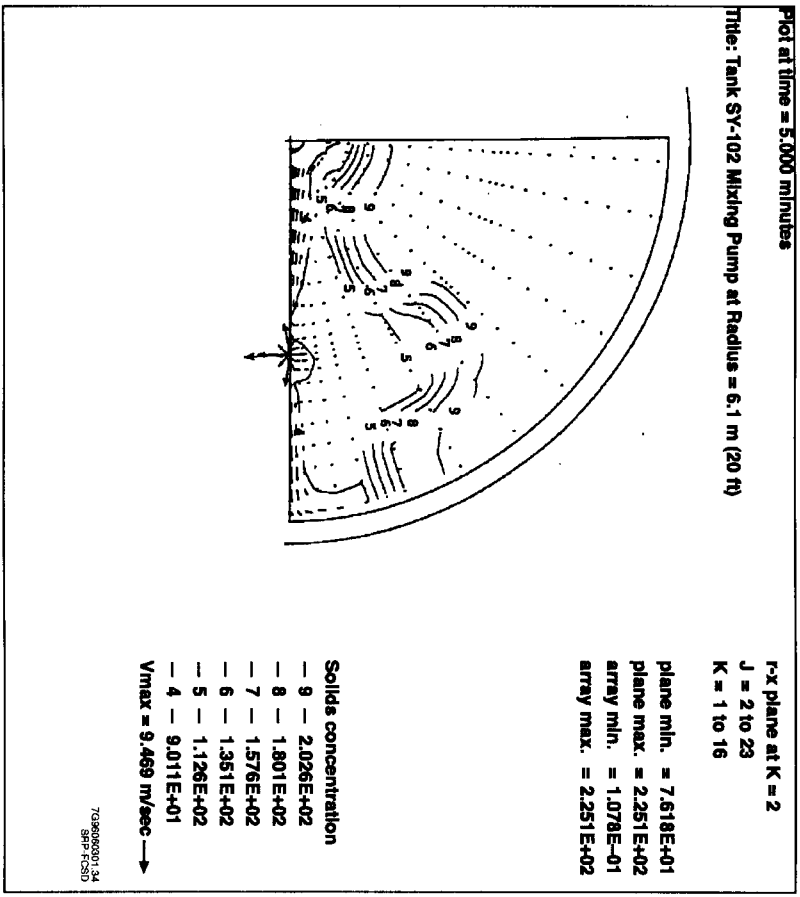

Figure 4-28. Predicted Vertical Distributions of Flow (m/s) and Solid 4 (with 10 Times Greater Settling Velocity) Concentration (kg/m3) on Vertical Plane 9 (2 O'clock Position) with Off-Center Jet at 5 Simulation Minutes.

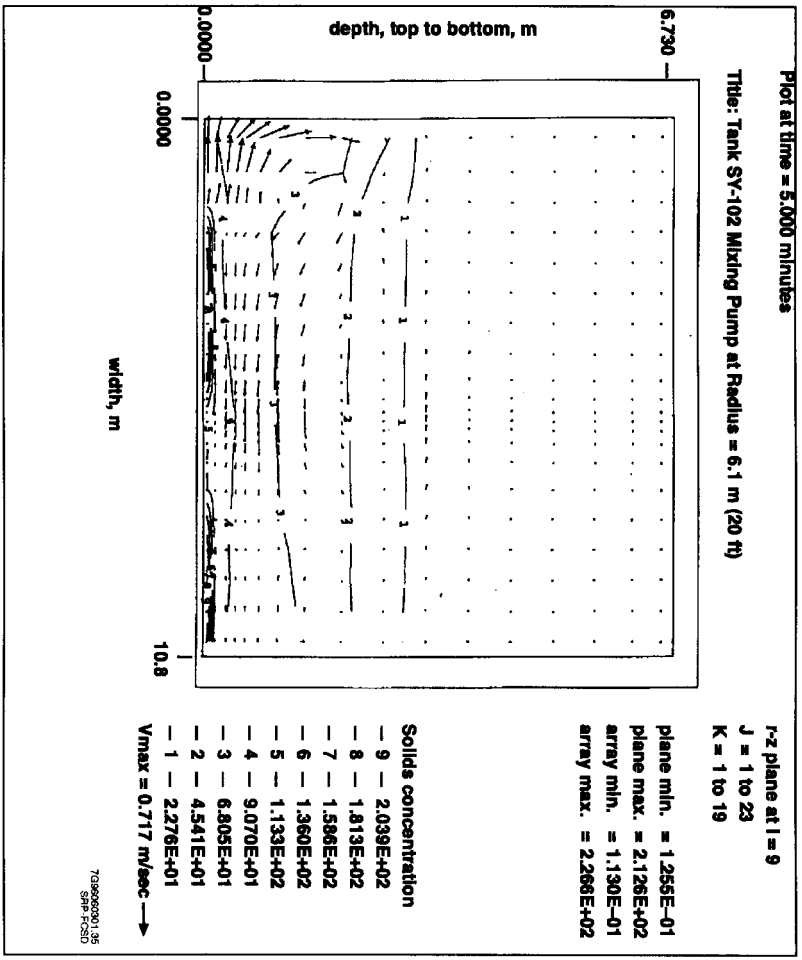

Figure 4-29. Predicted Horizontal Distributions of Flow (m/s) and Solid 4 (with 10 Times Greater Settling Velocity) Concentrations (kg/m3) at the Bottom of Tank with Off-Center Jet at 5 Simulation Minutes.

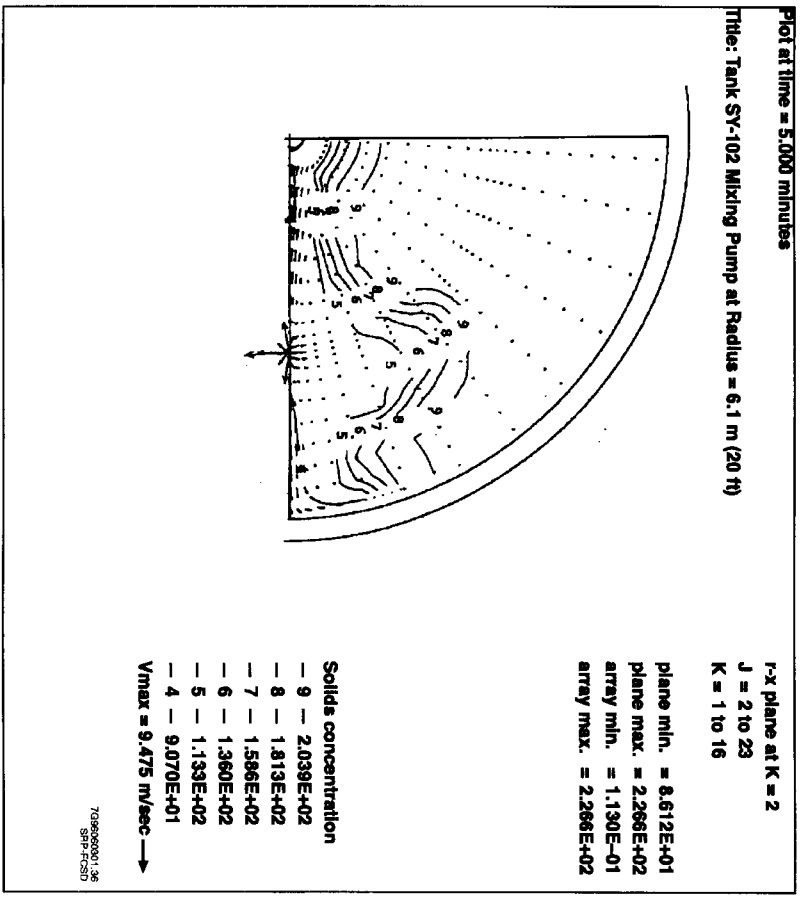

Figure 4-30. Schematic of an Air-lift Circulator.

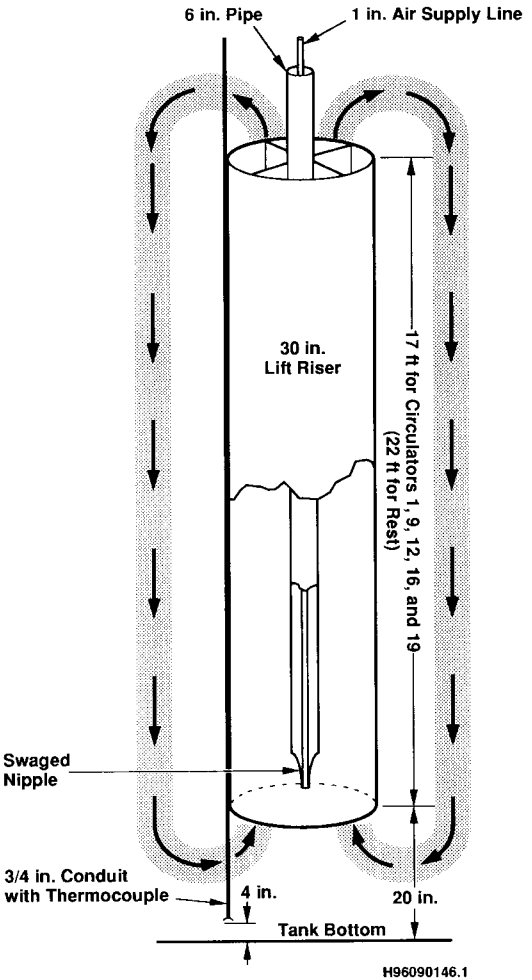

Figure 4-31. TEMPEST Predicted Velocity Field for Sludge Slurry at Bottom of Tank While Air Lift Circulators are Running.

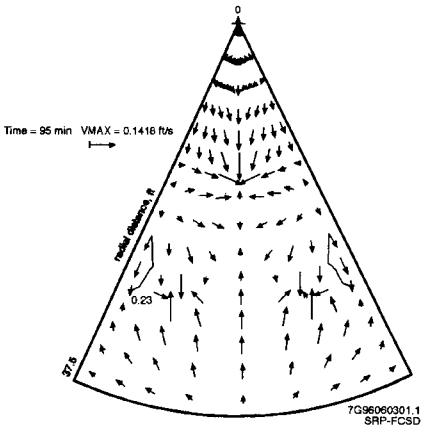

Figure 4-32. Temperature Profile and Velocity Profile for Heat Convection Simulation (Base Case).

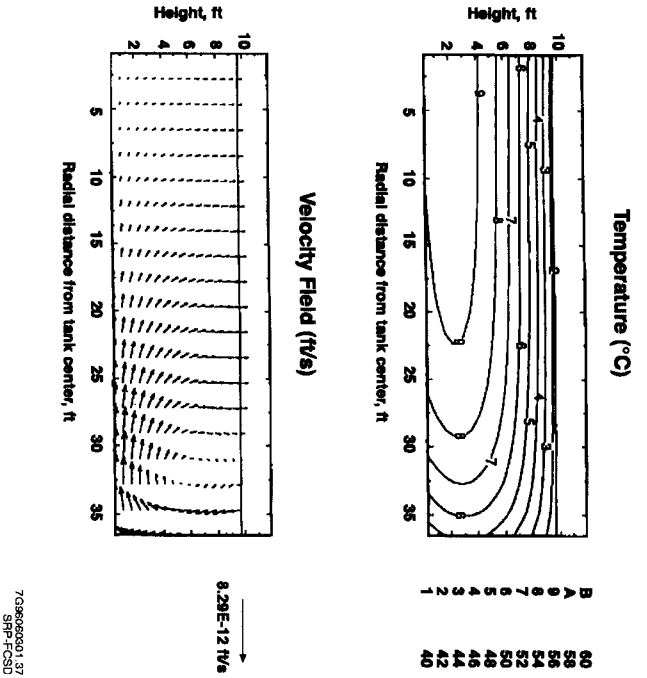

Figure 4-33. Temperature Profile and Velocity Profile for Heat Convection Simulation Range (High-Heat-Generation Case).

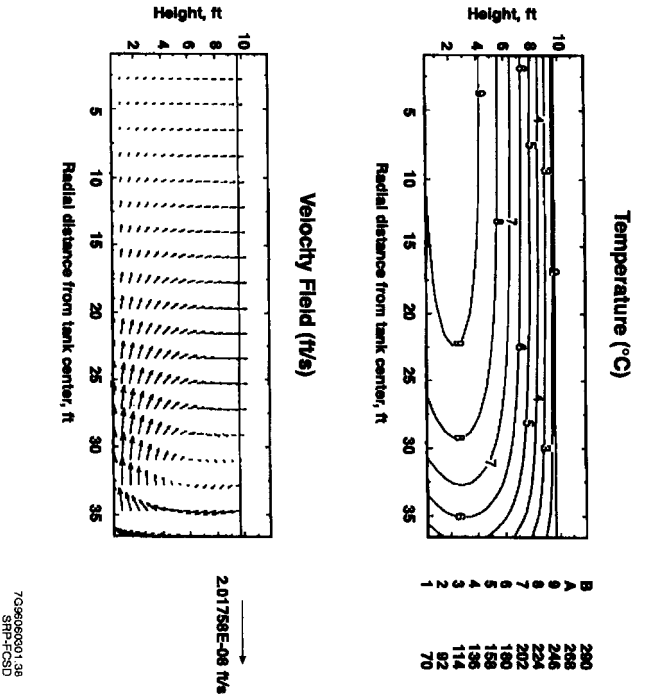

Table 4-1. Particle Size Distributions of Tank C-106 Sludge.

Solid Size Fractions	Particle Sizes (μm)	Percent weight	Settling Velocity[a] (mm/s)
1	5-10	35	0.076
2	10-15	11	0.19
3	15-20	5	0.36
4	20-25	12	0.58
5	25-30	4	0.88
5	30-35	0.8	0.88
6	35-40	8	1.6
7	40-45	10.8	2.0
8	45-50	7.4	2.5
9	50-55	6	3.1
	Total	100	

[a]Unhindered settling velocity is input to the model assuming the fluid is pure water at 37C. TEMPEST calculates hindered settling velocity for each particle size for the appropriate slurry conditions calculated at each node and time step.

Table 4-2. Maximum Segregation over the Initial Conditions Near the Bottom of the Hole.

Solid types	Initial condition	4 min (no yield stress)	7 min (yield stress)	20 min (no yield stress)
Solid 1	1	0.99	0.83	0.7
Solid 5	1	1.0	1.0	0.97
Solid 9	1	1.2	1.5	1.9

Table 4-3. Particle Size Distributions of Tank SY-102 Sludge.

Solid Size Fractions	Particle Size (μm)	Percent Volume	Settling Velocity[a] (mm/s)
1	10 - 20	7	0.081
2	20 - 30	8	0.24
3	30 - 40	8	0.49
4	40 - 50	19	0.81
5	50 - 60	30	1.2
6	60 - 100	25	2.5
7	100 - 175	3	7.1
	Total	100	

[a]Unhindered settling velocity is input to the model assuming the fluid is pure water at 37°C. TEMPEST calculates hindered settling velocity for each particle size for the appropriate slurry conditions calculated at each node and time step.

Table 4-4. Power Law Curve Fit Parameters for Tank SY-102 Wastes (DiCenso et al. 1995).

SY-102 Waste	Consistency Pa-s	Flow Behavior Index
Sample 1	0.013	0.808
Sample 2	0.014	0.791

Table 4-4. Simulation Input Parameters.

Parameter	Value
Fluid flow parameters	
Porosity of sludge	50 percent
Permeability of sludge	10^{-12} cm^2
Fluid density	1.4 gm/cm^3
Fluid viscosity	12.5 cP
Thermal conductivity parameters	
Thermal conductivity of sludge	0.434 W/m °C
Thermal conductivity of fluid	0.640 W/m °C
Boundary conditions	
Temperature of supernate	40°
Heat production from radioactive decay	2.66 W/m^3[a]
Heat losses from side walls	12%
Heat losses from bottom	22%

[a]From Crowe et al. 1993, p. 6-3

Table 4-5. Maximum Segregation Over the Initial Conditions near the SY-102 Tank Bottom.

Solid Types	Initial Condition	0.5 hr	1 hr	1.5 hr
Solid 1	1	0.91	0.91	0.93
Solid 4	1	0.96	0.96	0.97
Solid 7	1	1.4	1.4	1.3

This page intentionally left blank.

5.0 SCOPING RESULTS FOR STAGNANT SETTLING CASE

This chapter provides results based on a simplified one-dimensional analytical model. The conceptual model is based on a Double-Shell Tank (DST) that initially contains a uniformly mixed slurry. The slurry is then allowed to settle under stagnant conditions. The starting assumption is that the fissile material exists as discrete particles rather than within particles of mixed composition. If the fissile material can be shown to exist within particles of mixed composition that includes large amounts of neutron absorbers, fluid dynamic segregation calculations may be unnecessary.

This particular scenario could not result in a criticality because it results in the radionuclides being distributed uniformly across the tank floor. No single tank has sufficient fissile content to exceed an areal concentration of 240 g/ft^2 ^{239}Pu, which is the minimum areal concentration required to achieve criticality (Bratzel et al. 1996 and Waltar et al. 1996). To form a uniform layer inside a 75-ft diameter DST would require 1060 kg of ^{239}Pu. The total inventory in SY-102 is estimated at <42 kg (Tusler 1995); the inventory of C-106 may be as high as 100 kg (WHC 1995). Neither inventory approaches the minimum required.

However, the results provide some insight into the extent of segregation that might occur under differential settling (segregation) conditions. For example, while the larger particles settle faster and would be expected to be more concentrated near the bottom of a settled layer, each layer has a particle size distribution that includes particles of various sizes and densities. This distribution will tend to limit the degree to which fissile material can concentrate.

5.1 SIMPLIFIED SEDIMENTATION MODEL

In this simple conceptual model, a DST containing a uniform slurry is allowed to settle under stagnant conditions and the composition of the layers deposited are determined. The particles settle at their terminal settling velocity as calculated based on Stokes Law (see Equation 2.5). If the particle's Reynolds number exceeds 2, the friction factor is set equal to the following (Bird et al. 1960):

$$f = \frac{18.5}{N_{Re}^{\frac{3}{5}}} = \frac{18.5\mu^{\frac{3}{5}}}{(\rho D_p w)^{\frac{3}{5}}} \tag{5.1}$$

Where:

N_{Re} = particle Reynolds number
μ = dynamic viscosity
ρ = fluid density
D_p = particle diameter
w = settling velocity

Equation 5.1 is needed only to calculate the settling velocities of the largest particulates in the SY-102 particle size distribution and to bound sensitivity cases where the PuO_2 is set at the largest size. Thus, the calculated results are not sensitive to the selection of viscosity because within the Stokes Law region, the velocity of all particles is inversely proportional to the viscosity.

In the model, the individual particles settle until they reach the floor. The number and type of particles striking the floor over a given time are determined and their composition is used to represent the composition of a settled layer of sediment. The model does not calculate the accumulation of sediment, but determines when various particles reach the floor over time. The maximum fissile content of any layer of deposited sediment is then divided by the initial fissile content of the uniform slurry (both expressed as mass fraction of solids) to determine a factor increase in fissile concentration. Only the composition of the settled sludge is considered, not the degree to which the sludge layer is consolidated.

Initially, no hindered settling effects are considered. However, calculations including hindered settling effects are included at the end of this section, after the discussion of the more simple conceptual model results. Particle agglomeration is not explicitly considered in the model although the agglomeration behavior discussed in Appendix A is important for interpreting the results.

The uniform slurry is assigned a particle size distribution based on analysis of SY-102 or C-106 sludge samples as documented by Dicenso et al. (1995), Castaing (1994), and Weiss (WHC 1993a, and 1993b). Core samples were taken from tank SY-102 in 1988 (Scheele and Petersen) and 1990, and a supernatant sample was taken in 1994. Because no particle size distribution data was obtained from the 1990 core, the particle size distribution was taken from the 1988 sample. The particle size distribution was measured on the lower core segment (segment 102-SY-4B), which does not include the region of the core containing solids high in ^{239}Pu. Therefore, the particle size distribution does not include the high-^{239}Pu solids. We do not know whether the particle size distribution of the solids high in ^{239}Pu is similar to that measured.

The C-106 particle size distributions used for this analysis were taken from measurements made in 1977 as reported by Castaing (1994) and subsequent data collected by Weiss on a 1986 core (WHC 1993a, and 1993b). The 1986 sample was a composite of the entire core. We know little about the specifics of the measurement technique and sample preparation, including whether larger particles in the distribution may actually be agglomerates of smaller particles. The particle size distributions used for the modeling are provided in Table 5-1.

In all cases the fluid density was set to 1.0 g/cm^3 with a viscosity of 1.0 cP. Iron was assumed to exist as hematite with a density of 5.26 g/cm3; aluminum was assumed to exist as gibbsite with a density of 2.4 g/cm^3. The amount of iron and aluminum in the sludge was assigned based on waste characterization data (Castaing 1994, Dicenso et al. 1995). All other sludge components were arbitrarily assigned a density of 2.0 g/cm^3, which is believed to be conservatively low. The PuO_2 was assigned a density of either 11.4 or

6.0 g/cm^3. The density of 11.4 corresponds to crystalline PuO_2. In an aqueous environment, the density of less-crystalline hydrous PuO_2 may be lower than 11.4 because of the waters of hydration and some crystal disordering. Although definitive data is not available, several people who have worked with freshly-precipitated PuO_2 believe that the particle density is about 6 g/cm^3. The amount of plutonium assumed for C-106 simulations was set at 0.132 g/L sludge in C-106 corresponding to a conservative inventory of 100 kg. For SY-102, a concentration of 0.154 g/L is used based on an inventory of 41.4 kg plutonium and 71,000 gal of sludge (WHC 1995). These initial concentrations have little effect on the calculation of the degree of segregation, but do influence the impact of a given degree of segregation.

The particle volume within the distributions shown in Table 5-1 were assigned identities based on the sludge composition. No data on variations of sludge composition with particle size is available. Therefore, except where noted, the iron, aluminum, and "other" components were assumed to exist uniformly throughout the entire size distribution. The plutonium was distributed uniformly across the size distribution for some cases and given a fixed size in other cases. Iron, aluminum, and PuO_2 were explicitly tracked with their own densities in the calculation. All other sludge components were grouped into the category "other." Using the Weiss particle size distribution, the problem becomes one of tracking 18 sizes x 4 densities = 72 different particles, each with its own concentration determined from characterization data, as it settles to the floor of the tank.

5.2 SIMULATION RESULTS

The results of the simulations are summarized in Table 5-2. The factor increase represents the maximum increase in mass fraction PuO_2 (based on solids only) for any sediment layer in the sludge solids for the conditions shown. A value of "2" in Table 5-2 indicates that the mass fraction of PuO_2 has doubled from the initially uniform slurry.

5.2.1 Bounding Sensitivity Analysis

Additional bounding cases were calculated in which the PuO_2 is assigned the largest particle size in the sludge distribution. This provides the greatest potential for plutonium to segregate to the bottom of the sediment layer. These cases are not considered to be realistic because plutonium oxide particles would be expected to be small with an upper bounding size in the <2 to 8 μm range (see Section 7.2.5). These bounding cases are provided to indicate the sensitivity of the results to the upper bound for Pu particle size being established at larger than expected values. Table 5-3 presents the results for the three particle size distributions.

For the C-106 particle size distribution in Castaing (1994), the calculated enrichment factors indicate that, even under bounding assumptions, the fissile concentration just reaches the conservative waste model limit of 2.6 g/L of plutonium needed to attain criticality (see Rogers [1993] for the derivation of this value). For the Weiss particle size distribution though, the enrichment factor of 93.9 indicates a plutonium concentration in the settled sludge bottom layer of 12.4 g/L. This would be a worrisome degree of

concentration if it were actually to occur. Although it is not considered likely that PuO_2 particles would reach 90 μm, let alone be exclusively 90 μm, the case points out the importance of establishing a 10- to 20-μm or smaller upper bound on PuO_2. (See Section 7.2.5.) For SY-102, the degree of concentration is less severe because there is a larger quantity of larger particle sizes (the assumed neutron absorbers) within the sludge particle-size distribution.

5.2.2 Hindered Settling Effect

In the modeling described to this point the settling velocity of particles is not dependent on the local concentration of suspended solids. However, at high solids concentrations the settling velocity of particles is slowed (see Section 2.1.1.6 for more discussion). Calculations were performed to determine if hindered settling could have a significant effect on the degree of segregation just described. The results indicate that a hindered settling model has very little impact on the degree of segregation predicted. The hindered settling model was a form similar to equation 2.6:

$$w = w_0 (1 - C)^{4.7} \tag{5.2}$$

Where:

w = hindered fall velocity
w_0 = non-hindered fall velocity
C = volume fraction solids

Because of the dependence on local concentration, the problem requires much more intensive calculations than for the non-hindered settling case discussed in Section 5.2.1. The problem differs slightly in configuration from the earlier model in that it does simulate the formation and consolidation of the settled layer of solids. Thus, the distances of fall are slightly different for different particles depending on where in the bed they settle. Because of this difference, it is not expected that the hindered and non-hindered cases would agree exactly even if there were no effect of hindering on segregation. However, the models are sufficiently similar to determine if the hindered settling model has a significant effect on the degree of segregation.

The model described in section 5.1 was applied and compared to results obtained using the hindered settling model. Both simulations used the C-106, Castaing particle size distribution. Instead of placing all materials uniformly across the distribution, the material identities of the particle size distribution were assigned as follows:

- PuO_2 was assigned a particle size of 10 μm.
- Hematite was assigned particle size of 7.5 μm
- Gibbsite was assigned particle sizes of 7.5, 12.5, 17.5, and 22.5 μm.
- "Other" was assigned particle sizes of 22.5 μm through 52.5 μm.

This method of assigning compositions reduces the number of different types of particles to be tracked in the problem. Although there is no reason to believe that this distribution of composition accurately represents the sludge, the importance of this model is to look for differences between the results calculated for the hindered and non-hindered models. The results were calculated not only for the PuO_2 particle but also for each of the other particles in the problem. As can be seen in Table 5.4 the degree of segregation does not appear to be greatly influenced by the presence of the hindered settling effect. The degree of difference between results may be due to differences in the model configurations or be due to a very small effect of the hindered settling on the results. However, it is clear that the hindered settling does not have a significant effect on segregation.

5.2.3 Interpretation of Results from One-Dimensional Settling Calculations

The conservative waste model developed by Rogers (1993) describes a sludge that is at least as neutronically reactive as any known tank sludge composition. A safe plutonium concentration has been established for the conservative waste model sludge at 2.6 g/L for a sludge of infinite extent and optimal water moderation. Thus, for tank C-106, the initial concentration of 0.132 g/L must be concentrated by a factor of 20 to reach 2.6 g/L plutonium content. For any factor less than 20, the plutonium-concentrated sludge could not be made critical even if collected in large masses. In all of the cases evaluated, no sediment layer exceeded an increase in concentration of a factor of 10. This leaves a factor of 2 safety and indicates that it would be extremely difficult to reach a plutonium concentration sufficient to reach criticality.

The SY-102 model assumes a concentration of 0.154 g/L initially so that concentration by a factor of 17 is needed to reach the minimum safe concentration. If plutonium is assumed to be evenly distributed over all size ranges then this waste also has a factor of two safety between the minimum safe concentration and the maximum calculated plutonium sediment concentration after preferential settling. However, the particle size distribution of SY-102 is much different than C-106 in that 83.5% of the solids volume is associated with particles 35 μm or greater in diameter. Thus, when the plutonium is assumed to be 15 or 7.5 microns, the calculations indicate that the fissile material concentrates substantially in the upper levels of the sludge. For the monodisperse 15 μm PuO_2 particle, the concentration reaches 2.2 g/L which is close to the safe limit for a infinite mass of sludge. This concentrated layer contains 7.7% of the plutonium with only 0.5 wt% of the sludge. About 9.9% of the solids settle on top of this layer.

For a PuO_2 particle of 7.5 μm, which is the smallest SY-102 particulate in the measured distribution, the concentration factors are sufficient to exceed the 2.6 g/L safe level for infinite geometry providing plutonium concentrations of 4.9 and 3.0 g/L for PuO_2 densities of 11.4 and 6 g/cm^3 respectively. In the case of the 11.4 g/cm^3 PuO_2 material, the high concentration sediment layer contains 3% of the PuO_2 along with 0.1 wt% of the sludge. About 4.9% of the solids settle on top of this layer. In the case of the 6 g/cm^3 PuO_2 material, the high concentration sediment layer contains 7.7% of the PuO_2 along with 0.4 wt% of the sludge. Thus, it is possible to exceed the infinite safe limit in thin layers within the sediment. It should be

noted that the 240 g/ft^2 areal limit still applies such that regardless of the degree of concentration in any layer of sediment, criticality is not possible as long as the sludge settles into flat, uniform layers. This type of settling is expected for the slow settling materials that concentrate in the upper regions of the sludge. Also, the regions that exceed the safe limit for the 7.5 μm PuO_2 particles contain only 3%, or 7.7% of the PuO_2, dependent upon the assumed particle density of PuO_2 material, which corresponds to only 1.24 kg and 3.19 kg of PuO_2, respectively. The critical mass of plutonium needed for 4 g/L and 10 g/L plutonium concentrations in the conservative waste (sludge) model are 212.0 kg and 3.02 kg, respectively. Thus, even if the highest concentration layer were selectively collected from around the tank and dried to optimal water content, it still would not be sufficient to reach criticality.

Finally, particle flocculation is expected to interfere with segregation due to settling. If PuO_2 particles flocculate then the fluid dynamic properties of the flocs will not be significantly different than other flocs around them and the settling will not favor any particular material. Calculations indicate that 10 μm particles should be agglomerated at the conditions expected within the tanks and sludge settling tests indicate that no particles settle at velocities representative of submicron-sized particles indicating that flocculation is occurring among sub-micron particles (see Appendix A). Thus, for particles of 10 μm or less flocculation is expected. It is also expected that the maximum plutonium particle size is on the order of <2 to 8 μm (Section 7.2.5).

The results of the 1-D models indicate that if the upper bound for plutonium particle size is 10-20 μm or less, then it is extremely unlikely that segregation sufficient to achieve criticality will occur. However, this one-dimensional model is not sufficient by itself because it cannot address three-dimensional concerns that material might be selectively deposited in a localized area by fluid movements within the tank. This selective deposition is addressed by TEMPEST modeling presented in Section 4.0. Also, it cannot address processes where the transient settling behavior is important. Because of this, these issues are addressed by examining mineral separation processes from the mining industry (see Appendix B).

Table 5-1. Particle Size Volume Distributions Used in Modeling.

C-106 (Castaing 1994)		C-106 (WHC 1993)		SY-102 (Dicenso et al. 1995)	
Size, μm	Volume %	Size, μm	Volume %	Size, μm	Volume %
52.5	6.1	90	0.49	137.5	2.5
47.5	7.4	80	0.68	80	25
42.5	10.8	67	0.49	55	31
37.5	8	58	0.00	45	18
32.5	0.8	49	0.49	35	7
27.5	4	41	0.98	25	9
22.5	12	35	1.96	15	8
17.5	5	29	4.01	7.5	0.5
12.5	11	26	5.87		
7.5	36	21	8.31		
		18	11.24		
		15	13.49		
		13	18.87		
		11	14.37		
		9	10.26		
		7.8	3.42		
		6.5	2.54		
		5.5	2.54		

Table 5-2. Maximum Factor Increases in PuO_2 Mass Fraction in Sediment Layer.

Plutonium Distribution	Maximum Increase in Sediment PuO_2 Mass Fraction	
	PuO_2 density = 11.4 g/cm^3	PuO_2 density = 6.0 g/cm^3
C-106 (particle size distribution from Castaing, 1994)		
Uniform over all sizes	5.7	2.7
Monodisperse, 17.5 μm	4.1	6.6
Monodisperse, 7.5 μm	6.5	5.3
C-106 (particle size distribution by Weiss, WHC 1993)		
Uniform over all sizes	5.5	2.7
Monodisperse, 21.5 μm	9.3	5.5
Monodisperse, 5.5 μm	3.4	8.0
SY-102 (particle size distribution from Dicenso et al., 1995)		
Uniform over all sizes	7.5	3.9
Monodisperse, 15 μm	5.2	14.4
Monodisperse, 7.5 μm	32.1	19.3

Table 5-3. Bounding Sensitivity Cases for Maximum PuO_2 Particle Size.

Plutonium Distribution	Maximum Increase in Sediment PuO_2 Mass Fraction	
	PuO_2 density = 11.4 g/cm^3	PuO_2 density = 6.0 g/cm^3
C-106 (52.5 μm PuO_2, particle size distribution from Castaing, 1994)		
Monodisperse, 52.5 μm	19.8	9.6
C-106 (90.0 μm PuO_2, particle size distribution by Weiss, WHC 1993)		
Monodisperse, 21.5 μm	93.9	55.3
SY-102 (137.5 μm PuO_2, particle size distribution from Dicenso et al. 1995)		
Monodisperse, 15 μm	25.7	15.2

Table 5-4. Factor Increase in Mass Fraction Solids Concentration for Various Particles With and Without the Effect of Hindered Settling.

Composition	Size, μm	Non-Hindered	Hindered
"Other"[a]	52.5	3.9	4.2
"Other"	47.5	3.9	3.0
"Other"	42.5	4.1	3.4
"Other"	37.5	4.7	4.7
"Other"	32.5	5.4	6.7
"Other"	27.5	4.0	5.5
"Other"	22.5	3.8	5.1
$Al(OH)_3$	22.5	3.3	3.7
$Al(OH)_3$	17.5	3.8	4.0
$Al(OH)_3$	12.5	3.0	3.5
PuO2	10	5.3	6.7
$Al(OH)_3$	7.5	2.6	3.7
Fe_2O_3	7.5	4.0	3.9

[a]"Other" represents all sludge components except iron, aluminum and plutonium compounds and is calculated with a particle density of 2.0 g/cm^3.

6.0 EVALUATION OF 1/12-SCALE DATA FROM MIXING UNIFORMITY TESTS

Experimental evidence that particles segregate by size during mixer pump operation appears in Bamberger et al. (1995). That document describes a series of scaled mixing experiments that were performed to determine how much power was needed to maintain particles in suspension using mixer pumps. Although the potential for separation was not specifically studied, a small amount of data was collected that can be used to assess the potential for separation during mixer pump operation. This section provides a brief description of the experiments, a synopsis of some data relevant to separation and criticality, and a discussion of the additional data needs and activities that could be performed with the new data to as particle separation during actual operation of mixer pumps.

6.1 SCALED EXPERIMENTS

Experiments were conducted in a 1/12th-scale mixer pump and tank system for testing DST retrieval technologies. The 1/12th scale tank is installed in the 336 Building in the 300 Area of the Hanford Site. The system includes a 1/12th scale model of a Hanford Site DST, one simulated 1/12th scale mixer pump, which was mounted in the center of the tank, simulant preparation equipment, and instrumentation. A detailed description of the facility is available in Bamberger et al. (1996)

Fourteen experiments were conducted to determine the power required to suspend particulate materials using one centrally located mixer pump. The test matrix included four simulants and several flow rates. This matrix provided data to determine the influence of the following three factors on mixing behavior:

- Average particle diameter
- Pump power
- Mixture viscosity.

Based on the data taken, we can partly assess the influence these factorshave on separation.

The specific properties of the simulants were selected based on a scaling methodology described in Bamberger et al. (1996) and Liljegren (1993). This scaling methodology is based on the principle of similarity as described in Fox and McDonald (1973). When applied to using pumps to blend solids-liquid mixtures, the analysis indicates that eight dimensionless parameters must match to achieve similarity. According to the theory, if all parameters match, mixing will be similar in two vessels. The full theory was tested experimentally and found to apply to mixing solids when all dimensionless parameters match (Johnson 1994).

Matching all parameters when modeling a full-scale tank problem is not possible. As a compromise, we conducted the tests so that all paramters matched except the Reynolds number. This compromise was based on literature indicating that Reynolds number has a negligible effect above Re = 10^4 (Johnson 1994). Thus, all tests were performed in the fully turbulent region,

which is expected to apply during mixing in DSTs (i.e. the mixing of DSTs will be hydrodynamically turbulent) and where Reynolds numbers are much greater than 10.

Because flow was turbulent and all dimensionless parameters other than Reynolds number match those in the range anticipated for DSTs, the experiments are expected to closely mimic full-scale mixing behavior. Consequently, the data should be useful for determining the degree to which solids segregate during mixing operations in Hanford DST tanks.

6.2 TEST PROCEDURE

The 1/12 scale tests involved the following five major steps.

1. Prepare the simulant.
2. Run the pump at the desired power level until the mixture reaches equilibrium.
3. Collect bottle samples and analyze to determine the degree of suspension at equilibrium. Lower power level of pump and repeat Steps 2 and 3 until data for each simulant is collected at three power levels.
4. Turn off the mixer pump.
5. Collect and analyze solids from several locations in the settled area after settling is complete.

Bottle samples were analyzed to characterize the solids concentration, the viscosity, and the average diameter of solids in the suspension. The particle size distributions in the suspended slurry and the particle size distributions in settled solids are the data most relevant to criticality. More details related to the test procedure and data collected are provided in Bamberger et al. (1995).

6.3 PROPERTIES OF WELL-MIXED SIMULANTS

The settling behavior of tank wastewas studied using slurry simulants. The solids used to manufacture the simulants were either Minusil-10 or Minusil-40, which are manufactured silicon oxides of essentially uniform shape and size. The size is designated by the trailing number in the product name. The supernatant consisted of water or a sugar-water mixture. The solids in the simulant were selected to be fairly monodisperse (i.e. to be of one uniform size). However, settling behavior indicated that the simulants behaved as polydisperse mixtures.

Unlike tank waste, all simulant particulate material is expected to have the same specific gravity, which is approximately 2.6 g/cm^3 and all particles are of roughly similar shape. Therefore, all major differences in settling behavior during the experiments are caused by size variations. In DSTs,

settling behavior will vary depending on diameter, shape, and specific gravity of the waste particles.

Table 6-1 describes the mean diameter of particles in the simulants used during experiments. These sizes were measured from bottle samples collected during the final stage of simulant preparation. During this step, the 1/12th-scale mixer pump was run at a speed that allowed particles to be maintained in suspensionso they would achieve good mixing and suspension. Bottle samples were drawn and the samples were analyzed to determine the average particle size and the viscosity of the mixture. Different numbers of bottle samples were drawn depending on the specific test.

6.4 EFFECT OF PUMP POWER ON THE DIAMETER OF SUSPENDED PARTICLES

After complete mixing, the power level to the pump was lowered to model behavior that will occur in DSTs during waste retrieval. During this testing phase, some particle settling occurred and the concentration of suspended solids decreased. Additional settling occurred as power was lowered further. In addition, the average size of the particles in the suspended slurry decreased for all cases. The average diameters from a selected group of bottle samples are provided in Table 6-2; this data is from Bamberger et al. (1995). The selected bottles are the first set of bottle samples collected after the tank reached a steady degree of settling at the target pump power. Additional bottles were taken and analyzed but are not reported here.

Before we present the interpretation of this data, please note that the data is not fully analyzed. The magnitudes for the pump flow rates are taken directly from laboratory notebooks. The actual flow rate varied slightly around a steady state value, so more exact values require averaging of the complete data stream, which was not reported in Bamberger et al. (1996). In addition, the particle size data was often clipped as a result of the choice of bin increments selected for measurement purposes. The best selection of bin increments can only be made after one size histogram is obtained. Because the original experiment did not focus on particle segregation effects, this was not done. Additional analysis is required to evaluate the effect this clipping has on the diameter averages and standard deviations reported here. Because the effect of clipping on the precision of the data has not been assessed, all calculated numerical values will be stated in approximate terms, using only two significant digits. Additional analysis would allow more precise statement of the numerical values, however, the approximate values are adequate to describe trends.

The following trends appear in the data. The mean diameter of suspended particles decreases when the pump power is lowered. The mean particle diameter for simulant S1 decreased from 5.85 μm measured when fully mixed to about 5 μm when the pump operated at 20.8 gal/min. It decreased further to 2.5 when the pump flow rate was cut in half, and decreased again to 1.1 when the pump flow rate was cut to 5.4 gal/min. All four simulants behaved similarly. The most segregation is seen for simulant S1. This is probably because flow rates varied by a factor of four for this case and only a factor of two for the others.

Equally important, the standard deviation of the particle distributions

decreased as particles settled. For example, the standard deviation of the particle size distribution for the S1 simulant at the lowest power is 0.28 μm. This is approximately one quarter of the mean particle diameter. In contrast, the ratio of the standard deviation of the particle size to the average particle diameter in the original fully mixed simulant exceeded one half. This decrease in the standard deviation of the particle diameter always occurs with selective settling. It is a mathematical certainty. Even so, examining the ratio of the standard deviation to mean particle diameter is useful. This ratio decreases along with the mean particle diameter, which indicates that the suspended solids are becoming very monodisperse.

The particle size distribution of the suspended material is important for criticality because any material remaining suspended would settle if the pumps were turned off. Any particles still in suspension when the pump is turned off will settle as as very thin layers on top any unsuspended or previously settled material. This will be reflected in the measured size distributions in the settled bed presented later; these distributions did not exhibit a distinct layer of very small particles. After the agitation is stopped, remaining suspended fine particulates would tend to form a uniform layer of sediment and the quantity of plutonium is insufficient to achieve criticality in a uniform sludge layer in a DST regardless of the degree of segregation achieved.

6.5 SETTLED SOLIDS

After all tests with an individual simulant were completed, samples were collected from the settled bed of solids that formed on the bottom of the tank. Data is available for Simulants S2, S3, and S4. No data was collected for S1. Results for simulant S2 are described here. This simulant was selected because it has low viscosity, so tests were run at higher Reynolds number than for S3 and S4. S3 is a small diameter simulant, and is more representative of the sludge particle size in the Hanford tanks, but this test has not been examined in detail. The ideal typical case for a tank would be S1, which has both the lowest viscosity and the smallest particle size. Unfortunately, no settled solids data for S1 was collected in those tests.

Table 6-3 provides the volume mean and standard deviations at three radial locations for settled solids in Simulant S2. The table also lists the flow rate when the reported measurement points were first observed to fall in the settled layer. The data was taken by syringe from the settled solids layer after the liquid was drained from the tank.

The general trend is for the diameter of the settled solids to decrease with distance above the tank bottom. This is consistent with the size decreasing as pump power was turned down. The particles at the lower layers settled during the first series of tests when the pump power was relatively high; the particles in the upper layers settled during the later tests, or after the pump was turned off.

The diameter of the settled solids also appears to vary with radial location. The largest mean particle diameters are found at the smallest radial location of 28 in. because the solids settle preferentially near the outside wall. Only very large particles can settle near the pump nozzle when

the pump is operating at high speed.

When fully mixed, the volume average diameter of this simulant was roughly 22 μm, with a standard deviation near 13 μm. This settling pattern indicates that the large particles settled first, while the small particles settled last. However, the standard deviations of the particle sizes remain relatively large. For example, the measured sample taken from a radial location of 28 in. and an elevation of 0.25 in. has a mean diameter of 36 μm. However, the standard deviation is 20 μm, nearly two-thirds the mean diameter. This standard deviation exceeds that of the original batch. In all cases, the standard deviation for small particles is at least one-half the mean particle size. This makes strong segregation by size in settled layer unlikely, despite the strong segregations observed in the suspended solids. The apparent contradiction arises because the extremely monodisperse populations of particles consist of tiny populations of fines that remain suspended at low pump powers. When these fines settle, they form a very thin layer of solids that was not detectable using the simple sampling methods applied to the settled layer of solids.

6.6 IMPLICATIONS

The data presented here have a number of implications that are relevant to criticality. The most important is that segregation by size may occur in the tank. If specific compounds such as aluminum, iron, or plutonium oxides favor specific sizes, the segregation behavior extends to chemical species. The data suggest that segregation by size is noticeable, but not extremely strong. In all cases, large particles settle preferentially, but some small particles always settle with them. The degree of segregation will likely be greater with an initially broader size distribution than that used in these tests.

The effect of this measured segregation on the potential for criticality in Hanford tanks can not be quantified using these simple tests. However, the analyses presented in Sections 4.0 and 5.0 do provide our attempts. At a minimum, the 1/12th-scale tests do show segregation occurs but the separate layers still show significant variation in particle size distribution. Imposing compositional "worst case" distributions for the plutonium and neutron absorbers on the particle size distribution was performed in Section 5.0. The results suggest that the degree of particle segregation is not large enough to be of concern for realistic particle size distributions.

These 1/12th-scale tests corroborate the parameter that governs settling is expected to be the settling velocity of a particle, not the diameter. In our 1/12th-scale experiment, the settling velocity was always proportional to the square of the particle diameter.

Second, an analysis to predict the size and specific gravity of specific chemical constituents of the waste in Hanford Site tanks is required. If available, although we have found no data source to date, this chemical constituent data could be used with a predicted population density histogram to predict the concentration of individual chemical constituents (as discrete particles) in the settled layer.

Table 6-1. Particle Sizes and Viscosity of Simulants Used in Experiments.

Simulant	Volume mean particle size (μm)	Standard deviation (μm)	Viscosity of mixture (cP)
S1	5.85	3.19	1.50
S2	22.14 22.21 22.08	13.59 13.90 13.61	1.75 1.75 1.40
S3[1]	6.59 6.41 5.96	5.02 4.09 3.59	3.46 3.55 3.59
S4[1]	20.78 20.46 17.33	12.44 13.82 12.74	2.85 2.73 not measured

[1] From first runs for bottles B3H, B3M, and B3L.

Table 6-2. The Effect of Pump Power on the Size of Suspended Particles.

Simulant	Pump flow rate (gal/min)	Volume mean particle size (μm)	Standard deviation (μm)
S1	20.8	4.88 5.37 5.36	2.25 2.66 2.71
	10.5	2.35 2.64 2.92	1.08 2.64 2.92
	5.4	1.03 1.05 1.12	0.26 0.28 0.29
S2	18.79	12.22 9.22 9.07	9.58 7.44 6.82
	15.46	9.30 7.04 6.28	10.00 4.66 3.80
	10.6	4.82 4.84 4.52	3.02 2.94 2.39
S3	20.66	[1]5.88 5.95 6.03	3.49 3.49 3.54
	15.7	5.84 5.18 5.36	3.52 2.74 2.92
	10.5	4.77 6.06 4.62	2.45 5.37 2.26
S4	16.5	8.70 8.51 7.87	7.37 6.72 5.88
	15.7	7.49 7.59 7.49	5.89 5.64 5.19
	10.6	3.37 3.14 3.26	1.63 1.65 1.58

Table 6-3. Particle Diameters in Settled Solids for Simulant S2.

Radial Location (in.)	Elevation above tank bottom (in.)	Volume mean particle size (μm)	Standard deviation (μm)	Mixer pump flow during deposition (gal/min)
28	3.125	9.08	7.90	15.56
	1.125	26.28	12.99	18.79
	0.25	36.01	20.09	18.79
34	6.25	11.06	7.90	10.6
	5.375	19.02	10.88	15.56
	0.25	33.39	12.60	18.79
37.5	6.75	16.58	10.47	10.6
	5.00	18.55	10.55	15.56
	0.25	35.35	17.29	18.79

This page intentionally left blank.

7.0 CHEMICAL PROCESSES THAT CONTROL FATE OF PLUTONIUM AND NEUTRON ABSORBERS

This section focuses on the chemistry of plutonium and selected neutron absorbers. At present, expert opinion differs on whether precipitation or adsorption is the dominating process which partitions most of the plutonium between solid and solution phases in the tanks. We cover both views, but because existing literature on general actinides and Hanford Site tanks waste is not comprehensive, we cannot conclude which hypothesis is correct. We added an abbreviated test plan in Section 10.0. The tests outlined in the plan could be conducted in an attempt to determine which hypothesis is correct. The authors agree that the plutonium in the Hanford Site tanks, both currently and in the future, based on proposed retrieval activities or continued safe storage, will not be found in supernate solution or salt cake in high enough concentrations to cause a criticality. Also, the tank supernate will always have enough neutron absorber to promote subcriticality.

7.1 SOLUTION SPECIES

Plutonium in aqueous solutions exhibits multiple oxidation states (3+, 4+, 5+, 6+, and 7+) depending on factors such as pH, presence of complexants and reductants, and radiolysis; in some systems several oxidation states of this element may coexist at equilibrium (Choppin 1983). Typically, the lower oxidation states of plutonium are stable in highly acidic conditions. As alkalinity increases, the higher oxidation states tend to be stable. One factor that influences the solution speciation properties of plutonium, such as hydrolysis and complexation, is its dominant redox status. Therefore, to accurately assess the overall behavior of plutonium in solution, knowing the redox status of the system of interest is important.

7.1.1 Redox Status

Pu(III) is the stable redox species under highly acidic conditions and in the presence of a reducing agent. Pu(IV) species are stable under moderately reducing conditions. Pu(V) is stable under a narrow range of redox and pH conditions and has a strong tendency to disproportionate into IV and VI redox states (Choppin 1983). However, it has been pointed out that Pu(V) may be a stable and the dominant species only when present in ultra-trace (picomolar) concentration (Hanson 1980). Under oxidizing conditions Pu(VI) is the dominant form in solution. Typical oxidation potentials for plutonium are shown in Table 7-1.

The oxidation potentials indicate that increasing alkalinity results in a decreasing tendency for plutonium to form oxidized species. Disproportionation reactions are also involved in overall redox reactions of plutonium; however, typically the disproportionation mechanism is more important at high concentrations of plutonium and low concentrations of oxidizing agents (Cleveland 1979). Kinetics of plutonium redox reactions are significantly affected by the presence of complexing ligands. Data also shows that, because Pu(IV) forms stronger complexes than other redox species, its

oxidation or reduction to other forms is significantly retarded, and the redox conversion from other valence states to Pu(IV) is enhanced (Cleveland 1979).

Significant quantities of data have been collected for redox reactions of plutonium. However this data was derived from experiments conducted mainly in acid media to separate plutonium for defense purposes. Similar redox data for plutonium in highly alkaline, high ionic strength, mixed electrolyte medium, and at higher than ambient temperatures (similar to conditions that exist in tanks containing high-level waste [HLW]) is limited.

Recent experiments conducted by Yamaguchi et al. (1994) and Delegard (1995) on plutonium solubility in highly alkaline solutions in the presence of a reductant, $NaNO_2$, indicate that plutonium in solution exists mainly in the tetravalent state. Specifically, plutonium solubility experiments conducted by Delegard (1995) in a reductant-containing $NaOH/Na_2CO_3$ solution indicated that all detectable plutonium in solution existed in the tetravalent redox state. This suggests that, under ambient temperature conditions, and in HLW solutions containing mainly [$\geq$ 0.5M concentrations of NaOH, $NaNO_3$, $NaAl(OH)_4$, and $NaNO_2$], all the dissolved plutonium may exist in the tetravalent state.

7.1.2 Hydrolysis

Hydrolysis reactions of plutonium involve the formation of soluble complexes or solid phases with hydroxyl ions. Therefore, among other factors, plutonium hydrolysis species depend strongly on the concentration of hydroxyl ions in solution. Because the available data presented in Section 7.1.1 indicates that soluble plutonium in HLW tanks may exist mainly in the tetravalent state, all discussion of hydrolysis reactions will be restricted to Pu(IV) species. Pu(IV) hydrolyzes more readily than all other redox species of plutonium (Baes and Mesmer 1976). The order of hydrolysis of plutonium redox species follows the sequence Pu(IV) > Pu(III) > Pu(VI) > Pu(V). Depending on the total concentration of plutonium in solution, hydrolysis may also cause polymer formation. Typically polymerization occurs when total plutonium concentration in solution exceeds 10^{-6} M (Choppin 1983). Also, the presence of other complexing ligands inhibits polymer formation (Cleveland 1979). When total Pu(IV) concentration is $<10^{-6}$ M, hydrolysis reactions result in the formation of monomeric species. The speciation scheme can be expressed as:

$$Pu^{4+} + x\ OH^- = Pu\ (OH)_x^{x-4} \qquad (7.1)$$

Depending on the pH of the solution, the number of hydroxyls (x) coordinating plutonium may range from 1 to 4 or perhaps larger. Solubility data for tetravalent actinides (Rai and Ryan 1984, Rai et al. 1995) indicate lack of amphoteric behavior, thus the formation of $Pu\ (OH)_5^-$ species in solution appears to be unproven. However, solubility data obtained by Delegard (1987) in sodium hydroxide solutions ranging in concentration from 1 to 15 M, indicate amphoteric behavior that suggests the existence of negatively charged hydrolytic species of Pu(IV).

The stability constants for Pu(IV) hydrolytic species are listed in Table 7-2. The constants indicate that plutonium in the tetravalent state forms more stable complexes than plutonium in tri-, penta-, and hexavalent

states. Increasing hydroxyl concentration (increasing pH) results in the dominance of hydrolytic species with increasing numbers of OH^- coordinating with plutonium.

7.1.3 Complexation

Plutonium forms complexes with a number of inorganic and organic ligands. The tendency to form complexes depends on the ionic potential defined as a ratio of formal charge and the ionic radius of an ion. Among plutonium redox species, Pu(IV) exhibits the highest ionic potential, therefore Pu(IV) forms the strongest plutonium complexes with various ligands.

Typical Hanford Site HLW contains ligands such as NO_3, NO_2, CO_3, PO_4, SO_4 F, Cl, oxalate, citrate, EDTA, and HEDTA. Reviews of existing literature indicated that Pu(IV) complexes have been studied extensively because they occur during the plutonium separation process. The tabulated data shows that the Pu(IV) complexes containing NO_3, SO_4, F, and Cl form rather weak complexes, so these complexes may not be significant in Hanford Site HLW. Although phosphate, citrate, oxalate, and EDTA ligands form very strong complexes with Pu(IV) ion, the concentrations of these complexes will not be significant in Hanford Site HLW because the ligand concentrations in the waste solution are typically two orders of magnitude or more less than the strongly complexing hydroxyl ions. A sample calculation showed (Appendix F) that in a typical waste tank supernatant, the concentrations of Pu-hydroxyEDTA complexes would be insignificant as compared to the concentrations of Pu-hydroxycarbonate complexes. Typical stability constants for Pu(IV) complexes are tabulated in Table 7-3.

Based on solubility data, Lierse (1986) has suggested the existence of a series of Pu-carbonate complexes namely, $PuCO_3^{2+}$, $Pu(CO_3)_2^0$, $Pu(CO_3)_3^{2-}$, $Pu(CO_3)_4^{4-}$, and $Pu(CO_3)_5^{6-}$. However, there are no spectroscopic data to support the existence of these species. Because solubility data can be interpreted on the basis of any number of hypothetical species, the existence of such species are uncertain without additional confirmatory spectroscopic data.

Recently, based on solubility and spectroscopic data, Yamaguchi et al. (1994) showed that under alkaline conditions, Pu(IV)-OH-CO_3 mixed ligand complexes may form the dominant dissolved species in alkaline-carbonate solutions. Solubility experiments in high ionic strength solutions containing NaOH and Na_2CO_3 also have shown that plutonium mixed ligand species are the principal aqueous species (Delegard 1995). Photoacoustic spectroscopic data generated by Tait et al. (1995) has also confirmed the existence three different Pu(IV)-OH-CO_3 mixed ligand species, although these investigators could not determine the ligand stoichiometry. These investigators interpreted the data in terms of the existence of $Pu(OH)_x(CO_3)_y^{(3-x-2y)}$, $Pu(OH)_x(CO_3)_{y+1}^{(3-x-2y-2)}$, and $Pu(OH)_{x+1}(CO_3)_y^{(3-x-2y-1)}$ species. The distribution of these species as a function of pH and total aqueous carbonate concentrations is shown in Figures 7-1 and 7-2. The data indicates that the $Pu(OH)_{x+1}(CO_3)_y^{(3-x-2y-1)}$ species is dominant under all conditions examined in these experiments. The stoichiometries of these mixed ligand species for various values of x and a unit value of y were computed and compared with the stoichiometries of mixed ligand species predicted by Yamaguchi et al. (1994) in Table 7-4.

The data (Table 7-4) show that in all cases except two the predicted stoichiometry based on data presented by Tait et al. (1995) does not conform with stoichiometries of species predicted by Yamaguchi et al. (1994). Only in two cases, when x is 2 and y is 1, and when x is 1 and y is 2, does one of the predicted species $[Pu(OH)_2(CO_3)^{2-}]$ based on the data presented by Tait et al. (1995) agree with a species predicted by Yamaguchi et al. (1994). The stochiometries based on the suggested condition for charge $4-(x+2(y+1)) \leq -1$ from Tait et al. (1995) results in the set of species listed in the first column of Table 7-4. In a recent unpublished manuscript, Tait et al. (personal communication) indicate that x and y may be 1 and 2, respectively. Only one species from the speciation scheme of Tait et al. ($Pu(OH)_2(CO_3)_2^{2-}$)with either of the two species suggested by Yamaguchi et al. (1994). According to Yamaguchi et al. (1994) data, the dominant species at pH values above about 11 would be $Pu(OH)_4(CO_3)_2^{4-}$. The speciation scheme proposed by Tait et al. (1995) does not provide a comparable specie. Therefore, the data generated by Yamaguchi et al. (1994) and Tait et al. (1995) disagree about the number of complexes, their stochiometries, and the range of species dominance.

Although experimental data is available that confirms the existence of Pu(IV)-OH-CO_3 mixed ligand species, the existing data from spectroscopy and solubility are contradictory. Until the stoichiometry question is resolved, we chose to use the data set of Yamaguchi et al. (1994) in all speciation calculations. Predicted speciation of Pu(IV) species as a function of pH and carbonate concentrations are shown in Figures 7-3 and 7-4. The computations show that, at low carbonate concentrations (0.001M), various hydrolytic species predominate up to a pH value of about 6.5. At a pH between 6.5 and 10, $Pu(OH)_2(CO_3)^{2-}$ is the dominant aqueous species. At higher pH values, the neutral hydrolytic specie, $Pu(OH)_4^0$ makes up about 90 percent of the dissolved Pu(IV) species. With increasing carbonate concentration, the speciation picture shows significant changes. Under these conditions, the range of dominance of $Pu(OH)_2(CO_3)^{2-}$ species extends over about 7 orders of magnitude in (from a pH of about 3.5 to 10.5). At pH values above ~11, $Pu(OH)_4(CO_3)^{4-}$ will be the dominant aqueous species in solution.

The data suggests that the typical solution composition of HLW in Hanford Site tanks probably includes Pu(IV)-OH-CO_3 mixed ligand complexes as the dominant aqueous species. However, equilibrium calculations and/or spectroscopic measurements are needed to confirm the presence of these dominant species in HLW supernatants.

7.1.4 Ionic Strength Effects

Ionic strength is a measure of the total electrolyte concentration. This is defined as one half of the sum of the products of total concentrations and the charge on the electrolyte components in a waste solution. Ionic strength of a solution affects a number of reaction parameters related to complex formation, complex stability, solubility, and adsorption. Available stability data (up to 4M ionic strength) indicates that plutonium-complex species tend to become less stable with increasing ionic strength. For instance, the stability of $Pu(OH)^{3+}$ species decreases by about an order of magnitude when the ionic strength increases from 0 to 2M. The stability of a weaker complex such as $PuNO_3^{3+}$ also decreases by an order of magnitude when the ionic strength increases from 0 to 4M. However, the magnitude of

plutonium-complex stability constants in HLW solutions (typically ~9M) is difficult to assess because experimental data on solutions at these very high ionic strengths does not exist. Consequently, if we assume that the magnitude of change in stability is similar for all complex species, the type of dominant species can be expected to be the same even at higher ionic strengths. Thus, we will assume that the mixed hydroxide-carbonate solution species will predominate in the tank supernate liquids.

7.1.5 Temperature Effects

Higher than ambient temperatures will affect the reaction kinetics and chemical equilibrium of the HLW system. The bulk of published data on stability for hydrolytic and complex species for Pu(IV) was typically obtained at ambient temperatures. Therefore, to assess the effects of higher temperatures (up to boiling) on the supernatant chemistry of HLW stored in tanks, one needs to know how the ambient temperature stability constants change as a function of increasing temperature.

Literature review identified only one source of higher temperature complex stability data for plutonium species (Lemire and Tremaine 1980). The data used here was derived from their work using theoretical calculations instead of actual measurements. These calculations indicate that typically the stability constants of soluble Pu(IV) complexes (with inorganic ligands besides OH^-) increase by one or two orders of magnitude when the solution temperature increases from 25 °C to 100 °C.

7.1.6 Radiolysis Effects

Alpha emissions from ^{239}Pu produces free radicals, which are powerful redox agents. These free radicals may induce plutonium redox reactions resulting in the formation of various valence species. Such self-catalyzed Pu reactions are categorized as radiolytic effects. Most of the studies of radiolysis effects have been conducted in highly acidic solutions. Only a limited number of experiments have been conducted in which the radiolytic effects have been studied using near neutral or slightly alkaline solution. Available data shows that radiolysis in such solutions in the presence of ligands such as Cl, SO_4, NO_3, and CO_3 causes oxidation of reduced plutonium species (Sullivan 1983). Pikaev (1996) presented data on gamma-ray-induced radiolysis of alkaline aqueous solutions of neptunium and plutonium that showed the net reaction formed more reducing conditions and Pu(V) and Np(V) aqueous species were reduced to (IV) species. Camaioni et al. (1994) performed gamma irradiation tests on a simulated organic-rich Hanford Site tank waste supernatant and found that the net radiolysis species were reductants.

Two recent reports from Savannah River National Laboratory (SNL) using simulated HLW solutions similar to the supernatant solutions in Hanford tanks suggest the following. For solutions that contain NaOH, $NaNO_3$, $NaNO_2$, $NaAlO_2$, Na_2CO_3, and Na_2SO4 in concentrations similar to those found in Hanford tanks, the effects of gamma [^{60}Co] radiation of up to ~10^7 rads at a dose rate of 4 x 10^4 R/hr on Pu solubility was insignificant. However, at higher NaOH concentrations, concentrations of plutonium solution increased in small vials

that were irradiated and did not in control vials that contained plutonium hydrous oxide precipitates and the highly caustic solution. The experiment is summarized below and the reader is encouraged to read Karraker (1994, 1995).

Various simulated tank solutions with the components described earlier were prepared and inoculated with enough plutonium stock solution in 0.25 M nitric acid to cause plutonium precipitation. Small vials of the plutonium slurry were then gamma irradiated with a ^{60}Co source. After between 3 and 10 days of irradiation, the samples and the non-irradiated controls were analyzed for soluble plutonium based on filtration through 0.2-μm membranes. Based on wet chemical procedures some plutonium speciation data were also obtained. The plutonium speciation discussions are based on the assumption that only Pu(IV) would be retained on anion exchange resins while Pu(VI), Pu(V), and Pu(IV) polymer would not be strongly retained on the resin and could be easily rinsed out before rinsing the Pu(IV) with stronger reagents. All the data collected at SNL show solution plutonium concentrations below 0.02 g/L when Pu(IV) was the form used and 0.13 g/L when Pu(VI) was used. Although results indicate some increase in plutonium solution concentration in some solutions that are outside the range generally found in tanks, none of the results show solution concentrations above about one-tenth the minimum criticality value of 2.6 g/L amply discussed in Bratzel et al. (1996).

Karraker found that plutonium solution concentrations in the presence of excess hydrous plutonium-oxide, increased up to 5 to 10 times, versus unirradiated controls, in slurries that were irradiated and contained at least 2.75 M NaOH and contained $NaNO_3$ and $NaNO_2$. The effects were especially noted in solutions with NaOH concentrations above 6 M. When no sodium nitrite was present, plutonium solution concentrations did not increase until the hydroxide content reached >6 M. Karraker hypothesizes that the increased plutonium solubility may be caused by radiolysis species that are capable of oxidizing the Pu(IV) to a higher valence state. One possible reactive species that is formed by radiolysis is hydrogen peroxide [H_2O_2]. Karraker performed some experiments where H_2O_2 was added to NaOH solutions that contained plutonium precipitate/slurry and found that hydrogen peroxide did increase plutonium solubility when present in concentrations $>10^{-4}$ M. Further, the H_2O_2 degraded to water and oxygen with a half-life of between 100 and 300 minutes. If H_2O_2 is formed during radiolysis, it could be constantly supplied at a rate faster than it degrades naturally and could always be present in the waste tanks.

Karraker also used Pu(VI) stock solutions using a slight excess of permanganate in solution. The Pu(VI) acidic solution was mixed with simulated alkaline tank solution. A precipitate formed and the slurries were used in experiments like those just described. Control and irradiated slurries were filtered after several days and solution plutonium concentrations were measured. Aliquots of the filtrate were measured as created and after treatment with ferrous iron solution and $NaNO_2$ to reduce all the plutonium to the +4 valence state. Running both analyses allows one to estimate plutonium speciation. Karraker found that Pu(VI) is stable for at least 25 days. After irradiation, the observed plutonium concentration in solution drops as long as the hydroxide is below 8 M in pure NaOH solutions. The plutonium concentration drops in mixed NaOH, $NaNO_3$, and $NaNO_2$ solutions as long as the hydroxide is at least 4 M. However, the speciation of the solution plutonium remains (VI), which might conflict with the concept that the irradiation is

reducing the plutonium valence state. For similar tests where the plutonium stock solution was initially Pu(IV), the end speciation showed some transformation to Pu(VI) when only NaOH solutions were used. The higher the free hydroxide the more soluble plutonium converted to Pu(VI) in both the control and irradiated samples. No speciation work was performed in the presence of other salts, such as nitrite, nitrate, sulfate, or carbonate. This work is interesting but only scratches the surface of the radiolysis issue. The Karraker results might appear to conflict somewhat with the Russian results depending on the interpretation of why the plutonium valence state remaining in solution remains (VI), but the overall concentration drops. None of the work available considers the impacts of beta and alpha radiolysis, which exhibit different abilities to create radiolysis reactants, and the enormous amount of reactions that may form other reactive species or, conversely, rapidly consume radiolysis species. Quantifying the impacts of radiolysis on plutonium chemistry in the tanks is impossible. We conclude with one observation—that none of the observed plutonium solution concentrations in the tests discussed exceed 0.13 g/L which is 20 times below the plutonium concentration of concern to criticality.

No other radiolysis experimental data was found that is relevant for the highly alkaline and ionic strength solutions that are typical of Hanford Site HLW supernatants, which also typically contain reductive NO_2 anion. One other general review of radiation effects on solution chemistry was found (Serne 1989) that also suggests the issue is far from being understood. Although specific radiolysis data for actual tank solutions do not exist, several cited references and Delegard's solubility data (1995) indicate that the radiolysis effects on plutonium in Hanford Site HLW solutions maintain reducing conditions relative to plutonium aqueous chemistry.

7.2 SOLUBILITY

The concept of solubility/precipitation is well established from first principles. The concept often is used in bounding fate and transport analyses to estimate the distribution of actinides between the solution phase and the solid phase. For discussions and examples of why and how solubility is a valuable construct for addressing the fate of plutonium and other radionuclides, see Nitsche (1991), Pennders et al. (1985), Pryke (1985), Pryke and Rees (1986), Rai and Ryan (1984), and Rees (1985). Solubility constructs for pure or solid solution phases give an upper bound on the concentrations that one would expect to be in a mobile solution phase in equilibrium with solids; only cause lower amounts of the contaminant to be found in solution.

7.2.1 Precipitation of Plutonium Hydroxide Phase

In its simplest form, solubility calculations require one to identify the "solubility-controlling" solid and the predominant aqueous species that forms when the controlling solid dissolves. If several aqueous species contribute significantly to the overall solution concentration, their forms and stabilities also must be identified. Then one can use the thermodynamic solubility product or constant, K_{sp}, and the stability constants, K_i, that describe the formation of the predominant aqueous species to calculate the total solution concentration that should be present in the system of interest.

This is true inside a particular Hanford Site tank. We have determined that much literature is available that supports the choice of a partially crystalline Pu(IV) oxide described as $PuO_2 \bullet xH_2O$ as the "solubility-controlling" solid in the chemical environments inside the Hanford Site tank. Key references where efforts were made to directly determine the nature of the plutonium solid are Rai et al. (1980), Delegard (1987), and Yamaguchi et al. (1994). Other references that provide empirical data on observed plutonium solution concentrations in chemical environments similar to those inside the Hanford Site tank, but do not attempt to directly determine which solid phase is present, include Hobbs et al.(1993), Hobbs and Edwards (1993), Hobbs (1995), and Delegard et al. (1984, 1995). In a recent study involving waste supernatants, Hobbs and Karraker (personal communication) identified $PuO_2 \bullet xH_2O$ in the precipitated phase. The solubility data from Yamaguchi et al. (1994), Delegard (1995), Hobbs et al. (1993), and Hobbs (1995), plotted as a function of total carbonate concentration in Figure 7-5, show that in all these experiments, $PuO_2 \bullet xH_2O$ was most likely the solubility-controlling solid phase.

Some of the experiments conducted by Hobbs and his coworkers involved aluminum and iron. Plutonium and uranium were found to "coprecipitate" with the aluminum and iron. Hobbs (personal communication) believes that such phenomena are probably $PuO_2 \bullet xH_2O$ colloids being coagulated by aluminum and iron hydroxides rather than the formation of true solid solution phases. Coagulation is a proven chemical process that is used in water treatment plants to remove colloidal suspended impurities (Clark 1990). Solids resulting from coagulation differ from solid solution phases in two distinct ways. First, in coagulated mass, pure phase colloids are enclosed in the major phases (consisting of distinct gel phases), whereas, solid solutions constitute ions of comparable ionic radii substituting in a single solid phase. Second, in coagulated solid mass, the solubility of ions is controlled by each distinct relatively pure solid phase. Solid solutions control the solubility of all constituent ions in the discrete phase by the dissolution of the single solid solution phase. The plutonium solubility data, which agrees with the solubility of relatively pure phase $PuO_2 \bullet xH_2O$ (Figure 7-5), suggests that the precipitation of plutonium observed in Hobbs' experiments was more likely the result of coagulation rather than true solid solution formation with aluminum and iron hydroxides.

Identifying the predominant aqueous solution species one would expect to find in Hanford Site tanks is less certain, but likely candidates are $Pu(OH)_2(CO_3)_2^{2-}$ when the free hydroxide content is low (<0.01 M or ~pH≤10) and total carbonate is ≥0.1 M (see Section 7.1). At pH values of 12 to 13 and total inorganic carbon of ≥0.1 M, where carbonate is the predominant inorganic carbon species, the proposed soluble complex is $Pu(OH)_4(CO_3)_2^{4-}$ (see Section 7.1).

This selection is supported by data presented in Yamaguchi et al. (1994); Delegard (1995), where data in Delegard (1987) are reinterpreted; and Tait et al. (1995). We acknowledge that literature contains numerous articles for less alkaline, lower pH, and lower salinity waters common in lakes, rivers, and oceans that suggest the predominant aqueous species should be Pu(V) species. However, we find these reports unconvincing given the highly sensitive nature of speciation to key variables such as pH, eH, and the concentration of dissolved ligands such as carbonate.

Waste stream data from the Hanford Site (Agnew 1995, Agnew et al. 1996) indicate that the wastes was probably oversaturated with respect to $PuO_2 \bullet xH_2O$ (Figure 7-6). The degree of oversaturation of each waste stream can be more accurately evaluated using a chemical equilibrium code such as GMIN (see Felmy 1995) or Environmental Simulation Program (ESP v5.0) developed by OLI Systems Inc.. Given the $PuO_2 \bullet xH_2O$ as the "solubility-controlling" solid and the choice of either $Pu(OH)_2(CO_3)_2^{2-}$ or $Pu(OH)_4(CO_3)_2^{4-}$ as the dominant aqueous species, depending on pH and in the presence of at least 0.1 M total carbonate, we can now predict the total plutonium solution concentration in Hanford Site tanks. Expected plutonium solution concentrations for high-pH tanks should be ~10^{-7} M (0.025 ppm) at carbonate concentrations of ≥0.1 but ≤1.0 M as long as pH >12 and ~10^{-5} M (2.5 ppm) at carbonate concentrations of ≥1.0 M as long as pH >12. However, if pH is 10 or less, these solution plutonium values would increase by ~300 for tanks with high carbonate but little free hydroxide.

Based on studies by Rai and Ryan (1984), Delegard (1987), and Kim and Kanellakopulos (1989), we can assume that the $PuO_2 \bullet xH_2O$ in waste tanks is aging towards a more stable and partly crystalline phase. If this is so, the expected solution concentrations will be at least an order of magnitude less than the concentrations supported by freshly precipitated $PuO_2 \bullet xH_2O$, as shown in Figure 7-5. The cited laboratory studies by Hobbs and coworkers (the open circles in Figure 7-5) and Delegard (the open squares) corroborate the simple solubility estimates (the dashed and solid lines). Characterization data for supernatants and drainable solutions from Hanford Site waste tanks (Van Vleet 1993a, 1993b; Sederburg 1994; listed in Table 7-5) plot near or slightly below the lines, depending on specific tank carbonate and free hydroxide concentration (Figure 7-7). This relationship suggests that the plutonium-controlling solid is most likely $PuO_2 \bullet xH_2O$ or a less soluble, more crystalline (aged) $PuO_2 \bullet xH_2O$. Plutonium solution concentrations in the range of 0.1 to 100 ppm represented by the solubility considerations are thousands to about 30 times lower than the values needed to allow nuclear criticality to occur in solution. Bratzel et al. (1996) and Waltar et al. (1996) present more discussion on the plutonium concentrations necessary to reach criticality. Therefore, criticality is implausible in tank supernate solutions. In addition, to reach criticality, the following must occur.

- Plutonium solids must be rearranged (enriched)
- Plutonium-bearing or pure plutonium solids must be separated from the large excess of neutron absorber-bearing solids found in Hanford Site tank sludge.

Because of changes in ionic strength, the presence of other common inorganic ligands such as nitrate, nitrite, aluminate, sulfate, and phosphate are not expected to have any significant influence. The general impact of total dissolved salts (e.g., ionic strength) on thermodynamic activity and solubility also is not expected to change these estimates significantly. The key variables that control the solubility of plutonium in Hanford Site tanks are free hydroxide and carbonate content.

7.2.2 Organics Present in Hanford Site Tanks and their Influence on Solubility and Plutonium Speciation

Measurements of the total organic carbon content in supernate solution, sludge slurry, and perhaps salt cake have been taken for Hanford Site tanks. However, only a few tanks have been studied in enough detail to evaluate the types and amounts of organic components present in supernate and sludge. Data specific to Hanford Site tanks has been found in Campbell et al. (1994a, 1994b, 1994c), Campbell et al. (1995a, 1995b), Lokken et al. (1986), Pool and Bean (1994), Wahl et al. (1995), and WHC (1995b).

Much of the material in these documents describes the development of analytical procedures to measure selected organic compounds in the complex tank waste matrix. For the most part, they do not list copious analyses of tank samples. The task of measuring organic species in the complex highly radioactive tank phases is truly difficult. To date the organic analyses attempted have emphasized measuring chelating agents, chelating agent fragments, butyl phosphates, low-molecular-weight water-soluble organic acids and normal paraffin hydrocarbons (NPH).

To evaluate how well the organic analyses have identified the major organic compounds present in the tank materials, organic chemists have tried to calculate mass balances by comparing the organic carbon mass in the species identified with the total organic carbon measured in bulk material removed from the tanks. The bulk material consists of supernate solutions and solids, mainly sludge slurries.

Not all organic carbon is "seen" by all the techniques used to measure total organic carbon. Two commonly used methods to measure total organic carbon in tank materials are as follows:

- Hot persulfate oxidation, which acidifies a tank sample to drive off inorganic carbon. The remaining sample is then oxidized using a silver catalyst, heat, and persulfate to form carbon dioxide gas, which is collected and analyzed. This method assumes that the acidification and sparging do not liberate volatile organic material. Long-chain organics such as NPH, surfactants, acetone, butanol, benzene, and organic polymers do not react quantitatively using this technique.

- Combustion, where the sample is heated to 600 °C in the presence of oxygen gas. The resultant carbon dioxide is measured to quantify the organic carbon content.

Analysts feel that combustion may more accurately measure total organic carbon, but it is not generally used on actual tank samples. The hot persulfate method is favored, so the actual amount of organic carbon in the tanks may be ~0.5 to 2 percent by weight higher in tank solids and 0.5 to 1.5 percent higher in tank supernate than generally reported The types of organic carbon that have been found to predominate in aqueous phases in tank samples (chelators, chelator fragments, and low-molecular-weight organic acids) react fairly quantitatively using the persulfate technique, so we can

compare the mass of carbon species identified with the total organic carbon value to estimate how much organic carbon has not yet been identified.

The results of the mass balance check for the amount of organic carbon identified using detailed speciation techniques versus total organic carbon is improving. The current range is between 50 and 90 percent, with an average of 80 to 90 percent. This improvement is mostly because cation exchange techniques are now used to remove radioactive constituents, especially cesium and strontium, from tank samples. After the radioactive constituents are removed, the samples can be transferred from the hot cell to fume hoods for analysis using techniques that are specific for extracting organic materials. Being able to perform detailed work in a fume hood instead of being limited to the crude operations that can be performed in a hot cell lead to significant improvement in mass balance on organic carbon.

The following sample treatment and detailed organic analysis techniques are currently being used. To create hydrophilic samples, about 2 to 5 g of tank solids are stirred overnight with 10 to 20 mL of distilled water. The solution is filtered through 0.45-μm membranes in a hot cell. Newer procedures are then used to run the solution through a cation-exchange column (10 g of AG50W-X8 resin) to remove cationic radionuclides so the ion-exchange treated solution can then be removed from the hot cell. The water extract or a subsample is next taken to dryness using nitrogen blowdown techniques. The evaporites are then mixed with BF_3/methanol and heated to 100 °C for 1 hour to derivatize the hydrophilic organic species present. After cooling, chloroform is added and the resultant organic solution is added to an aqueous buffer solution of 0.1 M KH_2PO_4. The aqueous and chloroform phases are well mixed and allowed to separate. The chloroform phase, which contains derivatized organics, is saved for analysis by GC/MS (gas chromatography/mass spectrometry) to identify the organic species that are present and then by GC/FID (gas chromatography/flame ionization detection) to determine how much of each is present. Derivatization to form methyl esters of the organic compounds makes them easier to analyze using GC/MS.

This procedure was used to measure the water-soluble chelating agents, chelating agent fragments, and a few organic acids in the tank solids. Similar procedures were used on tank supernate solution with a one-to-one mix of supernate solution and distilled water. Another subsample of the water leachate (after cation exchange treatment) is run directly by LC and/or IC to quantify the low-molecular-weight organic acids (LMWA). LC/UV techniques were used to measure water-soluble LMWAs, such as the oxalic, glycolic, formic, succinic, and acetic acids present in the tanks as salts.

A second tank sample (tank solids or discrete organic solution phases) was equilibrated with an organic solvent three times (chloroform or methylene chloride) to leach hydrophobic organics from the tank material. The organic solvent extract was then concentrated by partial evaporation and analyzed by GC/MS to identify the hydrophobic organics, such as NPH, which are long-chained hydrocarbons (C_{12} to C_{15}), and tributyl phosphate (TBP) and its degradation products.

The results of organic speciation measurements on tank samples from double-shell tanks SY-101 and SY-103 are shown in Tables 7-6 through 7-9. Results for single-shell tank (SST) C-103 are shown in Tables 7-10 through

7-12. Tables 7-6 through 7-9 suggest the following conclusions for the two double-shell tanks.

- Oxalate, the predominant LMWA, is present at much higher levels in the sludge solids than in the supernate solution. This may be caused by the insolubility of many metal oxalates.

- Proportionately more chelators and chelator fragments were found in the supernate solution than in the solids. However, because the solids in the tanks can have higher total organic carbon (TOC), the absolute concentration of chelators in the solids can be as high or higher than in the supernate solution. EDTA is the predominant chelator present. The NPH content in tank samples analyzed to date is small (less than 7 percent of the total organic carbon).

In the mid 1980's Lokken et al. (1985) performed organic analyses on supernate solutions from double-shell tanks AN-107 and AZ-102, which have been categorized as "complex concentrate," using a derivatization technique similar to the one currently used. The analytes were then measured using GC/MS and GC/FTIR. NTA, HEDTA, EDTA and citric acid were identified at millimolar concentrations. The mass balance of total organic carbon was only 40 percent. Using HPLC techniques, some other classes of organic compounds, such as mono- and di-carboxylic acids, long-chained alkanes ranging from C_{23} to C_{35}, and phthalate esters, were identified. By the end of 1986, the mass balance had been improved to 75 percent. The final results for the AN-107 supernate waste solution are shown in Table 7-13. The report also describes organic aging studies performed on simulated "complex concentrate" for 85 days at room temperature and in the absence of radiation. Even under these mild conditions chelators such as EDTA and HEDTA showed significant degradation (approximately 70 percent), NTA showed no degradation, and citric acid showed 18 percent degradation. The chelator fragments identified were similar to those found in the actual waste, suggesting that EDTA and HEDTA would exhibit significant degradation in Hanford Site tanks. The degradation products identified accounted for only 41 percent of the loss of EDTA and HEDTA, which suggests that other fragments that are not amenable to GC/MS analysis, such as amines, were likely formed also.

The total organic carbon content of the "complex concentrate" waste liquor in Tank AN-107 is over four times higher than in tanks from the SY tank farm. The citric acid content in AN-107 supernate is about 10 times more concentrated and the HEDTA is at least an order of magnitude more concentrated, but the other chelators are present in about the same concentrations as found in the SY tanks' supernate solution and sludges. Fragments such as ED3A and IDA are also present in AN-107 at several times higher concentrations than are found in SY tank supernates. The AN-107 supernate contains numerous long-chained carboxylic acids not identified in the SY tanks. Conversely, the SY tank supernate solutions appear to contain shorter chained carboxylic acids. The hydrocarbon content in AN-107 solution is larger than in the SY samples and appears to contain compounds with longer chains than the NPH identified in SY tanks.

SST C-103 has a distinct organic solution layer floating on top. Some of this material was diluted 10,000 times with methylene chloride and analyzed

by GC/MS using the chemical ionization mode to determine molecular weight. High-resolution mass spectrometry also was used to improve our ability to identify the compounds. Table 7.10 lists the organic carbon species results for this organic layer. The relative weight of [TBP + DBBP] to [NPH] is about 2:1. The "missing" mass in the organic layer was mostly inorganic (perhaps colloidal suspension) matter that was identified by SEM to be metal-sulfate salts; alumino-silicate particles; calcium phosphate particles; and iron, chromium, and aluminum hydrous oxide particles.

A sample of tank C-103 aqueous supernate layer was mixed with equal portions of distilled water and extracted three times with methylene chloride. The organic extracts were then conditioned and evaporated to 1 ml volume and analyzed by GC/MS. The only organics (water-insoluble) found in the liquid phase were TBP at 80 ppm, DBBP at 7ppm, and NPH at ~1 to 3 ppm.

Data on the chemical composition of the aqueous phase (supernate solution) underlying the aforementioned discrete organic phase in Tank C-103 are shown in Table 7-11. The aqueous phase was measured for inorganic cations, anions, carbon, and radionuclides and for some physical properties such as viscosity and density, as well as for the water-insoluble organics just noted and the water-soluble organics mentioned in the next paragraph. Other data currently available on the water-soluble portion of supernate tank solids from Tank C-103 are shown in Table 7-12. The TOC values were determined using the persulfate oxidation method. The oxalate values were determined by ion chromatography. The TOC content of the tank liquids and solids from this SST is slightly lower than for the DST (see Table 7-6), but more oxalate is present in single-shell tank liquids than in DST liquids and less oxalate is present in SST solids than in DST solids.

From the few data available one can estimate that the tank supernate aqueous solutions may contain up to 3.8 mg of C/g of solution of EDTA, which is the strongest complexing agent for plutonium, iron, and aluminum, as well as most other metals present in the tanks (see the discussion of complex stability constants in Section 7.1 and Table 7-3 for details). One mole of EDTA contains 10 carbon moles, so the highest concentration of EDTA measured to date in supernate solution is ~0.04 M. All other identified chelating agents are present at lower concentrations. The highest concentration of LMWAs (about 2.0 mg C/mL) found in tank supernate solutions occurs in SSTs. One mole of oxalic acid contains two carbon atoms, thus the molarity of the supernate solution would be 0.15 M. The SST studied also had an immiscible liquid organic layer in consisting primarily of TBP and degradation products. TBP is a known complexing agent for plutonium. But the analyses for plutonium and other radionuclides in this discrete organic layer (see Table 7-11) are quite low compared to the aqueous phase. Further, the concentration of plutonium in either the organic liquid or the supernate is much lower than values needed to reach a criticality threshold where concern would occur.

Campbell et al. (1995b) state that Tank C-102 formerly contained a floating organic-solvent layer, but that much of this material was pumped to Tank C-103 and further salt-well pumping reduced the Tank C-102 liquid levels such that no free-standing liquids were present. Based on the data in Table 7-14, normal paraffin hydrocarbons are still present in the tank solids likely as coatings on the solids. An analysis of the head-space in Tank BY-108 suggests that it may have contained a discrete organic layer

floating on top of aqueous layers before interim stabilization by salt-well pumping. Tank C-103 currently does contain a discrete organic layer that has been verified by sampling (Postma et al. 1994). The solids in Tanks C-102 and C-103 are described as being sludge; the solids in Tank BY-108 is described as being salt cake. The solids (see Table 7-15) in the lower part of Tank BY-108 riser 17 and all solids from riser 16 appear to have less TOC and hydrophobic organics than tanks that originally had organic layers, but have sludge instead of salt cake as the solids.

Campbell et al. (1995a,b) describe several aging mechanisms that should change the nature and quantity of organics in the discrete organic layers present in some tanks, and likely in aqueous layers, although this is not stated in the reports. The high caustic content of the Hanford Site tanks should result in saponification of TBP to DBP (dibutyl phosphate) and, because DBP is much more water soluble than TBP, it should be extracted from the discrete organic phase into the aqueous fluids. Further, TBP undergoes radiolytic decomposition.

The NPH in the discrete floating organic layers in a few tanks is somewhat volatile under tank heat conditions. NPH decomposes radiolytically to carboxylic acids that are much more water soluble than NPH. Therefore the carboxylic acids will migrate towards the aqueous layers and some of the for long-chained acids perhaps precipitate and coat the inorganic sludges. Also, the passive ventilation systems present in some tanks has allowed some NPH to escape from the tank headspace.

At present we believe that the organic ligands present in Hanford Site tanks that could influence plutonium solubility are found at relatively low concentrations compared to free hydroxide and carbonate and most are also chemically unstable and are continually being transformed into molecules with even weaker complex-forming capabilities.

Delegard and Gallagher (1983) show in an empirical fashion that relatively high concentrations of chelating agents [HEDTA to 0.1 M, EDTA to 0.05 M, hydroxyacetate to 0.1 M, and citrate to 0.03M] did not increase the solubility of plutonium in tank environments. Toste et al. (1984, 1987) discuss procedures to analyze for specific chelating/complexing agents in complex waste streams and give data on an actual Hanford Site tank waste complex concentrate in which much of the soluble organic material is identified as degradation products of parent ligands commonly used to extract fission products.

Camaioni et al. (1995) also discuss ongoing work that shows radiation can degrade the complexing agents. Babad (personal communication 1996) says that the half-life data for EDTA measured by Camaioni et al. (1995) as a function of gamma dose rate equals about half the EDTA that degrades every 15 years. We presently consider the issue of organic constituents as insignificant to increasing plutonium solubility. To more quantitatively evaluate this factor, one could perform a few speciation calculations for supernate solutions with the highest concentration of EDTA presently found in tank supernates (~0.04 M).

7.2.3 Effects of Other Parameters on Plutonium Solubility

The possibility of large oxidation-reduction potential (Eh) and pH gradients in the tanks that could significantly affect plutonium are not considered credible at present. Some tanks (e.g., tanks AN-107 and C-106) may not contain as much free hydroxide as most other tanks, but evidence does not indicate that pH varies dramatically in individual tanks. The Eh in Hanford Site tanks was purposefully adjusted by adding sodium nitrite to lower the oxidation-reduction potential into a range that should minimize corrosion of the tank walls. The presence of excess nitrite can keep plutonium in the Pu(IV) valence state (Yamaguchi et al. 1994). This is consistent with the conclusions and choice of solubility-controlling solids and predominant aqueous plutonium species presented in this report. Eh is difficult to measure and many articles in the literature suggest that complex solutions and slurries with solids often show that some constituents are not in equilibrium with the measured Eh. We have found no evidence to suggest that plutonium or iron, a key neutron absorber that is also redox-sensitive, is behaving in unanticipated ways that could suggest that non-equilibrium reactions related to redox are dominant.

The effect of temperature on solubility for the chosen plutonium-controlling solid and predominant aqueous species is difficult to quantify. We have found sparse empirical data on the tank environment and only theoretical estimates of the thermodynamic data needed to calculate the effects of temperature using known chemical constructs that rely on enthalpy and heat-capacity measurements. Using the estimation technique presented by Lemire and Tremaine (1980), the solubility for amorphous Pu(IV) oxide/hydroxide would not be significantly affected by temperatures up to 100 °C. Required thermodynamic data for even the simple system, Pu-OH-H_2O, is not precisely known and is essentially nonexistent for complex systems, such as Pu-OH-CO_2-H_2O. This limits what we can say on this subject. Direct experimental observations of temperature effects on plutonium solubility in tank-related solutions are available in Hobbs et al. (1993), where tests at 60 °C showed no difference in observed plutonium solution concentrations from tests at room temperature.

The sparse literature available and calculations that extrapolate from tests involving few chemical components suggest that radiolysis will not have an important effect on plutonium solubility. Alpha decay is much more influential than beta or gamma decay in directly changing the solubility of solids, and the tanks do not contain high levels of alpha emitters. Also, the large inventory of solids in the tanks can readily buffer the hydrolysis species that form when ionizing radiation reacts with water. Some of the reaction products can change pH and Eh in the absence of large sources of buffering material (generally solids). Thus, our first impression is that radiolysis will not be a key parameter in changing the probability of nuclear criticality in Hanford Site tanks during continued inactive storage or active retrieval.

7.2.4 Solid Solution Phases

Plutonium recovery chemistry using the bismuth phosphate process depended on the tendency of plutonium to form solid solutions with bismuth and lanthanum ions. Studies conducted by Grebenshchikova et al. (1967a, 1967b) indicated that Pu(IV) formed solid solutions with lanthanum oxalates. Also,

tests by Hodgson et al. (1985) have shown that when zircalloy cladding removal wastes were treated with sodium hydroxide, transuranic constituents coprecipitated with zirconium hydroxide. As part of the plutonium separation process, data has been accumulated about the formation of plutonium solid solutions. This data (Coleman 1965, Penneman et al. 1980) about known Pu(IV) solid solutions is listed in Table 7-16.

Solid solution formation is a subset of coprecipitation phenomena in which two or more ions form a single solid phase. The solubility of a solid solution phase regulates the solution concentrations of each constituent ion at levels that may be significantly different from the solution concentrations of pure solid phases of each of the ions (Walton 1967). Typically, one of the conditions for solid solution formation is that the ionic radii of constituent ions should not differ significantly from each other (within 15 to 20 percent as cited in Walton 1967). Based on ionic radii data (Shannon 1976), we compared the ionic radii of Pu(IV) with those of other ions in the Hanford Site waste stream to determine which may potentially form solid solution phases with Pu(IV). The data show (Table 7-17) that only bismuth, cerium, lanthanum, thorium, uranium(IV), and zirconium are likely to form true solid solutions with Pu(IV). The Pu(IV) ion is too large to form solid solutions with either aluminum or iron in sixfold coordination. Therefore, the observed removal of Pu(IV) from suspended colloidal form by aluminum and Fe(III) hydroxide gels is probably a coagulation phenomenon, rather than the formation of thermodynamically definable solid solution phases, which involves removing Pu(IV) from the dissolved aqueous phase and substituting it into structural sites in gel phases.

Some experimental data confirms the potential formation of Pu(IV) solid solutions in certain Hanford Site waste streams. For instance, bench-scale tests on cladding removal wastes (CRW) conducted by Hodgson et al. (1985) showed that Pu(IV) can coprecipitate with lanthanum as a solid solution. Their data (Figure 7-8) showed that the decontamination factor (the ratio of initial plutonium concentration in solution to the plutonium solution concentration in equilibrium with the solid solution phase) ranged from 3 to 61 and was a function of lanthanum concentration. The decontamination factor (DF) of plutonium showed an exponential relationship with lanthanum concentration represented by Equation 7.2:

$$DF = 47.4e^{(219.0\,X)} - 46.6e^{(98.9X)} + 4108.6X \qquad (7.2)$$

where X represents the molar concentration of lanthanum.

These data showed that the mole fraction of plutonium in the lanthanum solid phase ranged from 2.9×10^{-3} to 3.18×10^{-2}, depending on the amount of lanthanum added to induce the precipitation of solid solution phases. Calculations indicate that, within the range of lanthanum concentrations used in these experiments, the resulting solid solutions would contain lanthanum/plutonium mole ratios of from 30 to 349. Hodgson et al. (1985) also indicated that when CRW was neutralized with sodium hydroxide, soluble transuranic elements were found to precipitate with zirconium hydroxide. The decontamination factors for Pu(IV) coprecipitating as solid solution with zirconium hydroxide were estimated to range from 10 to 100 (John L. Swanson, personal communication).

Available data indicate that some of the Hanford Site waste streams resulting from the bismuth phosphate process contained bismuth, lanthanum (used to coprecipitate plutonium in $BiPO_4$ and LaF_3 solid phases) and cerium (used as an oxidizer and a carrier precipitant for ^{144}Ce, a fission product). Waste streams containing Th(IV) were generated during the thoria campaigns of 1966 and 1970 (Agnew 1995). Therefore, Hanford waste streams containing constituents such as bismuth, cerium, lanthanum, and zirconium may have, on neutralization, precipitated as solid solution phases with Pu(IV). Although Hanford Site waste streams also contained uranium, Pu(IV) is unlikely to have coprecipitated with uranium solid phases because uranium in these wastes exist mainly in the U(VI) oxidation state (Agnew 1995).

7.2.5 Crystallization and Particle Size of Precipitated Phases

The upper size limit that crystalline particles may have and remain x-ray diffraction amorphous to analysis using standard mineralogy techniques can be estimated. Even crystalline particles will appear to be amorphous (showing no consistent lattice structure) if the average size of the particles is extremely small. Based on discussions in Klug and Alexander (1974), Bish and Post (1989), and Amonette and Zelazny (1994), we estimate that the minimum size that crystallites must reach to be measured by traditional powder x-ray diffraction as a very broad peak is 0.003 to 0.004 μm. According to Bartram (1967), crystallites smaller than 0.003 μm do not scatter the primary x-ray beam coherently; they contribute only to the background. Therefore, crystallites smaller than 0.003 μm have only short-range structural ordering and are x-ray amorphous. Peaks are still broad when the crystal size is up to nearly 0.1 μm (see Hsu 1977, p. 108), so literature must be reviewed carefully to attempt to discern whether the author is calling a mineral completely amorphous based on absolutely no diffraction patterns above a background noise, such as particles below 0.003 to 0.004 μm would give, or the author is calling very broad peaks amorphous. An author with this bent might call such very broad spectra resulting from particles as large as 0.1 μm amorphous.

A quantitative equation to estimate the crystallite size is known as the Scherrer equation and is defined as follows (Smith 1989):

$$D = (K \lambda)/[b \cos(\theta)] \tag{7.3}$$

where D = crystallite size in (Å)
- K = a shape constant (usually ~0.9)
- λ = the wavelength of the incident X-ray in (Å)
- b = the half-width of the diffraction profile of the sample (measured breadth minus instrumental blank breadth at same wavelength)
- θ = diffraction angle
- Å = angstroms (10^{-4} μm).

Equation 7.3 cannot be used to estimate the size of a crystal when the sample gives no peak distinguishable from the instrument background (where b becomes zero) but experts on XRD (x-ray diffraction) have used the value of 0.003 to 0.004 μm as an estimate.

If the initial precipitates formed by the fast neutralization of the Hanford Site acidic waste streams with sodium hydroxide are actually forming crystalline particles of less than 0.003 to 0.004 μm, the particles would appear amorphous to the traditional instrumentation (powder X-ray diffraction) used to identify solids with long-range structural ordering.

As described in various articles (e.g., Schwertmann and Cornell 1991, Stumm and Morgan 1981, Hsu 1977, and Cornell and Schwertmann 1979), many common oxides, such as aluminum, iron, copper, and zinc, appear to form very small crystallites that are interpreted as being amorphous at first, but grow and become "crystalline" with time. Schwertmann and Hsu prefer to think that the iron and aluminum crystallites, respectively, were essentially crystalline from the start, but the individual particles were too small to yield measurable x-ray diffraction patterns. These authors are considered by many earth scientists to be the leading experts on the mineralogy and soil chemistry of these two important compounds and several of us endorse their concepts.

Because small particles exhibit very large surface energy (Stumm and Morgan 1981) they are thermodynamically less stable than larger particles of the same mineral. This instability is a driving force for the small particles to agglomerate into more stable larger particles. Once the particles reach a size above perhaps 0.003 μm, they start looking crystalline to x-ray diffraction analyzers. In nature and in the laboratory, crystalline ferric oxides and aluminum oxides often are found as discrete particles of 0.1 to 10 μm.

Schwertmann and Cornell (1991) show that pure ferric oxides follow the stated trends and transform into several larger-sized crystalline forms in a few days to a few weeks, depending on the chemical and thermal conditions. Cornell and Schwertmann (1979), Hsu (1977), and others, concede that recrystallization to form larger particles can be retarded or inhibited by other dissolved species in the system. Some of the most efficient inhibitors of recrystallization are simple organic acids such as citrate and, to a much lesser extent, oxalate and fulvic acids from the decay of plant matter. Interestingly, these simple acids become much less effective at pH values of 11 or higher, which is the range most common in Hanford Site tanks.

Various mechanisms have been proposed to explain how crystalline growth to larger sizes is inhibited. One process is the adsorption of the organic acids onto either the very small crystals' surfaces or the larger crystals' surfaces that already appear crystalline, blocking further crystal growth. Another process could be the complexation of soluble iron to the extent that the system becomes undersaturated in iron and the crystals tend to redissolve to reestablish equilibrium. In some instances the organic acid does not stop crystal growth, but does change the type of ferric oxide that dominates (e.g., hematite vs. goethite). This is because the organic acid adsorbs onto specific sites on the surface of the iron oxide lattice. The presence of the organic acid blocks further growth (bonding of more ferric and oxide molecules) along that direction of the crystal. Because the difference between ferric oxide minerals often is only the number of molecules that attach to one or another axis in three-dimensional space, if one axis gets blocked, growth will occur on the other axes, which changes the type of mineral formed.

Hsu (1977) discusses the inhibition/retardation of particle growth for crystalline aluminum hydroxide (gibbsite and bayerite, $Al(OH)_3$) and aluminum oxyhydroxides (boehmite and diaspore, AlOOH). Anions, such as sulfate, phosphate, and silicate, that have a strong affinity for Al^{3+} in solution can tie up the Al^{3+} ions and sterically hinder the growth of the Al-OH polymer units that become the mentioned solids once enough have aggregated. The organic acids, such as citrate, impede aluminum hydroxide and oxyhydroxide in the same way as for the iron hydrous oxides (Kwong and Huang 1975). Again, the impact of these other ligands (anions) on the tank solutions is not easily quantified, but some indications are that the high pH, elevated temperatures, and long periods (~30 to 50 years) available for reaction, all favor the eventual recrystallization of partly crystalline products. Evidence in the Hanford Site, Savannah River, and Russian literature germane to defense waste tanks indicates that crystalline aluminum and iron hydroxide, oxide, and oxyhydroxide compounds are present (Hobbs 1995, and Zakharova and Ermolaev 1995). No literature studies have been identified that discuss the particle size or nature of plutonium solids within Hanford Site or other nuclear defense sludges. However, expecting that plutonium would act similarly to metals such as iron and aluminum for which some literature has been assimilated is logical.

Another interesting phenomenon related to particle size is the variability of a compound's solubility as a function of particle size. According to Stumm and Morgan (1981), finely divided particles (small crystallites) exhibit higher solubility than large crystals. Consequently, small crystals are thermodynamically less stable and should recrystallize into large ones. For particles smaller than about 1 μm or with a specific surface area greater than a few m^2/g, the surface energy is large enough to influence the surface properties of the particle and the free energy of the solid. Experimenters such as Schindler (1967) and Schindler et al. (1965) investigated the effect of particle size (and surface area of the particle) on the solubilities of ZnO, $Cu(OH)_2$, and CuO. Stumm and Morgan (1981) show that the solubility of the various compounds changes as a function of surface area by a theoretical ratio that relates the change in free energy of the particles to surface tension at the solid-solution interface. For ZnO, the solution concentration of zinc decreases by almost 30 times as the particle size of the ZnO increases from 0.0046 to 0.0560 μm, although these particle sizes are generally smaller than those usually measured for the aluminum and iron oxides. Further, the particle size plays a role in transforming one polymorph to another, such as $Cu(OH)_2$ to CuO or $Zn(OH)_2$ to ZnO. As discussed in Stumm and Morgan (1981), Schindler et al. describe how copper oxide that is 10 times more stable than copper hydroxide becomes less stable as the particle size decreases until, at a size of 0.004 μm, the CuO is less stable than the $Cu(OH)_2$. This is because the oxide exhibits a higher surface tension (interfacial energy) than the hydroxide and a cross-over in overall Gibbs free energy (thermodynamic stability) occurs as the particle size decreases for both compounds. The authors and cited experimental investigators suggest that this is why copper hydroxide forms first when acid solutions of copper ion are neutralized. This phenomenon may be another mechanism that explains why scientists find or claim that hydroxides form first during the rapid neutralization of acidic solutions, but that, with time, crystalline oxides are found.

As discussed previously, detailed solubility data as a function of particle size (and surface area of the particle) is available for only a few solids such as ZnO, $Cu(OH)_2$, and CuO. A literature search revealed that similar solubility vs particle size data for $PuO_2 \cdot xH_2O$ is not available. However, if we assume that the relationship between solubility and particle size for $PuO_2 \bullet xH_2O$ is similar to that for ZnO and $Zn(OH)_2$, the particle size of fresh and aged $PuO_2 \cdot xH_2O$ can be estimated. This implies that the differences in crystal structures of $Zn(OH)_2$ and $PuO_2 \bullet xH_2O$ do not affect the relationship.

Because freshly precipitated $PuO_2 \bullet xH_2O$ is x-ray amorphous, we can conclude that the bulk of this material may consist of particles smaller than 0.004 μm. Studies conducted by Andelman and Rozzell (1970) showed that the bulk of freshly precipitated $PuO_2 \bullet xH_2O$ exists as colloids that are not settlable thorough centrifuging. Studies of long-term aging of $PuO_2 \bullet xH_2O$ by Rai et al. (1980) and Delegard (1987) showed decreases in solubility, which indicates that particle growth occurred, along with a concomitant increase in crystallinity (long-range structural ordering). Further, x-ray diffraction data obtained on aged (over 3 years) $PuO_2 \bullet xH_2O$ precipitates showed that the precipitate had crystallized, resulting in particle growth and decreased solubility (Rai et al. 1980).

Therefore, assuming that the solubility-particle size relationship for zinc hydroxide precipitates observed by Schindler (1967) applies to $PuO_2 \bullet xH_2O$ precipitates, and using the data for equilibrium solubilities of fresh and aged precipitates from Rai et al. (1980) and Delegard (1987), we can calculate the following relationship for the average diameter of the smallest particle sizes that control plutonium solubility.

$$d \text{ (Angstroms)} = 2740 \exp (3 \times \Delta \log K_{sp}) + 35 \qquad (7.4)$$

Where d = particle diameter of plutonium oxide in angstroms
$\Delta \log K_{sp}$ = the difference in equilibrium solubility between the crystalline phase and a phase with lower crystallinity

The solubility data obtained by Rai et al. (1980) indicated that the solubilities between freshly precipitated and aged $PuO_2 \bullet xH_2O$ differed by about two orders of magnitude. Using this assumption, we can calculate that the smallest particles in aged $PuO_2 \bullet xH_2O$ material has an average diameter of about 0.3 μm. This calculation provides the smallest particle size that controls the solubility. The largest particle size can be estimated based on the particle-size distribution data obtained by Andelman and Rozell (1970). This data showed that the upper bound is approximately an order of magnitude higher than the smallest particle size in the plutonium-hydroxide colloidal mass. From this, we estimate that aged Pu(IV) oxyhydroxide has about 60 percent of the particles by mass less than 2 μm in size. About 40 percent of the mass of aged particles may range from about 2 to 8 μm in size. As shown by Andelman and Rozell (1970), ionic strength, presence of ligands, and other particulates will affect the particle size distribution of $PuO_2 \bullet xH_2O$.

In summary, one might infer that the particle sizes of precipitates in the Hanford Site tank sludge should be the same as that assessed from literature data. Some of the chemists on the review team believe that all the

metals present in the acid waste stream that form insoluble hydroxide-like phases, and probably those that form insoluble phosphate, sulfate, or carbonate compounds, follow a similar path. First, particles that range from less than nanometer (<0.001 μm) to 0.004 μm form, but have fixed chemical structures. Over time, these crystallites grow, driven by the thermodynamic need to shed excess surface energy, eventually reaching a threshold size that is identified as crystalline using traditional techniques, such as powder x-ray diffraction. Their size at this point is somewhere larger than 0.003 μm, depending on the author's criteria for calling the x-ray diffraction peaks sharp enough to qualify as crystalline. Crystalline compounds of these metal oxides/hydroxides formed in the laboratory or isolated from natural soils/sediments often range in size from 0.1 to 10 μm.

This crystal growth process has been recognized for at least a century. In early literature it is referred to as Ostwald Ripening. A succinct definition of Ostwald Ripening is the process wherein small crystals, which are more soluble than large ones, dissolve and reprecipitate onto larger particles.

The concept of solubility/precipitation is more well developed from first principles than is adsorption/desorption and is often used in bounding fate and transport analyses to estimate the distribution of contaminants between the solution and solid phases. Solubility constructs give an upper bound on the concentrations that one would expect to be in a mobile solution phase in equilibrium with solids, whereas any coincident adsorption-desorption reactions should only cause lower amounts of the contaminant to be found in solution. Because adsorption processes are less well understood and quantifiable than solubility, a complete review takes longer and can lead to less definitive results. Section 7.3 summarizes our findings on plutonium adsorption in tank-like environments.

7.3 ADSORPTION

Adsorption reactions are less well quantified than solubility reactions and generally lead to even lower concentrations of such materials as plutonium in solution. Most of the waste streams disposed of in tanks were acid liquids bearing high concentrations of dissolved metals such as aluminum, iron, chromium, manganese, bismuth, zirconium, uranium, etc., and low concentrations of plutonium that were neutralized with NaOH and sometimes carbonate-bearing solids. The rapid neutralization of acidic metal-bearing solutions with caustic leads to the precipitation of large amounts of oxyhydroxide solids (sludge).

Such neutralization not only precipitated the bulk of the metals in the waste, but coprecipitated and/or adsorbed various trace metals such as plutonium associated with reprocessing or waste management. Such sludge materials were allowed to settle in cascaded single-shell waste tanks. The essentially radionuclide-free supernate was then released to soil columns in a variety of engineered structures. Most reprocessing and product purification operations either used iron-containing reagents in sufficient quantities to moderate any fissile materials present or added iron-containing reagents during waste neutralization steps. Thus, the adsorption literature review

focussed on adsorption/coprecipitation of plutonium onto iron and aluminum and, to a much lesser extent, oxides of manganese, chromium, etc.

The same parameters that affect solubility were investigated:

1. Hydrolysis—pH effects
2. Soluble inorganic and organic complexation
3. Radiolysis
4. Redox
5. Ionic strength
6. Temperature effects on parameters 1 through 5
7. Time (aging, recrystallization).

7.3.1 Introduction

Adsorption is the process of net accumulation of ionic or molecular species at the interface between a solid phase and an aqueous phase. Adsorption differs from precipitation in that adsorption is a two-dimensional process and precipitation connotes a three-dimensional process of solid growth (Corey 1981). Although both these phenomena basically involve mass transfer of ionic and molecular species from aqueous phase to solid phase, the fundamental molecular processes differ significantly. Thus, data from any experiment that relies solely on monitoring mass transfer between liquid and solid phases without measuring other important factors cannot be used to distinguish between adsorption and precipitation.

The fact that mass transfer data fits any one of several adsorption isotherms does not confirm that adsorption is the controlling phenomenon. Extensive discussions about distinguishing between the two- and three-dimensional mass transfer processes (adsorption and precipitation) have been provided by Corey (1981) and Sposito (1986). The difficulty in distinguishing between these two processes based on insufficient and/or inadequate data led Sposito (1986) to formulate the following two rules:

- The adherence of experimental "sorption" data to an adsorption isotherm equation provides no evidence that the actual mechanism occurring is an adsorption process.

- The experimental observation than an ion-activity product is smaller than a corresponding solubility product constant provides no evidence that the principal mass transfer mechanism is adsorption.

The first rule is based on the fact that both adsorption and precipitation data can be fitted with well known isotherms. Data fit to an isotherm cannot be used as unequivocal proof that the principal process is adsorption. The second rule is based on formation of solid solutions possibly resulting in measured solubility products that are less than solubility products for pure precipitates. Another mechanism that can be misinterpreted as adsorption is the coagulation of pure-phase colloids by solid-phase substrates. This is especially true in the case of tri- and tetravalent cations such as lanthanides and actinides (Kinniburgh and Jackson 1981). These ions undergo strong hydrolysis resulting in precipitation of colloidal

hydroxides (Kepak 1971). These radiocolloids are hard to detect in the presence of a large amount of another solid, and their coagulation and settling with the other solids may lead to misinterpreting the observed reaction as true adsorption.

Following a detailed discussion of adsorption versus precipitation phenomena, Corey (1981) set forth the following six conditions that help interpret and judge the validity of existing adsorption data and also help guide investigators in designing appropriate adsorption experiments.

1. Even though bonding mechanisms are similar, specific adsorption is a two-dimensional phenomenon, whereas precipitation is a three-dimensional process.

2. Ions specifically adsorbed on substrates form solid solutions that are similar to solid solutions that form from the conventional precipitation process.

3. Relatively small deviations from theoretical concentrations may occur for precipitated solids at solubility equilibrium because particle size differs, polymorphic forms are present, or solid solutions form.

4. Concentrations of ions that are minor constituents in natural systems are usually controlled by either solid-solution equilibria or adsorption reactions.

5. Heterogeneous nucleation of a new solid phase involving adsorbed ions occurs only when a critical supersaturation is exceeded. Below critical supersaturation, ideal adsorption reactions may prevail.

6. Interpretations of many adsorption reactions are suspect because they are carried out in systems supersaturated with respect to potential new solid phases involving the ion of interest.

A review of adsorption and related processes led Davis and Hayes (1986) to conclude that interfacial reactions at solid surfaces such as adsorption, ion exchange, and precipitation are interrelated and that detailed studies are needed to identify the dominant mechanism.

During the last two decades, a class of adsorption models based on electrostatic interactions between adsorbates and sorbent surfaces has increasingly been used in interpreting experimental data. Detailed descriptions and comparisons of these models have been provided by Westall and Hohl (1980), Benjamin and Leckie (1981), Morel et al. (1981), Barrow and Bowden (1987), and Davis and Kent (1990). These models provide molecular-level interpretation of adsorption phenomena compared to non-electrostatic models (isotherm models). However, that these models can be applied to experimental data does not prove that adsorption is the controlling phenomenon in such experiments. Application of Corey's validity criteria and direct determination of species on solid surfaces via various spectroscopic techniques are also necessary to establish that adsorption is the dominant process in the system being investigated (Sposito 1986).

7.3.2 Adsorption Substrates in the Waste Tank Environment

The HLW generated during the plutonium separation process was rapidly neutralized (caustic strike) before storage in waste tanks. Experimental data from literature indicate that such rapid neutralization of acidic solutions containing iron and aluminum causes the formation of microcrystalline/x-ray amorphous ferric hydroxide (ferrihydrite) and aluminum hydroxide precipitates. Hanford Site HLW waste compositions indicate that these two solids form major adsorption substrates for plutonium in tank sludges. When no complexing ligands, such as dissolved carbonate, are present, freshly precipitated iron and aluminum hydroxides form. The fresh precipitates exhibit large surface areas and are capable of adsorbing large amounts of dissolved cationic species. Such high cationic adsorption capacities are caused by the large number of negatively charged adsorption sites that these substrates contain as a consequence of deprotonation of surface hydroxyl groups. Increasing the solution hydroxyl concentration (i.e., increasing pH) results in increasing deprotonation of surface hydroxyl groups. The cation adsorption capacities of these substrates increase as a function of increasing pH.

Most of the high-level radioactive waste solutions generated from chemical operations at the Hanford Site were acidic solutions containing metals dissolved in nitric acid. Concentrations of dissolved plutonium (typically $<10^{-5}$ M plutonium) that were not recovered in processing were also present in these waste solutions. Before sending the waste to underground tanks, the acid was neutralized with excess sodium hydroxide (containing unknown concentrations of sodium carbonate) to prevent corrosion of the carbon steel tanks. Metals, including plutonium, that were insoluble in basic solutions were precipitated as oxyhydroxides during neutralization. These oxyhydroxides are the major components of sludge in the tanks.

Concentrations of plutonium were very small compared to the other metals from the processing operations that were dissolved in the waste solutions (Braun et al. 1994). Typical mole ratios of iron/plutonium and aluminum/plutonium in the Hanford Site waste streams were 12,000 and 28,000, respectively, for bismuth phosphate waste; 1,400 and 132,000, respectively, for REDOX waste; 63,000 and 1,400,000, respectively, for PUREX aluminum-clad waste; 3,300 and 13,000, respectively, for PUREX Zirflex waste; and 100 and 7,400 respectively for plutonium finishing wastes. These ratios do not include iron added to the waste as a criticality control. In addition to iron and aluminum, other dissolved metals such as uranium, zirconium, manganese, bismuth, chromium, nickel, and tin were present in the acid waste and were precipitated as oxyhydroxides.

For example, the waste composition in tank C-106 (Sederburg 1994) consists mainly of sludge solids (746,000 L) and liquid supernate solution (182,000 L). The tank received tributyl phosphate waste from the uranium recovery process from 1954 to 1963, neutralized PUREX acid waste from 1958 to 1963, aluminum cladding waste from 1958 to 1963, PUREX organic wash waste from 1969 to 1974, and B Plant complexed waste from 1974 to 1978. This resulted in a sludge with high concentrations of iron, aluminum, silicon, and phosphate. The iron/plutonium and aluminum/plutonium mole ratios are about 4,500 and 5,800 in the sludge. The supernate solution has high concentrations of sodium

(4.0 M), nitrate (1.1 M), and carbonate (0.75 M). The plutonium concentration in the supernate is 0.0035 g/L (1.5×10^{-5} M).

In a nitric acid solution containing Pu(IV) as the only dissolved hydrolyzable metal ion, neutralization with sodium hydroxide, as required for waste solutions sent to the tanks, would produce plutonium polymer along with plutonium hydroxide. However, because of the low solubility of iron and aluminum hydroxides and their much higher initial concentrations in the waste solution, these compounds may precipitate first as the waste is neutralized and plutonium may be coprecipitated with them. A comparison of solubilities (with only dissolved hydrolytic species--no other complexants present) of crystalline $PuO_2 \bullet xH_2O$ (Allard 1982, Rai et al. 1980), amorphous $Fe(OH)_3$ (Lindsay 1979), and crystalline $Al(OH)_3$ (gibbsite) (Lindsay 1979) suggests this possibility. Assuming no significant kinetic differences, one could surmise that iron may precipitate before any plutonium can precipitate as plutonium oxyhydroxide during the waste neutralization process. Thus, the iron hydroxide sludge would be present and capable of adsorbing the plutonium from the solution before it could form its own precipitate. However, no experimental data derived under waste tank conditions exists to corroborate this hypothesis.

Amorphous iron is slightly less soluble than crystalline plutonium hydroxide and much less soluble than amorphous plutonium hydroxide. Because the waste contains thousands of times more iron and aluminum than plutonium, the possibility exists that a pure plutonium phase (plutonium hydroxide or polymer) may not form. Rather, the plutonium may be adsorbed on the iron and aluminum hydroxides that may precipitate first in much larger quantities.

Typical concentrations of plutonium in the acid wastes range from 10^{-5} to 10^{-6} M. At these low concentrations, incipient polymerization of plutonium hydroxide may require a relatively high pH. Also, polymerization is not instantaneous, but requires an induction period before it is formed (Toth et al. 1981). Although polymer formation is unlikely, any polymer that is formed has a strong affinity to adhere to other particles suspended in solution or on nearby surfaces (Dran et al. 1994).

Several likely coprecipitation mechanisms are important. First, sorption of plutonium hydroxide on the large surface areas of the solid metal oxyhydroxides is the most important mechanism. The sorption capacity (in terms of available sorption sites) for iron oxyhydroxide gel has been estimated to be about 500 μmoles/mole iron (Kinniburgh and Jackson 1981). This capacity greatly exceeds the molar ratios of plutonium/iron in the waste tank sludges, which range from about 0.016 to 10 μmole plutonium/mole of iron.

The hydrolysis of metal ions has been studied extensively (Baes and Mesmer 1976). As these hydrolysis reactions occur,a tendency has been shown for the ions to aggregate through hydroxyl bridging, forming dimers, trimers, or extensive polymeric networks that can reach colloid dimensions. These polymers can then condense with the loss of water to form oxygen-bridged polymeric species (Thiyagarajan et al. 1990). The polymers can contain more than one metal hydroxide (hydroxides of other metal ions present in the initial solution mixtures) bonded to the polymer. For example, if U(VI) is present during $PuO_2 \bullet xH_2O$ and $Th(OH)_4$ polymerization, the U(VI) is bonded through hydroxyl bridges to the polymer (Toth et al. 1981, 1984). Hydroxyl

bridge bonding is similar to that proposed for surface complexation models of sorption of hydrolyzable metal ions on oxide surfaces (Schindler 1981, Davis et al. 1978). Surface complexation models have been successfully used to predict sorption of uranyl ions onto amorphous iron oxyhydroxide, goethite, and hematite solids (Hsi and Langmuir 1985). Structures of uranyl (VI) complexes at the surface of clay minerals have been identified by Chisholm-Brause et al. (1994). These studies suggest that the trace levels of $PuO_2 \bullet xH_2O$ formed during neutralization of acidic wastes may be bonded to other oxyhydroxides that are present in much greater abundance in the sludge waste.

These observations indicate that sorption may be one of the mechanisms for removing plutonium from solution. However, because none of the experimental observations were conducted under precisely the conditions existing in Hanford Site waste tanks, some extrapolation is needed to determine that adsorption is the dominant mechanism.

Several changes take place as the precipitated substrates begin to age in the supernatant waste solution. One of these changes is the microcrystalline particles growing into larger crystalline particles that produce distinctive x-ray diffraction patterns. Experimental data shows that, with aging under very high pH conditions, ferric hydroxide precipitate converts to a well-crystallized oxyhydroxy mineral, goethite (FeOOH) and, with continued aging, to a crystalline oxide phase, hematite (Fe_2O_3). Similarly, the aluminum hydroxide precipitate converts first to a more crystalline gibbsite and, with continued aging, to an oxyhydroxy phase known as boehmite (AlOOH).

The second change that occurs as the precipitated substrates age to more crystalline phases is that in the cation adsorption capacity of the substrates with higher crystallinity is reduced. These materials with larger size crystallites contain smaller surface areas, and so have fewer ionizable surface hydroxyl sites. Goethite, hematite, and boehmite types of phases have been identified in some of the HLW sludges from the Hanford Site and Russia (Liu et al. 1995; Zakharova and Ermolaev 1995). However, data does not exist regarding the rate of crystallization of fresh precipitates when aged under very high ionic strengths, higher temperatures, and in the presence of high concentrations of both inorganic and organic ligands--conditions typically encountered in tanks containing HLW. Therefore estimating the relative proportions of different crystalline phases that currently exist in the waste tank sludges is difficult. Hanford site HLW sludge data (Appendix D) indicates that major waste constituents (aluminum and iron) not only exist as pure phase hydroxides and oxyhydroxides, but also as solid solution hydroxides, oxyhydroxides, silicates and phosphates. Therefore, it appears that the HLW sludge chemistry is much more complex than hypothesized precipitation of only hydroxide phases upon neutralization.

7.3.3 Tetravalent Plutonium Adsorption on Iron and Aluminum Oxide/hydroxide Substrates

Empirical data does not exist regarding adsorption of Pu(IV) species on iron- and aluminum-oxide/hydroxide substrates under typical HLW tank conditions (very high ionic strengths, higher temperatures, and high concentrations of both inorganic and organic ligands). However, a number of investigators have examined potential adsorption of plutonium on minerals, soils, and other geological substrates. Experiments conducted by Ticknor (1993) showed that plutonium sorbed on goethite and hematite from slightly basic solutions [(pH: 7.5) containing high dissolved salts, but extremely low bicarbonate concentrations (8.2×10^{-6} to 2.9×10^{-4} M)] with affinities reflected by distribution coefficients, K_d, ranging from 170 to 1,400 mL/g.

According to Pius et al. (1995), significant removal of Pu(IV) from solutions containing 0.1 to 1 M concentrations of sodium carbonate was observed with alumina, silica gel, and hydrous titanium oxide as substrates. These investigators also noted that the presence of carbonate lowered the sorption distribution coefficient for these adsorbents. However, even at 0.5 M carbonate, the coefficients were 60 mL/g, 1,300 mL/g, and 15,000 mL/g, respectively, for alumina, silica gel, and hydrous titanium oxide. In another study using bicarbonate solutions, the distribution coefficient for Pu(IV) sorption on alumina was lowered to about 30 mL/g at 0.5 M bicarbonate (Charyulu et al. 1991). However, one should note that the initial concentrations of Pu(IV) used by these investigators ranged from 8.4×10^{-6} to 4.2×10^{-5} M, which means that the solutions were probably supersaturated with respect to $PuO_2 \bullet xH_2O$ solid phase. Because the experimental conditions used by Pius et al. (1995), and Charyulu et al. (1991) do not fit Corey's criteria, the principal mechanism of plutonium removal from solution could have been precipitation as easily as adsorption.

Barney et al. (1992b) measured adsorption of plutonium from carbonate-free wastewater solutions onto commercial alumina adsorbents over a pH range of 5.5 to 9.0. Plutonium adsorption K_d values increased from about 10 mL/g at a pH of 5.5 to about 50,000 mL/g at a pH of 9.0. The slopes of the K_d compared to the pH curves were close to one, which indicated that one hydrogen ion is released to the solution for each plutonium ion that is adsorbed on the alumina surface. This behavior is typical of adsorption reactions of multivalent hydrolyzable metal ions with oxide surfaces. Changing the initial concentration of plutonium from about 10^{-9} to 10^{-10} M did not affect the Kd values, which showed that plutonium precipitation was not significant in these tests. Also, the initial plutonium concentrations were below the measured solubility limits of plutonium hydroxide. This experiment demonstrated that in carbonate-free systems, plutonium would be adsorbed on alumina substrates.

Delegard et al. (1984) performed tests to identify tank waste components that could significantly affect sorption of plutonium on three shallow sediments typical of the Hanford Site. They found that sorption was decreased by the chelating agents, 0.05 M ethylenediaminetetraacetate (EDTA) and 0.1 M N-2-hydroxyethylethylenediaminetriacetate (HEDTA), but not by low concentrations of carbonate (0.05 M). Delegard's data also showed that roughly a twofold increase in ionic strength caused an order of magnitude decrease in plutonium adsorption. Sorption of Pu(IV) on a Hanford Site

shallow sediment from a synthetic groundwater containing very low (0.003 M) carbonate ranged from about 5,000 mL/g to 30,000 mL/g (Barney 1992a).

Another study of Pu(IV) adsorption on goethite was conducted by Sanchez et al. (1985). The experimental conditions used by these investigators were evaluated for assessing whether the reaction being studied was indeed adsorption. The initial Pu(IV) concentrations used in their experiments were 10^{-10} and 10^{-11} moles per liter. These concentrations are well below the equilibrium saturation levels for $PuO_2 \bullet xH_2O$. The equilibrating solutions used in these experiments contained salts such as $NaNO_3$, NaCl, Na_2SO_4, and $NaHCO_3$ and did not contain any ionic constituents that may have potentially formed solid solution precipitates. Therefore, it is reasonably certain that the dominant reaction being studied was adsorption and not precipitation of pure or solid solution phases.

The Pu(IV) adsorption data obtained in 0.1 M $NaNO_3$ electrolyte medium (Figure 7-9) indicated an isotherm typical of metal and/or metal-like complex species adsorption on substrate (Benjamin and Leckie 1981). This indicates that Pu(IV) is adsorbing onto the ionized hydroxyl sites in the form of Pu^{4+} and its hydrolytic species, $PuOH^{3+}$, $Pu(OH)_2^{2+}$, $Pu(OH)_3^{+}$, and $Pu(OH)_4^{0}$, with metal ion and the metal-ion part of the complex adsorbing onto the surface. The adsorption isotherm obtained at the higher initial concentration (10^{-10} M) of total soluble Pu(IV) showed that the adsorption edge (pH value at which 50 percent adsorption occurs) increased towards a higher pH value, which is typical of the metal-like adsorption behavior of adsorbing species (Benjamin and Leckie 1981). Adsorption data for another tetravalent actinide (thorium) generated by LaFlamme and Murray (1987) (see Figure 7-10) and Righetto et al. (1988) confirms the typical adsorption behavior generally observed for higher valence actinides adsorbing onto iron and aluminum oxides, hydroxides, and oxyhydroxide surfaces.

The Pu(IV) adsorption data obtained in a medium of 0.1 M $NaNO_3$ represents the condition where only free cation and the hydrolytic species are the adsorbing species. Extensive experimental observations have shown that, when present, strong complexing agents have a significant effect on the metal ion adsorption (Benjamin and Leckie 1981). This modified adsorption behavior in the presence of complex-forming ligands is characterized by Benjamin and Leckie as ligand-like adsorption. Sanchez et al. (1985) also conducted experiments to examine the effect of dissolved carbonate (from 10 to 1,000 meq/L) on the adsorption of Pu(IV) on goethite. Their adsorption data showed that at a fixed pH value of 8.6, increasing carbonate concentration decreased the adsorption of plutonium (Figure 7-11). This data demonstrated that practically no Pu(IV) adsorption occurred on goethite when the total carbonate concentration approached 1,000 meq/l (0.5M CO_3).

Such complete suppression of Pu(IV) adsorption was attributed to the presence of anionic plutonium-hydroxy carbonate species in solution and to the fact that goethite at this pH contains mainly negatively charged sites that have negligible affinity to adsorb anionic species. This adsorption behavior of Pu(IV) in the presence of carbonate ions that form strong hydroxy carbonate complexes (see Section 7.1) is typical of ligand-like adsorption of metal ions described by Benjamin and Leckie (1981). Ligand-like adsorption is described as adsorption of a metal-ligand complex that is analogous to adsorption of the

free ligand species. Also, the metal-ligand complexes may not adsorb at all if these complexes are highly stable.

Th(IV) showed similar adsorption behavior in the presence of total carbonate concentrations ranging from 10 to 1,000 meq/l (LaFlamme and Murray 1987; see Figure 7-12). Righetto et al. (1988) conducted a study on adsorption of Th(IV) species, a surrogate for Pu(IV) on aluminum oxide surfaces. These data showed that in solutions containing 100 meq/l of carbonate concentration, significant reduction in Th(IV) adsorption occurred when pH increased from 8.5 to 9.8. This experiment (Righetto et al. 1988) also showed that under these pH conditions, the presence of an organic ligand also significantly retarded Th(IV) adsorption on aluminum oxide.

These data clearly demonstrate that increasing total carbonate and hydroxyl solution concentrations significantly decrease tetravalent actinide adsorption on iron and aluminum oxide, and oxyhydroxide surfaces. Using these data, we developed an adsorption envelope to represent the behavior of Pu(IV) on goethite in the presence of increasing carbonate concentrations and pH. The three-dimensional graph (Figure 7-13) represents the different degrees of Pu(IV) adsorption on goethite as a function of two variables (dissolved carbonate and hydroxyl concentrations). Two contour plots (Figures 7-14 and 7-15) are also provided to help visualize adsorption isopleths in carbonate-pH and carbonate- adsorption planes. The adsorption envelope (Figures 7-13 through 7-15) shows that Pu(IV) adsorption onto goethite may be completely suppressed under certain combinations of carbonate and hydroxyl concentrations.

Similar suppression of adsorption of higher valence state actinides in the presence of carbonate and hydroxyl ions has been observed by a number of investigators. Some of these studies include Pu(V) adsorption on goethite (Sanchez et al. 1985); adsorption of U(VI) on goethite (Tripathi 1984, Hsi and Langmuir 1985, Koehler et al. 1992), ferrihydrite (Payne et al. 1992), and clinoptilolite (Pabalan and Turner 1992); and Np(V) adsorption on ferrihydrite, hematite, and kaolinite (Koehler et al. 1992).

Although empirical data do not exist regarding adsorption of Pu(IV) species on iron- and aluminum-oxide/hydroxide substrates under typical HLW tank conditions (very high pH, significant carbonate concentrations, presence of other complex forming organic and inorganic ligands, high ionic strengths, high temperatures) we can use the existing experimental data to draw some conclusions regarding the adsorption of Pu(IV) on precipitated substrates.

- The tank supernatants are typically very highly alkaline and contain significant concentrations of dissolved carbonate.
- Pu(IV) in aqueous phase is likely to be present as anionic plutonium hydroxy and/or plutonium-hydroxy-carbonate species.
- Tank supernatants also contain other ligands that are known to retard or block the adsorption of Pu(IV) species.

These conditions led some chemists on the review team to conclude that plutonium adsorption onto hydrous oxides in waste tanks may not be a significant factor in plutonium partitioning between liquid and solid phases.

Other members of the team believe that the extraordinarily high pH, the large amount of iron and aluminum adsorbtion substrates present, the intimate mixing of fresh precipitates at the time of neutralization, and the hydroxly bridging of mixed oxides during aging will result in strong adsorption of the plutonium to the more common hydrous oxide tank sludge.

Figure 7-1. Distribution of Pu(IV)-Hydroxycarbonate Species as a Function of pH at Fixed Total Carbonate Concentration of 1.0 M (from Tait et al. 1995).

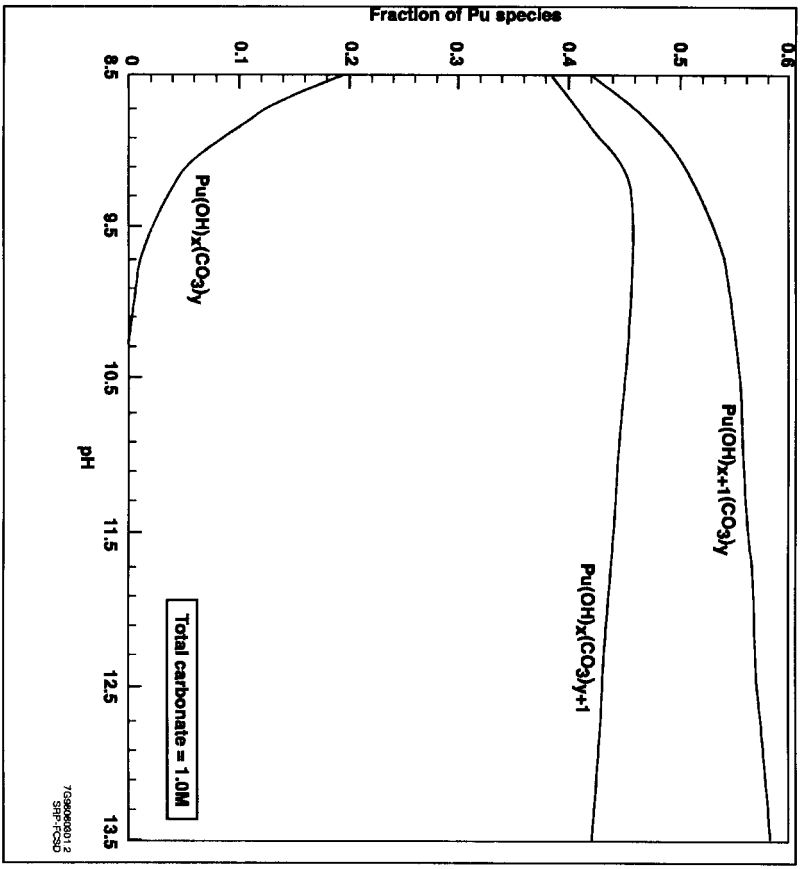

Figure 7-2. Distribution of Pu(IV)-Hydroxycarbonate Species as a Function of Total Carbonate Concentration at a Fixed pH of 8.5 (from Tait et al. 1995).

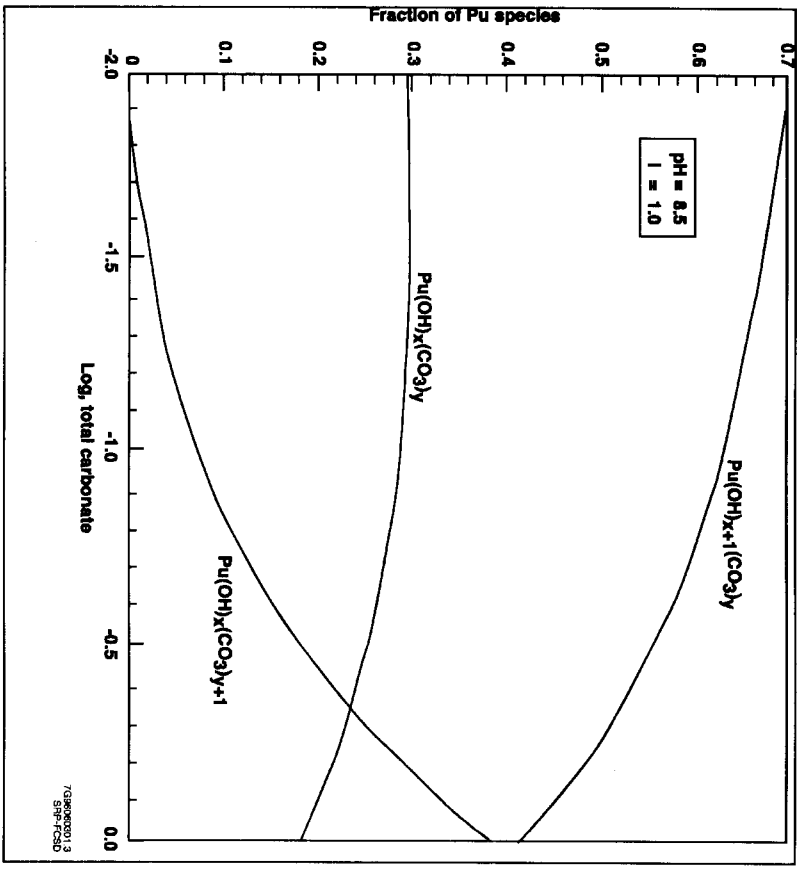

Figure 7-3. Computed Distribution of Pu(IV) Aqueous Species as a Function of pH at a Fixed Carbonate Concentration of 0.001 M.

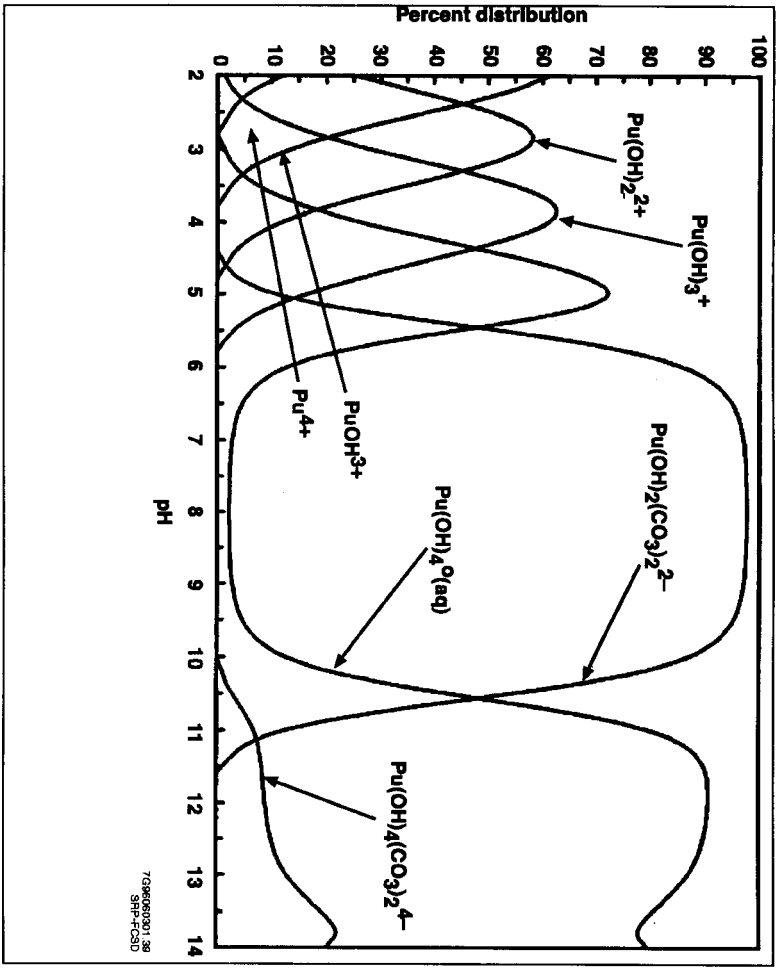

Figure 7-4. Computed Distribution of Pu(IV) Aqueous Species as a Function of pH at a Fixed Carbonate Concentration of 0.05 M.

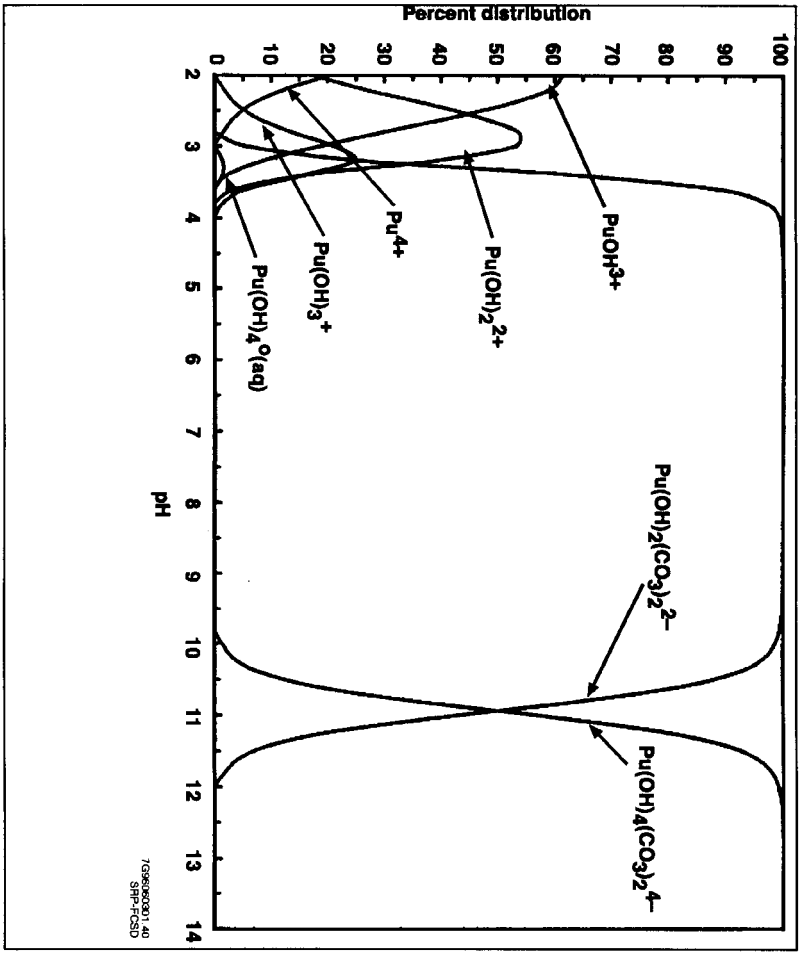

Figure 7-5. Experimental Data for Solubility of $PuO_2 \bullet xH_2O$ as a Function of pH and Total Carbonate Concentration.

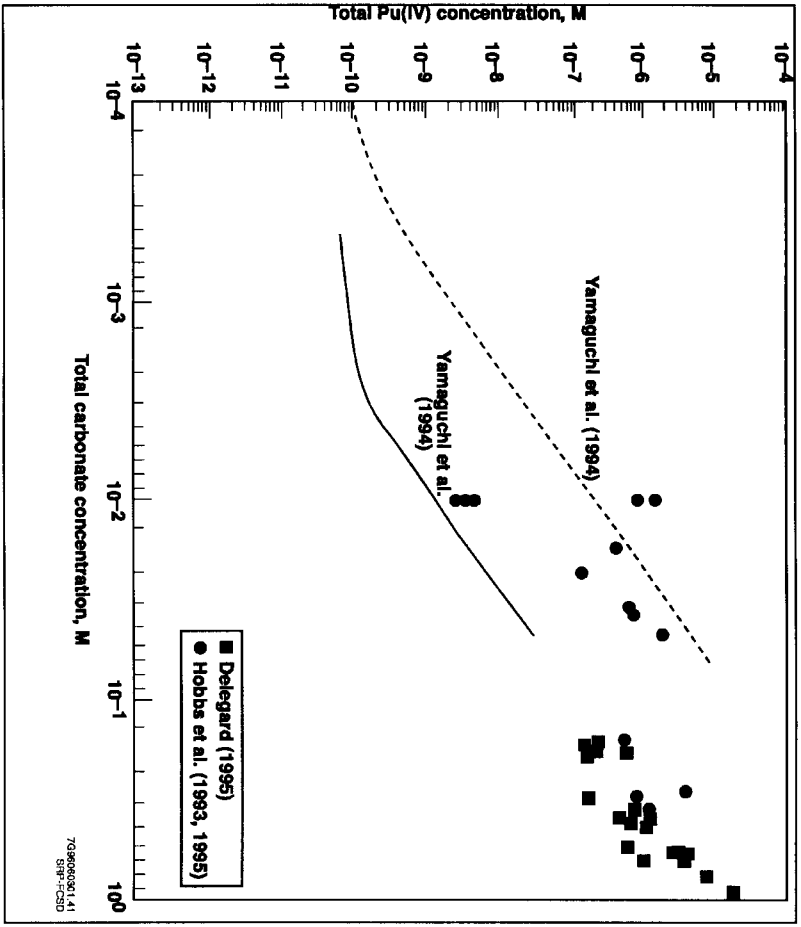

Figure 7-6. Hanford Waste Stream Data Compared with the Experimental Equilibrium Solubility of $PuO_2 \cdot xH_2O$.

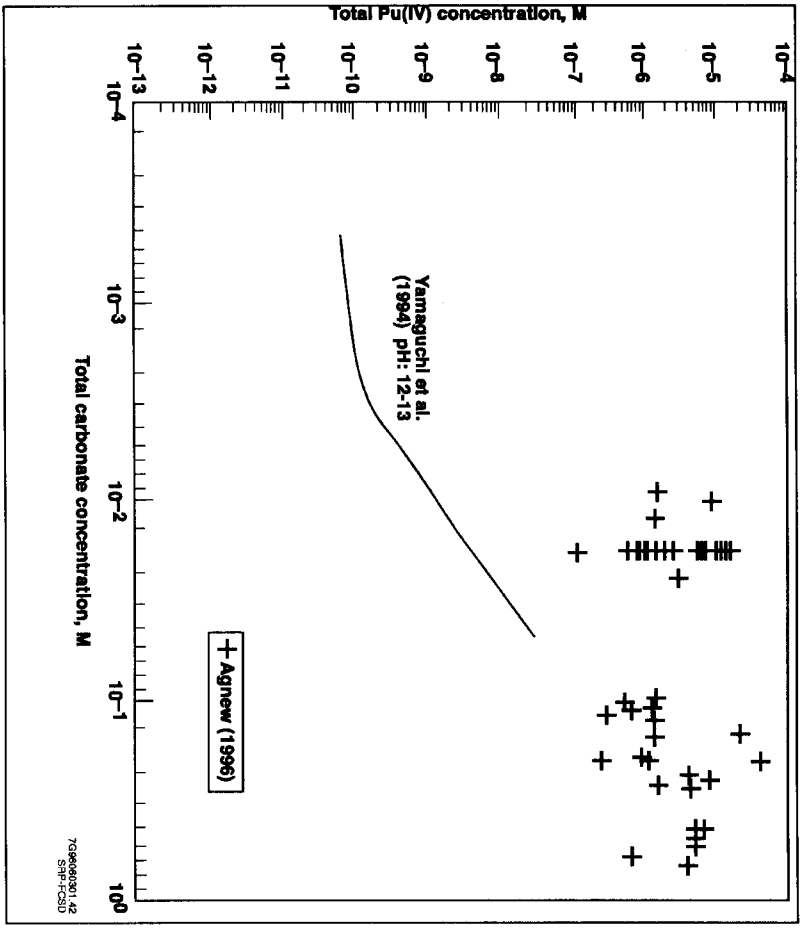

Figure 7-7. Hanford Waste Tank Supernatant Data Compared with Experimental Solubility Data for Solubility of Freshly Precipitated and Aged $PuO_2 \bullet xH_2O$ Solid.

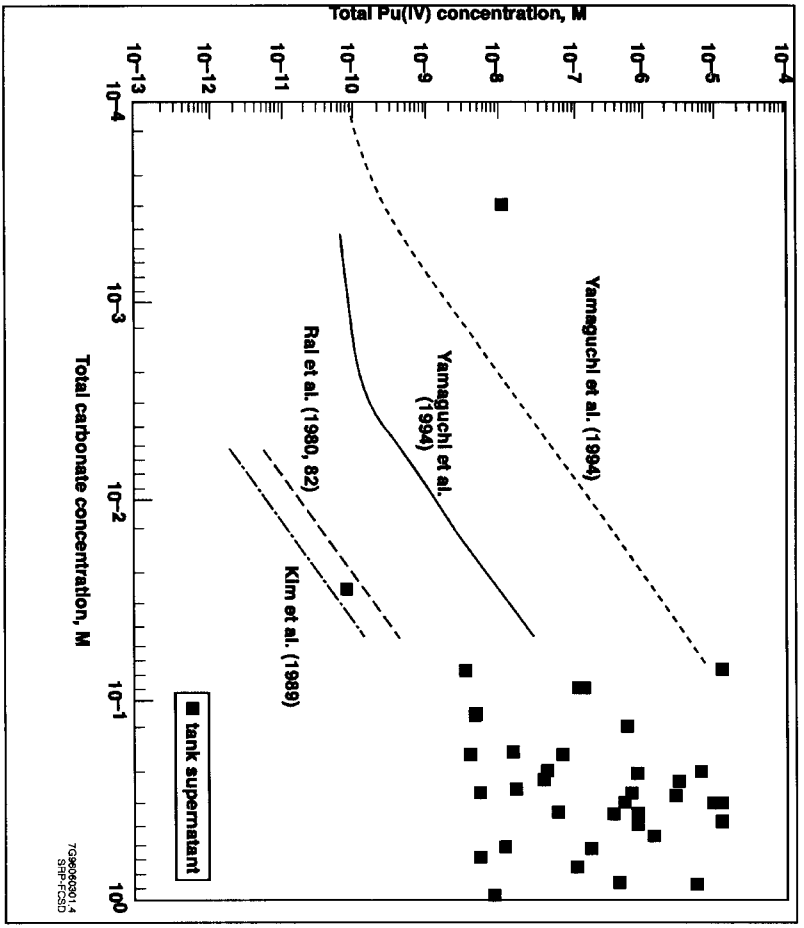

Figure 7-8. Experimental Data for Decontamination Factor of Plutonium in Cladding Removal Waste as a Function of Added Lanthanum Concentration.

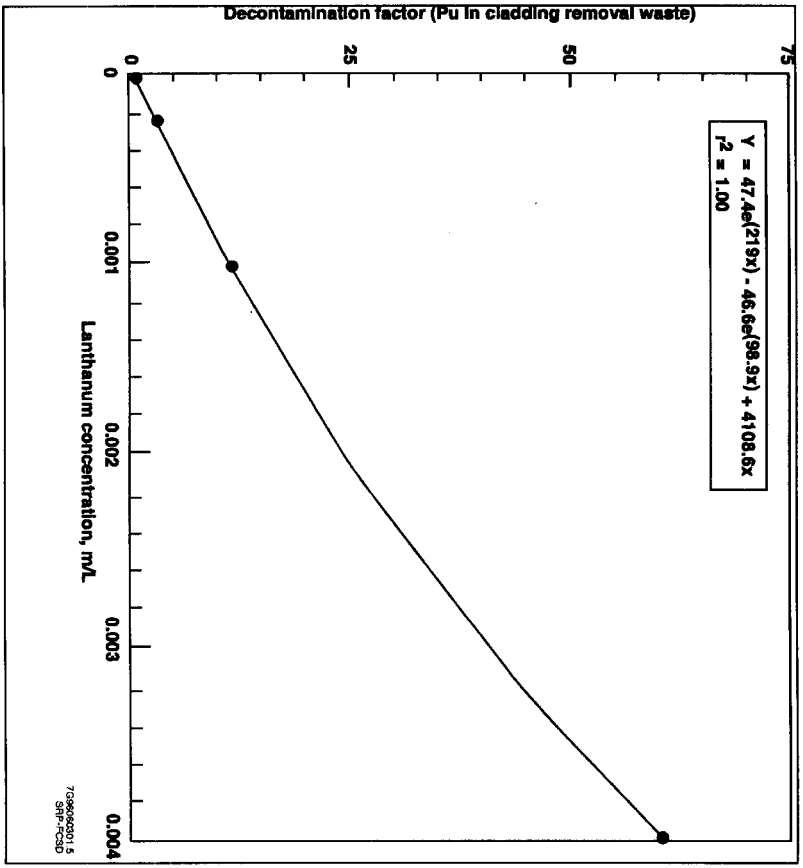

Figure 7-9. Adsorption Isotherms for Pu(IV) Adsorption on Goethite at Fixed Electrolyte Concentration.

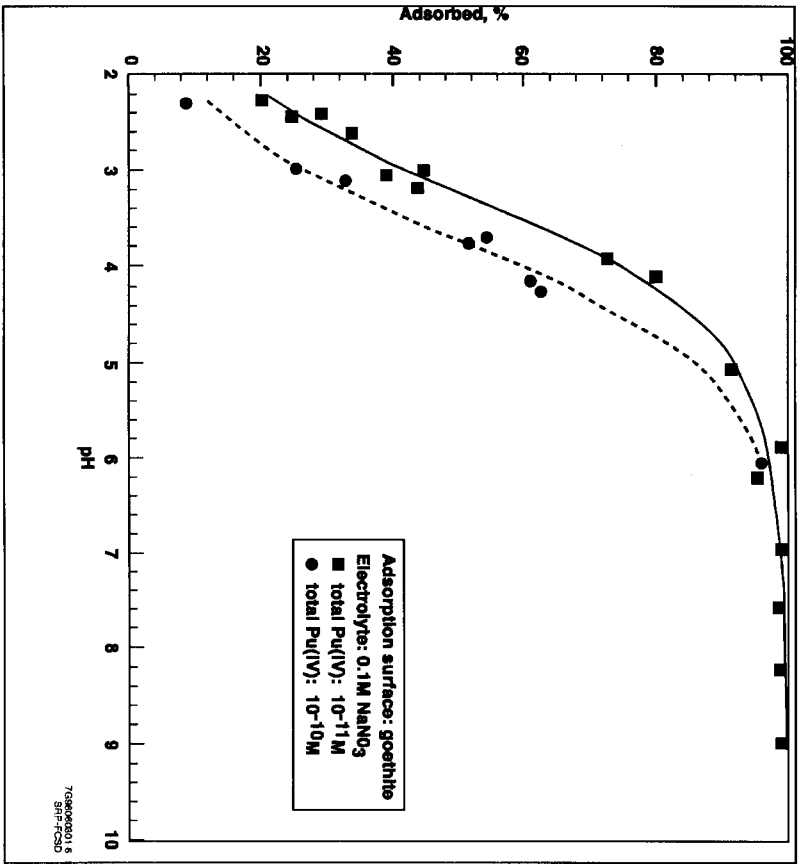

Figure 7-10. Adsorption Isotherms for Th(IV) Adsorption on Goethite at Fixed Electrolyte Concentration.

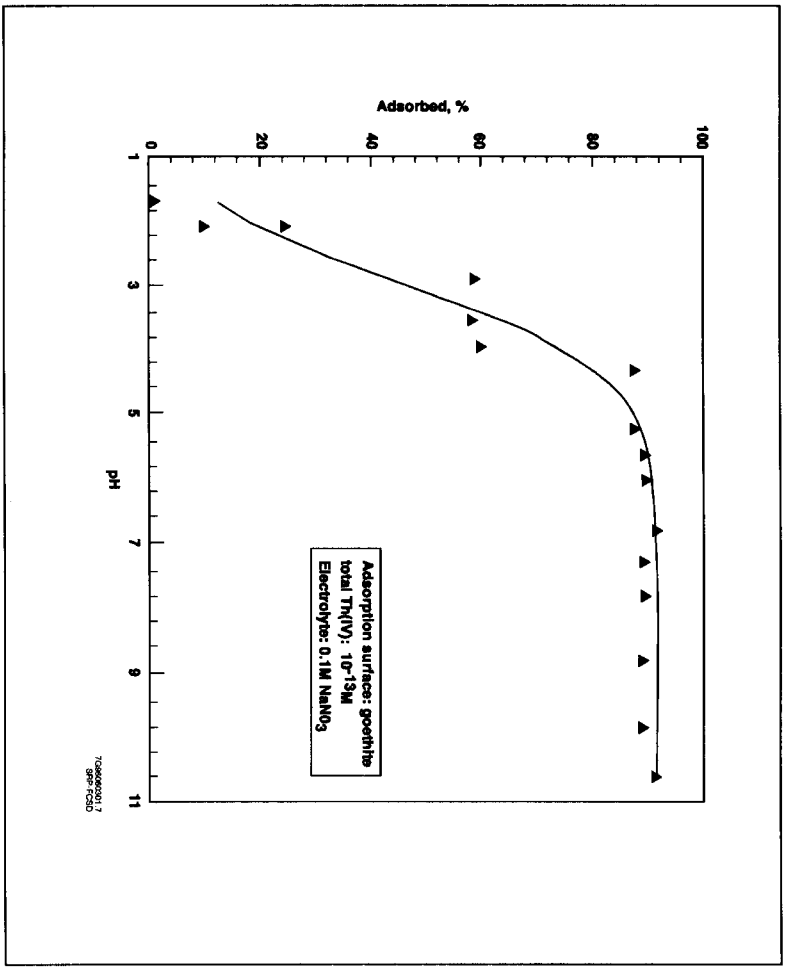

Figure 7-11. Experimental Data for Pu(IV) Adsorption on Goethite as a Function of Total Dissolved Carbonate Concentration at a Fixed pH Value of 8.6 (from La Flamme et al. 1987).

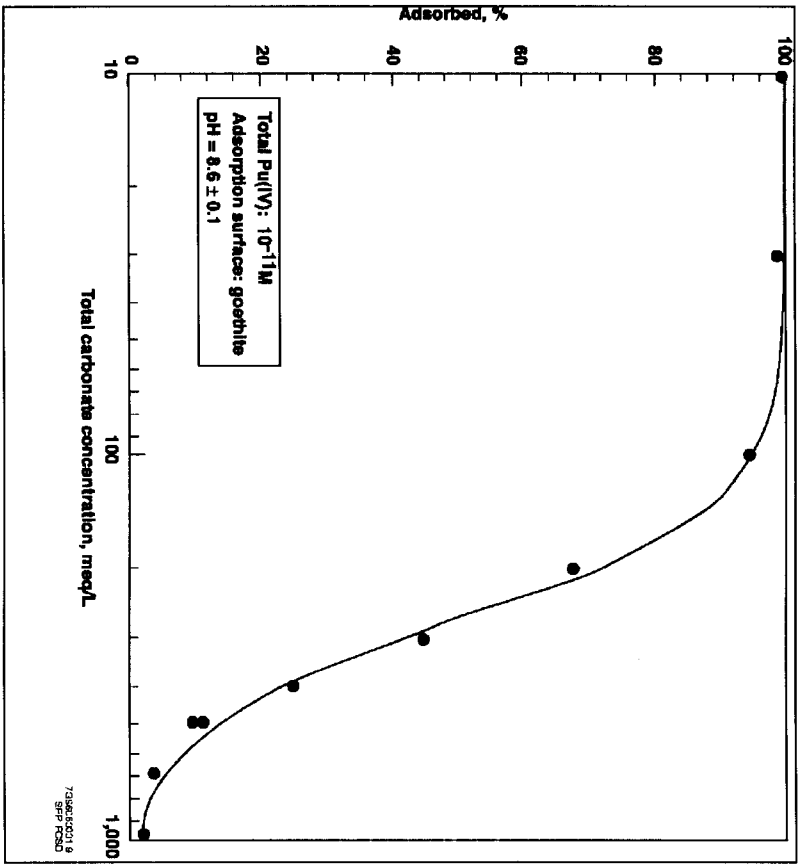

Figure 7-12. Experimental Data for Th(IV) Adsorption of Goethite Function of Total Dissolved Carbonate Concentration at a Fixed pH Value of 9.0 (from Sanchez et al. 1985).

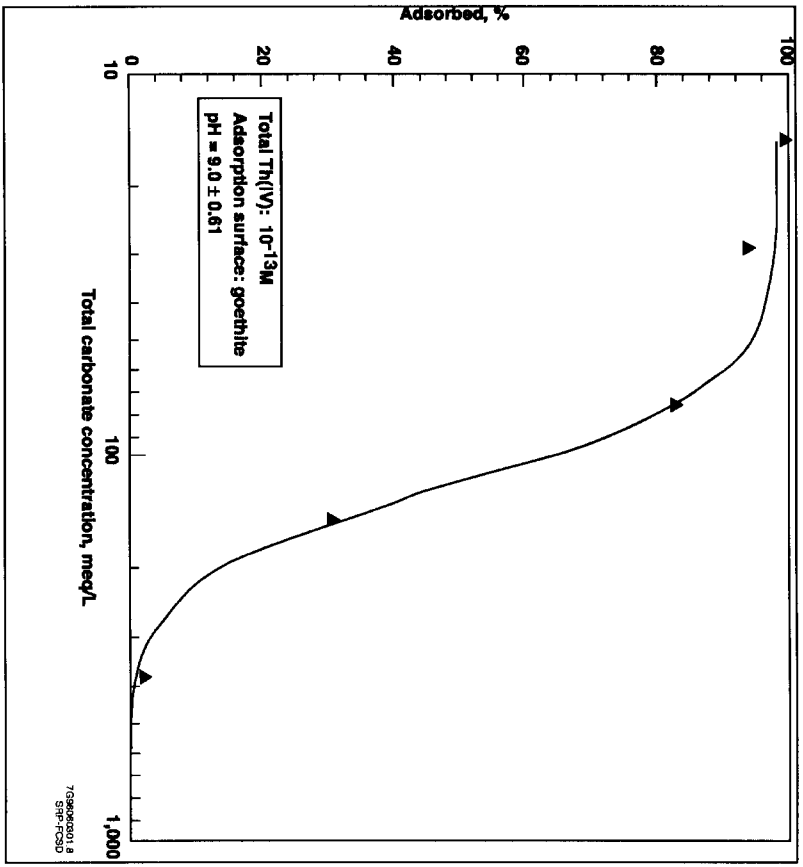

Figure 7-13. Estimated Pu(IV) Adsorption Envelope as a Function of pH and Total Dissolved Carbonate Concentration.

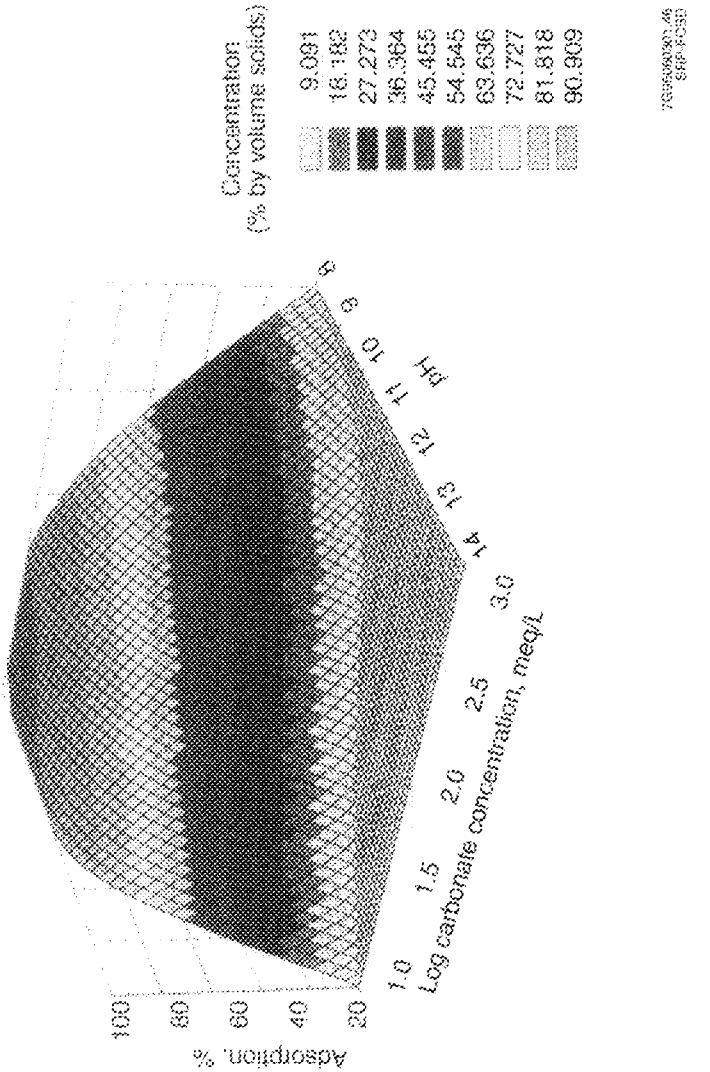

Figure 7-14. Estimated Pu(IV) Adsorption Isopleths with pH and Total Dissolved Carbonate as Variables.

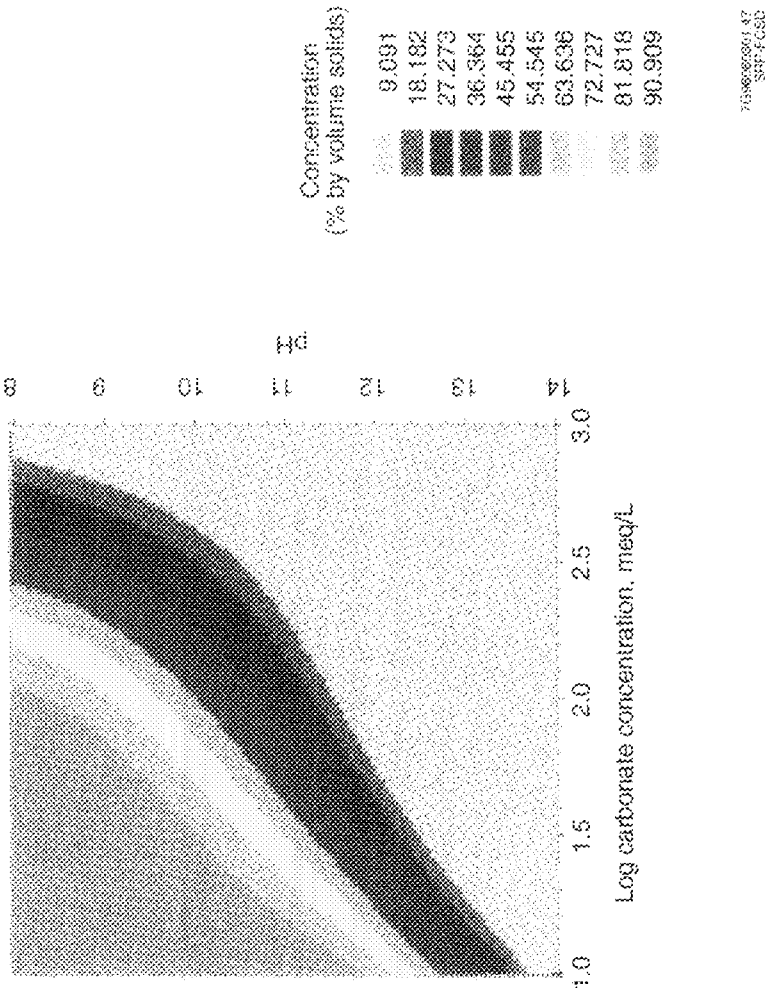

Figure 7-15. Estimated Pu(IV) Adsorption Isopleths as a Function of Total Dissolved Carbonate Concentration and at Various Fixed pH Values.

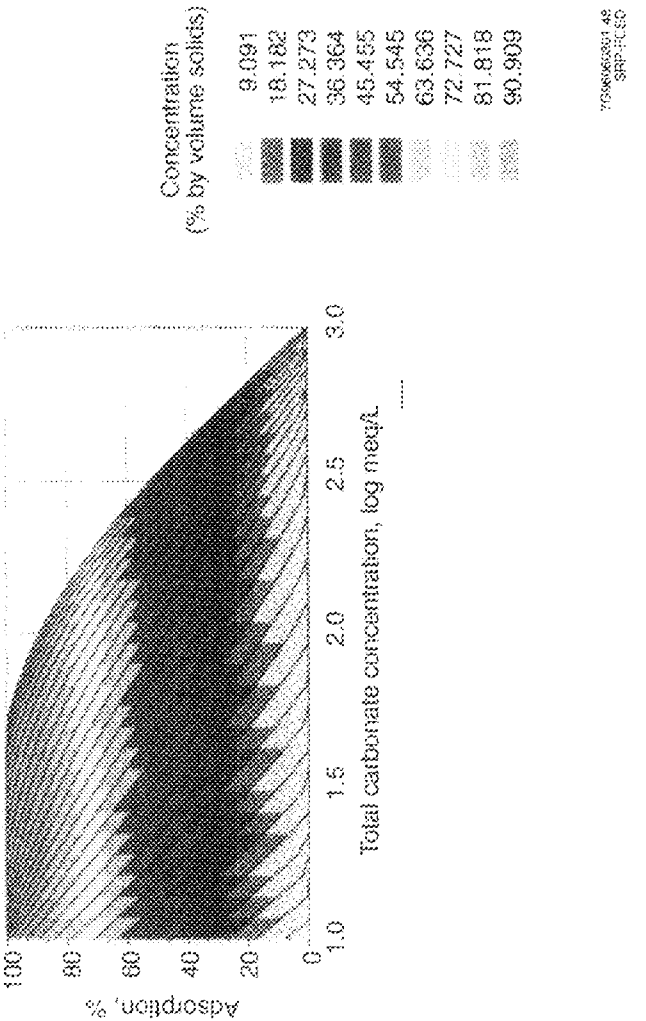

Table 7-1. Oxidation-Reduction Potentials for Plutonium.

Reaction	Oxidation Potentials (v)		
	pH=0	pH = 8	pH =14
Pu (III) → Pu (IV) + e^-	+0.982	-0.39	-1.04
Pu (IV) → Pu (V) + e^-	+1.17	+0.70	+0.52
Pu (V) → Pu (VI) + e^-	+0.916	+0.60	+0.16

Table 7-2. Stability Constants for Hydrolytic Species of Pu(IV).

Hydrolysis Reaction	log K
$Pu^{4+} + OH^- = Pu(OH)^{3+}$	13
$Pu^{4+} + 2\ OH^- = Pu(OH)_2^{2+}$	26
$Pu^{4+} + 3\ OH^- = Pu(OH)_3^{+}$	37
$Pu^{4+} + 4\ OH^- = Pu(OH)_4^{0}$	47

Table 7-3. Stability Constants for Pu(IV) Complexes.

Species	Log K	Species	log K
$PuCl^{3+}$	0.9	$Pu(OH)_2(CO_3)_2^{2-}$	34
PuF^{3+}	8	$Pu(OH)_4(CO_3)_2^{4-}$	50
$PuNO_3^{3+}$	1.8	$Pu(citrate)^{3+}$	~16
$PuSO_4^{2+}$	6	$Pu(Citrate)_2^{2+}$	~30
$Pu(SO_4)_2^0$	3.5	$PuOH(EDTA)^{2+}$	~17
$PuHPO_4^{2+}$	13	$Pu(C_2O_4)^{2+}$	~9
$Pu(HPO_4)_2^0$	24	$Pu(C_2O_4)_2^0$	~8
$Pu(HPO_4)_3^{2-}$	33	$Pu(C_2O_4)_3^{2-}$	~7
$Pu(HPO_4)_4^{4-}$	43	$Pu(C_2O_4)_4^{4-}$	~4

Table 7-4. Probable Stochiometries of Pu(IV)-OH-CO_3 Mixed Ligand Aqueous Species.

Tait et al. (1995)			Yamaguchi et al. (1994)
x = 1, y =1	x = 2, y =1	x = 3, y =1	
$PuOHCO_3^+$	$Pu(OH)_2CO_3^0$	$Pu(OH)_3CO_3^-$	$Pu(OH)_2(CO_3)^{2-}$
$PuOH(CO_3)^-$	$Pu(OH)_2(CO_3)_2^2$	$Pu(OH)_3(CO_3)^3$	$Pu(OH)_4(CO_3)_2^{4-}$
$Pu(OH)_2CO_3^0$	$Pu(OH)_3CO_3^-$	$Pu(OH)_4CO_3^{2-}$	--

Table 7-5. Total Dissolved Plutonium, Carbonate, and Hydroxyl Concentrations in Supernatants and Drainable Liquids from Single- and Double-Shell Tanks at the Hanford Site.*

Tank No.	Pu	CO_3	OH	Tank No.	Pu	CO_3	OH
	Total Concentration (-log M)				Total Concentration (-log M)		
AX-101	5.18	0.66	-0.45	SX-104	7.32	0.66	-0.30
AX-103	11.6	-0.04	-0.39	T-102	7.78	0.75	0.32
B-102	6.84	1.08	1.29	T-103	7.35	0.61	0.34
B-103	7.11	0.75	0.88	T-107	6.09	0.43	1.60
B-106	6.23	0.88	1.51	T-108	6.35	0.10	0.03
B-109	7.91	3.50	-0.11	T-109	6.71	0.27	0.42
BX-106	8.05	0.03	-0.32	T-112	6.90	1.08	0.31
BX-107	5.54	0.56	0.96	T-204	5.29	0.10	0.70
BX-109	7.17	0.45	0.96	TX-103	6.08	0.64	-0.14
BX-110	8.26	0.54	-0.14	TX-104	5.87	0.33	-0.48
BX-111	8.23	0.22	-0.54	TX-107	5.02	0.50	0.64
BX-112	6.11	0.46	1.14	TY-104	6.89	0.18	1.89
C-102	6.40	0.46	0.06	U-106	8.41	1.16	-0.07
C-106	4.83	0.13	0.90	U-202	8.37	0.75	-0.09
C-107	4.50	0.50	0.77	AN-104	6.15	0.55	-0.60
C-110	5.52	0.60	0.31	AN-107	5.22	-0.05	1.30
C-112	7.88	0.28	0.31	AW-105	10.10	1.55	0.49
C-201	3.83	0.41	0.47	AW-106	7.73	0.57	-0.41
C-204	8.31	0.94	1.72	AY-101	6.25	0.51	0.32
S-103	4.20	1.17	-0.07	AY-102	7.80	1.21	0.53

*All data from Van Vleet (1993a, b) except data for waste tanks C-106, and AY-102 are from Sederburg 1994).

Table 7-6. Organic Content (by Class) in Tank SY-101.

Core #	Chelators (mg C/g)	LMWA (mg C/g)	NPH (mg C/g)	Identified (%)
R4258 (solid)	4.7	3.3	1.44	87
R4259 (solid)	3.3	4.5	--	77
R4260 (solid)	4.8	4.4	0.41	91
R4261 (solid)	6.4	2.5	0.67	81
R4262 (solid)	2.2	5.8	0.02	73
R4263 (solid)	3.6	6.8	--	93

Table 7-7. Average Organic Content of SY-101 Core Samples.

Constituent (mg C/g)	Drainable Liquid	Solids
	composite segs 2-7	composite segs 10-14
TOC	10.9	11.1
NIDA	1.04	0.82
NTA	0.33	0.22
Citric acid	0.32	0.31
ED3A	0.30	0.28
EDTA	2.23	0.80
HEDTA	-	-
Other fragments	0.61	0.42
Succinic acid	0.07	0.05
Oxalic acid	1.8	5.7
Acetic acid	-	-
Formic acid	1.4	0.62
Glycolic acid	0.54	<
NPH	0.80	0.02
Mass balance on C	79%	83%

Table 7-8. Organic Carbon Analyses for Tank SY-103 Samples.

Constituent (mg C/g)	Drainable liquid composite segs 2-7	Solids composite segs 10-14
TOC	6.4	10.5
NIDA	0.2	0.16
NTA	0.14	0.16
Citric acid	0.42	0.56
ED3A	0.25	0.16
EDTA	0.55	0.65
HEDTA	0.03	<0.01
Other fragments	<0.01	0.14
Succinic acid	0.02	0.02
Oxalic acid	-	6.0
Acetic acid	0.6	0.7
Formic acid	1.2	0.9
Glycolic acid	-	tbd
NPH	tbd*	tbd
Mass balance on C	53%	90%

*To be determined.

Table 7-9. Summary of Organic Types in Tank Samples wt.%.

Type	Tank SY-101		Tank SY-103	
	Supernate	Solids	Supernate	Solids
chelators	44	26	23.4	18.3
LMWA	35	57	28.1	72.4
NPH	7	4	tbd*	tbd
Org. C Mass Bal.	86	87	51.5	90.7

* tbd = to be determined

Table 7-10. Organic Compounds and Other Inorganic Species Found in Organic Layer of Tank C-103.

Species	Weight %, unless noted
TBP	47.2
Tridecane (C_{13})	11.4
Tetradecane (C_{14})	6.0
Dodecane (C_{12})	2.8
DBBP	1.9
Pentadecane (C_{15})	0.9
Various branch alkanes	3.5
Water	1.3
Ammonia	<0.003
Water-soluble anions	<0.005
Water-soluble cations	<0.010
Gross Alpha Emmitters	550 (pCi/g)
Plutonium	$2.43 + 10^{-3}$ ppm
Gross Beta Emitters	$1.05 + 10^{+5}$ (pCi/g)
^{90}Sr	$5.5 + 10^{+5}$ (pCi/g)
^{137}Cs	$4.1 + 10^{+4}$ (pCi/g)
Others	$\sim 1.0 + 10^{+3}$ (pCi/g)
Total Mass Identified	75.0

Table 7-11. Analysis of Supernate Solution in Tank C-103.

Constituent	Concentration (units are ppm unless specified)
Gross Alpha Emitters	$4.35 + 10^{+4}$ pCi/mL
Gross Beta Emitters	$7.06 + 10^{+7}$ pCi/mL
^{137}Cs	$5.79 + 10^{+7}$ pCi/mL
^{60}Co	$5.11 + 10^{+4}$ pCi/mL
Cations	
Ammonia	0.23
Sodium	32,800
U	2100
K	320
Zr	300
Ni	72
Cr	57
Ca	5
Fe	3
Anions	
Nitrite	24,800
Sulfate	3,230
Nitrate	2,590
Phosphate	2,200
Floride	1,200
Chloride	430
Inorganic Carbon	5,175
Organic Carbon	7,200
pH	10
Density	1.078 g/mL @ 25°C
Viscosity	0.015-0.045 poise @ 25°C dependent on shear rate

Table 7-12. Organic Carbon Analyses on Tank C-103 Samples.

Sample #	Solids	
	TOC (mg C/g)	Oxalate (mg C/g)
Core 63-Seg. 2(upper)	8.5	2.66
Core 63-Seg. 2(lower)	10.2	--
Core 63-Seg. 3(upper)	7.6	1.94
Core 63-Seg. 3(lower)	8.9	--
Core 63-Seg. 4	4.5	2.32
Core 66-Seg. 3 (upper)	8.9	3.92
Core 66-Seg. 3 (lower)	--	2.96
Core 66-Seg. 4	9.2	2.96
	Liquids	
	TOC (mg/mL)	Oxalate (mg/mL)
Core 63-Seg. 1	7.71	3.36
Core 63-Seg. 2	7.61	--
Core 63-Seg. 4	--	3.36
Core 66-Seg. 1	--	3.14
Core 66-Seg. 2	--	3.1
Core 66-Seg. 3	--	2.96
Core 66-Seg. 4	--	2.73

Table 7-13. Organic Species Identified in Tank AN-107 Supernate Solution.

Compound	mM	mg C/mL
Chelates/Complexants		
Citric Acid	64.39	4.61
HEDTA	37.53	4.53
EDTA	31.41	3.77
Methane Tricarboxylic Acid*	17.32	1.45
NTA	7.33	0.53
Chelator Fragments	--	--
ED3A	17.91	1.72
HEDDA	2.39	0.26
E_2DTA	2.28	0.23
HEIDA	2.14	0.18
MeEDD'A	1.02	0.08
others	--	0.14
Carboxylic Acids		
Docos-13en-oic	2.50	0.67
Hexanedioic	2.04	0.15
Hexadecanoic	2.04	0.39
Phthalic	1.10	0.10
Nonanedioic	0.83	0.07
Tetradecanoic	0.68	0.12
Pentanedioic	0.60	0.04
Octadecanoic	0.54	0.11
Hydroxybutanedioic	0.33	0.01
Butanedioic	0.10	0.01
Alkanes		
C_{23} to C_{35}	7.77	2.50
Phthalate Esters		

Table 7-13. Organic Species Identified in Tank AN-107 Supernate Solution.

Compound	mM	mg C/mL
Dibutylphthalate	1.24	0.23
Dioctylphthalate	0.05	0.01
Total Organic Carbon		44.0

* Identification of this species is now considered erroneous (J. A. Campbell, personal communication 1996).

Table 7-14. Organic Species Measured in Tanks C-102 and C-204.

Sample Description	Species	Concentration (mg C/g)
C-102 Sludge Sample (drainable liquid minimal)		
Upper part of core	TOC	7.00
	NPH	7.97
	TBP	2.06
Lower part of core	TOC	6.00
	NPH	17.17
	TBP	2.74
C-204 Solids Sample (drainable liquid minimal)		
Auger core sample	TOC	60*
	NPH	trace
	TBP	330*
	DBP	2.5*
	EDTA	ND
	NTA	ND
	HEDTA	ND
	acetic acid	<0.1*
	formic acid	<0.1*
	oxalic acid	<0.1*

* per gram wet weight. Moisture content is ~55%; multiply values by 2.2 to get dry weight.
ND Not detected.

Table 7-15. Organic Species Measured in Tank BY-108.

Solid Sample (drainable liquid limited)		
Sample Description	Species	Concentration (mg C/g)
Riser 17, upper part of core	TOC	16.6
	NPH	ND
	TBP	ND
Riser 17, lower part of core	TOC	0.5
	NPH	ND
	TBP	ND
Riser 16	TOC	1.2
	NPH	ND
	TBP	ND

Table 7-16. Solid Solution Compounds Pu(IV).

Compound	Major Component Ions forming Solid Solutions with Pu(IV)					
	Bi (III)	Ce (III)	La (III)	Th (IV)	U(IV)	Zr(IV)
Hydroxide	•	•	•	•	•	•
Phosphate	•				•	•
Oxalate	•		•	•	•	
Iodate		•	•	•		•
Fluoride			•			
Peroxide				•		
Molybdate						•
Tungstate		•		•	•	
Arsenate	•					•
Pyrophosphate				•		
Hypophosphate				•		

Table 7-17. Differences in Ionic Radii Between Pu(IV) and Potential Solid Solution Forming Ions in Hanford Site Waste Streams (%).

Ions	Coordination Number*	
	VI	VIII
Bi(III)	-17	-18
Ce (III)	-15	-16
La(III)	-17	-17
Th(IV)	-9	-9
U(IV)	-3	-4
Zr(IV)	+19	+14
Al(III)	+61	--
Fe(III)	+33	--

* Ionic radii data from Shannon (1976).
-- Not applicable

CONTENTS

8.0 INTRODUCTION TO NATURAL ORE DEPOSIT EFFORTS 8-1
8.1 INTRODUCTION AND BACKGROUND 8-1
8.2 ORE-FORMING PROCESSES 8-2
8.2.1 Natural Ore-Forming Processes 8-2
8.2.2 Potential Ore-Forming Processes in Waste Tanks . . . 8-4
8.3 NATURALLY OCCURRING RADIOGENIC MINERALS 8-7
8.4 DATA NEEDS 8-8

LIST OF FIGURES

8-1 Settling Velocities for Gold Particles of Various Sizes and Degrees of Flatness F8-1

LIST OF TABLES

8-1 Comparison of Naturally Occurring Ore Deposits T8-1
8-2 Ore-Forming Processes T8-3

TERMS

8.0 INTRODUCTION TO NATURAL ORE DEPOSIT EFFORTS

8.1 INTRODUCTION AND BACKGROUND

Some processes occurring inside Hanford Site defense nuclear waste tanks may be analogous to those of natural ore deposits in which a trace material becomes highly enriched by naturally occurring processes. In the tank case we are interested in, processes whereby fissile particulate matter (i.e., precipitates of plutonium) could be concentrated. The common types of ore deposits are divided into those that form near the earth's surface and those that form under high temperature and pressure well below the earth's surface (Table 8-1). Ore bodies and waste tanks have many significant differences that must be considered, however. Most important of these is the amount of time required to form an ore body, which might take thousands to millions of years.Waste tanks, in most cases, have existed for at most four to five decades. Processes that take place in hydrothermal ore deposits, which were formed at great depths below the earth's surface under extremely high temperatures (300-600 °C) and pressures, are not applicable to near-surface Hanford Site waste tanks, the contents of which are generally ≤100 °C and under relatively low (atmospheric) pressure.

Based on available data on the contents of Hanford Site tanks (see Sections 7.0 and 9.0), which are limited to mainly bulk composition instead of detailed mineralogic contents, the bulk of the plutonium in tanks occurs in the bottom-residing sludge for either single or double-shell tanks; the plutonium in supernate liquid and salt cake is generally relatively low (<0.002 g Pu/L). A criticality concern would exist if the plutonium concentrations in any phase in the tanks increased to 2.6 g Pu/L (see Rogers 1993 or Waltar et al. 1996 for more details). For the sludge, this would require a minimum enrichment factor of 13 from the maximum level measured to date (0.19 g Pu/L). For an average tank the enrichment factor would be 50 to >100 where enrichment is defined as increasing the plutonium concentration in a volume of sludge while keeping all other constituents constant. According to calculations that assume homogeneous mixing of the sludge followed by differential settling into thin layers, a bed thickness of 18 cm with plutonium concentrations of 2.6 g/L would be required to reach criticality. The total mass of plutonium that would be present in this uniformly distributed sludge layer would be 1060 kg, which is about twice as much as the mass in the Hanford Site tank with the highest concentration of plutonium.

Depending on which neutralized waste streams were sent to that tank, sludge could contain a mixture of aluminum and iron oxyhydroxides, bismuth phosphate, calcium carbonate, and chromium and manganese oxides. Plutonium can be precipitated as discrete hydrous Pu(IV) oxide, coprecipitated within other selected metal oxides (solid solution formation), or sorbed onto other metal oxyhydroxides (mostly iron and aluminum), all of which are formed during neutralization from an acidic to an alkaline pH. However, little mineralogical data is available to establish the nature of the precipitates in the sludge. The plutonium may also exist as a phosphate compound, given the high phosphate concentrations in some of the tanks. Finally, some particulate plutonium oxide was likely present in the liquid waste stream sent to tank SY-102 from the Plutonium Finishing Plant.

8.2 ORE-FORMING PROCESSES

8.2.1 Natural Ore-Forming Processes

Table 8-1 classifies ore deposits into nine categories, which were extracted from the geologic literature. Further, seven natural ore-forming processes operate that can, individually or in combination, explain how the ore deposit types were formed. The seven ore-forming processes are listed in Table 8-2 and discussed in Sections 8.2.1.1 through 8.2.1.7.

8.2.1.1 Precipitation. Minerals can precipitate out of a solution as a result of changes in redox, pH, temperature, or pressure, which, either together or individually, could affect solubility and dissolution behavior. Precipitation may occur from silicate melts (i.e., magma) or from aqueous solutions. Particulates form as a result of spontaneous nucleation within the aqueous solutions or by nucleation on the enclosing surface (i.e., host rock) (Evans 1980). Precipitation was the dominant mechanism that occurred when Hanford Site acidic waste streams were neutralized in mixing/holding tanks before being pumped to the storage tanks. Continued changes in pH, redox, and temperature, as well as changes in the chemical environment as new waste was sluiced into the tanks or supernate liquid was pumped out to evaporators to open up space could promote some additional precipitation. That the precipitation would be isolated to small volumes within the tanks is less likely. The newly formed precipitates would most likely form in the supernate and settle into thin layers on the existing sludge surface. If precipitation occurred in the solution-saturated sludges, it would be expected to occur over large volumes unless very sharp gradients were created in the aforementioned parameters.

8.2.1.2 Mechanical Accumulation. Mechanical accumulation and concentration of ores (referred to as placer deposits) occur in nature when chemically resistant and mechanically durable constituents (e.g., elemental gold , magnetite [Fe_3O_4]), monazite [REE-phosphate]) are transported and reworked by stream currents or waves over long distances and times. The placer minerals are released from their matrix by weathering. The comminuted materials are eroded to bodies of water. Moving water sweeps away the lighter matrix and the heavier placer minerals sink to the bottom or are moved downstream short distances. Waves and shore currents also separate heavy minerals from light ones and coarse grains from fine ones. Eventually, the trace constituents derived from thousands of tons of rock or sediment matrix is concentrated into a relatively small volume.

The original process of filling SSTs (the cascading process where one tank received the slurry and when filled overflowed through connecting pipes to a second tank similarly connected to a third tank) could allow for some very limited differential accumulation. However, the possibility that enough plutonium would collect through differential accumulation to facilitate criticality events in the tanks is unlikely.

8.2.1.3 Magmatic Separation and Hydrothermal Alteration. Magmatic separation occurs in magma chambers buried deep within the earth's crust under extremely high temperatures and pressures. As temperature and pressure slowly decrease

over eons of geologic time, mineral crystals begin to form, the size of which depend on the rate of magma cooling. Depending on the composition of the melt, the first constituents to crystallize and settle are the heavier mafic minerals (e.g., iron- and magnesium-bearing). The last crystals to settle out are the lighter silicate minerals (e.g., quartz, K-feldspar, muscovite).

During magmatic activity, hot, aqueous, high-pressure (hydrothermal) solutions are generated. As the magma consolidates, these solutions become more concentrated in base metals and other elements that are not accommodated in the crystal lattices of the silicate minerals precipitate out of the consolidating magma. Hydrothermal alteration occurs when these high-pressure solutions are forced into the solid country rock along pores, fractures, and/or faults. During hydrothermal alteration these aqueous solutions can lead to precipitation of enriched ore bodies, as well as leaching/dissolution, lateral secretion, replacement, and recrystallization of the country rocks adjacent to the intrusion. Neither magmatic separation or hydrothermal ore formation is probable in Hanford Site tanks because the temperatures are 100's of degrees below those required in nature to form the ores.

8.2.1.4 Leaching and Dissolution. Leaching is the separation, selective removal, or dissolving out of soluble constituents from a rock or ore body by the action of percolating solutions. One clear distinction between ore deposits formed by leaching and tank environments is the lack of an open system in the tanks to carry away the dissolved material.

Dissolution is a process of chemical weathering by which mineral or rock constituents pass into solution (Bates and Jackson 1987). One common class of ore body formed by dissolution is a residuum-type ore. These types of ores are formed by the preferential leaching of one or more components of the country rock, leaving a residuum of the less soluble material in place. One of the more widely recognized ores formed by this process is bauxite (aluminum).

Several conditions appear to be necessary for these ores to form (Tole 1984, Tole et al. 1986). One is the composition of the host rock. Bauxite deposits form most readily on peraluminous-type (aluminum-rich, or silica-poor) materials. Therefore, many of these deposits are associated with nephelinites and nepheline syenites. Granites, diorites, etc., while composed of the same basic elements as the nepheline syenites, contain enough silica to weather to kaolin or similar silica-bearing minerals. Another apparent requisite for the formation of residuum-type deposits is the system's ability to transport the more soluble components away from the deposit. If the system is poorly drained, concentrations of the more reactive components (in this case silica) attain concentrations sufficient to form other phases locally, e.g., kaolin. Well drained systems transport dissolved silica and other soluble components away from the system, allowing for the aluminum concentrates to form. Finally, formation of residuum-type deposits generally require long time spans. The time required to form an ore body depends on the differences in the solubilities of the constituents. Large differences in solubility could cause ore to form rapidly, but more typically, the solubility of the individual components is similar, thus necessitating long time spans for deposits to form.

Processes involved in the formation of these residuum-type deposits do not apply to the concentration of elements in waste tanks. Because the tanks effectively contain all of the "deposited" elements, only limited opportunities occur for the more soluble elements to be carried away. Also, the long time periods required to form a viable residuum-type ore deposit also are many orders of magnitude longer than decades.

8.2.1.5 Lateral Secretion. Lateral secretion is a process whereby some constituents are concentrated or depleted adjacent to magmatic intrusions or zones of hydrothermal alteration. During lateral secretion, convectively driven fluids associated with consolidating magma draw metals and other constituents from the adjacent host rock and transport them to new sites of deposition (Bates and Jackson 1987). The large temperature differential needed for this process does not occur in the Hanford Site waste tanks.

8.2.1.6 Replacement. Replacement, an ion-exchange process, is "the dissolving of one mineral and the simultaneous deposition of another mineral in its place, without the intervening development of appreciable open spaces, and commonly without a change in the volume" (Edwards 1952). During replacement, old material diffuses out and new material diffuses in without a breakdown of the solid state (Bates and Jackson 1987). Good evidence for mineral replacement is the formation of pseudomorphs, where one mineral replaces another with contrasting crystal habits; the replacement mineral will conform to the crystal habit of the mineral it is replacing as it slowly transforms, one molecule at a time, from the original mineral to its psuedomorph. The Hanford Site tanks are unlikely to be able to create the necessary environment for this ore process to occur. Also, this process requires long time spans.

8.2.1.7 Recrystallization. Recrystallization involves the formation, essentially in the solid state, of new crystalline mineral grains in a rock. The new grains are generally larger than the original grains, and may have the same or a different mineralogical composition (Bates and Jackson 1987). For economical ore deposits, recrystallization has only been an important process for the subsurface ore types that require high temperature (>300 °C) and high pressures. Recrystallization to form highly enriched zones of trace components in tanks is not expected. The Ostwald ripening recrystallization covered in Section 7.2.5 is a different process where a trace component is not enriched in the designated volume; rather, the particle crystallinity is refined, increasing the particle size.

8.2.2 Potential Ore-Forming Processes in Waste Tanks

Of the seven common ore-forming processes listed in Table 8-2, only precipitation and mechanical accumulation might occur to some degree in waste tanks. The other five processes require either high temperature and pressure hydrothermal processes or surficial weathering (for leaching/dissolution). These processes require eons of geologic time and very specific environmental conditions to concentrate ore bodies. None of these conditions applies to the relatively young, shallowly buried tank wastes that are isolated from processes associated with surficial weathering or deep burial.

Precipitation of plutonium compounds could occur in tanks if the solubility of plutonium changes because of temperature or redox gradients or changes with aging within the tanks. (Pressure should not be a factor because it remains low and relatively constant.) Migration and segregation of tank constituents potentially could result in thermal gradients and redox gradients in the tanks, leading to precipitation of certain mineral phases, which might include plutonium hydroxide, plutonium phosphate, or some more complex combination of insoluble compounds. Plutonium-rich particles may also be concentrated during mechanical agitation of tank solids. In this case, the more dense precipitates would settle and accumulate toward the bottom of the tank. Because of its high density, discrete plutonium oxide particles would probably be among the first precipitates to settle out. The cascading action that occurred when the SST's were filled and the sluicing that will take place during retrieval could lead to mechanical accumulation. This would depend on the amount of turbulence and the sluicing frequency because the accumulation would be caused by the winnowing effects associated with multiple cycles of resuspension and settling. The possibility for a critical mass of plutonium forming depends on the following:

- Density and molecular composition of the plutonium-bearing precipitate (i.e., mineralogy) compared with that of the surrounding fluid

- Density and molecular composition of any other precipitates (i.e., iron, aluminum, and other transition metal oxides) compared with that of the surrounding fluid.

While continuous winnowing currents exist in tanks to create placer deposits similar to those found in nature, some mechanical accumulation could occur during infrequent tank additions when fluids transferred from one tank to another cascade between 4 and 10 m, depending on where the inlet pipe is located and how full the connected tanks are. For this reason, the mineralogical and chemical composition of the sludge and supernatant are important to determine the likelihood of a critical mass of plutonium existing in tanks. Possibly, more precipitation and preferential settling of plutonium might occur near the intake and outlet pipes as fluids cascade from one tank to the next. Also, during the mixing of DST tank contents with a mixer pump, as has been done recently to prevent the buildup of explosive gases, precipitates with a higher density (e.g., plutonium hydrous oxide or plutonium phosphate) could concentrate in areas of the tanks where stirring is less vigorous or incomplete. All these mechanical processes are discussed quantitatively in Sections 4.0, 5.0, and 6.0, and Appendices A and B.

The operation of mechanical concentration rests on a few basic principles involving chiefly the differences in specific gravity, size, and shape of particles, as affected by the velocity of a moving fluid. Stokes Law states that the settling velocity increases as the square of the diameter of the particle under laminar flow conditions:

$$v=Cd^2 \tag{8.1}$$

where d is the particle diameter in centimeters, and

$$C = [(ds-df)g]/18u \quad (8.2)$$

where ds = relative density of the solid
df = relative density of the fluid at a particular temperature
g = acceleration of gravity (980 cm/sec^2)
u = the viscosity of the fluid at a particular temperature.

Thus the settling velocity is influenced by the difference between the size and density of the particles and the density and viscosity of the suspending fluid (Lewis and McConchie 1994). Equations 8.1 and 8.2 assume that particles have the minimum amount of drag during settling (i.e., the particles are spheres). Thus, calculated settling velocities represent maximum velocities because individual particles are normally not spherical. A spherical pellet (higher Corey Shape Factor) has less specific surface than a thin, platy disc of the same weight, and therefore, will sink more rapidly. The influence of particle size and shape on settling velocity is demonstrated in Figure 8-1. The rate of settling in a fluid is also affected by the specific surface of particles. Of two spheres with the same weight but different sizes, the smaller with its lesser surface and, therefore, lesser friction in the fluid, sinks more rapidly. When current velocity decreases, much of the transported load settles out of suspension. Placer minerals will settle and drop out of solution where current slackens. Faster-moving water accentuates the differences in settling rate based on specific gravity. The specific surface is a factor also; of two equal-weight particles, the one with the larger specific surface is increasingly swept away from the other with increased water velocity. Thus flaky particles are easily separated from spherical particles, and fine materials are separated from coarse particles.

To determine the settling velocities of waste-tank particles we must first know the specific density and viscosity of the sludge and supernatant liquid, respectively, as well as the size and specific gravity of the precipitated particles. Except for density of the tank fluids, little data is available to calculate settling velocities for particles in waste tanks. In Hanford Site waste tanks, the relative density (df in equation 8.2) of the bulk sludge and supernatant range from 1.3-1.8 g/cm^3 to 1.0-1.5 g/cm^3, respectively (D.A. Reynolds, personal communication) but little data is available for the viscosity of the sludge or the density of plutonium-bearing particles versus other sludge components.

In general, settling velocity of particles of the same size differ by an order of magnitude from the lightest (quartz) to the heaviest (gold) particles (i.e., the densest particles settle up to 10 times as fast as less dense particles) settling in the same medium. It would appear that the viscosity of the suspending fluid has a greater influence on settling velocity than does particle density.

A possible mechanism for concentrating plutonium would be if plutonium-bearing compounds and other precipitates settled out preferentially during sluicing. The mechanical accumulation that takes place in tanks is significantly different from that of placer deposits. Except for the area close to the tank intake, the sluicing probably produces little turbulence because the fluids are cascading (like a waterfall) into a pool of preexisting fluids, salt cake, and sludge. Placer deposits form as a result of

continuously moving currents that winnow and segregate materials. However, no such currents occur within the tanks. Furthermore, placer ore deposits are impure; usually individual particles are mixed with or surrounded with any number of gangue minerals of little or no economic importance. Ore deposits of gold rarely exceed a grade of 1 troy ounce per metric ton, which is equivalent to a concentration of ~0.004-percent gold. Average ore grades at operating uranium mines range from 0.03-percent uranium to as high as 10-percent uranium but are most frequently less than 1-percent uranium (WWW 1996). The average crustal abundance of thorium is 12 ppm and for uranium, 2.7 ppm. We will say something about plutonium concentration in sludge here for comparison.

Another possible method for sorting, segregation, or mechanical accumulation of plutonium would be via ground shaking (i.e., earthquakes). Theoretically, this could redistribute tank contents into layers of contrasting density, with the densest particles migrating to the bottom. Earthquakes with notable magnitude are not common at the Hanford Site and thus will not be considered further. Another mechanism for concentrating plutonium is the artificial pumping or recirculation of tank contents, such as has been performed in one DST recently. If plutonium-rich precipitates are present and they have a significantly high density they could concentrate into "hot spots" or parts of the tank that are less turbulent or escape mixing. More detailed discussion and calculations are presented in the Fluid Dynamics sections (Sections 4.0, 5.0, and 6.0, and Appendices A and B) of this report; however, based on natural ore deposition phenomena/processes, the limited mechanical agitation, and time for agitation, relatively low temperatures, and small particle sizes present in the sludge, placer deposits of enriched plutonium are unlikely to exist in Hanford Site tanks.

8.3 NATURALLY OCCURRING RADIOGENIC MINERALS

Several radiogenic ore-forming minerals are found in nature; these include: autunite [$Ca(UO_2)_2(PO_4)2\bullet 10\text{-}12H_2O$], carnotite [$K_2(UO_2)_2(VO_4)_2\bullet nH20$], thorianite ($ThO_2$), torbernite [$Cu(UO_2)_2(PO_4)2\bullet 8\text{-}12H_2O$], tyuyamunite [$Ca(UO_2)_2(VO_4)_2\bullet nH_2O$], and uraninite ($UO_2$), also referred to as pitchblende. Uraninite is the most common uranium-producing mineral associated with uranium ore. Carnotite, autunite, torbernite, and tyuyamunite form as secondary minerals when groundwater leaches existing minerals, which leads to the remobilization and concentration of uranium into discrete ore bodies. None of the crystalline forms of these secondary uranium minerals or plutonium analogs are expected to be present in waste storage tanks. Depending on the pH of the mixture in a tank, a more likely component is some form of amorphous plutonium oxyhydroxide that may recrystallize to a more pure form of the oxide with time, or a plutonium-bearing solid-solution whereby plutonium substitutes for other cations (lanthanum, bismuth, or zirconium) into their hydrous oxide or phosphate solid, both of which are thought to exist in the Hanford Site tanks. Alternatively, plutonium may be present at such low concentrations that it does not form discrete solid phases and exists as a surface-adsorbed species onto the bulk sludge.

Natural thorium is of interest because it has the same valence as that likely for plutonium in the tank environment (+4), and thus could act as an analog for plutonium in ore bodies. The principal thorium-bearing mineral is monazite, a mixture of rare earth phosphates (thorium, cerium, lanthanum, YPO_4), containing 1- to 5-percent thorium dioxide and a smaller proportion of uranium. Monazite is associated with economic mineral sand deposits. Monazite is comparatively rare, occurring as an accessory mineral in granites, gneisses, aplites, pegmatites, silicic volcanic rocks (Gazzaz 1986), and as rolled grains in sands derived from the decomposition of such rocks (Hurlbut 1971, Mall and Mishra 1994). Monazite generally contains thorium concentrated up to 10 to 12 percent as ThO_2 (Mall and Mishra 1994) in sands as a placer deposit because of its resistance to chemical attack and its high specific gravity.

Monazite sands also are associated with other resistant and heavy minerals such as magnetite, ilmenite, rutile, and zircon (Jobe et al. 1993, Nagamalleswara 1994). The alluvial deposits, resulting from the weathering of granites, include a great deal of silica (sand). These are treated by standard ore-dressing methods to concentrate the monazite. The resulting dressed ore product may contain from 5 to 8 percent thorium, 0.15 to 0.25 percent uranium, and 50 percent other rare-earth elements, most in the form of phosphates (Glasstone and Sesonskeet 1981). Despite the long times available and continual agitation afforded by wave action, the monazite ore remains mixed with the more ubiquitous resistant (but significantly lighter) quartz sands. Monazite ore bodies do not show complete separation of heavy lanthanide- and actinide-rich minerals from more common minerals found in the earth's crust. Thorianite may also be present as a placer deposit in fluvial gravels according to Hurlbut (1971).

The specific gravity of uraninite is between 6.5 and 9, slightly lower than the value for thorium oxide (9.7). The non-crystalline and more oxidized minerals of uranium have lower specific gravities, so one would expect the density of hydrous plutonium oxide to be lower than the value for its crystalline oxide, 11.46. Thus, the settling velocities of freshly precipitated plutonium hydrous oxide particles of a fixed size should be lower than gold (specific gravity is 19.3), but faster than thorium and uranium minerals of the same fixed size.

8.4 DATA NEEDS

At present, the only process that could concentrate plutonium appears to be precipitation of a plutonium compound and preferential settling within the tanks. To determine how and when this settling might occur one needs to know the following information:

- The mineralogical composition and particle sizes of the plutonium-bearing precipitates and the "other" more ubiquitous sludge precipitates. Only if we know the mineral forms of all components can we determine the relative density, particle size distribution, and settling velocity of the precipitates.

- The amount of turbulence involved in the cascading and sluicing processes, how frequently effluent was added, and the volumes of effluent that were added to the tanks.

- The viscosity of the supernatant fluids and particle size distribution of sludges in the tank.

One interesting analysis that should be performed is determining the plutonium concentrations in tank sludges in existing cascading tank systems. A difference between the first tank and those downline would indicate that differential precipitation and settling of plutonium compounds occurs as fluids are passed from one tank to the next. If plutonium concentrations are similar in all three tanks, this would suggest that appreciable differential settling of plutonium is not occurring in the tanks.

This page intentionally left blank.

Figure 8-1. Settling Velocities for Gold Particles of Various Sizes and Degrees of Flatness (log-log scale).

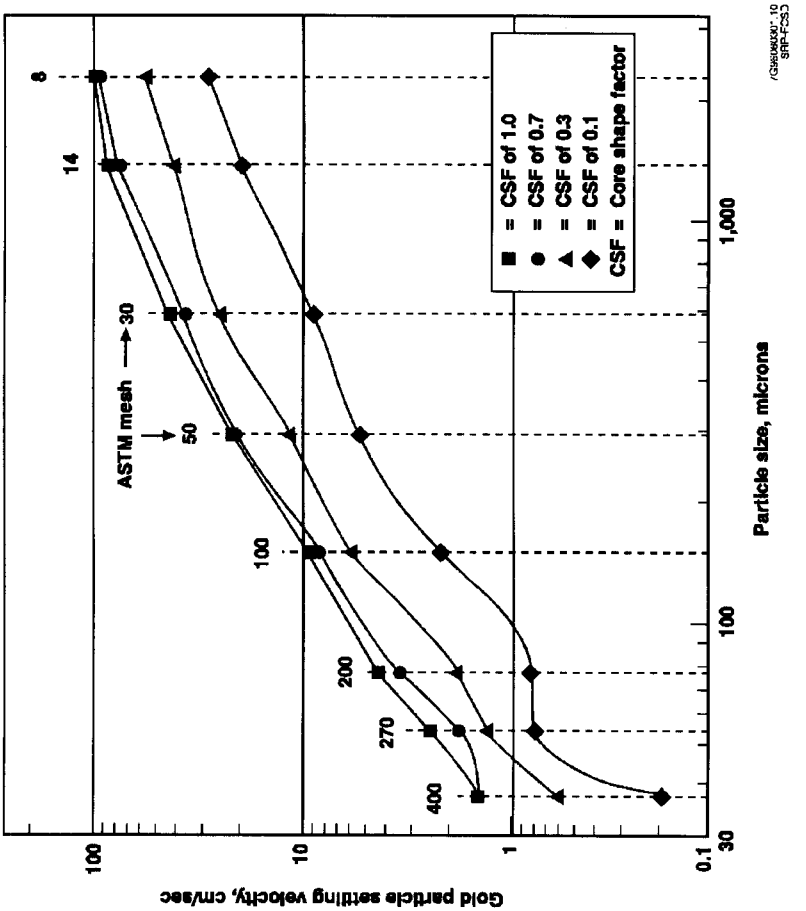

This page intentionally left blank.

Table 8-1. Comparison of Naturally Occurring Ore Deposits.

	Types of Ore Deposit	Ores of	Associated Minerals	Geometry	Processes Involved	Mechanisms Involved	Temperature/Pressure Regime	Examples
Surface Processes	Placer	Au, Cr, Fe, Th	cassiterite, chromite, columbite, copper, garnet, illmenite, magnetite, monazite, platinum, ruby, rutile sapphire, xenotime, zircon, monazite	lenticular	mechanical accumulation, chemical resistance, mechanical durability	Concentration in moving liquid medium (e.g., river current)	Ambient air temp and pressure	Placer gold deposits; mineral (e.g., monazite) sanddeposits
	Residual	Al, Fe, Ni, Co	gibbsite, boehmite, disapore, hematite, goethite	tabular, interlayered beds, lenses, and pockets	Leaching/dissolution	Intense and prolonged in-situ surficial chemical weathering in humid climate	Ambient air temp and pressure	Laterite (Fe-rich) and bauxite(Al-rich) deposits
	Supergene Enrichment	Al, Fe, Mn, Cu, Pb, Au, Ag	Sulfides, hematite, precious metals	lenticular, tabular	Leaching/reprecipitation, redox changes	Leaching and downward movement in zone of oxidation, followed by reduction and precipitation near water table interface	Near ambient temp(0-20°C), minor lithostatic pressure	Porphyry Copper Deposits
	Marine/Volcanic Exhalative	Cu, Pb, Zn, Ba, Au, Ag	Sulfides, precious metals	Discordant veins along open fractures, fissures, and caverns	Precipitation near underwater volcanic vent	Precipitation due to redox and temperature changes	Submarine volcanism and precipitation where hydrothermal fluids come in contact with marine sea water	Massive sulfide deposits
			Hypogene	*Enrichment*				
Subsurface Processes	telethermal	Pb, Zn, Cd, Ge, Hg	Native Au, Ag, Cu, Bi, sulfides, selenides, tellurides, quartz, carbonates, zeolites	Discordant veins, pipes, and stocks filling fractures and faults	Precipitation far from hydrothermal source	Near surface precipitation along open fractures, fissures, and caverns by very low temperature hydrothermal fluids	Low temp (+/-100°C) and pressure	Hg-Pb-Zn deposits
	epithermal	Pb, Zn, Au, Ag, Hg, Sb, Cu, Se, Bi, U	Native Au, Ag, Cu, Bi, sulfides, selenides, tellurides, quartz, carbonates, zeolites	Discordant veins, pipes, and stocks filling fractures and faults	Precipitation proximal to hydrothermal source	Near surface precipitation along fractures by relatively low-temperature hydrothermal fluids	Low Temp (50-200°C)and pressure	Gold veins
	mesothermal	Au, Ag, Cu, As, Pb, Zn, Ni, Co, W, Mo, U	sulfides, sulfosalts, pitchblende albite, quartz, sericite, chlorite, carbonates, montmorillonite	Tabular sheets, stocks, pipes, and fracture fillings, alteration haloes, stratiform	Replacement, precipitation by hydrothermal fluids	fracturing, injection, moderate hydrothermal alteration	Moderate temp (200-300°C) and pressure	Carbonatite, Mississippi-Valley type deposits
	hypothermal	Au, Sn, Mo, W, Cu, Pb, Zn, As	magnetite, sulfides, scheelite, garnet, mica, epidote, quartz, chlorite, tellurides	Discordant, irregular, veins, stocks, and fracture fillings; alteration haloes	Replacement, recrystallization, precipitation by hydrothermal fluids	fracturing, injection, intense hydrothermal alteration	High temp (300-600°C) and pressure	Skarn
	magmatic	Cr, Fl, Li, Be, Sn, Cs, Cu, Ni, Nb, Ta, U	chromite, beryl, lepidolite, tourmaline, feldspar, spodumene	Massive bodies and stopes	Magmatic separation, precipitation	Melting, stoping, hydrothermal alteration	Extreme temp (600-????°C) and pressure (XMb)	Pegmatites

Increasing Temperature and Pressure

Table 8-2. Ore-Forming Processes (from Evans 1980 and Jensen and Bateman 1981).

Step no.	Process description
1	Precipitation (solubility) a. Changes in temperature and pressure b. Changes in redox
2	Mechanical Accumulation
3	Magmatic Separation/Hydrothermal Alteration
4	Leaching/Dissolution
5	Lateral Secretion
6	Replacement (Ion Exchange)
7	Recrystallization

This page intentionally left blank.

9.0 PROPERTIES OF GENERATED WASTE RELEVANT TO CRITICALITY HAZARD

9.1 OBJECTIVE/SCOPE

This chapter characterizes the waste in the underground tanks using historical accounts of flows and compositions of waste stream inputs, waste treatment processes, and analytical results of recent waste samples from the tanks.

9.2 BACKGROUND

This section describes the waste streams that were added to the waste tanks and subsequent operations conducted on the waste. It describes the plutonium/uranium processing facilities, cesium and strontium removal facilities, and evaporation facilities, and their waste streams that were discharged to the tank farms. It also reports the chemical composition of the streams including densities, pH, volumes, and estimated solids contents. We also characterize waste streams that were returned to the tank farms after being removed and treated and describe in-farm treatment of the waste and operations affecting changes of the waste, including estimated resultant waste characterization.

9.2.1 Wastes from Plutonium Separations and Finishing Operations at Hanford

Plutonium separations processing began at the Hanford Site in 1944 at the bismuth phosphate plant and continued until 1990 when the PUREX plant was shut down. Facility flushing and waste treatment has continued after shutdown. Waste volume generation and transfers to the tank farms continue, although discharges contain little plutonium. U.S. Department of Energy, Headquarters accountability records report that 67.4 metric tons (MT) of plutonium (Roblyer 1994) were produced in the reactors at the Hanford Site. This includes 12.9 MT of nonweapons-grade plutonium (nominally 9 wt% or higher ^{240}Pu); the rest was weapons grade (nominally 6 wt% ^{240}Pu). This estimate agrees well with independently calculated plutonium production values based on thermal power generation and plutonium conversion factors representing the various reactor fuels. Using this approach, about 62.7 MT of plutonium was processed at the Hanford Site. About 4 MT of plutonium remains in the K Basins and 0.528 MT of was plutonium processed at West Valley, New York. Small quantities of miscellaneous fuels that were processed at the Hanford Site include plutonium recycle test reactor (PRTR), mixed oxide fuel (MOX), thorium fuel, and Shippingport reactor fuels (PWR).

Fuel types produced at the Hanford Site include aluminum-clad base fuel O3N, C5N, K5N, and aluminum-clad driver fuel O3E, C3E, and K5E irradiated in B, C, D, DR, F, H, KE, and KW reactors. Zirconium-clad base fuel, Mark IV, and zirconium-clad driver fuel, Mark IA, were irradiated in N Reactor.

Quantities of plutonium processed (Roetman et al. 1994) through each separations facility and percentage of the total amounts processed are shown in Table 9-1.

An estimate of the total plutonium discharged to the Hanford Site waste tanks is about 500 kg. An estimate of about 1,000 kg in waste tanks has been used for worst case criticality calculations because of uncertainties about the content of waste discharged to the tanks (Roetman et al. 1994).

The site contains 177 tanks; 149 are SSTs that have no current waste transfer activity and 28 are the newer DSTs. Tank diameters are given in Table 9-2. Figure 9-1 illustrates a typical waste configuration in the DSTs (unstabilized because waste transfers are fairly recent); Figure 9-2 illustrates the waste configuration for the SSTs. Sludge, which consists of solids with interstitial liquid containing water-insoluble chemicals that have precipitated from solution, forms the bottom layer in all the tanks. Salt cake was formed on top of the sludge in some tanks from the crystallization and precipitation of chemicals after the supernatant liquid was evaporated during volume reduction operations.

Figures 9-1 and 9-2 provide a perspective on the immense margin of subcriticality that exists if the tank waste is configured in a uniform pancake geometry and the fissile and neutron absorber materials are intimately mixed.

Waste management practices at the Hanford Site required waste to be transferred from separations and finishing facilities (or uranium, strontium and cesium recovery operations) to the low-carbon steel tanks only after low concentrations of plutonium were verified and the acid contents were neutralized with sodium hydroxide. The neutralization not only precipitated most of the fissile materials in the waste, but also coprecipitated various metal cations associated with reprocessing or waste management. Such materials were allowed to settle in SSTs, forming sludge layers. Most reprocessing and product purification operations contained sufficient uranium, zirconium, and/or aluminum or used enough iron-containing reagents to neutronically subdue any fissile materials present. The slow settling of alkali-insoluble materials tended to form pancake-like layers of solids in the waste tanks. As part of subsequent waste management efforts, operations were conducted to recover uranium, cesium, and strontium byproducts of fuel reprocessing from the waste. These operations also lowered heat loads in the tanks. All waste associated with these processes was made alkaline to prevent corrosion of the tanks.

To increase the storage capacity of the tanks, dilute waste supernatant solutions containing water-soluble salts produced by acid neutralization were heated to remove water. Two methods were used: in-tank solidification and successive-pass external evaporation, returning the concentrated waste to the tanks as evaporator bottoms. In both cases, the results were the same. Large quantities of water were removed, the solubility of the salts contained in the wastes was exceeded, and the salts were precipitated and settled out in the tanks, usually resulting in a five- to tenfold reduction in volume. The salts that settled in the tanks became salt cake that formed a layer on top of existing sludge inventories. The evaporation processes also concentrated both the free alkali (sodium hydroxide) and organic complexants in the waste, most of which remained in solution.

As part of an effort to reduce the potential of fluid leakage from SSTs, many of the tanks were salt-well pumped and most of the drainable liquids were transferred to DSTs. This further compacted both the sludge and salt cake layers. The resulting waste contained mainly non-drainable liquids, although some drainable waste remained.

9.2.2 Operational Controls on Waste Transfer

Current criticality controls (CPS-P-465-40000) require that waste transferred from reprocessing facilities to DSTs have a solution concentration limit of less than 0.013 g/L of plutonium (less than 0.05 g/gal). Fissile plutonium is defined as total ^{239}Pu and ^{241}Pu and equivalent ^{235}U and ^{233}U contents. This concentration limit is set to control the cumulative concentration of fissile material in tank solids at or below the operating value of 2.6 g/L as an upper value for settled waste in the tanks.

Plutonium fissile equivalence for ^{233}U is defined as "one gram of ^{233}U shall be assumed equivalent to one gram of ^{239}Pu." Plutonium fissile equivalence of ^{235}U is defined as "when the ^{235}U concentration in uranium exceeds 1 wt%, one gram of ^{235}U in excess of 1 wt% enrichment shall be assumed equivalent to one gram of plutonium." The ^{235}U content of postirradiated Mark IA fuel (preirradiated enrichment of 1.15 wt% ^{235}U average of inner and outer element) is 1.0 wt% when irradiated to 6 percent ^{240}Pu. This is the least irradiated Mark IA fuel processed. All other enriched fuels processed were irradiated to a greater extent and would have less ^{235}U. The 1 wt% ^{235}U value was determined by crediting the ^{238}U associated with ^{235}U as an adequate absorber for ^{235}U above natural concentration of 0.72 wt%. The ^{238}U could not also be credited as an absorber for plutonium calculations in this situation.

Neptunium-237 and ^{241}Am are not fissile isotopes but are fissionable in the presence of fast neutrons (Rogers 1996). These isotopes are both present in some waste tanks at low concentrations, but do not contribute to criticality because the tanks contain no fast neutron fields. When the hydrogen-to-actinide (^{237}Np and/or ^{241}Am) atom ratio is ≥ 5, these actinides are exempt from a need of specification (Tomlinson 1971). All waste has a hydrogen-to-actinide (^{237}Np and/or ^{241}Am) ratio greater than 5 because these actinides are present only at low concentrations and the water content of waste is greater than 5 wt%.

Further, the current controls on Hanford Site tank farms require that an auditable continuous inventory of plutonium and an assessment of the plutonium concentration both in the solids and supernatant shall be maintained for each tank. Waste discharged to the tank farms shall be alkaline (basic) with a pH of at least 8.0, unless a criticality safety evaluation shows that alkalinity control is not required. (A low pH by itself can not cause criticality.) Currently, specifications require that waste transferred to tanks have a pH of greater than 10 to control tank corrosion. Verification of compliance shall be documented before each transfer from a generating facility to the tank farms.

These or similar criticality controls were in place when waste was transferred to the SSTs in the past, as documented by (Oberg 1976). Presently waste from generating facilities cannot be transferred to SSTs, nor can

transfers be made between SSTs without an approved criticality review and documentation. No fissile material-bearing waste has been transferred to the SSTs since 1980.

9.2.3 Waste Properties Relevant to Criticality Hazard

Waste properties relevant to criticality in Hanford Site waste tanks include fissile material (^{239}Pu, ^{233}U, and ^{235}U) concentrations, neutron absorber concentrations, moderator concentrations, and any chemical or physical fissile material concentrating mechanisms (discussed in the other chapters of this report). Fissile materials are mainly in the sludges that have settled to the bottoms of the tanks. Fissile materials are quite insoluble in the tank waste caustic solutions and are at low concentrations in salt cakes and supernatant. Key parameters affecting criticality include the following:

- Plutonium mass inventory in each tank
- Plutonium concentration in tank waste
- Concentration and identity of neutron absorbers/moderators
- Tank geometry/operations/status.

Fissile materials are found mainly in sludge layers rather than in salt cake or supernatant liquid. Insoluble absorbers are also in the sludge layers. Absorbers of interest and their minimum subcriticality mass ratios (Rogers 1996) are listed in Table 9-3.

9.2.4 Activity Status of Tanks

SSTs have been inactive since 1981 and no wastes are scheduled to be added to them. The DSTs still receive wastes but, because no fuel separations operations are currently under way, the only waste received is from flushing of PFP and PUREX equipment, tanks, and cells. Any waste added to tank farm tanks is expected to have a very low plutonium concentration. Supernatant transfers from SSTs to DSTs occur infrequently.

9.3 WASTE STREAM CHARACTERIZATION

This section characterizes the waste streams routed to the tanks. Several aqueous separations, plutonium finishing, and waste treatment processes have been used at the Hanford Site since 1944. Each process generates its own distinctive fissile material-bearing aqueous waste discharged to the underground storage tanks. Both high- and low-level waste containing fissile material was discharged from these processes to the tank farms. The separations processes include the bismuth/phosphate process conducted at T Plant and B Plant from 1944 to 1956, the uranium recovery process conducted at U Plant from 1952 to 1959, the reduction oxidation (REDOX) process conducted at the REDOX facility from 1952 through 1966, and the plutonium-uranium extraction (PUREX) process conducted at the PUREX facility from 1956 to 1972 and 1983 to 1990. Plutonium finishing processes were conducted at the 234-5 (PFP) facility with wastes discharged to the tank farms from 1973 to the present. Uranium recovery and some cesium and

strontium scavenging were conducted at U Plant. Additional cesium and strontium recovery operations were conducted on first cycle waste from the bismuth phosphate process at T Plant and on tank farm supernatant pumped from some tanks to the AR vault for treatment.

9.3.1 Hanford Defined Waste

Recently, workers at Los Alamos National Laboratory (LANL) compiled currently available records from the Hanford Site on process flowsheets and waste transfers to tanks. The flowsheet data and old records on waste stream characterization were used to define a finite set of waste types that represent all the types created and sent to either tanks or cribs. This unique set of waste is called the Hanford Defined Waste (HDW) and is found in Agnew (1995). Coupled with all the records of transfers to tanks, out of tanks to recovery facilities and evaporators, and treated waste or concentrates back to tanks, the HDW have been used in a computer algorithm to define the contents in tanks, both total and split into sludge (with interstitial liquids) and supernate liquids (includes salt cake). The Agnew estimates of total plutonium inventories in the Hanford Site SSTs are listed in Table 9-4 and compared with three other independent estimates. As can be seen, the estimated plutonium content differs significantly between the SSTs. The plutonium inventory estimated for each of the DSTs using two sources is included in Table 9-5. Because plutonium concentration and content are the main concern for criticality, resolution of some of the uncertainties shown in the tables may be warranted.

This chapter is keyed toward evaluating the waste in the 29 larger tanks reported to contain more than 10 kg of plutonium or equivalent fissile material and the 4 smaller tanks (with 6.1 m diameter) containing more than 0.75 kg plutonium. The 10-kg and 0.75-kg fissile material screening values are set to allow focusing on the tanks of most interest to addressing the criticality issue. These screening values are a factor of 106 below the minimum critical areal density for Pu in pure water (240 g/ft^2) reported by Carter et al. (1969) for the tanks. Applying this areal density limit in water is conservative when compared to sludges. If the two sizes of tanks contain less than 10 kg or 0.75 kg fissile material, respectively, a concentrating mechanism of more than 100 would be required in the horizontal direction to approach a critical limit. This is considered incredible when the processes to add waste to the Hanford tanks are considered. The tanks with less than 10 kg or 0.75 kg of fissile material, as applicable, will be evaluated, but with less intensity unless analysis shows that they may contain higher quantities of plutonium. We have identified 33 tanks that have higher concentrations of plutonium than this screening value as determined by any one of four methods used. The tanks are listed in Table 9-6 and are shown in Tables 9-4 and 9-5 with asterisks.

The LANL waste model (Agnew 1996) can be used to help identify some criticality-related conditions in the waste tanks. Because, the current model was not designed to address criticality concerns, many neutron absorber concentrations are overestimated and the plutonium content is underestimated in some streams transferred to the tank farms. LANL has agreed to enter appropriate documented feed stream compositions that can be supplied into the

existing model in FYs 96 and 97 and issue a revision that would support the needs of criticality evaluations. Finally, not all waste transfer records and all actinide separation processing records have been released from classified storage. Therefore, some of the data cells in the following tables are blank at this time. Efforts will be made to complete the assessment of past records as they become declassified and available.

9.3.2 PUREX

As discussed earlier, 77.7 percent of the plutonium produced was separated using the PUREX process. The chronology of the separations discussions start with the most recent process, PUREX, and works backwards in time. Three main fuel types and some other miscellaneous fuels were reprocessed at the PUREX facility from 1956 to 1990. These fuel types include aluminum-clad fuel, thorium fuel, and zirconium-clad fuel. The quantities of fuel and aqueous waste streams directed to the tank farms are listed in Table 9-7. The following sections present the chemical content of the waste streams for the processing facility. The sections are organized by fuel type.

9.3.2.1 Zirconium-Clad Fuel Reprocessing Wastes. Zirconium-clad fuel was reprocessed at the PUREX facility during a number of campaigns. The dates, quantity of fuel, average exposure of fuel, and plutonium content are listed in the Table 9-8. The flowsheet values (Allen 1982), actual waste transfer volumes (from processing records), and sample analyses are given for each stream sent from the PUREX facility to the tank farms, waste fractionation facility, and/or 242 A Evaporator.

The N Reactor fuel elements consisted of uranium alloy 601 enriched to the appropriate ^{235}U content (natural 0.712 to 1.15 wt%) and clad with zircalloy 2. These fuel elements were irradiated at N Reactor then shipped to PUREX for reprocessing.

The aqueous waste streams from reprocessing this N Reactor fuel through the PUREX and REDOX reprocessing plants were transferred to tank farms, the waste fractionization facility, and the 242 A Evaporator. The nuclear material control records were used to determine quantities of plutonium, uranium, and neptunium discharged from separations facilities to the tank farms, waste fractionization facilities, and evaporators.

3920 MT of zircalloy-clad uranium was reprocessed at PUREX from 1983 to 1989 based on processing flow-sheet specifics for Mark IV and Mark IA fuel elements at an average preenrichment of 0.988% uranium-235 at N Reactor. Six campaigns were reprocessed at PUREX from 1983 to 1990; 2 fuels grade (greater than 9 wt% ^{240}Pu) and 4 weapons-grade (6 wt% ^{240}Pu) fuel. The fuel elements charged to a dissolver were always blended to maintain a ^{235}U content of less than 1 wt% in any single charge. Cold (unirradiated) uranium and recovered plutonium were recycled within the solvent extraction system as needed to blend for criticality control and to meet product specification requirements during these campaigns. As a result, the quantity of uranium processed through the solvent extraction system was considerably greater than the volume of uranium processed through the head end.

9.3.2.1.1 Zircalloy Decladding Waste. Zircalloy decladding waste quantities and compositions for the 1983-1990 campaigns discharged to AW-103 and AW-105 tanks are listed in Table 9-9 per flowsheet, process records, and the HDW model for comparison. Nuclear material control (NMC) process records were used to determine measured quantities of plutonium and uranium transferred to the specific waste tanks. The records are summarized in Appendix E. The NMC records indicate that 8.64 kg of plutonium and 11,697 kg uranium were transferred to the DSTs in zircalloy decladding waste from PUREX staging tank TK-E5 from 1983 to 1990. The zircalloy decladding waste consisted of one or two declad batches from each dissolver charge, a batch of spent metathesis solution, and a metathesis rinse batch, along with some tank water flushes and steam jet transfer dilutions. The quantities of plutonium, uranium, the volume of decladding waste transferred, and the associated uranium/plutonium mass ratios are shown by month for campaigns A01 through A06 in Appendix E. Appendix E also includes the underground tank receiving the waste and the fuel processed through the PUREX Head End and Solvent Extraction. References for this data are included in Appendix E.

The PUREX reprocessing plant records were used to determine actual volumes transferred from tank TK-E5 and a jet dilution of 5 vol% was applied to account for the water added to facilitate transfer to the tank farm. The total zirconium processed during the 1980's was calculated to be 284,000 kg based on the processing of 3,299 MTU of Mark IV fuel, 591 MTU Mark IA fuel, and 30 MTU of cold uranium (Mark IV) with cladding. The average amount of zirconium cladding for 0.94 wt% enriched fuel is 70.2 kg/MTU and for spike (enriched to average 1.15 wt%) fuel is 85.4 kg/MTU (PUREX Tech Manual). About 5 wt% (15,240 kg) of the zirconium (Schofield 1991) was processed through the PUREX HA column with the uranium feed stream and exited the PUREX plant in the neutralized zirflex current acid waste (NZCAW) waste stream from tank TK-F16. The remaining 95 wt% (269,000 kg) exited the PUREX plant from TK-E5 as decladding waste. The total uranium processed through the head end was 3920 MTU including the 30 MTU cold zircalloy 2-jacketed uranium at startup in 1983.

Decladding waste from the PUREX dissolvers was sampled in tanks D2 and E3 before centrifuging or in tank E5 (both 5,000-gal tanks) after centrifuging, nitrite addition, and neutralization. These tanks were agitated and duplicate samples were obtained for plutonium, uranium, and pH analysis. For samples taken from TK-D2 and -E3, solids were allowed to settle and the liquid analyzed for plutonium and uranium. For samples taken from TK-E5 after the waste had been centrifuged and neutralized, only sample solution and acid soluble fines were analyzed with the solution. Some plutonium and/or uranium as fine particulates and insoluble particulates may not have been accounted for by these sampling and analytical procedures. On verification that all batches contained less than 500 g plutonium, that the plutonium content was less than 0.013 g/L, and that the pH was greater than 12, the waste was transferred to the tank farm receiver tanks AW-103 or AW-105. Tank transfers were effected by steam jet, which resulted in about a 5 vol% water increase for each transfer. Water flushes were also used after each batch transfer of decladding solution, metathesis rinse of the dissolver, and dissolver rinse.

The total E5 waste volume transferred was 24,516,000 L including the 5 vol% jet dilution or 6254 L/MTU. The total uranium and plutonium determined by NMC sample analysis of each batch transfer were 11,697 kg and 8,638 g, respectively. The average uranium and plutonium concentration in the waste

was calculated to be 0.525 g/L of uranium and 0.00039 g/L of plutonium and is listed in the process records column of Table 9-10.

Maximum plutonium monthly average concentrations of up to 0.0012 g/L were observed in this decladding waste stream. This is well below the required limit concentration of 0.013 g/L plutonium for waste stream transfers to the tank farms.

Zircalloy 2 (Perry 1963) cladding contains 0.25 wt% iron, 0.05 wt% nickel, and 1.4 wt% tin. This amounts to an average iron content of 176 g/MTU and nickel content of 35 g/MTU processed through the PUREX dissolvers. Carbon steel shoes on the zircalloy fuel elements (Jacobs 1986) contributed about 130 g/MTU of iron if we assume that half the shoes were sent to the dissolver. Corrosion of the dissolver and dissolver coil during the coating removal process (Jacobs 1986) amounted to about 196 g/MTU of iron, 52 g/MTU of chromium, and 25 g/MTU of nickel.

The quantity and average composition of important criticality-related components of zirconium-clad fuel reprocessing waste streams from 1983 to 1990 are listed in Table 9-10. These figures are compared to the flowsheet values, the LANL HDW estimates, and PUREX process records. Based on process records that estimate sludge formation at 8.3 vol% determined by sludge accumulation in tank AW-103, the projected plutonium concentration is two orders of magnitude less than the 2.6-g/L criticality limit. Also, uranium, iron, and zirconium absorbers are projected to be present at much higher concentrations than needed to ensure that the associated plutonium concentrations remain subcritical.

9.3.2.1.2 Neutralized Zirflex Current Acid Waste. The aqueous NZCAW waste contained more than 99 percent of the nonvolatile fission products, plutonium and uranium losses from the HA column, and associated absorbers. This waste was treated in the PUREX Plant by concentrating in EF-6 and sugar denitrating in tank F15. After sugar denitration, the waste was agitated, sampled, and sent to F-16 for neutralization. Analysis was made for plutonium, uranium, iron, nickel, fluoride, and chromium as well as for pH. Metals were introduced to this stream by several mechanisms. Iron in this stream consists of iron that was added to uranium metal to form a stable fuel alloy in the reactor, ferrous ammonium sulfamate that was added as a reducing agent to the IBX and 2N columns, iron from dissolvers that corroded during the fuel dissolution process, and corrosion of the E-F6, 3WB, and 1UC concentrators, and T-U6 acid vacuum fractionator. Iron impurities in the PUREX uranium product were a negligible <40-ppm iron. Chromium and nickel were introduced by corrosion of the same vessels, as fuel impurities, and as a fission product in the irradiated fuel. Aluminum was introduced as aluminum nitrate in the dissolution process and as an alloying element in the uranium fuel.

The quantity and average composition of important criticality-related components of neutralized Zirflex current acid waste stream from 1983 to 1990 are listed in Table 9-11, which compares the flowsheet values, the LANL HDW estimates, and the process records. The projected plutonium concentration in the sludge formed in the tank farm tanks from this stream is more than two orders of magnitude less than the 2.6-g/L criticality limit and both iron and aluminum are present at much greater concentrations than those needed to

ensure subcriticality for the associated plutonium concentrations. This conclusion is supported by process records. The source and quantity of several important absorbers are listed in Table 9-12. The majority of this waste stream was received in tanks AZ-101 and -102. The actual volumes of waste transferred to the various receiving tanks are listed in Table 9-13.

9.3.2.1.3 Canyon Sump and Ammonia Scrubber Bottoms Waste. The canyon sump waste was received in Tank F-18, then sampled, neutralized, and discharged to tank farm tanks. Ammonia scrubber bottoms were transferred through Tank F18 periodically, but the quantity of waste from the scrubber bottoms was a very small fraction of the total waste. This canyon sump and ammonia scrubber waste stream was routed to Tanks AW-101, -102, -104, and -105 during the 1980s. Uranium is the only consistently significant insoluble neutron-absorber present in the canyon sump waste. Flowsheet, HDW model, and process records values for volume, specific gravity, volume percent solids, and plutonium and uranium content are compared in Table 9-14 with projected plutonium and uranium sludge content and the uranium-to-plutonium mass ratio of sludge as projected by process records.

9.3.2.1.4 Organic Wash Waste and Acid Fractionator Sump Waste. The organic wash waste and acid fractionator cell sump waste contained very small concentrations of plutonium in large quantities of waste and were not considered a concern. The volumes per MTU average 2716 L/MTU (see Appendix E) for organic wash waste and 1731 L/MTU (see Appendix E) for the acid fractionator cell waste. The amount of plutonium in each stream was very low, averaging 0.000101 g/L and 0.000017 g/L, respectively, and with average uranium-to-plutonium ratios of 4220 and 428. Few solids are associated with organic wash waste or acid fractionator cell sump waste. Some solids may form in the organic wash waste from the uranium and manganese content, but they would be expected to be only about 0.02 vol%. The chemical composition of the organic wash wastes indicated by the flowsheet and process records are shown in the Table 9-15. Only 182 g of plutonium were reported in the acid fractionator waste; 89 g went to AW-101 and 79 g went to AW-105. The low uranium-to-plutonium mass ratio (420) for the acid fractionator sump waste is not a criticality concern because of the low quantity of plutonium involved and because the waste stream was distributed to several tanks and mixed with other waste over a number of years.

The uranium content of the organic wash waste (average uranium-to-plutonium mass ratio of 4220) provided sufficient neutron absorption to maintain the waste much below the minimum required subcriticality value of 770. This waste was transferred to Tanks AW-101, AW-102, AW-103, AW-104, and AW-105. Tank AW 104 received 1094 g of plutonium from this stream between July 1986 and March 1990 at an average uranium-to-plutonium mass ratio of 2460. Tank AW-101 received 467 g of plutonium from this stream between July 1984 and March 1986 at a uranium-to-plutonium mass ratio of 3750. Tanks AW-102 received 80 g, AW-105 received 43 g, and AW-103 received 1 g from this stream. This waste transfer data is itemized in Appendix E.

9.3.2.2 Aluminum Clad Fuel Waste to Tank Farms. Irradiated aluminum clad fuels were processed at PUREX starting in January 1956 after cold runs were completed in the latter part of 1955. These runs continued through 1972 while other fuels were run intermittently. Aluminum cladding was removed from fuel

elements in the PUREX dissolver in boiling sodium nitrate solution while adding sodium hydroxide. The resulting solution was removed from the dissolvers and transferred to the C farm tanks from tank TK-D2. The dissolver was then rinsed with water that was transferred to the same C Farm tank. Typical O3N fuel elements contained about 42 g Al (as cladding and in AlSi bonding layer) per kg of uranium. The iron specification in the aluminum alloy (M-388) used for cladding after 1957 was between 0.45 and 0.77 wt%. An iron content of 0.5 wt% was assumed, which gives 209 g/MTU as a basis for the iron content in Table 9-16.

The composition of the aluminum cladding waste as listed in flowsheets, HDW, and process records is compared in Table 9-16. The projected plutonium concentration for sludge formed from this waste, assuming 6 vol% solids formation on settling in the tank farm, is 0.03 g/L, which is a factor of about 87 below the criticality limit of 2.6 g/L. Uranium, aluminum, and iron are present as insoluble neutron absorbers in sufficient quantity to ensure that the waste is subcritical. Uranium, by itself, is present at 2.2 times the concentration required to maintain this waste subcritical at the existing fissile content. The tanks receiving the cladding waste, quantities of waste transferred, time period of transfers, and sludge formation volume are listed in Table 9-17. Currently, we have only data for the last transfer to tank C-104. When the other records are declassified this table can be completed.

9.3.2.2.1 Neutralized Current Acid Waste (NCAW) for Aluminum Clad Fuel Processing. The aqueous NCAW waste from processing aluminum-clad fuel contained more than 99 percent of the nonvolatile fission products, plutonium and uranium losses from the HA column, and associated absorbers. This waste coming from the concentrator was originally neutralized and transferred to the A Tank Farm. In the early 1960's denitration was conducted with sugar, which reduced the amount of caustic that had to be added and the amount of waste that would have to be transferred. The sugar was destroyed in the process. After sugar denitration, the waste was agitated, sampled, and sent to Tank TK-F16 for neutralization. Analysis was made for plutonium and uranium, as well as for pH. Insoluble neutron absorbers were introduced to this stream by several mechanisms. Iron in this stream results from iron added to uranium metal to form a stable fuel alloy in the reactor, the addition of ferrous ammonium sulfamate as a reducing agent to the IBX, 2D, and 3A columns, and corrosion of the E-F6, 3WB, and 1UC concentrators and T-U6 acid vacuum fractionator. Iron impurities in the PUREX uranium product were negligible (<40 ppm). Chromium and nickel were introduced by corrosion of the same vessels, as fuel impurities, and as fission products in the irradiated fuel. Aluminum was introduced as an impurity in the uranium fuel. The sources and quantities of some insoluble neutron absorbers in this waste stream are listed in Table 9-18.

The quantity and average composition of important criticality-related components of the neutralized current acid waste stream from 1956 to 1967 are listed in Table 9-19, which compares the flowsheet values, the LANL HDW estimates, and the process records. The projected plutonium concentration in the sludge formed in the tanks from this stream is more than two orders of magnitude less than the 2.6-g/L criticality limit. Both iron and aluminum are present at much higher concentrations than needed to ensure subcriticality for

the associated plutonium concentrations. This conclusion is supported by process records. The majority of this waste stream was received in A Farm tanks.

Beginning in 1967, instead of being neutralized and going directly to the tank farm, this stream was sent to B Plant for strontium and cesium removal. Because the process records are being declassified and have not yet been evaluated, the values are not included in Table 9-18 at this time. It appears that the plutonium content should be near 0.002 g/L and this stream contains a high concentration of iron from the use of ferrous sulfamate reductant in the PUREX process and from corrosion of concentrators. If the sludge formed from this stream was 4 vol%, a resulting plutonium concentration of about 0.05 g/L would result. This is a factor of about 52 less than the criticality limit. Sufficient iron is present to provide an insoluble absorber-to-plutonium mass ratio of about 12,000, which results in a mass ratio sum of about 75. Sludge formed in the A Farm tanks from this stream is subcritical by a large margin.

9.3.2.2.2 Organic Wash Waste from Processing Aluminum-Clad Fuel. The organic wash waste from the Number 1 organic wash cycle (TK-G8) and Number 2 organic wash cycle (TK-R8) were transferred to the A Farm tanks with the boiling waste until 1969. After 1969 the organic wash waste was transferred to low-level waste in C Farm tanks. The organic wash waste contained very small quantities of plutonium in large quantities of waste and was not considered a concern. The amount of plutonium expected in this stream is very low, 0.0001 g/L. The process record uranium value given by Anderson (1990) of 0.036 g/L results in a uranium-to-plutonium ratio of about 360. Few solids are associated with organic wash waste. Some organic wash waste solids may form from the uranium and manganese content, but they would be expected to be only about 0.02 vol%. The chemical composition of the organic wash wastes, as indicated by Anderson (1990), is 0.04 M $NaNO_3$, 0.13 M Na_2CO_3, and 0.004M MnO_2. The low uranium-to-plutonium mass ratio (360) for the organic waste is not a criticality concern because of the low quantity of plutonium involved and because the waste stream was transferred intermittently with other waste streams to several tanks and mixed with other waste over a number of years.

9.3.2.2.3 Acid Fractionator Sump Waste. Acid fractionator sump waste was transferred to a crib during processing of aluminum-clad fuels. Therefore, none of this waste should have entered the Hanford Site tanks and it need not be considered further.

9.3.3 Thorium Fuel Waste to Tank Farms

Thorium was processed through the PUREX plant during two time periods. The quantities of thorium and ^{233}U processed during each period are listed in Table 9-7. Uranium-233 discharges to the tank farms during thorium fuel processing were from coating waste, high-level waste, canyon sump waste, organic wash waste streams, and plant flush waste. This waste was sent to Tank C-102 as the first tank in a cascading series of tanks during the 1966 campaign and to Tank C-104 as the first tank in a cascading series during the 1970-1971 campaign (Hess 1991).

The thorium fuel, received as powder and wafers, was packaged in aluminum cans. The aluminum cans were dissolved in sodium nitrate and sodium hydroxide solution and slurried from the dissolver carrying some thorium and uranium with them. This stream was centrifuged to remove entrained solids and the recovered solids were dissolved and added to the plant feed. The waste solution and slurry passing through the centrifuge was neutralized and transferred to C Farm (C-102 in 1966 and C-104 in 1970-1971). The composition of this stream is listed in Table 9-20 by flowsheet and process records for comparison. If the assumption is made that this stream contains about 5 vol% solids, it would form a sludge that contains 0.052 g/L ^{233}U, which is a factor of about 50 less that the criticality limit. Sufficient aluminum neutron absorber seems to be present to maintain this waste in a subcritical condition for the projected uranium concentration.

The neutralized thorium high-level waste (1WW) was accumulated in tank TK-F18 and transferred to C farm (tanks C-102 in 1966 and C-104 in 1970-1971). This waste came from the HA column, was concentrated in the EF-6 concentrator, sugar denitrated, neutralized in TK-F18, and then transferred to C Farm. The composition of this stream is compared by flowsheet and record values in Table 9-21. The projected ^{233}U concentration for sludge formed from this waste, assuming 4 vol% solids formation on settling in tanks, is 0.125 g/L, which is a factor of about 21 below the criticality limit of 2.6 g/L. Thorium, aluminum, and iron are present as insoluble neutron absorbers in sufficient quantities to ensure that the waste is subcritical. Thorium by itself is present at 3.5 times the concentration required to maintain this waste subcritical at the existing fissile content of this stream.

The thorium organic wash waste was accumulated in Tanks TK-G8 and TK-R8, neutralized, and transferred to the C Farm receiver tanks. The composition of this stream as listed in flowsheets and process records is compared in Table 9-22. The projected ^{233}U concentration for sludge formed from this waste, assuming 0.5 vol% solids formation on settling in tanks, is 0.3 g/L. This is a factor of about 9 below the criticality limit of 2.6 g/L. Thorium and manganese are present as insoluble neutron absorbers in sufficient quantity to ensure that the waste is subcritical.

Canyon sump waste was collected in Tank TK-F18, neutralized, and transferred to C farm tanks during the thorium campaigns. The waste uranium and thorium compositions of this stream are listed in Table 9-23. The projected ^{233}U concentration for sludge formed from this waste, assuming 0.2 vol% solids formation on settling in tanks, is about 3.1 g/L. This is just above the criticality limit of 2.6 g/L. Thorium is present on the average of 1.3 times the amount required to maintain the sludge formed from this stream in a subcritical condition. The quantity of sludge formed from this stream is small and, if distributed evenly over the tank sludge in a C farm tank, would amount to a sludge thickness of less than 1 cm. This waste was transferred between other waste transfers to the same C farm tank and would result in a mixed sludge with the cladding, 1WW, and organic wash waste. This stream does not present a criticality safety issue.

Plant flushes were made before starting the thorium runs and after completing them. These flushes were collected in Tanks TK-F18, TK-E5, TK-G8 and TK-R8, neutralized, and transferred to C Farm tanks. The waste uranium and thorium compositions of these flushes are listed in Table 9-24. The

projected ^{233}U concentration for sludge formed from this waste, assuming 0.1 vol% solids formation on settling in tanks, is about 3.6 g/L. This is above the criticality limit of 2.6 g/L. Thorium is present on the average of 0.96 times the amount required to maintain the sludge formed from this stream in a subcritical condition. The quantity of sludge formed from this stream is small and, if distributed evenly over the tank sludge in a C farm tank, would amount to a sludge thickness of less than 1 cm. This waste does not present a criticality safety issue in the tank farm.

9.3.4 REDOX

The REDOX process was the first continuous solvent extraction process used at the Hanford Site. It was developed at the Argonne National Laboratory. The REDOX process operated between 1952 and 1966 in the 202-S Building. Waste from the REDOX process was added to tank farm tanks as coating waste, high-level waste, and sump waste.

The REDOX process was a continuous counter-current column extraction process. The uranium and plutonium were separated from fission products and held in aqueous solution by manipulating the plutonium valence so that the two actinides could be preferentially extracted with hexone (methyl isobutyl ketone) and then separated from one another.

The design production or feed rate of the REDOX Plant was 3.1 tons of irradiated uranium reactor fuel per day. The product of the REDOX Plant was a liquid plutonium nitrate solution. The process was designed so that the high-level waste stream from REDOX would contain at least 10,000 ppm iron, with reference to plutonium.

Two types of waste were sent to underground tank storage: coating waste and REDOX high-level waste. The major components of the waste exiting the REDOX process were chromium, zirconium, iron, silicon, aluminum, sodium, and nitrate compounds.

Aqueous waste streams were directly transferred to underground tanks if analytical results were within the established limits for discharge. Initially, all of the liquid waste from the REDOX Plant was transferred to the S Tank Farm.

Based on two uranium and two plutonium purification cycles, detailed flowsheet data and process data, REDOX wastes transferred to tank farms are given in Table 9-25.

The REDOX aluminum-cladding waste is low in plutonium to give a projected sludge concentration of 0.04 g/L, assuming 6 vol% sludge formation on settling. It also has a uranium-to-plutonium mass ratio of 1284 and an aluminum mass ratio many times above the minimum required for neutron absorption to ensure subcriticality. The REDOX high-level waste is low in plutonium to give a projected sludge concentration of 0.005 g/L, assuming 4 vol% sludge formation on settling. It has a uranium-to-plutonium mass ratio of 1900, an iron-to-plutonium mass ratio of 893 and a chromium-to-plutonium mass ratio of 57,700. These add up to many times the minimum mass ratio sum required to ensure subcriticality in this waste stream.

9.3.5 Bismuth Phosphate Process Wastes

The bismuth/phosphate process was the first chemical process used at the Hanford Site to separate plutonium from irradiated reactor fuel elements. The bismuth/phosphate process operated between 1944 and 1956 in the 221-T Building and between 1945 and 1952 in the 221-B Building.

In this batchwise process, the plutonium valence was manipulated so the plutonium could be coprecipitated with bismuth phosphate, separated from uranium and the bulk of the fission products, and redissolved and reprecipitated several times for purification. Four major waste streams were sent to underground tanks from the bismuth phosphate process.

- Coating waste containing <0.1% of the plutonium
- Metal waste from extraction containing the greatest majority of the uranium, about 90 percent of the original fission product activity and 0.5 to 1.0 percent of the plutonium
- First decontamination cycle waste containing about 10 percent of the original fission product activity and 2 percent of the plutonium
- Second decontamination cycle waste containing less than 0.1 percent of the original fission product activity and about 1 percent of the plutonium.

The coating waste and the first decontamination cycle waste were combined initially but later kept separate for disposal.

The major cation components of the waste from the bismuth/phosphate process were uranium, silicon, chromium, iron, zirconium, bismuth, cerium, sodium, and aluminum. The major anion in most cases was nitrate, with lower concentrations of phosphate compounds. Typical compositions of the waste, as calculated from process flowsheets, are given in Table 9-28.

9.3.6 Uranium Recovery Waste Stream

Metal waste (waste containing the bulk of the uranium and fission products) from the bismuth phosphate plants were collected in underground storage tanks beginning in 1944. This waste was later removed from the underground tanks and processed through the Uranium Recovery Plant to recover uranium. The Uranium Recovery Plant began operation in 1952.

Uranium recovery waste consisted of combined, neutralized, and concentrated RAW and ROW streams. The composition and volume per metric ton of this waste stream transferred to the tank farms is listed in the Table 9-27. In November 1954, scavenging of the uranium recovery waste with ferrocyanide began. It resulted in the disposition of supernatant to the B-C Crib from the Uranium Recovery Plant and transfer of more concentrated waste to the tank farms. The projected plutonium concentration of sludge formed from this waste, based on a 4 vol% sludge formation volume, is less than 0.004 g/L. This is more than two orders of magnitude less than the criticality limit of 2.6 g/L. The uranium and iron content of this waste

provide an insoluble neutron absorber mass ratio sum of greater than 60, which results in waste conditions far below subcriticality.

9.3.7 Plutonium Finishing Plant Waste

PFP waste was transferred to the 242-T Evaporator Facility receiving tank (TK-R1) beginning in May 1973 because of a criticality concern in the cribs. Until then, PFP waste had been transferred to the cribs. PFP waste transferred to the 242-T Evaporator Facility consisted of high- and low-level salt waste and was transferred from the Z Plant D5 tank. This waste was neutralized in the 242-T Evaporator Facility and then concentrated in the 242-T Evaporator. The evaporator was shut down in 1976. PFP resumed operations in 1978 and its waste was routed to Tank TX-118 until 1981, when the PFP waste was diverted to the DST SY-102.

9.4 PLUTONIUM AND ABSORBER CONCENTRATIONS IN WASTE

Fissile and absorber material concentrations in the underground storage tanks have been calculated from actual analysis of only a few samples of tank waste. In general, the fissile materials are in the sludges formed in the underground tanks. These sludges were formed by settling/precipitation in the tanks from the introduced slurries. The fissile content of supernatant is less than 0.0005 g/L for most tanks. Salt cakes formed from evaporation of water from the supernatants also contain very low concentrations of fissile material and do not approach criticality.

The ratios of selected neutron absorbers to plutonium for the sludge fraction of tank contents were calculated for each tank using either predicted contents or actual measurements. The calculations were based on the following two sets of tank concentration and inventory information:

- Historical Tank Content Estimate (HTCE) Model Revision 3 estimates (Agnew et al. 1996)

- Estimates of average tank plutonium and absorber concentrations from sample data for a selected number of tanks based on tank characterization reports (TCR) (Hartley et al. 1996).

The elements analyzed as neutron absorbers were shown in Table 9-3.

The plutonium concentrations, which were given in activity units (pCi/g), had to be converted to mass units (ug/g) to calculate the mass ratios of the individual neutron absorbers to plutonium. The individual element-to-plutonium mass ratios were then divided by the element-specific minimum absorber-to-plutonium ratio needed to ensure subcriticality (Rogers 1996). The minimum subcritical ratios determine the minimum relative concentrations for the absorber materials that, if present individually with the plutonium, would provide subcriticality for any degree of moderation. Therefore, a ratio greater than 1.0 should indicate subcritical conditions. The individual absorber-to-plutonium ratios may be summed to give an overall assessment of the subcriticality conditions of the tank contents.

The subcriticality conditions in the tank can be further refined by summing the criticality ratios of the soluble and insoluble neutron absorbers separately. The sum of the criticality ratios for the insoluble neutron-absorbing elements demonstrates an added measure of subcriticality because there is added assurance that the insoluble elements will remain in close proximity with the plutonium in the tank sludge under the caustic tank conditions. The insoluble absorbers were: iron, chromium, bismuth, lanthanum, zirconium, nickel, manganese, and uranium.

Aluminum can become soluble under conditions associated with a pH of 14 or higher, so for this analysis, only 70 percent of the aluminum was assumed to be insoluble. Tables 9-28 and 9-29 give the total ratio sum and the ratio sum for the insoluble absorbers-to-plutonium for the sludge for the single- and double-shell tanks, respectively.

HTCE (Agnew et al. 1996) plutonium and absorber concentrations were estimated for 12 of the 28 DSTs and for all 149 SSTs. One of the SSTs, C-202, did not have criticality ratio estimates calculated because the HTCE analysis reported a 0.0 concentration for plutonium. The 14 tanks for which TCR sample tank average concentration contents were measured [see Hartley et al. (1996)] were all SSTs.

The tables contain 8 columns with the following information:

- Tank name
- Designation of tanks with high plutonium (using as *) [see Section 9.3.1 for discussion/rationale]
- The estimated total plutonium concentration in the tank solids (from Agnew et al. 1996)
- The sum of the ratio of all neutron absorbers-to-plutonium ratio using Agnew et al. (1996)
- The sum of the ratio of the insoluble neutron absorbers-to-plutonium ratio using Agnew et al. (1996)
- The average concentration of plutonium measured in tank solids from actual measurement (TCR)
- The sum of the ratio of all neutron absorbers-to-plutonium ratio using measured data (TCR)
- The sum of the ratio of insoluble neutron absorbers-to-plutonium ratio using measured data (TCR).

These evaluations show Tanks TX-118 and AW-103 as the only tanks with more than 10 kg plutonium to have a minimum total absorber-to-plutonium mass ratio sum of less than 10, which gives an order of magnitude safety factor regarding criticality assessment. These results support the conclusion that Hanford Site tank waste is subcritical, but additional evaluations are warranted.

In a separate analysis, we used Appendix C (Waste Sample Data and Analysis) of Braun et al. (1994), which describes analyses of tank sample concentrations for plutonium and absorber materials. The samples were taken from Hanford Site tank waste from 1974 to 1994, with the majority of the samples taken before 1989. Figure C-14 in Braun et al. (1994) is a histogram of the plutonium concentration in 221 solid samples; the maximum plutonium concentration was reported as 0.547 g/L. Figure C-24 in Braun et al. (1994) shows a histogram of the ratio sum for insoluble neutron absorbers for 236 solid samples. The insoluble absorbers used in the analysis were uranium, iron, manganese, chromium, and nickel. Eighteen of the 236 samples had ratio sums of less than 1, with about 55 samples having ratio sums of less than 10.

Each tank was evaluated for its potential for criticality based on the following eight criteria.

- Plutonium concentration <1 g/L
- Individual insoluble mass ratio for any absorber >1.0
- Sum of insoluble mass ratios >1.0
- Individual soluble mass ratio >10.0
- Sum of soluble mass ratios >10.0
- Thickness of sludge layer <20 in.
- For tanks with no sample information - similarity between tanks in a waste-type tank grouping that has at least one tank sampled and meet three of the first five criteria
- For tank groups or miscellaneous tanks that have no sample information - similar to tank groups with sample information or based on waste type.

Based on combinations of these criteria, all of the tanks were judged to be subcritical.

9.5 DISCUSSION OF ACTIVE TANKS (DOUBLE-SHELL TANKS)

As shown in Table 9-29 seven DSTs were estimated to have more than 10 kg plutonium. Because theses tanks are considered still active, they were evaluated in groups based on the types of waste received. The bulk of each tank's plutonium content is actually verified by analysis or is assumed to be in the waste sludge. The supernatant in these tanks contain almost negligible concentrations of plutonium. Salt cake inventory is not reported in these tanks except for AW-106, which is reported to contain 322,000 L of salt cake. Typical measured supernatant concentrations of plutonium are listed in Table 9-30.

PUREX zirconium decladding waste was received in Tanks AW-103 and AW-105 during the 1980's to form sludge layers on existing solids in the tanks. Neutralized current acid waste was received in Tanks AZ-101 and AZ-102. AW-106 received waste from several unrelated sources.

9.5.1 Waste in Tanks AW-103 and AW-105

A schematic of the waste in Tank AW-103 is shown in Figure 9-3, along with the waste introduction and core sample locations for the core sample obtained January 23, 1989. Core samples were obtained at about an 8.2-m radius in tanks AW-103 and AW-105. Results of the AW-103 core sample analysis listed in Table 9-31 for the composite of segments 4 and 5R indicate that the decladding waste, settled as sludge in the tank, has a plutonium concentration of 0.0327 g/L. Results of comparing the segment 4 and 5R composite analysis with the segment 6-10 (material from lower level in the sludge) segment composite analysis imply that a sludge heel existed in the tank before PUREX zirconium decladding waste was introduced in November 1983. The segment 6 through 10 composite analysis suggests that a heel of other waste with little plutonium and zirconium and more aluminum was present in Tank 103-AW before decladding waste was added in 1983. The decladding waste had substantial zirconium, while the initial heel had no significant zirconium and the heel contained significantly more aluminum than the zirconium cladding waste.

The Waste Tank Summary Report (Hanlon 1996) indicates a sludge content for AW-103 of 1,374,000 L and a supernatant content of 572,000 L. The same report indicates a sludge content of 1,124,000 L and a supernatant content of 288,000 L for AW-105. These sludge volumes are thought to have been representative of the sludge volume in 1989 and 1990 when sampling occurred. The quantity of sludge represented by core height is 7 full segments or 1,380,000 L for AW-103,and 4 full and one partial segment or 853,000 L for AW-105.

Table 9-31 also shows the results of the tank AW-105 sludge core sample analysis along with comparisons of projected sludge compositions based on process records for both tanks. Similar comparisons of the measured neutron absorber-to-plutonium mass ratios with process record estimated ratios are shown in Table 9-32.

Comparing process record sludge concentration projections with actual tank sample analysis for representative layers of waste, some significant differences are apparent. As determined by AW-103 and AW-105 sludge analysis, the plutonium content of the accumulated sludge is significantly higher than shown by NMC records of zirconium decladding waste batches transferred to these tanks during the 1980's. The zirconium content, as determined by sludge analysis and volume, is about a factor of two higher than was expected based on the total zirconium determined to be added to the two tanks from fuel elements processed in PUREX. We can not explain this discrepancy at this time. Either the chemical analysis for zirconium in the core material removed from the tank is incorrect or the flow sheets and process records are not accurate. However, we believe that the masses of fuel processed through the PUREX Plant are known, so actual quantities are known for the zirconium in decladding waste. This makes zirconium the most accurately known constituent in this waste stream.

Differences in plutonium content between the plant sending and the tank farm receiving the waste may be explained by sampling uncertainties in the plant batch-sampling procedures. The fines might not always have been representatively collected and analyzed. When NMC decladding waste samples were obtained from Tanks TK-D2 and TK-E3, collected solids were not analyzed. The plant centrifuge was assumed to have removed the solids before the waste was transferred to the TK-E5 neutralization tank. Starting in March 1994, when NMC samples were obtained from TK-E5, any undissolved fines from the samples were not analyzed. Some difficulties were observed in plutonium sampling by operating personnel (Harlow 1986) and the procedures were changed in 1987 to include analysis of fines.

Because fines were observed to be a concern in this stream, it could also be implied that fines may settle out of the supernatant unevenly in the tank farm receiving tank. The observation that the zirconium content of the sludge is greater than expected by a factor of about two could support a concern that uneven settling may have occurred. The waste was introduced into the tanks from near the top center of the tank through a pipe with an internal diameter of 0.957 cm angled about 20° from the horizontal and extending out less than 0.1 m. This angled pipe was rotated after each batch transfer to distribute the waste in different directions. The discharge rate of about 2.8 L/s would put the slurry at about an 8-m radius for a 7-m drop in elevation from the nozzle discharge point.

Obtaining core samples of the sludge as a function of radius in at least one of these receiving tanks and conducting a comparative analysis on the analytical results would be valuable. This would show whether the plutonium or zirconium is distributed unevenly.

Analysis of the 1990 AW-105 sludge sample showed a plutonium concentration of 0.063 g/L, which is about a factor of 50 less than the criticality concentration limit. Analysis of the 1989 AW-103 sample showed a concentration of 0.033 g/L, which is a factor of about 80 below the limit. The zirconium-to-plutonium mass ratio was 5111 in this AW-105 sample and 7697 in the AW-103 sample. These ratios are more than sufficient to ensure subcriticality. The insoluble absorber-to-plutonium mass ratios for AW-103 and AW-105 are listed in Table 9-32, along with the insoluble absorber-to-plutonium mass ratio sums. The insoluble neutron absorber-to-plutonium mass ratio sums for the upper sludge in these tanks are 3.2 for AW-103 and 2.7 for AW-105 and 8.5, as indicated by the process records. These results indicate that the decladding waste is below criticality.

9.5.2 Waste in Tank AW-106

The current Waste Tank Summary report (Hanlon 1996) indicates that tank AW-106 contains 799,000 L of sludge, 322,000 L of salt cake, and 912,000 L of supernatant. No sludge or salt cake samples were analyzed for this tank. Tusler (1995)suggests that the AW-106 sludge should be similar in chemical composition to AW-105 sludge, even though the sludge inventories are not related. Tusler concludes with a baseline recommended plutonium inventory of 13,988 g in AW-106. AW-105 received mainly PUREX zirconium-cladding waste starting in June 1984. Tank AW-106 received miscellaneous waste from A-106 in

1980, from B Plant in 1982, from AW-103 early in 1983. It also received miscellaneous waste from AW-102 from 1985 to 1989, from AP-105 in 1988, from AY-102 in 1989, and from an evaporator mini run in 1993 (Tusler 1995, Brevick 1995).

The tank HDW Model Rev 3 report (Agnew et al. 1996) indicates a much lower plutonium inventory in Tank AW-106 at 4310 g. It is recommended that the waste in this tank be core sampled and analyzed to provide supportive technical data for a more thorough evaluation of the criticality safety issue in this tank. In either case (Tusler baseline or HDW Rev 3), the plutonium concentration is more than one order of magnitude less than the criticality limit of 2.6 g/L and the waste is expected to be in a subcritical condition.

9.5.3 Waste in Tank AY-101

Tank AY-101 is reported (Hanlon 1996) to contain 314,000 L of sludge (76 cm deep) and 3,229,000 L of supernatant with no salt cake. Waste transfers into tank AY-101 include dilute noncomplexed waste from B Plant in 1981, dilute complexed waste from B Plant in 1983, waste from Tank AZ-102 in 1984, and miscellaneous smaller waste transfers from B Plant, PUREX [a very small amount of plutonium was added from NZCAW (22 g) and canyon sump waste (9 g)], saltwell pumping, and the 300 Area.

A sample containing supernatant and sludge (labeled 101-AY-1) was obtained from AY-101 December 29, 1994. This sample consisted of approximately 60 vol% settled solids and 40 vol% clear supernatant liquid. The liquid and settled solids were separated and analyzed and the results reported in an internal memo (Herting to Jones February 27, 1996). The settled solids were considered sludge. The sample represents a grab sample of the supernatant and sludge thought to be obtained near the top of the sludge in the tank.

The sludge (settled solids) analysis for plutonium and insoluble absorbers is listed in Table 9-33. The results listed are an average of a sample and a duplicate sample (very close agreement between sample and duplicate analysis) taken from the grab sample settled solids (Herting 1996a). Insoluble neutron absorber-to-plutonium ratios and ratio sums are also included in Table 9-34. The results show that the sludge plutonium concentration is two orders of magnitude less than the criticality limit of 2.6 g/L. The top portion of sludge in this tank contains sufficient insoluble absorbers (mass ratio sum of 19.8) present to preclude a criticality concern. Consideration should be given to obtaining and analyzing a full core sample of the sludge in this tank because the projected plutonium inventory (3.9 kg) implied by this grab sample evaluation is considerably less than the baselined (24 kg) and HDW Model Rev 3 (23 kg) values (see Table 9-5). Based on the sources of waste added to this tank, the grab sample evaluation appears more reasonable than the baselined or HDW Rev 3 values, but a good core sample evaluation of the sludge in this tank appears to be warranted. In either case, the plutonium concentration is more than one order of magnitude below the 2.6-g/L criticality limit. The insoluble neutron absorber-to-plutonium mass ratio is greater than 2 and the waste would be subcritical.

9.5.4 Waste in Tanks AZ-101 and AZ-102

Tank AZ-101 is reported (Hanlon 1996) to contain 132,000 L of sludge and 3,365,000 L of supernatant with no salt cake. Waste transfers to this tank included waste from Tank SY-102 in 1982, Tank AY-102 in 1983, and PUREX NZCAW in 1983 through 1986. According to NMC transfer records, 9,700 g of plutonium were added with this stream. Additional small volumes of noncomplexed waste were transferred to this tank.

Two core samples of AZ-101 waste were obtained in April and May 1989 and analyzed for chemical and radionuclide content. Before the tank was sampled, six sludge-level measurements were made and an average sludge level determination of 43 cm (17 in. or 177,000 L) was calculated. Two segments were obtained for each core. The first sample core obtained from riser #15F consisted of one segment with 280 g of supernatant and one segment consisting of 200 g of dark brown solids and 118 g of drainable liquid. The solids were soft, creamy, and sticky and did not maintain the cylindrical shape of the sampler after extrusion. Also, the solids obtained did not necessarily represent sludge strata in the tank because the second segment was obtained by suction from the bottom of the tank. Suction was used because the sampler was started at the bottom of the tank and could not be pushed or rotated. Analysis of the sample solids is listed in Table 9-34.

The second core sample was obtained from riser # 24D and consisted of two segments. The upper segment (#89-013) was 39.4 cm long, dark brown in color, retained its cylindrical shape after extrusion, and consisted of 305 g of solids with no drainable liquid. The lower segment (#89-014) was 48 cm long and consisted of 109 g drainable liquid and 208 g solids. Some concern about the strata representativeness of the lower segment is noted because about 17.9 cm of drainable liquid was present between the layers of solids. The total height of solids obtained in the samplers (39.4 cm in upper segment and 25.7 cm in lower segment) is in excess of the expected average solids height (43 cm) in the tank by about 22 cm. A composite sample was made from these two segments and analyzed. Results of the composite sample are listed in Table 9-34, along with the results from the first core and projected concentrations based on process records. Insoluble neutron absorber-to-plutonium mass ratios and ratio sums were calculated from these analyses. They are listed in Table 9-35, along with the projected mass ratios based on process records.

Four 1-cm-thick layer sections (subsamples L1, L2, L3, and L4) of these two segments were analyzed and reported in Hodgson (1995b). The results of these layer samples indicate that the solids at the bottom of the tank (about 6 cm from the bottom-sample L3) consist of waste with considerably greater aluminum, chromium, silver, manganese, sodium, chloride, nitrite, and sulfate than the three higher layers. The lower layer also had considerably lower concentrations of barium, calcium, cadmium, cerium, iron, nickel, and zirconium. The next layer sample (L4 obtained 44 cm up from the bottom of segment 2, not necessarily from the bottom of the tank, because liquid layers existed in the sample between these two locations) indicated that the layer consisted principally of the NZCAW waste with a minor mix of tank heel waste of L3 composition. These observations imply that AZ-101 had a heel of about 18 cm, then about 25 cm of NZCAW waste was added above it.

Results show that the bulk sludge plutonium concentration is about 0.16 g/L or less by sample analysis of the sludge in Tank AZ-101 and by projections from process record data, which is considerably less than the 2.6 g/L criticality limit. Sufficient insoluble absorber content (by factors of 8.6 to 13, mainly iron) is associated with the NZCAW sludge plutonium to ensure subcriticality by both sample analysis of the sludge in Tank AZ-101 and by projections from process record data.

9.5.5 Waste in Tank SY-102

Tank SY-102 is reported (Hanlon 1996) to contain 269,000 L of sludge and 1,169,000 L of supernatant with no salt cake. Tank SY-102 began receiving waste in 1977. Waste transferred to this tank from 1977 to 1981 was supernatant from the 241-S, -SX, -T, and -U tank farms (Jungfleish 1984) as feed to the 242-S and 242-A Evaporators. In 1981 SY-102 began receiving sludge and dilute noncomplexed waste from T Plant decontamination processes and dilute noncomplexed waste from 222-S Laboratory. In 1982 waste from PFP consisting of slurry and transuranic solids began being added to this tank. Salt well liquids from 200 West Area tanks were received in SY-102 until 1983 and after 1993.

The sludge accumulated in the tank is expected to have come from three sources. The first is precipitate of manganese dioxide and hydrous manganese hydroxide from wastes added in 1977. Some may have accumulated from transferring REDOX waste from S and SX tank farms before 1981. This waste contained high concentrations of aluminum, chromium, and iron. The third source was PFP slurry wastes added after 1981. The sludge from PFP wastes is expected to contain plutonium and ^{241}Am in it.

Three sampling and analysis events have occurred for Tank SY-102. The first core sample was obtained from riser 1B in October 1988. Push mode core samples were obtained in 1990 and a supernatant grab sample was obtained in 1994.

The 1988 core sample consisted of four segments. The top two (segments 1 and 2) consisted of supernatant and the bottom two (segments 3 and 4) consisted of sludge. The bottom sludge segment (4) contained 38.1 cm of recovered sludge. The top portion of this segment was analyzed and the results are listed in Table 9-36. Insoluble neutron absorber-to-plutonium mass ratios are given in Table 9-37.

Sludge sample analysis evaluations show low plutonium concentrations (0.018 g/L) and high concentrations of insoluble neutron absorbers. This ensures that this waste is in a highly subcritical condition. As the process records for the PFP wastes are obtained and evaluated, we expect them to support this conclusion.

As mentioned earlier in the report, Tank SY-102 is of special importance because a mixer pump will be installed in the tank. The mixer pump could rearrange the sludge particles. Analyses presented in Chapters 4, 5, and 6 suggest that discrete particle separation is not very likely and that the potential for this tank to go critical is extremely low, if not nonexistent.

9.6 SUMMARY AND CONCLUSIONS

The relevant criticality safety properties of Hanford Site underground stored waste was characterized in this chapter using currently available information. This chapter identified relevant fissile materials, neutron absorbers, and moderators related to criticality in waste streams sent to the tank farms and in the waste currently in the tanks. It also considered waste treatment processes that have been conducted on the waste over time. Additional information needed to provide more conclusive estimates of the contents of some of the tanks with the highest plutonium inventories is identified.

The approach to identifying properties relating to criticality in existing waste storage tanks was to determine the batchwise composition of discharges from the processing facilities to the tank farm storage tanks. NMC records were used for plutonium, uranium, and neptunium transfers because they have been well documented and reviewed for accuracy and because they identified the Hanford Site tanks that received each batch of waste. The NMC records included an accountability volume that was compared, where possible, to plant waste discharge volumes as supportive information. Where possible, the settled sludge concentration of fissile material and insoluble neutron absorbers in tanks that may contain fissile material in concentrations higher than 10 kg was determined based on the historical accumulation of process waste streams and by core sample analysis results. These two approaches to estimating inventories were compared and discrepancies discussed.

The results show that the fissile material concentrations in all of the Hanford Site tank waste is likely at subcritical values and that sufficient insoluble neutron absorbers are present to maintain subcritical conditions under safe storage and retrieval operations. Additional sampling of tank waste is recommended for some selected tanks to verify tank fissile material and insoluble absorber content.

We made the following final conclusions.

- The plutonium or equivalent plutonium concentration in most of the waste tank sludge is at least one to two orders of magnitude less than the 2.6-g/L criticality limit as determined by both process records and tank sample analysis results.

- The plutonium or equivalent plutonium concentration in the supernatant and salt cake in most tanks (those for which defensible data are available) is at least three orders of magnitude less than the 2.6-g/L criticality limit as determined by tank sample analysis.

- Process records and tank sample analysis indicate that the waste contains sufficient insoluble neutron absorbers to render the fissile material in a subcritical condition.

- Additional sampling and analysis of some tanks (tanks with high plutonium inventories) should be conducted to verify that the fissile and insoluble neutron absorber materials are at concentrations similar to the predictions, which clearly would maintain subcritical conditions.

- Any effort to remove the sludge waste (i.e. tank contents retrieval) or change its configuration (mixer pump operation, continued waste disposal, etc.) that may result in an increase in plutonium concentration and/or removal of insoluble neutron absorbers from the waste must be evaluated for effect on the criticality state of the waste before beginning the operation.

Figure 9-1. Schematic for the 28 DSTs at the Hanford Site.

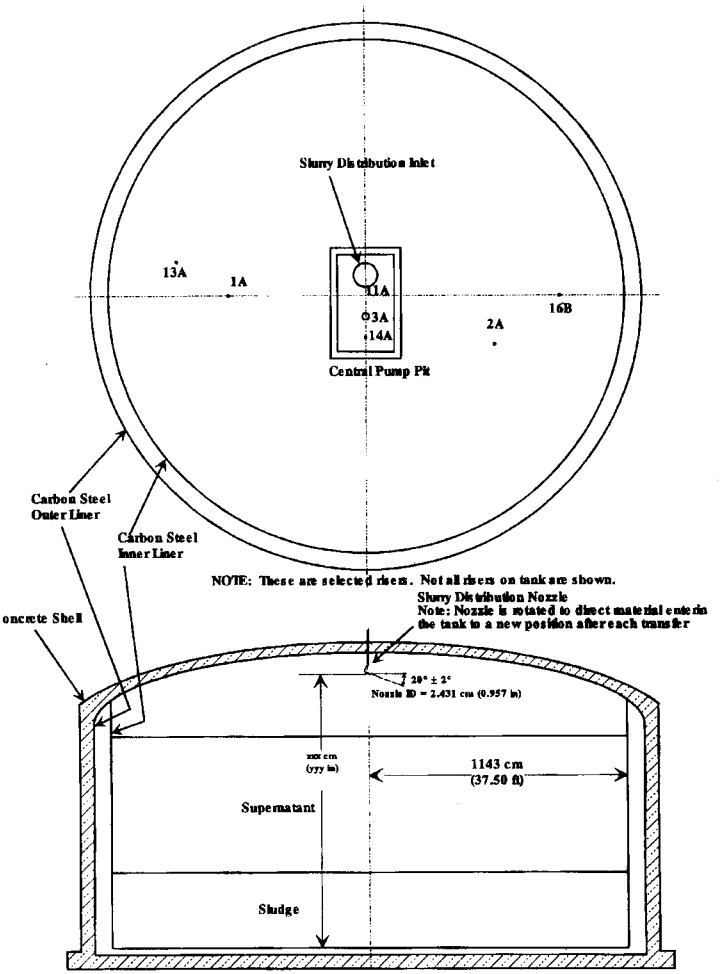

Figure 9-2. Schematic for the Two Types of SSTs at the Hanford Site.

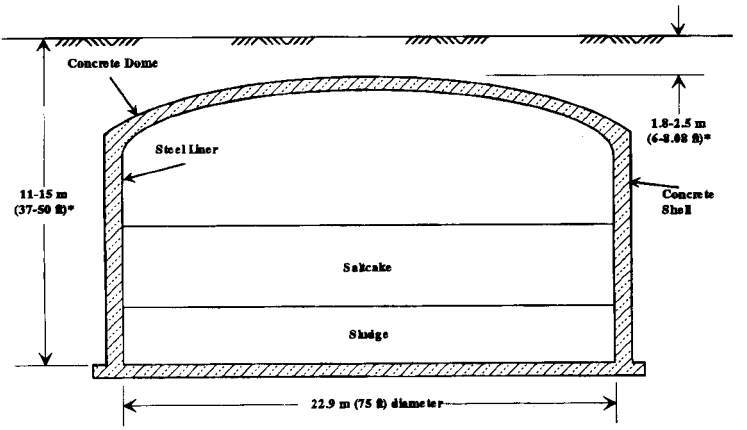

Single-Shell Tank (Types II, III and IV typical)

*Dimension and bottom profile varies with tank type

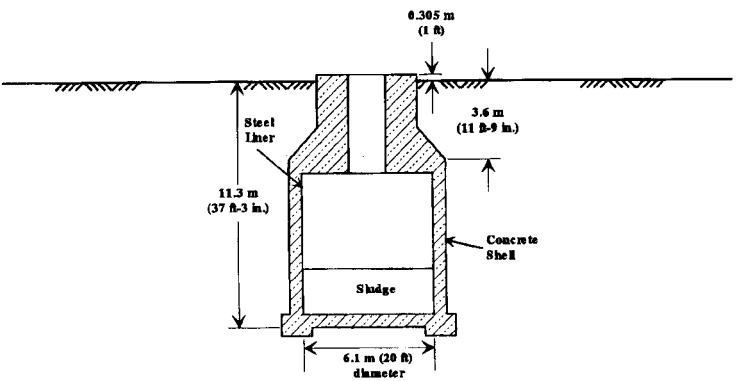

Single-Shell Tank (Type I)

Figure 9-3. Schematic of Tank AW-103 Showing Waste Introduction Location.

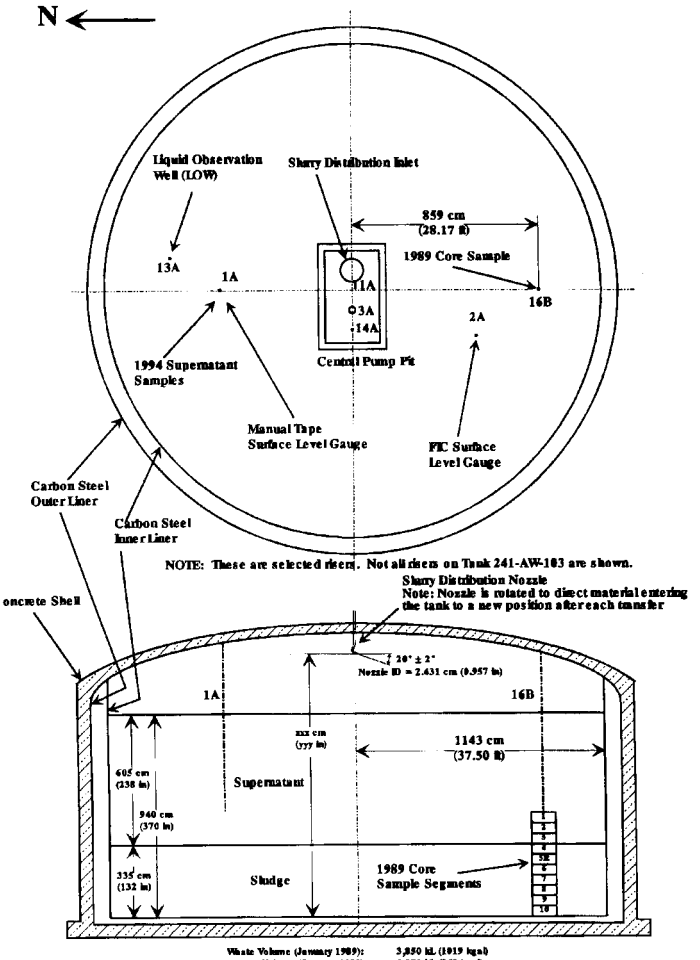

This page intentionally left blank.

Table 9-1. Plutonium Production by Plant.

	Quantity of plutonium processed (MT)	Mass of total plutonium (%)
Bismuth Phosphate T Plant B Plant	2.70	4.3
REDOX	11.27	18.0
PUREX	48.73	77.7

Table 9-2. Tank Diameters.

Tank type	No. of tanks	Diameter in m (ft)
SSTs	133 16	6.10 (20) 22.9 (75)
DSTs	28	22.9 (75)

Table 9-3. Minimum Subcriticality Mass Ratio for Selected Absorber Materials.

Insoluble absorbers (under tank waste conditions)	Minimum subcriticality mass ratio (absorber/fissile material)
Aluminum (assume 70% insoluble)	910
Bismuth	48,000
Boron	0.09
Cadmium	0.24
Calcium	770
Chromium	135
Copper	130
Iron	160
Lanthanum	121
Manganese	32
Mercury	5
Nickel	105
Silicon	1,400
Thorium	243
Uranium (natural)	770
Zirconium	4,000
Soluble absorbers	
Nitrogen	61
Phosphorus	1,300
Sodium	360

Table 9-4. Single-Shell Tank Plutonium Inventory Comparison. (7 sheets)

Tank	Waste Status Summary[a] (KL)			ASA source term and sample data[b]				HDW model (Rev. 3)[c] Pu (g)	WESTREN[d]		TRAC-summary TI-057 03/12/85[e]		HDW Model (Rev. 3)[c] ratio sum
	Sludge	Salt	Liquids	Sludge (g Pu/L)	Salt (g Pu/L)	Liquids (g Pu/L)	Total Pu (g)		Total Pu (Bq)	Pu (g)	Pu (Ci)	Pu (g)	
A-101[f]	11.4	3,596	0.0	6.52 E-04	4.40 E-03	4.40 E-03	15,828.70	3,730.00	4.46 E+12	1,943.13	2.00 E+03	32,258.06	234
A-102	56.8	83.27	15.1			1.80 E-03	27.25	792.00	4.57 E+10	19.90	3.00 E+02	4,838.71	20.8
A-103	1,385.3	0	18.9			5.00 E-04	9.46	702.00	7.36 E+12	3,205.16	4.00 E+02	6,451.61	6.19
A-104[f]	106.0	0	0.0	1.09 E-01			11,551.82	16,100.00	2.36 E+13	10,277.42	6.00 E+02	9,677.42	6.45
A-105[f]	71.9	0	0.0	1.40 E-01			10,053.72	1,760.00	1.00 E+13	4,354.84	2.00 E-06	3.23 E-05	59.6
A-106[f]	473.1	0	0.0	7.67 E-02		4.70 E-05	36,265.03	19,900.00	6.74 E+13	29,351.61	1.00 E+03	16,129.03	11.4
AX-101	11.4	2,820	0.0	5.00 E-05	5.00 E-05	5.00 E-05	141.56	4,700.00	1.06 E+11	46.16	3.00 E+02	4,838.71	42.6
AX-102	26.5	109.8	11.4		1.82 E-03	1.82 E-03	219.95	6,940.00	4.08 E+10	17.77	1.00 E+02	1,612.90	3.2
AX-103	7.6	416.4	0.0		4.20 E-05	4.20 E-05	17.49	1,670.00	2.86 E+11	124.55	0.00002	3.23 E-04	59.6
AX-104	26.5	0	0.0	1.49 E-01			3,934.51	647.00	1.42 E+13	6,183.87	3.00 E+02	4,838.71	59.6
B-101[f]	427.7	0	0.0	2.16 E-02			9,238.43	13,100.00	1.67 E+13	7,272.58	5.00 E+02	8,064.52	54.5
B-102	68.1	37.85	15.1		4.00 E-05	4.00 E-05	2.12	142.00	7.13 E+09	3.11	5.00 E+01	806.45	1,130
B-103	223.3	0	0.0			6.80 E-05	0.00	52.30	1.00 E+10	4.35	2.00 E+02	3,225.81	8,830
B-104	1,139.3	261.2	3.8	4.07 E-03	4.07 E-03		5,692.83	393.00		0.00	1.00 E+02	1,612.90	2,690
B-105	151.4	1,007	0.0	2.46 E-04	2.46 E-04		285.38	150.00	8.45 E+09	3.68	1.00 E+01	161.29	6,070
B-106	439.1	0	3.8			1.60 E-05	0.06	107.00	2.05 E+09	0.89	1.00 E+00	16.13	6,690
B-107	620.7	0	3.8	5.14 E-03			3190.60	79.60	7.49 E+12	3,261.77	4.00 E+01	645.16	4,160
B-108	355.8	0	0.0				0.00	71.10		0.00	4.00 E+00	64.52	6,030
B-109	480.7	0	0.0			3.34 E-06	0.00	1,660.00	3.58 E+09	1.56	5.00 E-01	8.06	335
B-110	927.3	0	3.8				0.00	485.00		0.00	2.00 E+02	3,225.81	1,240

Table 9-4. Single-Shell Tank Plutonium Inventory Comparison. (7 sheets)

Tank	Waste Status Summary[a] (KL)			ASA source term and sample data[b]				HDW model (Rev. 3)[c] Pu (g)	WESTREN[d]		TRAC-summary TI-057 03/12/85[e]		HDW Model (Rev. 3)[c] ratio sum
	Sludge	Salt	Liquids	Sludge (g Pu/L)	Salt (g Pu/L)	Liquids (g Pu/L)	Total Pu (g)		Total Pu (Bq)	Pu (g)	Pu (Ci)	Pu (g)	
B-111	893.3	0	3.8	2.81 E-03			2,510.06	2,560.00		0.00	3.00 E+01	483.87	223
B-112	113.6	0	11.4				0.00	189.00		0.00	4.00 E+00	64.52	949
B-201[g]	106.0	0	3.8	9.19 E-02			9,739.56	24.40	1.71 E+13	7,446.77		0.00	4,520
B-202[g]	102.2	0	0.0	1.01 E-02		1.15 E-06	1,032.17	23.50	9.47 E+11	412.40	2.00 E+02	3,225.81	4,520
B-203[g]	189.3	0	3.8	1.13 E-02			2,138.53	43.50	7.74 E+11	337.06	7.00 E-01	11.29	4,520
B-204[g]	185.5	0	3.8	1.28 E-02			2,373.95	42.70	4.35 E+12	1,894.35	7.00 E+00	112.90	4,520
BX-101	159.0	0	3.8	1.67 E-03			265.16	4,270.00	5.73 E+11	249.53	5.00 E+02	8,064.52	53.2
BX-102	363.4	0	0.0			1.89 E-06	0.00	591.00		0.00	3.00 E+01	483.87	541
BX-103	234.7	0	22.7			1.49 E-04	3.38	960.00	2.61 E+11	113.66	2.00 E-04	0.00	239
BX-104	363.4	0	11.4	1.23 E-02		3.44 E-04	4,473.23	254.00	7.88 E+12	3,431.61	6.00 E+01	967.74	9,440
BX-105	162.8	11.36	18.9	2.83 E-03	3.04 E-04	3.04 E-04	469.80	37.80	1.04 E+12	452.90	1.00 E-03	0.02	9,440
BX-106	143.8	0	0.0			1.22 E-04	0.00	328.00	2.71 E+08	0.12	1.00 E-03	0.02	879
BX-107	1,302.0	0	3.8	3.22 E-03		8.10 E-05	4,192.88	281.00	5.34 E+09	2.33	5.00 E+01	806.45	2,320
BX-108	98.4	0	0.0				0.00	23.80		0.00	5.00 E+00	80.65	2,000
BX-109	730.5	0	0.0			6.70 E-05	0.00	88.10	2.72 E+08	0.12	6.00 E+01	967.74	10,000
BX-110	772.1	0	11.4	1.06 E-03		2.26 E-06	818.49	619.00	1.12 E+07	0.00	2.00 E+01	322.58	1,070
BX-111	196.8	412.6	3.8			1.86 E-04	0.70	2,000.00	2.28 E+08	0.10	2.00 E+00	32.26	852
BX-112	620.7	0	3.8			2.16 E-04	0.82	209.00	2.09 E+10	9.10	1.00 E+01	161.29	1,940
BY-101	412.6	1,052	0.0				0.00	3,840.00		0.00	4.00 E-02	0.65	878
BY-102	0.0	1,048	0.0				0.00	3,440.00		0.00	4.00 E-03	0.06	849

Table 9-4. Single-Shell Tank Plutonium Inventory Comparison. (7 sheets)

Tank	Waste Status Summary[a] (KL)			ASA source term and sample data[b]				HDW model (Rev. 3)[c] Pu (g)	WESTREN[d]		TRAC-summary II-057 03/12/85[e]		HDW Model (Rev. 3)[c] ratio sum
	Sludge	Salt	Liquids	Sludge (g Pu/L)	Salt (g Pu/L)	Liquids (g Pu/L)	Total Pu (g)		Total Pu (Bq)	Pu (g)	Pu (Ci)	Pu (g)	
BY-103[f]	18.9	1,495	0.0				0.00	5,320.00		0.00	9.00 E+02	14,516.13	679
BY-104	151.4	1,385	0.0		1.97 E-03		2,729.06	1,940.00	6.28 E+12	2,734.84	2.00 E+02	3,225.81	1,200
BY-105	166.5	1,737	0.0		2.90 E-05	2.90 E-05	50.38	3,700.00		0.00	9.00 E+01	1,451.61	1,040
BY-106	359.6	2,070	0.0	1.93 E-05	1.93 E-05		46.85	5,950.00		0.00	3.00 E+01	483.87	918
BY-107	227.1	779.7	0.0				0.00	1,670.00		0.00	3.00 E+01	483.87	1,110
BY-108	582.9	280.1	0.0				0.00	710.00		0.00	3.00 E+01	483.87	1,920
BY-109	314.2	1,287	0.0				0.00	4,240.00		0.00	8.00 E-05	0.00	853
BY-110	389.9	1,117	0.0				0.00	2,340.00		0.00	5.00 E+01	806.45	1,150
BY-111	79.5	1,658	0.0				0.00	4,740.00		0.00	2.00 E-01	3.23	849
BY-112	18.9	1,083	0.0				0.00	3,090.00		0.00	1.00 E-04	0.00	852
C-101	333.1	0	0.0				0.00	4,470.00		0.00	1.00 E+02	1,612.90	63.9
C-102[f]	1,601.1	0	0.0	2.76 E-02		9.40 E-05	44,189.12	40,700.00	2.44 E+09	1.06	2.00 E+03	32,258.06	27.1
C-103[f]	234.7	0	503.4	1.54 E-03		1.54 E-03	1,135.13	17,000.00	4.47 E+11	194.66	3.00 E+02	4,838.71	9.79
C-104[f]	1,116.6	0	0.0	5.40 E-02		1.33 E-03	60,295.05	25,500.00	4.38 E+14	190,741.94	7.00 E+02	11,290.32	38.5
C-105[f]	492.1	0	18.9	7.40 E-02		1.32 E-02	36,662.25	6,990.00	9.50 E+13	41,370.97	2.00 E+03	32,258.06	49
C-106[f]	745.6	0	121.1	1.32 E-01		1.58 E-02	100,333.99	76,100.00	1.08 E+14	47,032.26	3.00 E+02	4,838.71	12.6
C-107[f]	1,040.9	0	0.0	3.44 E-02		7.45 E-03	35,806.10	9,220.00	2.20 E+12	958.06	3.00 E+02	4,838.71	69.1
C-108	249.8	0	0.0				0.00	20.60		0.00	9.00 E+01	1,451.61	11,100
C-109	234.7	0	15.1				0.00	4.80		0.00	1.00 E+00	16.13	47,100
C-110	669.9	0	3.8	3.94 E-03		2.47 E-03	2,648.91	90.30	3.08 E+10	13.41	1.00 E+02	1,612.90	4270

Table 9-4. Single-Shell Tank Plutonium Inventory Comparison. (7 sheets)

Tank	Waste Status Summary[a] (KL)			ASA source term and sample data[b]				HDW model (Rev. 3)[c] Pu (g)	WESTREN[d]		TRAC-summary TI-057 03/12/85[e]		HDW Model (Rev. 3)[c] ratio sum
	Sludge	Salt	Liquids	Sludge (g Pu/L)	Salt (g Pu/L)	Liquids (g Pu/L)	Total Pu (g)		Total Pu (Bq)	Pu (g)	Pu (Ci)	Pu (g)	
C-111	215.7	0	0.0				0.00	846.00		0.00	7.00 E+01	1,129.03	144
C-112	393.6	0	0.0	5.00 E-03		1.40 E-05	1,968.20	1,030.00	3.48 E+08	0.15	6.00 E+01	967.74	299
C-201	7.6	0	0.0	6.40 E-02			484.48	0.41	1.62 E+12	705.48	2.00 E-02	0.32	30,300
C-202	3.8	0	0.0				0.00	0.00		0.00	6.00 E-02	0.97	NA
C-203	18.9	0	0.0				0.00	1.64		0.00	6.00 E-03	0.10	14,600
C-204	11.4	0	0.0			1.35 E-06	0.00	0.82	4.43 E+08	0.19	2.00 E-05	0.00	19,900
S-101	923.5	647.2	45.4	6.80 E-04			628.01	6,510.00		0.00	2.00 E+02	3,225.81	208
S-102	15.1	2,063	0.0	1.31 E-03	1.01 E-03	1.01 E-03	2,103.29	2,090.00	7.01 E+07	0.03	2.00 E+01	322.58	3,900
S-103	37.9	836.5	64.3		1.70 E-03	1.70 E-03	1,529.61	1,350.00	2.00 E+12	870.97	2.00 E+00	32.26	3,900
S-104[f]	1,109.0	0	3.8	1.08 E-02			11,977.25	5,450.00	2.52 E+13	10,974.19	2.00 E+02	3,225.81	319
S-105	7.6	1,718	0.0		3.42 E-06	3.42 E-06	5.88	1,550.00		0.00	1.00 E+01	161.29	3,900
S-106[f]	106.0	1,692	15.1	4.96 E-02	5.75 E-06	5.75 E-06	5,266.42	7,080.00	1.89 E+13	8,230.65	1.00 E+00	16.13	26.1
S-107[f]	1,109.0	261.2	53.0	7.10 E-02	2.80 E-05	2.80 E-05	78,748.15	29,200.00	1.81 E+14	78,822.58	1.00 E+03	16,129.03	34.4
S-108	15.1	2,271	0.0	1.76 E-03	8.75 E-07	8.75 E-07	28.63	2,170.00	3.98 E+11	173.32	3.00 E+01	483.87	3,900
S-109	49.2	2,101	0.0	9.54 E-04	1.10 E-05	1.10 E-05	70.05	4,240.00	3.52 E+12	1,532.90	3.00 E+00	48.39	26.1
S-110	495.8	980.3	0.0				0.00	5,220.00	8.26 E+10	35.97	9.00 E+01	1,451.61	114
S-111	526.1	1,692	37.9	2.78 E-04	1.10 E-05	1.10 E-05	165.29	4,400.00	1.50 E+11	65.32	9.00 E+00	145.16	156
S-112	18.9	1,961	0.0		2.83 E-06	2.83 E-06	5.55	2,780.00	7.62 E+10	33.18	1.00 E+00	16.13	50.4
SX-101	423.9	1,298	3.8	1.36 E-04	1.36 E-04	4.63 E-06	234.82	1,910.00	6.09 E+14	265,209.68	2.00 E+02	3,225.81	1,130
SX-102	442.8	1,612	0.0	3.37 E-03	2.64 E-03	2.64 E-03	5,753.99	3,210.00		0.00	2.00 E+01	322.58	3,900
SX-103[f]	435.3	2,029	3.8	1.12 E-02	1.17 E-02	1.17 E-02	28,696.51	4,160.00	2.12 E+12	923.23	2.00 E+00	32.26	855

Table 9-4. Single-Shell Tank Plutonium Inventory Comparison. (7 sheets)

Tank	Waste Status Summary[a] (KL)			ASA source term and sample data[b]				HDW model (Rev. 3)[c] Pu (g)	WESTREN[d]		TRAC-summary TI-057 03/12/85[e]		HDW Model (Rev. 3)[c] ratio sum
	Sludge	Salt	Liquids	Sludge (g Pu/L)	Salt (g Pu/L)	Liquids (g Pu/L)	Total Pu (g)		Total Pu (Bq)	Pu (g)	Pu (Ci)	Pu (g)	
SX-104	514.8	1,809	0.0		7.80 E-04	7.80 E-04	1,411.20	3,270.00	5.59 E+09	2.43	2.00 E+02	3,225.81	1,240
SX-105	276.3	2,309	0.0	1.26 E-04	5.14 E-06	5.14 E-06	46.68	4,050.00	2.38 E+07	0.01	2.00 E+01	322.58	1,280
SX-106	45.4	1,760	230.9	5.00 E-03	5.66 E-04	5.66 E-04	1,353.96	2,730.00		0.00	3.00 E-04	0.00	822
SX-107	393.6	0	0.0				0.00	2,650.00	3.39 E+08	0.15	3.00 E+02	4,838.71	2,530
SX-108	329.3	0	0.0				0.00	1,040.00		0.00	3.00 E+02	4,838.71	993
SX-109	0.0	946.3	0.0				0.00	1,810.00		0.00	2.00 E+02	3,225.81	4,730
SX-110	234.7	0	0.0				0.00	335.00		0.00	3.00 E+02	4,838.71	1,840
SX-111	473.1	0	0.0	1.51 E-03		1.35 E-06	714.42	505.00	1.41 E+12	614.03	4.00 E+02	6,451.61	1,950
SX-112	348.2	0	0.0				0.00	302.00		0.00	2.00 E+02	3,225.81	2,160
SX-113	98.4	0	0.0				0.00	2.02		0.00	6.00 E+01	967.74	50,200
SX-114	685.1	0	0.0				0.00	1,300.00		0.00	4.00 E+02	6,451.61	1,150
SX-115	45.4	0	0.0	1.94 E-01			8,802.40	60.90	1.68 E+13	7,316.13	1.00 E+02	1,612.90	1,230
T-101[f]	382.3	0	3.8			4.70 E-05	0.18	11,400.00	1.07 E+09	0.47	5.00 E-05	0.00	9.63
T-102	71.9	0	49.2	1.26 E-03		2.90 E-05	92.04	1,980.00		0.00	1.00 E-06	0.00	24.3
T-103	87.1	0	15.1			1.40 E-05	0.21	1,980.00		0.00	1.00 E-01	1.61	22.3
T-104[f]	1,673.0	0	11.4	7.40 E-03		1.52 E-04	12,381.70	442.00	2.19 E+13	9,537.10	1.00 E+02	1,612.90	1,820
T-105	370.9	0	0.0	4.30 E-03		2.20 E-03	1,595.00	102.00		0.00	2.00 E+02	3,225.81	2,310
T-106	71.9	0	7.6	8.20 E-03		1.79 E-04	591.06	1,780.00	1.58 E+12	688.06	2.00 E+01	322.58	28.7
T-107	647.2	0	34.1	4.20 E-03		5.31 E-03	2,899.37	82.60	1.51 E+10	6.58	5.00 E+01	806.45	4,270
T-108	166.5	0	0.0			1.22 E-04	0.00	35.00		0.00	5.00 E+00	80.65	4,810

Table 9-4. Single-Shell Tank Plutonium Inventory Comparison. (7 sheets)

Tank	Waste Status Summary[a] (KL)			ASA source term and sample data[b]				HDW model (Rev. 3)[c] Pu (g)	WESTREN[d]		TRAC-summary TI-057 03/12/85[e]		HDW Model (Rev. 3)[c] ratio sum
	Sludge	Salt	Liquids	Sludge (g Pu/L)	Salt (g Pu/L)	Liquids (g Pu/L)	Total Pu (g)		Total Pu (Bq)	Pu (g)	Pu (Ci)	Pu (g)	
T-109	219.5	0	0.0			5.40 E-05	0.00	62.60		0.00	5.00 E-01	8.06	5,030
T-110	1,423.2	0	11.4			3.77 E-06	0.04	324.00		0.00	2.00 E+02	3,225.81	2,870
T-111	1688.1	0	0.0	3.94 E-03		1.35 E-06	6,651.15	370.00		0.00	1.00 E+02	1,612.90	2,920
T-112	227.1	0	26.5			3.00 E-05	0.79	44.60	1.81 E+09	0.79	2.00 E+02	3,225.81	2,710
T-201	106.0	0	3.8				0.00	24.40		0.00		0.00	4,520
T-202	79.5	0	0.0				0.00	18.30		0.00	3.00 E-01	4.84	4,520
T-203	132.5	0	0.0				0.00	30.50		0.00	3.00 E+00	48.39	4,520
T-204	143.8	0	0.0	1.51 E-03		1.52 E-03	217.18	33.10	4.54 E+10	19.77		0.00	4,520
TX-101	317.9	0	11.4			3.22 E-03	36.54	5,010.00		0.00	3.00 E-05	0.00	61.4
TX-102	0.0	821.3	0.0				0.00	879.00		0.00	9.00 E-08	0.00	9,440
TX-103	594.2	0	0.0			2.57 E-04	0.00	371.00	8.08 E+11	351.87	9.00 E-07	0.00	5,030
TX-104	0.0	242.2	3.8		1.39 E-03	1.39 E-03	341.73	199.00	1.94 E+12	844.84	3.00 E-04	0.00	9,440
TX-105	0.0	2,305	0.0		5.66 E-04	5.66 E-04	1,304.67	2,540.00		0.00	4.00 E-04	0.01	9,440
TX-106	0.0	1,715	0.0		2.00 E-05	2.00 E-05	34.29	1,370.00		0.00	3.00 E-08	0.00	4,410
TX-107	0.0	132.5	3.8		3.92 E-03	3.92 E-03	533.46	24.90	1.36 E+13	5,922.58	9.00 E-07	0.00	9,440
TX-108	0.0	507.2	0.0		7.90 E-05	7.90 E-05	40.07	395.00		0.00	6.00 E-01	9.68	15,200
TX-109	0.0	1,453	0.0		1.12 E-03	1.12 E-03	1,633.67	378.00		0.00	2.00 E+02	3225.81	1,820
TX-110	0.0	1,749	0.0		7.80 E-05	7.80 E-05	136.40	1,790.00		0.00	1.00 E+01	161.29	1,500
TX-111	0.0	1,400	0.0				0.00	1,410.00		0.00	1.00 E+00	16.13	1,180
TX-112	0.0	2,456	0.0				0.00	2,620.00		0.00	6.00 E-02	0.97	5030

Table 9-4. Single-Shell Tank Plutonium Inventory Comparison. (7 sheets)

Tank	Waste Status Summary[a] (KL)			ASA source term and sample data[b]				HDW model (Rev. 3)[c] Pu (g)	WESTREN[d]		TRAC-summary TI-057 03/12/85[e]		HDW Model (Rev. 3)[c] ratio sum
	Sludge	Salt	Liquids	Sludge (g Pu/L)	Salt (g Pu/L)	Liquids (g Pu/L)	Total Pu (g)		Total Pu (Bq)	Pu (g)	Pu (Ci)	Pu (g)	
TX-113	0.0	2,297	0.0				0.00	1,990.00		0.00	5.00 E+01	806.45	1,180
TX-114	0.0	2,025	0.0				0.00	2,100.00		0.00	5.00 E+00	80.65	4,730
TX-115	0.0	2,422	0.0				0.00	2,410.00		0.00	5.00 E-01	8.06	19,600
TX-116	0.0	2,388	0.0				0.00	958.00		0.00	6.00 E-10	0.00	5,660
TX-117	0.0	2,369	0.0				0.00	1,480.00		0.00	3.00 E-09	0.00	5,470
TX-118[f]	0.0	1,313	0.0	1.60 E-03	3.28 E-03	3.28 E-03	4,306.62	64,300.00	3.22 E+09	1.40	9.00 E+02	14,516.13	4.02
TY-101	446.6	0	0.0	5.05 E-03			2,255.48	163.00	5.15 E+12	2,242.74	2.00 E+02	3,225.81	2,100
TY-102	0.0	242.2	0.0		1.74 E-04		42.06	160.00	2.69 E+16	1.17 E+07	3.00 E+00	48.39	5030
TY-103	613.2	0	0.0	1.54 E-02			9,442.82	253.00	7.10 E+10	30.92	3.00 E+02	4838.71	4190
TY-104	174.1	0	0.0	5.62 E-03		3.60 E-05	978.50	1,140.00	1.80 E+12	783.87	8.00 E+00	129.03	19600
TY-105	874.3	0	0.0	1.78 E-03			1,556.32	66.70	1.20 E+12	522.58	7.00 E+01	1129.03	19600
TY-106	64.3	0	0.0	1.25 E-03			80.11	0.26	7.22 E+10	31.44	8.00 E+00	129.03	237000
U-101	83.3	0	11.4				0.00	9.00		0.00	2.00 E+00	32.26	9440
U-102	162.8	1,185	68.1	7.40 E-03	2.41 E-04	2.41 E-04	1,506.32	1,900.00	2.20 E+12	958.06	1.00 E-05	0.00	9,440
U-103	121.1	1,601	49.2	1.84 E-03	3.10 E-04	3.10 E-04	734.44	2,390.00	2.68 E+10	11.67	4.00 E-09	0.00	9,440
U-104	461.8	0	0.0	2.09 E-04			96.51	408.00	3.41 E+10	14.85	1.00 E-07	0.00	17,100
U-105	121.1	1,321	140.0	2.61 E-03			316.12	2,350.00	6.80 E+12	2,961.29	5.00 E-02	0.81	9,530
U-106	98.4	700.2	56.8		1.00 E-06	1.00 E-06	0.76	1,300.00	2.81 E+09	1.22	2.00 E-07	0.00	9,440
U-107[f]	56.8	1,363	117.3	9.20 E-03	1.00 E-05	1.00 E-05	537.13	14,000.00	1.04 E+12	452.90	7.00 E-05	0.00	26.2
U-108[f]	109.8	1,571	90.8	6.31 E-04	1.19 E-06	1.19 E-06	71.24	11,000.00	9.11 E+11	396.73	1.00 E+01	161.29	10.3
U-109[f]	181.7	1,499	71.9	7.62 E-02	4.25 E-03	4.25 E-03	20,519.81	6,780.00	5.28 E+13	22,993.55	6.00 E-02	0.97	50

Table 9-4. Single-Shell Tank Plutonium Inventory Comparison. (7 sheets)

Tank	Waste Status Summary[a] (KL)			ASA source term and sample data[b]				HDW model (Rev. 3)[c] Pu (g)	WESTREN[d]		TRAC-summary TI-057 03/12/85[e]		HDW Model (Rev. 3)[c] ratio sum
	Sludge	Salt	Liquids	Sludge (g Pu/L)	Salt (g Pu/L)	Liquids (g Pu/L)	Total Pu (g)		Total Pu (Bq)	Pu (g)	Pu (Ci)	Pu (g)	
U-110	704.0	0	0.0			3.73 E-06	0.00	88.00		0.00	2.00 E+02	3,225.81	4,850
U-111	98.4	1,147	0.0	2.63 E-04	7.27 E-04	7.27 E-04	859.65	1,120.00	5.94 E+10	25.87	2.00 E+00	32.26	4,020
U-112	170.3	0	15.1				0.00	989.00		0.00	3.00 E-01	4.84	120
U-201	15.1	0	3.8				0.00	644.00		0.00	9.00 E-11	0.00	26.1
U-202	15.1	0	3.8			1.15 E-06	0.00	644.00	4.04 E+08	0.18	1.00 E-10	0.00	26.1
U-203	7.6	0	3.8			1.72 E-06	0.01	325.00		0.00	1.00 E-10	0.00	26.1
U-204	7.6	0	3.8	2.53 E-03			19.15	322.00	2.20 E+10	9.58	3.00 E-11	0.00	26.1
Total inventory in grams							630,181.88	563,041.25		1.25 E+07 w/o TY-102 787791.15		347,629.09	

[a] Waste Tank Summary Report for Month Ending February 29, 1996, WHC-EP-0182-95.
[b] Tank Waste Source Term Inventory Validation, WHC-SD-WM-ER-400.
[c] Hanford Tank Chemical and Radionuclide Inventories: HDW Model Rev. 3, May 1996.
[d] Radionuclide and Chemical Inventories for the Single-Shell Tanks, WHC-SD-WM-TI-565, Rev. 1.
[e] Preliminary Estimation of the Waste Inventories in Hanford Tanks Through 1980, SD-WM-TI-057, Rev. 0-A.
[f] 22.9 m diameter tanks with greater than 10 kg plutonium.
[g] 6.1 m diameter tanks with greater than 0.754 kg plutonium.

Table 9-5. Double-Shell Tank Estimated Plutonium Inventory Comparison.

Tank	Waste status volume (KL)[a]			HDW Model (Rev. 3)[b] Pu (g)	Baselined[c] Pu (g)	HDW model (Rev. 3) ratio sum
	Sludge	Salt	Liquid			
AN-101	0	0	4,088	1,310	12.3	NA
AN-102	337	0	3,759	6,810	5,182	NA
AN-103	354[d]	0	68	6,720	70	2.71 E+01
AN-104	999	0	3,013	4,700	5,573	NA
AN-105	0	0	4,269	8700	140	NA
AN-106	64	0	1,514	708	344	NA
AN-107	507	0	3,494	4,580	3,077	NA
AP-101	0	0	2,790	463	13.7	NA
AP-102	0	0	4,156	2,620	5.1	NA
AP-103	0	0	95	887	0	NA
AP-104	0	0	3,157	0	8.7	NA
AP-105	0	0	583	4,940	1.6	NA
AP-106	0	0	405	2,280	1.7	NA
AP-107	0	0	95	0	0.3	NA
AP-108	0	0	106	946	0.5	NA
AW-101	318	0	3,948	8,890	3,490	1.09 E+04
AW-102	3.8	0	356	3,470	47.7	NA
AW-103[e]	1,374	0	572	18,100	44,791	4.62 E+01
AW-104	678	420	3,157	551	5,360	1.22 E+03
AW-105[e]	1,124	0	288	12,600	22,947	5.44 E+01
AW-106[e]	799	322	912	4,310	14,003	2.74 E+01
AY-101[e]	314	0	3,229	23,100	24,336	7.40 E+00
AY-102	121	0	3,630	9,650	8,702	2.85 E+01
AZ-101[e]	132	0	3,365	9,750	19,249	2.30 E+01
AZ-102[e]	360	0	3,259	12,500	27,186	1.62 E+01
SY-101	2,006[d]	0	71.9	7,470	1,472	NA
SY-102[e]	269	269	1,170	41,200	4,1387	1.35 E+01
SY-103	2,169[d]	0	632	3,750	3,670	NA

[a]Waste Tank Summary Report for Month Ending February 29, 1996, WHC-EP-0182-95.
[b]Hanford Tank Chemical and Radionuclide Inventories: HDW Model Rev. 3, May 1996.
[c]Baseline Report WHC-SD-WM-TI-640 as of January 1, 1995, plus updates to April 1996.
[d]Double-Shell Slurry.
[e]Tanks with estimated greater than 10 kg plutonium.

Table 9-6. Tanks With Enough Fissile Material To Warrant Further Consideration.

22.9-m diameter single-shell tanks					
A-101	A-104	A-105	A-106		
B-101					
BY-103					
C-102	C-103	C-104	C-105	C-106	C-107
S-104	S-106	S-107			
SX-103					
T-101	T-104				
TX-118					
U-107	U-108	U-109			
6.1-m diameter single-shell tanks					
B-201	B-202	B-203	B-204		
22.9-m diameter double-shell tanks					
AW-103	AW-105	AW-106			
AY-101					
AZ-101	AZ-102				
SY-102					

Table 9-7. Fuel Processed at PUREX and Associated Waste Volumes.

Fuel Type	Quantity of Fuel Charged (MT)	Cladding Waste Volume (l)	High Level Waste (CAW) (l)	Canyon Sump Waste (l)	Organic Wash Waste (l)	Acid Cell or Lab Waste (l)
Aluminum Clad	73,701 U	952,539,993				0
Thoria 1966 1970-1971	 188 Th [223 kg ^{233}U] 416 Th [628 kg ^{233}U]	1,400,000	859,200	1,154,000	3,749,000	1,060,000
Zirconium Clad 1983-90 1967-72	 3920 U 887 U	22,298,929	6,337,605	10,767,571	16,675,000	10,624,840
PRTR, SEFOR, Coproduct, Pu-Al Alloy, & Mixed Oxide						

Table 9-8. Zirconium-Clad Fuels Processed at PUREX.

Campaigns date	N Reactor fuel reprocessed through dissolvers (MTU)	Fuel exposure (average MWd/MTU)	^{235}U content average % total uranium	Plutonium content (kg)	Uranium processed through solvent extraction (MTU)
1983-1989 A01 through A06	3,920 (30 cold, 3,299 enriched to 0.94% and 591 to 1.15%)	1,281	0.80 (>0.72% 3,130 kg)	3,702	6,140
1967-1972	887	1,762		1,000	

MTU = metric tonnes of uranium.

Table 9-9. Decladding Waste Sludge Formation in AW-103 and -105 Receiver Tanks.

Tank	Time Receiving	Declad Waste Added (L)	Sludge Buildup (L)	Fraction Sludge Formation
AW-103	Oct 1983 - Dec 1988	13,470,000	1,031,400[a]	0.077
AW-105	June 1984 - Feb 1990	8,590,000	729,550[a]	0.085

Note:
[a]Difference between starting heel and ending sludge volume for these time periods.

Table 9-10. Plutonium and Associated Insoluble Absorbers in Zirflex Decladding Waste.

Waste property	Flowsheet[a]	Hanford-defined waste[b]	Process records[c]	Sludge content projected from process records	Mass ratio per process records (absorber/Pu)
Vol (L/MTU)	4,427	5,376	5,764		
Sp. gr.	1.07	--	1.06		
Settled vol% solids	--	10.5	8.1[d]		
Pu (g/L)	0.0013	0.00176	0.00039	0.0048	
U (g/L)	0.18	0.74	0.525	6.48	1,346
Fe (g/L)	--	2.2	0.087-0.117[e]	1.07-1.44[e]	223-300
La (g/L)	--	--			
Zr (g/L)	16.4	9.1	11.0	136	28,200

[a]G.K. Allen, et al., PFD-P-020-00001, Rev A4, Purex Flowsheet - Processing N Reactor Fuels, September 1985.
[b]S. F. Agnew, LA-UR-94-2657, Hanford Defined Wastes: Chemical and Radionuclide Compositions, September 1995.
[c]Appendix E information, Chemistry Laboratory Reports, Fuel Charging and Characterization Data, and Tank Farm Data.
[d]103-AW and 105-AW Tank Samples evaluation and Table 9.9.
[e]Based on iron content of zircalloy cladding and steel clips, and corrosion of the dissolver coils during zircalloy decladding. (letter from L. L. Jacobs to K. E. Plummer, March 14, 1986 and SAR 003). Iron added as ferric nitrate to AFAN starting in February 1985 (amounted to an additional 174 g/MTU or 0.028 g/L in waste stream).

Table 9-11. Neutralized Zirflex Current Acid Waste Transferred from TK-F16 (Based on MTU Irradiated Fuel Plus Cold Uranium Processed Through Solvent Extraction).

Waste property	Flowsheet[a]	Hanford defined waste[b]	Process records[c]	Projected sludge content based on process records	Mass ratio based on process records (insoluble absorber/Pu)
Vol (L/MTU)	885	699	1032		
sp. gr.	1.25	----	----		
Settled vol% solids	17	3.9	4.4		
Pu (g/L)	0.003	0.0034	0.0028	0.064	
U (g/L)	0.84	9.14	0.67 (1.1)[d]	15.2	239 (289)
Al (g/L)	----	9.18	12.4 (8.3)[d]	23.6	258 (assuming 70% insoluble) (2074)
Cr (g/L)	----	0	0.36	8.2	129
Fe (g/L)	----	6.55	5.57 (3.4)[d]	127	1989 (1214)
Ni (g/L)	----	0	0.17 (0.36)[d]	3.9	61 (95)
Zr (g/L)	----	0	3.8	86.4	1357

[a](Jacobs et al. 1985)
[b](Agnew 1995)
[c]Nuclear Material Control Records, Campaign Reports, Chemistry Laboratory Reports, Fuel Charging and Characterization Data, and Tank Farm Data.
[d]Average chemical analysis of numerous batches of waste, not a weighted average.

Table 9-12. Sources and Quantity of Some Insoluble Absorbers in the NZCAW.

Source	Sources and quantity of some insoluble absorbers in NZCAW (g/MTU)			
	Iron	Aluminum	Chromium	Nickel
Uranium alloy (601)[a]	325	750	<65	<100
SX reductant[b] IBX 2N	 3,535 493			
Dissolver corrosion[c]	200		53	25
Aluminum addition in dissolver[b]		12,000		
Concentrators corrosion[d]	1,200		318	150
Sodium hydroxide impurity[e]	<1			<1
Total	5,753	12,750	371	175

[a]Standard N Fuels Uranium (Weakly 1979)
[b]G.K. Allen, et al., PFD-P-020-00001, Purex Flowsheet - Processing N Reactor Fuels, 1982.
[c]Letter, L.L.Jacobs to K.E. Plummer N Basin Trip Report, March 1986
[d]Van der Cook, ARH-1649
[e]Kupfer 1996

Table 9-13. Sludge Volume Formed in Tanks from NZCAW.

Tank	Time period	Zirflex high level waste added (L)	Accumulated solids (L)	Solid volume fraction
AY-101	September 1983	10,688	[a]	----
AY-102	October 1983	252,145	[a]	----
AZ-101	Nov 1983 to April 1986	2,357,827	104,000 (≃10" sludge depth 7" to 17")	0.044
AZ-102	May 1984 to Mar 1990	1,971,219	Solids received by this stream indistinguishable since received other waste simultaneously	----
AZ-103	Sept 1985 to Dec 1985	47,384	[a]	----
AW-101	July 1984	47,971	[a]	----
AW-102		32,631	[a]	----
AW-104		182,774	[a]	----

Note:
[a] Insufficient solids to allow accurate solids build up measurement.

Table 9-14. PUREX Canyon Sump Waste Plus Ammonia Scrubber Bottoms Accumulated in Tank F-18.

Waste property	Flowsheet[a]	Hanford defined waste[b]	Process records[c]	Projected sludge content based upon process records (average)	Mass ratio based on process records (absorber/Pu)
Vol (l/MTU)	545	10,117[d]	1979		
sp. gr.	1.02	----	----		
Settled vol% solids	--	2	0.07[e]		
Pu (g/l)	0.003	0.000076	0.00081	1.1	
U (g/l)	1.8	0.11	1.59	2318	1963

[a] Jacobs et al. (1985)
[b] Agnew et al. (1996)
[c] Appendix E
[d] Includes organic wash and acid fractionator cell waste.
[e] Uranyl trioxide hydrate has a particle density of about 6 (Katz 1986), which gives a bulk density of about 3 and results in a settled sludge volume of about 0.07 vol% of the waste stream assuming uranium is the predominant metal contributor to solids.

Table 9-15. Organic Wash Waste Transferred from Tanks TK-G8 and TK-R8.

Waste property	Flowsheet[a]	Hanford defined waste[b]	Process records average[c]	Mass ratio insoluble absorber/Pu based on process records
Volume (l/MTU)	615	Included with canyon sump and acid fractionator waste	2,716	
sp. gr.	1.02			
Pu g/L	0.00026		0.000101	
U g/L	0.55		0.426	4220
Na_2CO_3 g/L	12.7			
$NaNO_3$ g/L	2.55			
MnO_2 g/L	0.52			
NaOH g/L	0.40			
$NaNO_2$ g/L	0.76			

[a]Jacobs (1985)
[b]Agnew et. al (1996)
[c]Appendix E

Table 9-16. Aluminum Cladding Waste.

Component	Flowsheet[a]	Hanford Defined Waste[b]	Process Records[c]	Projected sludge concentration	Projected Ratio Based On Process Records(Insoluble Absorber/Pu Ratio)	Projected Mass Ratio Sum Based on Process Records (Insoluble Absorber/Pu Ratio Sum)
Volume (L/MTU)	785	1442	1292			
Sp. gr.	1.27	1.15	1.19			
Settled vol% solids		8.1	6			
Pu (g/L)		0.00153	0.0017	0.03		
U (g/L)		2.78	2.9	58	1,706	2.2
Al (g/L)	57.5	23.0	32.4			
Fe (g/L)			0.16[d]	2.7	94.1	0.59
Na (g/L)	138.2		86			
Si (g/L)	0.20		0.56			
NO_3 (g/L)	9.1		37.2			
NO_2 (g/L)	78.7		41.4			
OH (g/L)	21.1		17			
Total						> 2.8

[a](Matheison and Nicholson 1968)
[b](Agnew et. al 1996)
[c](Anderson 1990)
[d](Kupfer 1996) Aluminum alloy iron content 209 g/MTU

Table 9-17. Sludge Formation in Receiving Tanks from Aluminum Cladding Removal Waste.

Tank	Time period	Aluminum cladding waste added (liters)	Accumulated solids (liters)	Solid volume fraction
C-104	1956			
C-105	1957			
C-106	1958			
C-101	1960			
C-102	1960 to 1965			
C-111	1957 to 1960			
C-112	1960 to 1961			
C-102	1965 to 1969			
C-107	1961 to 1962			
C-108	1961			
C-104	1970 to 1972	3816	108	2.5

Table 9-18. Sources and Quantity of Some Insoluble Absorbers in the NCAW.

Source	Sources and Quantity of Some Insoluble Absorbers in NCAW (g/MTU)			
	Iron	Aluminum	Chromium	Nickel
Uranium Alloy (501)[a]	125	<150	<65	<100
SX Reductant[b]				
IBX	1,041			
2DF	868			
3AS	729			
Dissolver Corrosion[c]	0		0	0
Concentrators Corrosion[d]	1,200		318	150
Total	3,963	<150	318	150

[a]Standard N Fuels Uranium (Weakly 1979)
[b]Matheison, W. E., G. A. Nicholson, Purex Chemical Flowesheet - Processing of Aluminum-Clad Fuels, ARH-214 Del, Feb. 15, 1968.
[c]Letter, L.L.Jacobs to K.E. Plummer N Basin Trip Report, March 1986
[d]Van der Cook, ARH-1649

Table 9-19. Neutralized Current Acid Waste from Aluminum Clad Fuel Processing.

Component	Flowsheet[a]	Hanford Defined Waste[b]	Process Records[c] 1956-1967 (Anderson 1990)	Mass Ratio Based on Process Records (Absorber/Pu)
Volume (L/MTU)	156	1,573	177	
Sp. gr.	1.14	----		
Settled vol% solids		3.9		
Pu g/l	0.00 18	0.00 14		
U g/l	0.06 7	2.55		
Al g/l		0	4.1	
Cr g/l		0.42	1.8	
Fe g/l	21.0	6.55	22.3	12,000
Na g/l	37.1	32.0	32.2	
PO_4 g/l	1.43	0	1.9	
SO_4 g/l	82	15.2	86.4	

[a](Matheison and Nicholson 1968)
[b](Agnew et. al 1996)
[c](Anderson 1990)

Table 9-20. Thorium-Aluminum Coating Waste from TK-E5.

Waste property	Flowsheet[a]	Hanford defined waste[b]	Process records[c]	Sludge content based upon process records (average)	Insoluble absorber to plutonium mass ratio based on process records (absorber/Pu)
vol (L/MTTh)	2,760	Not Specified	3,703		
sp. gr.	1.14				
settled vol% solids			(5)		
^{233}U (g/L) [total mass]	---		0.0026 [3.7kg]	0.052	
Th (g/L) [total mass]	0.32		0.26 [363 kg]	5.2	100
Al (g/L)	21.1		17.7		

[a]Smith 1970
[b]Agnew et. al 1996
[c]ARH-2127 PD PUREX Process Operation and Performance 1970 Thoria Campaign

Table 9-21. Thorium - Neutralized 1WW Waste from TK-F18.

Waste property	Flowsheet[a]	Hanford defined waste[b]	Process records[c]	Sludge content based upon process records (average)	Mass ratio based on process records (absorber/Pu)
vol (L/MTTh)	2,027	Not Specified	2,273		
sp. gr.	1.13				
settled vol% solids			4[d]		
^{233}U (g/L) [total mass]	0.0021		0.005 [4.3kg]	0.125	
Th (g/L) [total mass]	1.93		4.23 [3,632 kg]	106	845
Al (g/L)	9.18				
Fe (g/L)	1.4				

[a]Smith 1970
[b]Agnew et. al 1996
[c]ARH-2127 PD PUREX Process Operation and Performance 1970 Thoria Campaign
[d]Assumed value, not supported by tank farm sludge formation measurements related to waste volume transfers.

Table 9-22. Thorium - Organic Wash Waste from TK-G8 and TK-R8.

Waste property	Flowsheet[a]	Hanford defined waste[b]	Process records[c]	Sludge content based upon process records (average)	Mass ratio based on process records (absorber/Pu)
vol (L/MTTh)	4,250	Not specified	9,813		
sp. gr.	1.01				
settled vol% solids			(0.5)		
^{233}U (g/L) [total mass]			0.0015 [5.4 kg]	0.30	
Th (g/L) [total mass]			0.34 [1,271 kg]	68	228
$NaNO_3$ (g/L)	13.1				
Mn (g/L)	0.65				

[a]Smith 1970
[b]Agnew et. al 1996
[c]ARH-2127 PD PUREX Process Operation and Performance 1970 Thoria Campaign

Table 9-23. Thorium - Canyon Sump Waste from Tank TK-F18.

Waste property	Flowsheet[a]	Hanford-defined waste[b]	Process records[c]	Projected sludge content based upon process records (average)	Mass ratio based on insoluble absorber per process records (absorber/Pu)
vol (L/MTTh)	-----	Not Specified	3,054		
sp. gr.					
settled vol% solids			(0.2)		
^{233}U (g/L) [total mass]			0.0062 [7.2 kg]	3.1	
Th (g/L) [total mass]			1.97 [2,270 kg]	986	318

[a]Smith 1970
[b]Agnew et. al 1996
[c]ARH-2127 PD PUREX Process Operation and Performance 1970 Thoria Campaign

Table 9-24. Thorium - Flush and Lab Waste from PUREX.

Waste property	Flowsheet[a]	Hanford defined waste[b]	Process records[c]	Projected sludge content based upon process records (average)	Mass ratio based on process records (absorber/Pu)
vol (L/MTTh)	7,610	Not specified	9,142		
sp. gr.					
vol% solids			(0.1)		
^{233}U (g/L) [total mass]			0.0036 [12.4 kg]	3.6	
Th (g/L) [total mass]			0.84 [2,906 kg]	233	234

[a]Smith 1970
[b]Agnew et. al 1996
[c]ARH-2127 PD PUREX Process Operation and Performance 1970 Thoria Campaign

Table 9-25. Typical REDOX Waste Compositions.

Component	Al cladding		High level	
	Flowsheet[a]	Process records[b]	Flowsheet[a]	Process records[b]
Volume (L/MTU)	750	1,196	3425	2655
Sp. gr.	1.21	1.19	1.39	1.29
Pu, g/L	0.001	0.0026	0.0004	0.0001
U, g/L	1.33	3.34	0.15	0.19
$NaAlO_2$, M	1.91	1.2	0.93	1.2
NaOH, M	0.61	1.0	1.44	0.69
$NaNO_3$, M	0.80	0.6	4.37	4.83
$NaNO_2$, M	1.44	0.9	--	--
Na_2SiO_3, M	0.027	0.02	--	--
$Na_2Cr_2O_7$, M	--	--	0.10	0.066
Na_2SO_4, M	--	--	0.020	0.031
$Cr(OH)_3$, M	--	--	0.003	0.045
$Fe(OH)_3$, M	--	--	0.006	0.016

[a]Crawley (1960)
[b]Anderson (1990)

Table 9-26. Typical Bismuth Phosphate Waste Composition.

Component	Coating waste	Metal waste	First cycle waste	Second cycle waste
Gallons/MTU	377[a,b]	3,800	2,756[b]	2,400
Specific Gravity	1.18			
Pu, g/L	1.7 E-04	1.7 E-04	4.8 E-04	2.8 E-04
U, g/L	0.70	69.4	~0	~0
NaOH, M	0.39	--	--	--
$NaNO_3$, M	0.83	0.58	0.80	0.67
$NaAlO_2$, M	0.82	--	--	--
Na_2SiO_3, M	0.005	--	--	--
$NaNO_2$, M	0.62	--	--	--
Na_2CO_3, M	--	0.88	--	--
Na_2SO_4, M	--	0.25	--	--
Na_3PO_4, M	--	0.39	0.47	0.45
$Fe_2(SO_4)_3$, M	--	--	0.014	0.013
$(NH_4)_2SiF_6$, M	--	--	0.036	0.030
$(NH_4)_2SO_4$, M	--	--	0.014	0.013
$Cr(NO_3)_3$, M	--	--	0.002	0.002
NH_4NO_3, M	--	--	--	0.027

[a]Includes water and dilute nitric acid rinses.
[b]Coating waste and first cycle wastes mixed for disposal.

Table 9-27. Volume and Composition of Uranium Recovery Waste.

Waste property	Uranium recovery waste[a]	Hanford defined waste[b]	Process records
volume (l/MTU)	14,400	27,570	
% solids		2.8	
pH	>9.5	--	
sp. gr.	1.398	1.148	
Pu (g/L)	0.00014	0.000066	
U (g/L)	0.62	0.95	
Na (g/L)	174	89.9	
Fe (g/L)	1.34	0.11	
Cl (g/L)	0.98	3.64	
NO_3 (g/L)	383	160	
SO_4 (g/L)	33.0	13.6	
PO_4 (g/L)	23.8	12.4	
CO_3 (g/L)	--	11.5	

[a] HW-19140, Uranium Recovery Technical Manual, Chemical Development, November 10, 1951(see G.E. 1951).
[b] S. F. Agnew, LA-UR-94-2657, Hanford Defined Wastes: Chemical and Radionuclide Compositions, September 1995.

Table 9-28. Plutonium Criticality Ratios - Single-Shell Tanks. (5 sheets)

Tank Name	High Pu tanks	Agnew Pu conc (ug/g)	Agnew ratio sum	Agnew insolubles ratio sum	TCR mean Pu conc (ug/g)	TCR ratio sum	TCR insolubles ratio sum
A101	*	4.48	234.00	173.00	NA	NA	NA
A102		35.50	20.80	13.40	NA	NA	NA
A103		118.00	6.19	3.53	NA	NA	NA
A104	*	115.00	6.45	3.76	NA	NA	NA
A105	*	16.90	59.60	47.00	NA	NA	NA
A106	*	64.60	11.40	7.07	NA	NA	NA
AX101		21.90	42.60	32.30	NA	NA	NA
AX102		207.00	3.20	2.15	NA	NA	NA
AX103		16.90	59.60	47.00	NA	NA	NA
AX104		16.90	59.60	47.00	NA	NA	NA
B101	*	18.50	54.50	13.90	NA	NA	NA
B102		0.83	1,130.00	750.00	NA	NA	NA
B103		0.15	8,830.00	2,700.00	NA	NA	NA
B104		0.21	2,690.00	525.00	NA	NA	NA
B105		0.17	6,070.00	394.00	NA	NA	NA
B106		0.15	6,690.00	362.00	NA	NA	NA
B107		0.10	4,160.00	1,010.00	NA	NA	NA
B108		0.14	6,030.00	511.00	NA	NA	NA
B109		2.77	335.00	28.40	NA	NA	NA
B110		0.42	1,240.00	474.00	0.54	2,052.69	235.13
B111		2.42	223.00	135.00	1.58	453.02	80.13
B112		1.15	949.00	112.00	NA	NA	NA
B201		0.16	4,520.00	1,820.00	18.40	64.85	46.25
B202		0.16	4,520.00	1,820.00	NA	NA	NA
B203		0.16	4,520.00	1,820.00	NA	NA	NA
B204		0.16	4,520.00	1,820.00	NA	NA	NA
BX101		14.4	53.2	37.9	NA	NA	NA
BX102		2.05	541.00	125.00	NA	NA	NA
BX103		2.31	239.00	155.00	NA	NA	NA
BX104		0.06	9,440.00	6220.00	NA	NA	NA
BX105		0.06	9,440.00	6220.00	NA	NA	NA
BX106		1.57	879.00	56.90	NA	NA	NA

Table 9-28. Plutonium Criticality Ratios - Single-Shell Tanks. (5 sheets)

Tank Name	High Pu tanks	Agnew Pu conc (ug/g)	Agnew ratio sum	Agnew insolubles ratio sum	TCR mean Pu conc (ug/g)	TCR ratio sum	TCR insolubles ratio sum
BX107		0.17	2,320.00	522.00	0.93	960.18	101.70
BX108		0.19	2,000.00	442.00	NA	NA	NA
BX109		0.09	10,000.00	4,280.00	NA	NA	NA
BX110		0.61	1,070.00	121.00	NA	NA	NA
BX111		1.57	852.00	36.70	NA	NA	NA
BX112		0.25	1,940.00	266.00	NA	NA	NA
BY101		1.57	878.00	56.60	NA	NA	NA
BY102		1.64	849.00	31.30	NA	NA	NA
BY103	*	2.12	679.00	25.60	NA	NA	NA
BY104		1.02	1,200.00	152.00	NA	NA	NA
BY105		1.22	1,040.00	93.70	NA	NA	NA
BY106		1.51	918.00	55.10	NA	NA	NA
BY107		1.09	1,110.00	127.00	NA	NA	NA
BY108		0.56	1,920.00	386.00	0.75	2,009.56	397.83
BY109		1.59	853.00	32.30	NA	NA	NA
BY110		1.02	1,150.00	135.00	0.06	381.56	381.56
BY111		1.64	849.00	31.30	NA	NA	NA
BY112		1.70	852.00	32.90	NA	NA	NA
C101		9.22	63.90	29.80	NA	NA	NA
C102	*	16.70	27.10	13.80	NA	NA	NA
C103	*	51.30	9.79	4.80	NA	NA	NA
C104	*	15.60	38.50	24.50	NA	NA	NA
C105	*	8.59	49.00	19.60	NA	NA	NA
C106	*	66.40	12.60	8.07	NA	NA	NA
C107	*	6.38	69.10	23.90	NA	NA	NA
C108		0.06	11,100.00	4,770.00	NA	NA	NA
C109		0.01	47,100.00	33,600.00	5.55	161.41	83.51
C110		0.10	4,270.00	1,010.00	1.31	590.80	91.40
C111		2.86	144.00	48.30	NA	NA	NA
C112		1.78	299.00	185.00	0.98	2,514.46	1,955.79
C201		0.03	30,300.00	25,900.00	NA	NA	NA
C202		0.00	NA	NA	NA	NA	NA

Table 9-28. Plutonium Criticality Ratios - Single-Shell Tanks. (5 sheets)

Tank Name	High Pu tanks	Agnew Pu conc (ug/g)	Agnew ratio sum	Agnew insolubles ratio sum	TCR mean Pu conc (ug/g)	TCR ratio sum	TCR insolubles ratio sum
C203		0.05	14,600.00	11,100.00	NA	NA	NA
C204		0.04	19,900.00	16,100.00	NA	NA	NA
S101		4.48	208.00	102.00	NA	NA	NA
S102		0.18	3,900.00	3,110.00	NA	NA	NA
S103		0.18	3,900.00	3,110.00	NA	NA	NA
S104	*	3.17	319.00	84.40	4.59	256.85	72.76
S105		0.18	3,900.00	3,110.00	NA	NA	NA
S106	*	23.50	26.10	8.38	NA	NA	NA
S107	*	18.30	34.40	17.10	0.00	NA	NA
S108		0.18	3,900.00	3,110.00	NA	NA	NA
S109		23.50	26.10	8.38	NA	NA	NA
S110		5.85	114.00	78.90	NA	NA	NA
S111		4.33	156.00	112.00	NA	NA	NA
S112		12.80	50.40	27.70	NA	NA	NA
SX101		0.89	1,130.00	360.00	NA	NA	NA
SX102		0.18	3,900.00	3,110.00	NA	NA	NA
SX103	*	1.46	855.00	92.40	NA	NA	NA
SX104		0.76	1,240.00	472.00	NA	NA	NA
SX105		0.92	1,280.00	521.00	NA	NA	NA
SX106		1.58	822.00	59.70	NA	NA	NA
SX107		0.40	2,530.00	1,790.00	NA	NA	NA
SX108		1.22	993.00	232.00	NA	NA	NA
SX109		0.19	4,730.00	4,010.00	NA	NA	NA
SX110		0.75	1,840.00	1,110.00	NA	NA	NA
SX111		0.60	1,950.00	1,210.00	NA	NA	NA
SX112		0.50	2,160.00	1,420.00	NA	NA	NA
SX113		0.04	50,200.00	4,950.00	NA	NA	NA
SX114		1.13	1,150.00	401.00	NA	NA	NA
SX115		0.88	1,230.00	463.00	NA	NA	NA
T101	*	47.30	9.63	35.60	NA	NA	NA
T102		17.30	24.30	64.50	NA	NA	NA
T103		18.40	22.30	54.30	NA	NA	NA

Table 9-28. Plutonium Criticality Ratios - Single-Shell Tanks. (5 sheets)

Tank Name	High Pu tanks	Agnew Pu conc (ug/g)	Agnew ratio sum	Agnew insolubles ratio sum	TCR mean Pu conc (ug/g)	TCR ratio sum	TCR insolubles ratio sum
T104	*	0.20	1,820.00	243.00	2.28	220.18	43.89
T105		0.22	2,310.00	404.00	2.26	471.10	367.83
T106		16.50	28.70	31.30	NA	NA	NA
T107		0.10	4,270.00	1,020.00	NA	NA	NA
T108		0.14	4,810.00	869.00	NA	NA	NA
T109		0.18	5,030.00	786.00	NA	NA	NA
T110		0.18	2,870.00	870.00	NA	NA	NA
T111		0.18	2,920.00	1,260.00	2.26	275.55	157.90
T112		0.17	2,710.00	1,450.00	NA	NA	NA
T201		0.16	4,520.00	1,,820.00	NA	NA	NA
T202		0.16	4,520.00	1,820.00	NA	NA	NA
T203		0.16	4,520.00	1,820.00	NA	NA	NA
T204		0.16	4,520.00	1,820.00	NA	NA	NA
TX101		11.20	61.40	47.80	NA	NA	NA
TX102		0.06	9,440.00	6,220.00	NA	NA	NA
TX103		0.18	5,030.00	330.00	NA	NA	NA
TX104		0.06	9,440.00	6,220.00	NA	NA	NA
TX105		0.06	9,440.00	6,220.00	NA	NA	NA
TX106		0.15	4,410.00	3,390.00	NA	NA	NA
TX107		0.06	9,440.00	6,220.00	NA	NA	NA
TX108		0.06	15,200.00	7,630.00	NA	NA	NA
TX109		0.20	1,820.00	397.00	NA	NA	NA
TX110		0.24	1,500.00	319.00	NA	NA	NA
TX111		0.29	1,180.00	239.00	NA	NA	NA
TX112		0.18	5,030.00	330.00	NA	NA	NA
TX113		0.29	1,180.00	239.00	NA	NA	NA
TX114		0.19	4,730.00	323.00	NA	NA	NA
TX115		0.05	19,600.00	8,660.00	NA	NA	NA
TX116		0.17	5,660.00	355.00	NA	NA	NA
TX117		0.17	5,470.00	348.00	NA	NA	NA
TX118	*	214.00	4.02	2.10	NA	NA	NA
TY101		0.26	2,100.00	366.00	NA	NA	NA

Table 9-28. Plutonium Criticality Ratios - Single-Shell Tanks. (5 sheets)

Tank Name	High Pu tanks	Agnew Pu conc (ug/g)	Agnew ratio sum	Agnew insolubles ratio sum	TCR mean Pu conc (ug/g)	TCR ratio sum	TCR insolubles ratio sum
TY102		0.18	5,030.00	330.00	NA	NA	NA
TY103		0.17	4,190.00	1,870.00	NA	NA	NA
TY104		0.05	19,600.00	8,660.00	NA	NA	NA
TY105		0.05	19,600.00	8,660.00	NA	NA	NA
TY106		0.01	237,000.00	18,400.00	NA	NA	NA
U101		0.06	9,440.00	6,220.00	NA	NA	NA
U102		0.06	9,440.00	6,220.00	NA	NA	NA
U103		0.06	9,440.00	6,220.00	NA	NA	NA
U104		0.05	17,100.00	6,520.00	NA	NA	NA
U105		0.06	9,530.00	6,220.00	NA	NA	NA
U106		0.06	9,440.00	6,220.00	NA	NA	NA
U107	*	23.50	26.20	8.38	NA	NA	NA
U108	*	44.70	10.30	6.13	NA	NA	NA
U109	*	11.80	50.00	24.10	NA	NA	NA
U110		0.09	4,850.00	1,590.00	4.07	272.69	117.74
U111		0.14	4,020.00	2,430.00	NA	NA	NA
U112		4.10	120.00	46.20	NA	NA	NA
U201		23.50	26.10	8.38	NA	NA	NA
U202		23.50	26.10	8.38	NA	NA	NA
U203		23.50	26.10	8.38	NA	NA	NA
U204		23.50	26.10	8.38	NA	NA	NA

NA = not available.

Table 9-29. Neutron Absorber-to-Plutonium Mass Ratios for Solids in Double-Shell Tank.

Tank Name	High Pu Tanks	Agnew Pu Conc (ug/g)	Agnew Ratio Sum	Agnew Insolubles Ratio Sum	TCR Mean Pu Conc (ug/g)	TCR Ratio Sum	TCR Insolubles Ratio Sum
AN101		0.00	NA	NA	NA	NA	NA
AN102		0.00	NA	NA	NA	NA	NA
AN103		42.50	27.10	20.60	NA	NA	NA
AN104		0.00	NA	NA	NA	NA	NA
AN105		0.00	NA	NA	NA	NA	NA
AN106		0.00	NA	NA	NA	NA	NA
AN107		0.00	NA	NA	NA	NA	NA
AP101		0.00	NA	NA	NA	NA	NA
AP102		0.00	NA	NA	NA	NA	NA
AP103		0.00	NA	NA	NA	NA	NA
AP104		0.00	NA	NA	NA	NA	NA
AP105		0.00	NA	NA	NA	NA	NA
AP106		0.00	NA	NA	NA	NA	NA
AP107		0.00	NA	NA	NA	NA	NA
AP108		0.00	NA	NA	NA	NA	NA
AW101		0.07	10900.00	9500.00	NA	NA	NA
AW102		0.00	NA	NA	NA	NA	NA
AW103	*	9.87	46.20	11.80	NA	NA	NA
AW104		0.58	1220.00	1040.00	NA	NA	NA
AW105	*	8.92	54.40	18.60	NA	NA	NA
AW106	*	42.50	27.40	20.60	NA	NA	NA
AY101	*	103.00	7.40	4.55	NA	NA	NA
AY102		39.20	28.50	21.90	NA	NA	NA
AZ101	*	41.90	23.00	17.80	NA	NA	NA
AZ102	*	41.00	16.20	10.30	NA	NA	NA
SY101		0.00	NA	NA	NA	NA	NA
SY102	*	85.10	13.50	3.28	NA	NA	NA
SY103		0.00	NA	NA	NA	NA	NA

NA = not available

Table 9-30. Supernatant Plutonium Concentration for Double Shell Tanks with more than 10 kg of plutonium.

Tank	Date of Sample	Recent Supernatant Plutonium Concentration[a] (μg/l)
AW-103	September 1994	0.35
AW-105	August 1994	3.7
AW-106	November 1994	7.0
AY-101	October 1994	321
AZ-101	May 1989	11.4
AZ-102	August 1989	473
SY-102	March 1990	3.6

[a]Tusler (1995)

Table 9-31. AW-103 and AW-105 Tank Waste Analysis.

Sludge analyte	Sludge analysis (g/l)				
	AW-103 segments[a] based on 1.43 sp. gr.		AW-105 segments[b] based on 1.39 sp Gr for 3-6 and 1.50 sp. gr. for 7		Cladding waste projected concentrations based on process records[c]
	4-5R	6-10	3-6	7	
Pu	0.0327	0.0094	0.063	0.0058	0.0048
U	17.9	11.6	26.4	18.8	6.48
Al	3.46	11.0	4.89	54.9	
Cr	0.38	2.95	1.21	26.3	
Fe	1.13	1.16	7.90	29.1	1.07-1.44
La	3.62	0.23	3.54	0.25	
Zr	251.7	102.7	322	35.4	136

[a] (Hodgson and Tran 1995)
[b] (Tingey 1994)
[c] Calculated from Table 9-10

Table 9-32. AW-103 and AW-105 Sludge Insoluble Neutron Absorber-to-Plutonium Ratios.

Insoluble absorber	Tank AW-103 segments 4 and 5R absorber/Pu mass ratios and ratio sums		Tank AW-105 segments 3-6 absorber/Pu mass ratios and ratio sums		Process records projected for declad waste, absorber/Pu mass ratios and ratio sums	
U	547	----	419	-----	1346	----
Al	105	0.08	54.3	0.06		
Cr	12	0.09	19.2	0.14		
Fe	35	0.22	125	0.78	223	1.4
La	111	0.92	56.2	0.46		
Zr	7,697	1.92	5,111	1.28	28,200	7.1
Total		3.23		2.72		8.5

Table 9-33. AY-101 Sludge Analysis and Insoluble Absorber to Plutonium Mass Ratios.

Analysis	Settled sludge (average of sample and duplicate)	AY-101 insoluble absorber/Pu mass ratio	AY-101 insoluble absorber/Pu mass ratio sum
Sp. gr.	1.38		
Pu (g/l)	0.0124		
U (g/l)	Not Analyzed		
Al (g/l)	48.5 (70% of total)	3912	4.3
Fe (g/l)	16.6	1341	8.4
Mn (g/l)	2.8	226	7.1
Total			19.8

Table 9-34. AZ-101 Tank Sludge Analysis Compared to Projections from Process Records.

Sludge analyte	Sludge analysis of Cores 1 and 2 (g/l)		
	AZ-101 Core 1 solids[a] based on 1.7 sp. gr.	AZ-101 Core 2 solids[b] based on 1.67 sp. gr.	Projected NZCAW waste sludge concentrations based on process records[c]
	Segment 2 obtained by suction	Segments 1 and 2 composite	
Pu	0.095	0.16	0.064
U	----	16.4	15.2
Al	52.5	26.6	23.6
Cr	4.36	1.26	0.6
Fe	111	182	157
Ni	4.69	8.6	3.9
Zr	24.2	79.7	86.4

[a] (Letter from M. E. Peterson to A. J. Diliberto September 29, 1989)
[b] (Hodgson 1995)
[c] Taken from Table 9-11.

Table 9-35. AZ-101 Sludge Insoluble Neutron Absorber-to-Plutonium Ratios.

Insoluble absorber	Tank AZ-101 Core 1 segment 2 absorber/Pu mass ratios and ratio sums		Tank AZ-101 Core 2 segments 1 & 2 absorber/Pu mass ratios and ratio sums		Process records projected NZCAW insoluble absorber/Pu mass ratios and ratio sums	
U	----	----	124	-----	-----	----
Fe	1,168	7.30	1413	8.83	1946	12.2
Cr	46	0.34	8.6	0.14	----	----
Al (70%)	387	0.43	140	0.15	----	----
Ni	49.4	0.47	66.9	0.64	59	0.56
Zr	225	0.06	617	0.15	1331	0.33
Total		8.60		9.91		13.09

Table 9-36. Tank SY-102 Sludge Insoluble Neutron Absorber Analysis and Comparison to Projections from Process Records.

Sludge analyte	SY-102 Sludge insoluble absorber composition (g/L)	
	SY-102 cores 16 and 17 composite solids[a] based on 1.8 sp. gr.	Projected PFP waste sludge concentrations based on process records[b]
Pu	0.018	
U	3.5	
Al	82.1	
Ca	20.7	
Cr	34.0	
Fe	73.6	
Ni	1.85	
Mg	3.56	
Mn	19.6	

[a](Winters 1995)
[b]Records have not been declassified at this date.

Table 9-37. SY-102 Sludge Insoluble Neutron Absorber to Plutonium Ratios.

Insoluble absorber	Tank SY-102 core 16 and 17 sludges composite absorber/Pu mass ratios and ratio sums		Process records projected PFP insoluble absorber/Pu mass ratios and ratio sums[a]	
Al (70%)	3,193	3.51		
Ca	1,150	1.49		
Cr	1,889	14.0		
Fe	4,089	25.6		
Ni	103	0.98		
Mg	198	----		
Mn	1,089	34.0		
U	194	0.2500		
Total		79.8000		

[a]Records have not been declassified at this date.

10.0 LABORATORY EXPERIMENTS TO SUPPORT CRITICALITY ISSUES

Section 7.0 presented a detailed review of plutonium chemistry as it relates to criticality issues. All the available data reviewed indicated that plutonium in Hanford Site fuel reprocessing waste streams can potentially undergo three different types of reactions. These were precipitation as a distinct solid phase; precipitation as a solid solution with other components that are present in certain specific process-dependent waste streams (lanthanum, bismuth, and zirconium); and adsorption onto major hydroxide and/or oxyhydroxide components such as aluminum, iron, chromium, and manganese, etc. The available tank characterization data does not contain details on the speciation of plutonium in the waste phases (supernate, salt cake, and sludge). Therefore, the waste stream analyses were even less detailed, subsequent changes during aging in the tanks are largely uncharacterized, and no definite conclusion could be reached about the dominant chemical reactions and phase partitioning of plutonium in current waste tank environments. The review of plutonium chemistry relevant to waste tank environment raised the following questions:

1. During neutralization of the waste (for typical compositions of Hanford Site waste, see Agnew 1995), does plutonium form chemical bonds with the neutron absorbers (mainly iron and aluminum hydroxides) through mainly adsorption reactions?

2. To what extent does plutonium form solid solutions with compatible components such as lanthanum, bismuth, and zirconium on neutralization of waste streams?

3. Because Hanford Site waste streams were apparently oversaturated with respect to $PuO_2 \bullet xH_2O$ did plutonium precipitate as a distinct solid phase (coagulated by the large masses of iron and aluminum hydroxides)?

4. Does aging of the sludge solids release plutonium from neutron absorbers into separate solid phases that could settle out during retrieval?

5. What is the nature of aged solid phases (i.e., the extent to which iron and aluminum hydroxides have converted to oxyhydroxides and/or oxides) during decades of higher temperature aging in waste tanks?

6. What are the likely particle size distributions of neutron absorbing aluminum and iron solid phases and, if present, the distinct particles of $PuO_2 \bullet xH_2O$?

A set of experiments is being proposed to answer these important questions.

10.1 ADSORPTION EXPERIMENTS

To answer the first question and to reduce the differences that are likely to occur in interpreting the results of the experiments, the test plan should eliminate the possibility of forming separate plutonium phases that do

not contain neutron absorbers. This means that the concentration of plutonium in the test solutions should be far below the expected solubility limit for hydrated plutonium oxide under the conditions to be studied. Also, no metal ions other than neutron absorbers (iron and/or aluminum) should be present. The solutions should simulate the $NaNO_3$, $NaNO_2$, Na_2CO_3, and NaOH concentrations present in the neutralized waste stream solutions. Two sets of experiments need to be conducted with and without the presence of Na_2CO_3 to resolve the question whether in a typical Hanford waste stream environment, adsorption is likely to be a dominant mechanism. A measured lowering of the plutonium concentration in a solution that is known to be undersaturated with respect to $PuO_2 \bullet xH_2O$ during contact with iron or aluminum precipitate (formed before the plutonium is added) would prove that chemical bonding occurred between plutonium and the neutron absorbers. If adsorption does occur, aging the mixtures over a period of months and then performing desorption measurements on the solids would indicate the strength of the plutonium bonding to the neutron absorbers, mainly aluminum and iron hydroxides.

A second test would start with the plutonium, aluminum, and iron in acid solution. The next step would be to perform the neutralization reaction using NaOH. The resultant plutonium solution, as well as the solids, would be analyzed for plutonium concentration and solid morphology, mineralogy, and particle size, respectively. The slurry would be aged at a higher temperature in the presence of air. After set times the plutonium in solution and solid particles would be measured again to identify any changes. Specifically, one would look for amorphous solids turning into crystalline material, particle sizes increasing with time and whether concentration of plutonium in the solution increases or decreases. Care would be needed to keep the slurry pH constant; or at least the effects of pH (and other variables) would have to be considered when interpreting the change in plutonium concentration in the solution.

10.2 SOLID-SOLUTION FORMATION EXPERIMENTS

Experiments would be set up to test the potential solid solution formation of plutonium with waste stream components, such as $ZrO(NO_3)_2$, $La(NO_3)_3$, and $Bi(NO_3)_3$. Neutralization experiments are conducted with NaOH and Na_2CO_3 solutions with $NaNO_2$ as the holding reductant. These tests would not include all the other tank components, including aluminum, iron, chromium, manganese, PO_4, etc.

At least one additional experiment would use a Hanford Site tank waste composite that includes ligands such as hydroxide, nitrate, nitrite, carbonate, fluoride, chloride, phosphate, sulfate, and acetate, and metal ion components such as sodium, aluminum, silicon, iron, bismuth, potassium, zirconium, magnesium, calcium, strontium, chromium, manganese, nickel, boron, cerium, lead, and uranium in proportions that match overall Hanford Site tank waste from a given process, such as the bismuth phosphate or zirconium decladding processes. If warranted, several specific waste streams could be simulated using stable components traced with plutonium.

Following precipitation, aliquots of the precipitates would be aged at room temperature and at 90 °C (192 °F). Ultra-filtered sample solutions would be analyzed periodically for up to 1 year for plutonium concentration. After

6 months and again after 1 year, solid samples would be separated by a float/sink technique and analyzed using TEM/SEM/EDAX to determine whether the plutonium is hetero- or homogeneous; the bulk and surface morphology, primary particle size, and mineralogy of the major constituents; and the association of plutonium with the various particles within the precipitate matrix. This assumes that not enough plutonium will be present to observe discrete plutonium-rich particles. (TEM and SEM require about 0.1 percent by weight of an element to "see" it.) Settling studies would be performed to determine if plutonium preferentially reports to more- or less-buoyant phases. These characterization tests would be used to determine the extent to which plutonium is likely to partition into solid solution phases (especially in the first experiments with a simple set of components) or the extent to which plutonium would associate with particular types and sizes of solid phases in the waste tank environment after acid metal-rich waste streams are neutralized and aged.

10.3 PLUTONIUM SOLID PHASE FORMATION EXPERIMENTS

As discussed previously, Hanford Site waste streams apparently were oversaturated for $PuO_2 \bullet xH_2O$. Therefore, plutonium could have precipitated as a distinct solid phase and been coagulated by the large masses of iron and aluminum hydroxides. A set of experiments would be conducted with solutions oversaturated with respect to $PuO_2 \bullet xH_2O$ and containing $Fe(NO_3)_3$, and $Al(NO_3)_3$ and $NaNO_2$. These solutions would be neutralized with NaOH and Na_2CO_3. Aliquots of the resulting precipitates would be examined before and after aging at room temperature and at 90 °C (192 °F) using the TEM/SEM/EDAX techniques.

Because reverse strike (plutonium and metal acid mix added to base) was used to neutralize some of the Hanford Site waste streams, a reverse strike experiment will be conducted. In the reverse strike experiment, pH will be adjusted by adding an acid simulated waste stream to concentrated NaOH in the presence of $NaNO_2$ as a holding reductant. The precipitate will be examined in a fashion similar to the one used to examine the precipitates formed by the more common neutralization process (caustic titrated into the large volume of acid waste liquid) to determine the nature of resulting plutonium solid phase.

Following precipitation, the precipitate would be aged at room temperature and 90 °C (192 °F). Ultra-filtered sample solutions would be analyzed periodically for up to 1 year for plutonium concentration. After 6 months and again after 1 year, solid samples would be separated by float/sink technique and analyzed using SEM/EDAX to determine plutonium hetero/homogeneity within the precipitate matrix. Settling studies would be performed to determine the particle size distribution and whether plutonium preferentially reports to more- or less-buoyant phases or separates out in to a distinct solid phase.

10.4 TESTS ON ACTUAL HANFORD WASTE TANK SLUDGES

To more fully answer questions 4 through 6, it would be ideal to conduct tests on actual Hanford Site waste tank sludges. We would then compare the

results to those obtained using the simulated waste stream. Using physical separation methods, such as sink/float, using various liquids with increasing densities, any plutonium solid phases that are present would be expected to separate into the heavy (sink) fraction. Measuring plutonium in the fractions would determine where the plutonium resides in the tank. The measurements also would be used to characterize the plutonium-rich fractions. We would expect that the plutonium concentration would increase enough in the plutonium-rich fractions following separation from the dominant, but less dense, sludge matrix that the plutonium itself might be seen by TEM/SEM/EDAX. This would allow us to obtain much information specific to plutonium. Such characterization would also potentially resolve the question about whether aging of sludge solids causes a concomitant release of plutonium from neutron absorbers into separate solid phases that could preferentially settle out during retrieval.

Characterization of the major sludge components using analytical techniques such as selective extraction, x-ray diffraction, and particle size distribution also would help answer the following questions related to the nature of aged solid phases.

- To what extent have iron and aluminum hydroxides converted to more crystalline oxyhydroxides and/or oxides during decades of high-temperature aging in waste tanks?

- What are the likely particle size distributions of neutron-absorbing aluminum and iron solid phases and, if present $PuO_2 \bullet xH_2O \bullet$?

Data obtained by these characterization would be used to validate the data obtained through the more simple system bench-scale tests described in Sections 10.1 through 10.3.

11.0 REFERENCES

Ackers, P. and W. R. White, 1973, "Sediment Transport: New Approach and Analysis," in *J. of Hydr. Div.*, American Society of Civil Engineers, Vol. 99, pp. 2041-2060.

Agnew, S. F., 1995, *Hanford Defined Wastes: Chemical and Radionuclide Compositions*, LA-UR-94-2657, Rev. 2, Los Alamos National Laboratory, Los Alamos, New Mexico.

Agnew, S. F., J. Boyer, R. A. Corbin, T. B. Duran, J. R. FitzPatrick, K. A. Jurgensen, T. P. Ortiz, and B. L. Young. 1996, *Hanford Tank Chemical and Radionuclide Inventories: HDW Model Rev. 3.*, LA-UR-96-858, Los Alamos National Laboratory, Los Alamos, New Mexico.

Alam, A. M. Z. and J. F. Kennedy, 1969, "Friction Factors for Flow in Sand Bed Channels," in *J. of Hydr. Div.*, American Society of Civil Engineers, Vol. 95, pp. 1973-1992.

Allard, B., 1982, "Solubilities of Actinides in Neutral or Basic Solutions," in *Actinides in Perspective*, N. M. Edelstein, Ed., Pergamon Press.

Allen, G. K., 1976, *Estimated Inventory of Chemicals Added to Underground Waste Tanks, 1944 through 1975*, ARH-CD-610B, Atlantic Richfield Hanford Company, Richland, Washington.

Allison, J. D., D. S. Brown, and K. J. Novo-Gradac, 1990, *MINTEQA2/PRODEFA2, A Geochemical Assessment Model for Environmental Systems: Version 3.00 User's Manual*, EPA-600/3-91-021, U.S. Environmental Protection Agency, Athens, Georgia.

Amonette, J. A. and L. W. Zelazny, 1994, *Quantitative Methods in Soil Mineralogy*, SSSA Miscellaneous Pub., Soil Science Society of America, Inc., Madison, Wisconsin.

Andelman, J. B. and T. C. Rozell, 1970, *Plutonium in the Water Environment, I. Characteristics of Aqueous Plutonium*, Adv. Chem. Ser., Vol. 93, pp. 118-137.

Anderson, J. D., 1990, *A History of the 200 Area Tank Farms*, WHC-MR-0132, Westinghouse Hanford Company, Richland, Washington.

ARH, 1970, *Purex Process Operation and Performance 1970 Thoria Campaign*, ARH-2127 Declassified, Atlantic Richfield Hanford Company, Richland Washington.

Baes, C. F. and R. E. Mesmer, 1976, *The Hydrolysis of Cations*, John Wiley and Sons, New York, New York.

Bagnold, R. A., 1966, *An Approach to the Sediment Transport Problem from General Physics*, Geological Survey Professional Paper 422-I, U.S. Geological Survey, Washington, D.C.

Bamberger, J. A., P. S. Lowery, and L. M. Liljegren, 1990, *A Methodology to Predict the Uniformity of Double-Shell Tank Waste Slurries Based on Mixing Pump Operation*, PNL-7665, Pacific Northwest Laboratory, Richland, Washington.

Bamberger, J. A., L. M. Liljegren, C. W. Enderlin, P. A. Meyer, M. S. Greenwood, P. J. Titzler, and G. Terrones, 1996, *1/12-Scale Mixing Experiments to Characterize Double-Shell Tank Slurry Uniformity*, PNL-10820, Pacific Northwest Laboratory, Richland, Washington.

Barney, G. S., 1992a, *Adsorption of Plutonium on Shallow Sediments at the Hanford Site*, WHC-SA-1516-FP, Westinghouse Hanford Company, Richland, Washington.

Barney, G. S., K. J. Lueck, and J. W. Green, 1992b, "Removal of Plutonium From Low-Level Process Wastewaters by Adsorption," in *Environmental Remediation*, G. F. Vandergrift, D. T. Reed, and I. R. Tasker, Eds., ACS Symposium Series 509, American Chemical Society, Washington, D.C.

Barrow, N. J. and J. W. Bowden, 1987, "A Comparison of Models for describing the Adsorption of Anions on a Variable Charge Mineral Surface," in *J. Coll. Interfac. Sci.*, Vol. 119, pp. 236-250.

Bartram, S. F., 1967, "Crystallite-Size Determination from Line Broadening and Spotty Patterns," in *Handbook of X-Rays*, E. F. Kaelble, Ed., McGraw Hill, New York, New York.

Bates, R. L. and J. A. Jackson, 1987, *Glossary of Geology*, 3rd edition, American Geological Institute, Alexandria, Virginia.

Benjamin M. M. and J. O. Leckie, 1981, *Conceptual Model for Metal-Ligand-Surface Interactions during Adsorption*, Env. Sci. Tech., Vol. 15, pp. 1050-1056.

Bird, R. B., W. E. Stewart, and E. N. Lightfoot, 1960, *Transport Phenomena*, John Wiley and Sons, New York, New York.

Bish, D. L. and J. E. Post, 1989, *Modern Powder Diffraction*. Reviews in Mineralogy Volume 20, Mineralogical Society of America, Washington, D.C.

Blench, T., 1966, *Mobile-Bed Fluviology*, Dept. Tech. Ser. University of Alberta, Edmonton, Alberta, Canada.

Bratzel, D. R. and F. M. Jungfleisch, 1980, "Evaluation of Waste Storage Tank Physical and Chemical Characterization Data," No. 65453-80-265, in *Laboratory Reports for WHC-SD-WM-ES-244*, Westinghouse Hanford Company, Richland, Washington.

Bratzel, D. R., W. W. Schulz, R. Vornehm, A. E. Waltar, H. Babad, G. S. Barney, J. Greenborg, L. H. Rodgers, R. E. Felt, D. W. Jeppson, C. A. Rogers, K. N. Schwinkendorf, T. S. Vail, R. J. Serne, G. A. Whyatt, 1996, *Tank Farm Nuclear Criticality Review*, WHC-SD-WM-TI-725, Rev. 0, Westinghouse Hanford Company, Richland, Washington.

Braun, D. J., L. D. Muhlestein, T. B. Powers, and M. D. Zentner, 1994, *High Level Waste Tank Subcriticality Safety Assessment*, WHC-EP-0687, Westinghouse-Hanford Company, Richland, Washington.

Brevick, C. H., 1995, *Historical Tank Content Estimate for the Southeast Quadrant of the Hanford 200 East Areas*, WHC-SD-WM-ER-350, Westinghouse Hanford Company, Richland, Washington.

Brown, C. B., 1950, "Sediment Transportation," in *Engr. Hydr.*, H. Rouse, ed., John Wiley and Sons, New York, New York.

Brownlie, W. L., 1981a, *Prediction of Flow Depth and Sediment Discharge in Open Channels*, Report KH-R-43A, W. M. Keck Laboratory of Hydraulics and Water Resources, California Institute of Technology, Pasadena, California.

Brownlie, W. L., 1981b, *Compilation of Alluvial Channel Data: Laboratory and Field*, Report KH-R-43B, W. M. Keck Laboratory of Hydraulics and Water Resources, California Institute of Technology, Pasadena, California.

Brownlie, W. L., 1983, "Flow Depth in Sand-Bed Channels," *J. of Hydr. Div.*, American Society of Civil Engineers, Vol. 109, pp. 959-990.

Camaioni, D. M., W. D. Samuels, B. D. Lenihan, S. A. Clauss, K. L. Wahl, and J. A. Campbell, 1994, *Organic Waste Tank Safety Program Waste Aging Studies*, PNL-10161, Pacific Northwest Laboratory, Richland, Washington.

Campbell, J. A., S. Clauss, R. Lucke, K. Grant, G. Mong, V. Hoopes, J. Rau, B. Lerner, and R. Steele, 1994a, *Flammable Gas Safety Program Analytical Methods Development: FY 1993 Progress Report*, PNL-9062, Pacific Northwest Laboratory, Richland, Washington.

Campbell, J. A., R. B. Lucke, S. A. Clauss, G. M. Mong, K. E. Grant, J. K. Rau, F. V. Hoopes, R. K. Steele, B. D. Lerner, and K. L. Wahl, 1994b, *Waste Tank Organic Safety Program Analytical Methods Development: FY 1994 Progress Report*, PNL-10128, Pacific Northwest Laboratory, Richland, Washington.

Campbell, J. A., R. B. Lucke, S. A. Clauss, G. M. Mong, K. E. Grant, J. K. Rau, F. V. Hoopes, K. L. Wahl, B. D. Lerner, and R. K. Steele, 1994c, *Flammable Gas Safety Program Analytical Methods Development: FY 1994 Progress Report*, PNL-10127, Pacific Northwest Laboratory, Richland, Washington.

Campbell, J. A., S. A. Clauss, K. E. Grant, F. V. Hoopes, G. M. Mong, J. K. Rau, R. Scheele, and K. L. Wahl, 1995a, *Flammable Gas Safety Program Organic Analysis and Analytical Methods Development: FY 1995 Progress Report*, PNL-10776, Pacific Northwest Laboratory, Richland, Washington.

Campbell, J. A., R. M. Bean, K. L. Wahl, G. M. Mong, K. E. Bell, K. B. Wehner, A. D. Rick, R. J. Ray, D. B. Bechtold, B. R. Wels, R. W. Schroeder, J. W. Ball, B. D. Valenzuela, J. M. Frye, S. L. Fitzgerald, P. P. Bachelor, B. Griffin, R. K. Fuller, A. B. Banally, and S. M. Parong, 1995b, *Analysis of Samples from Hanford Waste Tank 241-C-103*, PNL-10531, Pacific Northwest Laboratory, Richland, Washington.

Carter, R. D., G. R. Keil, and K. R. Ridgeway, 1969, *Criticality Handbook, Vol. II*, Atlantic Richfield Hanford Company, Richland, Washington.

Castaing, B. A., 1994, *101-AY, 102-AY, and 106-C Data Compendium*, WHC-SD-TI-578, Rev. 1, Westinghouse-Hanford Company, Richland, Washington.

Charyulu, M. M., I. C. Pius, A. Kadam, M. Ray, C. K. Sivaramakrishnan, and S. K. Patil, 1991, "The Behavior of Plutonium in Aqueous Basic Media," *J. Radioanal. and Nucl. Chem.*, Vol. 152, (2), pp. 479-485.

Chisholm-Brause, C., S. D. Conradson, C. T. Buscher, P. G. Eller, and D. E. Morris, 1994, "Speciation of Uranyl Sorbed at Multiple Binding Sites on Montmorillonite," *Geochim. Cosmochim. Acta*, Vol. 58, (17), pp. 3625-3631.

Choppin, G. R., 1983, "Aspects of Plutonium Solution Chemistry," in *Plutonium Chemistry*, W. T. Carnall and G. R. Choppin, eds., ACS Sym. Ser. 216, pp. 213-230, Washington, D.C.

Clark, R. M., 1990, "Water Supply," in *Standard Handbook of Environmental Engineering*, R. A. Corbitt, ed. McGraw Hill, New York, pp. 5.1-5.225.

Cleveland, J. M., 1979, *The Chemistry of Plutonium*, American Nuclear Society, LaGrange Park, Illinois.

Colby, B. R., 1964a, "Practical Computation of Bed-Material Discharge," in *J. of Hydr. Div.*, American Society of Civil Engineers, Vol. 90, pp. 217-246.

Colby, B. R., 1964b, *Discharge of Sands and Mean Velocity Relationships in Sand-Bed Streams*, Prof. Paper 462-A, United Sates Geological Survey, Washington, D.C.

Coleman, G. H., 1965, *The Radiochemistry of Plutonium*, NAS-NS 3058, National Academy of Sciences-National Research Council, U.S. Atomic Energy Commission, Washington, D.C.

Corey R. B., 1981, "Adsorption vs Precipitation," in *Adsorption of Inorganics at Solid-Liquid Interfaces*, M. A. Anderson and A. J. Rubin, eds., Ann Arbor Science, Ann Arbor, Michigan, pp. 161-182.

Cornell, R. M., and U. Schwetmann, 1979, "Influence of Organic Anions on the Crystallization of Ferrihydrite," *Clays and Clay Minerals*, Vol. 27, pp. 402-410.

Crawley, D. T. and M. K. Harmon, 1960, *REDOX Chemical Flowsheet HW-No. 6*, HW-66203, Declassified, Hanford Atomic Works, Richland, Washington.

Cross, M. M., 1965, "Rheology of Non-Newtonian Fluids: A New Flow Equation for Systems," *J. Colloid Sci.*, Vol. 20, pp. 417-437.

Crowe, R. D., M. Kummerer, and A. K. Postma, 1993, *Estimation of Heat Load in Waste Tanks Using Average Vapor Space Temporatures*, WHC-EP-0709, Westinghouse Hanford Company, Richland, Washington.

Dabak, T. and O. Yucel, 1987, "Modeling of the Concentration and Particle Size Distribution Effects of the Rheology of Highly Concentrated Suspensions," *Powder Tech.*, Vol. 52, pp. 193-206.

Davis J. A. and K. F. Hays, 1986, "Geochemical Processes at Mineral Surfaces: An Overview," in *Geochemical Processes at Mineral Surfaces*, J. A. Davis and K. F. Hays, eds., ACS Symp Ser. 323, pp. 2-19.

Davis J. A. and D. B. Kent, 1990, "Surface Complexation Modeling in Aqueous Geochemistry," in *Mineral-Water Interface Geochemistry*, M. F. Hochella, Jr. and A. F. White, Eds., Rev. in Miner. Ser. Vol. 23, pp. 177-260.

Davis, J. A., R. O. James, and J. O. Leckie, 1978, "Surface Ionization and Complexation at the Oxide/Water Interface," *J. Coll. Inter. Sci.*, Vol. 63, pp. 480-499.

Delegard, C. H., 1995, "Carbonate Complexes of Plutonium in Alkaline Solution," in *Calcination/Dissolution Chemistry Development Fiscal Year 1995*, WHC-EP-0882, pp. 4-25 to 4-31, Westinghouse Hanford Company, Richland, Washington.

Delegard, C. H., 1987, "Solubility of $PuO_2 \bullet xH_2O$ in Alkaline Hanford High-Level Waste Solution," *Radiochim. Acta*, Vol. 41, pp. 11-21. (Also published as RHO-RE-SA-75 P, Rockwell Hanford Company, Richland, Washington.)

Delegard, C. H., G. S. Barney, and S. A. Gallagher, 1984, *Effects of Hanford High-Level Waste Components on the Solubility and Sorption of Cobalt, Strontium, Neptunium, Plutonium, and Americium*, ACS Symp. Ser. Vol. 246, pp. 95-112. (Also published as RHO-RE-SA-18 P, Rockwell Hanford Company, Richland, Washington in 1983.

Delegard, C. H. and S. A. Gallagher, 1983, *Effects of Hanford High-Level Waste Components on the Solubility of Cobalt, Strontium, Neptunium, Plutonium, and Americium*, RHO-RE-ST-3P, Rockwell Hanford Company, Richland, Washington.

DiCenso, A. T., L. C. Amato, W. I. Winters, 1995, *Tank Characterization Report for Double-Shell Tank 241-SY-102*, WHC-SD-WM-ER-366, Rev. 0, Westinghouse Hanford Company, Richland, Washington.

Dran, J. C., G. D. Mea, V. Noulin, J. C. Petit, and V. Rigato, 1994, "Interaction of Pseudocolliods with Mineral Surfaces: The Fate of the Scavenged Cation," *Radiochim. Acta*, Vol. 66/67, pp. 221-227.

DuBoys, P., 1879, "Le Rohne et les Rivieres a Lit Affoullable," *Anneles des et Chausses*, Series 5, Vol. 18, pp. 141-195.

Dunn, I. S., 1959, "Tractive Resistance of Cohesive Channels," *J. Soil Mech. Foun. Div.*, ASCE, NO. SMC, Proc. Paper 2062, pp. 1-24.

Einstein, H. A. 1950, *The Bed Load Function for Sediment Transportation in Open Channels*, Technical Bulletin 1026, U.S. Department of Agriculture, Soil Conservation Service, Washington, D.C.

Einstein, H. A., and N. Barbarossa, 1952, "River Channel Roughness," *Trans.* ASCE, Vol. 117, pp. 1112-1146.

Edwards, A. B., 1952, "The Ore Minerals and their Textures," *J. Proc. Royal Soc. New South Wales*, Vol. 85, pp. 26-46.

Ellwood, K. R. J., G. C. Georgiou, T. C. Papanatasiou, and J. O. Wilkes, 1990, "Laminar Jets of Bingham-Plastic Liquids," *J. Rheology*, Vol. 34, pp. 787-813.

Engelund, F., 1966, "Hydraulic Resistance of Alluvial Streams," *J. Hydr. Div.*, Vol. 92, pp. 315-327.

Engelund, F. and E. Hansen, 1967, *A Monograph on Sediment Transport in Alluvial Streams*, Teknisk Vorlab, Copenhagen, Denmark.

Engelund, F. and J. Fredsoe, 1976, "A Sediment Transport Model for Straight Alluvial Channels," *Nordic Hydrology*, Vol. 7, pp. 293-306.

Evans, A. M., 1980, *An Introduction to Ore Geology*, Elsevier, New York.

Eyler, L. L., 1983, *Sediment Settling and Resuspension in Waste Storage Tanks with Air Injection Circulators*, Letter Report FATE-83-109, Pacific Northwest Laboratory, Richland, Washington.

Eyler, L. L., D. S. Trent, J. A. Fort, 1993, *TEMPEST: A Computer Program for Three-Dimensional Time-Dependent Computational Fluid Dynamics*, Volume 2: User's Manual, Version T, Mod 2. PNL-8857, Vol 2. Rev. 1., Pacific Northwest Laboratory, Richland, Washington.

Fan, S., ed., 1988, *Twelve Selected Computer Stream Sedimentation Models Developed in the United States*, Subcommittee on Sedimentation Interagency Advisory Committee on Water Data, Federal Energy Regulatory Commission, Washington, D.C.

Felmy, A. R., 1995, "GMIN, A Computerized Chemical Equilibrium Program Using a Constrained Minimization of the Gibbs Free Energy: Summary Report," in *Chemical Equilibrium and Reaction Models*, R. H. Loeppert, A. P. Schwab and S. Goldberg, eds., SSSA Special Publication Number 42, American Society of Agronomy, Inc., Madison, Wisconsin.

Flaxman, E. M., 1962, "Channel Stability in Undisturbed Soils," *J. Hydr. Div.* Vol. 89, pp. 87-96.

Fox and McDonald, 1973, *Introduction to Fluid Dynamics*, John Wiley and Sons, New York, New York.

Frankel, N. A. and A. Acrivos, 1967, "On the Viscosity of A Concentrated Suspension of Solid Spheres," *Chem. Eng. Sci.*, Vol. 22, pp. 847-853.

Garde, R. I. and K. G. R. Raju, 1966, "Resistance Relationship for Alluvial Channel," *J. Hydr. Div.*, Vol. 95, pp. 77-100.

Gazzaz, M., 1986, "Geochemistry of Radioelements in Silicic Volcanic Rocks of the Northern Arabian Shield," *Arab J. Nucl. Sci. Appl*, Vol. 27, pp. 291-307.

GE, 1951, *Uranium Recovery Technical Manual*, HW-19140, Declassified, General Electric Company, Richland, Washington.

Glasstone S. and A Sesonske, 1981, *Nuclear Reactor Engineering*, Third Edition, Robert E. Krieger Publishing Company, Malabar, Florida.

Govier G. W. and K. Aziz, 1972, *The Flow of Complex Mixture in Pipes*, Robert E. Krieger Publishing Company, Malabar, Florida.

Graf, W. H., 1971, *Hydraulics of Sediment Transport*, McGraw-Hill Book Co., Inc., New York, New York.

Grebenshchikova, V. I., R. V. Bryzgalova, and I. V. Chernitskaya, 1967, "The Coprecipitation of Plutonium with Lanthanum Oxalate," in *Coprecipitation and Adsorption of Radioactive Elements*, V. M. Vdovenko, Ed., Israel Program of Scientific Translations, Jerusalem, Israel.

Hanlon, B. M., 1996, *Waste Tank Summary Report for Month Ending February 29, 1996*, WHC-EP-0182-95, Westinghouse Hanford Company, Richland, Washington.

Hanson, H. D., 1980, *Transuranics in the Environment*, DOE/TIC-22800, U.S. Department of Energy, Washington, D.C.

Hargraves, R. B., 1980, *Physics of Magmatic Processes*, Princeton University Press, Princeton, New Jersey.

Harlow, D. G., 1985, letter to D. C. Bartholomew, *Interim Head End/Solvent Extraction/Plutonium Oxide Conversion Campaign Report, September 1985*, Letter #65940-85-534, November 7, 1985, Rockwell Hanford Company, Richland Washington.

Hartley, S. A., 1996, *A Comparison of Historical Tank Content Estimates (HTCE) Model and Sample-Based Estimates of Hanford Waste Tank Contents*, PNNL-draft, Pacific Northwest Laboratory, Richland, Washington.

Haynie, R. B. and D. B. Simons, 1968, "Design of Stable Channels in Alluvial Materials," *J. Hydr. Div.*, Vol. 94, pp. 1399-1420.

Henderson, F. M., 1966, *Open Channel Flow*, The Macmillan Company, New York, New York.

Hess, A., letter to S. D. Godfry, *Review of Records for Source of U-233 in Tank 104-C*, August 19, 1991, No. 29210-91-030, Westinghouse Hanford Company, Richland, Washington.

Hobbs, D. T. and T. B. Edwards, 1993, *Solubility of Plutonium in Alkaline Salt Solutions*, WSRC-TR-93-131, Westinghouse Savannah River Company, Aiken, South Carolina.

Hobbs, D. T., T. B. Edwards, and S. D. Fleischman, 1993, *Solubility of Plutonium and Uranium in Alkaline Salt Solutions*, WSRC-TR-93-056, Westinghouse Savannah River Company, Aiken, South Carolina.

Hobbs, D. T., 1995, *Effects of Coprecipitation on the Concentrations of Uranium and Plutonium in Alkaline Salt Solutions*, WSRC-TR-95-0462, Westinghouse Savannah River Company, Aiken, South Carolina.

Hodgson, K. M., 1995, *Tank Characterization Report for Double-Shell Tank 241-AZ-101*, WHC-SD-WM-ER-410, WestingHouse Hanford Company, Richland, Washington.

Hodgson, K. M. and T. T. Tran, 1995, *Tank Characterization Report for Double-Shell Tank 241-AW-103*, WHC-SD-WM-ER-455, WestingHouse Hanford Company, Richland, Washington.

Hodgson, K. M., D. L. Herting, W. W. Schulz, L. A. Bray, and J. L. Swanson, 1985, "Content and Removal of TRU Elements from Aqueous Zirconium Cladding Waste," in *Proc. Intl. Symp. Actinide/Lanthanide Separations*, G. R. Choppin, J. D. Navratil, and W. W. Schulz. Eds., World Scientific. Philadelphia, Pennsylvania.

Hsi, C. K. D. and D. Langmuir, 1985, "Adsorption of Uranyl onto Ferric Oxyhydroxides: Application of the Surface Complexation Site-Binding Model," in *Geochim. Cosmochim. Acta* Vol. 49, pp. 1931-1941.

Hsu, P. H., 1977, "Aluminum Hydroxides and Oxyhydroxides," in *Minerals in Soil Environments*, Soil Science Society of America, Inc., Madison, Wisconsin.

Hurlbut, C. S., 1971, *Dana's Manual of Mineralogy*, John Wiley and Sons, New York, New York.

Inglis, C. C., 1968, "Discussion of Systematic Evaluation of River Regime by C. R. Neill and V. J. Galey," in *J. Of Waterways and Harbors Division*, Vol. 94, pp. 109-114.

Jackson, R. R. and R. L. Walser, 1977, *Purex Process Operation and Performance: 1970 Thoria Campaign*, ARH-2127, Atlantic Richfied Hanford Company, Richland, Washington.

Jacobs, L. L., 1986, Letter sent March 14, 1986, *N Basin Trip Report Clarification*, to K. E. Plummer, Westinghouse Hanford Company, Richland, Washington.

Jacobs, L. L., G. K. Allen, and D. W. Reberger, 1985, *Purex Flowsheet - Processing N Reactor Fuels*, PFD-P-020-00001, Rev A4, Westinghouse Hanford Company, Richland, Washington.

Jansen, P. Ph., L. Van Bendegom, J. Van Den Berg, M. De Vries, and A. Zanen eds., 1979, *Principles of River Engineering—The Non-Tidal Alluvial River*, Pitman Publishing Limited, London, England; San Francisco, California; and Melbourne, Australia.

Jensen, M. L. and A. M. Bateman, 1981, *Economic Mineral Deposits*, John Wiley and Sons, New York, New York.

Jobe, K., E. B. Ledger, P. Sharp, M. C. Crocker, 1993, *Radiostratigraphy and Heavy Mineral Content of the Weches Formation (Eocene), Nacogdoches County, Texas*, AAPG Bulletin 77:9, p. 1588-1509, American Association of Professional Geologists, Washington, D.C.

Johnson, J. S., 1994, *An Investigation into Jet Mixing Similarity Parameters Proposed for Solid-Liquid Mixtures*, Masters Thesis, Washington State University, Pullman, Washington.

Jopling, A. V., 1964, "Laboratory Study of Sorting Processes Related to Flow Separation," in *J. Geophy. Res.*, Vol. 69, pp. 3403-3418.

Jungfleisch, F. M., 1984, *Preliminary Estimation of the Waste Inventories in Hanford Tanks Through 1980*, SD-WM-TI-057, Westinghouse Hanford Company, Richland, Washington.

Kalyon, D. M., P. Yaras, B. Aral, and U. Yilmazer, 1993, "Rheological Behavior of a Concentrated Suspension: A Solid Rocket Fuel Simulant," in *J. Rheology*, Vol. 37, pp. 35-53.

Karim, M. F. and J. F. Kennedy, 1981, *Computer-Based Predictions for Sediment Discharge and Friction Factor of Alluvial Streams*, IIHR Report No. 242, Iowa Institute of Hydraulic Research, University of Iowa, Iowa City, Iowa.

Karraker, D. G., 1994, Radiation Effects on the Solubility of Plutonium in Alkaline High Level Waste, WSRC-MS-94-0278X (Rev. 2), Westinghouse Savannah River Company, Aiken, South Carolina.

Karraker, D. G., 1995, *Plutonium (VI) Solubility Studies in Savannah River Site High-Level Waste Supernate*, WSRC-TR-95-0244, Westinghouse Savannah River Company, Aiken, South Carolina.

Kennedy, J. F., 1963, "The Mechanics of Dunes and Antidunes in Erodible-Bed Channels," in *J. Fluid Mech.*, Vol. 16, Part 4, pp. 521-544.

Kepak, F. 1971, "Adsorption and Colloidal Properties of Radioactive Elements in Trace Concentrations," in *Chem. Rev.*, Vol. 71, pp. 357-370.

Kim, J. I. and B. Kanellakopulos, 1989, "Solubility Products of Plutonium(IV) Oxide and Hydroxide," in *Radiochim. Acta*, Vol. 48, pp. 145-150.

Kinniburgh D. G. and M. L. Jackson, 1981, "Cation Adsorption by Hydrous Metal Oxides," in *Adsorption of Inorganics at Solid-Liquid Interfaces*, M. A. Anderson and A. J. Rubin, eds., Ann Arbor Science, Ann Arbor, Michigan.

Klug, H. P. and L. E. Alexander, 1974, *X-ray Diffraction Procedures for Polycrystalline and Amorphous Materials*, Wiley and Sons Publishing, New York, New York.

Koehler M., E. Wieland, and J. O. Leckie, 1992, "Metal-Ligand Interactions During Adsorption of Uranyl and Neptunyl on Oxides and Silicates," in *Proc. of 7th Int. Symp. on Water-Rock Interaction -WRI7. V1: Low Temp. Env.*, Y. K. Kharaka A. S. Maest., A. A. Balkema, eds., Rotterdam, Netherlands.

Krone, R. B., 1962, *Flume Studies of the Transport of Sediment in Estuarial Shoaling Processes*, Hydraulic Engineering Laboratory and Sanitary Engineering Research Laboratory, University of California at Berkeley, California.

Krupka, K. M. and R. J. Serne, 1996, *Performance Assessment of Low-Level Radioactive Waste Disposal Facilities: Effects on Radionuclide Concentrations by Cement/Ground-Water Interactions*, NUREG/CR-6377, U.S. Nuclear Regulatory Commission, Washington, D.C.

Kupfer, M. J., 1996, *Interim Report on Determining Best Basis Total Chemical and Radionuclide Inventories in Hanford Site Tank Wastes*, WHC-SD-WM-TI-740, Westinghouse Hanford Company, Richland, Washington.

Kwong, N. G. and P. M. Huang, 1975, "Influence of Citric Acid on the Chrystallization of Aluminum Hydroxides," in *Clays and Clay Minerals*, Vol. 23, pp. 164-165.

LaFlamme, B. D. and J. W. Murray, 1987, "Solid/Solution Interaction: The Effect of Carbonate Alkalinity on Adsorbed Thorium," in *Geochim. Cosmochim. Acta.*, Vol. 332, pp. 351-357.

Lane, E. W., 1947, "Report of the Subcommittee on Sediment Terminology," in *Transactions, American Geophysical Union*, Vol. 28, No. 6, pp. 936-938.

Laursen, E. M, 1958, "The Total Sediment Load of Streams," in *J. Hydr. Div.*, Vol. 54, pp. 1-36.

Leliavsky, S., 1966, *An Introduction to Fluvial Hydraulics*, Dover Publications, Inc., New York, New York.

Lemire, R. J. and P. R. Tremaine, 1980, "Uranium and Plutonium Equilibria in Aqueous Solutions to 200 °C," in *J. Chem. Eng. Data*, Vol. 25, pp. 361-370.

Lewis, D. W., and D. McConchie, *Analytical Sedimentology*, Chapman and Hall, New York, New York.

Lide, D. R., 1995, *CRC Handbook of Chemistry and Physics*, CRC Press, New York, New York.

Lierse, Ch., 1985, *Chemical Behavior of Plutonium in Natural Aquatic System: Hydrolysis, Carbonate Complexation and Redox Reaction*, Ph. D. Thesis, Technische Universitat Munchen, Germany.

Liljegren, L. M., 1993, *Similarity Analysis Applied to the Design of Scaled Tests of Hydraulic Mitigation Methods for Tank 241-SY-101*, PNL-8518, Pacific Northwest Laboratory, Richland, Washington.

Lindsay, W. L., 1979, *Chemical Equilibria in Soils*, John Wiley and Sons, New York, New York.

Liu, J., L. R. Pederson, and L. Q. Wang, 1995, *Solid-Phase Characterization in Flammable-Gas-Tank Sludges by Electron Microscopy*, PNL-10723, Pacific Northwest Laboratory, Richland, Washington.

Lokken, R. O., R. D. Scheele, D. M. Strachan, and A. P. Toste, 1986, *Complex Concentrate Pretreatment: FY 1986 Progress Report*, PNL-7687, Pacific Northwest Laboratory, Richland, Washington.

Lovera, F. and J. F. Kennedy, 1969, "Friction-Factors for Flat-Bed Flows in Sand Channels," *J. of Hydr. Div.*, American Society of Civil Engineers, Vol. 95, pp. 1227-1234.

Maddock, T., Jr., 1976, "Equations for Resistance to Flow and Sediment Transport in Alluvial Channels," *Water Resour. Res.*, Vol. 12, pp. 11-21.

Maddock, T., Jr., 1969, *The Behavior of Straight Open Channels with Movable Beds*, Professional Paper 622-A, United Sates Geological Survey, Washington, D.C.

Mahoney, L. A. and D. S. Trent, 1995, *Correlation Models for Waste Tank Sludge and Slurries*, PNL-10695, Pacific Northwest Laboratory, Richland, Washington.

Mall, J. and B. B. Mishra, 1994, "Occurrence of Monazite in Some Alluvial Soils of North Bihar," *Current Sci.*, Vol. 66, pp. 158-160.

Matheison, W. E. and G. A. Nicholson, 1986, *PUREX Chemical Flowsheet-Processing of Aluminum-clad Fuels*, ARH-214 DEL, Atlantic Richfield Hanford Company, Richland, Washington.

McNown, J. S., J. Malaika, and R. Pramanik, 1951, "Particle Shape and Settling Velocity," *Transactions*, 4th Meeting of the International Association for Hydraulic Research, Bombay, India, pp. 511-522.

Mehta, A. J., E. J. Hayter, W. R. Parker, R. B. Krone, A. M. Teeter, 1989a, "Cohesive Sediment Transport I: Process Description," *J Hydr. Div.*, Vol. 115, pp. 1076-1093.

Meyer-Peter, E., and R. Muller, 1948, "Formulas for Bed-Load Transport," *Report on Second Meeting of International Association for Hydraulic Research*, Stockholm, Sweden, pp. 39-64.

Morel, F. M. M., J. G. Yeastad, and J. C. Westall, 1981, "Adsorption Models: A Mathematical Analysis in the Framework of General Equilibrium Calculations," in *Adsorption of Inorganics at Solid-Liquid Interfaces*, M. A. Anderson and A. J. Rubin, eds., Ann Arbor Science, Ann Arbor, Michigan, pp. 262-294.

Mostafa, M. G. and R. M. McDermin, 1971, "Discussion of Sediment Transportation Mechanics: Hydraulic Relations for Alluvial Streams by the Task Committee for Preparation of Sedimentation Manual, Committee of Sedimentation of the Hydraulic Division, Vito A. Vanoni, Chmn.," *J. Hydr. Div.*, Vol. 97, pp. 1770-1780.

Nagamalleswara, R. B., 1994, "Radiometric, Magnetic Susceptibility and Mineralogical Studies in Some Beach Placers of Andhra Pradesh, East Coast of India," *J. Geol. Soc. India*, Vol. 43, pp. 669-675.

Nakato, T., 1990, "Tests of Selected Sediment-Transport Formulas," *J. Hydr. Div.*, Vol. 116, pp. 362-379.

National Research Council, 1983, *An Evaluation of Flood-Level Prediction Using Alluvial-River Models*, National Academy Press, Washington, D.C.

Nichols, W. E., N. J. Aimo, M. Oostrom, and M. D. White, 1996, *STOMP: Subsurface Transport Over Multiple Phases. Application Guide*, PNNL-12216, Pacific Northwest National Laboratory, Richland, Washington.

Nitsche, H., 1991, "Solubility Studies of Transuranium Elements for Nuclear Waste Disposal: Principles and Overview," *Radiochim. Acta*, Vol. 52/53, pp. 3-8.

Nordin, C. F., Jr., 1989, "River Meander Model I: Development," in *J. Hydr. Div.*, Vol. 115, pp. 1433-1450.

Oberg, G. C., 1979, *Miscellaneous Facilities Criticality Prevention Specifications*, RHO-MA-149, Rockwell Hanford Operations, Richland, Wahington.

Onishi, Y., 1994a, "Sediment Transport Models and Their Testing," in *Computer Models of Free Surface and Pressurized Flow*, M. H. Chaudrey, and L. W. Mays eds., NATO ASI Series E, Applied Sciences, Vol. 274, pp. 281-312.

Onishi, Y., 1994b, "Contaminant Transport Models in Surface Waters," in *Computer Models of Free Surface and Pressurized Flow*, M. H. Chaudrey and L. W. Mays, eds., NATO ASI Series E, Applied Sciences, Vol. 274, pp. 313-341.

Onishi, Y., H. C. Graber, and D. S. Trent, 1993, "Preliminary Modeling of Wave-Enhanced Sediment and Contaminant Transport in New Bedford Harbor," in *Nearshore and Estuarine Cohesive Sediment Transport*, A. J. Mehta, ed. American Geophysical Union, pp. 541-557.

Onishi, Y., and J. D. Hudson, 1996, *Waste Mixing and Diluent Selection for the Planned Retrieval of Hanford Tank 241-SY-102: A Preliminary Assessment* , PNNL-10927, Pacific Northwest National Laboratory, Richland, Washington.

Onishi, Y., H. C. Reid, D. S. Trent, 1995, *Dilution Physics Modeling: Dissolution/Precipitation Chemistry*, PNL-10815, Pacific Northwest Laboratory, Richland Washington.

Pabalan, R. T. and D. R. Turner, 1992, "Sorption Modeling for HLW Performance Assessment," *Re. On Res. Act. For Calender Year 1991*, W. C. Patrick, ed., CNWRA 91-01A, San Antonio, Texas, Cen. Nuc. Waste Reg. Analysis, pp. 8-1 to 8-66.

Partheniades, E., 1962, *A Study of Erosion and Deposition of Cohesive Soils in Salt Water*, thesis presented to the University of California at Berkeley, California.

Payne T. E., K. Sekine, J. A. Davis, and T. D. Waite, 1992, "Modeling of Radionuclide Sorption Processes in the Weathered Zone of the Koongarra Ore Body," in *Alligator Rivers Analogue Project Annual Report, 1990-1991*, P. Duerden, ed., Aus. Nuc. Sci. Tech. Org, pp 57-85.

Pennders, R. M. J., M. Prins, and M. J. Frissel, 1985, "The Influence of Environmental Factors on the Solubility of Pu, Am, and Np in Soil-Water Systems," in *Speciation of Fisson and Activation Products in the Environment*, Elsevier Science Publishing Co. Inc., New York, New York, pp 38-46.

Penneman, R. A., R. G. Haire, and M. H. Lloyd, 1988, "Polymolybdates as Plutonium (IV) Hosts," in *Actinide Separations*, J. D. Navratil and W. W. Schulz, eds., ACS Symp. Ser. 117, Am. Chem Soc., Washington, D.C.

Perry, J. H., 1963, *Chemical Engineers' Handbook, Fourth Edition*, McGraw-Hill Book Company, New York, New York.

Pikaev, A., 1996, *Gamma Radiolysis of Alkaline Aqueous Solutions of Neptunium and Plutonium*, poster at Chemistry of the Actinides and Technetium in Alkaline Media Meeting, Battelle Auditorium, April 2, 1996, Richland, Washington.

Pius, I. C., M. M. Charyulu, B. Venkataramani, C. K. Sivaramakrishnan, and S. K. Patil, 1995, "Studies on Sorption of Plutonium on Inorganic Ion Exchangers from Sodium Carbonate Medium," in *J. Radioanal. Nucl. Chem. Letters*, Vol. 199, Issue 1, pp. 1-7.

Pool, K. H. and R. M. Bean, 1994, *Waste Tank Organic Safety Project Analysis of Liquid Samples from Hanford Waste Tank 241-C-103*, PNL-9403, Pacific Northwest Laboratory, Richland, Washington.

Postma, A. K., D. B. Bechtold, G. L. Borsheim, J. M. Grigsby, R. L. Guthrie, M. Kummerer, M. G. Plys, and D. A. Turner, 1994, *Safety Analysis of Exothermic Reaction Hazards Associated With the Organic Liquid layer in Tank 241-C-103*, WHC-SD-WM-SARR-001, Westinghouse Hanford Commpany, Richland, Washington.

Pryke, D. C. and J. H. Rees, 1986, "Understanding the Behaviour of the Actinides Under Disposal Conditions: A Comparison Between Calculated and Experimental Solubilities," in *Radiochim. Acta*, Vol. 40, pp. 27-32.

Pryke, D. C., 1985, "A Simple Model for the Calculation of Actinide Solubilities in a Repository for Nuclear Waste," in *Speciation of Fisson and Activation Products in the Environment*, Elsevier Science Publishing Co. Inc., New York, New York, pp. 157-161.

Rai, D. and J. L. Ryan, 1984, "Solubility Constraint: An Important Consideration in Safety Assessment of Nuclear Waste Disposal," in *Mat. Res. Soc. Symp. Proc.*, Vol. 26, pp. 805-815.

Rai, D., R. J. Serne, and D. A. Moore, 1980, "Solubility of Plutonium Compunds and Their Behavior in Soils," in *Soil Sci. Soc. J.*, Vol. 44, pp. 490-495.

Rai D., A. R. Felmy, D. A. Moore, and M. J. Mason, 1995, "The Solubility of Th(IV) and U(IV) Hydrous Oxides in Concentrated $NaHCO_3$ and Na_2CO_3 Solutions," in *Mat. Res. Soc. Symp. Proc.*, Vol. 353, pp. 1143-1150.

Rai, D. and J. L. Ryan, 1984, "Solubility Constraint: An Important Consideration in Safety Assessment of Nuclear Waste Disposal," in *Mat. Res. Soc. Symp. Proc.*, Vol. 26, pp. 805-815.

Rai, D., R. J. Serne, and D. A. Moore, 1980, "Solubility of Plutonium Compounds and Their Behavior in Soils," in *Soil Sci. Soc. J.*, Vol. 44, pp. 490-495.

Raudkivi, A. J., 1967, *Loose Boundary Hydraulics*, Pergamon Press, New York, New York.

Rees, J. H., 1985, "The Theoretical Derivation of Solubilities of Long-Lived Radionuclides in Disposal," *J. Nucl. Mater.*, Vol. 130, pp. 336-345.

Reynolds, D. A. and D. L. Herting, 1984, *Solubilities of Sodium Nitrate, Sodium Nitrite, and Sodium Aluminate in Simulated Nuclear Waste*, RHO-RE-ST-14P, Rockwell Hanford Operations, Richland, Washington.

Richards, K., 1982, *Rivers—Form and Process in Alluvial Channels*, Methuen and Co., Ltd., London, England and New York, New York.

Richardson, J. F. and W. N. Zaki, 1954, "Sedimentation and Fluidisation: Part I," in *Trans. Instn. Chem. Engrs*, Vol. 32, p.35-53.

Righetto, L., G. Bidoglio, B. Marcandalli, and I. R. Bellabono, 1988, "Surface Interactions of Actinides with Alumina Colloids," *Radio Chimica Acta*, Vol. 44/45, pp. 73-75.

Roblyer, S. P., 1994, *Plutonium and Tritium Produced in the Hanford Site Production Reactors*, WHC-SD-CP-RPT-014, Westinghouse Hanford Company, Richland, Washington.

Roetman, V. E., 1994, *Estimation of Plutonium in Hanford Site Waste Tanks Based on Historical Records*, WHC-EP-0793, Rev. 0, Westinghouse Hanford Company, Richland, Washington.

Rogers, C. A., 1993, *An Analytical Model For Evaluating Subcritical Limits for Waste in Hanford Site Storage Tanks*, WHC-SD-SQA-CSA-20356, Rev. 0, Westinghouse Hanford Company, Richland, Washington.

Rogers, C. A., K. N. Schwinkendorf, and H. Harris, 1996, *Criticality Parameters for Tank Waste Evaluation*, WHC-SD-SQA-CSA-507, Rev. 0, Westinghouse Hanford Company, Richland, Washington.

Rouse, H., 1937a, "Modern Conceptions of the Mechanics of Fluid Turbulence," in *Trans.* ASCE, Vol. 102, pp. 463-543.

Rouse, H., 1937b, "Nomogram for the Settling Velocity of Spheres," in *Division of Geology and Geography Exhibit D of the Report of the Commission on Sedimentation, 1936-37*, pp. 57-64, National Research Council, Washington, D.C.

Rouse, H, 1950, *Engineering Hydraulics*, John Wiley and Sons, New York, New York.

Sanchez, A. L., J. W. Murray, and T. H. Sibley, 1985, "The Adsorption of Pu(IV) and (V) of Goethite," in *Geochim. Cosmochim. Acta.*, Vol. 49, pp. 2297-2307.

Scheele, R. D. and M. E. Petersen, 1989, *Results of the Characterization of Samples of Waste from Double-Shell Tank 102-SY*, Pacific Northwest Laboratory, Richland, Washington.

Schindler, P., H. Althaus, F. Hofer, and W. Minder, 1965, "Loslichkeitsproduckte von Metalloxiden und - hydroxiden: Loslichkeitsprodukte von Zinkoxid, Kupferxide und Kupferoxid in Abhangigkeit von Teilchengrosse und molarer Oberflache. Ein Beitrag zur Thermodynamik von Grenzflachen fest-flussig," *Helv. Chim. Acta*, Vol. 48, pp. 1204-1215.

Schindler, P., 1967, "Heterogeneous Equilibria Involving Oxides, Hydroxides, Carbonates, and Hydroxide Carbonates," in *Equilibrium Concepts in Natural Water Systems*, Adv. Chem. Ser. No. 67, pp. 196-221, American Chemical Society, Washington, D.C.

Schindler, P., 1981, "Surface Complexes at Oxide-Water Interfaces," in *Adsorption of Inorganics at Solid-Liquid Interfaces*, M. A. Anderson and A. J. Rubin, eds., Ann Arbor Science, Ann Arbor, Michigan, pp. 1-50.

Schofield, J. S., 1991, Letter *Estimation of Neutralized Current Acid Waste and Neutralized Cladding Removal Waste Constituents*, to S. L. Barker at Westinghouse Hanford Company , Richland, Washington sent July 18, 1991.

Schwertmann, U. and R. M. Cornell, 1991, *Iron Oxides in the Laboratory*, Verlagsgesellschaft mbH, VCH Publishing, New York, New York.

Sederburg, J. P., 1994, *Chemical Compatibility of Tank Wastes in Tanks 241-C-106, 241-AY-101, and 241-AY-102*, WHC-SD-WM-ES-290, Westinghouse Hanford Company, Richland, Washington.

Serne, R. J., 1989," Radiation Effects on Chemistry," in *Engineering Geology*. 26:319-329.

Shannon, R. D., 1976, "Revised Effective Ionic Radii and Systematic Studies of Interatomic Distances in Halides and Chalcogenides," in *Acta Cryst.*, Vol. A32, pp. 751-767.

Shen, H. W. and C. S. Hung, 1972, "An Engineering Approach to Total Bed Material Load by Regression Analysis," in *Proc. of the Sedimentation Syst.*, pp. 14.1-14.17.

Shergold, F. A., 1946, "The Effects of Sieve Loading on the Results of Sieve Analysis of Natural Sands," in *J. Soc. Chem. Ind.*, Vol. 65, pp. 245-249.

Shields, A., 1936, "Anwendung der Aenlichkeitsmechanik und der Turbulenzforschung auf die Geschiebebewegung," in *Mitteilungen der Preussischen Versuchsanstalt fur Wasserbau und Schiffbau*, Berlin, Germany, English translation ("Application of Similitude Mechanics and the Research on Turbulence to Bed-Load Movement") by W. P. Ott and J. C. van Uchelen, California Institute of Technology, Pasadena, California.

Shulits, S., 1935, *The Schoklitsch Bed-Load Formula*, Engineering, London, England, pp. 644-646 and 687.

Simons, D. B. and F. Senturk, 1977, *Sediment Transport Technology*, Water Resource Publications, Denver, Colorado.

Simons, D. B. and E. V. Richardson, 1966, *Resistance to Flow in Alluvial Channels*, Professional Paper 422J, U.S. Geological Survey, Washington, D.C.

Smerdon, E. T. and R. P. Beasley, 1961, "Critical Tractive Forces in Cohesive Soil," *Ag. Eng.*, St. Joseph, Michigan, pp. 26-29.

Smith, D. K., 1989, "Computer Analysis of Diffraction Data," in *Modern Powder Diffraction*, Reviews in Mineralogy, Vol 20, pp. 183-216, Mineralogical Society of America, Washington, D.C.

Smith, G. F., 1970, *Purex Plant Chemical Flowsheet for the 1970 Thorium Campaign*, ARH-1748, Atlantic Richfield Hanford Company, Richland, Washington.

Sposito, G., 1986, "Distinguishing Adsorption from Surface Precipitation," in *Geochemical Processes at Mineral Surfaces*, J. A. Davis and K. F. Hays, eds, ACS Symp Ser. 323, Am. Chem. Soc., Washington, D.C.

Stumm, W. and J. J. Morgan, 1981, *Aquatic Chemistry*, 2nd. Edition, John Wiley and Sons Publishing, New York, New York.

Sullivan, J. C., 1983, "Reaction of Plutonium Ions with Products of Water Radiolysis," in *Plutonium Chemistry*, W. T. Carnall and G. R. Choppin, eds. ACS Sym. Ser. 216, pp 241-249.

Sundborg, A., 1956, "The River Klaralven, a Study of Fluvial Processes," in *Geografiska Annaler*, pp. 127-316.

Tait, C. D., S. A. Ekberg, P. D. Palmer, and D. E. Morris, 1995, *Plutonium Carbonate Speciation Changes as Measured in Dilute Solutions with Photoacoustic Spectroscopy*, LA-12886-MS, Los Alamos National Laboratory, Los Alamos, New Mexico.

Tank Waste Science Panel, 1991, *Chemical and Physical Processes in Tank 241-SY-101: A Preliminary Report*, PNL-7595, Pacific Northwest Laboratory, Richland, Washington.

Teeter, A. M., 1988, *New Bedford Harbor Project--Acushnet River Estuary Engineering Feasibility Study of Dredging and Dredged Material Disposal Alternatives--Report 2, Sediment and Contaminant Hydraulic Transport Investigations*, U.S. Army Corps of Engineers Waterways Experiment Station, Viscksburg, Mississippi.

Theis, C. V., 1935, "The Relation Between the Lowering of the Piezometric Surface and the Rate and Duration of Discharge of a Well Using Groundwater Storage," in *Trans. Amer. Geophys. Union*, Volume 2, pp. 519-524.

Thiyagarajan, P., H. Diamond, L. Soderholm, E. P. Horwitz, L. M. Toth, and L. K. Felker, 1990, "Plutonium(IV) Polymers in Aqueous and Organic Media," in *Inorg. Chem.*, Volume 29, pp. 1902-1907.

Ticknor, K. V., T. T. Vandergraaf, and D. G. Juhnke, 1986, *The Effect of Laboratory Time-Scale Hydrothermal Alteration on Igneous Rok Coupon Radionuclide Sorption/Desorption*, TR-376, Atomic Energy of Canada Limited Research Company, Chalk River, Ontario, Canada.

Ticknor, K. V., 1993, "Actinide Sorption by Fracture-Filling Minerals," *Radiochim. Acta*, Vol. 60, pp. 33-42.

Tingey, J. M. and Simpson. B. C., 1994, *Characterization Information for Double Shell Tank 241-AW-105*, WHC-SD-WM-TI-649 Rev. 0, Westinghouse Hanford Company, Richland, Washington.

Tingey, J. M. and B. C. Simpson, 1995, *Waste Characterization; Double-Shell Tank; AW-105*, WHC-SD-WM-ER-455, Westinghouse Hanford Company, Richland, Washington.

Toffaleti, F. B., 1969, "Definitive Computations of Sand Discharge in Rivers," in *J. of Hydr. Div.*, Vol. 95, pp. 225-248.

Tole, M. P., 1984, "Some Implications of the Role of Kinetics in Enhancing Element Transport," *in Hydrochemical Balances in Freshwater Systems*. E. Ericksson, Ed. pp. 79-86. International Association of Hydrological Sciences, Publication No. 150.

Tole, M. P., A. C. Lasaga, C. Pantano, W. B. White, 1986, "The Kinetics of Dissolution of Nepheline ($NaAlSiO_4$)," *Geochim Cosmochim Acta*, Vol. 50, pp. 379-392.

Tomlinson, R. E., 1971, *Technical Criteria for the Prevention of Criticality*, ARH-468, Atlantic Richfield Hanford Company, Richland, Washington.

Toste, A. P., R. B. Lucke, T. J. Lechner-Fish, D. J. Hendren, and R. B. Myers, 1987, "Organic Analyses of Mixed Nuclear Wastes," *Waste Management '87, Volume 3*, pp. 323-329, R. G. Post, ed. University of Arizona Press, Tucson, Arizona.

Toste, A. P., L. J. Kirby, and T. R. Pahl, 1984, "Role of Organics in the Subsurface Migration of Radionuclides in Groundwater," *ACS Symp. Ser. 246*, pp. 95-112, American Chemical Society, Washington, D.C.

Toth, L. M., H. A. Friedman, and M. M. Osborne, 1981, Plymerization of Pu(IV) in Aquous Nitric Acid Solution, *J. Inorg. Nucl. Chem.*, Vol. 43, pp. 2929-2934.

Toth, L. M., H. A. Friedman, G. M. Begun, and S. E. Doris, 1984. "Raman Study of Uranyl Ion Attachment to Thorium(IV) Hydrous Polymer," *J. Phys. Chem.* 88: 5574-5577.

Trent, D. S., and L. L. Eyler, 1993, *TEMPEST: A Computer Program for Three-Dimensional Time Dependent Computational Fluid Dynamics*, PNL-8857 Vol. 1, Version T, Mod 2, Pacific Northwest Laboratory, Richland, Washington.

Trent, D. S. and L. L. Eyler, 1989, *TEMPEST: A Three Dimensional Time-Dependent Computer Program for Hydrothermal Analysis, Volume 1: Numerical Methods and Input Instructions*, PNL-4348, Vol. 1, Rev. 2, Pacific Northwest Laboratory, Richland, Washington.

Trent, D. S. and T. E. Michener, 1993, *Numerical Simulation of Jet Mixing Concepts in Tank 241-SY-101*, PNL-8559, Pacific Northwest Laboratory, Richland, Washington.

Tripathi, V. S., 1984, *Uranium(VI) Transport Modeling: Geochemical Data and Submodels*, Ph.D. dissertation, Stanford University, Stanford, California.

Tusler, S.A., 1995, *Double-Shell Tanks Plutonium Inventory Assessment*, WHC-SD-WM-TI-640, Rev. 0, Westinhouse Hanford Company, Richland Washington.

Van der Cook, R. E. and R. L. Walser, 1970, *Purex Alternate Reductant Study*, ARH-1649, Atlantic Richfield Hanford Company, Richland Washington.

Van Rijn, L. C., 1984a, "Sediment Transport, Part I: Bed Load Transport," *J. Hydr. Div.*, American Society of Civil Engineers, Vol. 110, pp. 1431-1456.

Van Rijn, L. C., 1984b, "Sediment Transport, Part II: Suspended Load Transport," *J. Hydr. Div.*, American Society of Civil Engineers, Vol. 110, pp. 1613-1641.

Van Vleet, R. J., 1993a, *Radionuclide and Chemical Inventories for the Double Shell Tanks*. WHC-SD-WM-TI-543, Rev. 1, Westinghouse Hanford Company, Richland, Washington.

Van Vleet, R. J., 1993b, *Radionuclide and Chemical Inventories for the Single Shell Tanks*, WHC-SD-WM-TI-565, Rev. 1, Westinghouse Hanford Company, Richland, Washington.

Vanoni, V. A., ed., 1975, *Sedimentation Engineering*, ASCE Manuals and Reports on Engineering Practice, American Society of Civil Engineers, New York, New York.

Wadell, H., 1932, "Volume, Shape, and Roundness of Rock Particles," *J. Geol.*, Vol. 40, pp. 443-451.

Wahl, K. L., J. A. Campbell, S. A. Clauss, K. E. Grant, B. D. Lerner, G. M. Mong, A. K. Sharma, C. E. Petersen, A. J. Saenz, S. A. Bryan, I. E. Burgeson, R. D. Scheele, and R. L. Sell, 1995, *Waste Tank Organic Safety Program Advanced Organic Analysis and Analytical Methods Development: FY 1995 Progress Report*, PNL-10777, Pacific Northwest Laboratory, Richland, Washington.

Walsh, D. E. and P. D. Rao, 1986, *A Study of Factors Suspected of Influencing the Settling Velocity of Fine Gold Particles*. MIRL Report No. 76, Mineral Industry Research Laboratory, University of Alaska, Fairbanks, Alaska.

Waltar, A. E., H. Babad, G. S. Barney, R. S. Felt, J. Greenborg, L. H. Rodgers, R. J. Serne, G. A. Whyatt, D. R. Bratzel, and E. J. Lipke, 1996, *Criticality Safety Assessment of Tank 241-C-106 Remediation*, WHC-SD-W320-CSA-001, Rev. 0, Westinghouse Hanford Company, Richland, Washington.

Walton, A. G., 1967, *The Formation and Properties of Precipitates*, Intersci. Pub., New York, New York.

Weakly, E. A., 1979, *Fuels Engineering Technical Handbook*, UNI-M-61, United Nuclear, Inc. Richland, Washington.

Westall, J. and H. Hohl, 1980, "A Comparison of Electrostatic Models for Oxide/Solution Interface," *Adv. Coll. Interfac. Sci.*, Vol. 12, pp. 265-294.

WHC, 1995a, *90-Day Safety Screen Results for Tank 241-C-103, Push Mode Core Samples 63 and 66*, WHC-SD-WM-DP-099, Rev. 0B, Westinghouse Hanford Company, Richland, Washington.

WHC, 1993a, *Laboratory Reports for WHC-SD-WM-ES-244*, WHC-MR-0419, Westinghouse Hanford Company, Richland Washington, contains letter from Weiss, R. L. to T. R. Pauly, dated April 14, 1987, "Additional Analyses on Core Samples from Tanks 241-C-105 and 241-C-106," Internal Letter No. 65453-87-050, Rockwell International, Richland, Washington.

WHC, 1993b, *Laboratory Reports for WHC-SD-WM-ES-244*, WHC-MR-0419, Westinghouse Hanford Company, Richland, Washington, contains letter from J. E. Horton of 222-S Laboratory to W. R. Christensen, dated July 22, 1977, and *Subreport: 102AY Data: Results of the Characterization of 102-AY Solids, Washed Solids and Supernatant* R. D. Scheele, M. E. Petersen, J. M. Tingey, 1990, Pacific Northwest Laboratory, Richland, Washington.

WHC, 1995a, *Tank Waste Source Term Inventory*, 1995, WHC-SD-WM-ER-400, Westinghouse Hanford Company, Richland, Washington.

WHC, 1995b, *90-Day Safety Screen Results for Tank 241-C-103, Push Mode Core Samples 63 and 66*, WHC-SD-WM-DP-099, Rev. 0B, Westinghouse Hanford Company, Richland, Washington.

White, C. M., 1940, "The Equilibrium Grains on the Bed of a Stream," in *Proc. Royal Soc.*, London, Series A, Vol. 174, pp. 322-338.

White, M. D. and M. Oostrom, 1996a, *STOMP: Subsurface Transport Over Multiple Phases. Theory Guide*, PNNL-11217, Pacific Northwest National Laboratory, Richland, Washington.

White, M. D. and M. Oostrom, 1996b, *STOMP: Subsurface Transport Over Multiple Phases. User's Guide*, PNNL 12218, Pacific Northwest National Laboratory, Richland, Washington.

Willingham, C. E., 1994, *Thermophysical Properties of Hanford High-Level Tank Wastes - A Preliminary Survey of Recent Data*, PNL-9419, Pacific Northwest Laboratory, Richland Washington.

Winters, W. I., 1995, *Tank Characterization Report for Double-Shell Tank 241-SY-102*, WHC-SD-WM-ER-366, Rev. 0., Westinghouse Hanford Company, Richland, Washington.

Whyatt, G. A., R. J. Serne, S. V. Mattigod, Y. Onishi, M. R. Powell, J. H. Westsik, Jr., L. M. Liljegren, G. R. Golcar, K. P. Recknagle, P. M. Doctor, V. G. Zhirnov, J. Dixon, D. W. Jeppson, and G. S. Barney, 1996, *The Potential for Criticality in Hanford Tanks Resulting from Retrieval of Tank Waste*, PNNL-11304, Pacific Northwest National Laboratory, Richland, Washington.

WWW, 1996, *Radioactivity in Nature and Mineralogy and Ore Grade*, two web sites found at addresses: [http://www.sph.umich.edu//~bbusby/natural.htm] and [http://www.uilondon.org/uore.html] respectively.

Yamaguchi, T., Y. Sakamoto, and T. Ohnuki, 1994, "Effect of the Complexation on Solubility of Pu(IV) in Aqueous Carbonate System," in *Radiochim. Acta.*, Vol. 66/67, pp. 9-14.

Yang, C. T. and A. Molinas, 1982, "Sediment Transport and Unit Stream Power Function," in *J. Hydr. Div.*, American Society of Civil Engineers, Vol. 108, pp. 774-793.

Yang, C. T., 1973, "Incipient Motion and Sediment Transport," in *J. Hydr. Div.*, American Society of Civil Engineers, Vol. 99, pp. 1679-1704.

Yang, C. T., 1979, "Unit Stream Power Equations for Total Load," in *J. Hydr. Div.*, Vol. 40, pp. 123-138.

Zakharova E. V. and V. M. Ermolaev, 1995, "Transformation of Solid Phases during Storage of Radioactive Sludge in Tanks," *Radioactive Waste Management and Environmental Remediation Session*, American Society of Mechanical Engineers Proceedings 1995 Annual Meeting, pp 129-132.

Zandi, I. and G. Govatos, 1967, "Heterogeneous Flow of Solids in Pipelines," *J. of Hydr. Div.*, American Society of Civil Engineers, Vol. 93, pp. 145-159.

Znamenskaya, N. S., 1967, "The Analysis of Estimating of Energy Losses by Instantaneous Velocity Distribution of Streams with Movable Bed," *Proceedings, Twelfth Congress of the International Association for Hydraulic Research*, Vol. 1, pp. 27-30.

This page intentionally left blank.

APPENDIX A

FLOCCULATION OF WASTE PARTICLES

This page intentionally left blank.

APPENDIX A

FLOCCULATION OF WASTE PARTICLES

Sludge in Tank C-106 will be retrieved by sluicing it with AY-102 supernatant and returning the resulting slurry to AY-102 where it will settle. The sludge has low concentrations of plutonium and excess concentrations of neutron absorbers, primarily iron and aluminum, which prevent criticality in the sludge. Plutonium particles in the sludge may have a density and settling velocity that could differentiate it from other particles during transport and settling. These differences could result in concentration of plutonium and segregation of plutonium from neutron absorbers.

The analysis described here was performed in an effort to determine whether flocculation of solid particles will prevent discrete waste solids from segregating according to their individual settling velocities. If a plutonium particle flocculates with other sludge particles, the unique density and settling velocity of the plutonium particle will be masked by the properties of the flocculant. Therefore, the driving force, the different settling velocities of individual particles, that promotes segregation would be eliminated. If the rapid flocculation of the particles can be shown to effectively bond the plutonium-containing solids to other waste solids, the criticality concerns associated with particle segregation can be dismissed.

Calculations were done to predict whether the individual waste particles will agglomerate under the conditions expected during C-106 waste retrieval. These calculations require that certain properties of the waste solids and supernate be quantified. When the needed data were not available, conservative assumptions were made. The calculations predict that particles in the size range of about 1 to 10 μm will flocculate rapidly, if the salt concentration in the retrieval fluid is maintained at about 0.10 molar or higher and the pH exceeds 10.0. Particles smaller than about 1 μm are expected to be weakly flocculated.

Comparing these predictions with observed waste particle settling data for Hanford tank sludge indicates that the assumptions used for the flocculation calculations are conservative. That is, studies on Hanford sludge suggest that flocculation is the predominant control on individual sludge particles across a large range of sizes including particles in the less than 1 μm to several tens of μm range. The settling rate data imply that the small particles are effectively captured within the flocs formed by the larger particles. Thus, segregation of individual waste particles is not expected to occur if the salt concentration is at least 0.1 molar in the supernate and the mixing intensity is low enough to permit flocculation.

A.1 BACKGROUND

Derjaguin, Landau, Verwey, and Overbeek developed the DLVO theory describing colloidal flocculation and coagulation. This appendix prepresents their standard approach to predicting the tendency of colloidal systems to flocculate and coagulate. The DLVO theory is explained in textbooks such as Hiemenz (1986). The theory's concept is simple. The magnitude of the

repulsive forces between particles is compared to the magnitude of the interparticle attractive forces. If the attractive forces exceed the repulsive forces, the particles are expected to flocculate or coagulate.

Particles can group together in two distinct ways depending on the nature of the interparticle attractive and repulsive forces. Particles are said to flocculate when they are loosely bound together at a small, but nonzero interparticle distance. The interparticle distance corresponds to the distance where the sum of the attractive forces minus the sum of the repulsive forces is at a maximum. The particles are prevented from approaching closer than this distance by the repulsive forces. Particles are said to be coagulated when the attractive forces are sufficient to overcome the repulsive forces at all possible interparticle separation distances.[1] The surfaces of coagulated particles are in contact with each other.

Particles dispersed in a liquid often develop a surface charge. The surface charge can arise through the adsorption of ions onto the particle surface or through the addition or removal of protons from molecules at the particle surface.[2] Metal hydroxide and oxide particles are often found to have a positive surface charge at low pH, zero charge at a pH between about 6 and 8, and a negative charge at high pH (Hunter 1981). At the pH range of interest for tank waste applications (pH of 10 or higher), the hydrous metal oxide sludge solids will be negatively charged. High liquid pH results in particles that are more strongly negatively charged. Particle agglomeration tends to be inhibited by the negative charges.

As two negatively charged particles approach each other, their respective electric fields interact and a repulsive force develops. The magnitude of this repulsive force can be estimated using Coulomb's law and classical electrostatics. However, the nature of the interaction between particles is more complicated than that assumed by Coulomb's law, which assumes point charges separated by a distance. Each charged solid particle submerged in a liquid is surrounded by a cloud of oppositely charged ions. Negatively charged particles are surrounded by a diffuse cloud of cations (positively charged). As two particles approach each other, these ion clouds interact and generate a force of repulsion. The work done by moving two spherical particles of radii a_1 and a_2 together from an initial large separation distance to a separation of h is given by the following equation (Shaw 1980):

---

[1]If the net interparticle force is repulsive at some distances, the particles may still coagulate provided that the magnitude of the net repulsion is on the order of the forces generated by thermal motions.

[2]Other mechanisms can result in the development of particle surface charge, but these are not described here.

$$\phi_R(h) = \frac{64\pi\varepsilon a_1 a_2 k^2 T^2 \Upsilon_1 \Upsilon_2}{(a_1 + a_2) e^2 z^2} \exp(-\kappa h) \tag{A.1}$$

where ε = permittivity of the interparticle medium, C^2/Nm^2
κ = Debye parameter as given by Equation (A.2), m^{-1}
T = absolute temperature, K

Y_i = charge-dependent parameter for particle i as given by Equation (A.3)
e = electron charge = 1.6×10^{-19} C
z = valence of the salt ions in solution, 1.0 is used here
k = Boltzmann's constant = 1.38×10^{-23} J/K.

The measurement unit for ϕ_R as given in Equation A.1 is joules. The value of the Debye parameter, which is also called the inverse double-layer thickness, is given by

$$\kappa = \left(\frac{2e^2 N_A c z^2}{\varepsilon k T}\right)^{\frac{1}{2}} \tag{A.2}$$

where N_A = Avogadro's number = 6.02×10^{23} molecules/mole
c = concentration of z:z electrolyte, moles/m^3
k = Boltzmann's constant = 1.38×10^{-23} J/K

The value of the charge-dependent parameter used in Equation A.1 is given by:

$$\Upsilon_i = \tanh\left(\frac{ze\psi_i}{4kT}\right) \tag{A.3}$$

In Equation A.3, the term ψ_i is the surface charge (in volts) of particle number i.

Equations A.1, A.2, and A.3 were used to estimate the repulsive force between particles of various sizes. A temperature of about 300 K (roughly 80 °F) was used for all calculations. The DLVO predictions were found to be relatively insensitive to variations in temperature over the range of 290 K to 380 K (63 to 225 °F), which covers the range of temperatures expected during waste retrieval.

A combination of dipole-dipole and induced dipole-dipole interactions at the molecular level generate attractive forces between particles (Hiemenz 1986). The magnitude of the attractive force is a function of the particle sizes, shapes, and compositions and the properties of the fluid medium between the particles.

For spheres, the attractive potential (in joules) is given by Equation A.4.

$$\Phi_A(h) = -\frac{A}{6}\left[\frac{2a_1a_2}{h^2+2a_1h+2a_2h} + \frac{2a_1a_2}{h^2+2a_1h+2a_2h+4a_1a_2} + \ln\left(\frac{h^2+2a_1h+2a_2h}{h^2+2a_1h+2a_2h+4a_1a_2}\right)\right] \tag{A.4}$$

In this equation, term A, the Hamaker constant, accounts for the portion of the attractive force that depends on the composition of the particles. The Hamaker constant is a complicated function of the dielectric and polarizability properties of the particles and the surrounding fluid medium.

The net interaction potential, Φ_{net}, is given by summing the repulsive potential, which has a positive magnitude, with the attractive potential, which has a negative magnitude. The resulting formula allows the nature of the interaction to be determined. If the net potential is negative, the particles attract. If the net potential is positive, the particles repel. The net interaction potential is given by:

$$\Phi_{net}(h) = \Phi_R(h) + \Phi_A(h) \tag{A.5}$$

The net interaction potential function is usually plotted in units of kT versus particle separation distance (h) as measured between the nearest particle surfaces (as opposed to the center-to-center distance). Units of kT, which is Boltzmann's constant times absolute temperature, are used to directly compare the magnitude of the net force with the forces generated by molecular vibrations.[3] A typical plot of three different net interaction potentials is shown in Figure A-1. Curve (a) shows a positive net interaction at essentially all interparticle distances. No flocculation or coagulation is predicted for this case. Curve (b) shows a positive net interaction potential at separations of about 5 to 20 nm, but the net force is attractive (negative potential) at distances greater than about 20 nm. Flocculation, but not coagulation, is predicted for this case. Curve (c) shows a net negative interaction for all separations. Rapid, irreversible coagulation is predicted.

The curves in Figure A-1 were generated by selecting different surface charge values for particles 0.5 μm in diameter surrounded by a 0.01 molar monovalent salt solution. Section A.2 describes why we chose the values for the Hamaker constant and particle surface charge used to calculate the net interaction potentials expected during C-106 retrieval.

---

[3]Thermally induced molecular vibration forces are the source of Brownian motion in particles suspensions.

A.2 ASSUMPTIONS USED FOR DLVO CALCULATIONS

To perform the DLVO calculations for the tank waste conditions during retrieval we had to make two key assumptions. First, the magnitude of the Hamaker constant had to be determined. Second, the magnitude of the particle surface charge had to be estimated. The temperature and salt concentrations expected during retrieval were also estimated, but a sound basis exists for selecting the specific values for both of these parameters. Insufficient data are available to accurately estimate the waste surface charge and effective Hamaker constant, so conservative assumptions were made.

The Hamaker constant used for the DLVO calculations was 0.8×10^{-20} J. This value was selected based on an examination of the range of reported Hamaker constants for inorganic compounds. No Hamaker constant data were found for plutonium compounds. Russel et al. (1989, p. 148) reports effective Hamaker constants for a variety of substances (e.g., silica, calcite, and calcium fluoride) in water. The reported Hamaker constants range from 0.83×10^{-20} to 5.32×10^{-20} J. A lower Hamaker constant implies a smaller attractive force, so, to be conservative, we selected a Hamaker constant at the low end of typical values. The actual effective Hamaker constants for the waste solids are likely to be larger than 0.8×10^{-20} J, but without relevant data, the use of the lower Hamaker constant is justified.

The particle surface charges were all assumed to be -200 mV. [Many metal oxides and hydroxides are negatively charged at high pH (Hunter 1981)]. The predominant neutron absorber particles (iron and aluminum oxides and hydroxides) are expected to have a negative surface charge. Any plutonium oxide or hydroxide particles also are expected to be negatively charged at high pH, but surface charge data for plutonium compounds is not available. Grebenshchikova and Davydov (1965) report that the charge on Pu(IV) hydroxide particles is negative at pH values higher than about 8.5.

A surface charge magnitude of -200 mV was selected based on the known typical range of particle zeta-potentials. Zeta-potential is s related to, but not equal to, the particle surface charge. The zeta-potential is smaller than the particle surface charge by an amount that depends on the salt concentration in the liquid (Hiemenz 1986, p. 768). Zeta-potential is defined as the electrostatic potential at the surface of shear. The shear surface is that distance from the particle surface at which the ions are not bound so tightly as to prevent viscous flow. Hunter (1981, p. 49) states that the absolute magnitude of zeta-potential is usually less than about 150 mV.

Fortunately, the DLVO calculations are relatively insensitive to the magnitude of the surface charge when the surface charge absolute magnitude is higher than 100 mV. Because the typical range of zeta-potentials at high pH implies that the surface charge on the waste particles could credibly be more negative than -150 mV, a value of -200 mV was chosen for the DLVO calculations. After some preliminary calculations, we found the difference between the DLVO predictions for an assumed -100 mV surface charge and a -200 mV surface charge is minimal, so this assumption likely is not overly conservative.

Zeta-potential measurements have been made on waste simulant solids.[4] At high pH (11.8), the zeta-potential was reported to be about -50 mV. The salt concentration in the liquid was not measured, so the magnitude of the particle surface potential cannot be reliably estimated. It seems reasonable, though, that the surface potential was more negative than -60 mV. The zeta-potential measurements on waste simulants, which contained the same chemical species as expected in Hanford tank supernates, provide added assurance that the assumed -200 mV surface potential for the DLVO calculations is reasonable.

The biggest uncertainty in the input parameters for the DLVO calculations is clearly the estimated Hamaker constant. The assumed value of 0.8×10^{-20} J could credibly be about an order of magnitude too low. The effect of a larger Hamaker constant on the calculations is to make flocculation or coagulation more likely. Because a conservatively low Hamaker constant has been assumed here, instances where flocculation or coagulation occurs are likely, even though the DLVO calculations might predict no flocculation or coagulation.

A.3 ANALYSIS OF FLOCCULATION MODELING RESULTS

The DLVO suspension stability calculations performed imply that the concentration of salt expected in the liquid during retrieval is high enough to ensure rapid particle flocculation. This conclusion applies provided the existing AY-102 supernate is used as the retrieval fluid for sluicing the waste from C-106. Using a more dilute supernate or dilute sodium-hydroxide/nitrite (the term inhibited, as in corrosion-inhibiting, is used at the Hanford Site) water also is predicted to result in the formation of flocs, but the flocs will be weaker and it is not clear whether the weak flocculation will be sufficient to prevent particle segregation.

Rapid flocculation of particles is expected to prevent the separation of plutonium-laden particles from the rest of the sludge/waste solids, which act as neutron absorbers. It has been suggested that differences in density and settling velocities between the plutonium-laden solids and the other waste solids (primarily metal hydroxides and oxides) may allow plutonium to become concentrated near either the bottom or the top of a settled solids layer, depending on whether the settling velocity of the plutonium particles is greater than or less than that of the non-plutonium particles. This is unlikely to occur because all the particles in the slurry are expected to participate in rapid flocculation, which will inhibit segregation of individual waste solids. The resulting flocs, which may contain both plutonium and non-plutonium solids, will all have similar settling properties. This will prevent the segregation of plutonium from the non-plutonium solids.

---

[4]Virden, Jud W., J. Liu, B. C. Bunker, V. S. Stenkamp, and L. Song. *Solids Formation and Sludge Dissolution: Final Report for FY1994*. TWRSPP-94-092. Letter Report prepared for Westinghouse Hanford Company by the Pacific Northwest Laboratory, Richland, Washington.

This conclusion assumes that the mixing intensity applied to the slurry during settling is relatively low. More intense mixing may inhibit floc formation and permit some degree of particle segregation. This conclusion is justified in the following sections.

A.3.1 Salt Effects on the Electrostatic Double-Layer

The concentration of salt in the tank supernatant liquid determines whether flocculation will occur. At high pH, the waste solids are expected to be negatively charged. In the absence of significant dissolved salts, the particles repel each other electrostatically and no flocculation takes place. When salt is added, the dissolved ions reduce the influence of the electrostatically repulsive particles. The interparticle attractive forces (Van der Waals and London Dispersion forces) can overcome the electrostatic repulsion if enough salt is added. When this happens, the particles can flocculate or coagulate.

Figure A-2 shows the net interaction potential plotted as a function of interparticle separation for four different particle sizes. The interaction potential is the sum of the interparticle attractive and electrostatic repulsive forces. Attractive forces are assigned a negative sign, so a negative net interaction potential indicates a net attractive force between the particles. The units used to express the interaction potential are in terms of kT, which is the product of Boltzmann's constant (1.38E-23 J/K) and absolute temperature (300 K). Units of kT are used because this allows the magnitude of the interparticle forces to be compared to the magnitude of thermal forces from molecular vibrations. If the magnitude of a net attractive or repulsive force is on the order of a few kT or less, it is unlikely to influence the interparticle behavior significantly because the force will be masked by thermal forces.

The net interaction potentials shown in Figure A-2 indicate that flocculation is predicted for particles larger than about 2 μm in diameter when the salt concentration is 0.021 molar (equal to that of inhibited water). The curve for 2-μm particles shows that the minimum interaction potential is about -7 kT. In practice, colloidal systems with net interaction potentials between about -15 kT and -3 kT have been found to form very weak flocs, which are easily disturbed by the combination of thermal and applied shear forces (Hiemenz 1986, p. 727). When the interaction potential is lower than about -15 kT, however, the attractive forces are stronger and the flocs are more resistant to disturbance.

The attractive forces are predicted to be dominant for 10-μm particles, as shown in Figure A-2 (minimum net interaction potential of -35 kT). However, gravity and inertia become important when compared to colloidal forces for particles larger than about 5 μm, so DLVO calculations for particles larger than about 5 μm should be applied cautiously. The buoyed weight of a 10-μm-diameter sludge particle (assumed spherical) is on the order of 10^{-11} N. For comparison to the colloidal forces, the maximum net attractive force indicated in Figure A-2 is used. The maximum attraction is given by the maximum positive slope of the net interaction potential curve. In Figure A-2, the maximum attractive force between 10-μm particles is estimated to be 0.5×10^{-11} N. In Figure A-3, the maximum force for the

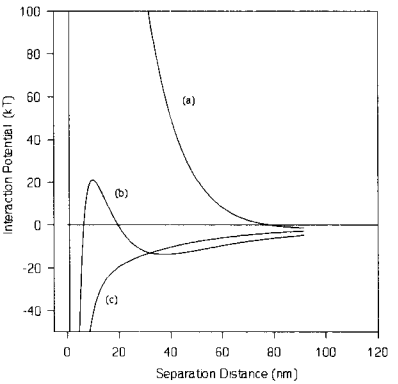

Figure A-1. Example DLVO Interaction Plot.

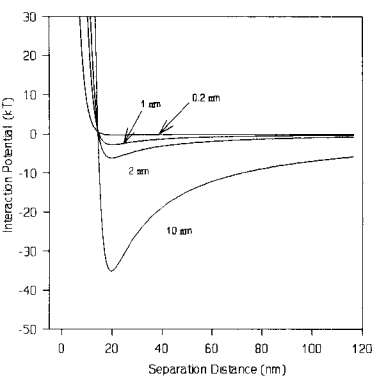

Figure A-2. 0.021 M Salt and -200 mV DLVO Calc.

maximum force for the 10-μm particles is about 1.2×10^{-11} N. For 10-μm particles, then, the gravitational force is approximately equal to the net attractive force.

A.3.2 Sensitivity to Surface Charge Assumption

The net interaction potential plots for particles in a 0.1 molar salt solution are shown in Figure A-3. A salt concentration of 0.1 molar was selected because it represents the current salt concentration in the AY-102 supernate.[5] Provided that AY-102 supernate is used as the retrieval fluid for C-106 sluicing, the particles will be exposed to salt concentrations of 0.1 molar or greater.[6] Figure A-3 shows that particles on the order of 2 μm and larger are expected to flocculate together. Smaller particles will be bound less strongly together.

The net interaction potential for a 0.10 M salt concentration and a -100 mV assumed surface charge is shown in Figure A-4. The curves in Figures A-3 and A-4 are essentially identical. This indicates that the DLVO calculations are relatively insensitive to the assumed surface charge when the surface charge is less than -100 mV and the salt concentration is 0.1 M or higher.

A.3.3 Flocculation Rate

The flocculation rate at 0.10 M salt concentration is expected to be rapid. Because the interaction potentials are all predicted to be negative (net attraction), there is no potential energy barrier to slow the flocculation of particles. The flocculation rate will be controlled by the rate at which the particles encounter one another, which is a function of both mixture agitation and particle diffusion. Hunter (1993, p. 442) states that the rate of flocculation in the absence of an appreciable potential energy barrier is on the order of seconds to minutes. Thus, the waste solids are expected to flocculate rapidly once the mixing intensity is sufficiently reduced to avoid destroying the flocs as they form.

Because the flocculation is expected to be rapid, appreciable particle-size segregation before flocculation occurs is unlikely.

A.3.4 Selective Agglomeration

In some colloidal systems, selective agglomeration of particles can occur. Selective agglomeration would be of concern for criticality analyses if, for example, the plutonium-containing particles preferentially

---

[5]The sodium cation concentration in the Tank AY-102 supernate is reported by Castaing (1994) to be 2150 mg/L, which is 0.093 M.

[6]As sludge is retrieved from C-106, the salt concentration in the liquid is expected to increase as the soluble fraction of C-106 solids dissolves.

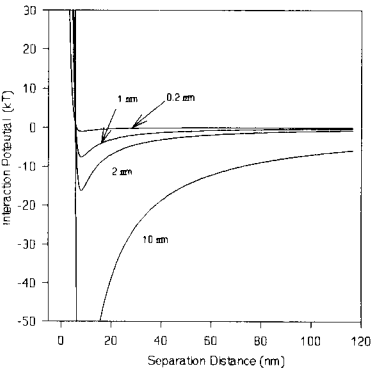

Figure A.3. 0.10 M Salt and -200 mV DLVO Calc.

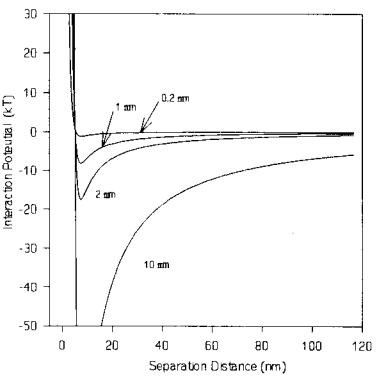

Figure A.4. 0.10 M Salt and -100 mV DLVO Calc.

flocculated/coagulated with each other rather than with the neutron absorbers. Selective agglomeration can occur when one or more species of particles in a suspension either have no significant surface charge or are oppositely charged compared to the other particles in the suspension. If, for example, all the neutron-absorber particles possess a large negative charge while the plutonium-containing particles have only a weak negative charge, the plutonium-containing particles could selectively agglomerate with each other rather than with the neutron absorbers. Alternatively, if the plutonium-containing particles have a positive charge, they will agglomerate preferentially with the negatively charged absorber particles rather than with other plutonium-containing particles.

Selective agglomeration should not occur in suspensions of tank waste solids provided that the solution pH is maintained above about 10. At pH of greater than 10, the neutron-absorber particles and the plutonium-containing particles should all possess a significant negative surface charge, which will prevent selective agglomeration. Zeta-potential measurements made on simulated waste solids (primarily neutron-absorbing oxides and hydroxides of iron and aluminum) demonstrate that the neutron-absorbing particles possess a negative surface charge more negative than about -22 mV at a pH of 10.0.[7] Zeta-potential data for specific plutonium compounds have not been found, but tests conducted on Pu^{4+} solutions by Grebenshchikova and Davydov (1965) indicate that the resulting $Pu(OH)_4$ particles are negatively charged at pHs greater than about 8.5. Transition from a positive charge to a negative charge at a pH of about 8.0 to 8.5 is similar to that reported for the neutron-absorbing solids.

Retrieval operations conducted at lower solution pH may be vulnerable to selective agglomeration effects. If the solution pH is expected to decrease to below 10 during operations, a more thorough analysis of the potential for selective agglomeration must be conducted.

A.3.5 Floc Destruction by Viscous Shear

The DLVO calculations conservatively predict that some degree of particle flocculation should be observed at 0.1 M salt (and higher). Particle coagulation is not predicted, however. Because flocculation forms relatively weakly bonded particle aggregations, vigorous mixing might effectively prevent the formation of flocs. Under conditions of moderate to intense mixing, localized particle segregation may be possible by applying enough shear to inhibit flocculation, but not enough mixing intensity to prevent the largest particles from settling to the tank floor.

A spherical particle subjected to a uniform shear field will experience shearing and extensional forces on the order of F_{shear}, which is given by:

where μ = liquid viscosity, Pascal-sec

---

[7]Virden, Jud W., J. Liu, B. C. Bunker, V. S. Stenkamp, and L. Song. *Solids Formation and Sludge Dissolution: Final Report for FY1994*. TWRSPP-94-092. Letter Report prepared for Westinghouse Hanford Company by the Pacific Northwest Laboratory, Richland, Washington.

$$F_{shear} = \mu\gamma\pi d^2 \tag{A.6}$$

γ = shear rate, s^{-1}
d = particle diameter, m

The maximum attractive force for 2-μm particles in a 0.1 M salt solution (for the assumed surface potential and Hamaker constant) is estimated from Figure A-3 to be about 7×10^{-12} N. Equation A.6 predicts that 2-μm particles in a moderately intense 100 s^{-1} shear field will experience about 1.2×10^{-12} N of force. A more intense shear field of 500 s^{-1} will apply a force approximately equal to that of the interparticle attractive force. Tbis shows that if the slurry is exposed to moderately intense mixing, flocculation may be inhibited.

This comparison of shear and interparticle attractive forces is over-simplified. A more rigorous treatment of the problem would be required to determine what level of mixing intensity causes enough shear to inhibit flocculation. Unless this further analysis is completed, the conclusion that flocculation will prevent particle segregation should be applied specifically to weakly mixed sludge settling scenarios. The TEMPEST simulations shown in Chapter 4.0 suggest that the AY-102 receiver tank is a weakly mixed settling scenario.

A.3.6 Implications of Hot-Cell Sludge Settling Tests

Samples of waste solids have been withdrawn from many of the Hanford Site tanks. Settling rate tests were conducted on some samples, but not on solids from tank C-106. Therefore, data from other waste tanks were used in this analysis. Of great interest to the criticality issue resolution work is the fate of plutonium-containing particles during settling. As described earlier, if the settling velocities of the plutonium-containing particles are appreciably different from those of the neutron-absorbing particles, plutonium might possibley reach concentrations of concern during waste retrieval and handling operations.

The fate of plutonium-containing particles has not been tested directly. Such testing would involve settling waste slurries from an initially well-mixed condition either under gentle or no agitation. The resulting sediment bed would be analyzed to determine whether the plutonium concentration increased in any portion of the bed. These types of tests are proposed and discussed further in Chapter 10.0.

Even though plutonium segregation by settling has not been measured, the existing waste solids' settling velocity data provide information relevant to the particle flocculation analysis presented here.

The DLVO calculations presented in Figures A-2 through A-4 indicate that particles larger than roughly 2 μm are expected to flocculate in a 0.10 M retrieval fluid. Particles smaller than about 1 μm will be very weakly bonded to any particles with which they might happen to flocculate, depending on the validity of the surface charge and Hamaker constant assumptions used for the

DLVO calculations.[8] Determining the fate of the particles that are smaller than 1 μm is important. Do they remain dispersed and subsequently settle on the layer of flocculated larger particles or do they participate in the flocculation?

The answer to this question appears to be that the smaller particles participate in the flocculation process and settle along with the larger particles. This conclusion is based on the observed settling behavior of waste solids.

Waste solids settling tests conducted to date were performed by first diluting the solids with either water or tank supernate, then mixing the slurry well, and then measuring the rate at which the interface between the settling solids and the clear supernate progresses downward. It has been observed in settling tests of solids from tanks SY-102 (Winters 1995) and C-107[9] that the supernate above the settling slurry is relatively clear. The maximum rate at which the supernate/slurry interface moves downward provides an indication of the settling velocities of the smallest particles, or smallest flocs within the slurry. Unhindered settling velocity for a sphere in a viscous liquid is given by Stokes' law,

$$v = \frac{2}{9} \frac{R^2 (\Delta\rho) g}{\mu} \tag{A.7}$$

where v = particle settling velocity, m/s
R = particle radius, m
$\Delta\rho$ = density difference between particle and fluid, kg/m^3
g = gravitational acceleration, 9.8 m/s^2
μ = fluid viscosity, Pa-sec

Winters (1995) reports that the maximum settling velocity for a 2:1 dilution of SY-102 solids with water was 0.42 cm/h. Assuming an effective settling particle density of roughly 2500 kg/m^3 [2.5 g/cm^3], ($\Delta\rho$ = 1500 kg/m^3), and a fluid viscosity of 1.1 cP (based on supernate salt concentration measurements given by Winters), the particle diameter corresponding to a settling velocity of 0.42 cm/h is about 1.3 μm.

It must be stressed, however, that Stokes' law applies only to relatively dilute particle suspensions in which the settling rate is controlled by the interaction between the particle and the surrounding fluid. In more concentrated suspensions, the interactions between particles can

---

[8]The DLVO calculations presented in Figures A.2 through A.4 apply to equal particle sizes. That is, $a_1 = a_2$. Calculations were also done to examine the interaction potentials between particles of different sizes. The magnitude of the interaction potential is determined largely by the size of the smaller particle, so statements made based on $a_1 = a_2$ DLVO calculations are expected to apply equally well to $a_1 <> a_2$ particle interactions.

[9]Personal Communication with K. P. Brooks, who is currently conducting settling tests using C-107 solids in a radioactive hot-cell.

significantly decrease the observed settling rate. This is relevant because the SY-102 settling velocity data presented by Winters were obtained from a concentrated suspension. The 2:1 dilution of SY-102 solids had a density of 1290 kg/m^3, 36.5 wt% solids, and an apparent viscosity at low shear rates of about 10 to 15 cP. With such a high concentration of solids, the settling is expected to be much slower than that observed in more dilute suspensions. Settling velocities for C-107 solids exhibit unhindered settling only for slurry concentrations of less than about 15 wt%. Thus, the SY-102 settling velocity data are not expected to be representative of unhindered settling and the Stokes' law equation does not apply. Because of this, the 1.3-μm particle/floc size estimated by Stokes' law may be much smaller than the actual particle/floc size.

The maximum settling velocities for C-107 solids have thus far been observed to be on the order of 5-15 cm/h, which is much faster than the SY-102 solids in hindered settling. The C-107 solids were settled at much lower concentrations ranging from 4.5 wt% to about 10 wt%. The solids were washed with inhibited water and allowed to settle, so the salt concentration used was relatively low (about 0.021 M). Under these conditions the initial interface settling rate was about 15 cm/h when the initial solids concentration was 4.5 wt%. Using a particle density of 2500 kg/m^3 and a supernate viscosity of 0.55 cP (the test was run at 50°C), Stokes' law implies an effective particle/floc diameter of about 5.3 μm.

Recall that the interface settling rate provides an estimate of the settling velocities of the smallest particles/flocs in the suspension. Thus, the particles/flocs of the C-107 solids settling in inhibited water are expected to be larger than about 5 μm. Because the number-average particle size of the C-107 solids has been measured at about 0.6 μm,[10] flocculation clearly is occurring in the C-107 slurry, even at the relatively low salt concentration of inhibited water.

Because the settling velocity data imply that even the smallest settling particles/flocs are considerably larger than 1 μm, we can reasonably conclude that the sub-micron particles are flocculating along with the larger particles and settling as flocs with an effective (aerodynamic) diameter on the order of 5 to 10 μm, or more.

Possibly, the small particles flocculate with each other and with the larger particles, and are protected from disrupting forces by the structure of the larger particles in the floc. Alternatively, the Hamaker constant and surface charge used to develop the DLVO interaction potential curves may be overly conservative. Regardless, we can reasonably conclude that particle flocculation and/or coagulation takes place at salt concentrations on the order of 0.1 M and higher. If slurries containing sufficient salt are allowed to settle, rapid flocculation and coagulation are expected to prevent particles from settling according to their individual settling velocities.

---

[10]Personal communication with P. A. Smith (PNNL). The particle size distribution data for the C-107 solids will be included in the report prepared by K. P. Brooks (PNNL) at the end of fiscal year 1996.

A.4 TEM EVIDENCE FOR PARTICLE FLOCCULATION

Several analytical tools have been used to characterize the particle size, the mineralogy and speciation of selected elements in the sludge to aid in interpreting sludge leaching. The tools used include transmission electron microscopy (TEM); two x-ray absorption spectroscopy (XAS) techniques, XANES (x-ray absorption near-edge spectroscopy) and EXAFS (x-ray absorption fine structure spectroscopy); Raman spectroscopy and nuclear magnetic resonance (NMR) spectroscopy. Finally, two "direct" particle size analyzers have been employed sparingly to measure particles and agglomerates of sludge. For particles/agglomerates larger than 1 μm in size, an optical particle analyzer that counts/sizes individual particles using light attenuation techniques was used. For particles/agglomerates that are smaller than 1 μm, a second device that is based on photon correlation spectroscopy, (Microtrac system from Leeds and Northrup) was used.

Data of interest to us was obtained using TEM and relates particle size, crystallinity and mineralogy with the tendency to agglomerate. The TEM is a useful tool for characterizing tank sludge because it provides data on size, morphology, chemical composition, and mineralogy on solids down to a size of 1 to 10 nanometers (0.001 to 0.01 μm). Sludge samples from 10 tanks have been reported: AW-105, B-111, BX-107, C-109, C-112, S-104, SY-101, SY-103, T-104, and T-111. Further, several tank sludge simulants and "pure" phases of aluminum hydroxide, iron hydroxide, and calcium phosphate have been studied. Pertinent references from which the following observations were taken include Virden et al. (1994a, 1994b), LaFemina et al. (1994a, 1994b), LaFemina et al. (1995a, 1995b, 1995c), Liu et al. 1995, Lui (1995), and Bunker et al. (1995).

General conclusions that can be gleaned from these references follow. Sludge in Hanford Site tanks consists of very small primary particles, both amorphous and crystalline, that readily agglomerate to form larger particles. The primary individual particles range in size from a few nanometers to several μm, but most primary particles are submicron in size, between 0.010 and 0.050 μm. Over 90% of the particles (includes both primary particles and agglomerates) characterized are not chemically or mineralogically distinct in size. Most of the individual crystallites (primary particles) are less than 0.05 μm in size. The largest primary particles found are crystalline salt particles such as $NaNO_3$ and $NaOH \bullet 4H_2O$ or gibbsite. The more common submicron primary particles are usually agglomerated to form clusters with sizes from submicron to a few microns. A few agglomerates reach sizes of tens to a few hundred microns. These large particles are easily disaggregated into smaller aggregates using mechanical energy. In general, agglomerates usually contain several types of primary particles with diverse chemical and mineralogic compositions. The agglomerates exist in irregular fractal shapes. These findings support the conclusion that the Hanford sludges do not contain significant quantities of crystalline particles of fixed composition with sizes larger than a few microns. Instead the sludge is random-composition aggregates of many submicron sized primary crystallites that often attach with other agglomerates to form clusters that can reach tens to a few hundred microns in size. These clusters readily break apart with minimal mechanical energy to agglomerates with a size distribution between tens of nanometers to at the extreme a few microns.

Some specific TEM measurements on samples from Hanford tanks follow.

Dried sludge from tank AW-105 consists of two different materials, a pure white powder and a brown-orange mud. The white powder contains two highly crystalline materials. The primary aggregates of the first crystals appear to be bi-modal is size; 0.1 to 0.5 μm and 1 to 2 μm. The material is alkali salt, likely $NaNO_3$ and KNO_3. The smaller sized particles are thought to represent fresh precipitate that occurs when the sample is dried to perform the TEM analysis; the larger sized particles are assumed to be "native" in the sludge. The second crystalline phase has primary particles of <0.01 μm size and agglomerates up to about 1 μm. The material is ZrO_2 and represents about 20 percent by volume of the bulk sample.

The orange-brown sludge material from this core contains five types of small aggregates with primary particles all being nanometer-sized. On a volume basis, the various particles were 50 percent boehmite [AlOOH], 30 percent zirconia [ZrO_2], 15 percent goethite [ferric oxide], and smaller amounts of a ferric-chromic oxide and sheet-like alumino-silicate clay-like material. The sample appears to also contain a trace of calcium carbonate (calcite).

TEM analyses of sludge from tank C-112 showed most of the particles are fine grained (<0.01 μm) but many agglomerates and a few crystalline aluminum- and uranium-bearing particles reach 5 to 10 μm in size. The fine-grained particles are primarily calcium phosphate, iron/nickel hydrous oxides, aluminum hydroxide, and iron hydroxide. Crystalline boehmite [AlOOH] and gibbsite [$Al(OH)_3$] were positively identified in this sludge sample.

Extended X-ray Absorption Fine Structure (EXAFS) characterization of sludge from tanks C-109 and C-112 show that stable strontium (and by inference ^{90}Sr) in the sludge is incorporated into calcium carbonate crystals, mainly the aragonite form (70%) and calcite (10%), and hydroxyapatite [$Ca_5(OH)(PO_4)_3$].

Sludge from T-111, a tank containing two types of bismuth phosphate waste, shows a large amount of crystalline sodium hydrogen phosphate. The material is agglomerated to sizes up to 100 μm that break apart on washing in a sodium nitrite/hydroxide solution into smaller agglomerates of 5 μm. These smaller agglomerates in turn consist of primary particles with mean sizes of 0.05 μm. Other particles consist of iron, bismuth, and silicon in a fairly fixed ratio although no x-ray diffraction patterns were observed that would suggest that the compound is crystalline. The compound is inferred to be amorphous bismuth ferrite [$Fe_2Bi(SiO_4)_2OH$]. Less common particles that appear to be crystalline include hydroxyapatite [$Ca_5(OH)(PO_4)_3$] with a rod-like habit with 0.1-μm size; Jacobsite [Fe_2MnO_4] with a plate-like habit and 0.5-μm size; goethite [FeOOH] with rod-like habit with 0.5-μm size; and lanthanum pyrophosphate [$La_4(P_2O_7)_3$] with irregular shape and crystallite size of 0.5 μm.

In summary, numerous crystalline and amorphous compounds have been found in Hanford Site sludge using a combination of analytical tools with emphasis on TEM . Numerous aluminum phases have been identified including crystalline boehmite, gibbsite, sodium aluminate, aluminum phosphate, and unidentified aluminosilicates (clay/zeolites). Amorphous aluminum hydroxide and alumino-silicates are also present. Common iron phases include bismuth ferrite, some goethite and more commonly amorphous iron hydroxide. Numerous phosphate phases are found in bismuth phosphate waste, including crystalline sodium

phosphate, calcium phosphates, aluminum phosphates and lanthanum pyrophosphate. Calcium carbonates have also been found. Stable strontium is often associated with these phases, as well as with the calcium phosphate phase [$Ca_5(OH)(PO_4)_3$]. Crystalline zirconia [ZrO_2] has been found in sludge from a tank that received cladding removal waste. Chromium phases are generally amorphous with trivalent chromium associated with aluminum and iron hydroxides and hexavalent chromium present with bismuth oxide. Infrequently crystalline bismuth oxide, Jacobsite [iron-manganese oxide], uranyl oxide of undetermined stoichiometry, and bismuth iron phosphate are found. Plutonium is present at such low concentrations that it cannot be found using any of the solids characterization techniques discussed.

All of the solids characterization data from TEM lead to the following conclusions regarding particle size. Although techniques such as TEM show that most of the primary particles (both by numbers and volume percent) in tank sludges are smaller than 0.1 μm in diameter, measurements of particle size based on indirect techniques such as sedimentation or light scattering indicate that most of the particles are larger than 1 μm. This apparent discrepancy between the two types of data is because sludge slurries are heavily agglomerated. Further, it is important to understand that an agglomerate with an effective diameter of ~1 μm does not behave like a primary particle having the same diameter.

Sludge can be discussed on several length scales, each of which provides useful information. The smallest length scale, the size of primary particles or discrete crystallites, can be measured with TEM and particles are found between 0.005 and 0.05 μm. The primary particles in tanks are agglomerated and range in size from 0.1 to 10 μm. Finally, the fractal agglomerates or clusters associate to form large flocs that range anywhere from 10 μm to perhaps 1 mm. The size of these flocs is determined by the level of shear and Brownian motion present in the solution that supports the flocs. The more shear and motion, the greater the tendency for the flocs to break apart into smaller agglomerates. Retrieval operations supply ample kinetic energy to break up large flocs, but they could reform as settling commences. Very high shear can also break up agglomerates into discrete primary particles, which given the normal conditions in Hanford Site tanks, should rapidly reagglomerate once the high inputs of kinetic energy dissipate.

A.4 REFERENCES

Bunker, B. C., P. J. Bruinsma, G. L. Graff, C. R. Hymas, X. S. Li, J. R. Phillips, D. R. Rector, P. A. Smith, L. Song, J. M. Tingey, and Y. Wang, 1995, *Colloidal Studies for Solid/Liquid Separation*, TWRSPP-95-045, Pacific Northwest Laboratory, Richland, Washington.

Castaing, B. A., 1994, *AY-101, AY-102, and C-106 Data Compendium*, WHC-SD-WM-TI-578, Rev. 1., Westinghouse Hanford Company, Richland, Washington.

Grebenshchikova, V. I. and Y. P. Davydov, 1965, "State of Pu(IV) in the Region of pH = 1.0 to 12.0 at a Plutonium Concentration of 2×10^{-5} M," in *Soviet Radiochemistry*, Vol. 7:2, pp 191-195.

Hiemenz, P. C., 1986, *Principles of Colloid and Surface Chemistry*, 2nd Ed., Marcel Dekker, Inc., New York, New York.

Hunter, R. J., 1981, *Zeta Potential in Colloid Science*, Academic Press, New York, New York.

Hunter, R. J., 1993, *Foundations of Colloid Science, Volume 1*, Clarendon Press, Oxford, England.

LaFemina, J. P., J. W. Virden, J. Liu, L. Song, A. R. Felmy, N. G. Colton, J. A. Franz, J. C. Linehan, D. L. Blanchard, B. C. Bunker, and M. L. Balmer, 1994a, *Tank Waste Treatment Science: Report for the Second Quarter FY 1994*, TWRSPP-94-027, Pacific Northwest Laboratory, Richland, Washington.

LaFemina, J. P., J. W. Virden, J. Liu, L. Song, V. S. Stenkamp, A. R. Felmy, E. A. Jenne, D. Rai, R. W. Fulton, N. G. Colton, J. G. Hill, G. S. Anderson, S. E. Faulk, J. A. Franz, J. C. Linehan, W. J. Shaw, C. D. Carlson, D. L. Balanchard, J. A. Campbell, S. Conradson, R. L. Gordon, N. J. Hess, J. C. Hutton, M. M. Lamourex, R. W. Stromatt, D. L. Styris, K. L. Wahl, B. C. Bunker, and M. L. Balmer, 1994b, *Tank Waste Treatment Science: Report for the Third Quarter FY 1994*, TWRSPP-94-086, Pacific Northwest Laboratory, Richland, Washington.

LaFemina, J. P., G. S. Anderson, D. L. Blanchard, P. J. Bruinsma, B. C. Bunker, N. G. Colton, S. D. Conradson, J. L. Cox, J. C. Hutton, A. R. Felmy, R. L. Gordon, G. L. Graff, N. J. Hess, J. G. Hill, E. A. Jenne, M. M. Lamourex, J. Liu, B. M. Rapko, D.R. Rector, P. A. Smith, L. Song, D. L. Styris, L. E. Thomas, A. J. Villegas, and Y. Wang, 1995a, *Tank Waste Treatment Science Task Quarterly Report for October-December 1994*, PNL-10762, Pacific Northwest Laboratory, Richland, Washington.

LaFemina, J. P., G. S. Anderson, D. L. Blanchard, P. J. Bruinsma, B. C. Bunker, I. E. Burgeson, Y. L. Chen, N. G. Colton, S. D. Conradson, A. R. Felmy, R. L. Gordon, G. L. Graff, N. J. Hess, J. G. Hill, J. C. Hutton, C. R. Hymas, E. A. Jenne, M. M. Lamourex, X. S. Li, J. Liu, G. J. Lumetta, L. Rao, B. M. Rapko, D. R. Rector, J. R. Rustad, P. A. Smith, L. Song, S. M. Sterner, D. L. Styris, L. E. Thomas, J. M. Tingey, S. M. Tingey, A. J. Villegas, and Y. Wang, 1995b, *Tank Waste Treatment Science Task Quarterly Report for January- March 1995*, PNL-10763, Pacific Northwest Laboratory, Richland, Washington.

LaFemina, J. P., D. L. Blanchard, P. J. Bruinsma, B. C. Bunker, I. E. Burgeson, Y. L. Chen, N. G. Colton, S. D. Conradson, A. R. Felmy, R. L. Gordon, N. G. Gotts, G. L. Graff, N. J. Hess, J. C. Hutton, C. R. Hymas, M. M. Lamourex, X. S. Li, J. Liu, G. J. Lumetta, J. R. Phillipos, B. M. Rapko, D.R. Rector, J. R. Rustad, P. A. Smith, L. Song, S. M. Sterner, L. E. Thomas, J. M. Tingey, S. M. Tingey, L. Q. Wang, and Y. Wang, 1995c, *Tank Waste Treatment Science Task Quarterly Report for April-June 1995*, PNL-10764, Pacific Northwest Laboratory, Richland, Washington.

Lui, J, 1995, *TEM Characterization of Tank Sludge Simulants*, TWRSPP-95-033, Pacific Northwest Laboratory, Richland, Washington.

Liu, J., L. R. Pederson, L. Q. Wang, 1995, *Solid-Phase Charcterization in Flammable-Gas-Tank Sludges by Electron Microscopy*, PNL-10723, Pacific Northwest Laboratory, Richland, Washington.

Russel, W. B., D. A. Saville, and W. R. Schowalter, 1989, *Colloidal Dispersions*, Cambridge University Press, Cambridge, Massachusetts.

Shaw, D. J., 1980, *Introduction to Colloid and Surface Chemistry*, 3rd Ed., Butterworths, Boston, Massachusetts.

Virden , J. W., B. C. Bunker, and J. Lui, 1994a, *Solids Formation and Sludge Dissolution: Results of Transmission Electron Microscopy on Tank Sludge Simulant*, TWRS-PP-94-028, Pacific Northwest Laboratory, Richland, Washington.

Virden, J. W., J. Liu, B. C. Bunker, V. S. Stenkamp, and L. Song, 1994b, *Solids Formation and Sludge Dissolution: Final Report for FY1994*, TWRSPP-94-092, Pacific Northwest Laboratory, Richland, Washington.

Winters, W. I., 1995, *Tank Characterization Report for Double-Shell Tank 241-SY-102*, WHC-SD-WM-ER-366, Rev. 0., Westinghouse Hanford Company, Richland, Washington.

This page intentionally left blank.

APPENDIX B

GRAVITY CONCENTRATION

This page intentionally left blank.

APPENDIX B
GRAVITY CONCENTRATION

This appendix reviews mining literature concerning particle segregation using gravity concentration. Gravity concentration is one of the earliest known methods for separating heavy minerals such as gold and tin oxide from the lighter components of the ore. The mining literature was reviewed to determine if the mechanisms that achieve the gravity separations are applicable to separating plutonium-rich particles from neutron-absorber sludge particles in the tanks. Chapters 4.0, 5.0, and 6.0 present our critical analyses, using various fluid dynamic tools, of the potential for particle separation in tanks. We state in several places that the analyzes to not include all possible mechanism and processes such as momentum-driven processes that are too complicated to be easily reduced to simple mathematical algorithms. In this appendix we review some of these difficult-to-quantify processes that challenge existing mathematical algorithms. We are particularily looking for evidence that ore-milling processes that are engineered to separate different particles could occur spontaneously within tanks during the various operations used to transfer or retrieve waste, remove liquid, or to remove heat from tanks. Our goal is to review ore-milling operations to understand the basic principles and to evaluate whether past and future Hanford Site tank operations could reproduce the necessary conditons and driving forces.

Gravity concentration separates minerals according to their relative density. Four approaches to gravity concentration shown in Figure B-1 are as follows (Burt 1980, 1986 and Clarkson 1984).

- **Density Separations**. A fluid with an apparent density between those of the materials to be separated is selected so that the lighter components will float while the heavier components will settle.

- **Stratification Separations**. The materials to be separated are subjected to repeated vertical pulsation of the carrier fluid so that the heavier materials segregate beneath the lighter ones. Jigs and jigging are typical of stratification equipment.

- **Flowing Film Separations**. The separations are achieved by the relative movement of the particles in a slurry flowing down an inclined plane. Sluices, pinched sluices, Reichert Cones, palongs, and spiral separators are flowing film separators.

- **Shaking Separations**. The mineral components separate in a flowing film with an imposed oscillating or orbital horizontal shear force. Shaking tables and the Bartles-Mozley and Crossbelt concentrators are typical shaking separators.

Particles can also be separated by centrifugal methods. These would include centrifuges and cyclones.

B.1 DENSITY SEGREGATION

Plutonium in the tanks will not segregate by density because all the particles of concern have densities greater than supernatants and would have a tendency to settle. Only in situations where a particle was induced to float in an aqueous solution would density segregation become a possible concern. Flotation can be induced in the following three ways (Tchobanoglous and Burton 1991).

- Injecting air while the slurry is under pressure, then releasing the pressure so that small air bubbles form
- Bubbling air directly into the slurry
- Saturating the slurry with air, then applying a vacuum (Tchobanoglous and Burton 1991).

Flotation can be enhanced by adding chemicals to alter the surface or structure of the particles so that air bubbles are more easily trapped or adsorbed. More analysis of chemically-enhanced froth flotation was performed by Columbia University School of Mines and is found in Whyatt et al. (1996). Whyatt et al. (1996) conclude that the types of organics used to enhance froth flotation are not similiar to the types of organics present in the Hanford Site tanks and that the pH of tank supernate is outside the range where the chemical additives work effectively to suspend fine particles in the hydrophobic froth.

B.2 STRATIFICATION

In stratification processes such as jigging, particles are sorted based on their movement in a bed through which a fluid is passed vertically. The bed is dilated by the upward movement of the fluid and is contracted by the downward movement. In typical mining applications, the cycle frequency would be on the order of 100 to 300 cycles per minute. Four mechanisms have been proposed to describe the process. These are differential acceleration at the beginning of the fall, hindered settling, attaining the minimum potential energy level, and interstitial trickling.

Figure B-1. Gravity Concentration Methods.

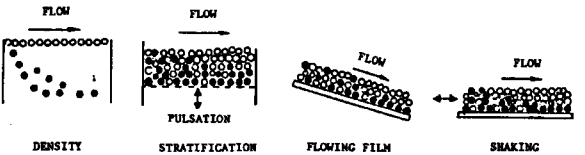

At the top of the upward, dilation pulse, the particles have zero velocity and begin to fall with accelerations and velocities that are functions of particle density and independent of particle size. The heavier particles will have a larger initial acceleration and travel farther than lighter particles over a finite time before terminal velocities are attained. Thus, if the cycle frequency is high enough that the fall time is short and the number of falls is large, the separations can be achieved based on the relative accelerations of the particles.

With hindered settling, higher particle concentrations result in increased particle interactions. These increased interactions increase the apparent density of the slurry so that individual particles settle as if they were in a more dense fluid than the actual slurry fluid. This changes the apparent ratio of settling velocities for particles of different sizes and stratification occurs. This theory is not universally accepted.

Another mechanism for stratification is that a bed of particles will seek its minimum potential energy level. A uniform mixture of light and heavy particles with a center of gravity at its center will rearrange so that the heavier particles are on the bottom, thereby lowering the center of gravity and reducing the potential energy of the system. The jigging operation serves to fluidize the bed to release the potential energy.

Interstitial trickling can contribute to the stratification achieved by jigging operations. Because all particles do not travel the same distance during a bed dilation cycle, they come to rest at different instants. Coarse particles may remain in suspension for a shorter time and bridge together. Finer particles can still settle through the interstices between the larger particles during the bed settling phase of the cycle.

B.3 FLOWING FILM SEPARATIONS

Flowing film separations rely on the following mechanisms for achieving separations.

- Thin film separations where the film thickness and particle size are similar and the rate of shear on the fluid is small
- Flowing film concentration where the particle slurry experiences continuous shear
- Flowing film concentration enhanced with riffles to form mini centrifugal concentrators.

Thin film separations require laminar flow down a smooth inclined plate. Under these conditions, a parabolic velocity profile is created in the fluid. The fluid velocity is zero at the plate surface and reaches its peak at the film/air interface. Particles in contact with the plate surface are forced to slide or roll down the incline by the fluid action. The fluid must provide the force necessary to overcome any sliding or rolling resistances. Because of the fluid velocity profile, the larger and lighter particles will tend to move farther than smaller and heavier particles. Mineral particles typically distribute in the general downslope sequence of fine heavies, coarse heavies and fine lights, and coarse lights. Thin film separations work with film thicknesses up to about 10 particle diameters.

When a slurry of sufficient particle concentration is subjected to flow, particle collisions and interactions result in a stress normal to the direction of fluid flow. This is known as the Bagnold force. The resulting force on the particles can be shown to decrease with increasing particle density and increase with increasing particle size. Under such conditions, larger particles tend to move to the fluid surface where the shear strain is less and smaller particles tend to move to the bottom of the particle bed where the shear strain is greatest (Holtham 1992). The resulting distribution of particles is coarse lights on top, followed by fine lights and coarse heavies, and fine heavies on the bottom.

Sluice boxes may incorporate riffles perpendicular to the flow path to enhance the recovery of heavy particles. The riffles form eddies or vortexes in the fluid between the riffles such that the heavier particles are ejected from the vortex while lighter particles are swept away. The riffles also allow the heavier particles to settle and prevent them from being carried away by the bulk fluid flow. To be effective, the fluid flow must be high enough to create the vortices between riffles yet slow enough that the particles do not remain in suspension.

For all flowing film separations, fluid velocities must be low enough that the particles are not simply maintained in suspension because of fluid turbulence.

B.4 SHAKING DEVICES

The mechanisms by which shaking tables achieve particle segregation are complex and not clearly understood (Burt 1986). The shaking induces shear in the bed similar to the flowing film concentrators. This makes Bagnold forces important. Thin fluid films are typically used so that particle rolling and sliding becomes important. Shaking tables typically include riffles to improve recovery. The resulting separating mechanisms can oppose one another with the dominant mechanism being determined by operating parameters. Operating experience indicates that for a feed material with fine particles, one should use less water, less feed, higher frequencies, and shorter strokes with low riffles. These conditions are similar to those for the Bartles-Mozley concentrator described in the following paragraph.

Most gravity separation devices used in the mining industry are effective in recovering minerals with particle sizes down to approximately 100 μm. Figure B-2, from Burt (1986), shows typical operating ranges for gravity concentration equipment. Smaller particle (<100 μm) slurries are referred to as slimes and require low-capacity approaches such as the Bartles-Mozley concentrator, Crossbelt concentrator or centrifuges to achieve significant separations of the finer particles down to approximately 5 μm in size. Recoveries of cassiterite (tin ore, SnO_2, ρ = 6.99) particles in excess of 50 percent at 5 μm and 80 percent at 10 μm have been achieved with Bartles-Mozley devices. The Bartles-Mozley concentrator uses smooth decks inclined to less than 2° to minimize the slurry velocity (Mills and Burt 1979). The device operates with a slurry film thickness of between 0.5 and 1 mm. An orbital shear is imposed on the film via the deck. A typical shear rate would be on the order of 4.5 to 5 m/min. Recovery is highest when the velocity ratio, defined as the fluid film velocity divided by the shear rate, is less than 1.0 (Mills and Burt 1979). The roughness profile of the deck has an important affect on the recovery of the fines (Sivamohan and Forssberg 1986). For example, a wooden deck with a roughness profile of 30 to 40 μm demonstrated significantly greater retention of fines compared to a stainless steel deck with a roughness profile of 0.25 to 0.50 μm.

B.5 COMPARISON TO TANK WASTE CONDITIONS

The only waste phase for which criticality could potentially be an issue is tank sludge. Tank sludge particulates, includling both primary particulates and agglomerates, are fine with sizes ranging from less than 1 nanometer (0.001 μm) to about 100 μm. Much of the material classified as >10 μm likely is actually agglomerates of smaller particles. Plutonium, the most important fissile material in the tanks is believed to exist as very fine particulate and, in any case, should be less than about 10 μm. As shown in Figure B-2, many of the devices used commercially to achieve segregation by density would fail to achieve significant segregation for tank sludge becasue sludge is too fine-grained. The devices that could potentially achieve the segregation fall into the categories of centrifugal devices and shaking devices including shaking tables, Bartles-Mozley Concentrators, and Bartles-Mozley Crossbelt Concentrators.

Figure B-2. Typical Particle Sizes Recovered for Various Gravity Concentration Devices.

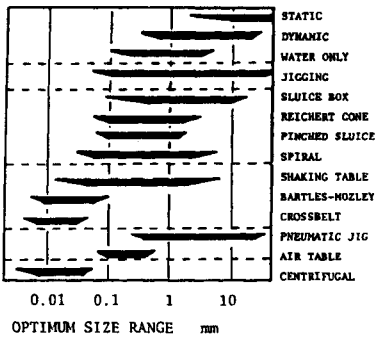

Centrifugal devices include centrifuges and cyclones. Both rely on creating centrifugal forces to separate the heavy particles and therefore require specialized equipment configurations that are not considered applicable to any known tank operating activity or pieces of equipment in tanks (risers, air lift circulators, liquid level wells, etc.).

Density separations are not expected under current tank operating conditions. The densities of the fissile material particles and neutron poisons are both greater that the density of the supernatants. Although some of the tanks include spargers (air-lift circulators), the bubbles formed are too large to create excessive flotation of the particles. Commercial flotation devices typically use fine bubbles and may add chemicals to enhance the flotation process.

Slime concentrators typically rely on a shaking mechanism to achieve segregation of the particles in a thin flowing film. Different-sized particles and different-density particles are segregated because they traverse the surface at different velocities. This phenomenon is not expected to occur to any great degree in the tank for several reasons. First, although segregation could occur in the layer of fluid moving across the tank floor, no collection device would be used to selectively collect the slower moving particles. In the separator, this is achieved by shaking the surface in an eccentric manner to force particles on the surface to exit preferentially to one side of the device. Turbulence would also interfere with the segregation. In the separator, the film is kept very thin to ensure laminar flow conditions. Turbulence would tend to lift particles from the surface and result in mixing that would disrupt the segregation process. Therefore, while some segregation from this mechanism is conceptually possible in Hanford

tanks, no mechanism is present to achieve the degree of segregation needed or to continuously segregate fissile material in such a way to collect it into a critical configuration.

B.6 SUMMARY

Because the sludge in Hanford Site tanks is fine grained and the supernatant solution exhibits high pH and salinity, the chemical environment in tanks does not promote efficient particle separation using the ore-dressing processes described. Further, the separations processes that are amenable to fine particles in the range of a few to tens of microns rely on continual acceleration (shaking or centrifugation) under narrowly controlled conditions and specialized riffles or flow impediments to optimize separation. The tank operations that restrict acceleration to a level where turbulence is avoided are of too short a duration to effectively separate significant quantities of sludge. Also, the tanks do not contain the specially constructed riffles and baffles that are required to make the commercial equipment work effectively.

B.7 REFERENCES

Burt, R. O., 1980, "Slime Recovery by Gravity Concentration - A Viable Alternative?" In: *Fine Particles Processing*, American Institute of Mining, Metallurgical, and Petroleum Engineers, Inc., New York, New York.

Burt, R. O., 1986, "Selection of Gravity Concentration Equipment," in *Design and Installation of Concentration and Dewatering Circuits*, Society of Mining Engineers, Littleton, Colorado.

Clarkson, R., 1984, "The Use of Nuclear Tracers to Evaluate the Gold Recovery Efficiency of Sluiceboxes," *CIM Bulletin*, Vol. 87, No. 979, pp 29-37.

Holtham, P. N., 1992, "Particle Transport in Gravity Concentrators and the Bagnold Effect," *Minerals Engineering*, Vol. 5, No. 2, pp 205-221.

Mills, C., and C. R. Burt, 1979, "Thin Film Gravity Concentrating Devices and the Bartles-Mozley Concentrator," *Mining Magazine*, Vol 141(1), pp 32-39.

Sivamohan, R. and K. S. E. Forssberg, 1986, "Progress in Gravity Concentration - Theory and Practice," in *Advances in Mineral Processing*, Society of Mining Engineers, Littleton, Colorado.

Tchobanoglous, G., and F. L. Burton, 1991, *Wastewater Engineering Treatment, Disposal, and Reuse*, McGraw Hill, Inc., pp 242-248.

Whyatt, G. A., R. J. Serne, S. V. Mattigod, Y. Onishi, M. R. Powell, J. H. Westsik, Jr., L. M. Liljegren, G. R. Golcar, K. P. Recknagle, P. M. Doctor, V. G. Zhirnov, J. Dixon, D. W. Jeppson, and G. S. Barney, 1996, *The Potential for Criticality in Hanford Tanks Resulting from Revrieval of Tank Waste*, PNNL-11304, Pacific Northwest National Laboratory, Richland, Washington.

This page intentionally left blank.

APPENDIX C

ANALYSIS TO DETERMINE THE VOLUME OF AIR ENTRAINED BY A SINGLE AIR LIFT CIRCULATOR

This page intentionally left blank.

APPENDIX C: ANALYSIS TO DETERMINE THE VOLUME OF AIR ENTRAINED BY A SINGLE AIR LIFT CIRCULATOR.

This analysis was performed to determined whether an air lift circulator is capable of entraining 2100 gpm of liquid. Analysis requires understanding the geometric features of an air lift circulator and applying correlations to predict the flow in the appropriate geometry. This discussion is organized as follows. The geometry of the air lift circulator is provided first. Correlations to predict the flow in that geometry follow. The predicted pressure drop as a function of target gas and liquid flow rates are provided at the end of the discussion.

C.1 ABSTRACT REPRESENTATION OF THE AIR-LIFT CIRCULATOR.

Air is supplied at the bottom of an open ended pipe which is enclosed in a larger diameter shroud, Figure C.1. The larger diameter shroud extends somewhat below the air supply pipe. The buoyant air released from the air supply pipe rises inside the shroud, and in the process entrains some liquid into the bottom of the shroud. The total flow rate of entrained liquid depends on air supply rate, the geometry of the air-lift circulator and the physical properties of the liquid.

In the Hanford tanks, the system is complicated by the fact that the liquid is a slurry which contains suspended solids. There are no specific correlations in the literature to predict the pressure drop in suspension of solid-liquid mixtures using gas bubbles. So, it will be assumed here that the slurry is a liquid with a density and viscosity equal to the slurry density.

This assumption is justified if the suspended particles are relatively small which is the case of Hanford slurries and sludges. In any case, the assumption is consistent with the goal of the analysis, which is to determine whether the entrained liquid flow rate used in a TEMPEST prediction documented by Eyler (1983 & 1984) is reasonable. The TEMPEST analysis made similar assumptions regarding flow of the mixture. So, any uncertainty resulting from treating the slurry mixture as a liquid is also embedded in the result of the TEMPEST simulation.

C. 2 METHOD OF ANALYSIS.

The flow rate inside the shroud may be predicted by recognizing that the pressure drop calculated for flow outside the shroud must be equal to that calculated flow inside the shroud. That is, pressures at points 3 and 1 in Figure C.1 can be determined without knowledge of the gas flow rate through understanding of single phase flow relations that apply outside the shroud. In addition, the pressure difference between 3 and 1 depends on the gas and liquid flow rates inside the shroud. If the gas flow rate is known, then entrained liquid flow rate will take on the value that ensures that pressure differences between points 3 and 1 must be the same when calculated using relations that apply outside the shroud and when calculated using those that apply inside the shroud.

Because there are no flow losses outside the shroud, the pressure drop everywhere outside the air-lift circulator can be predicted using Bernoulli's equation along a stream line connecting the free surface of the liquid and the entrance of the shroud. This gives a second relation for the pressure difference between points 1 and 3, $P_1 - P_3$, which depends on the entrained liquid flow rate entering the air-lift circulator.

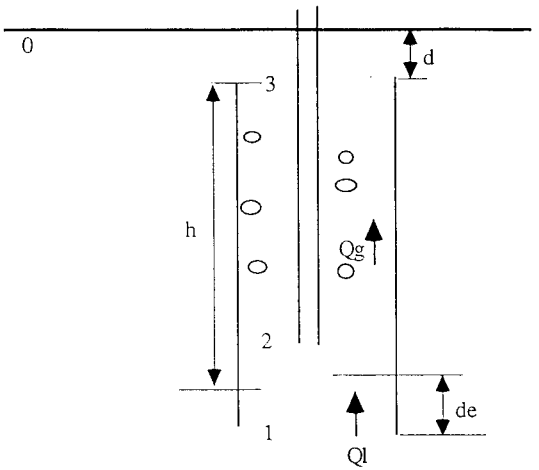

Figure C.1 Schematic Representation of the Air Lift Circulator.

The pressure drop inside the air-lift circulator can be analyzed by dividing the air lift circulator into two regions. This first is the region from points 1 to 2 which describes developing single phase flow. The second is the loss from points 2 to 3, which we will predict using a correlation for gas-liquid flow in a vertical pipe. The sum of the pressure drop in the two regions is the pressure difference between points 1 and 3, $P_1 - P_3$. This pressure difference will depend on the unknown entrained liquid flow rate Q_l, the known gas flow rate Q_g and the air-lift circulator geometry.

The two methods of relating the pressure drop $P_1 - P_3$ to the entrained liquid flow rate, Q_l result in two equations and two unknowns. Thus the system can be manipulated to obtain the solution for the entrained liquid flow rate.

The algebraic equations will now be described.

The pressure difference between the free surface and the shroud entrance, point 0 and point 1 respectively, is described by Bernoulli's equation for single phase flow:

$$P_1 - P_0 = \rho_L g(h+d) - \tfrac{1}{2}\rho_L V_{L1}^2 = \rho_L g(h+d) - \rho_L Q_{L1}^2 / 2A^2 \qquad \text{(C.1)}$$

where P_1 = the static pressure at point 1;
P_0 = the static pressure at point 0 ;
ρ_L = the density of the slurry between the surface and point 1;
h = the height of the external tube or shroud;

d = the immersion depth of the top of the tube;
g = the acceleration due to gravity;
A = the cross-sectional area of the shroud;
Q_{L1} = the entrained liquid, or slurry, flow rate and
V_{L1} = the velocity of the liquid at point 1.

The static pressure at the exit of a pipe with subsonic flow is equal to the local ambient pressure. So, the pressure difference between the surface and point three varies hydrostatically. This can be quantified by:

$$P_3 - P_0 = \rho_L g(d) \tag{C.2}$$

where P_3 = the static pressure at point 3.

Taking the sum of (C.1) and (C.2) results in

$$P_1 - P_3 = \rho_L gh - \tfrac{1}{2}\rho_L V_{L1}^2 = \rho_L gh - \rho_L Q_{L1}^2 / 2A^2 \tag{C.3}$$

Equation (C.3) may be used to determined the pressure drop based on flow that occurs outside the air lift circulator.

The pressure drop between points 1 and 2 cannot be determined exactly, but may be bounded. The upper bound is estimated from loss coefficients for flow at a pipe entry and the frictional loss for fully developed flow in the short entry region.

$$P_1 - P_2 = \rho_l g(d_e) + \left(K_{loss} + f\, d_e / D\right)\rho_l V_l^2 / 2 \tag{C.4}$$

where K_{loss} = the loss coefficient associated with developing flow;
d_e = the distance between the air-lift circulator entrance and the exit of the gas supply tube (see Figure C.1);
D = the diameter of the shroud and
f = the friction factor in single phase flow.

The lower bound is $P_1 - P_2 = 0$. The upper bound estimate will under predict the entrained flow rate, and is used here.

More refined estimates are not possible because published values of K_{loss} account for the entire loss that accrues during flow development. In the case of an air lift circulator, the liquid flow is not fully developed at the air injection point, so the pressure loss is smaller.

The pressure drop between points 2 and 3 must be predicted based on correlations for the pressure drop in a gas-liquid flow. Several correlations to predict the pressure drop in the gas-liquid flow in vertical circular pipes are published in Govier and Aziz (1987). However, Govier and Aziz recommend that the correlations for gas-liquid mixtures may be applied to predict flow of crude oil, which often contains some entrained particulate.

Because of the existence of the air lift supply tube inside the shroud, the air lift circulator is not a circular pipe. Instead, it is an annulus with a very small internal pipe. Govier and Aziz provide no recommendations to account for the difference between annular flow and

pipe flow. So, to estimate the flow in the annulus, the correlations for pipe flow were adapted by substituting the hydraulic diameter of the annulus for the diameter of the pipe. This is commonly recommended in flow of single phase fluids.

The hydraulic diameter D_h is defined as $D_h = 4A/P$ where A is the cross-sectional area of the flow region and P is the perimeter of the flow region. For a circular pipe, the hydraulic diameter and the diameter are equal.

Only one of the correlations recommended in Govier and Aziz (1987) apply to large diameter pipes. This was the correlation recommended by Ros (1961) and extended by Duns and Ros (1963); this correlation was selected to predict the entrained liquid flow rate in the air lift circulator.

The Ros correlation involves numerous intermediate steps to calculate the pressure drop. The procedure is described here in an order that facilitates calculation, rather than one that describes the phenomenology of two-phase flow.

The Ros correlation states that the pressure drop ΔP in the two phase region can be decomposed into three parts. These are the hydrostatic pressure head ΔP_{HH}, the change in kinetic energy with height ΔP_{KE} and the frictional pressure loss, ΔP_f. The sum of the three contributions equals the total pressure drop. So,

$$\Delta P = \Delta P_{HH} + \Delta P_{KE} + \Delta P_f \tag{C.5}$$

The hydrostatic head can be calculated using

$$\Delta P_{HH} = \left[E_g \rho_g + \left(1 - E_g\right)\rho_l\right] g z \tag{C.6}$$

where E_g = the average volume fraction of the gas in the two-phase region;
ρ_g = the density of the gas in the two-phase region;
ρ_l = the density of the liquid in the two-phase region and
z = the length of the region containing both liquid and gas phases.

For most gas-liquid pipe flows, including the one under consideration, Ros recommends neglecting the kinetic energy change. So, $\Delta P_{KE} = 0$.

The frictional pressure drop is estimated using

$$\Delta P_f = \frac{2 f_r V_{SL}^2 \rho_L}{D_h}\left(1 + \frac{V_{SG}}{V_{SL}}\right) z \tag{C.7}$$

where f_r = the friction factor in gas-liquid flow;
V_{SL} = the superficial liquid velocity and
V_{SG} = the superficial gas velocity.

The superficial liquid and gas velocities may be determined respectively using $V_{SG} = \frac{Q_g}{A}$ and $V_{SL} = \frac{Q_L}{A}$; where Q_L is the volumetric flow rate of liquid and Q_g is the volumetric flow rate of gas.

To evaluate (C.6), and (C.7), we require a model to predict the gas volume fraction E_g and the friction factor f_r in a vertical gas-liquid flow. The procedure to predict these is now described.

The first step of the procedure requires specifying the flow rates of the liquid and gas phase and determining the physical properties of both phases. The second step involves computing the magnitude of four dimensionless parameters. These are:

The liquid velocity number

$$N_{VL} = V_{SL}\sqrt[4]{\rho_L / g\sigma} \tag{C.8}$$

The gas velocity number

$$N_{VG} = V_{SG}\sqrt[4]{\rho_L / g\sigma} \tag{C.9}$$

The pipe diameter number

$$N_D = D_H\sqrt[4]{\rho_L / g\sigma} \tag{C.10}$$

and the liquid viscosity number

$$N_L = \mu_L\sqrt[4]{g / \rho_L\sigma^3} \tag{C.11}$$

where σ = the surface tension of the slurry in air and
μ_L = the viscosity of the slurry.

The next step is to identify the flow regime. For brevity, this discussion will focus on the region referred to as "Region I" by Ros. This is also referred to as the bubble and slug or froth flow regime. In this regime, the liquid phase is continuous and the gas phase is discontinuous and forms bubbles. We will focus on this region because it is based data for a range of pipe diameters that includes that of the air lift circulators.

Region I occurs when $N_{Vg} < L_1 \div L_2 N_{VL}$, where L_1 and L_2 are functions of N_D. The functional relation is illustrated in Figure 8.21 in Govier and Aziz (1987). The flow in the air lift circulator is predicted to fall in this region. In this region, the friction factor is calculated as follows. First, the slip number, N_s, is calculated using:

$$N_s = F_1 + F_2 N_{VL} + F_3\left(\frac{N_{VG}}{1+N_{VL}}\right) \tag{C.12}$$

with

$$F_3' = F_3 - \frac{F_4}{N_D}\,. \tag{C.13}$$

where $F1$ = is an empirical constant,
$F2$ = is an empirical constant,
$F3$ = is an empirical constant and
$F4$ = is an empirical constant.

The values of $F1$, $F2$, $F3$ and $F4$ are provided as a function of N_L in Figure 8.20 in Govier and Aziz (1987). The slip velocity, S, is then calculated using

$$S = N_s \Big/ \sqrt[4]{\rho_L / g\sigma}\,. \tag{C.14}$$

The gas void fraction E_G may then be calculated using

$$S = \frac{V_{SG}}{E_G} - \frac{V_{SL}}{(1-E_G)}\,. \tag{C.15}$$

The hydrostatic pressure head may then be determined using (C.6).

The remaining steps are those to determined the frictional pressure drop, ΔP_f (see equation C.7) The friction factor is determined using

$$f_r = f_1\left(\frac{f_2}{f_3}\right) \tag{C.16}$$

where f_r = is an empirical constant,
$f1$ = is an empirical constant,
$f2$ = is an empirical constant and
$f3$ = is an empirical constant

The magnitude of f_1, is determined from Figure 8.23 in Govier and Aziz (1987), which is a modified Moody diagram. The magnitudes of f_2 and f_3 account for hold up effects. f_2 is obtained as a function of $f_1 \, V_{SG}/V_{SL} \, N_D^{2/3}$ and is shown in Figure 8.24 in Govier and Aziz (1987). f_3 is determined algebraically using

$$f_3 = 1 + f_1\sqrt{V_{SG}/50\ V_{SL}}\,. \tag{C.17}$$

Once f_r is determined, it may be used to evaluate the frictional pressure drop using (C.7).

Finally, the pressure drop between points 1 and 3 can be determined using

$$P_1 - P_3 = \rho_l g(d_e) + \left(K_{loss} + f\,{}^{d_e}\!/_{D}\right)\rho_l V_l^2/2 + \Delta P \qquad \text{(C.18)}$$

where ΔP is calculated using C.5.

C.3 RESULTS OF ANALYSIS

The procedure described in C.2 was applied to verify that the entrained flow rate in the air lift circulator could meet or exceed 2100 gpm used by Eyler (1983 & 1984). The entrained rate is possible if the pressure drop inside the air lift circulator caused by a specific air and liquid flow rate is less than that outside the circulator.

Values of the pressure drop were predicted using the following parameters:

Air flow rate: 50 scfm minimum (George et al. 1996). The lower bound on the entrained liquid flow rate was obtained by applying the ideal gas law to obtain the volumetric flow rate at the hydrostatic pressure at the entrance of the shroud. It was assumed that the shroud entrance was submerged 30 ft below the free surface of the liquid. This provided a very conservative value for the air flow rate because the correlations predict lower liquid entertainment rates for lower air flow rates. The values used was 26.5 cfm.

Temperature: > 200 ^{0}F (George et al. 1996).

Height of air-lift circulator 22 ft long and 17 ft long.

Diameter of Air lift circulator shroud 30 inches (George et al. 1996).

Diameter of air supply line 1".

Distance between bottom of air supply line and bottom of air lift circulator 6".

Entrained liquid flow rate used by Eyler (1983 & 1984): 2100 gpm.

The physical properties used of the entrained fluid were estimated to be equal to those of water at standard conditions. The density of the slurry is expected to exceed this value.

The pressure drop between points 1 and 3 determined using C.3 and that determined using C.18 are provided in Table C.1; these values correspond to the physical properties just described. In both cases, the pressure drop that would occur when 2100 gpm was entrained in the shroud was less than the pressure drop outside the shroud; that is the value based on C.18 was less than that calculated using C.3. This implies that 2100 gpm can be entrained for the physical properties evaluated.

The same procedure was then used to predict the pressure drop using all properties described previously and one modification. The specific gravity of the slurry was assumed to be s.g. = 2. This is an upper bound estimate for the specific gravity. The flow rate of at least 2100 gpm was also found to be achieved for this specific gravity.

The pressure drops are provided in Table C.2. Higher pressure drops were achieved both inside and outside the shroud; this is a hydrostatic effect. However, the pressure drop inside the shroud was smaller than outside, indicating that more than 2100 gpm of fluid would be entrained.

The pressure drop inside and outside the shroud were then predicted using all properties applied to the predictions in Table C.1 except that the viscosity of the liquid was assumed to be 2 cP. The pressure drop predictions are provided in Table C.3. The entrained flow rate of 2100 gpm was found to be achieved. In fact, the numerical predictions were entirely insensitive to the viscosity of the fluid in the range applied. This is typical of turbulent pipe flows.

The conclusions of this analysis were that the air lift circulators will entrain at least 2100 gpm for the range of physical properties anticipated in Hanford Tanks. This suggests that the parameters selected by Eyler (1983 & 1984) are applicable to predict the suspension of solids in DST's.

Table C.1. Pressure drop predicted assuming that the slurry has physical properties equal to that of water at standard conditions.

Height of air lift circulator (ft)	Pressure Drop $P_3 - P_1$ (Pa)	
	Based on C.3	Based on C.18
22	6.57×10^4	6.23×10^4
17	5.04×10^4	4.81×10^4

Table C.2. Pressure drop predicted assuming that the slurry has a specific gravity of s.g.= 2; other properties same as Table C.1.

Height of air lift circulator (ft)	Pressure Drop $P_3 - P_1$ (Pa)	
	Based on C.3	Based on C.18
22	1.31×10^5	1.26×10^5

Table C.3. Pressure drop predicted assuming that the slurry has a viscosity of 2 cP; other physical properties same as Table C.1.

Height of air lift circulator (ft)	Pressure Drop $P_3 - P_1$ (Pa)	
	Based on C.3	Based on C.18
22	6.57×10^4	6.23×10^4

C.4 REFERENCES

Eyler, L.L. 1984. Three-Dimensional Numerical Simulation of Settling and Resuspension of Solids in Storage Tanks with Air Injection Circulators. PNL-SA-11586, Pacific Northwest Laboratories, Richland, Washington. Presented at the Slurry Transport Association Ninth International Technical Conference on Slurry Transportation March 1984.

Eyler , L. L. 1983. Sediment Settling and Resuspension in Waste Storage Tanks with Air Injection Circulators. FATE-83-109, Pacific Northwest Laboratories, unpublished, Richland, Washington.

Govier, G.W. and K. Aziz. 1987. **The Flow of Complex Mixtures in Pipes.** Krieger Publishing Company, Malabar, Florida

George, K. , R.P. Raven M. Tiffany, and L.E. Ross. 1996. Tank Farm Plant Operating Procedure. TO-200-030 Rev. E-7.

Ros, N.C.J. J. 1961 Petrol. Technology **13**, 1037

Duns, H, and R.C.J. Ros. 1963 Sixth World Petroleum Congress, Section 2, Paper No. 22, Frankfurt

This page intentionally left blank.

APPENDIX D

PATHWAYS OF IRON HYDROXIDES, OXYHYDROXIDES, AND OXIDES

This page intentionally left blank.

APPENDIX D

LIMITED SOLUBILITY SOLID PHASES IN HANFORD WASTE TANK SLUDGES

D.1 HANFORD SLUDGE CHARACTERIZATION STUDIES

The high-level waste (HLW) generated during the plutonium separation process was rapidly neutralized (caustic strike—direct, or reverse) before storage in waste tanks. Direct caustic strike involved adding caustic (sodium hydroxide containing unknown concentrations of sodium carbonate) to the waste whereas, reverse caustic strike involved titrating the acidic waste into a caustic solution. Experimental data from literature indicate that such rapid neutralization of iron and aluminum containing acidic solutions results in the formation of microcrystalline/x-ray amorphous compounds of limited solubilities. These compounds may consist of hydroxides, silicates, phosphates, and carbonates depending on the types and concentrations of various ligands present in the waste streams. In addition to iron and aluminum, other dissolved metals such as bismuth, cerium, chromium, lanthanum, manganese, lead, nickel, uranium, and zirconium that were present in the acid waste streams upon neutralization may have precipitated as compounds of limited solubilities (hydroxides, oxyhydroxides, silicates, and phosphates).

Recently, sludge samples from a number of Hanford Site waste tanks have been collected and characterized as to their physical and chemical properties (Colton et al. 1994, Liu et al. 1995, Lumetta et al. 1996, Temer and Villareal 1995, 1996). These tanks have been categorized based on the major type of waste being stored (Hill et al. 1995). The waste types and the grouping of these sludge-characterized tanks (19 single-shell and 4 double-shell tanks) are tabulated in Tables D-1 and D-2). According to Hill et al. (1995), group I (consisting of 22 single-shell tanks [SST]) is the most significant category of tanks because it contains (by volume) 37 percent of salt cake, 12 percent of sludge, 21 percent of supernatant, 42 percent of interstitial liquid, and 28 percent of the total waste volume of all the 149 single-shell tanks.

The characterization of sludges from 21 SST, and 4 DST conducted by Colton et al. (1994), Liu et al. (1995), Lumetta et al. (1996), Temer and Villareal (1995, 1996) consisted of measuring physical properties such as the settling properties and size distribution of particles. Also, the chemical characterization of sludges included total chemical and radiological analyses, solubilities in water and in an alkaline solution, compound identification using x-ray and electron diffraction, and chemical analyses using electron beam techniques (scanning and transmission electron microscopy with x-ray analysis). Both water soluble and insoluble solid phases were identified in these characterization studies. However, data collected about only water-insoluble solid compounds (from sludges) are listed in Table D-3.

The data shows that aluminum in Hanford Site waste tank sludges may exist in a number of compounds of limited solubilities such as, aluminum hydroxide, boehmite [α-AlOOH], amorphous and crystalline aluminosilicates of variable composition, sodium aluminate [$NaAl(OH)_4$], variscite [$AlPO_4 \cdot 2H_2O$], chromium-substituted gibbsite [$Al_{(1-x)}Cr_x(OH)_3$], and cancrinite [$Na_4Al_3(SiO_4)_3CO_3$].

Table D-1. Types of Wastes Stored in Selected Single- and Double-Shell Hanford Site Tanks.

SORWT Group[a]	Tank #	Waste types[b]				Watch List Status[c]
		Primary	Secondary	Tertiary	Other	
I	S-107	R	EB	CW	IX-MIX	N
III	BY-104	TBP-F	EB-ITS	CW	IX	F
III	BY-110	TBP-F	EB-ITS	1C	CW	F
IV	S-104	R	-	-	-	N
IV	SX-108	R	-	-	-	H
V	BX-105	TBP	CW	IX	EB	N
V	BX-109	TBP	CW	1C	IX	N
VII	B-202	224	-	-	-	N
X	C-107	1C	CW	SRS	-	N
X	T-107	1C	CW	R	LW	F
X	U-110	1C	CW	R	LW	N
XII	BX-107	1C	TBP	CW	IX	N
XIII	C-108	TBP-F	1C	CW	OWW	F
XIII	C-109	TBP-F	1C	CW	IX	F
XIII	C-112	TBP-F	1C	CW	IX	F
XV	T-111	2C	224	DW	-	O
XVI	B-110	2C	5-6	FP	IX	N
XVI	B-111	2C	5-6	FP	IX	N
XXII	TY-104	TBP	1C-F	DW	MIX-R	F
Ungrouped	B-104	2C	EB	TBP	1C	N
Ungrouped	T-104	1C	-	-	-	N
DS tank	AW-105	PL	CWR	EB	DW	N
DS tank	SY-101	R	EB	DW	CW	G
DS tank	SY-102	DW	Z	-	-	N
DS tank	SY-103	R	EB	DW	CW	G

[a]Groupings based on Hill et al. (1995)
[b]See Table D-2 for waste definitions. Tanks may contain wastes from several processes. Primary: Waste contribiting to the highest sludge volume, Secondary: Waste contribiting to the second highest sludge volume, Tertiary: Waste contribiting to the third highest sludge volume, Other: Mixture of wastes contributing lesser sludge volumes.
[c]F: ferrocyanide, G: Gas generation, H: High-heat, N: Non-watch status, O: Organics.

Table D-2. Description of Selected Waste Types Stored in Hanford Site Waste Tanks.

Waste	Description
1C	First decontamination cycle waste from $BiPO_4$ process (~24% is cladding waste)
1C-F	1C waste scavenged with ferrocyanide additions
2C	Second decontamination cycle waste from $BiPO_4$ process
224	Final decontamination waste from $BiPO_4$ process
5-6	Waste from Tank 5-6 at B Plant resulting boil-over from $BiPO_4$ process
CW	Aluminum cladding waste (after 1964 Zircalloy cladding) from PUREX process
CWR	Cladding (aluminum and zircalloy) waste from REDOX process
DW	Decontamination waste from T Plant containing mainly 0.24M $NaNO_2$ solution
EB	Slurry product from the evaporators
EB-ITS	In-tank solidifed EB waste
FP	Fission products waste produced in B Plant and Hot Semiworks
IX	Ion exchange waste from the cesium recovery process at the B Plant
IX-MIX	IX and miscellaneous wastes
LW	Waste from the 222-S Laboratory
MIX-R	Miscellaneous waste with R waste (high-level waste from the REDOX process)
OWW	Organic solvent wash waste from the PUREX Plant
PL	Low-level waste from PUREX plant
R	High-level waste from the REDOX process
SRS	Sludge feed from strontium-extraction process at the B Plant
TBP	Uranium extraction process waste from U Plant
TBP-F	Uranium extraction process waste from U Plant, scavenged with ferrocyanide additions
Z	Plutonium Finishing Plant waste

This page intentionally left blank.

Table D-3. Compounds of Limited Solubility Identified in Selected Hanford Waste Tank Sludges. (2 sheets)

Compounds		Hanford Waste Tanks (Characteristic Groups based on SORWT Model[a])																								
		I	III		IV		V		VII	X			XII	XIII			XV	XVI		XXII	Ungrouped		Double Shell Tanks			
Name	Composition	S-107	BY-104	BY-110	S-104	SX-108	BX-105	BX-109	B-202	C-107	T-107	U-110	BX-107	C-108	C-109	C-112	T-111	B-110	B-111	TY-104	B-104	T-104	AW-105	SY-101	SY-102	SY-103
Al-hydroxide	$Al(OH)_3$			●			●	⊖				●	⊕	●	●	●			⊕			⊕	⊖		⊕	⊕
Boehmite	AlOOH	●	●		●	●			⊖	●[b]	●	●			●	⊖							●		●[b]	
Al-silicate (am)	variable	⊖	⊕			⊕				⊕			●									●				●
Al-silicate (cr)	variable				⊖[c]		●				●		●	⊖	⊖	⊖[d]			⊖	⊕	⊕	●[e]	⊖		⊖	
Na Aluminate	$NaAl(OH)_4$											⊖												●		
Variscite	$AlPO_4 \cdot 2H_2O$										⊖		●									●				
Cr- gibbsite	$Al_{(1-x)}Cr_x(OH)_3$																							●	●	⊖
Cancrinite	$Na_4Al_3(SiO_4)_3CO_3$											⊕			⊕	⊖			⊖							
Ferrihydrite	$Fe(OH)_3$												●			●	●	●	●	●		●	⊖		⊖	
Goethite	α-FeOOH	⊕	⊕	●[f]	⊖	⊕	●	●		●		⊕		⊕	⊕		●						⊕		⊕[g]	
Fe-Bi silicate	$Fe_2Bi(SiO_4)_2OH$			⊕[h]					●[i]		●		●				●		●		●	●				
Fe-Bi phosphate	?										⊖		⊕					●[j]								
Cr- ferrihydrite	$Fe_{(1-x)}Cr_x(OH)_3$		⊖										⊖				⊖					⊖	⊖			
Jacobsite	Fe_2MnO_4					⊕						⊕[k]					⊖									
Theophrastite	$Ni(OH)_2$		⊖	⊖										●	⊕	⊖			⊖	⊖						
Bi Oxide	Bi_2O_3											⊕[l]	⊕		⊕		⊕		⊖[m]	●						
Uranyl hydroxide	$UO_2(OH)_2$	●	⊖[n]	●[n]	⊖	●	●	●			●			⊕		●[n]				●	⊕				⊖	
Calcite/aragonite	$CaCO_3$						⊕								⊕[p]	●							⊖			
Hydroxyapatite	$Ca_5(PO_4)_3OH$		●	●				⊕	⊖					●	⊕	●[p]	●			⊖					⊖[q]	
La- Pyrophosphate	$La_4(P_2O_7)_3$																⊕									

Table D-3. Compounds of Limited Solubility Identified in Selected Hanford Waste Tank Sludges. (2 sheets)

Compounds		Hanford Waste Tanks (Characteristic Groups based on SORWT Model[a])																								
		I	III		IV		V		VII	X			XII	XIII			XV	XVI		XXII	Ungrouped		Double Shell Tanks			
Name	Composition	S-107	BY-104	BY-110	S-104	SX-108	BX-105	BX-109	B-202	C-107	T-107	U-110	BX-107	C-108	C-109	C-112	T-111	B-110	B-111	TY-104	B-104	T-104	AW-105	SY-101	SY-102	SY-103
Zr Oxidehydrate	$ZrO_2 \cdot xH_2O$	⊕								⊕													●			
Pb-OH-phosphate	$Pb_5(PO_4)_3OH$									⊕					⊕											
Grimaldite	CrOOH			⊕								⊖						⊕								
+Quartz	SiO_2														⊕	⊖									⊖	

●: >10 wt %, ⊕: 2 - 9 wt%, ⊖: <2 wt%. [a]SORWT Model -applicable to only single shell tanks (Hill et al. 1995). [b]$(Al_2O_3)_x \cdot y\ H_2O$, [c]K-Al silicate (Temer and Villarreal, 1995), [d]$NaAlSi_3O_8$ and $Al_2Si_2O_5(OH)_4$, [e]Na-Al silicate, [f]maghemite (γ-Fe_2O_3), [g]akagenite (β-FeOOH),

[h]Fe-silicate (amorphous), [i]Mn-La-Fe-Bi silicate (Temer and Villareal, 1995), [j]$BiPO_4$, [k] $Fe_{(1-x)}Mn_xOOH$, [l]$Bi_{(1-x)}Mn_xO_3$, [m]$Bi_{(1-x)}Cr_x(OH)_3$, [n]β-U_3O_8, [o]$CaSO_4$, [p]hydroxyapatite and $Mg_3(PO_4)_2$, [q]$CaFPO_3 \cdot 2H_2O$, [r]$SiO_2 \cdot x\ H_2O$ (amorphous),

Data Sources: AW-105, B-111, BX-107, C-112, S-104, SY-101, SY-102, SY-103, T-104, and T-111 (Liu et al. 1995). B-110, C-109, C-112, and U-110 (Colton et al., 1994). BY-104, BY-110, C-107, S-107, and SX-108 (Lumetta et al. 1996).

B-104, B-202, BX-105, BX-109, C-108, S-104, T-107, and TY-104 Temer and Villarreal, 1995, 1996)

Many of these compounds may have formed initially on caustic additions to the acidic wastes. Some of these compounds may also have formed from alteration of precipitated compounds during decades of aging within the tank environment.

D.2 ALUMINUM-CONTAINING SOLID PHASES

Precipitation experiments conducted by Barnhisel and Rich (1965), and Hsu (1966) indicated that rapid caustic addition (resulting in neutral or alkaline conditions) to Al-bearing solutions results in precipitation of bayerite [β-$Al(OH)_3$] or nordstrandite [γ-$Al(OH)_3$] or both whereas, slow caustic titration (with pH conditions below neutral) precipitates gibbsite [α-$Al(OH)_3$]. Hsu (1977) also indicated that if anions such as phosphate and silicate are present during neutralization, phases such as phosphates and silicates may form instead of hydroxide phases. Other experimental data obtained by Hsu (1966) and Chesworth (1972), showed that neutralization of aluminum-containing high ionic strength solutions result in the formation of boehmite-like (pseudoboehmite) precipitates. Presence of carboxylic acids also promotes the formation of pseudoboehmite (Kodama and Schnitzer, 1980; Violante and Violante, 1980; Kwong and Huang 1981; Violante and Huang 1985). Data obtained by Violante and Violante (1980) showed that the type of carboxylic acid, the molar ratio of Al to carboxylic acid, and the pH influence the type of aluminum hydroxide precipitates.

Data from the Hanford waste tanks (Table D-3) indicate that boehmite (α-AlOOH) is the dominant Al-bearing solid phase in many of the tanks which have high ionic strength conditions thus conforming with experimental observations of Hsu (1977) and Chesworth (1972). In waste tanks (U-110, C-109, C-112, AW-105, and SY-102) in which aluminum hydroxide or aluminum silicate phases coexist with boehmite, it likely that all these phases are at equilibrium, or phase conversion may be occurring indicating disequilibrium conditions. In some of the tanks aluminosilicate phases seem to predominate indicating the influence of silicate in controlling the nature of precipitating aluminum-solid phases. It is interesting to note that in tanks BX-107 and T-104, the dominant aluminum-solid phases are the silicates and phosphates, which suggests that other ligands are present during the rapid neutralization of waste streams results in solid phases other than hydroxides or oxyhydroxides. Phase stability relationships (Lindsay 1979) suggest that varicite [$AlPO_4 \cdot 2H_2O$] may have existed in certain Hanford Site waste streams even before the caustic strike. One of the waste tanks (SY-101) contains a sodium aluminate phase. Occurrence of this phase has been attributed to very high hydroxyl concentrations (Liu et al. 1995). Minor to trace amounts of cancrinite has been found in some of the tanks (U-110, C-109, C-112, and B-111). Because we lack experimental data it is difficult to assess whether cancrinite was one of the initial aluminum-bearing solid phases that precipitated during the neutralization process or formed during the decades-long aging of sludges.

D.3 IRON-CONTAINING SOLID PHASES

Our literature review indicated that significant amount of data exists about the formation and transformation of iron hydroxides, oxyhydroxides, and oxides. The data has been summarized by Schwertmann and Taylor (1989) and Schwertmann and Cornell (1991). The formation and transformation pathways for various hydrolytic iron compounds are schematically shown in Figure D-1. Available data (Schwertmann and Cornell 1991) indicate that the formation of iron hydroxide, oxyhydroxide, and oxide phases depend mainly on Eh-pH conditions, presence of ligands, rate of oxidation, time and temperature during aging of precipitates. The data indicate that rapid neutralization of acidic Fe(III) solutions results in the formation of ferrihydrite. Depending on pH and temperature conditions ferrihydrite is known to transform into either goethite or hematite. This is the most probable pathway for the formation of iron hydroxide and oxyhydroxide compounds in Hanford HLW. When subjected to caustic strikes and concomitant high pH conditions, Fe(III) containing HLW may have initially precipitated ferrihydrite-like compounds. On aging this precipitate subsequently may have altered to goethite and/or hematite. Sludge characterization data (Table D-3) show that in a number of waste tanks, goethite is the principal Fe-oxyhydroxide phase. Presence of goethite indicates almost a complete transformation of ferrihydrite in these tank sludges. Other tanks (BX-107, C-112, T-111, B-110, B-111, T-104, and AW-105) contain mainly ferrihydrite or a mixture of ferrihydrite and goethite suggesting that no or partial transformation of initially precipitated iron-hydroxide material. Maghemite (γ-Fe_2O_3) has been identified in tank BY-110 sludge indicating a transformation pathway either through the initial formation of green rust or magnetite. Also, akaganeite (ß-FeOOH) has been found as the principal iron-bearing phase in sludge from tank SY-102 indicating partial neutralization and aging in the presence of chloride. Iron also occurs as a ferric bismuth silicate solid phase in a number of tanks (T-107, BX-107, T-111, B-111,B-104, and T-104) that contain neutralized waste streams from the bismuth phosphate process. A few tanks contain minor or trace amounts of iron-bismuth phosphate. In some cases, ferric bismuth silicate and ferric bismuth phosphate phases coexist with ferric-hydroxide and oxyhydroxide phases. Such coexistence of iron-bearing solid phases in tank sludges suggests that the presence of other cationic and anionic constituents such as bismuth, silicon, and PO_4 in waste streams also control the type of iron solid phases that precipitate.

D.4 OTHER SOLID PHASES

Data in Table D-3 show that U in HLW waste streams has precipitated mainly as a hydroxide except in two cases (BY-110, and C-112) where U is found as an oxidic phase (ß-U_3O_8). Bismuth in wastes originating from bismuth phosphate process is found in the form of bismuth oxide, ferric bismuth silicate, bismuth phosphate, and ferric bismuth phosphate. Lanthanum in sludges has been detected in the form of pyrophosphates (AW-105, T-111). Zirconium in neutralized cladding removal wastes apparently precipitates as a hydrated oxide (S-107, C-107, AW-105). Other waste stream constituents such as calcium and lead, have been found mainly in the form of hydroxyphosphate.

Figure D-1. Formation and Transformation Pathways of Iron Hydroxides, Oxyhydroxides, and Oxides.

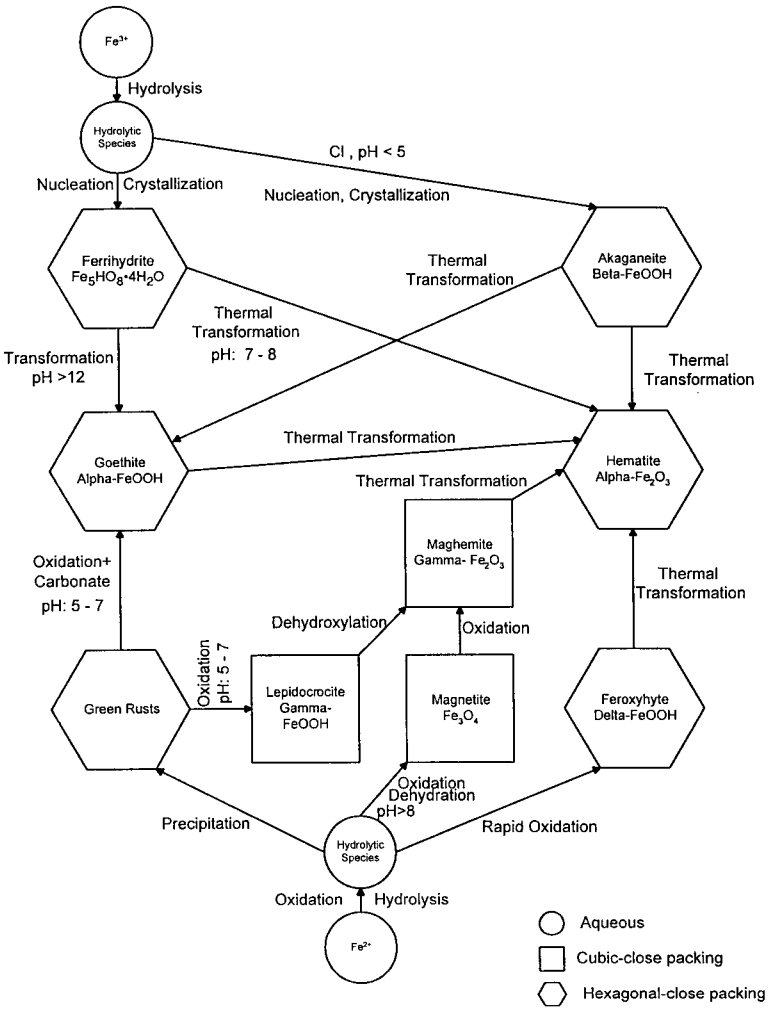

Minor constituents in the waste streams, such as chromium and manganese, have been found either as a pure phase or as solid solutions with major components. For instance, chromium occurs as grimaldite (CrOOH) in sludges of waste tanks BY-110, U-110, and B-110 whereas, it is found in solid solution forms with aluminum (SY-101, SY-102, and SY-103), iron (BY-104, BX-107, T-111, T-104, and AW-105), and bismuth (B-111). Manganese is found in solid solution phases with iron (SX-108, U-110, T-111), and bismuth (U-110).

Solid phases of plutonium and other radionuclides present in trace concentrations in sludges were not detected because of limitations of the analytical techniques used in the characterization studies. Depending on the solid matrix, compound identification using XRD requires each phase be present at least 1 wt%. Electron beam techniques (SEM and TEM) can detect compounds if they are present in minimum concentrations of 0.1% by weight. Because total concentrations of plutonium in Hanford Site sludges are well below these detection limits, it is not feasible to detect plutonium solid phases, unless these solids are separated and concentrated using appropriate processes. However, we can expect that plutonium solid phase forms in the sludges will be analogous to the solid phases of minor elements (plutonium can exist either as a pure phase or as solid solution phases) depending on the electrolyte chemistry of the waste stream, rate and degree of neutralization, and time and temperature of aging of resulting sludges.

In summary, the compound identification data collected from the sludge characterization studies indicates that

- On rapid neutralization, aluminum and iron (major components of acidic waste streams) precipitate as hydroxides, silicates, and phosphates. These compounds occur as pure and solid solution phases depending on the waste chemistry (type and concentrations of other constituents such as bismuth, chromium, and manganese).

- Microcrystalline aluminum and iron hydroxide phases upon aging transform into crystalline phases such as boehmite and goethite.

- Uranium in sludges occurs mainly as a hydroxide phase and in three cases as an oxide phase.

- Minor constituents in waste streams (chromium and manganese) occur as pure phases and also as solid solutions with major constituents (aluminum, iron, and bismuth) as a function of waste chemistry.

- Although solid phases of plutonium and other trace constituents were not identified (because of limitations in analytical techniques) in sludges, by analogy, plutonium in sludges is expected to occur as a pure phase or as solid solutions.

D.6 REFERENCES

Barnhisel, R. I., and C. I. Rich, 1963, "Gibbsite Formation from Aluminum Interlayers in Montmorillonite," *Soil Sci. Soc. Am. Proc.*, Vol. 27, pp. 632-635.

Chesworth, W., 1972, "The Stability of Gibbsite and Boehmite at the Surface of the Earth," *Clays and Clay Miner*, Vol. 20, pp. 369-374.

Colton, N. G., 1994, *Estimated Bulk Compositions for SST Sludges*, TWRSPP-94-086, "Tank Waste Treatment Science: Report for the Fourth Quarter FY 1994," Pacific Northwest Laboratory, Richland, Washington.

Hill, J. G., G. S. Anderson, and B. C. Simpson, 1995, *The Sort on Radioactive Waste Type Model: A Method to Sort Single-Shell Tanks into Characteristic Groups*, PNL-9814, Rev. 2, Pacific Northwest Laboratory, Richland, Washington.

Hsu, P. H., 1966, "Formation of Gibbsite from Aging Hydroxy-Aluminum Solutions," *Soil Sci. Soc. Am. Proc*, Vol. 30, pp. 173-176.

Hsu, P. H., 1977, "Aluminum Hydroxides and Oxyhydroxides," in *Minerals in Soil Environments*, Soil Sci. Soc. Am., Madison, Wisconsin.

Kodama, H., and M. Schnitzer, 1980, "Effect of Fulvic Acid on the Crystallization of Aluminum Hydroxide," *Geoderma*, Vol. 24, pp. 195-205.

Kwong K. F., and P. M. Huang. 1981. Comparison of the Influence of Tannic Acid and Selected Low-molecular Organic Acids on Precipitation Products of Aluminum. *Geoderma*, Vol. 26, pp. 179-193.

Lindsay, W. L. 1979, *Chemical Equilibria in Soils*, John Wiley & Sons, New York, New York.

Liu, J, L. E. Thomas, Y. L. Chen, and L. Q. Wang, 1995, *Sludge Characterization Studies*, TWRSPP-95-019, "Tank Waste Treatment Science: Report for the Third Quarter FY 1995," Pacific Northwest Laboratory, Richland, Washington.

Lumetta, G. J., B. M. Rapko, M. J. Wagner, J. Liu, and Y. L. Chen, 1996, *Washing and Caustic Leaching of Hanford Tank Sludges: Results of FY 1996 Studies*, PNNL-11278, Pacific Northwest National Laboratory, Richland, Washington.

Schwertmann U. and R. M. Taylor, 1989, "Iron Oxides," in *Minerals in Soil Environments*, Soil Sci. Soc. Am., Madison, Wisconsin.

Schwertmann, U. and R. M. Cornell, 1991, *Iron Oxides in the Laboratory*. Verlagsgesellschaft mbH, VCH Publishers, Weinheim, Germany.

Temer, D. J. and R. Villareal, 1995, *Sludge Washing and Alkaline Leaching Tests on actual Hanford Tank Sludge: A Draft Report on Samples TY-104 and C-107*, LAUR-95-3211, Los Alamos National Laboratory, Los Alamos, New Mexico.

Temer, D. J. and R. Villareal, 1996, *Sludge Washing and Alkaline Leaching Tests on actual Hanford Tank Sludge: A Draft Report on Samples B-104 and BX-109*, LAUR-96-1986, Los Alamos National Laboratory, Los Alamos, New Mexico.

Violante, A. and P. Violante, 1980, "Influence of pH, Concentration and Chelatng Power of Organic Anions on the Synthesis of Aluminum Hydroxides and Oxyhydroxides," *Clays and Clay Miner*, Vol. 28, pp. 425-434.

Violante, A. and P. M. Huang, 1985, "Influence of Inorganic and Organic Ligands on the Formation of Aluminum Hydroxides and Oxyhydroxides," *Clays and Clay Miner*, Vol. 33, pp. 181-192.

APPENDIX E

FUEL PROCESSED AT PUREX AND PUREX-TO-TANK FARM WASTE TRANSFER DATA SINCE 1983

This page intentionally left blank.

APPENDIX E

FUEL PROCESSED AT PUREX AND PUREX-TO-TANK FARM WASTE TRANSFER DATA SINCE 1983

The Appendix E tables contain the quantities of fuel processed through the PUREX dissolvers and solvent extraction system since 1983. Plant transfers to the double shell tank farms are listed by campaign and by month. Waste volumes (both nuclear material control and plant discharge), uranium and plutonium content, average plutonium concentrations, and uranium to plutonium mass ratios are listed by tank farm receiving tank as a summary, by campaign, and by month. Waste transfers for the PUREX plant cleanout after shutdown are also included in these tables.

Table E1 Summary of all Post 1983 Waste Transfers from PUREX to Tank Farms

Table E2 Summary and Monthly Transfers of E5 (Zirflex Decladding) Waste to Tank Farms

Table E3 Summary and Monthly Transfers of F16 (Neutralized Zirflex Current Acid) Waste to Tank Farms

Table E4 Summary and Monthly Transfers of F18 (Canyon Sump) Waste to Tank Farms

Table E5 Summary and Monthly Trnasfers of G8 and R8 (Organic Wash) Waste to Tank Farms

Table E6 Summary and Monthly Transfers of U3 and U4 (Acid Fractionator Sump) Waste to Tank Farms

This page intentionally left blank.

Table E-1. Summary of all Post 1983 Waste Transfers from PUREX to Tank Farms (includes Campaigns A01 thru A06 and cleanout period). (4 sheets)

Waste stream	AW-101	AW-102	AW-103	AW-104	AW-105	AY-101	AY-102	AZ-101	AZ-102	AZ-103	AN-102	AP-108	Totals
Summary of plutonium (g)													
E5	22		4548	193	3897				1				8661
F18	3434	759	58	4405	7813	9		36	289		0	26	16829
F16	8	246		628		22	65	9700	6974	118			17761
G8&R8	467	80	1	1103	43						0		1694
U3&U4	89	7	0	7	82							0	185
TOTALS	4020	1092	4607	6336	11835	31	65	9736	7264	118	0	26	45130
Summary of uranium (g)													
E5	18742		7190155	73981	4415113				3529				11701520
F18	4546538	1457180	75397	10838714	16103448	24377		59610	599343		2434	117486	33824527
F16	30500	6372		130193		7526	14833	1408938	2111285	72317			3781964
G8&R8	1751155	430116	15133	2730977	2222685						3673		7153739
U3&U4	33735	12634	107	21915	248169							1923	318483
TOTALS	6380670	1906302	7280792	13795780	22989415	31903	14833	1468548	2714157	72317	6107	119409	56780233
U/Pu	1587	1746	1580	2177	1942	1029	228	151	374	613	#DIV/0!	4593	1258
Summary of transfer volumes (L)													
E5	25511	0	9919701	208889	6316039	0	0	0	11008	0	0	0	16481148
F18	2005863	524415	28970	5090256	2643106	8599	0	36463	31230	0	23289	152757	10544948
F16	31458	19657	0	138622	0	8036	168533	2357827	1270276	28374	0	0	4022783
G8&R8	4649600	1259075	12934	6252267	2808527	0	0	0	0	0	19224	0	15001627
U3&U4	3327744	817749	28526	4324354	1863554	0	0	0	0	0	0	112945	10474872
TOTALS	10040176	2620896	9990131	16014388	13631226	16635	168533	2394290	1312514	28374	42513	265702	56525378

Table E-1. Summary of all Post 1983 Waste Transfers from PUREX to Tank Farms (includes Campaigns A01 thru A06 and cleanout period). (4 sheets)

Waste stream	AW-101	AW-102	AW-103	AW-104	AW-105	AY-101	AY-102	AZ-101	AZ-102	AZ-103	AN-102	AP-108	Totals
E-5 Transfer volumes (L)													
Campaign 1		4070		2704819		907776							
Campaign 2		21441		2312351		1646763							
Campaign 3				181964		920118							
Campaign 4				1884678		1383010							
Campaign 5				497723	191949	466870							
Campaign 6				2319928		991502				11008			
Cleanout Period				18238	16940								
TOTALS		25511	0	9919701	208889	6316039	0	0	0	11008	0	0	0
F-18 Transfer volumes (L)													
Campaign 1		276285				931108							
Campaign 2		1075453	48302				8599		21475				
Campaign 3		207162	63299						14988				
Campaign 4		446963	412814	14964	151508					9623			
Campaign 5					1227478								
Campaign 6				14006	3486133					10773			
Cleanout Period					225137	1711998				10834		23289	152757
TOTALS		2005863	524415	28970	5090256	2643106	8599	0	36463	31230	0	23289	152757

Table E-1. Summary of all Post 1983 Waste Transfers from PUREX to Tank Farms (includes Campaigns A01 thru A06 and cleanout period). (4 sheets)

Waste stream	AW-101	AW-102	AW-103	AW-104	AW-105	AY-101	AY-102	AZ-101	AZ-102	AZ-103	AN-102	AP-108	Totals
F-16 Transfer volumes (L)													
Campaign 1		18126					8036	9388	802173	56155			
Campaign 2		13332							1099326				
Campaign 3									287940		28374		
Campaign 4			19657					16151	168388	501329			
Campaign 5								43293		313157			
Campaign 6					123496			99701		399635			
Cleanout Period					15126								
TOTALS		31458	19657	0	138622	0	8036	168533	2357827	1270276	28374	0	0
G8 & R8 Transfer volumes (L)													
Campaign 1		1065130		12934		2797761							
Campaign 2		2586881	73276			10766							
Campaign 3		456404	236602										
Campaign 4		541185	949197		518115								
Campaign 5					2318154								
Campaign 6					3298801								
Cleanout Period					117197							19224	
TOTALS		4649600	1259075	12934	6252267	2808527	0	0	0	0	0	19224	0

Table E-1. Summary of all Post 1983 Waste Transfers from PUREX to Tank Farms (includes Campaigns A01 thru A06 and cleanout period). (4 sheets)

Waste stream	AW-101	AW-102	AW-103	AW-104	AW-105	AY-101	AY-102	AZ-101	AZ-102	AZ-103	AN-102	AP-108	Totals
U3 & U4 Transfer volumes (L)													
Campaign 1		321667				1272155							
Campaign 2		2148109	97983	28526		91847							
Campaign 3		137413	157533										
Campaign 4		720555	536911		278115								
Campaign 5					1694447								
Campaign 6			25322		1863485								
Cleanout Period					488307	499552							112945
TOTALS		3327744	817749	28526	4324354	1863554	0	0	0	0	0	0	112945

Table E-2A. Summary and Monthly Transfers of E5 (Zirflex Decladding) Waste to Tank Farms (includes cleanout period)
Summary of E5 Waste for Campaigns A01 thru A06.

	Campaign #							
	A01	A02	A03	A04	A05	A06		
NMC Data								
Vol (L) =	3616665	3980555	1102083	3267687	1156542	3322438	16445970	35178
Pu (g) =	1900	1397	725	1931	1236	1449	8638	23
U (kg) =	4105.164	3050.21	608.837	2032.081	550.827	1350.285	11697.404	38.951
MTU =	992.0	1119.7	212.3	868.15	125.68	550.742	3868.572	0
Tank E-5 Vol (L)=	4231252	5043354	1443518	4363915.9	1526388	4628647	21237075	45564
Plant Vol (incl Jet Dilution) (L)=	4442814.6	5295521.7	1515693.9	4582111.7	1602707.4	4860079.4	22298929	47842
Plant to NMC Waste vol ratio =	1.23	1.33	1.38	1.40	1.39	1.46	1.36	1.36
Plant Waste Volume (L) per MTU=	4479	4729	7139	5278	12752	8825	5764	not applicable
Avg Pu g/Plant L=	0.000428	0.0002638	0.0004783	0.0004214	0.0007712	0.0002981	0.0003874	0.0004807
Avg U g/Plant L=	0.924	0.576	0.402	0.443	0.344	0.278	0.525	0.814
Avg U to Pu Ratio =	2161	2183	840	1052	446	932	1354	1694

Note:

Plant Vol for Cleanout Period has been calculated by multiplying NMC vol by 1.36/1.05 (the avg ratio for the Campaigns).

Table E-2B. Summary and Monthly Transfers of E5 (Zirflex Decladding) Waste to Tank Farms (includes cleanout period)
Summary of E5 Waste for Campaigns A01 thru A06.

Tank #	A01			A02			A03			A04		
	NMC Pu (g)	NMC U (g)	U/Pu	NMC Pu (g)	NMC U (g)	U/Pu	NMC Pu (g)	NMC U (g)	U/Pu	NMC Pu	NMC U (g)	U/Pu
AW-101	0	5252	#DIV/0!	22	13490	613						
AW-103	1379	2935054	2128	750	1583943	2112	67	75168	1122	929	1162195	1251
AW-104												
AW-105	521	1164858	2236	625	1452777	2324	658	533669	811	1002	869886	868
AZ-102												
TOTALS	1900	4105164	2161	1397	3050210	2183	725	608837	840	1931	2032081	1052

Tank #	A05			A06			Tank totals for all campaigns			Cleanout period		
	NMC Pu (g)	NMC U (g)	U/Pu	NMC Pu (g)	NMC U (g)	U/Pu	NMC Pu (g)	NMC U (g)	U/Pu	NMC Pu	NMC U (g)	U/Pu
AW-101							22	18742	852			
AW-103	582	277763	477	820	1156032	1410	4527	7190155	1588	21	34835	1659
AW-104	191	69865	366				191	69865	366	2	4116	2058
AW-105	463	203199	439	628	190724	304	3897	4415113	1133			
AZ-102				1	3529	3529	1	3529	3529			
TOTALS	1236	550827	446	1449	1350285	932	8638	11697404	1354	23	38951	1694

Table E-2C. Summary and Monthly Transfers of E5 (Zirflex Decladding) Waste to Tank Farms (includes cleanout period)
Summary of E5 Waste for Campaigns A01 thru A06.

Month	NMC volume transfers (L)				NMC Pu (g)				NMC U (g)					PUREX summary volumes (L)	Plant to NMC waste vol ratio	Processed fuel HE MTU
	AW-101	AW-103	AW-105	Total	AW-101	AW-103	AW-105	Total	AW-101	AW-103	AW-105	Total	U/Pu			
Sep-83				0				0				0	#DIV/0!	0		
Oct-83		12874		12874				0				0.876	#DIV/0!	14425	1.18	
Nov-83		123196		123196		45		45		0.876		50.569	1124	138039	1.18	incl below
Dec-83		247014		247014		194		194		50.569		369.856	1906	276775	1.18	incl below
Jan-84		441153		441153		256		256		369.856		667.523	2608	494304	1.18	incl below
Feb-84		166133		166133		151		151		667.523		466.703	3091	186149	1.18	incl below
Mar-84		464672		464672		363		363		466.703		267.753	738	609882	1.38	incl below
Apr-84		413513		413513		157		157		267.753		504.9	3216	542736	1.38	474
May-84		289818		289818		70		70		254.795		254.795	3640	380386	1.38	91
Jun-84		355277	7241	362518		59	0	59		185.856	4.392	190.248	3225	475805	1.38	94
Jul-84	4070	84196	366913	455179	0	48	130	178	5,252	66.938	368.147	440.337	2474	597422	1.38	147
Aug-84	0		462492	462492			381	381			761.671	761.673	1999	607021	1.38	incl below
Sep-84	0	106973	71130	178103		36	10	46		99.285	30.646	129.931	2825	233760	1.38	186
Total	4070	2704819	907776	3616665	0	1379	521	1900	5,252	2935.054	1164.858	4105.164	2161	4556703.87	1.32	992

Table E-2C. Summary and Monthly Transfers of E5 (Zirflex Decladding) Waste to Tank Farms (includes cleanout period)
Summary of E5 Waste for Campaigns A01 thru A06.

Notes:

1. HE MTU data was taken from monthly Campaign Reports. Purex Volume information therein did not appear reliable because Volumes reported (although inclusive of chemical addition and flushes) were less than NMC recorded volumes for Nov-Dec '83 and certain other months.

2. The Flowsheet data and sample analyses were used to calculate factors which were multiplied by NMC volumes to give Plant Transfer volumes.

   For Oct 83 to Feb-84 the factor was (1000+8300)/8300 = 1,120
   For Mar 84 to Sep-84 the factor is 9345/(9364-2245) = 1,313

   Plant to HMC Waste Vol ration includes a further Jet Dilution factor of 1.05.

3. June-84 SX MTU figure has been calculated from Campaign letter report information.

4. ERR implies 0 g Pu yielding an infinite U/Pu ratio.

Table E-2D. Summary and Monthly Transfers of E5 (Zirflex Decladding) Waste to Tank Farms (includes cleanout period)
Summary of E5 Waste for Campaigns A01 thru A06.

Month	NMC volume transfers (L)				NMC Pu (g)				NMC U Loss (kg)					PUREX summary volumes		Processed fuel HE MTU	Processed Fuel HE MTU
	AW-101	AW-103	AW-105	Total	AW-101	AW-103	AW-105	Total	AW-101	AW-103	AW-105	Total	U/Pu	(Gal)	(L)		
Sep-84	0	37668	96446	134114	0	6	12	18	0	19.678	28.871	48.549	2697	incl below	incl below	incl below	42.5
Oct-84	0	0	19816	19816	0	0	2	2	0	0	3.602	3.602	1801	incl below	incl below	incl below	0.0
Nov-84	0	13975	114188	128163	0	32	51	83	0	31.912	161.231	193.143	2327	107200	405752	1.51	24.4
Dec-84	0	0	340531	340531	0	0	144	144	0	0	494.282	494.282	3433	97200	367902	1.13	105.3
Jan-85	0	340929	126130	467059	0	107	46	153	0	404.189	45.705	449.894	2940	147800	559423	1.26	137.5
Feb-85	0	361404	0	361404	0	119	0	119	0	290.59	0	290.59	2442	115300	436411	1.27	95.4
Mar-85	0	443780	0	443780	0	117	0	117	0	232.994	0	232.994	1991	147100	556774	1.32	156.1
Apr-85	4817	512895	0	517712	0	131	0	131	0.283	219.093	0	219.376	1675	166000	628310	1.27	138.4
May-85	0	255443	13989	269432	0	84	0	84	0	161.704	0.502	162.206	1931	92200	348977	1.36	65.6
Jun-85	0	166988	0	166988	0	75	0	75	0	59.387	0	59.387	792	59500	225208	1.42	36.5
Jul-85	16624	156901	241228	414753	22	72	144	238	13.207	68.145	184.862	266.214	1119	145739	551621	1.40	111
Aug-85	0	22368	444409	466777	0	7	172	179	0	96.251	362.209	458.46	2561	164019	620813	1.40	144.6
Sep-85	0	0	250026	250026	0	0	54	54	0	0	171.513	171.513	3176	90400	342164	1.44	52.4
CAMPAIGN A02 TOTAL	21441	2312351	1646763	3980555	22	750	625	1397	13.49	1583.943	1452.777	3050.21	2183	1332458.2	5043354.4	1.33	1119.7

E5 Waste Summary for CAMPAIGN A05

NMC Data
Vol (L) = 3980555
Pu (g) = 1397
U (kg) = 3050.21
MTU = 1119.700
Tank E-5 Vol (L) = 5043354
Plant Vol (incl Jet Dilution) (L) = 5295522
Plant to NMC Waste vol ration = 1.33
Plant Waste Volume (L) per MTU = 4729

Notes:

1. Campaign 3 E-5 transfers began in Oct-85.
2. Campaign A01 E-5 transfers ended on Sep 10, 1984.
3. Purex Volume and HE MTU data have been obtained from monthly campaign reports issued as internal letters.
4. July and Aug-85 Volumes have been ratioed from NMC data using a factor of 1.33 (includes 5% Jet Dilution).

Table E-2E. Summary and Monthly Transfers of E5 (Zirflex Decladding) Waste to Tank Farms E-5 Data Tabulations -- Campaigns 3&4.

Month	NMC Volume Transfers (L)			E-5 Volume (Purex Summaries)		Processed Fuel	E-5 Waste Summary for Campaign A03 (Oct-Dec 85)	
	AW-103	AW-105	Total (L)	gal	L	HE MTU	NMC Data	
Oct-85	0	321806.8	321806.8	109483.0	414393.0	65.4	Vol (L) =	1102082.7
Nov-85	0	440219.7	440219.7	154540.5	584935.7	109.7	Pu (g) =	725
Dec-85	181964.3	158091.9	340056.2	117355.1	444189.2	37.2	U (kg) =	608.837
CAMPAIGN A03 TOTAL	181964.3	920118.4	1102082.7	381378.6	1443517.9	212.3	MTU =	212.300
Jan-86	239694.2	0	239694.2	87612.2	331612.1	48.25	Plant Vol (incl Jet Dilution) (L)=	1515693.8
Feb-86	358643.1	25269.4	383912.5	137123.8	519013.7	105.3	Plant to NMC Waste vol ratio =	1.38
Mar-86	256183.6	378736.2	634919.8	223073.9	844334.8	208.9	Plant Waste Volume (L) per MTU=	7139
Apr-86	0	434617.2	434617.2	151697.9	574176.4	104.3	Avg Pu g/Plant L=	0.0004783
May-86	27300.1	357423.2	384723.3	131566.8	497980.3	98.76	Avg U g/Plant L=	0.402
Jun-86	190052	66744.7	256796.7	88647.9	335532.3	65.52	Avg U to Pu Ratio =	840
Jul-86	429347.3	57000.6	486347.9	168519.9	637847.7	131.04		
Aug-86	383457.2	63218.6	446675.8	160719.9	608324.6	105.98		
Sep-86	0	0	0	3987.8	15093.9	0.1		
CAMPAIGN A04 TOTAL	1884677.5	1383009.9	3267687.4	1152950.0	4363915.9	868.15		
	NMC Pu (g)		Total Pu (g)				E-5 Waste Summary for Campaign A04 (Jan-Sep '86)	
Oct-85	0	152	152					
Nov-85	0	350	350				NMC Data	
Dec-85	67	156	223				Vol (L) =	3267687.4
CAMPAIGN A03 TOTAL	67	658	725				Pu (g) =	1931

Table E-2E. Summary and Monthly Transfers of E5 (Zirflex Decladding) Waste to Tank Farms E-5 Data Tabulations -- Campaigns 3&4.

	NMC Volume Transfers (L)			E-5 Volume (Purex Summaries)		Processed Fuel	E-5 Waste Summary for Campaign A03 (Oct-Dec 85)	
							U (kg) =	2032.081
Jan-86	64	0	64				MTU =	868.15
Feb-86	136	5	141				Tank E-5 Vol (L)=	4363915.9
Mar-86	284	329	613				Plant Vol (incl Jet Dilution) (L) =	4582111.7
Apr-86	0	302	302				Plant to NMC Waste vol ratio =	1.40
May-86	10	229	239				Plant Waste Volume (L) per MTU=	5278
Jun-86	59	43	102				Avg Pu g/Plant L=	0.0004214
Jul-86	162	25	187				Avg U g/Plant L=	0.443
Aug-86	214	69	283				Avg U to Pu Ratio =	1052
Sep-86	0	0	0					
CAMPAIGN A04 TOTAL	929	1002	1931					
Oct-85	0	95.949	95.949	631			E5 Waste SUMMARY for CAMPAIGNS A03 & A04	
Nov-85	0	320.203	320.203	915				
Dec-85	75.168	117.517	192.685	864			NMC Data	
CAMPAIGN A03 TOTAL	75.168	533.669	608.837	840			Vol (L) =	4369770.1
							Pu (g) =	2656
Jan-86	122.468	0	122.468	1914			U (kg) =	2640.918
Feb-86	302.924	10.526	313.45	2223			MTU =	1080.45
Mar-86	235.624	153.008	388.632	634			Tank E-5 Vol (L)=	5807433.8
Apr-86	0	268.672	268.672	890			Plant Vol (incl Jet Dilution) (L)=	6097805.5
May-86	21.71	273.616	295.326	1236			Plant to NMC Waste vol ratio =	1.40
Jun-86	80.182	35.319	115.501	1132			Plant Waste Volume (L) per MTU=	5644
Jul-86	262.812	24.527	287.339	1537			Avg Pu g/Plant L=	0.0004356

Month

Table E-2E. Summary and Monthly Transfers of E5 (Zirflex Decladding) Waste to Tank Farms E-5 Data Tabulations – Campaigns 3&4.

	NMC Volume Transfers (L)			E-5 Volume (Purex Summaries)		Processed Fuel	E-5 Waste Summary for Campaign A03 (Oct-Dec 85)	
Aug-86	136.475	104.218	240.693	851			Avg U g/Plant L=	0.433
Sep-86	0	0	0	#DIV/0!			Avg U to Pu Ratio =	994
CAMPAIGN A04 TOTAL	1162.195	869.886	2032.081	1052				
A03 U/Pu	1122	811	840					
A04 U/Pu	1251	868	1052					
A03 & A04 E-5, U/Pu =	1242	846	994					

NOTE:

In reviewing U/Pu ration, the total mass of Pu should also be considered. ERR indicates - g Pu yielding an infinite U/Pu ratio.

Month

Table E-2F. Summary and Monthly Transfers of E5 (Zirflex Decladding) Waste to Tank Farms E-5 Data Tabulations – Campaigns 3&4.

Month	NMC Volume Transfers (L)				E-5 Volume (Purex Summaries)		Plant to NMC Waste Vol Ratio	Processed Fuel
	AW-101	AW-103	AW-105	Total (L)	gal	L		HE MTU
Sep-84	0	37668	96446	134114	incl below	incl below	incl below	42.5
Oct-84	0	0	19816	19816	incl below	incl below	incl below	0.0
Nov-84	0	13975	114188	128163	107200	405752	1.51	34.4
Dec-84	0	0	340531	340531	97200	367902	1.13	105.3
Jan-85	0	340929	126130	467059	147800	559423	1.26	137.5
Feb-85	0	361404	0	361404	115300	436411	1.27	95.4
Mar-85	0	443780	0	443780	147100	556774	1.32	156.1
Apr-85	4817	512895	0	517712	166000	628310	1.27	138.4
May-85	0	255443	13989	269432	92200	348977	1.36	65.6
Jun-85	0	166988	0	166988	59500	225208	1.42	36.5
Jul-85	16624	156901	241228	414753	145739	551621	1.40	111
Aug-85	0	22368	444409	466777	164019	620813	1.40	144.6
Sep-85	0	0	250026	250026	90400	342164	1.44	52.4
CAMPAIGN A02 TOTAL	21441	2312351	1646763	3980555	1332458.23	5043354.4	1.33	1119.7
Month	NMC Pu (g)				E5 Waste Summary for CAMPAIGN A05			
Sep-84	0	6	12	18				
Oct-84	0	0	2	2	NMC Data			
Nov-84	0	32	51	83	Vol (L) =			3980555
Dec-84	0	0	144	144	Pu (g) =			1397
Jan-85	0	107	46	153	U (kg) =			3050.21
Feb-85	0	119	0	119	MTU =			1119.700
Mar-85	0	117	0	117	Tank E-5 Vol (L)=			5043354.4
Apr-85	0	131	0	131	Plant Vol (incl Jet Dilution) (L)=			5295522.12

Table E-2F. Summary and Monthly Transfers of E5 (Zirflex Decladding) Waste to Tank Farms E-5 Data Tabulations -- Campaigns 3&4.

May-85	0	84	0	84	Plant to NMC Waste vol ratio =			1.33
Jun-85	0	75	0	75	Plant Waste Volume (L) per MTU=			4729
Jul-85	22	72	144	238	Pu g/Plant L=			0.000263808
Aug-85	0	7	172	179	U g/Plant L=			0.576
Sep-85	0	0	54	54	U to Pu Ratio =			2183
CAMPAIGN A02 TOTAL	22	750	625	1397				
Month	NMC U Loss (kg)							
Sep-84	0	19.678	28.871	48.549	2697			
Oct-84	0	0	3.602	3.602	1801			
Nov-84	0	31.912	161.231	193.143	2327			
Dec-84	0	0	494.282	494.282	3433			
Jan-85	0	404.189	45.705	449.894	2940			
Feb-85	0	290.59	0	290.59	2442			
Mar-85	0	232.994	0	232.994	1991			
Apr-85	0.283	219.093	0	219.376	1675			
May-85	0	161.704	0.502	162.206	1931			
Jun-85	0	59.387	0	59.387	792			
Jul-85	13.207	68.145	184.862	266.214	1119			
Aug-85	0	96.251	362.209	458.46	2561			
Sep-85	0	0	171.513	171.513	3176			
CAMPAIGN A02 TOTAL	1583.943	1452.777	3050.21	2183				

Table E-2F. Summary and Monthly Transfers of E5 (Zirflex Decladding) Waste to Tank Farms E-5 Data Tabulations -- Campaigns 3&4.

From E-5 in May-88	6575	0 = SUM
	16170	
	15846	
	SUM =	
	TOTAL =	0

Monthwise Tank Receipts (L) from E-5 in July-87
AW-103-> 12407 14399 <-AW-105
Plant Waste Volume per MTU = #VALUE

Notes:

1. Campaign 3 E-5 transfers began in Oct-85.
2. Campaign A01 E-5 transfer ended on Sep 10, 1984.
3. Purex Volume and HE MTU data have been obtained from monthly campaign reports issued as internal letters.
4. July and Aug-85 Volumes have been ratioed from NMC data using a factor of 1.33 (includes 5% Jet Dilution).

Table E-2G. Summary and Monthly Transfers of E5 (Zirflex Decladding) Waste to Tank Farms E-5 Data Tabulations -- Campaigns 3&4.

Month	NMC Volume Transfers (L)				NMC Plutonium (g)				NMC Uranium (kg)				PUREX Summary Vol		Processed Fuel MTU	Month
	AZ-102	AW-103	AW-105	Total	AZ-102	AW-103	AW-105	Total	AZ-102	AW-103	AW-105	Total	gal	L		
Jan-88	0	57442.7	0	57442.7	0	28	0	28	0	35.544	0	35.544	28266	106986.8	11.1	Jan-88
Feb-88	0	287353.4	0	287353.4	0	328	0	328	0	179.039	0	179.039	115293.0	436384.0	62	Feb-88
Mar-88	0	275784.2	0	275784.2	0	226	0	226	0	77.003	0	77.003	94485.0	357625.7	41.67	Mar-88
Apr-88	0	0	0	0	0	0	0	0	0	0.000	0	0	0.0	0.0	0	Apr-88
May-88	0	0	51323.5	51323.5	0	0	1	1	0	0.000	9.778	9.778	19013.0	71964.2	4.86	May-88
Jun-88	0	318399.5	67398	385797.5	0	58	1	59	0	131.854	18.496	150.35	137473.0	520335.3	76.64	Jun-88
Jul-88	0	250754.7	0	250754.7	0	30	0	30	0	87.354	0	87.354	87762.0	332179.2	39.38	Jul-88
Aug-88	0	565870	18203.6	584073.6	0	81	0	81	0	310.607	0.045	310.652	218530.0	827136.1	98.5	Aug-88
Sep-88	0	190567.6	227949.7	418517.3	0	16	80	96	0	113.307	25.033	138.34	174477.0	660395.4	92.062	Sep-88
Oct-88	11007.5	129929.6	149006.7	289943.8	1	12	78	91	1.091	74.396	16.934	92.421	110560.0	418469.6	52.79	Oct-88
Nov-88	0	211383.5	195855.2	407238.7	0	27	275	302	0	117.222	11.318	128.54	139433.8	527756.9	45.38	Nov-88
Dec-88	0	89885.4	63252.3	153137.7	0	42	152	194	0	65.250	1.556	66.806	52513.1	198762.1	17.51	Dec-88
Jul-89	0	0	19871.3	19871.3	0	0	3	3	0	0	0.258	0.258	6347.0	24023.4	0	Jul-89
Nov-89	0.0	0	12024.9	12024.9	0	0	2	2	2.438	0.000	0.631	3.069	3766.0	14254.3	0	Nov-89
Dec-89	0	0	134618.4	134618.4	0	0	26	26	0	0	88.262	88.262	47248.3	178834.8	0	Dec-89
Jan-90	0	0	15371.6	15371.6	0	0	9	9	0	0	9.247	9.247	4760.2	18017.4	0	Jan-90

Table E-2G. Summary and Monthly Transfers of E5 (Zirflex Decladding) Waste to Tank Farms E-5 Data Tabulations -- Campaigns 3&4.

Feb-90	0	0	36627.1	36627.1	0	0	1	1	0	0	9.166	9.166	11230.9	42509.0	19.95	Feb-90
TOTALS	11007.5	2319927.9	991502.3	3322437.7	1	820	628	1449	3.529	1156.032	190.724	1350.285	1222892.3	4628647.356	550.742	TOTALS

E5 Waste Summary for CAMPAIGN A06

NMC Data
Vol (L) = 3322437.7
Pu (g) = 1449
U (kg) = 1350.285
MTU = 550.742
Tank F-16 Vol (L) = 4628647.356
Plant Vol (incl Jet Dilution) (L) = 4860079.723
Plant to NMC Waste vol ratio = 1.46
Plant Waste Volume (L) per MTU = 8824.6
Pu g/Plant L = 0.000298143
U g/Plant L = 0.27783
U to Pu Ratio = 932

	Vol, gal	U, kg
Jan-85	3.14E+04	
Feb-85	2.54E+04	152.3
Mar-85	3.91E+04	118.8
Apr-85	8.08E+04	336.1
May-85	1.67E+04	311.5
Jun-85	3.98E+04	117.8
Jul-85		255
Aug-85		
Sep-85	1.64E+04	
		107

NMC Campaign Report Summary

From Campaign Letter Reports

Plant Waste Volume per MTU = 5768
Pu g/Plant L = 0
U g/Plant L = 0.000

= SUM

Table E-3A. Summary and Monthly Transfers of F16 (Neutralized Zirflex Current Acid) Waste to Tank Farms (includes Campaigns A01 thru A06 and cleanout period).

	Campaign #							
NMC Data	A01	A02	A03	A04	A05	A06	Summary	Cleanout period March 91
Vol (L) =	893878	1112658	316313.5	705524.5	356450.6	622833	4007657.6	15126
Pu (g) =	3119	4293	1306	5006	2006	2031	17761	0
U (kg) =	767.258	564.174	136.039	672.808	1292.261	349.109	3781.649	0.315
MTU =	1282	2141.7	344.790	1193.079	297.335	880.875	6139.779	0
Tank F-16 Vol (L) =	1132531	1893988	503812	1113806	512144.6	879533	6035814	22761
Plant Vol (incl Jet Dilution) (L) =	1189157.6	1988687.4	529002	1169496	537751.83	923509.65	6337604.7	23899
Plant to NMC Waste vol ratio =	1.33	1.79	1.67	1.66	1.51	1.48	1.58	1.58
Plant Waste Volume (L) per MTU=	928	928.6	1534	980	1809	1048.4	1032.2	not applicable
Avg Pu g/Plant L=	0.00262	0.0021587	0.0024688	0.0042805	0.0037303	0.0021992	0.0028025	0
Avg U g/Plant L=	0.645	0.284	0.257	0.575	2.403	0.378	0.597	0.013
Avg U to Pu Ratio =	246	131	104	134	644	172	213	#DIV/0!

Note:
Plant transfer Volumes were not available for the cleanout period. The NMC The NMC vol was multiplied by 1.58/1.05 to obtain the Plant Vol. implies 0 g Pu yielding an infinite U/Pu ratio.

Table E-3B. Summary and Monthly Transfers of F16 (Neutralized Zirflex Current Acid) Waste to Tank Farms (includes Campaigns A01 thru A06 and cleanout period).

Tank #	A01			A02			A03			A04		
	NMC Pu	NMC U	U/Pu	NMC Pu	NMC U (g)	U/Pu	NMC Pu (g)	NMC U (g)	U/Pu	NMC Pu (g)	NMC U (g)	U/Pu
AW-101	6	28744	4791	2	1756	878						
AW-102										246	6372	26
AW-104												
AY-101	22	7526										
AY-102	0	9388	#DIV/0!							2	108	54
AZ-101	3054	705806		4291	562418	131	1188	63722	54	1167	76992	66
AZ-102	37	15794								3591	589336	164
AZ-103							118	72317	613			
TOTALS	3119	767258	246	4293	564174	131	1306	136039	104	5006	672808	134
Campaign #	A05			A06			Tank Totals			Cleanout Period		
TANK #	NMC Pu (g)	NMC U (g)	U/Pu	NMC Pu (g)	NMC U (g)	U/Pu	NMC Pu (g)	NMC U (g)	U/Pu (g)	NMC Pu	NMC U	U/Pu
AW-101							8	30500	3813			
AW-102							246	6372	26			
AW-104				628	129878	207	628	129878	207	0	315	#DIV/0!
AY-101							22	7526	342			
AY-102	17	628	37	46	4709	102	65	14833	228			
AZ-101							9700	1408938	145			
AZ-102	1989	1291633	649	1357	214522	158	6974	2111285	303			
AZ-103							118	72317	613			
TOTALS	2006	1292261	644	2031	349109	172	17761	3781649	213	0	315	#DIV/0!

Table E-3C. Summary and Monthly Transfers of F16 (Neutralized Zirflex Current Acid) Waste to Tank Farms
F16 Data Tabulations -- Campaign A01.

Month								Volumes		Purex Summary	
	AW-101	AY-101	AY-102	AZ-101	AZ-102	Totals	Month	gal	L	Vol Ratio	NMC Waste SX MTU
Sep-83		8036				8036	Sep-83		11628	1.52	
Oct-83			9388			9388	Oct-83		13584	1.52	
Nov-83				22049		22049	Nov-83		31905	1.52	incl below
Dec-83				35794		35794	Dec-83		51794	1.52	incl below
Jan-84				104236		104236	Jan-84	incl below	incl below		incl below
Feb-84				33863		33863	Feb-84	incl below	incl below		incl below
Mar-84				84821		84821	Mar-84	incl below	incl below		incl below
Apr-84				105436		105436	Apr-84	120000	454200	1.45	491
May-84				43871	19015	62886	May-84		90996	1.52	154
Jun-84				80801	25744	106545	Jun-84	35000	132475	1.31	153
Jul-84	7827			102361		110188	Jul-84	29100	110144	1.05	178
Aug-84				89500		89500	Aug-84	incl below	incl below		incl below
Sep-84	10299			99441	11396	121136	Sep-84	62300	235806	1.18	306
CAMPAIGN A01 TOTAL	18126	8036	9388	802173	56155	893878	TOTALS	246400	1132531.391	1.33	1282

Table E-3D. Summary and Monthly Transfers of F16 (Neutralized Zirflex Current Acid) Waste to Tank Farms F16 Data Tabulations – Campaign A01.

Month	NMC Pu (g)						NMC U (kg)					Totals	U/Pu
	AW-101	AY-101	AY-102	AZ-101	AZ-102	Totals	AW-101	AY-101	AY-102	AZ-101	AZ-102		
Sep-83		22				22		7.526				7.526	0
Oct-83			0			0			9.388			9.388	#DIV/0!
Nov-83				26		26				20.907		20.907	1
Dec-83				63		63				115.177		115.177	2
Jan-84				315		315				38.646		38.646	0
Feb-84				73		73				26.642		26.642	0
Mar-84				245		245				13.832		13.832	0
Apr-84				265		265				34.944		34.944	0
May-84				172		172				97.986	5.944	103.93	1
Jun-84				491	31	522				52.262	8.061	60.323	0
Jul-84	6			313	5	324	19.254			34.515		53.769	0
Aug-84				721		721				204.148		204.148	0
Sep-84	0			370	1	371	9.49			66.747	1.789	78.026	0
CAMPAIGN A01 TOTAL	6	22	0	3054	37	3119	28.744	7.526	9.388	705.806	15.794	767.258	0

Table E-3D. Summary and Monthly Transfers of F16 (Neutralized Zirflex Current Acid) Waste to Tank Farms F16 Data Tabulations – Campaign A01.

Notes:

1. Purex Volume and HE MTU data have been obtained from monthly campaign reports issued as internal letters.

2. Purex Vol for Sep-Dec'83 & May'84 in Campaign reports is less than NMC volumes. For these months, Purex xfers are calc using a factor based on flowsheet informationon chemical additions and flushes. NMC volumes are multiplied by (4.7+2.1)/4.7 = to obtain Purex Volumes.

3. June-84 SX MTU figure has been calculated from Campaign letter report information.

4. ERR implies 0 g Pu yielding an infinite U/Pu ratio.

F16 Waste Summary for CAMPAIGN A01 (Sep'83-Sep'84)

NMC Data
Vol (L) = 893878
Pu (g) = 3119
U (kg) = 767.258
MTU = 1282
Tank F16 Vol (L) = 1132531.391
Plant Vol (incl Jet Dilution) (L) = 1189157.961
Plant to NMC Waste vol ratio = 1.33
Plant Waste Volume (L) per MTU = 928
Pu g/Plant L = 0.002622864

Table E-3E. Summary and Monthly Transfers of F16 (Neutralized Zirflex Current Acid) Waste to Tank Farms F16 Data Tabulations -- Campaign A01.

Month	NMC Volume Transfers (L)			NMC Plutonium (g)			NMC Uranium (kg)				Purex Summary Volume		Plant NMC Ratio	Processed Fuel MTU
	AW-01	AZ-101	Total	AW-101	AZ-101	Total	AW-101	AZ-101	Total		gal	L		
Sep-84		6041	6041		0	0		0.077	0.077	Sep-84	incl below	0.0	0.00	incl below
Oct-84	3604		3604	0		0	1.362		1.362	Oct-84	incl below	0.0	0.00	incl below
Nov-84		37598	37598		62	62		137.501	137.501	Nov-84	36900	139667	2.96	98
Dec-84		82842	82842		558	558		45.948	45.948	Dec-84	35400	133989	1.62	239
Jan-85		117520	117520		428	428		30.530	30.53	Jan-85	53600	202876	1.73	269
Feb-85		74996	74996		289	289		6.997	6.997	Feb-85	32100	121499	1.62	110
Mar-85	9728	92778	102506	2	307	309	0.394	54.405	54.799	Mar-85	43900	166162	1.62	257
Apr-85		129681	129681		481	481		57.516	57.516	Apr-85	62300	235806	1.82	212
May-85		108676	108676		227	227		48.308	48.308	May-85	41400	156699	1.44	153.9
Jun-85		43539	43539		161	161		1.587	1.587	Jun-85	16000	60560	1.39	66.4
Jul-85		104081	104081		576	576		98.841	98.841	Jul-85	46747	176938	1.70	305
Aug-85		160186	160186		751	751		44.464	44.464	Aug-85	71946	272316	1.70	282.4
Sep-85		141388	141388		451	451		36.244	36.244	Sep-85	60100	227479	1.61	149
TOTAL	13332	1099326	1112658	2	4291	4293	1.756	562.418	564.174	TOTAL	500393.2365	1893988.4	1.70	2141.7

F16 Waste Summary for CAMPAIGN A02

NMC Data
Vol (L) = 1112658
Pu (g) = 4293
U (kg) = 564.174
MTU = 2141.7
Tank F-16 Vol (L) = 1893988.4
Plant Vol (incl Jet Dilution) (L) = 198887.8
Plant to NMC Waste vol ratio = 1.79
Plant Waste Volume (L) per MTU = 929
Pu g/Plant L = 0.0021587
U g/Plant L = 0.284
U to Pu Ratio = 131

Notes

1. Purex Volumes were not available for July & Aug'85. For these months, the NMC volume was multiplied by a factor of 1.70 to obtain Purex volumes. An additional factor of 1.05 is applied due to Jet Dilution (see Summary).

Table E-3F. Summary and Monthly Transfers of F16 (Neutralized Zirflex Current Acid) Waste to Tank Farms F-16 Data Tabulations - Campaign 3&4.

Month	NMC volume transfers (L)						F-16 Volume (Purex Summarics)		Processed Fuel	NMC Data	
	AZ-101	AZ-102	AZ-103	AW-102	AY-102	TOTAL (L)	gal	L	SX MTU		
Sep-85	0.0	0.0	14386.0	0	0	14386	6045	22881			
Oct-85	51312.1	0.0	13987.8	0	0	65300	24628	93218	51.60	Vol (L) =	316313.5
Nov-85	117030.7	0	0	0	0	117031	51550	195115	152.33	Pu (g) =	1306
Dec-85	119596.9	0	0	0	0	119597	50885	192598	140.86	U (kg) =	136.039
CAMPAIGN A03 TOTAL	287939.7	0	28373.8	0	0	316314	133108	503812	344.79	MTU =	344.790
										Tank F-16 Vol (L)=	503811.89
Jan-86	12135.1	0	0	0	0	12135	4719	17862	18.70	Plant Vol (incl Jet Dilution) (L)=	529002.49
Feb-86	50856	0	0	0	0	50856	22549	85346	186.91	Plant to NMC Waste vol ratio =	1.67
Mar-86	95218.9	38561.3	0	0	0	133780	59792	226315	243.05	Plant Waste Volume (L) per MTU=	1534
Apr-86	10177.9	132392.9	0	0	0	142571	58237	220428	109.07	Avg Pu g/Plant L=	0.0024688
May-86	0	30874.6	0	8445.8	0	39320	19764	74808	139.79	Avg U g/Plant L=	0.257
Jun-86	0	112501.9	0	0	0	112502	41341	156477	73.61	Avg U to Pu Ratio =	104
Jul-86	0	43932.1	0	11210.8	0	55143	25604	96911	196.74		
Aug-86	0	66944.9	0	0	0	66945	32773	124045	215.18		
Sep-86	0	76121.3	0	0	16151	92272	29488	111614	10.03		
CAMPAIGN A04 TOTAL	168387.9	501329.0	0.0	19656.6	16151.0	705525	294268	1113806	1193.08		

Table E-3F. Summary and Monthly Transfers of F16 (Neutralized Zirflex Current Acid) Waste to Tank Farms F-16 Data Tabulations - Campaign 3&4.

			NMC Pu (g)			TOTAL Pu(g)	Note: SX MTU for Sep 85 was accounted for in Campaign 2.			F-16 Waste Summary for CAMPAIGN A04 (Jan-Sep'86)	
Sep-85	0	0	89	0	0	89					
Oct-85	98	0	29	0	0	127					
Nov-85	517	0	0	0	0	517				NMC Data	
Dec-85	573	0	0	0	0	573				Vol (L) =	705524.5
CAMPAIGN A03 TOTAL	1188	0	118	0	0	1306				Pu (g) =	5006

Table E-3F. Summary and Monthly Transfers of F16 (Neutralized Zirflex Current Acid) Waste to Tank Farms F-16 Data Tabulations - Campaign 3&4.

										U (kg) =	672.808
Jan-86	10	0	0	0	0	10				MTU =	1193.079
Feb-86	283	0	0	0	0	283				Tank F-16 Vol (L)=	1113805.5
Mar-86	822	229	0	0	0	1051				Plant Vol (incl Jet Dilution) (L) =	1169495.8
Apr-86	52	734	0	0	0	786				Plant to NMC Waste vol ratio =	1.66
May-86	0	393	0	135	0	528				Plant Waste Volume (L) per MTU=	980
Jun-86	0	274	0	0	0	274				Avg Pu g/Plant L=	0.0042805
Jul-86	0	908	0	111	0	1019				Avg U g/Plant L=	0.575
Aug-86	0	944	0	0	0	944				Avg U to Pu Ratio =	134
Sep-86	0	109	0	0	2	111					
CAMPAIGN A04 TOTAL	1167	3591	0	246	2	5006				F-16 Waste summary for CAMPAIGNS A03 & A04	
										NMC Data	
			NMC U Loss (kg)			TOTAL U (kg)	U/Pu			Vol (L) =	1021838
Sep-85	0	0	62.728	0	0	62.728				Pu (g) =	6312
Oct-85	3.349	0	9.589	0	0	12.938	102			U (kg) =	808.847
Nov-85	32.644	0	0	0	0	32.644	63			MTU =	1537.869
Dec-85	27.729	0	0	0	0	27.729	48			Tank F-18 Vol (L)=	1617617.4
CAMPAIGN A03 TOTAL	63.722	0	72.317	0	0	136.039	104			Plant Vol (incl Jet Dilution) (L)=	1698498.3

Table E-3F. Summary and Monthly Transfers of F16 (Neutralized Zirflex Current Acid)
Waste to Tank Farms F-16 Data Tabulations - Campaign 3&4.

										Plant to NMC Waste vol ratio =	1.66
Jan-86	19.054	0	0	0	0	19.054	1905			Plant Waste Volume (L) per MTU=	1104
Feb-86	23.273	0	0	0	0	23.273	82			Avg Pu g/Plant L=	0.00372
Mar-86	34.121	8.452	0	0	0	42.573	41			Avg U g/Plant L=	0.476
Apr-86	0.544	32.486	0	0	0	33.030	42			Avg U to Pu Ratio =	128
May-86	0	180.765	0	4.951	0	185.716	352				
Jun-86	0	51.058	0	0	0	51.058	186				
Jul-86	0	273.151	0	1.421	0	274.572	269				
Aug-86	0	8.096	0	0	0	8.096	9				
Sep-86	0	35.328	0	0	0.108	35.436	319				
CAMPAIGN A04 TOTAL	76.992	589.336	0	6.372	0.108	672.808	134				
A03 U/Pu	54	#DIV/0!	613	#DIV/0!	#DIV/0!						
A04 U/Pu	66	164	#DIV/0!	26	54						
"A03 & A04 F-16, U/Pu="	60	164	613	26	54						

NOTES:

Campaign A03 Sep-85 transfers (approx. 10 vol% of month's total) were not merged with Campaign A02 because of high U and Pu amounts.

Sep-85 'Plant vol' was back calculated by multiplying NMC vol by 1.67/1.05 Campaign A05 F-16 transfers commence in March-87.

ERR indicates 0 g Pu yielding an infinite U/Pu ratio

Table E-3G. Summary and Monthly Transfers of F16 (Neutralized Zirflex Current Acid) Waste to Tank Farms F-16 Data Tabulations (NZCAW Waste) - Campaign A05.

Month	NMC Volume Transfers (L)			NMC Plutonium (g)			NMC Uranium Loss (kg)			Purex Summary Volume			Processed Fuel
	AZ-102	AY-102	TOTAL	AZ-102	AY-102	TOTAL	AZ-102	AY-102	TOTAL	U/Pu	gal	L	SX MTU
Mar-87	13981.4	0	13981.4	2	0	2	0.454	0	0.454	227	4819.00	18239.9	16.77
Apr-87	44510.5	10919	55429.5	1009	2	1011	1086.937	0.1	1087.037	1075	27358.00	103550.0	18.85
May-87	38505.9	0	38505.9	92	0	92	41.084	0	41.084	447	15993.00	60533.5	5.917
Jun-87	35993.5	0	35993.5	49	0	49	21.896	0	21.896	447	14319.00	54197.4	0
Jul-87	50279.2	0	50279.2	373	0	373	51.392	0	51.392	138	21981.00	83198.1	95.923
Aug-87	61719.4	12344.4	74063.8	264	4	268	44.941	0.149	45.09	168	14779.00	55938.5	79.534
Sep-87	68167.5	0	68167.5	200	0	200	44.929	0	44.929	225	28979.00	109685.5	80.341
Oct-87	0	0	0	0	0	0	0	0	0	#DIV/0!	0.00	0.0	0
Nov-87	0	0	0	0	0	0	0	0	0	#DIV/0!	0.00	0.0	0
Dec-87	0	20029.8	20029.8	0	11	11	0	0.379	0.379	34	7081	26801.6	0
CAMPAIGN	313157.4	43293.2	356450.6	1989	17	2006	1291.633	0.628	1292.261	644	135309.00	512144.57	297.34
F16 Waste Summary for CAMPAIGN A05													
NMC Data													
Vol (L) =		356450.6											
Pu (g) =		2006											
U (kg) =		1292.261											
SX MTU =		297.335											
Tank F16 Vol (L) =		512144.565											
Plant Vol (incl Jet Dilution) (L) =		537751.7933											
Plant to NMC Waste vol ratio =		1.51											
Plant Waste Volume (L) per MTU =		1809											
Pu g/Plant L =		0.003730346											
U g/Plant L =		2.403											
U to Pu Ratio =		644											

Table E-3H. Summary and Monthly Transfers of F16 (Neutralized Zirflex Current Acid) Waste to Tank Farms F-16 Data Tabulations (NZCAW Waste) - Campaign A06.

Month	NMC Volume Transfers (L)				NMC Plutonium (g)				NMC Uranium (kg)				Purex Summary Volume		Processed Fuel MTU
	AZ-102	AW-104	AY-102	TOTAL	AZ-102	AW-104	AY-102	TOTAL	AZ-102	AW-104	AY-102	TOTAL	gal	L	
Jan-88															11.1
Feb-88	28277.4	7495.4	0	35772.8	87	22	0	109	4.502	0.421	0	4.923	19380.0	73353.3	62
Mar-88	0	56261.4	0	56261.4	0	438	0	438	0	112.809	0	112.809	23766.0	89954.3	89.5
Apr-88	0	0	10282.3	10282.3	0	0	11	11	0	0.000	1.147	1.147	3922.0	14844.8	0
May-88	0	0	0	0	0	0	0	0	0	0.000	0	0	0.0	0.0	20.805
Jun-88	49335.2	8450.8	0	57786	220	21	0	241	18.186	5.722	0	23.908	24318.0	92043.6	136.543
Jul-88	16277.8	16751.3	0	33029.1	119	74	0	193	2.011	1.377	0	3.388	14953.0	56597.1	52.63
Aug-88	33673.3	15730.5	0	49403.8	143	37	0	180	4.574	9.250	0	13.824	22687.0	85870.3	160.74
Sep-88	60997.9	0	0	60997.9	123	0	0	123	6.291	0.000	0	6.291	28369.0	107376.7	87.18
Oct-88	58484.7	6118.1	0	64602.8	167	33	0	200	7.627	0.200	0	7.827	30360.0	114912.6	112.937
Nov-88	19102.9	12688.8	89419.1	121210.8	56	3	35	94	2.006	0.099	3.562	5.667	10925.3	41352.3	43.71
Dec-88	36018.8	0	0	36018.8	32	0	0	32	9.701	0.000	0	9.701	13599.2	51473.0	30.82
Jun-89	11308.4	0	0	11308.4	1	0	0	1	0.464	0	0	0.464	3965.7	15010.2	0
Feb-90	46953.7	0	0	46953.7	386	0	0	386	156.722	0	0	156.722	20752.2	78547.1	72.91
Mar-90	39205.0	0	0.0	39205	23	0	0	23	2.438	0.000	0	2.438	15376.0	58198.2	0
TOTAL	399635.1	123496.3	99701.4	622832.8	1357	628	46	2031	214.522	129.878	4.709	349.109	232373.4	879533.32	880.875

F16 Waste Summary for CAMPAIGN A06 (Jan'88-Mar'90)

Vol (L) =	622832.8	
Pu (g) =	2031	
U (kg) =	349.109	
MTU =	880.875	
Tank F-16 Vol (L) =		879533.32
Plant Vol (incl Jet Dilution) (L) =		923509.98
Plant to NMC Waste vol ratio =		1.48
Plant Waste Volume (L) per MTU =		1048.4
Pu g/Plant L =	0.0021992	
U g/Plant L =		0.3780241
U to Pu Ratio =	172	

Table E-4A. Summary and Monthly Transfers of F18 (Canyon Sump) Waste to Tank Farms (includes Campaigns A01 thru A06 and cleanout Period).

NMC Data	Campaign #						Summary	Cleanout Period
	A01	A02	A03	A04	A05	A06		Jun'90-Mar'96
Vol (L) =	1207393	1132354	285449.2	1035872	1227478	3510911	8399457.2	2124015
Pu (g) =	1653	1605	553	1481	2005	2463	9760	7069
U (kg) =	2660.918	2399.407	427.166	3354.235	3528.493	6865.957	19236.176	14588.351
MTU =	1282	2141.7	344.790	1193.079	297.335	880.875	6139.779	0
Tank F-18 Vol (L)=	1471870	1358450	302504	1225883	1629904	4266218	10254829	2589275.4
Plant Vol (incl Jet Dilution) (L) =	1545463.5	1426372.5	317629	1287177	1711399.2	4479528.9	10767571	2718739.2
Plant to NMC Waste vol ratio =	1.28	1.26	1.11	1.24	1.39	1.28	1.28	1.28
Plant Waste Volume (L) per MTU=	1206	666.0	921	1079	5756	5085.3	1753.7	Not Applicable
Avg Pu g/Plant L=	0.00107	0.0011252	0.001741	0.0011506	0.0011716	0.0005498	0.0009064	0.0026001
Avg U g/Plant L=	1.722	1.682	1.345	2.606	2.062	1.533	1.786	5.366
Avg U to Pu Ratio =	1610	1495	772	2265	1760	2788	1971	2064

Note:

(1) Plant transfer volumes were not available for the Cleanout period. The NMC vol was multiplied by 1.28/1.05 to obtain the Plant Vol. (2) 12728 g of Neptunium were present in the Jan-93 transfer to tank AZ-102.

Campaign # ->	A01			A02			A03			A04		
	NMC Pu	NMC U	U/Pu	NMC Pu	NMC U	U/Pu	NMC Pu	NMC U	U/Pu	NMC Pu	NMC U	U/Pu
TANK #	(g)	(g)		(g)	(g)		(g)	(g)		(g)	(g)	
AW-101	861	788457	916	1496	2241774	1499	496	318580	642	581	1197727	2061
AW-102				66	74925	1135	55	107307	1951	638	1274948	1998
AW-103										3	741	247
AW-104										106	432737	4082
AW-105	792	1872461	2364									
AY-101				9	24377	2709						
AZ-101				34	58331	1716	2	1279	640			
AZ-102										153	448082	2929
TOTALS	1653	2660918	1610	1605	2399407	1495	553	427166	772	1481	3354235	2265

Table E-4B. Summary and Monthly Transfers of F18 (Canyon Sump) Waste to Tank Farms (includes Campaigns A01 thru A06 and cleanout Period).

Campaign #	A05			A06			Tank Totals			Cleanout Period		
	NMC Pu	NMC U	U/Pu	NMC Pu	NMC U	U/Pu	NMC Pu	NMC U	U/Pu	NMC Pu	NMC U	U/Pu
TANK #	(g)	(g)		(g)	(g)		(g)	(g)		(g)	(g)	
AW-101							3434	4546538	1324			
AW-102							759	1457180	1920			
AW-103				55	74656	1357	58	75397	1300			
AW-104	2005	3528493	1760	2278	6707805	2945	4389	10669035	2431	16	169679	
AW-105							792	1872461	2364	7021	14230987	2027
AY-101							9	24377	2709			
AZ-101							36	59610	1656			
AZ-102				130	83496	642	283	531578	1878	6	67765	11294
AP-108										26	117486	4519
AN-102										0	2434	#DIV/0!
TOTALS	2005	3528493	1760	2463	6865957	2788	9760	19236176	1971	7043	14468431	2054

Table E-4C. Summary and Monthly Transfers of F18 (Canyon Sump) Waste to Tank Farms
F-18 Data Tabulations -- Campaign A01

Month	NMC Volume Transfers (L)			NMC Plutonium (g)			NMC Uranium (kg)			Month	PUREX Vol Trans	Fuel
	AW-101	AW-105	TOTAL	AW-101	AW-105	TOTAL	AW-101	AW-105	TOTAL		L	SX MTU
Nov-83	0	164626	164626	0	98	98	0	826.211	826.211	Nov-83	200687	incl below
Dec-83	0	128833	128833	0	41	41	0	83.537	83.537	Dec-83	157054	incl below
Jan-84	0	100307	100307	0	80	80	0	255.066	255.066	Jan-84	122279	incl below
Feb-84	0	147774	147774	0	65	65	0	62.948	62.948	Feb-84	180144	incl below
Mar-84	0	133500	133500	0	101	101	0	157.075	157.075	Mar-84	162743	incl below
Apr-84	0	78117	78117	0	286	286	0	93.948	93.948	Apr-84	95228	491
May-84	0	51662	51662	0	19	19	0	53.794	53.794	May-84	62978	154
Jun-84	0	111405	111405	0	101	101	0	287.119	287.119	Jun-84	135808	153
Jul-84	83663	14884	98547	92	1	93	123.786	52.763	176.549	Jul-84	120133	178
Aug-84	79052	0	79052	35	0	35	104.62	0.000	104.62	Aug-84	96368	306
Sep-84	113570	0	113570	734	0	734	560.051	0.000	560.051	Sep-84	138447	incl above
TOTAL	276285	931108	1207393	861	792	1653	788.457	1872.461	2660.918	TOTAL	1471870	1282

NMC Data	
Vol (L) =	1207393
Pu (g) =	1653
U (kg) =	2660.918
MTU =	1282
Tank F-18 Vol (L) =	1471870
Plant Vol (incl Jet Dilution) (L) =	1545463
Plant to NMC Waste vol ratio =	1.28
Plant Waste Volume (L) per MTU =	1206
Pu g/Plant L =	0.00107
U g/Plant L =	1.722
U to Pu Ratio =	1610

Notes:

1. Purex Summary Volume given in monthly Campaign Reports for the months of Nov & Dec'83 is less than volumes in NMC records. The same holds true for certain other months in Campaign A01. Thus, the monthly Campaign report volumes are considered unreliable; Purex volume transfers are obtained by multiplying the NMC volumes by an avg Plant:NMC vol ratio of the other Campaigns The factor used to obtain Plant Vol is 1.28/1.05.

2. SX MTU figures have been obtained from the monthly Campaign Reports. MTU figure given for April-84 includes the period Nov-83 thru April-84 MTU figure shown for Aug-84 includes August thru mid-Sep-84.

Table E-4D. Summary and Monthly Transfers of F18 (Canyon Sump) Waste to Tank Farms F-18 Data Tabulations -- Campaign A02.

Month	NMC Volume Transfers (L)					NMC Plutonium (g)					NMC Uranium (kg)					PUREX Summary Vol		Processed
	AW-101	AW-102	AY-101	AZ-101	Total	AW-101	AW-102	AY-101	AZ-101	Total	AW-101	AW-102	AY-101	AZ-101	Total	gal	L	Fuel MTU
Sep-84	45969				45969	12				12	74.187				74.187	incl below	0.0	incl below
Oct-84	66526				66526	65				65	218.732				218.732	incl below	0.0	incl below
Nov-84	99475				99475	164				164	426.539				426.539	78300.0	296365.5	98
Dec-84	130644		8599		139243	233		9		242	168.441		24.377		192.818	40500.0	153292.5	239
Jan-85	106285				106285	87				87	126.488				126.488	31400.0	118849.0	269
Feb-84	104352				104352	103				103	118.889				118.889	25400.0	96139.0	110
Mar-85	160549				160549	153				153	336.108				336.108	39100.0	147993.5	257
Apr-85	52985	39585			92570	18	11			29	46.473	45.547			92.02	29593.1	112009.7	212
May-85	42414	8717			51130.855	134	55			189	88.459	29			117.837	16700.0	63209.5	153.9
Jun-85	131380				131380	213				213	254.91				254.91	39800.0	150643.0	66.4
Jul-85	51761				51761	124				124	242.863				242.863	20376.2	77123.9	305
Aug-85	54195			11643	54195	13			32	45	68.838			53.208	122.046	21334.4	80750.6	282.4
Sep-85	28918			9832	28918	177			2	179	70.847			5.123	75.97	16400.0	62074.0	149
TOTAL	1075453	48302	8599	21475	1132353.9	1496	66	9	34	1605	2241.774	74.925	24.377	58.331	2399.407	358903.6	1358450.1	2141.7

F18 Waste Summary for CAMPAIGN A02

NMC Data

Vol (L) =		1132353.9
Pu (g) =	1605	
U (kg) =	2399.407	
MTU =	2141.7	
Tank F-16 Vol (L) =		1358450.1
Plant Vol (incl Jet Dilution) (L) =		1426372.6
Plant to NMC Waste vol ratio =		1.26
Plant Waste Volume (L) per MTU=		666.0
Pu g/Plant L =		0.0011252
U g/Plant L =		1.68217
U to Pu Ratio =		1495

NOTE:

For April-85, the Plant Vol reported in Purex waste vol summary (80,800 gal) appears to " be abnormally high as compared to the NMC vol.
For this month, the Plant vol has therefore been calculated by multiplying the NMC" vol by the factor 1.27/1.05.

F18 Waste Summary for CAMPAIGN A02

NMC Data		
Vol (L) =		1132353.9
Pu (g) =	1605	
U (kg) =	2399.407	
MTU =	2141.7	
Tank F-16 Vol (L) =		1358450.1
Plant Vol (incl Jet Dilution) (L) =		1426372.6
Plant to NMC Waste vol ratio =		1.26
Plant Waste Volume (L) per MTU=		666.0
Pu g/Plant L =		0.0011252
U g/Plant L =		1.68217
U to Pu Ratio =		1495

NOTE:

For April-85, the Plant Vol reported in Purex waste vol summary (80,800 gal) appears to " be abnormally high as compared to the NMC vol.
For this month, the Plant vol has therefore been calculated by multiplying the NMC" vol by the factor 1.27/1.05.

Table E-4E. Summary and Monthly Transfers of F18 (Canyon Sump) Waste to Tank Farms
F-18 Data Tabulations -- Campaigns 3&4

Month	NMC Volume Transfers (L)							F-18 Volume (PUREX Summaries)		Proceed Fuel	F-18 Waste Summary for Campaign A03 (Oct-Dec '85)	
	AW-101	AW-102	AW-103	AW-104	AZ-101	AZ-102	TOTAL (L)	gal	L	SX MTU	NMC Data	
Oct-85	89362	63299.2	0	0	14988.2	0	167649.4	44751.2	169383.3	51.6	Vol (L) =	285449.2
Nov-85	23015.8	0	0	0	0	0	23015.8	6794.3	25716.6	152.33	Pu (g) =	553
Dec-85	94784	0	0	0	0	0	94784	28376.3	107404.1	140.86	U (kg) =	427.166
CAMPAIGN A03 Total	207161.8	63299.2	0	0	14988.2	0	285449.2	79921.8	302504.0	344.79	MTU =	344.790
											Tank F-18 Vol (L)=	302503.9752
Jan-86	227327.5	0	0	0	0	0	227327.5	56007.8	211989.7	18.7	Plant Vol (incl Jet Dilution) (L)=	317629.1739
Feb-86	106458	0	0	0	0	0	106458	37657.5	142533.7	186.91	Plant to NMC Waste vol ratio =	1.11
Mar-86	70827.9	48782.6	0	0	0	0	119610.5	39365.1	148997.0	243.05	Plant Waste Volume (L) per MTU=	921
Apr-86	27108.5	85623.9	0	0	0	0	112732.4	39080.5	147919.6	109.07	Avg Pu g/Plant L=	0.001741024
May-86	0	80848.4	0	0	0	0	80848.4	25225.4	95478.1	139.793	Avg U g/Plant L=	1.345
Jun-86	0	79321.9	14963.6	0	0	0	94285.5	30347.0	114863.4	73.606	Avg U to Pu Ratio =	772
Jul-86	15241.1	118237.3	0	50887.4	0	9623	193988.8	62086.1	234995.8	196.74		
Aug-86	0	0	0	49139.1	0	0	49139.1	16360.7	61925.2	215.18		
Sep-86	0	0	0	51481.7	0	0	51481.7	17749.2	67180.7	10.03	F-18 Waste Summary for CAMPAIGN A04 (Jan-Sep'86)	
CAMPAIGN A04 Total	446963.0	412814.1	14963.6	151508.2	0.0	9623.0	1035871.9	323879.3	1225883.2	1193.08		

Table E-4E. Summary and Monthly Transfers of F18 (Canyon Sump) Waste to Tank Farms
F-18 Data Tabulations -- Campaigns 3&4

											NMC Data	
				NMC Pu (g)			TOTAL Pu(g)	NaOH (gal)	NaOH (L)	NaOH/Plt Vol	Vol (L) =	1035871.9
Oct-85	160	55	0	0	2	0	217	1619	6128	0.04	Pu (g) =	1481
Nov-85	27	0	0	0	0	0	27	290	1098	0.05	U (kg) =	3354.235
Dec-85	309	0	0	0	0	0	309	1475	5583	0.06	MTU =	1193.079
CAMPAIGN A03 Total	496	55	0	0	2	0	553		avg ratio =	0.05	Tank F-18 Vol (L)=	1225883.2
											Plant Vol (incl Jet Dilution) (L) =	1287177.397
Jan-86	97	0	0	0	0	0	97	1452	5496	0.02	Plant to NMC Waste vol ratio =	1.24
Feb-86	191	0	0	0	0	0	191	1440	5450	0.05	Plant Waste Volume (L) per MTU=	1079
Mar-86	289	74	0	0	0	0	363	1245	4712	0.04	Avg Pu g/Plant L=	0.00115058
Apr-86	2	242	0	0	0	0	244	1397	5288	0.05	Avg U g/Plant L=	2.606
May-86	0	196	0	0	0	0	196	1191	4508	0.06	Avg U to Pu Ratio =	2265
Jun-86	0	107	3	0	0	0	110	1465	5545	0.06		
Jul-86	2	19	0	45	0	153	219	1460	5526	0.03	SUMMARY for CAMPAIGNS A03 & A04	
Aug-86	0	0	0	14	0	0	14	610	2309	0.05	NMC Data	
Sep-86	0	0	0	47	0	0	47	395	1495	0.03	Vol (L) =	1321321.1
CAMPAIGN A04 Total	581	638	3	106	0	153	1481		avg ratio =	0.04	Pu (g) =	2034
											U (kg) =	3781.401

Table E-4E. Summary and Monthly Transfers of F18 (Canyon Sump) Waste to Tank Farms
F-18 Data Tabulations -- Campaigns 3&4

			NMC U Loss (kg)				TOTAL U (kg)	U/Pu			MTU =		1537.869
Oct-85	87.632	107.307	0	0	1.279	0	196.218	904			Tank F-18 Vol (L) =		1528387.211
Nov-85	20.749	0	0	0	0	0	20.749	768			Plant Vol (incl Jet Dilution) (L) =		1604806.571
Dec-85	210.199	0	0	0	0	0	210.199	680			Plant to NMC Waste vol ratio =		1.21
CAMPAIGN A03 Total	318.58	107.307	0	0	1.279	0	427.166	772			Plant Waste Volume (L) per MTU=		1044
											Avg Pu g/Plant L=		0.001267442
Jan-86	393.64	0	0	0	0	0	393.64	4058			Avg U g/Plant L=		2.356
Feb-86	266.498	0	0	0	0	0	266.498	1395			Avg U to Pu Ratio =		1859
Mar-86	422.738	310.56	0	0	0	0	733.298	2020					
Apr-86	111.292	213.681	0	0	0	0	324.973	1332					
May-86	0	248.572	0	0	0	0	248.572	1268					
Jun-86	0	283.077	0.741	0	0	0	283.818	2580					
Jul-86	3.559	219.058	0	156.459	0	448.082	827.158	3777					
Aug-86	0	0	0	79.258	0	0	79.258	5661					
Sep-86	0	0	0	197.02	0	0	197.02	4192					
CAMPAIGN A04 Total	1197.727	1274.948	0.741	432.737	0	448.082	3354.235	2265					

Table E-4E. Summary and Monthly Transfers of F18 (Canyon Sump) Waste to Tank Farms
F-18 Data Tabulations -- Campaigns 3&4

A03 U/Pu	642	1951	#DIV/0!	#DIV/0!	640	#DIV/0!							
A04 U/Pu	2061	1998	247	4082	#DIV/0!	2929							
"A03 & A04, F-18, U/Pu="	1408	1995	247	4082	640	2929							

NOTES:

Campaign A03 Sep-85 transfers (approx. 30 vol% of month's total) were merged with Campaign A02.
Campaign A05 Sep-86 transfers (approx. 10 vol% of month's total) were merged with Campaign A04.

Purex vol reported in Purex Summary sheets (164061 gal) for May-86 is 8 times the NMC vol for that month. The former appears to be erroneous.Therefore NMC vol is multiplied by 1.27/1.05 to obtain Purex vol for May-86.

ERR indicates 0 g Pu yielding an infinite U/Pu ratio.

Table E-4F. Summary and Monthly Transfers of F18 (Canyon Sump) Waste to Tank Farms
F18 Data Tabulations -- Campaign A06.

Month	NMC VOLUME TRANSFERS (L)				N M C Plutonium (g)				N M C Uranium (kg)				PUREX Summary Vol		Processed
	AW-104	AW-103	AZ-102	TOTAL	AW-104	AW-103	AZ-102	TOTAL	AW-104	AW-103	AZ-102	TOTAL	gal	L	Fuel MTU
Nov-87	183395.4			183395.4	115			115	227.651			227.651	61493.0	232751.0	0
Dec-87	108601.9			108601.9	33			33	208.445			208.445	34890.0	132058.7	0
Jan-88	267426.5			267426.5	8			8	577.156			577.156	85280.0	322784.8	11.1
Feb-88	183793.9			183793.9	69			69	214.768			214.768	55220.0	209007.7	62
Mar-88	263038.2			263038.2	260			260	175.696			175.696	85810.0	324790.9	89.5
Apr-88	220773			220773	3			3	150.291			150.291	59982.0	227031.9	0
May-88	57234.5			57234.5	28			28	198.695			198.695	23521.0	89027.0	20.805
Jun-88	83153.4	14005.6		97159	291	55		346	429.809	74.656		504.465	29303.0	110911.9	136.543
Jul-88	219838.5		10772.9	230611.4	400		130	530	432.609		83.496	516.105	79534.0	301036.2	52.63
Aug-88	60458.2			60458.2	40			40	61.886			61.886	19775.0	74848.4	160.74
Sep-88	62579.7			62579.7	47			47	105.515			105.515	20930.0	79220.1	87.18
Oct-88	47329.9			47329.9	291			291	193.159			193.159	16469.0	62335.2	112.937
Nov-88	115084.1			115084.1	122			122	517.82			517.82	71835.0	271895.5	43.71
Dec-88	15869.4			15869.4	7			7	22.854			22.854	4780.7	18094.9	30.82
Jan-89	86329.4			86329.4	56			56	263.28			263.28	11382.3	43082.0	0
Feb-89	346381.6			346381.6	22			22	86.218			86.218	112374.3	425336.7	0
Mar-89	199111.8			199111.8	69			69	850.762			850.762	128701.5	487135.2	0
Apr-89	318245.4			318245.4	11			11	222.554			222.554	21422.7	81084.9	0
May-89	56642.5			56642.5	13			13	26.128			26.128	17510.0	66275.4	0
Jun-89	59140.6			59140.6	6			6	12.543			12.543	18121.0	68588.0	0
Jul-89	37232.3			37232.3	12			12	23.61			23.61	11911.8	45086.2	0
Aug-89	12776.6			12776.6	6			6	38.205			38.205	3971.6	15032.5	0

Table E-4F. Summary and Monthly Transfers of F18 (Canyon Sump) Waste to Tank Farms
F18 Data Tabulations -- Campaign A06.

Sep-89	13579.1			13579.1	3			3	6.763			6.763	4257.6	16115.0	0
Oct-89	41324.6			41324.6	37			37	139.823			139.823	14025.0	53084.6	0
Nov-89	55202.3			55202.3	33			33	122.201			122.201	22192.8	83999.7	0
Dec-89	211279.12			211279.12	23			23	505.487			505.487	59362.7	224687.8	0
Jan-90	29268.6			29268.6	17			17	2.649			2.649	9012.8	34113.4	0
Feb-90	28270.2			28270.2	12			12	570.757			570.757	9088.0	34398.1	72.91
Mar-90	22670.3			22670.3	51			51	62.599			62.599	7459.5	28234.2	0
Apr-90	63662.6			63662.6	184			184	222.527			222.527	16467.4	62329.1	0
May-90	16439			16439	9			9	35.345			35.345	11054.5	41841.3	0
TOTAL	3486132.62	14005.6	10772.9	3510911.12	2278	55	130	2463	6707.805	74.656	83.496	6865.957	1127138.2	4266218.087	880.875

Table E-4F. Summary and Monthly Transfers of F18 (Canyon Sump) Waste to Tank Farms
F18 Data Tabulations -- Campaign A06.

Month	From Campaign Letter Reports					
	Vol, gal					
Jan-85	3.14E+04	U, kg	Pu, g			
Feb-85	2.54E+04	152.3	91.6			
Mar-85	3.91E+04	118.8	103			
Apr-85	8.08E+04	336.1	154.4			
May-85	1.67E+04	311.5	29.7			SUM =
Jun-85	3.98E+04	117.8	188.2		"TOTAL, (L) = "	#REF!
Jul-85		255	214		Fr sent to AW-105 =	
Aug-85						
Sep-85	1.64E+04					
		107	306			
	NMC Campaign Report Summary					
	A01	Pu, g	U, kg			
	A02	807	3428			
	A03	1577	2300			
	A04	691	457			
	A05	1375	3392			
	A06-A	234	89.2			
	A06-B	1255	2630			
	A06-C	800	2768			
	SUM =	273	332			
		7012	15395.5			

Table E-4G. Summary and Monthly Transfers of F18 (Canyon Sump) Waste to Tank Farms
F18 Data Tabulations for Plant Cleanout Period.

		AW-104			AP-108			AN-102			AZ-102			AW-105	
	Vol (L)	U (g)	Pu (g)	Vol (L)	U (g)	Pu (g)	Vol (L)	U (g)	Pu (g)	Vol (L)	U (g)	Pu (g)	Vol (L)	U (g)	Pu (g)
Jun-90	13593	37927	4												
Jul-90	14793	10607	3												
Aug-90	15683	5505	4												
Oct-90	31622	73864	2												
Nov-90	16825	5838	1												
Dec-90	38546	3168	1												
Jan-91	16569	2387	0												
Feb-91	16432	3341	0												
Mar-91	30302	8627	0												
Apr-91	30772	18415	1												
May-91				10181	3635	0									
Jun-91				46945	53666	23									
Jul-91				14122	13684	2									
Sep-91				12284	26287	0									
Oct-91				15647	15975	1									
Dec-91				11569	1144	0									
Jan-92				25571	654	0									
Apr-92				16438	2441	0									
Jul-92							23289	2434	0						

Table E-4G. Summary and Monthly Transfers of F18 (Canyon Sump) Waste to Tank Farms
F18 Data Tabulations for Plant Cleanout Period.

Jan-93										10834	67765	6			
Feb-93													11186	2584	1
May-93													14468	661	2
Jun-93													15925	72463	8
Jul-93													13158	89	0
Oct-93													26738	698790	5
Nov-93													65833	1904501	10
Dec-93													15426	3178	0
Jun-94													15585	206031	150
Aug-94													27655	448849	249
Sep-94													59010	1054423	620
Nov-94													60110	542129	527
Dec-94													61319	171344	137
Jan-95													42987	790146	947
Feb-95													84109	2026882	1813
Mar-95													87833	2474665	1936
Apr-95													37087	879306	518
May-95													308025	2052039	13
Jun-95													357944	55059	8
Jul-95													44449	115623	61
Aug-95													14346	907	1

Table E-4G. Summary and Monthly Transfers of F18 (Canyon Sump) Waste to Tank Farms
F18 Data Tabulations for Plant Cleanout Period.

Sep-95													24413	206744	0
Oct-95													40792	81190	3
Nov-95													182788	428333	6
Feb-96													59265	4209	3
Mar-96													41547	10842	3
TOTALS	225136.692	169679	16	152757	117486	26	23289	2434	0	10834	67765	6	1711998	14230987	7021
TOTAL FOR ALL TANKS:			Vol (L)	U (g)	Pu (g)		NOTE: 12728 g of Neptunium were present in the Jan-93 transfer to tank AZ-102								
			2124014.692	14588351	7069										

Table E-5A. Summary and Monthly Transfers of G8 & R8 (Organic Wash) Waste to Tank Farms (includes Campaigns A01 thru A06 and Cleanout Period)

	CAMPAIGN #						SUMMARY	Cleanout Period
NMC Data	A01	A02	A03	A04	A05	A06		136421
Vol (L) =								9
Pu (g) =	3875825	2670923	693006.7	2008497	2318154	3298801	14865206.7	43.307
U (kg) =	133	286	84	298	568	316	1685	0
MTU =	2531.527	1121.784	283.456	855.649	1562.745	755.271	7110.452	145516
Tanks F8 & G8 Vol (L) =	1282	2141.7	344.790	1193.079	297.335	880.875	6139.779	152791.52
Plant Vol (incl Jet Dilution) (L) =	4134213	2848985	759190	2142892	2507287	3488381	15880947.8	1.12
Plant to NMC Waste vol ratio =	4340923.65	2991434.25	797149	2250037	2632651.35	3662800.05	16674995.19	Not Applicable
Plant Waste Volume (L) per MTU =	1.12	1.12	1.15	1.12	1.14	1.11	1.12	
Avg Pu g/Plant L =	3386	1396.8	2312	1886	8854	4158.1	2715.9	
Avg U g/Plant L =	0.00003	9.560635E-05	0.000105375	0.000132442	0.000215752	8.62728E-05	0.00010105	5.89038E-05
Avg U to Pu Ratio =	0.583	0.375	0.356	0.380	0.594	0.206	0.426	0.283
	19034	3922	3374	2871	2751	2390	4220	4812
						Note: Plant transfer volumes were not available for the Cleanout Period. The NMC vol was multiplied by 1.12/1.05 to obtain the Plant Vol.		

Campaign # ->	A01			A02			A03			A04		
TANK #	NMC Pu (g)	NMC U (g)	U/Pu	NMC Pu (g)	NMC U (g)	U/Pu	NMC Pu (g)	NMC U (g)	U/Pu	NMC Pu (g)	NMC U (g)	U/Pu
AW-101	89	295367	3319	285	1105925	3880	71	200895	2830	22	148968	6771
AW-102				1	14201	14201	13	82561	6351	66	333354	5051
AW-103	1	15133	15133									
AW-104							0	0		210	373327	1778
AW-105	43	2221027	51652	0	1658	#DIV/0!						
TOTALS	133	2531527	19034	286	1121784	3922	84	283456	3374	298	855649	2871

Table E-5A. Summary and Monthly Transfers of G8 & R8 (Organic Wash) Waste to Tank Farms (includes Campaigns A01 thru A06 and Cleanout Period)

Campaign # ->	A05			A06			Tank Totals			Cleanout Period		
TANK #	NMC Pu (g)	NMC U (g)	U/Pu	NMC Pu (g)	NMC U (g)	U/Pu	NMC Pu (g)	NMC U (g)	U/Pu	NMC Pu (g)	NMC U (g)	U/Pu
AW-101							467	1751155	3750			
AW-102							80	430116	5376			
AW-103							1	15133	15133			
AW-104	568	1562745	2751	316	755271	2390	1094	2691343	2460	9	39634	4404
AW-105							43	2222685	51690			
AN-102										0	3673	#DIV/0!
TOTALS	568	1562745	2751	316	755271	2390	1685	7110432	4220	9	43307	#DIV/0!

Table E-5B. Summary and Monthly Transfers of G8 & R8 (Organic Wash) Waste to Tank Farms

G-8 & R-8 Data Tabulations -- Campaign A01														
	NMC VOLUME TRANSFERS (L)								Waste Volume (PUREX Transfers) TOTAL (L)			Processed Fuel		
	G-8			R-8										
Month	AW-101	AW-103	AW-105	AW-101	AW-103	AW-105	TOTAL (L)		R8 & G8		SX MTU			
Sep-83						90207	90207		96221					
Oct-83						104425	104425		111387					
Nov-83			139655			96131	235786		251505		incl below			
Dec-83			224052			126736	350788		374174		incl below			
Jan-84			190847			83814	274661		292972		incl below			
Feb-84			150996			78477	229473		244771		incl below			
Mar-84			278466			112772	391238		417321		incl below			
Apr-84			280264			33965	314229		335178		491			
May-84			264445			113169	377614		402788		154			
Jun-84		12934	211871			144284	369089		393695		153			
Jul-84	233057		42358	196866		30827	503108		536649		178			
Aug-84	164990			168957			333947		356210		306			
Sep-84	199080			102180			301260		321344		incl above			
CAMPAIGN A01 TOTAL	597127	12934	1782954	468003	0	1014807	3875825		4134213.333		1282			

			NMC Pu (g)				TOTAL Pu(g)	
Sep-83						0	18	
Oct-83						18	27	
Nov-83			9			0	10	
Dec-83			1			0	2	
Jan-84			1			0	2	

NOTE:
Purex Vol given in monthly Campaign Reports are Accountability vol.
The avg ratio of Plant: NMC vol, 1.12/1.05 for the other campaigns, is used to calculate the Vol of Purex waste transfers.

G8 &R8 Waste Summary for CAMPAIGN A01
(Sep'83-Sep-'84)

Table E-5B. Summary and Monthly Transfers of G8 & R8 (Organic Wash) Waste to Tank Farms

Feb-84			0			1	3	
Mar-84			2			0	6	
Apr-84			4			0	7	
May-84			2			1	6	
Jun-84		1	2	0		0	10	
Jul-84	5		2	0		0	84	
Aug-84	77			0			84	
Sep-84	7						140	
CAMPAIGN A01 TOTAL	89	1	23	0	0	20	133	
			NMC U Loss (kg)				Total U (kg)	U/Pu
Sep-83						44.77	44.770	2487
Oct-83						117.211	117.211	4341
Nov-83			116.083			238.265	354.348	35435
Dec-83			158.075			813.636	971.711	485856
Jan-84			35.32			19.877	55.197	27599
Feb-84			4.938			10.855	15.793	5264
Mar-84			7.784			43.138	50.922	8487
Apr-84			91.835			0.747	92.582	13226
May-84			131.864			25.853	157.717	26286
Jun-84		15.133	291.072			64.604	370.809	37081
Jul-84	41.283		4.385	17.832		0.715	64.215	764
Aug-84	42.832			73.758			116.590	1388
Sep-84	100.675			18.987			119.662	855
CAMPAIGN A01 TOTAL	184.79	15.133	841.356	110.577	0	1379.671	2531.527	19034

NMC Data	
Vol (L) =	3875825
Pu (g) =	133
U (kg) =	2531.527
MTU =	1282.000
Tank G8 & R8 Vol (L) =	4134213.333
Plant Vol (incl Jet Dilution) (L) =	4340924
Plant to NMC Waste vol ratio =	1.12
Plant Waste Volume (L) per MTU =	3386
Avg Pu g/Plant L =	3.06386E-05
Avg U g/Plant L =	0.583
Avg U to Pu Ratio =	19034

		AW-101	AW-103	AW-105	
	Pu (g)	89	1	43	
	U (kg)	295.367	15.133	2221.027	

Table E-5C. Summary and Monthly Transfers of G8 & R8 (Organic Wash) Waste to Tank Farms.

	G-8 & R-8 Data Tabulations -- Campaign A02									
	NMC VOLUME TRANSFERS (L)							Waste Volume (PUREX Transfers)	Processed Fuel	
	G-8			R-8				TOTAL (L)		
Month	AW-101	AW-102	AW-105	AW-101	AW-102	AW-105	TOTAL (L)	R8 & G8	SX MTU	
								38303	incl below	
Oct-84	13531			22378			35909	403876	98	
Nov-84	162175			216459			378634	238213	239	
Dec-84	132889		10766	79670			223325	237026	269	
Jan-85	195054			27158			222212	358164	110	
Feb-85	257004			78775			335779	265097	257	
Mar-85	180254			68274			248528	209840	212	
Apr-85	94758	32392		56584	12991		196725	184593	153.9	
May-85	135431			9732	27893		173056	163667	66.4	
Jun-85	63363			90075			153438	277887	305	
Jul-85	174492			86027			260519	230505	282.4	
Aug-85	194710			21388			216098	241813	149	
Sep-85	142686			84014			226700	2848984.533	2141.7	
CAMPAIGN A02 TOTAL	1746347	32392	10766	840534	40884	0	2670923			

Table E-5C. Summary and Monthly Transfers of G8 & R8 (Organic Wash) Waste to Tank Farms.

			NMC Pu (g)				TOTAL Pu(g)	
Oct-84	0			0			0	
Nov-84	89			0			89	
Dec-84	23		0	0			23	
Jan-85	26			0			26	
Feb-85	66			0			66	
Mar-85	23			0			23	
Apr-85	0	0		0	1		1	
May-85	12			0	0		12	
Jun-85	5			3			8	
Jul-85	4			0			4	
Aug-85	15			0			15	

NOTE:

Purex Vol given in monthly Campaign Reports are Accountability vol. The avg ratio of Plant: NMC vol, 1.12/1.05 for the other campaigns, is used to calculate the Vol of Purex waste transfers.

G8 &R8 Waste Summary for CAMPAIGN A02
(Oct'84-Sep'85)

NMC Data

Vol (L) =	2670923
Pu (g) =286	
U (kg) =	1121.784
MTU =2141.700	
Tank G8 & R8 Vol (L) =	2848984.533
Plant Vol (incl Jet Dilution) (L) =	2991433.76
Plant to NMC Waste vol ratio =	1.12
Plant Waste Volume (L) per MTU =	1397
Avg Pu g/Plant L =	9.56063E-05
Avg U g/Plant L =	0.375
Avg U to Pu Ratio =	3922

Table E-5C. Summary and Monthly Transfers of G8 & R8 (Organic Wash) Waste to Tank Farms.

Sep-85	19			0			19					
CAMPAIGN A02 TOTAL	282	0	0	3	1	0	286					
			NMC U Loss (kg)				Total U (kg)	U/Pu				
Oct-84	0.643			0.341			0.984	#DIV/0!				
Nov-84	153.731			44.841			198.572	2231		AW-101	AW-102	AW-105
Dec-84	88.522		1.658	71.995			162.175	7051	Pu (g)	285	1	0
Jan-85	121.401			8.458			129.859	4995	U (kg)	1105.925	14.201	1.658
Feb-85	194.451			82.948			277.399	4203				
Mar-85	100.347			38.765			139.112	6048				
Apr-85	29.694	2.194		13.019	1.923		46.830	46830				
May-85	26.844			2.623	10.084		39.551	3296				
Jun-85	11.544			57.543			69.087	8636				
Jul-85	20.402			7.251			27.653	6913				
Aug-85	11.154			6.652			17.806	1187				
Sep-85	8.746			4.01			12.756	671				
CAMPAIGN A02 TOTAL	767.479	2.194	1.658	338.446	12.007	0	1121.784	3922				

Table E-5D. G-8 & R-8 Data Tabulations (Organic Wash Waste) -- Campaigns A03 and A04.

	NMC VOLUME TRANSFERS (L)								Plant Volume (PUREX Summaries)					
	G-8			R-8					G-8		R-8		TOTAL (L)	Processed Fuel
Month	AW-101	AW-102	AW-104	AW-101	AW-102	AW-104	TOTAL (L)		gal	L	gal	L	R8&G8	SK MTU
Oct-85	87491	80463.8	0	18480.3	60166.4		246601.5		48553	183772	22685.78	85865.7	269637.3819	51.6
Nov-85	132768.3	32430.3	0	17009.8	41934		224142.4		49346	186774	17024.7	64438.5	251212.6832	152.35
Dec-85	135068.9	21607.8	0	65586.1	0		222262.8		44326	167773	18643.7	70566.4	238339.7846	140.86
CAMPAIGN A03 TOTAL	355328.2	134501.9	0	101076.2	102100.4		693006.7		142224	538319	58354.18	220870.6	759189.8496	344.79
Jan-86	53980.2	0	0	57831.8			111812		15207	57557	17030.9	64462.0	122019.4296	18.7
Feb-86	152038.2	0	0	83720.8			235759		42821	162076	23687.1	89655.7	251731.9473	186.91
Mar-86	97989.1	92513	0	42371.9	10609.4		243483.4		53690	203215	14896.7	56384.0	259599.3348	243.05
Apr-86	0	217446	0	27813.3	63858.6		309117.9		62741	237473	26958	102056.0	339509.3903	103.07
May-86	0	190240.2	0		35449.9		225690.1		53639	203025	10002.2	37858.3	240883.3046	139.795
Jun-86	0	118583.7	0		47580.5		166164.2		33371	126310	13407.2	50746.3	177056.2819	75.695
Jul-86	0	77160.3	85489.1		84994.1	19541.6	267185.1		45665	172843	29630.4	112151.1	284994.3759	196.74
Aug-86	0	0	186785.2		10761.9	93412.7	290959.8		52654	199296	25451.4	96333.5	295629.4689	215.18
Sep-86	0	0	132886.4	25439			158325.4		38068	144086	7234.532692	27382.7	171468.5092	10.05
CAMPAIGN A04 TOTAL	304007.5	695943.2	405160.7	237176.8	253254.4	112954.3	2008496.9		397855	1505882	1.68E+05	637009.6	2142892.042	1195.08
									Note: Sep-86 G8 and R8 Purex Volumes have been proportionately divided between Campaigns 4 and 5, based on NMC volume ratios.					-
			NMC Pu (g)				TOTAL Pu(g)							-
Oct-85	7	4	0	0	0		11							
Nov-85	47	9	0	0	0		56							
Dec-85	17	0	0	0			17							
CAMPAIGN A03 TOTAL	71	13	0	0	0		84							

Table E-5D. G-8 & R-8 Data Tabulations (Organic Wash Waste) -- Campaigns A03 and A04.

Jan-86	7	0	0	0			7							
Feb-86	14	0	0	0			14							
Mar-86	1	13	0	0	0		14							
Apr-86	0	39	0	0	0		39							
May-86	0	7	0		0		7							
Jun-86	0	3	0		0		3							
Jul-86	0	4	6		0	0	10							
Aug-86	0	0	81		0	0	81							
Sep-86	0	0	123	0			123							
CAMPAIGN A04 TOTAL	22	66	210	0	0	0	298							
			NMCC U Loss (kg)				Total U (kg)	U/Pu						
Oct-85	18.188	34.973	0	2.458	6.688		62.307	5664						
Nov-85	94.967	22.297	0	7.338	17.617		142.219	2540						
Dec-85	54.242	0.986	0	23.702			78.93	4643						
CAMPAIGN A03 TOTAL	167.397	58.256	0	33.498	24.305	0	283.456	3374						
Jan-86	2.131	0	0	7.266			9.397	1342						
Feb-86	74.428	0	0	25.244			99.672	7119						
Mar-86	22.494	35.569	0	6.898	1.347		66.308	4736						
Apr-86	0	88.203	0	9.829	10.24		108.272	2776						
May-86	0	106.8	0		19.418		126.218	18031						
Jun-86	0	36.248	0		8.325		44.573	14858						

Table E-5D. G-8 & R-8 Data Tabulations (Organic Wash Waste) -- Campaigns A03 and A04.

Jul-86	0	14.353	31.12		10.456	17.192	73.121	7312		
Aug-86	0	0	120.086		2.395	19.648	142.129	1755		
Sep-86	0	0	185.281	0.678			185.959	1512		
CAMPAIGN A04 TOTAL	99.053	281.173	336.487	49.915	52.181	36.84	855.649	2871		
A03 U/Pu	2358	4481	#DIV/0!	#DIV/0!	#DIV/0!	#DIV/0!				
A04 U/Pu	4502	4260	1602	#DIV/0!	#DIV/0!	#DIV/0!				
A03 & A04 G8-R8, U/Pu for AW-101 =				2766						
A03 & A04 G8-R8, U/Pu for AW-102 =				4026	NOTE: ERR indicates 0 g Pu yielding an infinite U/Pu ratio.					
A03 & A04 G8-R8, U/Pu for AW-104 =				1778						

CAMPAIGN A03

	AW-101	AW-102	AW-104	
Pu(g)	71	13		0
U(kg)	200.895	82.561	0	

CAMPAIGN A04

	AW-101	AW-102	AW-104	
Pu(g)	22	66		210
U(kg)	148.968	333.354	373.327	

G8 & R8 Waste Summary for CAMPAIGN A03 (OCT-DEC'85)

NMC Data

Vol (L) =	693006.7
Pu (g) =	84
U (kg) =	283.456
MTU =	344.790
Tank G8 & R8 Vol (L) =	759189.8496
Plant Vol (incl Jet Dilution) (L) =	797149.3421
Plant to NMC Waste vol ratio =	1.15
Plant Waste Volume (L) per MTU =	2312
Avg Pu g/Plant L =	0.000103575
Avg U g/Plant L =	0.356
Avg U to Pu Ratio =	3374

G8 & R8 Waste Summary for CAMPAIGN A04 (Jan-Oct'86)

NMC Data

Vol (L) =	2008496.9
Pu (g) =	298
U (kg) =	855.649
MTU =	1193.079
Tank G8 &R8 Vol (L) =	2142892.0
Plant Vol (incl Jet Dilution) (L) =	2250036.644
Plant to NMC Waste vol ratio =	1.12
Plant Waste Volume (L) per MTU =	1886
Avg Pu g/Plant L =	0.000132442
Avg U g/Plant L =	0.380
Avg U to Pu Ratio =	2871

G8 & R8 Waste SUMMARY for CAMPAIGNS A03 & A04

NMC Data

Vol (L) =	2701503.6
Pu (g) =	382
U (kg) =	1139.105
MTU =	1537.869
Tank G8 & R8 Vol (L) =	2902081.892
Plant Vol (incl Jet Dilution) (L) =	3047185.987
Plant to NMC Waste vol ratio =	1.13
Plant Waste Volume (L) per MTU =	1981
Avg Pu g/Plant L =	0.000125362
Avg U g/Plant L =	0.374
Avg U to Pu Ratio =	2982

Table E-6A. Summary and Monthly Transfers of U3 & U4 (Acid Fractionator Sump) Waste to Tank Farms (includes Cleanout Period).

				CAMPAIGN #				SUMMARY	Cleanout Period			
	A01		A02	A03	A04	A05	A06		(Jun'95-Jan'96)			
NMC Data												
Vol (L) =	1593822		2366465	294947	1535580	1694447	1888807	9374067.5	1100804			
Pu (g) =	113		45	16	1	7	0	182	3			
U (kg) =	19.338		22.491	3.959	17.304	5.623	9.16	77.875	240.608			
MTU =	1282		2141.7	344.790	1195.079	297.335	880.875	6139.779	0			
Tanks U3 & U4 Vol (L)=	1700077		2569305	317392	1646217	1912142	1973762	10118895.1	1184674.781			
Plant Vol (incl Jet Dilution) (L) =	1785080.85		2697770.25	333261	1728528	2007749.1	2072450.1	10624839.86	1243908.52			
Plant to NMC Waste vol ratio =	1.12		1.14	1.13	1.13	1.18	1.10	1.13	1.13			
Plant Waste Volume (L) per MTU=	1392		1259.6	967	1449	6752	2352.7	1730.5	not applicable			
Avg Pu g/Plant L=	0.00006		1.66804E-05	4.80103E-05	0.0000006	0.0000035	0	1.71297E-05	0.0000024			
Avg U g/Plant L=	0.011		0.008	0.012	0.010	0.003	0.004	0.007	0.193			
Avg U to Pu Ratio =	171		500	247	17304	803	#DIV/0!	428	80203			
Campaign # ->		A01			A02			A03			A04	
TANK #	NMC Pu (g)	NMC U (g)	U/Pu	NMC Pu (g)	NMC U (g)	U/Pu	NMC Pu (g)	NMC U (g)	U/Pu	NMC Pu (g)	NMC U (g)	U/Pu
AW-101	36	9084	252	41	21202	517	11	1346	122	1	2103	2103
AW-102				2	357	179	5	2613	523	0	9663	#DIV/0!
AW-103				0	107	#DIV/0!						
AW-104										0	5538	#DIV/0!
AW-105	77	10254	133	2	825	413						
TOTALS	113	19338	171	45	22491	500	16	3959	247	1	17304	17304
Campaign # ->		A05			A06			Tank Totals			Cleanout Period	

Table E-6A. Summary and Monthly Transfers of U3 & U4 (Acid Fractionator Sump) Waste to Tank Farms (includes Cleanout Period).

TANK #	NMC Pu (g)	NMC U (g)	U/Pu	NMC Pu (g)	NMC U (g)	U/Pu	NMC Pu (g)	NMC U (g)	U/Pu	NMC Pu (g)	NMC U (g)	U/Pu
AW-101							89	33735	379			
AW-102				0	1	#DIV/0!	7	12634	1805			
AW-103							0	107	#DIV/0!			
AW-104	7	5623	803	0	9159	#DIV/0!	7	20320	2903	0	1595	#DIV/0!
AW-105							79	11079	140	3	237090	79030
AP-108										0	1923	#DIV/0!
TOTALS	7	5623	803	0	9160	#DIV/0!	182	77875	428	3	240608	80203

Note:

Plant transfer volumes were not available for the cleanout period. The NMC vol was multiplied by 1.13/1.05 to obtain Plant Vol.
"ERR indicates 0 g Pu, yielding an infinite U/Pu ratio."

Table E-6B. Summary and Monthly Transfers of U3 & U4 (Acid Fractionator Sump) Waste to Tank Farms
U3 & U4 Data Tabulations – Campaign A01.

	NMC VOLUME TRANSFERS (L)					Waste Volume (PUREX Transfers)		
	U-3		U-4				Total (L)	Processed Fuel
Month	AW-101	AW-105	AW-101	AW-105	TOTAL (L)		R8 & G8	SX MTU
Sep-83		119161		32626	151787		161906	
Oct-83		49686		16606	66292		70711	
Nov-83		68665		16371	85036		90705	incl below
Dec-83		50042		17367	67409		71903	incl below
Jan-84		189697		28870	218567		233138	incl below
Feb-84		112124			112124		119599	incl below
Mar-84		180438		41290	221728		236510	incl below
Apr-84		149209		25679	174888		186547	491
May-84		68794		13097	81891		87350	154
Jun-84		73927		18506	92433		98595	153
Jul-84	63589		19540		83129		88671	178
Aug-84	68166		23052		91218		97299	306
Sep-84	78534		68786		147320		157141	incl above
CAMPAIGN A01 TOTAL	210289	1061743	111378	210412	1593822		1700076.8	1282
		NMC Pu (g)			TOTAL Pu(g)			
Sep-83		0		1	1			
Oct-83		1			1			
Nov-83		2			2			
Dec-83		1			1			
Jan-84		4			4			
Feb-84		2			2			
Mar-84		5		3	8			

Table E-6B. Summary and Monthly Transfers of U3 & U4 (Acid Fractionator Sump) Waste to Tank Farms
U3 & U4 Data Tabulations -- Campaign A01.

Apr-84		3		5	8			
May-84		29		1	30			
Jun-84		19		1	20			
Jul-84	12		4		16			
Aug-84	6		8		14			
Sep-84	2		4		6			
CAMPAIGN A01 TOTAL	20	66	16	11	113			
		NMC U Loss (kg)			Total U (kg)	U/Pu		
Sep-83		0.573		0.328	0.901	901		
Oct-83		0.642		0.039	0.681	681		
Nov-83		1.272		0.027	1.299	650		
Dec-83		1.157		0.769	1.926	1926		
Jan-84		0.886		0.702	1.588	397		
Feb-84		0.56			0.560	280		
Mar-84		0.221		0.12	0.341	43		
Apr-84		0.403		0.523	0.926	116		
May-84		1.031		0.445	1.476	49		
Jun-84		0.213		0.343	0.556	28		
Jul-84	7.197		0.172		7.369	461		
Aug-84	0.261		0.121		0.382	27		
Sep-84	0.322		1.011		1.333	222		
CAMPAIGN A01 TOTAL	7.78	6.958	1.304	3.296	19.338	171		

Table E-6B. Summary and Monthly Transfers of U3 & U4 (Acid Fractionator Sump) Waste to Tank Farms
U3 & U4 Data Tabulations – Campaign A01.

NOTE:

Purex Vol given in Campaign A01 monthly Report are Accountability vol.
"The avg ratio of Plant: NMC vol, 1.12/1.05 for the other campaigns," is used to calculate the Vol of Purex waste transfers.
G8 &R8 Waste Summary for CAMPAIGN A01
(Sep'83-Sep-'84)

NMC Data

Vol (L)			=	1593822	
Pu (g)			=	113	
U (kg)			=	19.338	
MTU				=	1282.000
Tank G8 & R8 Vol (L)		=	1700076.8		
Plant Vol (incl Jet Dilution) (L)	=	1785080.6			
Plant to NMC Waste vol ratio		=	1.12		
Plant Waste Volume (L) per MTU	=	1392			

Avg Pu g/Plant L	=	6.33E-05
Avg U g/Plant L	=	0.011
Avg U to Pu Ratio	=	171

	AW-101		AW-105
Pu (g)	36		77
U (kg)	9.084	10.254	

Table E-6C. Summary and Monthly Transfers of U3 & U4 (Acid Fractionator Sump) Waste to Tank Farms
U3 & U4 Data Tabulations (Acid Fractionator Sump Waste) -- Campaign A02

	NMC VOLUME TRANSFERS (L)							Waste Volume (PUREX Transfers)	
		U-3				U-4		TOTAL (L)	Proceed Fuel
Month	AW-101	AW-102	AW-103	AW-105	AW-101	AW-102	TOTAL (L)	R8 & G8	SX MTU
Sep-84	25513						25513	27700	
Oct-84	48350				24347		72697	78928	incl below
Nov-84	58782				23258		82040	89072	98
Dec-84	80650			67079	68413		216142	234668	239
Jan-85	150424			24768	62552		237744	258122	269
Feb-85	173784				62550		236334	256591	110
Mar-85	161812				63653		225465	244791	257
Apr-85	106713	75270			43760	22713	248456	269752	212
May-85	97418				22737		120155	130454	153.9
Jun-85	142221				48611		190832	207189	66.4
Jul-85	176998		28526		38008		243532	264406	305
Aug-85	222575				40941		263516	286103	282.4
Sep-85	140345				63694		204039	221528	149
CAMPAIGN A02 TOTAL	1585585	75270	28526	91847	562524	22713	2366465	2569304.857	2141.7

Table E-6C. Summary and Monthly Transfers of U3 & U4 (Acid Fractionator Sump) Waste to Tank Farms
U3 & U4 Data Tabulations (Acid Fractionator Sump Waste) -- Campaign A02

				NMC (Pu)			TOTAL Pu(g)		
Sep-84	1						1		
Oct-84	2						2		
Nov-84	2				1		3		
Dec-84	2			2	2		6		
Jan-85	3			0	0		3		
Feb-85	9				3		12		
Mar-85	9				4		13		
Apr-85	2	2			1	0	5		
May-85	0				0		0		
Jun-85	0				0		0		
Jul-85	0		0		0		0		
Aug-85	0				0		0		
Sep-85	0				0		0		
CAMPAIGN A02 TOTAL	30	2	0	2	11	0	45		

Table E-6C. Summary and Monthly Transfers of U3 & U4 (Acid Fractionator Sump) Waste to Tank Farms
U3 & U4 Data Tabulations (Acid Fractionator Sump Waste) -- Campaign A02

			NMC U Loss (kg)				Total U (kg)		
Sep-84	0.026						0.026		
Oct-84	0.040				0.028		0.068		
Nov-84	1.618				0.086		1.704		
Dec-84	0.093			0.067	0.265		0.425		
Jan-85	0.253			0.758	0.099		1.110		
Feb-85	0.730				0.064		0.794		
Mar-85	1.750				1.566		3.316		
Apr-85	0.255	0.293			1.916	0.064	2.528		
May-85	1.793				0.018		1.811		
Jun-85	1.087				0.05		1.137		
Jul-85	1.466		0.107		0.137		1.710		
Aug-85	3.858				0.879		4.737		
Sep-85	1.925				1.2		3.125		
CAMPAIGN A02 TOTAL	14.894	0.293	0.107	0.825	6.308	0.064	22.491		

Table E-6C. Summary and Monthly Transfers of U3 & U4 (Acid Fractionator Sump) Waste to Tank Farms
U3 & U4 Data Tabulations (Acid Fractionator Sump Waste) – Campaign A02

NOTE:

Purex Vol given in Campaign A02 monthly Report is Accountability vol.
"The avg ratio of Plant: NMC vol, 1.14/1.05 for the other campaigns," is used to calculate the Vol of Purex waste transfers.

U3 & U4 Waste Summary for CAMPAIGN A02
(Sep'84-Sep'85)

NMC Data Vol (L)	=	2366465
Pu (g)	=	45
U (kg)	=	22.491
MTU	=	2141.700
Tank U3 & U4 Vol (L)	=	2569304.857
Plant Vol (incl Jet Dilution) (L)	=	2697770.1
Plant to NMC Waste vol ratio	=	1.14
Plant Waste Volume (L) per MTU	=	1260
Avg Pu g/Plant L	=	1.66804E-05
Avg U g/Plant L	=	0.008
Avg U to Pu Ratio	=	500

	AW-101	AW-102	AW-103	AW-105
Pu (g)	41	2	0	2
U (kg)	21.202	0.357	0.107	0.825

Note: ERR indicates 0 g Pu, yielding an infinite U/Pu ratio.

Table E-6D. Summary and Monthly Transfers of U3 & U4 (Acid Fractionator Sump) Waste to Tank Farms U-3 & U-4 Data Tabulations – Campaigns A03 and A04.

	NMC VOLUME TRANSFERS (L)							Plant Volume (PUREX Summaries)				U3 & U4 Waste Summary CAMPAIGN A03
		U-3			U-4				U3 & U4		Proceed Fuel	
Month	AW-101	AW-102	AW-104	AW-101	AW-102	AW-104	TOTAL (L)		gal	L	SX MTU	NMC Data
												Vol (L) = 294946.5
Oct-85	0	72737.9	0	0	21862.9		94600.8		2.70E+04	102359.3	51.6	Pu (g) = 16
Nov-85	71030.8	35946.9	0	0	0		106977.7		3.03E+04	114651.4	152.33	U (kg) = 3.959
Dec-85	66382.5	0	0	0	26985.5		93368		2.65E+04	100381.2	140.86	MTU = 344.790
CAMPAIGN A03 TOTAL	137413.3	108684.8	0	0	48848.4	0	294946.5		83855.2	317391.9	344.79	Tank U3 &U4 Vol (L) = 317391.932
												Plant Vol (incl Jet Dilution) (L) = 333261.5286
Jan-86	129791.8	0	0	19596.8			149388.6		4.40E+04	166709.6	18.7	Plant to NMC Waste vol ratio = 1.13
Feb-86	170333.3	0	0	20078.3			190411.6		5.41E+04	204689.4	186.91	Plant Waste Volume (L) per MTU = 967
Mar-86	69916.5	139241.4	0		19844		229001.9		6.45E+04	243953.5	243.05	Avg Pu g/Plant L = 4.80105E-05
Apr-86	0	176647.5	0	0	14632.1		191279.6		5.45E+04	206227.6	109.07	Avg U g/Plant L= 0.012
May-86	146521.5	0	0		41775		188296.5		5.29E+04	200254.9	139.793	Avg U to Pu Ratio = 247
Jun-86	164316.7	0	0		44015.8		208332.5		5.84E+04	221201.1	73.606	
Jul-86	0	79416.1	83380.5		21339.1	29629.7	213765.4		6.06E+04	229194.2	196.74	
Aug-86	0	0	92164			20858.4	113022.4		3.24E+04	122659.7	215.18	
Sep-86	0	0	22146			29935.9	52081.9		1.36E+04	51327.2	10.03	
CAMPAIGN A04 TOTAL	680879.8	395305.0	197690.5	39675.1	141606.0	80424.0	1535580.4		4.35E+05	1646217.2	1195.08	

Table E-6D. Summary and Monthly Transfers of U3 & U4 (Acid Fractionator Sump) Waste to Tank Farms U-3 & U-4 Data Tabulations – Campaigns A03 and A04.

												U3 & U4 Waste Summary for CAMPAIGN A04
				NMC Pu (g)			TOTAL Pu(g)					
Oct-85		0		0			0		Campaign 3			NMC Data
Nov-85	10	5					15		AW-101	AW-102	AW-104	Vol (L) = 1535580.4
Dec-85	1				0		1	Pu (g)	11	5	0	Pu (g) = 1
CAMPAIGN A03 TOTAL	11	5	0	0	0	0	16	U (g)	1.346	2.613	0	U (kg) = 17.304
												MTU = 1193.079
Jan-86	0			0			0					Tank U3&U4 Vol (L) = 1646217.2
Feb-86	0			1			1		Campaign 4			Plant Vol (incl Jet Dilution) (L) = 1728528.104
Mar-86	0	0		0			0		AW-101	AW-102	AW-104	Plant to NMC Waste vol ratio = 1.13
Apr-86		0			0		0	Pu (g)	1	0	0	Plant Waste Volume (L) per MTU = 1449
May-86	0				0		0	U (g)	2.103	9.663	5.538	Avg Pu g/Plant L= 5.78527E-07
Jun-86	0				0		0					Avg U g/Plant L=0.010
Jul-86		0			0	0	0					Avg U to Pu Ratio =17304
Aug-86			0			0	0					
Sep-86			0			0	0					
CAMPAIGN A04 TOTAL	0	0	0	1	0	0	1					

Table E-6D. Summary and Monthly Transfers of U3 & U4 (Acid Fractionator Sump) Waste to Tank Farms U-3 & U-4 Data Tabulations – Campaigns A03 and A04.

												U3 & U4 Waste Summary for CAMPAIGNS A03 & A04
				NMC U Loss (kg)			Total U (kg)	U/Pu				NMC Data
Oct-85		0.143			0.571		0.714	#DIV/0!				Vol (L) = 1830526.9
Nov-85	1.224	0.533					1.757	117				Pu (g) = 17
Dec-85	0.122				1.366		1.488	1488				U (kg) = 21.263
CAMPAIGN A03 TOTAL	1.346	0.676	0	0	1.937	0	3.959	247				MTU = 1537.869
												Tank U3&U4 Vol (L) = 1963609.174
Jan-86	0.051			0.025			0.076	#DIV/0!				Plant Vol (incl Jet Dilution) (L) = 2061789.632
Feb-86	0.357			0.349			0.706	706				Plant to NMC Waste vol ratio = 1.13
Mar-86	0.084	0.151			7.561		7.796	#DIV/0!				Plant Waste Volume (L) per MTU = 1341
Apr-86		0.572			0.565		1.137	#DIV/0!				Avg Pu g/Plant L = 8.245265-06
May-86	0.335				0.19		0.525	#DIV/0!				Avg U g/Plant L=0.010
Jun-86	0.224				0.025		0.249	#DIV/0!				Avg U to Pu Ratio =1251
Jul-86		0.56	0.138		0.039	0.617	1.354	#DIV/0!				
Aug-86			3.454			0.064	3.518	#DIV/0!				
Sep-86			0.226	0.678		1.039	1.943	#DIV/0!				
CAMPAIGN A04 TOTAL	1.051	1.283	3.818	1.052	8.38	1.72	17.304	17304				
A03 U/Pu	122	135	#DIV/0!	#DIV/0!	#DIV/0!	#DIV/0!		Note: ERR indicates 0 g Pu yielding an infinite U/Pu ratio				
A04 U/Pu	#DIV/0!	#DIV/0!	#DIV/0!	1052	#DIV/0!	#DIV/0!						
A03 & A04 U3-U4, U/Pu for AW-101 =				287								
A03 & A04 U3-U4, U/Pu for AW-102 =				2455								

Table E-6E. Summary and Monthly Transfers of U3 & U4 (Acid Fractionator Sump) Waste to Tank Farms

	U-3 & U-4 Data Tabulations - Campaign A05							
Month	NMC VOLUME TRANSFERS (L)			PUREX Summary Vol			Processd Fuel	
	U-3	U-4	TOTAL	U-3 & U-4			SX MTU	Purex: NMC Vol ratio
	AW-104	AW-104	AW-104		gal	L		
Oct-86	145904.9	107813.8	253718.7		75747	286702.1	0	1.13
Nov-87	41812.9	50378.4	92191.3		27523	104176.2	0	1.13
Dec-86	0	0	0		0	0.0	0	1.11
Jan-87	51357.9	21347.4	72705.3		21243	80404.8	0	1.38
Feb-87	46116.4	48253.5	94369.9		34386	130151.0	0	1.07
Mar-87	71144.8	23405.7	94550.5		26770	101324.5	16.77	1.11
Apr-87	23544.6	21716.1	45260.7		13248	50143.7	18.85	1.13
May-87	42785.6	0	42785.6		12730	48183.1	5.917	1.08
Jun-87	44594.9	61900.6	106495.5		30552	114882.3	0	1.07
Jul-87	71385.1	68077	139462.1		39407	149155.5	95.923	
Aug-87	134470.5	86561.4	221031.9		64521	244212.0	79.534	1.10
Sep-87	75180.3	92168.2	167348.5		46834	177266.7	80.341	1.06
Oct-87	51438.2	47267.8	98706		27776	105132.2	0	1.07
Nov-87	148843.6	21297.4	170141		50795	192259.3	0	1.13
Dec-87	95680.3	0	95680.3		33857	128148.7	0	1.34
CAMPAIGN A05 TOTAL	1044260	650187.3	1694447.3		505189	1912142	297.335	1.13

Table E-6E. Summary and Monthly Transfers of U3 & U4 (Acid Fractionator Sump) Waste to Tank Farms

	NMC Pu (g)			
	U-3	U-4	TOTAL	
Oct-86	0	1	1	
Nov-86	0	0	0	
Dec-86	0	0	0	
Jan-87	0	0	0	
Feb-87	0	0	0	
Mar-87	0	0	0	
Apr-87	0	0	0	
May-87	0	0	0	
Jun-87	0	0	0	
Jul-87	1	0	1	
Aug-87	0	0	0	
Sep-87	0	0	0	
Oct-87	0	5	5	
Nov-87	0	0	0	
Dec-87	0	0	0	
CAMPAIGN A05 TOTAL	1	6	7	

NOTE: For the months Oct-Dec'86 and Nov'87 the reported Purex waste transfer vol is less than NMC vol. These Purex vol figures are apparently in error. For these months, NMC vol is multiplied by the factor 1.13, to obtain Purex transfer vol.

U3 & U4 Waste Summary for CAMPAIGN A05
(Oct'86-Dec'87)

NMC Data

Vol (L) =	1694447.3
Pu (g) =	7
U (kg) =	5.623
SX MTU =	297.335
Tank U3 & U4 Vol (L) =	1912141.97
Plant Vol (incl Jet Dilution) (L) =	2007749.069
Plant to NMC Waste vol ratio =	1.18
Plant Waste Volume (L) per MTU =	6752

Table E-6E. Summary and Monthly Transfers of U3 & U4 (Acid Fractionator Sump) Waste to Tank Farms

	NMC U Loss (kg)					Pu g/Plant L = 3.48649E-05
	U-3	U-4	TOTAL	U/Pu		U g/Plant L = 0.003
Oct-86	0.261	0.408	0.669	669.0		U to Pu Ratio = 803
Nov-86	0.011	0.013	0.024	#DIV/0!		
Dec-86	0	0	0	#DIV/0!		
Jan-87	0.034	0.002	0.036	#DIV/0!		
Feb-87	0.016	0.006	0.022	#DIV/0!		
Mar-87	0.252	0.281	0.533	#DIV/0!	Note: ERR indicates 0 g Pu, yielding an infinite U/Pu ratio.	
Apr-87	0.033	0.016	0.049	#DIV/0!		
May-87	0.054	0	0.054	#DIV/0!		
Jun-87	0.005	0.095	0.1	#DIV/0!		
Jul-87	0.904	0.556	1.46	1460.0		
Aug-87	0.334	0.238	0.572	#DIV/0!		
Sep-87	0.904	0.352	1.256	#DIV/0!		
Oct-87	0.164	0.042	0.206	41.2		
Nov-87	0.449	0.112	0.561	#DIV/0!		
Dec-87	0.081	0	0.081	#DIV/0!		
CAMPAIGN A05 TOTAL	3.502	2.121	5.623	803.3		

Table B-6F. Summary and Monthly Transfers of U3 & U4 (Acid Fractionator Sump) Waste to Tank Farms U-3 & U-4 Data Tabulations (Acid Fractionator Sump Waste) -- Campaign A06.

Month	NMC VOLUME TRANSFERS (L)			NMC Plutonium (g)			NMC Uranium (kg)			PUREX Summary Vol		Processed Fuel
	U-3	U-4	TOTAL	U-3	U-4	TOTAL	U-3	U-4	TOTAL	U-3 & U-4		
	AW-104	AW-104	AW-104	AW-104	AW-104	AW-104	AW-104	AW-104	AW-104	gal	L	SX MTU
Jan-88	72506	17789	90294	0	0	0	0.059	0.151	0.210	32532	123134	11.1
Feb-88	135217	46792	182008	0	0	0	0.169	0.827	0.996	51538.00	195071	62
Mar-88	156860	74792	231652	0	0	0	0.484	1.045	1.529	64052.00	242437	89.5
Apr-88	54065	25805	79870	0	0	0	0.062	0.016	0.078	22635.00	85673	0
May-88	106620	0	106620	0	0	0	0.112	0.000	0.112	29845.00	112963	20.805
Jun-88	81264	0	81264	0	0	0	0.790	0.000	0.790	16380.00	61998	136.543
Jul-88	46308	19984	66292	0	0	0	0.073	0.003	0.076	25433.00	96264	52.63
Aug-88	102884	0	102884	0	0	0	0.757	0.000	0.757	29139.00	110291	160.74
Sep-88	82250	20734	102984	0	0	0	0.038	0.060	0.098	29425.00	111374	87.18
Oct-88	67241	0	67241	0	0	0	1.142	0.000	1.142	12203.00	46188	112.937
Nov-88	45640	0	45640	0	0	0	0.366	0.000	0.366	18991.40	71882	43.71
Dec-88	24272	19158	43430	0	0	0	0.036	0.003	0.039	11694.30	44263	30.82
Jan-89	43621	0	43621	0	0	0	0.913	0.000	0.913	11734.80	44416	0.00
Feb-89	49385	0	49385	0	0	0	0.007	0.000	0.007	13232.6	50085	0
Mar-89	54405	0	54405	0	0	0	0.044	0.000	0.044	14518.8	54954	0
Apr-89	49190	0	49190	0	0	0	0.157	0.000	0.157	13111	49625	0
May-89	27343	0	27343	0	0	0	0.007	0.000	0.007	7085	26817	0
Jun-89	46387	20239	66627	0	0	0	0.013	0.395	0.408	17847.8	67554	0
Jul-89	47546	0	47546	0	0	0	0.029	0.000	0.029	12676.6	47981	0
Aug-89	23698	0	23698	0	0	0	0.004	0.000	0.004	6431	24341	0
Sep-89	23221	0	23221	0	0	0	0.010	0.000	0.010	6210	23505	0
Oct-89	23925	0	23925	0	0	0	0.004	0.000	0.004	6417	24288	0
Nov-89	47850	0	47850	0	0	0	0.088	0.000	0.088	12832	48569	0

Table B-6F. Summary and Monthly Transfers of U3 & U4 (Acid Fractionator Sump) Waste to Tank Farms U-3 & U-4 Data Tabulations (Acid Fractionator Sump Waste) -- Campaign A06.

Dec-89	44875	0	44875	0	0	0	0.010	0.000	0.010	12056	45632	0
Jan-90	49440	21019	70459	0	0	0	0.040	0.507	0.547	18944.2	71704	0
Feb-90	20746	0	20746	0	0	0	0.001	0.000	0.001	5546	20992	72.91
Mar-90	50121	20295	70416	0	0	0	0.471	0.266	0.737	18959	71760	0
CAMPAIGN A06 TOTAL	1576877.47	286607.17	1863484.64	0	0	0	5.886	3.273	9.159	521469.5	1973762	880.875

NOTES:

In Jan-88 there was one NMC transfer from U3 tank to AW-102 of 25322 L, containing 0 g Pu and only 0.001 kg U. This transfer has been accounted for in the Summary.

For Jan & Feb-88 the SX MTU was not available. The HE MTU has been used for these months.

ERR (see Summary) indicates 0 g Pu, yielding an infinite U/Pu ratio."

U3 & U4 Waste Summary for CAMPAIGN A06
(Jan'88-Mar'90)

NMC Data	
Vol (L) =	1888806.64
Pu (g) =	0
U (kg) =	9.16
MTU =	880.875
Tank U3 & U4 Vol (L) =	1973762.058
Plant Vol (incl Jet Dilution) (L) =	2072450.16
Plant to NMC Waste vol ratio =	1.10
Plant Waste Volume (L) per MTU =	2352.7
Pu g/Plant L=	0
U g/Plant L =	0.00442
U to Pu Ratio =	#DIV/0!

Table E-6G. Summary and Monthly Transfers of U3 & U4 (Acid Fractionator Sump) Waste to Tank Farms U3 & U4 Data Tabulation for Plant Cleanout Period.

	AW-104			AP-108			AW-105		
	Vol (L)	U (g)	Pu (g)	Vol (L)	U (g)	Pu (g)	Vol (L)	U (g)	Pu (g)
Jun-90	47400	176	0						
Aug-90	17539	496	0						
Oct-90	30056	149	0						
Nov-90	55503	136	0						
Jan-91	189482	484	0						
Feb-91	44655	28	0						
Mar-91	77857	101	0						
Apr-91	25815	25	0						
Jun-91				32639	1432	0			
Oct-91				16571	319	0			
Dec-91				8398	63	0			
Jan-92				21696	37	0			
Apr-92				33641	72	0			
Jul-92							19687	15	0
Aug-92							9997	74	0
Sep-92							77164	189	0
Oct-92							18799	207	0
Nov-92							19774	4	0
Dec-92							17020	11	0
Jan-93							19113	12	0

Table E-6G. Summary and Monthly Transfers of U3 & U4 (Acid Fractionator Sump) Waste to Tank Farms U3 & U4 Data Tabulation for Plant Cleanout Period.

Feb-93							41359	11	0
Mar-93							33648	247	0
May-93							24362	105	0
Oct-93							19231	1154	0
Dec-94							17939	1044	0
Jan-95							20093	1172	0
Jul-95							17568	2264	0
Sep-95							24369	206744	0
Dec-95							47170	2322	2
Jan-96							72259	21515	1
TOTALS	488307	1595	0	112945	1923	0	499552	237090	3
TOTAL FOR ALL TANKS:			Vol (L)	U (g)	Pu (g)				
			1100804	240608	3				

APPENDIX F

CONCENTRATION RATIO OF PLUTONIUM (IV) HYDROXYCARBONATE AND PLUTONIUM(IV) HYDROXY-EDTA COMPLEXES

This page intentionally left blank.

APPENDIX F

CONCENTRATION RATIO OF PLUTONIUM (IV) HYDROXYCARBONATE AND PLUTONIUM(IV) HYDROXY-EDTA COMPLEXES

Concentrations of $Pu(OH)_4(CO_3)_2^{4-}$, and $Pu(OH)EDTA^-$ in a typical waste tank supernatant can be compared to evaluate the significance of organic complexes of Pu(IV). For this purpose, we chose tank B-109 in which the estimated concentration of EDTA is about an order of magnitude higher than carbonate concentration.

The formation of $Pu(OH)_4(CO_3)_2^{4-}$ complex is represented by the reaction:

$$Pu^{4+} + 4OH^- + 2CO_3^{2-} = Pu(OH)_4(CO_3)_2^{4-} \quad (1)$$

According to the mass action law, the concentration of the complex is related to the concentrations of the unbound species by the relationship:

$$[Pu(OH)_4(CO_3)_2^{4-}] = K_1^c[Pu^{4+}][OH^-]^4[CO_3^{2-}]^2 \quad (2)$$

where [ ] represents concentrations, and K_1^c is the conditional equilibrium constant for reaction (1).

Experimental data listed in Weigel et al. (1986) indicates that Pu(IV) forms a hydroxy complex with EDTA ligand. The stoichiometry of this complex has been indicated to be $Pu(OH)EDTA^-$. This is the only known Pu-EDTA complex and, at present, we have no evidence for the existence of other Pu-EDTA complexes. The formation of $Pu(OH)EDTA^-$ complex from unbound component reactant species can be represented by the reaction

$$Pu^{4+} + OH^- + EDTA^{4-} = Pu(OH)EDTA^- \quad (3)$$

The concentration of $Pu(OH)EDTA^-$ is related to the unbound reactant species by the relationship

$$[Pu(OH)EDTA^-] = K_3^c[Pu^{4+}][OH^-][EDTA^{4-}] \quad (4)$$

where [ ] represents concentrations, and K_3^c is the conditional equilibrium constant for reaction (3). The concentration ratio of complexes $[Pu(OH)_4(CO_3)_2^{4-}$ and $Pu(OH)EDTA^-]$ can be computed using the equations (2) and (4)

$$[Pu(OH)_4(CO_3)_2^{4-}]/[Pu(OH)EDTA^-] = K_1^c[Pu^{4+}][OH^-]^4[CO_3^{2-}]^2/K_3^c[Pu^{4+}][OH^-][EDTA^{4-}] \quad (5)$$

This relationship can be further simplified to

$$[Pu(OH)_4(CO_3)_2^{4-}]/[Pu(OH)EDTA^-] = K_1^c[OH^-]^3[CO_3^{2-}]^2/K_3^c[EDTA^{4-}] \quad (6)$$

The conditional constants, K_1^c and K_3^c (for ionic strength of 0.2) were calculated from data listed by Yamaguchi et al. (1994) and Weigel et al. (1986). Assuming that the free (unbound) concentrations of the ligands are

equivalent to the total concentrations found in tank B-109

$$[OH^- = 1.29M,\ CO_3^{2-} = 3.17x10^{-4}M,\ \text{and EDTA} = 8.13x10^{-3}]$$

we can compute the concentration ratio as:

$$[Pu(OH)_4(CO_3)_2^{4-}]/[Pu(OH)EDTA^-] = 3.02x10^{49}[1.29]^3[3.17x10^{-4}]^2/7.24x10^{16}[8.13x10^{-3}] \quad (7)$$

From equation (7) the concentration ratio $[Pu(OH)_4(CO_3)_2^{4-}]/[Pu(OH)EDTA^-]$ is calculated to be 1.1 x 10^{28}. The magnitude of this ratio indicates that in tank supernatants (in which carbonate concentrations are typically higher than concentrations of organics such as EDTA), the dominant Pu(IV) species would be Pu-hydroxycarbonate complexes and that the concentrations of Pu-organic complexes such as $Pu(OH)EDTA^-$ would be insignificant.

Recall that we purposefully selected a tank with high EDTA and low CO_3^{2-} concentrations. As shown in equation (6), the ratio of $Pu(OH)_4(CO_3)_2^{4-}$ to $Pu(OH)EDTA^-$ complexes varies as the cube of the free hydroxide, square of the free carbonate, and inversely with the free EDTA concentrations. Tanks with low hydroxide and carbonate but high EDTA supernatant concentrations would lower the ratio, but it would take an unrealistic combination of these three variables (condition not encountered so far in Hanford tank supernatants) to lower the ratio to a point where $Pu(OH)EDTA^-$ complex becomes significant.

REFERENCES

Weigel, F., J. J. Katz, and G. T. Seaborg, 1986, "Plutonium," in *The Chemistry of Actinide Elements*, Chapman and Hall, London, England.

Yamaguchi, T., Y. Sakamoto, and T. Ohnuki, 1994, "Effect of Complexation on the Solubility of Pu(IV) in Aqueous Carbonate System," *Radiochim. Acta.*, Vol. 66/67, pp. 9-14

DISTRIBUTION SHEET

To	From	Page 1 of 3
Distribution	Safety Issue Resolution	Date
Project Title/Work Order		EDT No. 61375B
Fluid Dynamics, Particulate Segregation, Chemical Processes, Natural Ore Analog and Tank Inventory Discussions that Relate to the Potential for Criticality in Hanford Tanks		ECN No.

Name	MSIN	Text With All Attach.	Text Only	Attach./ Appendix Only	EDT/ECN Only
U.S. Department of Energy, Richland Operations Office					
D. H. Alexander	S7-51	X			
C. L. Sohn	S7-51	X			
U.S. Department of Energy					
H. Calley 19901 Germantown Road Germantown, MD 20874		X			
R. E. Felt 850 Energy Drive, MS 1222 Idaho Falls, ID 83401		X			
Westinghouse Hanford Company					
H. Babad	S7-14	X			
G. S. Barney	T5-12	X			
R. K. Biyani	L5-31	X			
D. R. Bratzel (5)	S7-14	X			
L. M. Calderon	R3-01	X			
R. J. Cash	S7-14	X			
M. L. Cowen	A2-34	X			
G. L. Dunford	A2-34	X			
S. J. Eberlein	R2-12	X			
J. Greenborg	H0-35	X			
J. W. Hagan	R3-01	X			
D. W. Jeppson	L5-31	X			
J. J. Klos	R2-54	X			
E. J. Lipke	A2-34	X			
R. M. Marusich	A2-34	X			
C. A. Rogers	A3-34	X			
T. S. Vail	R2-54	X			
A. E. Waltar	H0-32	X			
Central Files (orig. +1)	A3-88	X			
Document Processing Center	A3-94	X			

DISTRIBUTION SHEET

To	From	Page 2 of 3
Distribution	Safety Issue Resolution	Date
Project Title/Work Order		EDT No. 613758
Fluid Dynamics, Particulate Segregation, Chemical Processes, Natural Ore Analog and Tank Inventory Discussions that Relate to the Potential for Criticality in Hanford Tanks		ECN No.

Name	MSIN	Text With All Attach.	Text Only	Attach./ Appendix Only	EDT/ECN Only
Battelle Columbus					
R. W. Tayloe Room 11-10-070 505 King Avenue Columbus, OH 43201		X			
Lawrence Livermore National Laboratory					
L. Gray Mail Stop: L-394 7000 East Avenue Livermore, CA 94550		X			
MACTC					
Y. G. Noorani	S7-73	X			
Los Alamos National Laboratory					
T. P. McLaughlin Mail Stop: F-691 Bikini Atol Road SM 30 Warehouse Los Alamos, NM 87545		X			
Pacific Northwest National Laboratory					
J. W. Brothers (2)	K8-07	X			
J. P. LaFemina	K9-91	X			
S. V. Mattigod	K6-81	X			
L. G. Morgan	K6-48	X			
Y. Onishi (3)	K9-33	X			
A. W. Prichard	K8-34	X			
R. J. Serne (7)	K6-81	X			
G. A. Whyatt (5)	P7-19	X			
Bechtel Hanford Company					
P. G. Doctor	H0-02	X			

DISTRIBUTION SHEET

To	From	Page 3 of 3
Distribution	Safety Issue Resolution	Date
Project Title/Work Order		EDT No. 613758
Fluid Dynamics, Particulate Segregation, Chemical Processes, Natural Ore Analog and Tank Inventory Discussions that Relate to the Potential for Criticality in Hanford Tanks		ECN No.

Name	MSIN	Text With All Attach.	Text Only	Attach./ Appendix Only	EDT/ECN Only
M. Chew & Associates					
R. Vornehm 7008 Regency Road Knoxville, TN 37931		X			
Oak Ridge National Laboratory					
E. Whitesides 510 Lakewood Road Kingston, TN 37763		X			
Westinghouse Savannah River Company					
M. Thompson Savannah River Site Building 773-51A Aiken, SC 29808		X			
W2S Company					
W. W. Schulz 5314 Arustos Court, NE Albuquerque, NM 87111		X			